UNIVERSIDAD COMPLUTENSE DE MADRID
FACULTAD DE CIENCIAS QUÍMICAS
Departamento de Química Analítica

TESIS DOCTORAL

Estudio del papel de la molécula CD69 en la regulación de la inflamación y angiogénesis mediante estrategias bioanalíticas

MEMORIA PARA OPTAR AL GRADO DE DOCTOR

PRESENTADA POR

Raquel Sánchez Díaz

Directores

María Pilar Martín Fernández
José Luis Luque García

Madrid, 2018

UNIVERSIDAD COMPLUTENSE DE MADRID

FACULTAD DE CIENCIAS QUÍMICAS
Departamento de Química Analítica
Doctorado en Química Avanzada

TESIS DOCTORAL

Estudio del papel de la molécula CD69 en la regulación de la inflamación y angiogénesis mediante estrategias bioanalíticas

Memoria para optar al grado de Doctor presentada por:

RAQUEL SÁNCHEZ DÍAZ

Directores:

María Pilar Martín Fernández

José Luis Luque García

Madrid, 2017

UNIVERSIDAD COMPLUTENSE DE MADRID

Facultad de Ciencias Químicas

Departamento de Química Analítica

Doctorado en Química Avanzada (R.D. 1393/2007)

Título de la Tesis

Estudio del papel de la molécula CD69 en la regulación de la inflamación y angiogénesis mediante estrategias bioanalíticas

Tesis Doctoral presentada por

Raquel Sánchez Díaz para optar al grado de Doctor

Tesis Doctoral dirigida por los Doctores

María Pilar Martín Fernández y Jose Luis Luque García

Madrid 2017

Madrid, 03 de Abril de 2017

La Doctora María Pilar Martín Fernández, *Assistant Professor* y jefe de grupo de "*Moléculas Reguladoras de los Procesos Inflamatorios*" del Área de Patofisiología Vascular del Centro Nacional de Investigaciones Cardiovasculares (CNIC) CERTIFICA:

Que el trabajo de investigación titulado "***Estudio del papel de la molécula CD69 en la regulación de la inflamación y angiogénesis mediante estrategias bioanalíticas***", ha sido realizado por Doña Raquel Sánchez Díaz, bajo mi codirección y asesoramiento, considerando que es apto para su defensa ante tribunal y reúne las condiciones exigibles para optar al grado de Doctor.

Y para que así conste extiendo el presente certificado en Madrid a 3 Abril de 2017.

Firmado, Dra. M. Pilar Martín.

Assistant Professor
Group Leader *Regulatory Molecules* Lab.
Vascular Pathophysiology Area
Centro Nacional de Investigaciones cardiovasculares (CNIC)
28029 Madrid, Spain
Phone: +34 91 453 1200-ext 2009
pmartinf@cnic.es
web: http://www.cnic.es/es/inflamacion/moleculas/index.php

Universidad Complutense de Madrid
Dpto. Química Analítica - Facultad de CC. Químicas - Ciudad Universitaria. 28040 Madrid
Tfno.: 34 913944331 Fax: 34 913944329 E-mail: depquian@ucm.es

Madrid, 03 de Abril de 2017

José Luis Luque García, Profesor Contratado Doctor del Departamento de Química Analítica de la Facultad de Ciencias Químicas de la Universidad Complutense de Madrid, CERTIFICA:

Que el trabajo de investigación titulado: "***Estudio del papel de la molécula CD69 en la regulación de la inflamación y angiogénesis mediante estrategias bioanalíticas***", ha sido realizado por Doña Raquel Sánchez Díaz, bajo mi codirección y asesoramiento, considerando que es apto para su defensa ante tribunal y reúne las condiciones exigibles para optar al grado de Doctor.

Y para que así conste, extiendo el presente certificado en Madrid a 3 de Abril de 2017.

Fdo: Dr. José L. Luque García
Dpto. Química Analítica
Facultad de Ciencias Químicas
Universidad Complutense de Madrid
Ciudad Universitaria s/n 28040 Madrid, España
Tel. 913944212

ÍNDICE

ABREVIATURAS Y ANGLICISMOS

ANOVA: Analisis de la varianza *(Analysis Of Variance)*

APCs*:* Células presentadoras de antígeno *(Antigen Presenting Cells)*

AU: unidades arbitraries *(Arbitrary Units)*

BM : Medula ósea *(Bone Marrow)*

CD4SP: Linfocitos CD4 simples positivos.

CH : Hipersensibilidad de contacto. *(Contac Hypersensitivity)*

CIA: Artritis inducida por colágeno. (*Collagen Induced Arthritis)*

CTLA-4: Antigeno -4 asociado al linfocito T citotoxico *(Cytotoxic T Lymphocyte Antigen-4)*

CTLD: Dominio de lectina tipo C *(C- type lectin domain)*

DC: Células dendríticas*. (Dendritic cells)*

DIGE: *Difference gel electrophoresis*

DR/DRep: Animales dobles reportero

EAE: Encefalomielitis autoimmune experimental *(Experimental Autoimmune Encephalomyelistis)*

EAM*:* Miocarditis experimental autoinmune *(Experimental Autoimmune Myocarditis)*

ELISA*:* *Enzyme Linked Immuno Sorvent Assay*

FACS: *Fluorescence Activated Cells Sorting*

FMT: Tomografía Molecular de Fluorescencia *(Fluorescence Molecular Tomography)*

FoxP3*:* *Forkhead Box Protein 3*

FTOC: Cultivo organotípico de timos fetales *(Fetal Thymus Organ Culture)*

GFP: Proteína verde fluorescente *(Green Fluorecent Protein)*

GITR: Receptor de TNFα inducido por glucocorticoides *(Glucocorticoid-Induced TNF receptor)*

HIF1α: Factor 1-alfa inducible por hipoxia *(Hypoxia Induced Factor I)*

HUVEC: Células endoteliales humanas de cordon umbilical *(Human Umbilical Endothelial Cells)*

I: Ionomicina

ICAT*: Isotope-coded affinity tag*

ICPL: *Isotope Coded Protein Label*

IFNγ: Interferon gamma

IL: Interleuquina

IS: Isquemia

iTRAQ*: Isobaric tags for Relative and Absolute Quantification*

iTreg: Células T reguladoras inducibles

KO: ***knock-out***

mAB: anticuerpo monoclonal

Me-LN: Ganglios linfáticos del mediastino *(Mediastinun Lymph Nodes)*

MFI: Media de la intensidad de la fluorescencia

MLEC: Células endoteliales de pulmon *(Mouse Lung Endothelial Cells)*

MHC: Complejo mayor de histocompatibilidad *(Major Histocompatibility Complex)*

miRNA: microRNA

mRNA: RNA mensajero

MS: Espectrometría de masas*. (Mass spectrometry)*

MS-LN: Ganglios linfáticos mesentéricos *(Mesenteric Lymph Nodes)*

NFκB: Factor nuclear kappa beta

NKs: Células *natural killer*

NX: Nefrectomía

OVA : Albúmina de huevo (*Ovoalbumin*)

PBLs: Linfocitos de sangre periférica (Periferal Blood Lymphocytes)

PBMCs: Células mononucleares de sangre periférica *(Peripheral Blood Mononuclear Cells)*

P-LN: Ganglios linfáticos periféricos *(Peripheral Lymph Nodes)*

PAD: Enfermedad arterial periférica *(Peripheral Arterial Disease)*

PDF: Fluido de diálisis peritoneal (*Peritoneal Dialysis Fluid)*

PHA: Fitohemaglutinina

PI3K: Fosfatidil inositol 3 quinasa *(Phosphatidil Inositol 3P)*

PMA: Forbol 12 Miristato 13 Acetato

P+I: *PMA+IONOMICINA*

PO-LN: Ganglios linfáticos poplíteos *(Popliteal Lymph Nodes)*

pTreg: células t reguladoras periféricas *(Peripheral Treg)*

qPCR: Reacción en cadena de la polimerasa (*Polimerase chain reaction*) cuantitativa

RFP: Proteína roja fluorescente *(Red Fluorecent Protein)*

ROCK1: Rho-associated, coiled-coil-containing protein kinase 1

RHOA: *Ras homolog gene family, member A*

Rho GDI 1: Rho GDP dissociation factor 1

RORγt: Factor de transcripción nuclear huérfano relacionado con el ácido retinoico gamma t *(Retinoic Acid-Related Orphand Receptor gamma1)*

RU: Unidades relativas *(Relative units)*

SD: Desviación estántar *(Standar Deviation)*

SILAC: Marcaje metabólico con isótopos estables *(Stable isotope labeling with amino acids in cell culture)*

$S1P_1$: Receptor de la esfingosina 1 fosfato 1 *(Sphingosine 1- phosphate receptor 1)*

$S1P_3$: Receptor de la esfingosina 1 fosfato 3 *(Sphingosine 1- phosphate receptor 3)*

Sorting: Análisis preparativo para separación de células mediante citometría de flujo

SOSC1: Supresor de señalización de citoquinas 1 *(Suppressor Of Cytokine Signaling 1)*

STAT´s: Transductores de señal y activadores de la transcripción. *(Signal Transducers and Activators of Transcription)*

TCR: Receptor de los linfocitos T *(T Cell Receptor)*

Tconv: Linfocitos T convencionales

TGFβ: Factor de crecimiento transformante beta.

Th: Linfocitos T colaboradores *(T helper)*

TLR: *Toll Like Receptor*

TNF: Factor de necrosis tumoral *(Tumor Necrosis Factor)*

Tr1: Células T reguladoras tipo1 *(regulatory T cells type 1)*

Treg: Células T reguladoras *(Regulatory T cell)*

tTreg: Células T reguladoras del timo (*Thymus regulatory T cells*)

UTR: Región no traducida *(UnTraslated Region)*

VEGF: Factor de crecimento vascular endotelial. (***Vascular endothelial growth factor)***

VSCM: Células vasculares de músculo liso (*Smooth Vascular Muscle Cells)*

WB: *Western Blot*

WT: Fenotipo salvaje *(Wild Type)*

OBJETIVOS

Los objetivos de esta tesis doctoral han sido los siguientes:

1. Estudiar el papel de CD69 en los procesos fibroproliferativos, mediados por la respuesta immune de células Th17 y T reguladoras.

2. Estudiar el papel de CD69 en el desarrollo de las células T reguladoras generadas en el timo y en la función y homeostasis de estas células en tejidos en estados patológicos y fisiológicos.

3. Testar el papel del receptor CD69 en la regulación de la respuesta inmune implicada en procesos de angiogénesis post-isquemia.

4. Estudiar, mediante técnicas bioanalíticas, las rutas de señalización de las células endoteliales en procesos de angiogénesis, así como el papel de CD69 en estos procesos.

RESUMEN

El antígeno CD69 es una proteína transmembrana expresada en leucocitos tras su activación y que persiste en infiltrados leucocitarios de tejidos inflamados en diversas enfermedades crónicas y autoinmunes. Se ha descrito que los ratones deficientes en CD69 muestran una respuesta inflamatoria exacerbada en modelos animales de estas enfermedades, lo que confiere a esta molécula un importante papel como regulador de la respuesta inmune. En este trabajo hemos analizado el papel inmunomodulador de CD69 en la generación de fibrosis tras diálisis peritoneal, encontrando que este receptor regula el balance entre las células Th17 y T reguladoras (Treg) en enfermedades que cursan con procesos fibro-proliferativos. La inhibición de las repuestas Th17 por CD69 en estos procesos limita la síntesis de citoquinas pro-inflamatorias como el TGFβ o la IL-6, íntimamente ligadas a la proliferación de fibroblastos, por lo que los animales deficientes en CD69 presentan una fibrosis severa de la membrana peritoneal, incluso en condiciones urémicas. Los experimentos con animales reconstituidos con precursores hematopoiéticos demostraron que la expresión de CD69 en células linfoides es la responsable del control de los procesos fibro-proliferativos.

Las células Treg son esenciales para el mantenimiento de la homeostasis inmune y del control de las células Th17 y su activación exacerbada en reacciones autoinmunes. En esta tesis se ha abordado el estudio del papel de CD69 en la función y la diferenciación de las Treg, así como el análisis de los mecanismos moleculares implicados en estos procesos. Hemos caracterizado una población de células Treg Foxp3^{+} CD69^{+} que expresa el receptor de manera constitutiva y que es esencial para el desarrollo de las repuestas reguladoras y la supresión de las células T convencionales *in vitro* e *in vivo*. La expresión de CD69 en estas células está acompañada por un incremento en la expresión de otros recetores inmuno-reguladores como el CTLA-4, GITR o ICOS, un aumento de la secreción de TGFβ y una potente actividad supresora. Estos mecanismos, regulados por CD69 a través de la activación de las vías de ERK y STAT5, están inhibidos tras el bloqueo del receptor con anticuerpos anti-CD69, demostrando el papel clave de esta molécula en estos procesos. La terapia con células Treg Foxp3^{+} CD69^{+} en animales deficientes en CD69 con tolerancia inmunológica desregulada, revierte el fenotipo de estos animales eficientemente previniendo la inflamación en un modelo de asma.

Aunque la implicación del microRNA-155 (miR-155) y su promotor BIC en el desarrollo de las células T reguladoras en el timo está muy estudiada, la vía de activación del miR-155 que conduce a la diferenciación de las células tTreg no se había definido. En este trabajo mostramos que la regulación de la expresión de CD69, mediante silenciamiento por shRNA o transfección de miR-155, es crítica para la diferenciación de células tTreg y la homeostasis de pTreg mediante la regulación de BIC/miR-155 y su diana, el supresor de la señalización de citoquinas 1 (SOCS1). La ausencia de CD69 inhibe la fosforilación y activación de Stat5 conduciendo a una menor

transcripción de BIC/miR155 y a un incremento de la expresión de SOCS1, inhibiendo de este modo la diferenciación de tTregs en embriones, animales adultos y quimeras hematopoiéticas $CD69^{-/-}$. En consecuencia, los ratones *miR155*$^{-/-}$ tienen deficiencia en células Treg $CD69^{+}$, mientras que la sobre-expresión de miR-155 induce la expresión del receptor CD69, lo que sugiere que ambas moléculas se activan concomitantemente en un bucle de retroalimentación positivo. Nuestros datos demuestran que el receptor CD69 actúa como una molécula clave y no redundante en el proceso de diferenciación de células T reguladoras en el timo, contribuyendo de una manera muy importante a preservar los mecanismos de homeostasis inmune.

Las enfermedades cardiovasculares causadas por isquemia tienen un importante componente inflamatorio. Aunque la mayoría de estudios se han realizado en el compartimento mieloide, también se ha relacionado a los linfocitos Th17 y Treg de la inmunidad adaptativa como moduladores antagónicos de los procesos de neo-vascularización post-isquemia. En este trabajo demostramos la implicación del receptor CD69 en procesos de angiogénesis, desde dos puntos de vista; el papel de CD69 como mediador inmune a través de la regulación del balance entre células Th17 y Treg y su papel como regulador de distintos procesos angiogénicos en las células endoteliales. Hemos encontrado que las células Th17 se inducen tras la isquemia activando la transcripción del miR-721 por estas células y su secreción a la sangre. Estos procesos están exacerbados en los animales deficientes en CD69, cuya expresión de este miRNA regula negativamente la expresión de sus genes diana Meox2 y CUX1 en el tejido isquémico. Estos genes, de la familia de factores de transcripción homeobox, tienen propiedades anti-angiogénicas que regulan los procesos de revascularización tras la isquemia. En consecuencia, los animales $CD69^{-/-}$, así como las quimeras hematopoiéticas que no expresan el receptor en el compartimento linfoide, realizan la revascularización de los tejidos isquémicos de un modo más eficiente que los animales $CD69^{+/+}$.

Debido a la complejidad de procesos biológicos que forman parte de la angiogénesis, realizamos un análisis proteómico, mediante la técnica de SILAC, comparando las células endoteliales de pulmón procedentes de animales $CD69^{+/+}$ y $CD69^{-/-}$ activadas *ex vivo*. El análisis bioanalítico mediante esta técnica nos ha permitido identificar una serie de proteínas involucradas en estos procesos como la *Rho GDP dissociation inhibitor 1* (Rho GDI 1) o la *PDZ and LIM domain protein 1*. La activación de la Rho GDI 1 induce la inactivación de RhoA/ROCK1 lo que favorece la activación de la vía AKT/mTOR y la inducción de HIF-1α y por lo tanto de la angiogénesis, reforzando la hipótesis del papel anti-angiogénico del receptor CD69 en las células endoteliales. Por otro lado, las proteínas con dominios LIM están implicadas en la movilización del citoesqueleto celular que tiene un papel fundamental en el reclutamiento de proteínas como los receptores de efrinas, que estabilizan los receptores de VEGF en la membrana de la célula endotelial promoviendo la activación y proliferación de las mismas. Este estudio reveló un inesperado e importante papel de CD69 en las células endoteliales así como en los procesos de neo-vascularización post-isquemia postulando esta molécula como una diana terapeútica en esta patología.

En resumen, en esta tesis se han estudiado varias funciones del receptor inmune CD69 en procesos fibro-proliferativos, de generación de tolerancia inmunológica, de diferenciación de las células T reguladoras y de la

revascularización post-isquemia. El estudio de todos estos procesos, de enorme importancia en numerosas patologías inflamatorias crónicas, autoinmunes y cardiovasculares, que parecen estar regulados por la molécula CD69 han revelado numerosas proteínas y miRNAs esenciales en estas enfermedades. El análisis bioanalítico por SILAC de las células endoteliales reveló numerosos procesos y proteínas regulados por CD69, este estudio abre nuevas vías de investigación que postulan esta molécula como moduladora de distintas proteínas y procesos en enfermedades autoinmunes y cardiovasculares.

SUMMARY

The CD69 antigen is a transmembrane protein expressed in leukocytes upon activation and that persists in leukocyte infiltrates of inflamed tissues in various chronic and autoimmune diseases. CD69 deficient mice have been reported to exhibit an exacerbated inflammatory response in animal models of these diseases, which gives this molecule an important role as a regulator of the immune response. In this study we have analyzed the role of CD69 in the generation of fibrosis after peritoneal dialysis, and found that this receptor regulates the balance between Th17 and T regulatory cells (Treg) in diseases that occur with fibroproliferative processes. Inhibition of Th17 responses by CD69 in these processes limits the secretion of pro-inflammatory cytokines such as TGFβ or IL-6, intimately linked to fibroblast proliferation, whereby CD69 deficient animals exhibit severe fibrosis of the Peritoneal membrane, even under uremic conditions. Experiments with animals reconstituted with hematopoietic precursors demonstrated that the expression of CD69 in lymphoid cells is responsible for the control of fibroproliferative processes.

Treg cells are essential for the maintenance of immune homeostasis and control of Th17 cells and their exacerbated activation in autoimmune reactions. This Thesis has addressed the study of the role of CD69 in the function and differentiation of Tregs, as well as the analysis of the molecular mechanisms involved in these processes. We have characterized a population of $Foxp3^+$ $CD69^+$ Treg cells that expresses the receptor in a constitutive way and is essential for the development of regulatory responses and the suppression of conventional T cells *in vitro* and *in vivo*. The expression of CD69 in these cells is accompanied by an increase in the expression of other immunoregulatory receptors such as CTLA-4, GITR or ICOS, an increase in TGFβ secretion and potent suppressor activity. These mechanisms, regulated by CD69 through the activation of ERK and STAT5 pathways, are inhibited after receptor blockade with anti-CD69 antibodies, demonstrating the key role of these molecules in these processes. Adoptive therapy with $Foxp3^+$ $CD69^+$ Treg cells in CD69 deficient animals, with deregulated immunological tolerance, reverses the phenotype of these animals efficiently by preventing inflammation in an asthma model.

Although the involvement of microRNA-155 (miR-155) and its promoter BIC in the development of regulatory T cells in the thymus is well studied, the miR-155 activation pathway leading to differentiation of tTreg cells is not well defined. In this work, we show that the regulation of CD69 expression by silencing by shRNA or miR-155 transfection is critical for the differentiation of tTreg cells and pTreg homeostasis by the regulation of BIC / miR-155 and its target, the suppressor of cytokine signaling 1 (SOCS1). The absence of CD69 inhibits Stat5 phosphorylation and activation leading to lower BIC / miR155 transcription and increased SOCS1 expression,

thereby inhibiting the differentiation of tTregs in embryos, adult animals and CD69$^{-/-}$ hematopoietic chimeras. As a consequence, miR155$^{-/-}$ mice are deficient in CD69^{+} Treg cells, whereas overexpression of miR-155 induces CD69 receptor expression, suggesting that both molecules are activated concomitantly in a positive feedback loop. Our data demonstrate that the CD69 receptor acts as a key and non-redundant molecule in the process of differentiation of regulatory T cells in the thymus, contributing in a very important way to preserving the mechanisms of immune homeostasis.

Cardiovascular diseases caused by ischemia have an important inflammatory component. Although most studies have been performed in the myeloid compartment, Th17 and Treg lymphocytes of adaptive immunity have also been implicated as antagonistic modulators of post-ischemic neo-vascularization processes. In this study, we demonstrate the implication of the CD69 receptor in angiogenesis processes, from two points of view; the role of CD69 as an immune mediator by regulating the balance between Th17 and Treg cells and its role as a regulator of different angiogenic processes of endothelial cells. We have found that Th17 cells are induced after ischemia by activating the transcription of miR-721 by these cells and their secretion into the blood. These processes are exacerbated in animals deficient in CD69 whose expression of this miRNA negatively regulates the expression of their target genes Meox2 and CUX1 in the ischemic tissue. These genes, from the family of homeobox transcription factors, have anti-angiogenic properties that regulate the revascularization processes after ischemia. Consequently, CD69 $^{-/-}$ animals, as well as hematopoietic chimeras that do not express the receptor in the lymphoid compartment, revascularize ischemic tissues more efficiently than CD69 $^{+/+}$ animals.

Due to the complexity of biological processes that are part of angiogenesis, we performed a proteomic analysis, using the SILAC technique, comparing the lung endothelial activated cells from CD69 $^{+/+}$ and CD69$^{-/-}$ animals *ex vivo*. The bioanalytical analysis by means of this technique has allowed us to identify a group of proteins involved in these processes as the Rho GDP dissociation inhibitor 1 (Rho GDI 1) or the PDZ and LIM domain protein 1. Activation of Rho GDI 1 induces the inactivation of RhoA / ROCK1, which favors the activation of the AKT / mTOR pathway and the induction of HIF-1α and thus of angiogenesis, reinforcing the hypothesis of the anti-angiogenic role of the CD69 receptor in endothelial cells. On the other hand, proteins with LIM domains are involved in the mobilization of the cellular cytoskeleton that plays a fundamental role in the recruitment of proteins such as ephrin receptors, which stabilize VEGF receptors in the endothelial cell membrane promoting its activation and proliferation. This study revealed an unexpected and important role of CD69 in endothelial cells as well as post-ischemia neo-vascularization processes, postulating this molecule as a therapeutic target in this pathology.

In summary, this Thesis has studied several functions of the CD69 immune receptor in fibroproliferative processes, generation of immune tolerance, differentiation of regulatory T cells and post-ischemia revascularization. The study of all these processes, of enormous importance in many chronic inflammatory, autoimmune and

cardiovascular pathologies, that appear to be regulated by the CD69 molecule, have revealed numerous proteins and essential miRNAs in these diseases. The bioanalytical analysis by SILAC of endothelial cells revealed numerous processes and proteins regulated by CD69, this study opens new avenues of investigation that postulate this molecule as modulator of different proteins and processes in autoimmune and cardiovascular diseases.

I. INTRODUCCIÓN

I. INTRODUCCIÓN

1. LAS RESPUESTAS INMUNITARIAS

El sistema inmune tiene como función fundamental la defensa frente a agentes extraños, ya sean microorganismos, macromoléculas o compuestos químicos. Su mecanismo de acción consta de dos tipos de respuesta, las reacciones inmediatas conocidas como respuesta inmune innata y las reacciones tardías o respuesta inmune adaptativa. La respuesta inmune innata constituye la primera línea de defensa frente a los microorganismos patógenos y se caracteriza por constituir mecanismos de respuestas rápidos que eliminen los agentes infecciosos. La respuesta inmune adaptativa constituye un método de defensa más específico que se activa tras la exposición a un agente infeccioso, aumentando su intensidad y capacidad de respuesta en las siguientes exposiciones a dicho patógeno. Esta respuesta está constituida por la inmunidad humoral y la inmunidad celular.

La inmunidad humoral se caracteriza por la producción de anticuerpos por los linfocitos B, cuya función es reconocer específicamente antígenos, neutralizándolos para que sean eliminados por diversos mecanismos efectores. En la inmunidad celular participan los linfocitos T que se dividen fundamentalmente en dos grandes poblaciones con distintas características. Los linfocitos T $CD8^+$ tienen función citotóxica o citolítica, eliminando las células que presentan antígenos extraños como las células infectadas por virus u otro tipo de patógenos. Los linfocitos T $CD4^+$ o colaboradores (T *helper, Th*) actúan de puente entre la inmunidad innata y la adaptativa favoreciendo la proliferación y diferenciación de otros linfocitos y reclutando células de la respuesta inmune innata.

2. LA RESPUESTA INMUNE ADAPTATIVA

La respuesta inmune adaptativa consta de tres etapas: la primera etapa o fase de reconocimiento del antígeno, segunda etapa o fase de activación de los linfocitos y la tercera fase efectora. En la fase de activación, los linfocitos T vírgenes requieren de las señales proporcionadas por las células presentadoras de antígeno (*Antigen-Presenting Cell*, APC). El antígeno es presentado por las APCs a las células T en el contexto de las moléculas del complejo mayor de histocompatibilidad (*Major Histocompatibility Complex,* MHC). Tras el reconocimiento de un antígeno a través del receptor de células T (*T cell receptor*, TCR) específico y la activación de este clon de linfocitos T, se produce una

respuesta que implica la síntesis de proteínas, entre las que se encuentran las citoquinas, que estimulan la proliferación y función de los linfocitos de manera autocrina así como de otras células efectoras de la respuesta inmune.

2.1. RESPUESTAS TH1 Y TH2

Las células T $CD4^+$ se han clasificado tradicionalmente en dos subpoblaciones Th1 y Th2 dependiendo de su función efectora y del patrón de citoquinas secretadas (Mosmann and Coffman, 1989; Swierkosz et al., 1979) y (Tada et al., 1978). Las células Th1 se caracterizan por la secreción de interferón gamma (IFN-γ) como mecanismo para regular la inmunidad celular. Su diferenciación tiene lugar tras la producción de interleuquina (IL)-12 e IFN-γ por parte de las APC y de las células *Natural Killers* (NK), respectivamente (Napolitani et al., 2005; Szabo et al., 2003). El factor de trascripción Stat4 (*Signal Transducers and Activators of Trascription 4*) media el proceso de expresión de estas citoquinas, que desencadenan la inmunidad celular mediante la diferenciación de células Th1 (Trinchieri et al., 2003). Stat4 es fosforilado por el receptor de la IL-12 induciendo su homodimerización y translocación al núcleo, una vez allí activa el factor de trascripción T-bet que es el regulador principal de la diferenciación de las células T $CD4^+$ hacia el linaje Th1.

Las células Th2 se caracterizan por la secreción de IL-4, IL-5 e IL-13, entre otras, mediando en la respuesta inmune humoral y las respuestas alérgicas. La citoquina IL-4 media la diferenciación hacia el linaje Th2 ya que la activación del receptor de esta citoquina fosforila el factor de transcripción Stat6 (Glimcher and Murphy, 2000). La internalización de homodimeros de Stat6 al núcleo induce la expresión de la proteína 3 de unión de GATA (GATA3), que junto con cMaf favorece la diferenciación de las células Th2 (Zheng and Flavell, 1997) (Figura 1).

2.2. RESPUESTAS TH17

En la última década se ha caracterizado un nuevo sub-tipo de células T $CD4^+$ helper, las células Th17 (Harrington et al., 2006; Weaver et al., 2006). Los linfocitos Th17 se caracterizan por expresar un patrón de citoquinas entre las que se encuentran la IL-17A, IL-17F, IL-21 e IL22. La diferenciación hacia el linaje Th17 está mediada por las citoquinas IL-6, TGF-β e IL-1β, entre otras. El receptor de IL-6 en la célula T induce la fosforilación del factor de trascripción Stat3, que a su vez regula transcripcionalmente el receptor nuclear *huérfano* relacionado con el Ácido Retinoico γt (*Retinoic Acid-Related Orphan Receptor gamma* t, RORγt), que dirige la diferenciación de las células Th17 (Ivanov et al., 2006; Yang et al., 2007). La expresión de la citoquina IL-21 producida por las células NK o las NKT, junto con el TGF-β es otra vía

alternativa de la de la diferenciación hacia Th17 (Korn et al., 2007), además la IL-21 es también producida por las células Th17 potenciando su diferenciación de manera autocrina. La IL-23 producida por las células presentadoras y algunas células estromales, estabiliza la población de células Th17 y permite su expansión manteniendo una expresión sostenida de las citoquinas específicas y, por tanto, de la respuesta inmune (Bettelli et al., 2007).

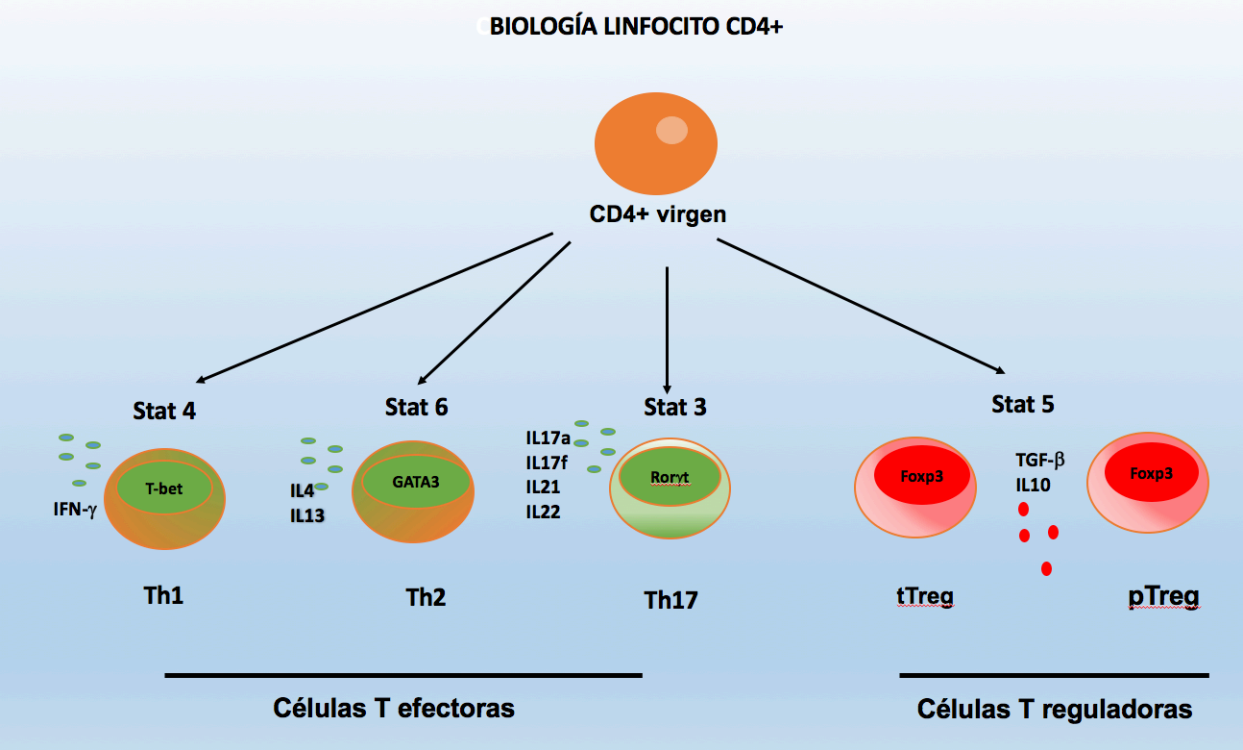

Figura 1: Esquema de diferenciación de los linfocitos T *helper* CD4$^+$. Cuando un linfocito T virgen se expone a un antigen, puede diferenciarse a dos tipos de subpoblaciones de células según la función que vaya a ejercer, efectora o reguladora. En el esquema se detallan, los subtipos de poblaciónes así como los principales factores de transcripción que dan lugar a la diferenciación de cada tipo celular y las citoquinas expresadas por las diferentes poblaciones de células.

Estas células median en procesos inflamatorios y están relacionadas con la patogénesis de muchas enfermedades autoinmunes (Bettelli et al., 2007). La autoinmunidad es un estado de reactividad anómalo del sistema inmune frente a los antígenos propios, debido a fallos en los mecanismos de tolerancia o eliminación de células T auto-reactivas. Algunas enfermedades autoinmunes en las que las células Th17 juegan un papel fundamental son la psoriasis (Krueger et al., 2007), la artritis reumatoide (Kirkham et al., 2006), las enfermedades inflamatorias intestinales (Duerr et al., 2006), el asma (Barczyk et al., 2003), la miocarditis autoinmune (EAM) (Rangachari et al., 2006) la encefalomielitis (Kebir et al., 2007) o la hipersensibilidad por contacto (He et al., 2006; Nakae et al., 2002).

La defensa frente a patógenos infecciosos es otra importante función de los linfocitos Th17, llevada a cabo mediando en la inflamación con predominio de reclutamiento de neutrófilos al tejido inflamado. La inmunidad mediada por linfocitos Th17 es particularmente importante en las mucosas protegiendo al organismo frente a una gran variedad de hongos, bacterias y otros microorganismos (Aujla et al., 2008; Ouyang et al., 2008).

2.3. LINFOCITOS T REGULADORES

La respuesta inmune está regulada mediante un balance entre células efectoras y células T reguladoras (Treg). Estas células se generan en el timo y su función es controlar la respuesta inflamatoria tanto en los órganos linfoides secundarios como en los tejidos inflamados, con el fin de mantener la homeostasis del sistema inmune y evitar un efecto nocivo de una respuesta inflamatoria exacerbada (Ohkura et al., 2013). La mayoría de células Treg se caracterizan por la expresión de la cadena α del receptor de la IL-2 (CD25) y el factor de trascripción FoxP3 (*Forkhead box Protein 3*). La activación de CD25 por IL-2 induce la fosforilación de Stat5 que es el encargado de activar FoxP3 (Burchill et al., 2008; Lio and Hsieh, 2008). La trascripción de FoxP3 interviene en la diferenciación y función supresora de una parte importante de las células Treg (Fontenot et al., 2003; Hori et al., 2003; Wan and Flavell, 2007) (Figura 2).

Las moléculas CD25 y FoxP3 también son expresadas por otros tipos celulares de forma inducible (Kmieciak et al., 2009), por lo que no son exclusivas de las Treg. Otras moléculas expresadas por las Treg y que caracterizan esta población son: CTLA-4 (*Cytotoxic T Lymphocyte Antigen-4*), que interviene en la función supresora de las células Treg y en el control de la homeostasis del sistema inmune (Read et al., 2000); GITR (*glucocorticoid-induced TNF receptor*) que participa en el control de la función de las células Treg; CD27 que también es miembro de los receptores de TNF que se expresa en las células T vírgenes y desaparece en las células T efectoras, pero mantiene su expresión en las Treg (Mack et al., 2009;

Ruprecht et al., 2005). La baja o nula expresión de CD127 (la cadena α del receptor de la IL7) las diferencia de las células T efectoras activadas (Liu et al., 2006; Seddiki et al., 2006). Se han definido dos tipos de células Treg en función de su localización, aunque ambas se producen en el timo. Las células Treg que se encuentran en el timo (tTreg) y las que se encuentran en la periferia (pTreg). En general, las células tTreg responden a antígenos propios y las que se generan en la periferia responden a antígenos extraños, lo que hace suponer que estas dos subpoblaciones de células Treg ejercen diferentes funciones (Hsieh et al., 2006; Jordan et al., 2001; Kretschmer et al., 2005). Las células Treg ejercen su función supresora inhibiendo la actividad efectora de los linfocitos T $CD4^+$ y $CD8^+$ impidiendo su diferenciación, activación o proliferación mediante el contacto célula-célula o a través de la secreción de citoquinas supresoras como la IL-10 o TGF-β (Chen et al., 2003; Collison et al., 2007; Roncarolo et al., 2006). Otro mecanismo efector de las Treg es a través de perforinas o granzimas cuya actividad citotóxica elimina las células T efectoras (Gondek et al., 2005; Grossman et al., 2004). Las células Treg también pueden ejercer su función supresora en células presentadoras de antígeno (*Dendritic Cells, DCs*), atenuando su actividad presentadora y co-estimuladora (Mellor and Munn, 2004; Qureshi et al., 2011) así como en neutrófilos y otras células inflamatorias a través de la actividad ecto-ATP difosfohidrolasa del receptor CD39 (Fabbiano et al., 2015).

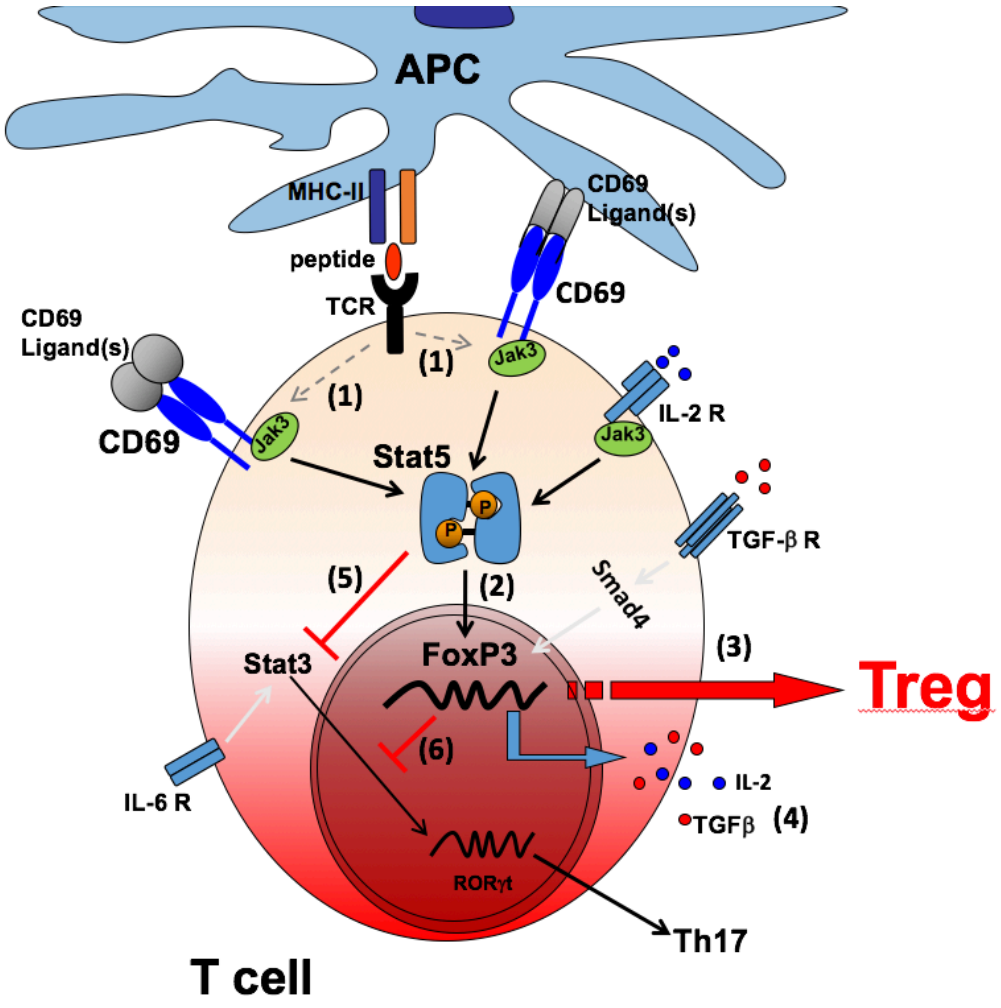

Figura 2: Esquema de las principales vías que intervienen en la diferenciación de las células treg. El reconocimiento por el TCR del antigeno presentado por la APC junto con la activación de CD69 y el IL-2R inducen la fosforilación de la quinasa Jak3 (1). La interacción de Jak3 con Stat5 induce su fosforilación, dimerización y entrada al núcleo (2). Stat5 en el núcleo activa el factor de transcripción FoxP3 que favorece la diferenciación de las células Treg (3). Como consecuencia de la activación de FoxP3 se producen IL2 y TGFβ (4). La inhibición de la activación de Stat3, tanto por Stat5 (5) como por Foxp3 (6), inhiben la transcripción de Rorγt y por lo tanto, diferenciación hacia Th17.

3. ENFERMEDADES INFLAMATORIAS Y AUTOINMUNES

Las enfermedades relacionadas con el sistema inmune suponen un amplio campo, en el que se pueden encontrar implicadas enfermedades en las que el sistema inmune se comporta de manera patológica como pudieran ser los procesos de autoinmunidad, el rechazo de trasplantes o la hipersensibilidad. Además el sistema inmune está implicado en procesos patológicos como la aterosclerosis, enfermedades infecciosas, enfermedades cardiovasculares y procesos neoplásicos. El conocimiento del funcionamiento de la respuesta inmune es crucial para el desarrollo de terapias para todas estas enfermedades.

3.1. AUTOINMUNIDAD

Las enfermedades autoinmunes, que afectan a un 5% de la población mundial, se caracterizan por un fracaso en la tolerancia frente a los antígenos propios, que deriva en respuestas inmunes anómalas (O'Shea and Paul, 2010). En los procesos de autoinmunidad participan las células Th1 mediante la inducción de la inflamación y el daño tisular. La producción de IFN-γ por parte de las de las células T $CD4^+$ participa en el desarrollo de diferentes enfermedades autoinmunes como la diabetes tipo I y la esclerosis múltiple, (Powrie and Coffman, 1993). Junto con las células Th1, las células Th17 juegan un papel fundamental en el desarrollo de las enfermedades autoinmunes. Los animales deficientes en IL-23 son resistentes a desarrollar encefalomielitis experimental (*Experimental Autoimmune Encelomyelitis,* EAE) (Langrish et al., 2005). Además los animales deficientes en la subunidad p19 del receptor de la IL-23, que no desarrollan respuestas Th17, son resistentes a distintas enfermedades autoinmunes como la artritis (Nakae et al., 2003), la EAE (Komiyama et al., 2006), la miocarditis (*Experimental Autoinmune Myocarditis*, EAM) (Rangachari et al., 2006; Sonderegger et al., 2006) y o la hipersensibilidad de contacto (He et al., 2006).

3.2. ENFERMEDADES ALÉRGICAS

Estas enfermedades están determinadas por la influencia de factores genéticos y medioambientales, como la exposición a distintos alérgenos, infecciones o la contaminación ambiental. Los procesos alérgicos están relacionados con reacciones inflamatorias crónicas mediadas por inmunoglobulina E (IgE) y se caracterizan por una respuesta inmediata al antígeno, que en muchas ocasiones puede tener consecuencias patológicas graves. La inflamación bronquial cursa con presencia de eosinófilos e hipertrofia de las células musculares lisas bronquiales debido a la hiperreactividad generada por los antígenos. Este tipo de reacciones alérgicas, que clásicamente estaban relacionadas únicamente con las

respuestas tipo Th2, tienen un importante componente Th17 (Nakae et al., 2002). Hay un incremento en los niveles de IL-17 en los pulmones y lavados broncoalbeolares (BAL) o suero de los pacientes asmáticos (Molet et al., 2001). En modelos de asma alérgico murino mediado por eosinófilos, se ha demostrado que la IL-17 media la inducción de una población de Th2 específica de alérgeno en la fase de sensibilización (Nakae et al., 2002). También se ha descrito que el reclutamiento de los eosinófilos es menor en los ratones deficientes para el receptor de la IL-17 (IL-17R) (Schnyder-Candrian et al., 2006).

4. CD69 Y LA FAMILIA DE LECTINAS TIPO C

4.1 CARACTERIZACIÓN BIOQUÍMICA Y ESTRUCTURAL DE CD69

Las lectinas tipo C son un grupo de proteínas que se caracterizan por poseer un dominio de reconocimiento de carbohidratos (*Carbohydrate Recognition Domain,* CDR). Estás moléculas se dividen en siete subfamilias en función de su estructura, la localización relativa del dominio CDR en relación a los otros dominios, y el grado de similitud estructural y funcional entre los diferentes dominios CDR (Drickamer and Taylor, 1993; Santis et al., 1994). CD69 pertenece a la subfamilia de proteínas transmembrana tipo II, en las que el dominio de reconocimiento de carbohidratos (CTLD, *C- type lectin – like Domain*) ha perdido la capacidad de unir Ca^{2+} a lo largo de la evolución. El gen de CD69 se localiza en el brazo largo del cromosoma 6 en ratón, y en el cromosoma 12 en humano (Lopez-Cabrera et al., 1993); (Ziegler et al., 1994). Este gen se encuentra dentro de la región llamada "*Complejo Natural Killer*" (NKC), que comprende varios genes de la familia de las lectinas tipo C específicas para las células NK (Figura 3A). CD69 pertenece al grupo V de las lectinas tipo C con dominio receptor NK (*NK Domain,* NKD) (Weiss et al., 1998). CD69 es una proteína transmembrana con un dominio CTLD unido a la región citoplasmática N-terminal mediante una región transmembrana (Lopez-Cabrera et al., 1993). Es una glicoproteína homodimérica de unos 60kDa, formada por dos cadenas polipeptídicas idénticas que se diferencian por su estado de glicosilación (de 33 a 27kDa) y que están unidas mediante puentes disulfuro (Sanchez-Mateos and Sanchez-Madrid, 1991) (Figura 3B).

CD69 no une monosacáridos ni polisacáridos mostrando muy baja afinidad por los fucoidanos (Childs et al., 1999). Hasta hace poco no se conocían los ligandos naturales de CD69, pero recientemente se ha demostrado que la galectina 1, expresada en la membrana de células dendríticas, se une a CD69 y la unión de ambos interviene en la función y diferenciación de células Th17 (de la Fuente et al., 2014). Por otro lado, la interacción dependiente de glicosilación entre CD69 y el complejo S100A8/S100A9 favorece la diferenciación de las células Treg (Lin et al., 2015).

A

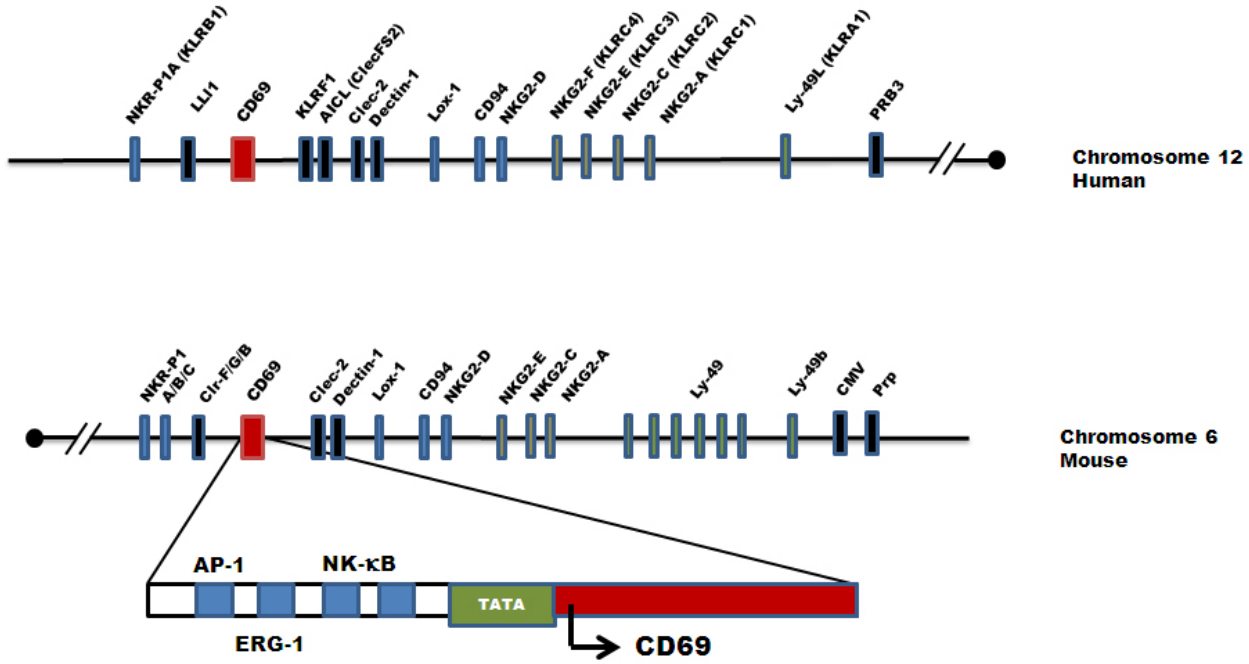

B

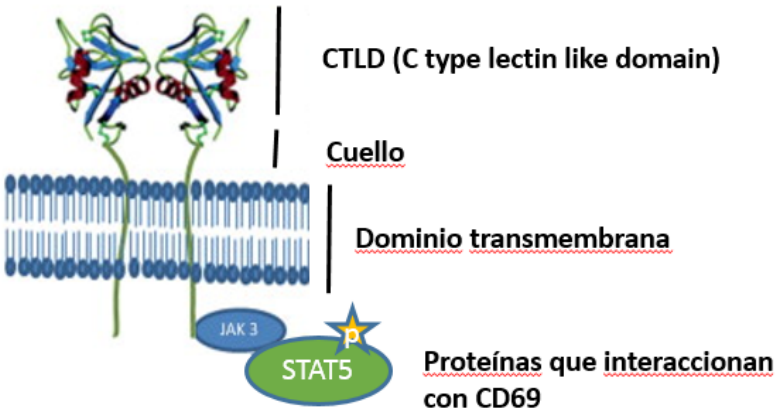

Figura 3: Localización y estructura de CD69. **(A)** Esquema representativo de la localización cromosómica y genes circulantes de CD69 en humano y ratón. **(B)** Estructura del homodímero de CD69 expresado en la membrana de la célula y la interacción con proteínas del citosol.

4.2. REGULACIÓN DE LA TRANSCRIPCIÓN DE CD69

La expresión de CD69 durante la activación de linfocitos T requiere síntesis *de novo* (Cebrian et al., 1988) que puede ser inducida por multitud de estímulos, como el tratamiento con anticuerpos monoclonales frente a CD3/TCR o CD2 y agentes activadores de la proteína quinasa C como los ésteres de forbol, o el tratamiento con lectinas mitogénicas como la fitohemaglutinina (Cebrian et al., 1988). También se ha descrito la expresión de CD69 de forma independiente de antígeno mediante las citoquinas IL-2, TNFα, IL-6 (Unutmaz et al., 1994) e IL-15, que aumenta la expresión de CD69 en células T y NKs (Kanegane and Tosato, 1996; McInnes et al., 1997).

Los estímulos anteriormente descritos intervienen en la expresión de CD69 a través de la activación molecular de la PKC (Cebrián et al. ,1988). De manera parcialmente independiente a esta vía se ha descrito que Ras y su efector Raf están implicados en la expresión de CD69 dependiente de TCR-CD3 (D'Ambrosio et al., 1994). La activación del receptor por anticuerpos monoclonales anti CD69 en presencia de esteres de forbol, provoca un incremento de Ca^{2+} dentro de la célula que activa la quinasa ERK, la expresión de los genes IL-2 e IFNγ y la proliferación de las células T (Testi et al., 1989; Zingoni et al., 2000). En nuestro grupo se ha demostrado que la inducción de CD69 en células T inhibe la diferenciación de las células Th17 a través de la activación de la ruta de señalización Jak3/Stat5, tanto en humano como en ratón (Martin et al., 2010a). La cola citoplasmática de CD69 activa la fosforilación de la vía Jak3/Stat5 inhibiendo la expresión del factor de trascripción RORγt e impidiendo la diferenciación de las células Th17. El bloqueo del receptor de la IL2 inhibe la vía Jak3/Stat5 restableciendo la activación de RORγt y la diferenciación de las células Th17 (Martin et al., 2010a) (Figura 2).

Con respecto a la regulación transcripcional de la expresión de CD69, se ha encontrado una secuencia TATA en la región 5´, 30 pares de bases antes del inicio de la trascripción y varias secuencias putativas de unión de diferentes factores de trascripción como NF-KB, Egr-1 y AP1 que intervendrían en la expresión de éste gen (Lopez-Cabrera et al., 1995). Otros estímulos como los ésteres de forbol o la estimulación por vía del TCR inducen la activación de factores de trascripción como AP-1, EGR y ATF/CREB, que actúan para regular el promotor de CD69 (Castellanos Mdel et al., 2002) (Figura 3A).

4.3. EXPRESIÓN CELULAR DE CD69

CD69 se expresa en la membrana de todas las células derivadas de la médula ósea tras activación, excepto en los eritrocitos (Testi et al., 1994). La expresión en la membrana entre 2 y 4 horas tras la activación celular hace que se considere a CD69 dentro del grupo de genes tempranos inducidos en el

proceso de activación leucocitaria (Lopez-Cabrera et al., 1993)Su expresión constitutiva *in vivo* está restringida a algunos tipos celulares; los timocitos sometidos a procesos de selección en el timo, una población de células Treg y determinadas células residentes (Barthlott et al., 1997; Sanchez-Mateos et al., 1989; Swat et al., 1993). CD69 se encuentra fundamentalmente expresado en la membrana de células presentes en el tejido inflamado de enfermedades como la artritis reumatoide y la hepatitis viral crónica (Garcia-Monzon et al., 1990; Laffon et al., 1991), así como en los leucocitos responsables del rechazo a trasplantes (Mampaso et al., 1993). También se han encontrado niveles elevados de CD69 en lesiones ateroscleróticas, en los linfocitos involucrados en procesos alérgicos (Caspar-Bauguil et al., 1998; Hartnell et al., 1993), en los linfocitos que infiltran tumores (Coventry et al., 1996)y en infecciones persistentes (Zajac et al., 1998).

Otras células que expresan CD69 son las células B del manto de los ganglios linfáticos, en células $CD4^+$ de los centros germinales, plaquetas (Testi et al., 1990), neutrófilos (Gavioli et al., 1992), eosinófilos (Nishikawa et al., 1992) basófilos (Escribano et al., 1997)células de Langerhans (Bieber et al., 1992) y monocitos periféricos (De Maria et al., 1994).

4.4. CD69 COMO MOLÉCULA INMUNO-MODULADORA

Se ha demostrado que la molécula CD69 actúa como mediadora en procesos inflamatorios funcionando como regulador negativo de la inflamación. En el modelo murino de artritis inducida por colágeno (*Collagen-Induced* Arthritis, CIA) se observó que los ratones deficientes en CD69 desarrollan formas exacerbadas de la enfermedad. Estos animales *CD69-/-* presentan menos niveles de TGF-β, mecanismo por el cual CD69 podría estar regulando la inflamación (Sancho et al., 2003).

En otros trabajos con animales deficientes en CD69 se han encontrado evidencias que apuntan en la misma dirección y postulan a CD69 como una molécula inmunoreguladora. La deficiencia de CD69 exacerba la respuesta inmune en el asma alergico, dermatitis de contacto, miocarditis autoinmune y colitis. En el modelo de asma alérgico inducido con ovoalbúmina o en el modelo de hipersensibilidad de contacto inducida por oxazolona (*Contact Hypersensitivity,* CHS), los efectos inflamatorios mediados por las células T efectoras están exacerbados en los animales *CD69-/-,* así como en animales WT tratados con anticuerpos anti-CD69 que bloquean la señalización del receptor (Martin et al., 2010b). En el modelo de miocarditis autoinmune, los animales deficientes en CD69 muestran una mayor inflamación en el corazón mediada por células Th17 (Cruz-Adalia et al., 2010).En el modelo de colitis CD69 actúa como regulador negativo del proceso inflamatorio favoreciendo la función de células Treg $FoxP3^+$, que favorecen la tolerancia oral y disminuyen los efectos adversos de la colitis (Radulovic et al., 2013). En

definitiva, CD69 actúa como un modulador negativo de la inflamación regulando el balance entre las células Th17 proinflamatorias y las células Treg antiinflamatorias, tanto en homeostasis como en procesos inflamatorios patológicos (Martin and Sanchez-Madrid, 2011). CD69 regula negativamente la diferenciación hacia células Th17 mediante la activación de la ruta de señalización Jak3/Stat5, impidiendo la activación del factor de transcripción RORγt tanto en humano como en ratón. Además, favorece la expresión de las citoquinas IL-2 y TGF-β implicadas en la diferenciación de los linfocitos T $CD4^+$ hacia células Treg mediante la activación de su factor de trascripción FoxP3 (Cortes et al., 2014).

Otros datos que apoyan la función reguladora de CD69 en la respuesta inflamatoria es la identificación de poblaciones de linfocitos T $CD69^+$, que se comportan como las células Treg induciendo anergia y efectos reguladores. En un modelo de lupus en ratón se han encontrado poblaciones de linfocitos $CD4^+$ $CD69^+$ en los infiltrados inflamatorios y en tejidos linfoides que inhiben la producción de IL-2, y favorecen la generación de células Th17 (Ishikawa et al., 1998). En estudios clínicos en pacientes con esclerosis sistémica se ha encontrado que la expresión de CD69 en sus células Treg es menor que en individuos sanos, y además esta menor expresión de CD69 se relaciona con una menor producción de TGFβ y, por lo tanto, con una menor capacidad supresora de estas células (Radstake et al., 2009).

Asimismo, se ha identificado una población de linfocitos T reguladores (linfocitos $CD69^+CD4^+CD25^-$), inducidos en respuesta a tumores, que no expresan FoxP3 y no producen IL-10, pero sí expresan IL-122 (la cadena β del receptor de la IL-2) y producen TGF-β1, siendo así capaces de suprimir la progresión del tumor, ya que CD69 mantendría alta la expresión de TGF-β1 a través de la activación de ERK1/2, y favorecería la función inmuno-supresora de este tipo de células (Han et al., 2009). También se han encontrado este tipo de células $CD69^+CD4^+CD25^-$ en pacientes trasplantados con un menor riesgo de sufrir la enfermedad de injerto contra huésped (GVHD *Graf Versus Host Disease*) (Lu et al., 2012). CD69 está asociado con la generación de células Treg del timo, que se producen mediante la activación de las células dendríticas plasmacitoides, residentes en el timo, que promueven la diferenciación de células Treg $CD4^+$ $CD25^+$ $FoxP3^+$, a partir de timocitos $CD4^+CD8^+$ que expresan niveles altos de CD69 (Martin-Gayo et al., 2010). Por último, hay estudios que demuestran la relación de CD69 con la migración de los linfocitos a órganos linfoides periféricos mediante el receptor de la esfingosina 1 fosfato (*Sphingosine-1-phosphate receptor 1,* $S1P_1$) demostrándose que en animales deficientes en CD69, esta molécula se encuentra up-regulada favoreciendo que haya más migración a órganos linfoides periféricos (Lamana et al., 2011).

5. ANGIOGÉNESIS Y LA ENFERMEDAD ARTERIAL

Ante un proceso de isquemia se desencadenan diversos procesos fisiológicos para intentar paliar la falta de oxígeno en el tejido isquémico. Estos procesos implican la activación de mecanismos de crecimiento y proliferación de nuevos capilares, que aporten oxígeno al tejido dañado, y que se conocen en términos generales como angiogénesis y neo-vascularización. En general la angiogénesis se refiere a la formación de capilares a partir de otros ya existentes, que comienza con la activación de células endoteliales y un incremento de la permeabilidad vascular, seguido de una rotura de la membrana basal, migración de células endoteliales, invasión de matriz extracelular, invasión de la matriz intersticial, formación de la membrana basal y, por último, formación del lumen del capilar. El concepto de neo-vascularización en respuesta a isquemia tisular, avanzó gracias al descubrimiento de la vasculogénesis post-natal, ya que antes se pensaba que el proceso de neo-vascularización ocurría sólo durante el desarrollo embrionario y se atribuía el proceso de formación de nuevos vasos en adultos, a un mecanismo de angiogénesis. Actualmente se considera que la vasculogénesis en adultos, se refiere a la formación de nuevos vasos mediante la agregación de primitivos precursores endoteliales (*Endothelial Progenitor Cells,* EPCs), que de hecho se encuentran en la sangre periférica de adultos y evidenciando su reclutamiento en procesos de neo-vascularización en tejido isquémico (Asahara et al., 1997).

5.1. ENFERMEDAD ARTERIAL PERIFÉRICA

Las enfermedades cardiovasculares que cursan con isquemia, como la enfermedad de la arteria coronaria (*coronary artery disease*, CAD) o la enfermedad arterial periférica (*peripheral artery disease*, PAD) son un problema de salud a nivel mundial. La PAD**,** es una enfermedad común pero grave. Se produce cuando el exceso de colesterol y otras grasas que circulan en la sangre se acumulan en las paredes de las arterias que suministran sangre a los brazos y piernas. Esta acumulación, llamada placa de ateroma, que estrecha las arterias puede acabar reduciendo o bloqueado el flujo sanguíneo. Se manifiesta de manera más común en las arterias de las piernas, pero también puede presentarse en las arterias que llevan sangre del corazón a la cabeza, los brazos, los riñones y el estómago. A pesar de los progresos que se han hecho en los tratamientos de revascularización, muchos pacientes no son candidatos para estos tratamientos (Padilla et al., 2007). La estimulación de la angiogénesis mediante la administración exógena de factores de crecimiento o mediante la activación de la expresión de determinados genes, es un campo emergente pero todavía no bien desarrollado, que permitiría la recuperación de la isquemia de músculo cardiaco y esquelético (Doi et al., 2007). El uso de VEGF-A (*Vascular endothelial growth factor A*) se presentó como una mejora a corto plazo, pero no ha llegado a

suponer beneficios a largo plazo (Seppo Ylä-Herttuala, 2007). El trasplante de EPCs promueve neo-vascularización terapéutica, aunque el éxito de éste tipo de tratamientos no es todo lo efectivo que se esperaba (Sica et al., 2006; Yuyama et al., 2002). Se sabe que los linfocitos $CD4^+$ y $CD8^+$ juegan un papel fundamental en neo-vascularización post-isquemia a través de la activación de las vías B7/CD28 y CD40/CD40L. CD28 interviene en la generación y homeostasis de las células $CD4^+$ $CD25^+$ Treg que participan en neo-vascularización post-isquémica a través del control de las células efectoras de la respuesta inmune. Por otro lado, las células Th17 participan activamente en el proceso de neo-vascularización, ya que el acumulo de células inflamatorias en la zona isquémica como monocitos, neutrófilos y macrófagos, induce la expresión de citoquinas pro-inflamatorias como la IL-6 que favorece la diferenciación de los linfocitos T $CD4^+$ al subtipo de linfocitos Th17 productores de la citoquina IL-17 que estimula la producción de IL-1β y VEGF-A, estimulando así la (Sica et al., 2006)balance entre las células Th17 y las células Treg podría constituir una nueva estrategia a la hora de abordar el tratamiento de las enfermedades que cursan con isquemia (Hata et al., 2011; Zouggari et al., 2009). A la hora de abordar nuevos tratamientos para las enfermedades que cursan con isquemia, es necesario tanto el conocimiento de los procesos que controlan la angiogénesis y neo-vascularización, como la identificación de nuevos factores pro-angiogénicos más eficaces a la hora de acelerar la revascularización de tejidos isquémicos.

5.2. MÉTODOS DE ESTUDIO DE ANGIOGÉNESIS

Existen diferentes métodos para el estudio del proceso de angiogénesis, incluyendo estudios *in vitro* que implican la realización de cultivos de células endoteliales que permiten la evaluación de su capacidad de migración y proliferación. Entre estos métodos cabe destacar los ensayos con matrigel que permiten evaluar la capacidad de respuesta de las células endoteliales a determinados estímulos angiogénicos, estimando la capacidad que tienen estas células de formar tubos o capilares (Kubota et al., 1988); los ensayos de recuperación de la herida, que permiten evaluar la capacidad de migración de estas células (Lampugnani, 1999) siendo la migración y la capacidad de formación de tubos, dos características fundamentales que deben poseer las células endoteliales. También existen métodos *ex vivo* que permiten evaluar este tipo de capacidades en las células endoteliales, tales como los ensayos con anillos aórticos, que permiten evaluar la angiogénesis teniendo en cuenta la interacción de las células endoteliales con la matriz extracelular y con las células perivasculares que median en los procesos de angiogénesis y neo-vascularización (Nicosia and Ottinetti, 1990a, b). A pesar de la utilidad de estos ensayos, la información que se obtiene no es suficiente para comprender los procesos de angiogénesis,

ya que en estos mecanismos interviene, entre otros, el sistema inmune, cuyo papel queda excluido en este tipo de ensayos. Por este motivo, es necesario el desarrollo de modelos animales para comprender mejor los procesos que intervienen en los mecanismos de angiogénesis y neo-vascularización. El modelo de *Hind Lind Isquemia* se ha desarrollado en ratones, ratas y conejos (Deindl and Schaper, 2005; Liddell et al., 2005), en concreto, el modelo murino de *Hind Lind Isquemia* se reportó por primera vez 1998 (Couffinhal et al., 1998). En dicho modelo se practica una incisión en la piel de la mitad superior de la extremidad posterior derecha, se descubre la arteria femoral, se liga la parte distal y la parte proximal de la arteria, cortándose el fragmento entre las ligaduras. El proceso de perfusión se monitoriza mediante la técnica de láser doppler y se representa como el Ratio de Reperfusión, que se calcula como el cociente entre el flujo existente en la pata isquémica y el flujo de la pata no isquémica. Para este modelo se ha descrito que las diferentes cepas de ratones presentan diferentes patrones de recuperación de las isquemia, recuperándose mejor los animales C57BL/6 que los animales BALBc, los diferentes patrones de recuperación se deben a las diferencias genéticas en la vasculatura colateral que presentan ambas cepas (Helisch et al., 2006).

6. MICRO-RNAS

Los micro-RNAs (miRNAs) son pequeñas moléculas de RNA no codificante que se caracterizan por poseer un tamaño de entre 20 a 24 nucleótidos de longitud. Están implicados en la regulación post-trascripcional de la expresión génica uniéndose al dominio 3´UTR (*untraslated region*) del RNA mensajero (mRNA) específico impidiendo su traducción a proteína o provocando su degradación (Pillai, 2005). Fueron identificados por primera vez en el nematodo *Caenorhabditis elegans*, a principios de la década de 1990 (Lee et al., 1993; Wightman et al., 1993), pero fue en 2001 cuando se acuño el término miRNA (Lagos-Quintana et al., 2001; Lau et al., 2001; Lee and Ambros, 2001) . Se estima que un solo miRNA puede regular la expresión de entre cientos y miles de genes diana (Griffiths-Jones, 2004; Lewis et al., 2005; Miranda et al., 2006). La primera vez que se relacionó a un miRNA con una enfermedad fue con la Leucemia de células B (Calin et al., 2002). En 2008 se descubrió que los miRNAs no sólo están presentes en el interior de las células, si no que se encuentran también en el exterior, pudiendo incluso ser secretados en vesículas producidas por las células como los exosomas que los protegen de su degradación. (Chen et al., 2008; Lawrie et al., 2008; Mitchell et al., 2008). Esta presencia de los miRNAs en el medio extracelular, sugiere que éstas moléculas podrían intervenir en procesos de comunicación intercelular (Zernecke et al., 2009; Zhang et al., 2010). Todos estos avances han puesto de manifiesto el importante papel de estas moléculas en el control de la regulación post-transcripcional. La identificación

de los perfiles de expresión de miRNAs, proporcionaría gran cantidad de información para desentrañar los mecanismos que regulan los diferentes procesos que ocurren en el interior de la célula, postulando a éstas pequeñas moléculas como biomarcadores de procesos tanto fisiológicos como patológicos, constituyendo así una potencialmente importante herramienta diagnóstica (Kosaka et al., 2010).

6.1. BIOLOGÍA DEL MICRORNA-155

El miRNA-155 (miR-155) se procesa a partir de un tránscrito primario en el gen hospedador llamado "BIC". En el ratón se encuentra localizado en el cromosoma 16 y en humano en el cromosoma 21. Participa en la regulación de procesos tanto fisiológicos cómo patológicos interviniendo en la inhibición de crecimientos tumorales, procesos infecciosos y atenuando enfermedades cardiovasculares.

Se expresa moderadamente en células madre hematopoyéticas (*Hematopoietic Stem Cells*, HSCs) y su expresión es mucho menor en células hematopoyéticas maduras. La expresión del transcrito BIC y del miR-155 maduro se induce rápidamente en linfocitos B y T después de la exposición a un antígeno (Haasch et al., 2002; O'Connell et al., 2010; Taganov et al., 2006; Thai et al., 2007), desempeñando un papel importante en procesos inmunológicos. El miR-155 participa en procesos de inmunidad innata incrementándose su expresión en monocitos, macrófagos y células dendrítricas una vez expuestas a estímulos inflamatorios (Brown et al., 2007; O'Connell et al., 2010; Taganov et al., 2006). En macrófagos, las citoquinas pro-inflamatorias como TNFα o IFNγ aumentan el procesamiento del miR -155 maduro. Este incremento supone la activación de la ruta de NF-κB/Jnk perfilándolo como una molécula que participa en la respuesta inmune innata (Baltimore et al., 2008; Kluiver et al., 2007; O'Connell et al., 2010; Yin et al., 2008a), aunque todavía queda por conocer sus dianas y dilucidar su papel en la respuesta inflamatoria en macrófagos (Baltimore et al., 2008). Este miRNA también podría actuar de puente entre la respuesta inmune innata y la adquirida, ya que se ha descrito que las células dendríticas deficientes en miR-155 son incapaces de desencadenar la activación de las células T tras la exposición a un antígeno (Rodriguez et al., 2007). Con respecto a la inmunidad adaptativa, este miRNA participa en la respuesta inmune mediada por linfocitos B. Está implicado en el desarrollo de los centros germinales disminuyendo la producción de IgG1 ya que la proteína PU.1 es diana de este miRNA. La inhibición de la transcripción de PU.1 regula negativamente el *swich* de inmunoglobulinas hacia IgG1 (Vigorito et al., 2007). Otra diana del miR-155 es la proteína citidina deamidasa (*Cytidine Deamidase*, AID) que interviene en el proceso de hipermutación somática. El miR-155 también está implicado en la respuesta inmune mediada por las células T interviniendo en las respuestas Th1 y Th2 a través de la regulación de la proteína c-Maf (Costinean et al., 2006; Rodriguez et al., 2007). El factor de trascripción FoxP3,

específico de células Treg, tiene sitio de unión en el promotor del miR-155 (BIC), y esto se correlaciona con una mayor expresión de este miRNA en células Treg y células T convencionales (Cobb et al., 2006; Zheng et al., 2007). La proteína SOCS1 es otra diana del miR-155, que interviene en la diferenciación las células Treg y en la función y diferenciación de las células Th17 mediante la modulación de la activación de la ruta Jak/Stat.

La relación del miR-155 con el sistema cardiovascular se debe en parte al papel regulador que realiza en el sistema inmune, ya que en pacientes con síndrome coronario agudo (ACS) está disminuida su expresión en células mononucleares de sangre periférica (*Peripheral Blood Mononuclear cell,* PBMCs). Esta disminución se correlaciona con un incremento en la diferenciación de los linfocitos pro-inflamatorios Th17 (Yao et al., 2011). Se ha encontrado que el miR-155, mediante el control de la actividad de los macrófagos, regula la hipertrofia cardiaca a través de un mecanismo indirecto, dependiente de la inflamación (Heymans et al., 2013). Asimismo, a partir de la regulación de la función de los macrófagos, promueve la aterosclerosis (Nazari-Jahantigh et al., 2012; Wei et al., 2013) y los efectos perjudiciales de la *diabetes mellitus* (DM) como la micro-angiopatía, que se atribuyen a la activación de una vía pro-apoptótica regulada por el miR-155 en los precursores de médula ósea de estos pacientes (Spinetti et al., 2013).

Finalmente, se ha relacionado este miRNA con procesos tumorales. Está muy relacionado con leucemias, encontrándose altamente expresado en los blastos de medula ósea procedentes de pacientes con leucemia mieloide aguda (AML) subtipo M4 y M5 (O'Connell et al., 2008). Se le relaciona con expansión y proliferación de monocitos y macrófagos de medula ósea y regula ciertas dianas como UT.1, relacionada con desordenes hematopoyéticos y mielo-proliferativos (O'Connell et al., 2008). El miR-155 se encuentra también altamente expresado en varios tipos de tumores sólidos como el cáncer de mama. Hay más de 147 dianas reguladas por este miRNA relacionadas con cáncer de pecho e implicadas en procesos de apoptosis, diferenciación, angiogénesis, proliferación y transición del epitelio mesenquimal (Mattiske et al., 2012). También es considerado indicador de mala prognosis en carcinoma de tiroides (Nikiforova et al., 2008), cáncer de colon, cáncer cervical y cáncer de pulmón.

6.2. EL MICRORNA-721

Este miRNA fue identificado por primera vez en 2006 en el sistema nervioso central de ratón (Wheeler et al., 2006) y posteriormente fue descrito en embriones pre-implantados de ratón (Yang et al., 2008). Se encuentra codificado en el cromosoma 5 de ratón, en los intrones 4 y 5 de la proteína CUX1. No se ha descrito un homólogo de este miRNA en humano, pero sí que se ha encontrado en el cromosoma 8 un

fragmento similar al de ratón en 18 nucleótidos de los 21 que presenta la secuencia madura de este miRNA (Wheeler et al., 2006). El miR-721, por su homología de secuencia, pertenece a la familia de miRNAs-130/301/721, que se ha descrito que intervienen en la generación de células madre pluripotentes inducibles (IPS) a través de la represión del factor de transcripción Meox2 (Pfaff et al., 2011)La proteína Meox2 es un factor de transcripción de tipo *Homeobox*. Su regulación por el miR-721 se produce mediante la degradación del RNA mensajero. Se relaciona esta proteína con el desarrollo de las extremidades a nivel embrionario, y está implicada en la regulación del ciclo celular a través de la proteína P21 (Douville et al., 2011). Además, en células endoteliales es un regulador negativo de la angiogénesis a través de NF-KB (Cantile et al., 2008). Meox 2 en el contexto de angiogénesis y el sistema circulatorio se expresa en cardiomiocitos, células vasculares de musculo liso (*vascular smooth muscle cells*, VSMCs), fibroblastos cardiacos y células endoteliales, y previene la proliferación de la vasculatura a través de la sobreexpresión de p21 y p16. También interviene en la regulación de la función de los fibroblastos a través de TGFβ, que se encuentra disminuida en la zona de lesión después de un infarto. Su sobrexpresión favorece la proliferación de miofibroblastos (Gremel et al., 2011). Todos estos datos parecen relacionar al miR-721 con procesos de angiogénesis, neo-vascularización y remodelado cardiovascular.

7. ESTRATEGIAS BIOANALÍTICAS PARA LA IDENTIFICACIÓN Y CUANTIFICACIÓN DE PROTEÍNAS

En los últimos tiempos se han producido enormes avances en el campo de la biotecnología, que han resultado de gran ayuda en el campo de la investigación biológica. En concreto, el avance tecnológico experimentado por la espectrometría de masas (*mass spectrometry*, MS), la ha convertido en una de las alternativas más prometedoras en los estudios de biología post-genómica. En este ámbito, los métodos bioanalíticos de cuantificación de proteínas basados en marcaje metabólico, tales como SILAC (*Stable Isotope Labeling by Aminoacids in Cell Culture*) son de especial interés, ya que proporcionan una alta sensibilidad y reproducibilidad, con un error global inferior al 5%, lo que permite su aplicación tanto en la proteómica de expresión como en la funcional. No obstante, la espectrometría de masas *per se* no es una técnica cuantitativa, ya que moléculas distintas proporcionan respuestas espectrométricas diferentes. En este ámbito, los métodos analíticos de cuantificación de proteínas basados en marcaje isotópico son destacables. Además de para identificar diferencias de expresión entre dos muestras celulares o de tejidos, resultan especialmente atractivos para el estudio de mecanismos moleculares y de cambios funcionales relevantes entre dos o más estados biológicos.

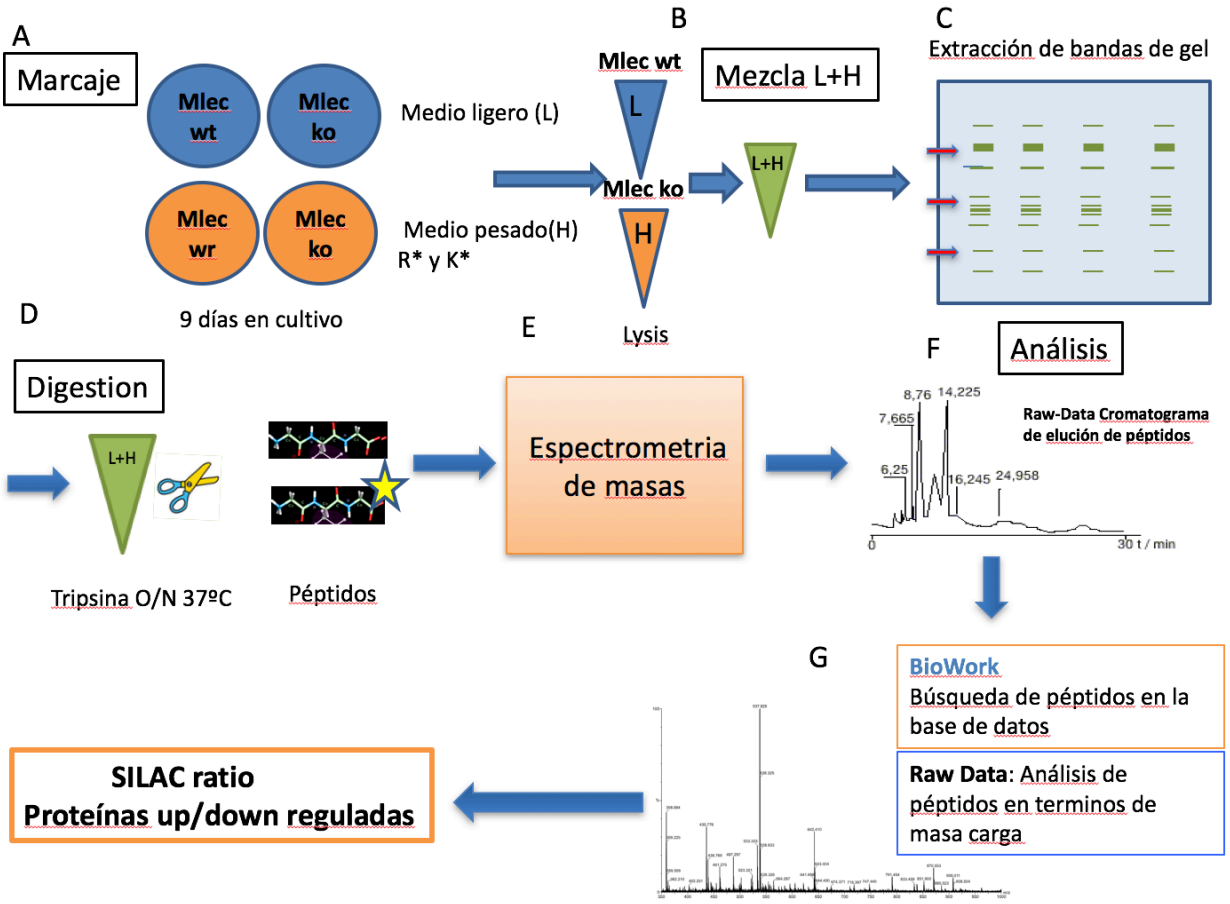

Figura 4: Esquema de trabajo de un experimento de SILAC. Fase de marcaje metabólico (A), fase de preparación de extractos de proteína (B), extracción de bandas de gel(C), digestión con tripsina (D), análisis por espectómetro de masas (E) y análisis informático de los datos (F y G). Mlec: *mouse lung endothelial cells*. WT: wild type. KO: $CD69^{-/-}$. R*: arginina ^{13}C; K*: lisina ^{13}C.

Dentro de estos métodos de cuantificación se puede distinguir entre los basados en marcaje metabólico y los basados en marcaje químico. La principal diferencia entre ambos grupos de métodos es la etapa del proceso analítico en la cual se realiza el marcaje. Mientras que en los métodos de marcaje metabólico (SILAC, ^{15}N) (Ong et al., 2002) éste se realiza antes de comenzar el tratamiento de muestra (purificación, fraccionamiento, digestión, etc.), el marcaje químico se realiza a nivel de proteínas (DIGE, ICAT, ICPL) (Marouga et al., 2005; Turecek, 2002) o de péptidos (iTRAQ, ^{18}O) (Canas et al., 2006; Lopez-Ferrer et al., 2006; Zieske, 2006), lo que conlleva que las muestras a comparar deben ser tratadas por separado hasta el punto en el que se realiza el marcaje. Esto implica que cualquier error introducido durante dicho tratamiento de muestra se verá reflejado en los resultados finales, incrementando, por tanto, la dificultad de discernir si la diferencia final de expresión proteica observada es consecuencia de la

diferencia intrínseca entre los estados biológicos que se están comparando, o es debida a un error introducido durante las operaciones previas del proceso analítico. Este problema es especialmente importante cuando las diferencias esperadas entre los sistemas que se están comparando no son muy grandes, o cuando los tratamientos de muestra que se requieren conllevan una alta variabilidad. Éste es el caso de muchos de los métodos de fraccionamiento y purificación celular usados normalmente, tales como el fraccionamiento nuclear o, aún en mayor grado, la inmunoprecipitación. Dicho problema es inexistente en el caso de los métodos de marcaje metabólico, ya que la mezcla de las muestras a comparar es previa al propio tratamiento de muestra, de forma que cualquier error que pueda ser introducido durante estas etapas no se reflejará en los resultados finales. Otra ventaja de los métodos metabólicos es que aseguran una eficacia del marcaje del 100%. Los métodos de marcaje químico, por el contrario, implican una etapa de derivatización que podría no ser completa, lo que supone una potencial introducción de productos secundarios que limitarían la sensibilidad del análisis. La principal desventaja de los métodos metabólicos respecto de los métodos químicos es que, mientras los segundos pueden aplicarse a cualquier proteoma (células, tejidos, fluidos, etc.), el marcaje metabólico está limitado al uso de sistemas vivos, principalmente cultivos celulares. No obstante, actualmente se está ampliando su campo de aplicación a cultivos primarios (Spellman et al., 2008) e incluso a organismos completos (Kruger et al., 2008).

7.1. PROTEÓMICA Y ANGIOGÉNESIS

En los últimos tiempos los avances en proteómica basados en la MS han resultado ser de gran utilidad a la hora de entender el comportamiento de las células endoteliales y se postula que la proteómica moderna puede suponer un gran impulso para avanzar en el campo de la angiogénesis (Zanivan et al., 2012). En 2003 se publicó el primer estudio proteómico en HUVECS (*Human Umbilical Vein Endothelial Cells*); en el que se identificaron 53 proteínas de lisado de éstas células mediante TOF MS (Bruneel et al., 2005), varios años más tarde el número de proteínas aumentó a 162 de las cuales 8 estaban diferencialmente expresadas después de un estímulo pro-apoptótico (Bruneel et al., 2005) después de esto la MS se convirtió en una técnica de gran importancia en el campo de la angiogénesis y en particular en la biología de las células endoteliales. Hay muchos estudios que comparan cambios en patrones de expresión de proteínas en las células endoteliales en diferentes estados, el más ambicioso ha llegado a detectar 5000 proteínas, de las cuales cientos de ellas estaban diferencialmente expresadas en respuesta a factores inflamatorios como TNFα, INFγ y IL1-β (Gautier et al., 2014). Otros estudios, usando la técnica de marcaje estable con O^{18}, han encontrado 3800 proteínas diferencialmente

expresadas en HUVECS en respuesta al factor pro-angiogénico VEGF, algunas de las cuales no se habían descrito nunca como dependientes de este factor (Jorge et al., 2009).
La MS ha avanzado de tal modo que permite identificar, de manera muy precisa, modificaciones post-traduccionales en las proteínas, esto es también de gran interés en el campo de la angioénesis, ya que las modificaciones post-traduccionales son críticas a la hora de regular la función y los mecanismos de acción en las células endoteliales. Se han encontrado 1288 sitios de fosforilación en células endoteliales tratadas con angiotensina I y han servido para establecer una conexión entre la angiotensina y el factor de transcripción FOXO I (Verano-Braga et al., 2012).

Otro de los esfuerzos en los avances en la tecnología de la MS están dirigidos a analizar la composición de proteínas en los diferentes compartimentos sub-célulares llegando incluso a analizarse el secretoma producido por las células endoteliales en cultivo (Burghoff and Schrader, 2011). Este estudio ha sido muy importante para conocer los mecanismos de comunicación paracrina entre las células endoteliales y las células presentes en el estroma, llegándose a demostrar que en función de las proteínas o péptidos secretados se puede regular incluso la proliferación de tumores (Franses and Edelman, 2011).

Los últimos avances en MS de alta resolución y la exactitud del método de cuantificación que nos proporciona la técnica de SILAC, los postula como métodos candidatos para avanzar en los conocimientos en el campo de la angiogénesis y de las células endoteliales.

II. MATERIALES Y MÉTODOS

II. MATERIALES Y MÉTODOS

1. ANIMALES UTILIZADOS EN EL ESTUDIO

Los ratones CD69$^{-/-}$ (Knock out para el gen CD69) fueron generados en el fondo 129/Sv (Lauzurica et al., 2000) y se retrocruzaron durante al menos 12 generaciones con animales de fondo genético C57BL/6 y BALB/c (Martin et al., 2010a),. Para los experimentos de asma tolerogénico *in vivo*, se utilizaron hembras CD69$^{+/+}$ y CD69$^{-/-}$, de 10 a 12 semanas de edad, en el fondo genético BALB/c. Los ratones C57BL/6 Ly5.1 (CD45.1^{+}) se adquirieron en el Laboratorio Jackson (B6.SJL-Ptprca Pepcb/BoyJ: 002014). Los ratones Rag2$^{-/-}$ γc$^{-/-}$ (Knock out para los genes Rag 2γ e IL2rγ) fueron cedidos por la Dra. María Luisa Toribio (Centro de Biología Molecular, CSIC), se cruzaron con ratones C57BL/6 CD69$^{-/-}$, para generar ratones con el genotipo Rag2 WT y dobles knock out para IL2rγ$^{-/-}$/CD69$^{-/-}$.

Los ratones doble reporteros (DR) FoxP3-mRFP/IL17e-GFP también con fondo genético C57BL/6 fueron generados y cedidos por el laboratorio del doctor Richard Flavell (Yale University School of Medicine, 400 New Haven, CT). Los animales DR se cruzaron con los ratones C57BL/6 CD69$^{-/-}$ para generar los animales, Foxp3-mRFP/IL17 e-GFP/CD69$^{+/-}$ (heterocigotos para el gen CD69), y Foxp3-mRFP/IL17 e-GFP/CD69$^{-/-}$ (KO para el gen de CD69), hermanos de camada. Esta cepa de ratones doble reportero Foxp3-mRFP/IL-17 e-GFP se caracteriza por llevar insertado en el *locus* del gen Foxp3 una proteína fluorescente roja monomérica y en el locus de IL17 una proteína fluorescente verde que se expresan en una sola copia a la par que se expresan los genes de Foxp3 e IL17, constituyendo una herramienta fundamental para seguir la expresión de estos genes. Los ratones Mirn155$^{-/-}$ fueron proporcionados por la Dra. Rinako Nakagawa (Instituto Francis Crick, Londres). Todos los animales fueron alojados y utilizados en las instalaciones del CNIC en la zona libre de patógenos específicos (SPF). Los procedimientos con animales fueron aprobados por el comité ético de experimentación animal del CNIC y de la Comunidad Autónoma de Madrid y realizados de conformidad con las directrices que marca el Instituto Europeo de Salud; Directiva 407 2010/63/UE del Parlamento Europeo relativa a la protección de los animales utilizados para fines científicos (Diario Oficial de la Unión Europea, Vol. 53:33-79, 409, 2010).

2. CIRUGÍAS Y PROCEDIMIENTOS ANIMALES

2.1. RATONES URÉMICOS Y TRATAMIENTO CON PDF

Para generar la uremia, se realizó una nefrectomía de 5/6. Los animales fueron anestesiados por inhalación con 4% de isoflurano y 2% de oxígeno. Para la analgesia se inyectó por vía intramuscular 0,05-0,1 mg/kg de buprenorfina (Temgesic) de 15 a 30 minutos antes de la cirugía. Al animal anestesiado se le afeitó el abdomen y se le colocó en una almohadilla calefactora. Después de la preparación del animal, se le realizó una incisión en la línea media ventral a través de la piel, seguida de una incisión a lo largo de la línea alba, después de ambas incisiones y mediante laparotomía, el riñón izquierdo se liberó de su cápsula con pinzas de cirugía y algodones mojados. En este punto, el riñón pudo ser fácilmente colocado sobre una almohadilla para heridas, situada en la parte superior del peritoneo. Con el riñón colocado sobre la almohadilla, se eliminó con una cuchilla eléctrica monopolar su tercera parte anterior y su tercera parte posterior, el tercio restante del riñón izquierdo se volvió a colocar en la cavidad abdominal. Siguiendo el mismo procedimiento, el riñón derecho se retiró de la cavidad abdominal, se liberó de su cápsula y se realizó una ligadura total con sutura insoluble que incluye la vena del riñón, la arteria y la uretra. Después de la ligadura, el riñón derecho se extirpó del cuerpo (Figura 5).

Para analizar la uremia en los animales se extrajeron 200 µl de sangre mediante punción facial antes de la nefrectomía, y los días 10 y 54 post-nefrectomía. Se analizaron los niveles de urea y creatinina presentes en el suero, usando el equipo Dimension RxL Max Integrated Chemistry System.

La implantación del catéter para el tratamiento con el fluido peritoneal se realizó como se indica anteriormente (Gonzalez-Mateo et al., 2008) y en el caso de los animales nefrectomizados, dicha implantación se realizó 10 días después de la nefrectomía (Figura 5). El tratamiento con el fluido peritoneal (PDF-4, 25% de glucosa, pH 5.5, Stay Safe; FreseniusMedical Care) se realizó diariamente durante 40 días con 2 ml de PDF por animal en todos los grupos experimentales (animales WT y $CD69^{-/-}$, 10 animales por grupo; animales WT y $CD69^{-/-}$ nefrectomizados de 8 a 10 animales por grupo y quimeras hematopoieticas $Rag2^{-/-}\gamma c^{-/-}$ $CD69^{+/+}$ ó $CD69^{-/-}$ 10 animales por grupo). El tratamiento con el anticuerpo 2.2 ó el control de isotipo 2.8 se realizó con 100 µg de anticuerpo diluido en el fluido peritoneal cada 2 días, durante los 40 días que dura el tratamiento.

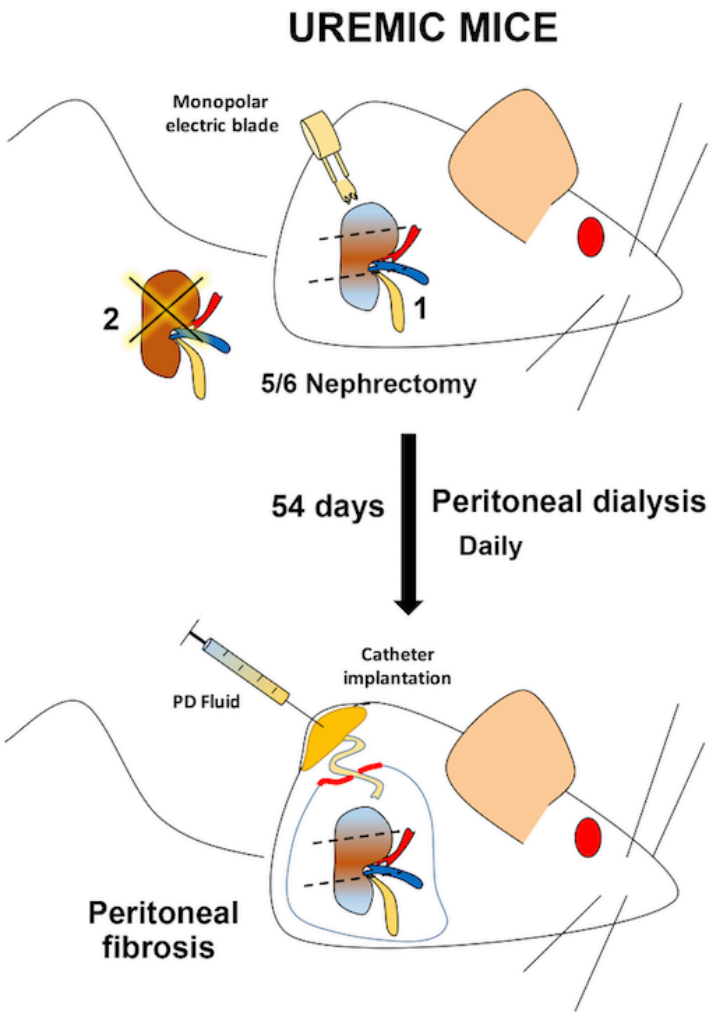

Figura 5. Generación de ratones urémicos. La figura ilustra una nefrectomía de 5/6 realizada por laparatomía del riñón derecho y posterior daño de 2/3 del riñón izquierdo mediante una cuchilla eléctrica. El riñón con el daño se introdujo de nuevo en la cavidad peritoneal antes del tratamiento con el líquido de diálisis, que se administró mediante la implantación de un catéter peritoneal.

2.2 ANÁLISIS DE CITOQUINAS

Una vez terminado el tratamiento de los animales sometidos a PDF, se lavó su cavidad peritoneal con 2 ml de solución salina. Inmediatamente después, los ratones se sacrificaron y se recolectó su lavado peritoneal. La solución se centrifugó, y el sobrenadante se analizó para ver la producción de citoquinas y quimiocinas mediante citometría de flujo, utilizando la Técnica FlowCytomix (Bender MedSystems GmbH). Los datos fueron analizados con el software FlowCytomix Pro 2.2 (Bender MedSystems GmbH).

2.3 QUIMERAS DE MÉDULA OSEA

QUIMERAS MIXTAS PARA EL TRATAMIENTO CON PDF

Hembras WT y CD69$^{-/-}$ de entre 10-12 semanas de edad, fueron irradiadas letalmente con dos dosis de 6.5 Gy, 24 horas más tarde se las administró por vía intravenosa 4x10^{6} células de BM procedentes de animales Rag2$^{-/-}\gamma c^{-/-}$ y animales CD69$^{-/-}$ ó CD69$^{+/+}$mezcladas en una proporción de 3:1, respectivamente. Antes del tratamiento con PDF durante 40 días se esperaron 10 semanas para la reconstitución de los progenitores de médula ósea.

QUIMERAS PARA LOS EXPERIMENTOS DE DIFERENCIACIÓN DE TTREG

Las hembras receptoras Rag2$^{-/-}\gamma c^{-/-}$ de 8 a 12 semanas de edad fueron irradiadas con una dosis sub-letal de 0.6 Gy de radiación γ. Al día siguiente de la irradiación se les administró de forma intravenosa una mezcla 1:1 de células de médula ósea de animales Foxp3 mRFP/CD69$^{+/+}$/CD45.1 y Foxp3 mRFP/CD69$^{-/-}$ /CD45.2. Se esperó al menos 10 semanas para la reconstitución, y la contribución de los diferentes precursores de la médula ósea de los donantes se determinó por FACS.

QUIMERAS TOTALES C57BL/6 PARA LOS EXPERIMENTOS DE ISQUEMIA

Hembras receptoras C57BL/6 WT para CD69 de 8 a 12 semanas, fueron irradiadas letalmente con dos dosis de radiación γ de 6.5 Gy. El día después de la irradiación se les administró por vía intravenosa 10^{6} precursores de medula ósea procedentes de animales Foxp3-mRFP/IL17e-GFP/CD69$^{+/+}$ ó Foxp3-mRFP/IL17e-GFP/CD69$^{-/-}$. Después del tiempo necesario para la reconstitución y tras comprobar su correcta reconstitución, se procedió a realizar la isquemia en la extremidad posterior izquierda.

QUIMERAS MIXTAS RAG2$^{-/-}\gamma c^{-/-}$ PARA LOS EXPERIMENTOS DE ISQUEMIA

Las hembras receptoras Rag2$^{-/-}\gamma c^{-/-}$ de ocho a doce semanas de edad fueron irradiadas con una dosis de 0.6 Gy de radiación γ, al día siguiente a la irradiación se les administró de forma intravenosa 10^{6} células de precursores de médula ósea de animales Rag2$^{-/-}\gamma c^{-/-}$ y de precursores Foxp3-mRFP/IL17 e-GFP/CD69$^{+/+}$ ó Foxp3-mRFP/IL17 e-GFP/CD69$^{-/-}$ mezcladas en una proporción 3:1, respectivamente. Tras el tiempo necesario para la reconstitución, unas 10 semanas, se analizó por FACS la contribución de los diferentes precursores de médula ósea de los donantes. Si los niveles de poblaciones linfoides y mieloides fueron correctos, se sometió al animal al proceso de isquemia. En estas quimeras el endotelio y el componente mieloide es WT para CD69, siendo el componente linfoide CD69$^{+/+}$ o CD69$^{-/-}$, por lo que este tipo de quimeras son ideales para el estudio del papel de CD69 en el compartimento linfoide en los procesos de neovascularización.

2.4 EXPERIMENTOS DE ASMA TOLEROGÉNICA CON ANTÍGENO NO PATÓGENO Y *ADOPTIVE TRANSFER* DE CÉLULAS ITREG O PTREG

Para analizar la función *in vivo* de las Treg, se utilizó el modelo de tolerancia a antígeno no patógeno descrito por de Heer et al., 2004. El día 0 del experimento, se inyectó intratraqueal 800 µg de OVA libre de LPS (Calbiochem) a los ratones BALB/c $CD69^{+/+}$ o BALB/c $CD69^{-/-}$. El día 19 del experimento se inyectaron los animales receptores con 5×10^6 células iTregs diferenciadas *in vitro* o con 2×10^5 pTreg purificadas mediante *sorting*. El día 20 de el experimento, los ratones recibieron durante 3 días consecutivos y por un periodo de 30 min, 3 aerosoles de OVA (10mg/ml en PBS o PBS como control), usando un nebulizador. Las células Treg se diferenciaron cómo se describe en el apartado de diferenciación de células Treg específico para éste experimento. La purificación de las células pTreg se realizó de bazos y se separaron por *sorting* las células $CD4^+$ $CD25^+$ $CD69^+$ o $CD69^-$.

2.5 *IN VIVO* FMT 1500

Los ratones se inyectaron de forma intravenosa con 4 nmoles de sonda Neutrophil Elastase 680 FAST (PerkinElmer, Inc.). Las imágenes se tomaron *in vivo* utilizando el tomógrafo de fluorescencia molecular FMT 1500 (PerkinElmer, Inc.). Los datos de fluorescencia recogidos se analizaron mediante la versión 1.1 del software del sistema FMT 2500, que cuantifica de manera tridimensional la cantidad total de fluorescencia emitida en el pulmón, obteniendo un valor de la concentración de la sonda en picomoles.

2.6 CULTIVOS DE LÓBULOS DE TIMO FETAL

Se retiraron los úteros de los ratones hembra en los tiempos gestacionales apropiados, y los embriones se colocaron en una placa de Petri con PBS frío para la extracción de los embriones y posteriormente los lóbulos de los timos. Para cultivar los lóbulos de timo fetal, se colocaron filtros de 0,8 µm de poro de membrana de nitrocelulosa (Millipore) sobre esponjas Gelfoam de 12-7 mm embebidas en medio IMDM, atemperado y suplementado con FCS al 10%, L-glutamina, antibióticos y β-mercaptoetanol.

Los FTOCs se mantuvieron de 4 a 14 días en cultivo, reemplazado el medio cada 3 días. El anticuerpo monoclonal anti-CD69 (2.2) o el anticuerpo control de isotipo (2.8) se añadió (50 µg/ml) al medio de cultivo y se reemplazó cada 3 días. Al final del periodo de cultivo, se prepararon suspensiones celulares a partir de los lóbulos de timo que se analizaron por FACS.

2.7. ISQUEMIA DE LAS EXTREMIDADES POSTERIORES. MODELO DE ENFERMEDAD ARTERIAL PERIFÉRICA (PAD)

Los animales se anestesiaron por inhalación de isofluorano. Se realizó una incisión en la porción media de la extremidad posterior izquierda, y se descubrió la arteria femoral (Figura 6). La parte proximal de la arteria femoral y la porción distal de la arteria safena se ligaron y se retiró el fragmento de arteria entre ambas ligaciones. La neovascularización se evaluó en los días 1, 3, 7, 14, 21 y 28 después de la isquemia (Figura 6) mediante *Lasser Doppler* (Moor LDI 2 IR y analizadas con el software de análisis *moor LDI Windows based control, processing and analysis*). Este método nos permitió evaluar la perfusión del miembro después de la lesión isquémica, expresado en forma del ratio isquemia/reperfusión, en el que se relacionan el miembro isquémico y no isquémico del mismo animal. La técnica de *Lasser Doppler* se aplica para la monitorización del flujo sanguíneo, en muchas ramas de la medicina y la fisiología. Se basa en la aplicación de un haz de luz láser de bajo poder energético sobre la piel y otros tejidos. Los movimientos de las partículas sanguíneas, presentes en la red microvascular de la zona monitorizada, causan un efecto Doppler sobre el haz de luz, que es medido y recogido por un receptor que procesa la información. La transformación de la información en un código de colores, se representa en un monitor, generándose un mapa de intensidades de flujo que permite una fácil interpretación visual y su cuantificación para comparar las áreas problema con las áreas control. Las medidas de flujo periférico (*peripheral flows* FP) se representa en *Flux* que son unidades arbitrarias comunes para todos los aparatos que realizan éste tipo de medidas y que se calibran usando una señal de flujo estándar generada en condiciones igualitarias. En el caso concreto de las medidas que hemos realizado en este trabajo, en el que queremos analizar diferencias de flujo locales entre distintas zonas y que además tienen que ser comparadas con exploraciones consecutivas en igualdad de condiciones, hemos usado las unidades relativas RU, que calcula el flujo en función la media de los valores reales de flujo obtenidos en un espacio y tiempo determinados (J.R. González-Escalada, 1999). Por otra parte, la neovascularización se evaluó por inmunohistoquímica una vez sacrificado el animal mediante el marcaje con anti-CD31 que permitió evaluar la formación de nuevos vasos en el músculo abductor izquierdo del animal; el músculo abductor derecho fue usado como control.

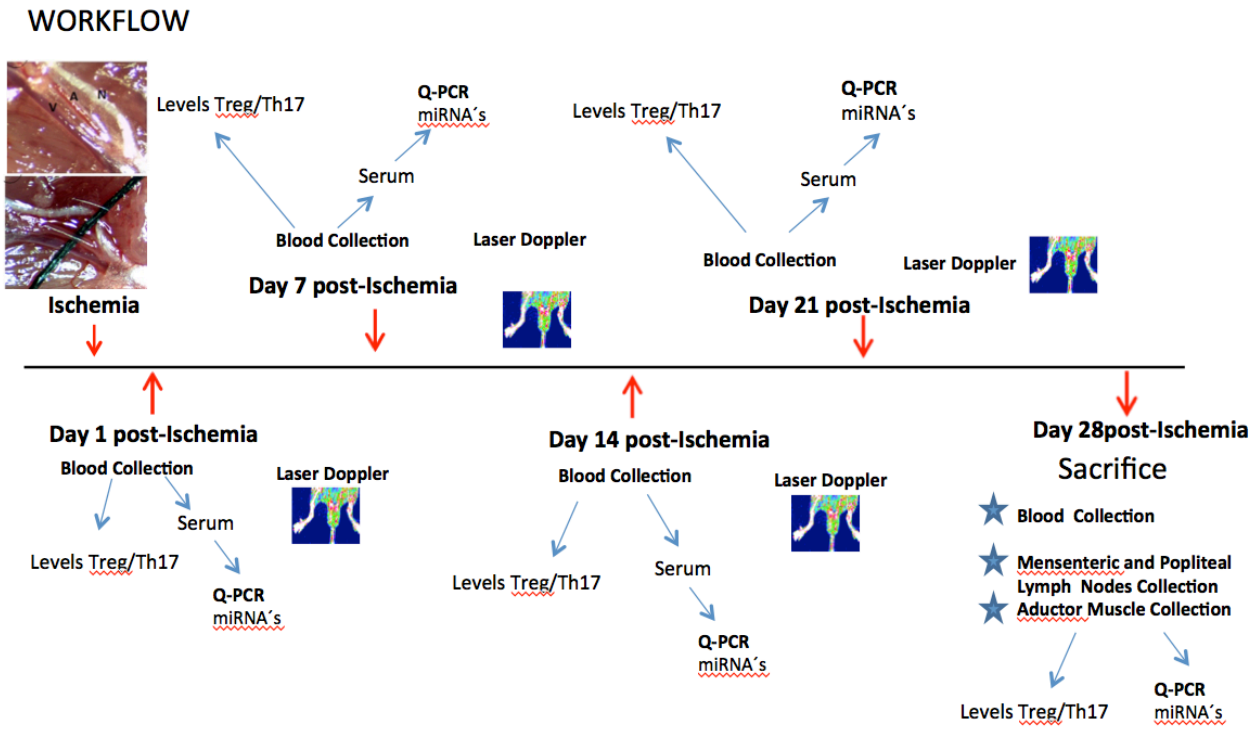

Figura 6. Esquema representativo de un experimento estándar de isquemia de la arteria femoral y monitorización del proceso de revascularización del músculo abductor. Se analizaron los ratones a día 1, 7, 14, 21 y 28 después de la cirugía por *Laser Doppler* y se tomaron muestras de sangre para el análisis de las respuestas Th17/Tregs por FACS, y de suero para analizar el contenido en miRNAs. En la mayoría de experimentos, si no se indica lo contrario, se sacrificaron los ratones a día 28 y se tomaron muestras de sangre (linfocitos periféricos y suero), ganglios linfoides y músculo. **A**: arteria, **V**: vena, **N**: nervio.

3. Producción del anticuerpo 2.2 y su control de isotipo 2.8

El anticuerpo murino mAb-2.2 (IgG1-K), específico para CD69 de ratón, fue generado como se describe en Esplugues et al., 2003. Se purificó a partir de sobrenadantes concentrados del hibridoma productor usando una columna de proteína G (GE), una vez purificado el anticuerpo se dializó ampliamente contra PBS, y se almacenó a -20°C. Se procedió de igual manera con el control de isotipo 2.8.

4. TINCIONES CELULARES Y ANÁLISIS DE FACS

4.1 MARCAJES DE CITOMETRÍA USADOS EN LOS EXPERIMENTOS DE TRATAMIENTO CON PDF

Las suspensiones celulares obtenidas de lavado peritoneal se tiñeron en tampón de FACS (PBS, BSA 0,5%, EDTA 0.5µM, NaN_3 0,1%) con anticuerpos específicos de ratón conjugados con diferentes fluorocromos CD3, CD45, CD4, CD8a, B220, CD11c, CD11b, Ly6C, CD69, Ly6G, IFN-γ, IL-4 e IL-17 (BD Biosciences) y FoxP3 (eBiosciences).

Antes de la tinción intracelular para IL17, IFN-γ e IL-4, las células fueron re-estimuladas durante 4 horas con 50 ng/ml de PMA, 500 ng/ml de ionomicina en presencia de 1 mg/ml de Brefeldina A. Después de la estimulación se procedió primero a la fijación celular con paraformaldehido al 2% en PBS y a su posterior permeabilización con saponina al 0.5% en tampón de FACS. Para la tinción intracelular de Foxp3, se utilizó el kit de tinción Foxp3 (eBioscience).

4.2 TINCIONES CELULARES REALIZADAS PARA ANALIZAR LA FUNCIÓN Y DIFERENCIACIÓN DE CÉLULAS TREG

Para el análisis de neutrófilos en los lavados broncoalveores se marcaron en tampón de FACS con los anticuerpos GR-1 y CD11b de BD y se consideraron neutrófilos las células que expresaban altos niveles de ambos marcadores. Las suspensiones celulares se obtuvieron de los diferentes órganos de animales adultos (timo, bazo y ganglios linfáticos) o timos fetales, y se incubaron en tampón de FACS, con anticuerpos específicos de ratón conjugados con diferentes fluorocromos contra CD4, CD8, CD69, CD45.1 y CD45.2 de BD Biosciences.

Para la tinción STAT5 y fosfo-STAT5 intracelular, se separaron células tTreg Foxp3-mRFP$^+$ CD69$^+$ y CD69$^-$ mediante *sorting* en FACSAria III (BD). Una vez sorteadas las células, se fijaron con 0,2% paraformaldehído y se permeabilizaron con metanol al 90%. Las células se incubaron con el anticuerpo anti fosfo-STAT5 (Tyr 694) (*Cell Signaling*), o con Alexa Fluor 647 anti-fosfo-STAT5 (Tyr 694). Se usó de control de isotipo el anticuerpo Alexa Fluor 647 IgG1 también de Beckton Dickinson.

Los PBL humanos fueron obtenidos después de la separación con gradiente de densidad con Ficoll de *buffy coat* procedentes de diferentes donantes humanos sanos. Las células se mantuvieron en medio RPMI suplementado con FCS al 10%, HEPES 20 mM, L-glutamina, antibióticos, aminoácidos no esenciales, piruvato de sodio y β-mercaptoetanol. Los PBL tratados se incubaron con anticuerpos específicos de humano anti-CD4, CD25, CD69 (BD Biosciences) y Foxp3 (Miltenyi Biotec), conjugados con diferentes fluorocromos.

4.3 TINCIONES CELULARES REALIZADAS PARA ANALIZAR LOS EXPERIMENTOS DE ISQUEMIA

Para evaluar los niveles de células Th17 y Treg en los animales Foxp3-mRFP/IL17e-GFP/CD69$^{+/+}$, Foxp3-mRFP/IL17e-GFP/CD69$^{-/-}$ o en las quimeras descritas en el apartado de procedimientos con animales sometidos a isquemia de la extremidad posterior, se extrajeron 50 µl de sangre de la vena caudal, se aislaron los linfocitos por gradiente de densidad con Ficoll y se marcaron con el anticuerpo anti-CD4 (BD). Para evaluar los niveles de células Th17 antes del marcaje, las células fueron incubadas durante 4 horas con PMA, Ionomicina y Brefelfina, para su posterior marcaje con el anticuerpo anti-CD4 de BD. Los niveles de células Th17 y Treg se evaluaron antes de la isquemia y los días 1, 3 y 7 post-isquemia.

Las células marcadas se analizaron en un citómetro de flujo LSRFortessaTM (BD) equipado con cuatro láseres (405, 488, 561 y 640 nm) ó en un BD FACS Canto II, y los datos fueron analizados con FlowJo v10.0.4. (Tree Star).

5. DIFERENCIACIONES *IN VITRO* DE CÉLULAS TREG.

En todos los casos las células se mantuvieron en medio RPMI suplementado con FCS al 10%, HEPES 20 mM, L-glutamina, antibióticos, aminoácidos no esenciales, piruvato de sodio y β-mercaptoetanol.

5.1 ENSAYOS DE SUPRESIÓN CON CÉLULAS TREG

Las células Tconv se obtuvieron de suspensiones celulares de bazos o ganglios linfáticos mesentéricos y se incubaron con los siguientes anticuerpos biotinilados: anti-CD8, CD19, B220, MHCII, CD11c, IgM, DX5 y CD11b (BD) seguido de una incubación con *microbeads* (esferas magnéticas, Miltenyi) conjugadas con estreptavidina. Las células T CD4^{+} se seleccionaron negativamente con el separador auto-MACS Pro (Miltenyi). Las células Tconv obtenidas, se cultivaron con anticuerpo anti-CD3 pegado a placa (1 µg/mL), anti-CD28 soluble (2 µg/ml) y esplenocitos irradiados deplecionados de células T. Las células Treg Foxp3-RFP se purificaron mediante *sorting* en el que se separó la población de células Foxp3-mRFP/CD69^{+} y la población Foxp3-mRFP/CD69^{-}. Se co-cultivaron células Tconv solas, Tconv + células Foxp3-mRFP CD69^{+} y Tconv + células Foxp3-mRFP CD69^{-}. La proliferación de células T se evaluó 48 h tras la tinción de células Tconv CD4^{+} mediante el análisis de la dilución del trazador celular CellTraceViolet.

5.2 DIFERENCIACIÓN DE CÉLULAS TREG PARA LOS EXPERIMENTOS DE *ADOPTIVE TRANSFER*

Para la diferenciación de la células Treg se inyectaron intraperitonealmente ratones CD69$^{+/+}$ y CD69$^{-/-}$ con 10 µg OVA en 2 mg alum, 5 días después se sacrificaron los animales y se purificaron las células CD4^{+}

de bazo y de ganglios linfáticos mesentéricos, mediante selección negativa con *microbeads* de Miltenyi, estas células se expandieron *in vitro* en presencia de TGF-β, IL-2, APC irradiadas y péptido de OVA.

5.3 EXPERIMENTOS DEL BLOQUEO DEL RECEPTOR DE LA INTERLEUQUINA 2

Se diferenciaron Treg inducibles de ratones Foxp3-mRFP/CD69$^{+/+}$, ratones Foxp3-mRFP/CD69$^{-/-}$, Il2rγ$^{-/-}$ CD69$^{-/-}$ y Il2rγ$^{-/-}$. Para ello se aislaron células T CD4^{+} vírgenes de estos ratones, y se co-cultivaron 72 h con células presentadoras de antígeno irradiadas en presencia de anti-CD3 unido a placa (2 μg/ml) y anti-CD28 soluble (2 μg/ml) y TGFβ recombinante (10 ng/ml) e IL-2 (2ng/ml). Las últimas 9 h, las células fueron incubadas con o sin inhibidor de JAK 3 (CAS 202475 60 3 Calbiochem) (10 μg/ml).

5.4 EXPERIMENTOS CON ANTICUERPOS BLOQUEANTES DE CD69

Se diferenciaron Treg inducibles de ratones Foxp3-mRFP/CD69$^{+/+}$y ratones Foxp3-mRFP/CD69$^{-/-}$ del mismo modo que los experimentos de bloqueo del receptor de la IL-2. Después de la diferenciación, las células Treg fueron cultivadas 4h con el anticuerpo anti 2.2 ó con el control de isotipo 2.8.

6. CULTIVO DE CÉLULAS ENDOTELIALES DE PULMÓN DE RATÓN

Las células endoteliales de pulmón de ratón *(Mouse Lungs Endothelial Cells,* MLECS) se extrajeron de los pulmones de animales CD69$^{+/+}$ y CD69$^{-/-}$. Una vez sacrificados los animales por dislocación cervical, se extrajeron los pulmones de la cavidad torácica, y una vez limpios de coágulos y grasa, se trocearon en una placa Petri hasta obtener una pasta de tejido pulmonar que se digirió con colagenasa. Tras extraer las células de tejido pulmonar, se procedió primero a hacer una selección negativa con el anticuerpo anti-CD16/CD32 FcϒRIII de BD, para eliminar fundamentalmente los macrófagos alveolares, y una vez plaqueadas las células de la selección negativa, se esperó a que se formasen colonias de unas 20 células. En este punto, se procedió a hacer la selección positiva de las células endoteliales con el anticuerpo anti-ICAM II (BD). Se plaquearon las células seleccionadas positivamente y se cultivaron en DMEN F12, suplementado con 20% de suero, antibióticos, heparina y EGF (factores de crecimiento endotelial) hasta su expansión apropiada para trabajar con ellas. La pureza del cultivo de MLEC se evaluó por citometría de flujo con los anticuerpos anti-CD31 y CD45.1. Para los diferentes experimentos siempre se usaron cultivos con al menos el 85% de pureza. Para los experimentos en los que se evaluaron los niveles de miR-721 y de las proteínas Meox2 y Cux1 en las células endoteliales, se estimularon O/N con 50 ng/ml de PMA, 500 ng/ml de ionomicina o con TNFα a 20 ng/μl.

7. TRANSFECCIONES TRANSITORIAS DE MIRNA

Las células PBL (10^6) se transfectaron transitoriamente con 50 pM de anti miR-155 (AM12601 Ambion) con el reactivo Lipotransfectina (Niborlab) de acuerdo con la instrucciones del fabricante. Se usó como control negativo un anti-miR Scramble (AM1701 negativo control # 1 Ambion). Las células transfectadas fueron estimuladas con anticuerpo anti-CD3 unido a placa (OKT3; 3 µg/ml) durante 24 horas.

Las PBL ($0,5x10^6$) se transfectaron con 50 pM de Pre-miR hsa-miR-155 o Pre-miR control negativo (Ambion) usando Lipofectamina RNA iMAX (Invitrogen). Las células transfectadas se estimularon durante 4 h con 50 ng/ml de PMA y 750 ng/ml de ionomicina (P + I). Después de ambos tipos de transfecciones y estimulaciones, los niveles de CD69 y fosfo-STAT5 fueron monitorizados por citometría de flujo, y los niveles transcripcionales de hsa-miR-155 y SOCS1 fueron analizados por qPCR.

8. PLASMIDOS E INFECCIONES LENTIVIRALES

Los plásmidos lentivirales pLKO contenían secuencias silenciadoras para CD69 (shCD69) (Sigma Aldrich) (TRCN0000057693; TRCN0000057694; TRCN0000057695) y fueron clonadas en el vector lentiviral pLKO. Se usó como control el mismo plásmido pLKO vacío, es decir, sin secuencia silenciadora (Sigma Aldrich) (Ref. SHC001).

Las secuencias shCD69 utilizadas fueron las siguientes:

SHCD69 1 (5'-3'): CCGGGCATGGAATGTGAGAAGAATTCTCGAGAATTCTTCTCACATTCCATGCTTTTTG;

SHCD69 2 (5'-3'): CCGGAGGCCAATACACATTCTCAATCTCGAGATTGAGAATGTGTATTGGCCTTTTTTG;

SHCD69 3 (5'-3'): CCGGGTGGTCAAATGGCAAAGAATTCTCGAGAATTCTTTGCCATTTGACCACTTTTTG.

La producción de los lentivirus se realizó en células HEK-293 cultivadas en DMEM con FBS al 10% (Sigma Aldrich), L–glutamina y antibióticos. Las HEK-293 se transfectaron de forma transitoria mediante el método del fosfato de calcio, con los plásmidos de la polimerasa y la envuelta lentiviral, 8.9 y PMD2G (suministrados por F. Sánchez-Madrid, Hospital de la Princesa, España) y el plásmido PLKO que expresa la secuencia shCD69 ó el plásmido PLKO control. El sobrenadante que contenía las partículas lentivirales, se recogió 48 horas después de parar la transfección y se concentró mediante ultracentrifugación a 26000 rpm durante 2 horas (Optima L-100 XP Ultracentrifuge Beckman).

Las PBL aisladas de donantes sanos (10^7) fueron infectadas con partículas LV diluidas en RPMI a una multiplicidad de infección (*multiplicity of infection*, MOI) de 10, durante 5 horas. Después de la incubación, se reemplazó el medio de infección por RPMI completo suplementado con 10% de FBS. Doce horas después, las células infectadas se seleccionaron con puromicina durante 48 horas. Se estimularon las células seleccionadas con el anticuerpo anti-CD3 unido a placa (OKT3; 3 µg/mL) durante 24 horas y después de la estimulación, los niveles de CD69 se monitorizaron por citometría de flujo y los niveles de miRNA-155 fueron analizados por qPCR

9. *WESTERN BLOT* Y TINCIONES INMUNOHISTOQUÍMICAS

9.1 EXPERIMENTOS CON TREG OBTENIDAS *EX VIVO*

Los lisados de proteínas de células tTreg Foxp3-mRFP $CD69^+$ y $CD69^-$ sorteadas se prepararon en tampón PD (Tris HCl 40 mM, pH 8.0, NaCl 0.5 M, EDTA 6 mM, EGTA 6 mM y 0,1% de NP40) que contenían el cóctel de inhibidores de proteasas (Complete Mini, Roche). Se cargaron 20 µg de lisado de proteína en geles de SDS-poliacrilamida al 12% y se electrotransfirieron a membrana de nitrocelulosa (BioRad). Los anticuerpos primarios para el inmunoblotting fueron los siguientes: anti β-actina, anti SOCS 1 y anti STAT5 (Santa Cruz); anti fosfo-STAT5 (Cells Signaling).

9.2 EXPERIMENTOS DE ISQUEMIAS.

Los lisados proteicos de músculo aductor se realizaron en 500 µl de buffer PD suplementados con inhibidores de proteasas y fosfatasas y la disgregación del tejido se realizó en un triturador ultraturrax durante aproximadamente 30´´, después de la homogenización del tejido se incubo 20´ en hielo para favorecer la lisis de las células extraídas del tejido y se centrifugó a 13000 rpm para separar la fracción soluble proteica de los lípidos y restos celulares. Se cargaron 20 µg de lisado de proteína en geles de SDS-poliacrilamida al 10% ó 12% y se transfirieron a membrana de nitrocelulosa (BioRad). Los anticuerpos primarios utilizados fueron los siguientes: P-AKT, RHOA y HIF2α (Cell Signaling); S1P1 y S1P3 (Cayman); β-actina y ROCK1, (Santa Cruz), Endoglina (BD) y HIF 2α (Abcam).

9.3 TINCIONES INMUNOHISTOQUÍMICAS.

Se realizaron cortes histológicos de 4 µm de músculo esquelético incluidos en parafina, que fueron introducidos en Tampón Tris para desenmascarar el antígeno usando el sistema DAKO PTlink a pH 9 para CD31 y pH 6 para Meox2. Después se incubó con 3% de H_2O_2 para bloquear la peroxidasa endógena con suero fetal bovino durante 30 minutos, las secciones se incubaron 45 minutos a temperatura ambiente con los anticuerpos primarios anti-CD31 (Abcam ab28364) y anti-Meox-2 (Abcam ab117551). El anticuerpo secundario para la tinción de CD31 es Dako Envision Flex HRP anti-rabbit (K4003) y para Meox-2 es Goat anti-mouse HRP (DAKO P0447), el revelado de la tinción se realizó con el sustrato DAB (DAKO K3468). En ambos casos la evaluación cuantitativa de la expresión de proteínas se realizó con el escáner de fluorescencia Oddisey y se analizó con el software de análisis Image Studio Lite v4.0 (LICOR).

10. EXTRACCIÓN DE RNA Y ANÁLISIS DE LA EXPRESIÓN GÉNICA

EL RNA y microRNA de fragmentos de membrana peritoneal de unos 0.5 cm^2 ó de 2 a 6 x 10^4 células tTregs purificadas por *sorting* de timos de ratón o de 10^6 PBLs humanas, se extrajeron con miRNeasy mini kit (Qiagen), seguido del tratamiento con DNAsa para eliminar el DNA genómico con el kit Turbo DNAse-free (Ambion). Para el tratamiento con DNAsa de las membranas peritoneales y de las células PBLs, se usaron 0.5 µg de RNA. Para las tTreg debido a la poca cantidad obtenida, se trató todo lo que se extrajo con la DNAsa.

Para el análisis de la expresión de Fibronectina, Colageno, TGF-β, IL-6, IL-1β, SOCS-1, Foxp3, MEOX2, CUX1 y BIC, se realizó la transcripción inversa (RT) utilizando el kit High Capacity cDNA reverse transcription kit (Applied Biosystems). Para las q-PCRs de de los genes Fibronectina, Colageno, TGF-β, IL-6, IL-1β, SOCS-1, Foxp3, MEOX2 y CUX1 se usó SYBR green PCR master mix (Applied Biosystems) y los genes de GAPDH y β-Actina de ratón y humanos se usaron como control de expresión endógena.

Cebadores usados para amplificar los genes murinos:

SOCS-1, (F) 5'-CTGCGGTTCTATTGGGGAC-3', (R) 5'-AAAAGGCAGTCGAAGGTCTCG-3'.

Foxp3, (F) 5'-CACCCAGGAAAGACAGCAACC-3', (R) 5'-GCAAGAGCTCTTGTCCATTGA-3'.

CD69, (F) 5'-CCCTTGGGCTGTGTTAATAGTG-3', (R) 5'-AACTTCTCGTACAAGCCTGGG-3'

GAPDH, (F) 5'-TGAAGCAGGCATCTGAGGG-3', (R) 5'-CGAAGGTGGAAGAGTGGGAG-3'.

Colágeno, (F) 5'-CCAGAGTGGAACAGCGATTAC-3', (R) 5'-GCAGGCGAGATGGCTTATTT-3'.

Fibronectina, (F) 5'-GCAAACCTATAGCTGAGAAGTC-3', (R) 5'-CAAGTACAGTCCACCATCATC-3'.

TGF-β, (F) 5'-GGAACTCTACCAGAAATATAGCAACAATTC-3´, (R) 5'-TGTAATCCGTCTCCTTGGTTCAG-3'.

IL-6, (F) 5'-GAGGATACCACTCCCAACAGACC-3', (R) 5'-AAGTGCATCATCGTTGTTCATACA-3'.

IL-1β, (F) 5'-TGGTGTGTGACGTTCCATT-3', (R) 5´-CAGCACGAGGCTTTTTTGTTG-3'.

β-Actina, (F) 5'-AAGGAGATTACTTGCTCTGGCTCCTA-3', (R) 5'-ACTCATCGTACTTCCTGCTTGCTGAT-3'.

MEOX2, (F) 5'-GCTGCCCGAGAAAAGGAACT-3', (5) 5'-TCGTTTGCTAGTGAGTCCCC-3'

CUX1, (F) 5'-TGATGCCACCGCAACAGTATT-3´, (R) 5'-GCGTAAATCCTCTGGAGTGTTCT-3'

Cebadores usados para amplificar genes humanos:

SOCS-1, (F) 5'-TTTTCGCCCTTAGCGTGAAGA-3', (R) 5'-GAGGCAGTCGAAGCTCTCG-3.'

GAPDH, (F) 5'-AATGGACTGGTCGTGGAG-3', (R) 5'-CCCTCCAGGGGATCGTTTG-3'.

La expresión de BIC, promotor de miRNA-155, se analizó por q-PCR utilizando TaqMan Master mix Universal y la sonda TaqMan específica para BIC (ID Mm01716204-m1 e ID Hs01374570-m1) (Applied Biosystems).

La expresión de los microRNAs se analizó utilizando TaqMan MicroRNA Reverse Transcription Kit para hacer las retrotrascripciones inversas, y para la q-PCR se usó TaqMan Universal PCR Master mix (Applied Biosystems). Como cebadores o sondas se usaron los ensayos de TaqMan específicos de cada microRNA, mmu-miR-155-5p (Ref. 002571), hsa-miR-155-5p (Ref. 002287), .hsa-miR-721-5p (Ref: 001657). Las sondas sno135 snRNA (Ref. 001230) y sno202 snRNA (Ref: 001232) se usaron como controles de expresión endógenos. En todos los casos, el análisis por q-PCR se realizó con un termociclador ABI Prism 7900HT 384 (Applied Biosystems). La expresión génica relativa se determinó usando el método $2^{-\Delta\Delta CT}$.

11. MARCAJE METABÓLICO DE CÉLULAS ENDOTELIALES

Entre los métodos de cuantificación de proteínas basados en espectrometría de masas, se escogió la técnica de SILAC (*Stable Isotope Labeling by Aminoacids in Cell Culture)* por ser el más apropiado y exacto para comparar las proteínas de dos poblaciones celulares de genotipos diferentes. El procedimiento general seguido para marcar estas células se muestra en la Figura 3, y consiste en cultivar las dos poblaciones celulares a comparar de la siguiente forma; La población A (MLEC CD69$^{+/+}$) se cultivó en DMEN F12 (Sigma) que contenía aminoácidos ligeros (R y K) y la población B (MLEC CD69$^{-/-}$) en un medio similar pero conteniendo R y K pesados, SILAC DMEN F12 (Dunnde Cells) (Figura 7A). Los aminoácidos pesados fueron isótopos estables (no radiactivos) que contenían ^{13}C en lugar de ^{12}C. La incorporación de estos aminoácidos proporcionó un incremento conocido en la masa del péptido comparada a su versión ligera (por ejemplo 6 Da en el caso de usar $^{13}C_6$-Lys) que no puede atribuirse a ningún otro cambio químico. En este caso concreto, las poblaciones celulares que se compararon fueron células primarias, que necesitaron unos aportes nutricionales diferentes a los de las líneas celulares inmortalizadas, por lo que ambos medios de cultivo se suplementaron con Insulina, Trasferrina y Selenio (ITS, Sigma), que sustituyó a los suplementos especiales que permiten el mantenimiento en cultivo de las MLEC y que son incompatibles con los experimentos de SILAC, ya que llevaban aminoácidos libres que impedirían la incorporación de los aminoácidos marcados. Una vez se consiguió un marcaje del 100% (tras 6 doblajes de la población), los dos cultivos se mezclaron y se extrajeron las proteínas. El extracto de proteínas fue separado mediante electroforesis en gel SDS-PAGE al 10% de entrecruzamiento y las bandas visualizadas mediante tinción con azul de Coomassie. El gel se cortó en 20 bandas horizontales que se destiñeron con una disolución 50:50 de 25 mM bicarbonato amónico-acetonitrilo. Posteriormente se realizó una digestión en gel de cada banda mediante adición de tripsina 12.5 ng/μl preparada en 25 mM bicarbonato amónico. Tras incubar las bandas 16 h a 37ºC y en agitación suave, se extrajeron los péptidos mediante extracciones secuenciales con acetonitrilo y ácido fórmico al 5% en agua (Figura 7A y B).

La mezcla de péptidos fue analizada empleando un sistema de nanocromatografía líquida (Eksigent) equipado con una precolumna de C18 (0.3 x 10 mm) y una columna analítica de fase inversa C18 HPLC PepMap (75μm x 15 cm). La separación cromatográfica de los péptidos fue llevada a cabo en modo gradiente desde un 5% hasta un 95% de acetonitrilo en fase acuosa al 0.1% de ácido fórmico. Las carreras cromatográficas se realizaron en 120 min a un flujo de 200 nl/min. El eluído fue conectado directamente con un *emitter* de acero inoxidable en una fuente de ionización por *electrospray* (Figura

7C). Los péptidos fueron analizados y fragmentados en un espectrómetro de masas de trampa de iones lineal (LTQ XL, Thermo) operando en modo dependiente de datos y alternando ZoomScans con MS/MS de los 3 picos más intensos de cada *full scan* realizado entre un rango de masas de 400 y 1600 u. La ventana de masas de los *ZoomScan* fue fijada en 12 Da para permitir visualizar la envoltura isotópica de la mayoría de péptidos con carga 2^+ y 3^+. Las moléculas de carga 1^+ fueron excluidas de los análisis de MS/MS. Las energías de colisión normalizadas fueron fijadas al 35% con una exclusión dinámica aplicada en periodos de 3 min para evitar la fragmentación repetitiva de los mismos iones.

Los archivos *.raw* generados fueron convertidos a archivos *.mgf* para poder realizar la búsqueda en el motor MASCOT (MatrixScience) equipado con una base de datos descargada del NCBInr conteniendo 34966 secuencias de proteínas de ratón. Para llevar a cabo las búsquedas, se fijaron como modificaciones variables la oxidación de metioninas y $^{13}C_6$-Arg y $^{13}C_6$-Lys. Asimismo, se fijó la tripsina como enzima proteolítica y se permitió hasta 1 missed-cleavage. La exactitud en los iones precursores y en los fragmentos de masas fue fijada en 1.2 y 0.3 Da, respectivamente. Los valores de score cut-off en MASCOT fueron fijados en 38 ($p<0.05$) para los péptidos y en 45 ($p<0.01$) para las proteínas. El porcentaje de falsos positivos fue calculado usando una base de datos reversa.

En los espectros de masas obtenidos, cada péptido apareció como un doblete, el de menor masa (péptido ligero) correspondió a la población A, mientras que el de mayor masa (pesado) correspondió a la población B. Debido a que ambos péptidos fueron químicamente idénticos, excepto por su diferencia de masa, se comportaron de forma igual en todos los pasos del proceso analítico, incluyendo la etapa de separación cromatográfica, con lo que se consiguió que ambos péptidos co-eluyeran y fueran analizados y detectados por el espectrómetro en el mismo momento. De esta manera, se pudieron relacionar directamente las intensidades de pico observadas en el espectro, con las concentraciones relativas de las proteínas a las cuales pertenecen dichos péptidos en las poblaciones celulares que se compararon.

Para llevar a cabo la cuantificación relativa se utilizó el programa QuiXoT y los cocientes SILAC se expresaron como intensidad de los péptidos pesados (^{13}C) dividida entre la intensidad de los péptidos ligeros (^{12}C). Las funciones moleculares y celulares de las proteínas que se encontraron alteradas (Cociente SILAC diferente de 1) se analizaron empleando las anotaciones de Gene Ontology (GO).

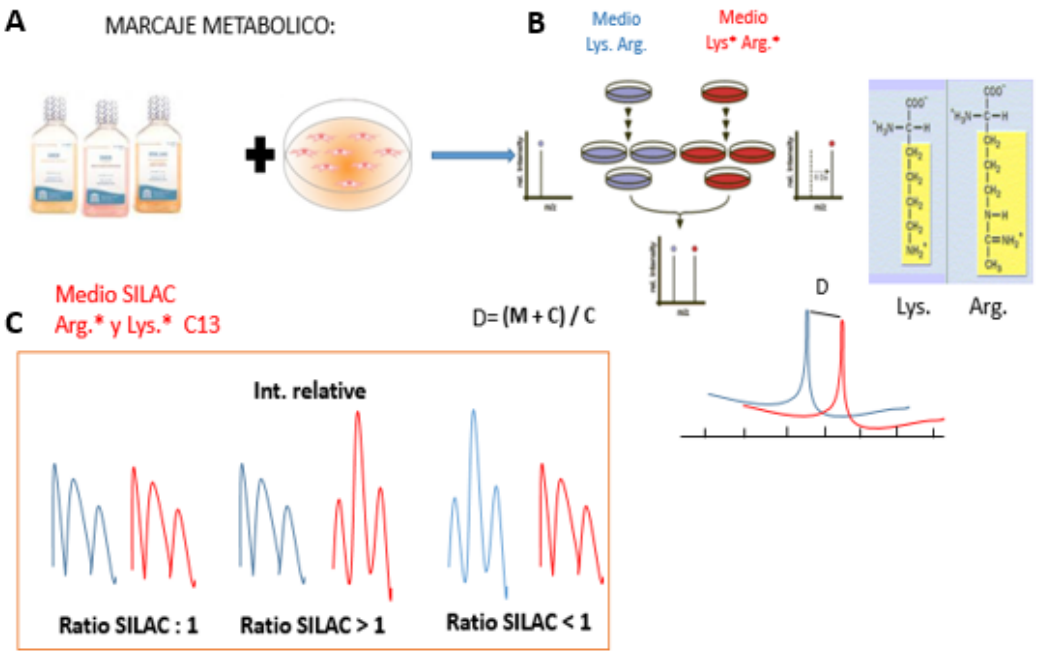

Figura 7. Esquema representativo que muestra como se realiza un experimento de marcaje metabólico (A) Cultivo celular con los dos diferentes medios ligero y pesado**. (B)** Mezcla de las dos poblaciones celulares**. (C)** esquemarepresentativo para la comparación de las diferentes intensidades realtivas que conduce a determinar el ratio SILAC .

III. RESULTADOS

III. RESULTADOS

1. ESTUDIO DEL PAPEL DE CD69 EN LA RESPUESTA TH17 Y LA REGULACIÓN DE FIBROSIS

Los pacientes con un fallo renal crónico (*end-stage renal disease*, ESRD) sometidos a diálisis peritoneal desarrollan una fibrosis peritoneal progresiva debido entre otros motivos a la exposición continua al fluido peritoneal con el que se desarrolla la técnica . El desarrollo de fibrosis limita el uso de esta técnica en pacientes con fallo renal crónico a periodos limitados de tiempo, por lo que hace necesario buscar otras alternativas para asegurar la supervivencia de estos pacientes. Datos recientes apuntan a la inflamación mediada por las células Th17 como un factor fundamental para el desarrollo de la fibrosis en el peritoneo (Liappas et al., 2017; Rodriguez-Diez et al., 2014). El antígeno leucocitario CD69 modula el establecimiento y la progresión de la inflamación mediante el control del equilibrio entre las células Th17 y las células T reguladoras (Treg) (Martin and Sanchez-Madrid, 2011) sin embargo, su papel en la fibrosis tisular sigue siendo ampliamente desconocida. Hemos explorado el papel de CD69 en la fibroproliferación utilizando un modelo de de fibrosis peritoneal en ratón inducida por la exposición al líquido de diálisis en estado normal o urémico.

1.1. CD69 CONTROLA LA FIBROSIS PERITONEAL EN CONDICIONES URÉMICAS

Generamos ratones urémicos *wild type* (WT) y CD69$^{-/-}$ mediante la ablación de un riñón y el daño irreversible en 2/3 del restante (nefrectomía de 5/6, Figura 8A). Estos animales se trataron con solución salina o líquido de diálisis peritoneal (*Peritoneal Dyalisis Fluid*, PDF) durante 40 días. Al final del estudio se observó un aumento significativo de la fibrosis peritoneal en ambos ratones expuestos a PDF en comparación con ratones expuestos a solución salina, desarrollándose fibrosis e infiltrado leucocitario exacerbado en ratones CD69$^{-/-}$ (Figura 8B y C). Estos datos fueron confirmados por la detección de niveles de mRNAs de colágeno I y fibronectina así como TGF-β, IL-6, e IL-1β, encontrandose estos tránscritos aumentados en la membrana peritoneal de animales CD69$^{-/-}$ en comparación con ratones WT expuestos a PDF (Figura 8D y E). Además, el nivel de IL-17 en el efluente peritoneal aumentó muy significativamente en ratones CD69$^{-/-}$ expuestos a PDF, mientras que los niveles de IFN-γ e IL-4 no mostraron diferencias significativas entre los grupos (Figura 9).

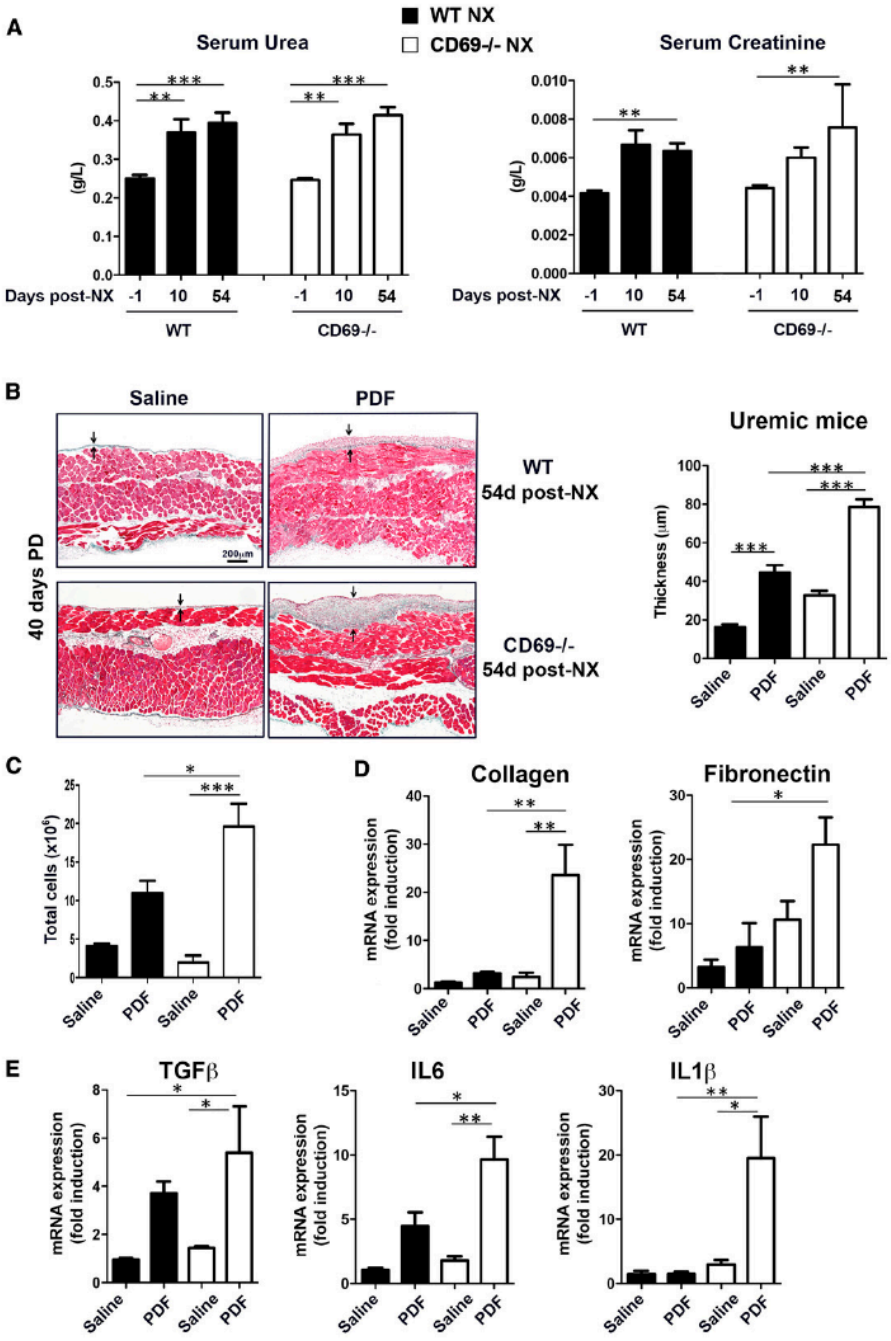

Figura 8. CD69 regula la fibrosis en ratones con función renal deficiente. Los ratones WT y CD69$^{-/-}$ sometidos a nefrectomía (NX) de 5/6 fueron tratados con solución salina o PDF durante 40 días. **(A)** Niveles séricos de urea y creatinina antes de la nefrectomia y 10-54 días después de la nefrectomía en los grupos tratados con solución salina o PDF. **(B)** Evaluación de la fibrosis por tinción *Tricrómico de Masson* en ratones CD69$^{-/-}$ y WT 54 días después de la nefrectomía. Las flechas indican el grosor de la membrana peritoneal. El panel derecho muestra la cuantificación de la fibrosis de la membrana peritoneal en ratones urémicos (n=10). **(C)** Recuento total de células mononucleares en el efluente peritoneal en cada grupo de ratones. La fibrosis e inflamación en el tejido peritoneal de ratones urémicos WT y CD69$^{-/-}$ se evaluó por qPCR de colágeno I y fibronectina **(D)** y citoquinas pro-

inflamatorias **(E),** respectivamente. Las barras de error muestran la SD (n=6). Los datos se analizaron por ANOVA y post-test de Bonferroni para comparar los diferentes grupos por pares (*P<0.05, ** P<0.01, *** P<0,001).

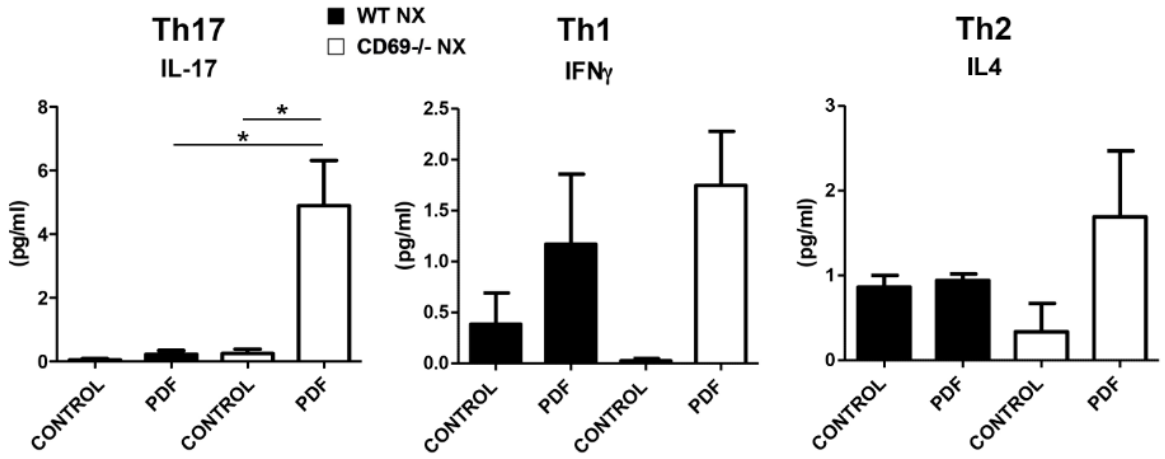

Figura 9. Expresión de citoquinas en la cavidad peritoneal de ratones urémicos WT y CD69$^{-/-}$. Los ratones nefrectomizados se trataron con solución salina o PDF durante 40 días. La producción de citocinas asociadas a las células T *helper* se evaluó mediante análisis por citometría de flujo (Flow cytomix). Las barras muestran la media y SD (n≥6). Los datos se analizaron por ANOVA y post-test de Bonferroni para comparar los diferentes grupos por pares (* P <0.05, ** P <0.01, *** P <0.001).

El reclutamiento de linfocitos T CD4^{+} y CD8^{+} a la membrana peritoneal inducido por PDF fue similar en ratones WT y CD69$^{-/-}$ (Figura 10A). Aunque los niveles de Th17 aumentaron tanto en ratones WT como en ratones CD69$^{-/-}$ tratados, el número de Th17 fue significativamente mayor en los últimos. El número de Treg también aumentó en ratones WT y CD69$^{-/-}$ tratados con PDF, alcanzando significación estadística sólo en el grupo CD69$^{-/-}$. Asimismo, el aumento del ratio Th17/Treg sólo alcanzó significación estadística en ratones CD69$^{-/-}$ (Figura 10B). Los monocitos y neutrófilos se reclutaron de manera similar en ratones WT y CD69$^{-/-}$ (Figura 10C). Cabe destacar que el número de células en el infiltrado inflamatorio fue generalmente menor en ratones CD69$^{-/-}$ nefrectomizados con respecto a los no nefrectomizados expuestos a PDF, mientras que el espesor de la membrana fibrosada fue similar en ambos grupos de ratones CD69$^{-/-}$. Por el contrario, los animales WT urémicos tratados mostraron niveles mayores de fibrosis e infiltrado en comparación con ratones no uremico WT. Estos datos sugieren que la uremia aceleró el proceso inflamatorio por lo que la curva de inflamación estaba en su fase de declinación en los animales CD69$^{-/-}$ pero no en ratones WT expuestos a PDF 40 días. En conjunto, nuestros resultados confirman el papel regulador de CD69 en estos procesos.

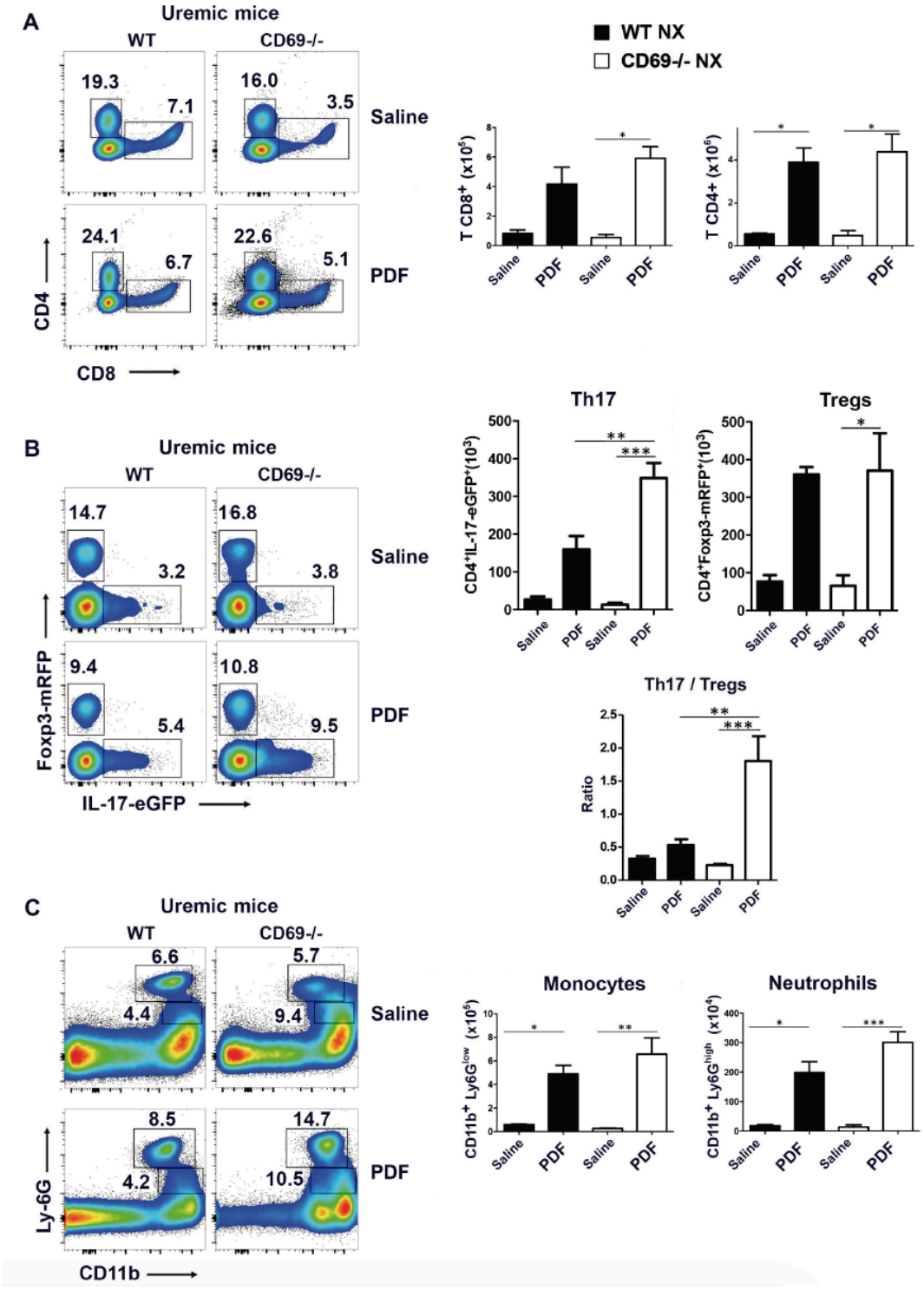

Figura 10. Infiltrado en el efluente peritoneal en animales sometidos a nefrectomía de 5/6. (A) Izquierda, diagramas de densidad representativos del análisis de células T $CD8^+$ y $CD4^+$ por citometría de flujo en los efluentes peritoneales de ratones uremicos $CD69^{-/-}$ dobles reporteros Foxp3-mRFP e IL-17-eGFP o WT hermanos de camada. Los números indican el porcentaje de células incluidas en los recuadros. Derecha, evaluación de los números totales de células T $CD8^+$ y $CD4^+$ en ratones tratados durante 40 días con solución salina o PDF. **(B)**

Izquierda, diagramas de densidad representativos del análisis por citometria de flujo de los niveles de células $CD4^+$ $Foxp3\text{-}RFP^+$ (Treg) e $IL\text{-}17^+$ (Th17) en los diferentes grupos experimetales. Derecha, cuantificación y ratio de Th17/Tregs de los diferentes grupos. **(C)** Diagramas representativos del análisis por citometria y cuantificación de monocitos ($CD11b^+$ $Ly6G^{low}$) y neutrófilos ($CD11b^+$ $Ly6G^{high}$) en efluentes peritoneales. Los datos se analizaron por ANOVA y post-test de Bonferroni para comparar los diferentes grupos por pares (* P <0.05, ** P <0.01, *** P <0.001).

1.2. EL BLOQUEO DE CD69 IMITA LA RESPUESTA EXACERBADA DE LOS ANIMALES DEFICIENTES EN $CD69^{-/-}$

Para demostrar la relevancia de la expression en la membrana de CD69 en la inflamación y posterior fibrosis producida por la exposición a PDF, tratamos animales WT con un anticuerpo monoclonal (mAb) neutralizante de CD69 (2.2) que regula la expression de la molécula en la membrana, o su control de isotipo (2.8). Los ratones $CD69^{-/-}$ tratados con 2.2 se utilizaron como control. Los animales WT tratados con anti-CD69 mostraron un aumento de la fibrosis peritoneal en respuesta a la exposición a PDF, en comparación con los animales WT tratados con 2.8 y similar a la fibrosis encontrada en los ratones $CD69^{-/-}$ tratados con anti-CD69 (Figura 11A). Del mismo modo las células Th17, pero no Th1 o Th2, de animales WT y $CD69^{-/-}$ tratados con 2.2 aumentaron considerablemente (Figura 11B). También hubo aumento significativo en el número de Treg en ratones $CD69^{-/-}$, aunque no en animales WT tratados con 2.2 (Figura 11C). El aumento de la inflamación en ratones tratados con el anticuerpo 2.2, se acompañó con un menor reclutamiento de neutrófilos en WT en comparación con $CD69^{-/-}$ (Figura 11D). Estos datos indican que, aunque parcialmente, el tratamiento de animales WT con mAb anti-CD69 reproduce los resultados obtenidos con los animales $CD69^{-/-}$, demostrando la relevancia de la expresión de CD69 en la membrana de las células T en esta patología.

1.3. LA EXPRESIÓN DE CD69 EN EL COMPARTIMENTO LINFOIDE REGULA LA FIBROSIS

Para excluir los efectos de la expresión de CD69 en el compartimento mieloide y acotar el estudio a su expresión en las células linfoides, los animales WT y $CD69^{-/-}$ fueron irradiados y reconstituidos con una mezcla de precursores de médula ósea (*bone marrow*; BM) de $Rag2^{-/-}\gamma c^{-/-}$: $CD69^{-/-}$ o $Rag2^{-/-}\gamma c^{-/-}$: WT en proporción 3:1, respectivamente. Los precusores $Rag2^{-/-}\gamma c^{-/-}$, deficientes en compartimento linfoide y más numerosos, generan animales quiméricos con células mieloides WT por competición en el nicho de BM, siendo el compartimento linfoide WT o $CD69^{-/-}$ en cada caso (Figuras 12 y 13A). Las quimeras $Rag2^{-/-}\gamma c^{-/-}$:$CD69^{-/-}$ generaron mayor fibrosis peritoneal inducida por PDF que las quimeras $Rag2^{-/-}\gamma c^{-/-}$:WT, indicando que la expresión de CD69 en el compartimento linfoide es fundamental para controlar la respuesta fibroproliferativa después del tratamiento con PDF (Figura 13B). Un análisis de las

subpoblaciones T helper reveló un aumento significativo en células Th17 pero no en Th1 o Th2 en los ratones reconstituidos con BM Rag2$^{-/-}$γc$^{-/-}$:CD69$^{-/-}$ en comparación con las quimeras Rag2$^{-/-}$γc$^{-/-}$: WT, en respuesta a la exposición a PDF (Figura 13C). Por lo tanto, estos datos muestran de forma inequívoca que la expresión de CD69 dentro del compartimiento linfoide controla la respuesta Th17 y el desarrollo de la fibrosis en el peritoneo después del tratamiento con PDF.

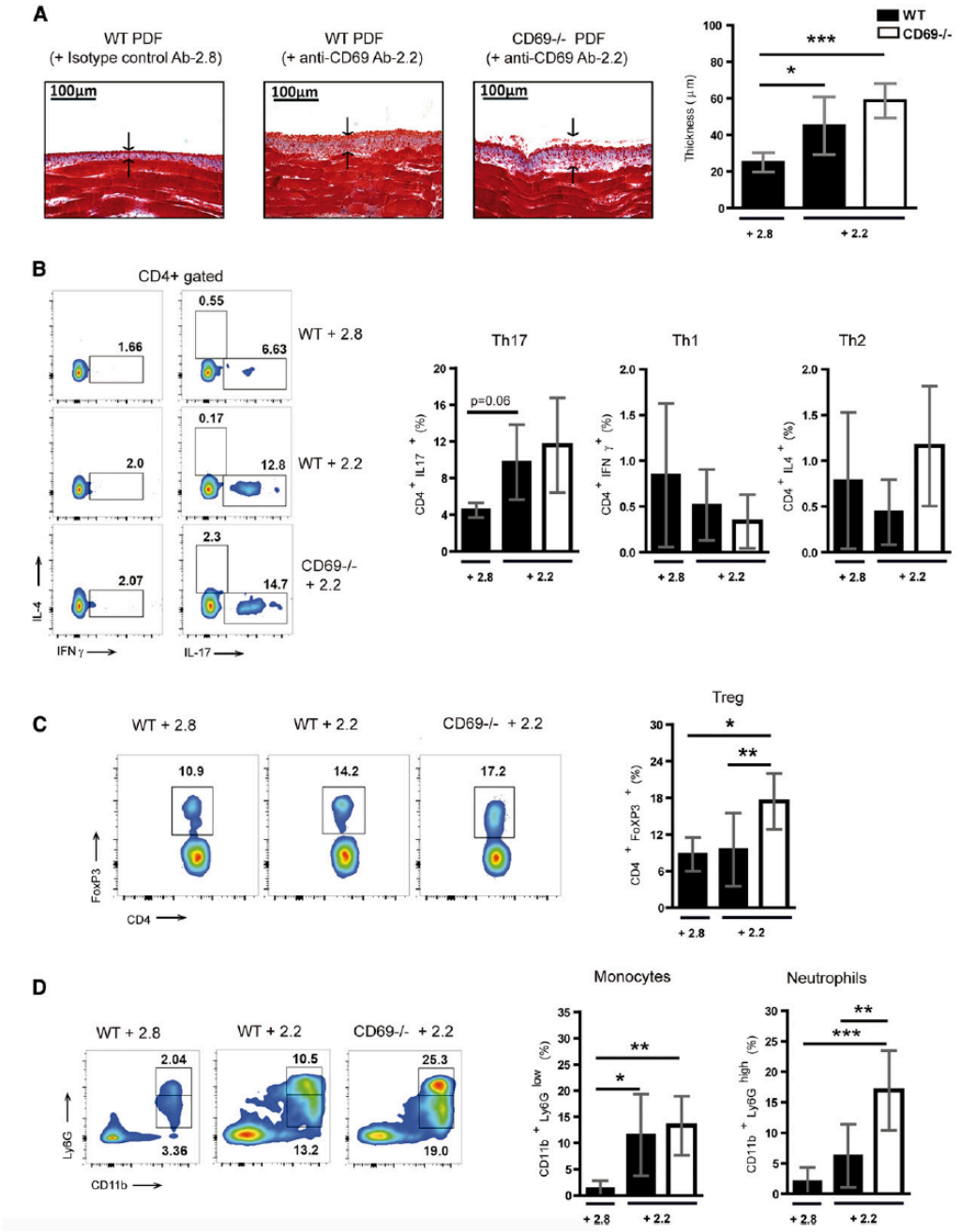

Figura 11. El bloqueo con anti-CD69 en ratones WT reproduce el fenotipo de ratones CD69$^{-/-}$ tras diálisis con PDF. Los ratones WT y CD69$^{-/-}$se trataron intraperitonealmente con PDF durante 40 días, combinado con anticuerpo anti-CD69 (2.2) o control de isotipo (2.8), cada 5 días. **(A)** Fibrosis de la membrana peritoneal analizada por

inmunohistoquímica con tinción de Tricrómico de Masson en los diferentes grupos. Las flechas indican el espesor de la membrana, cuantificado en μM en los histogramas. **(B-D)** Análisis por citometría de flujo de los efluentes peritoneales y cuantificación de los porcentajes de leucocitos. Los recuadros muestran el porcentaje de células Th1, Th2, Th17 (B), Treg (C) y mieliodes, CD11b^{+} Ly6G^{low} (monocitos) y CD11b^{+} Ly6G^{high} (neutrófilos) (D). Los datos se analizaron por ANOVA y post-test de Bonferroni para comparar los diferentes grupos por pares (* P <0.05, ** P <0.01, *** P <0.001).

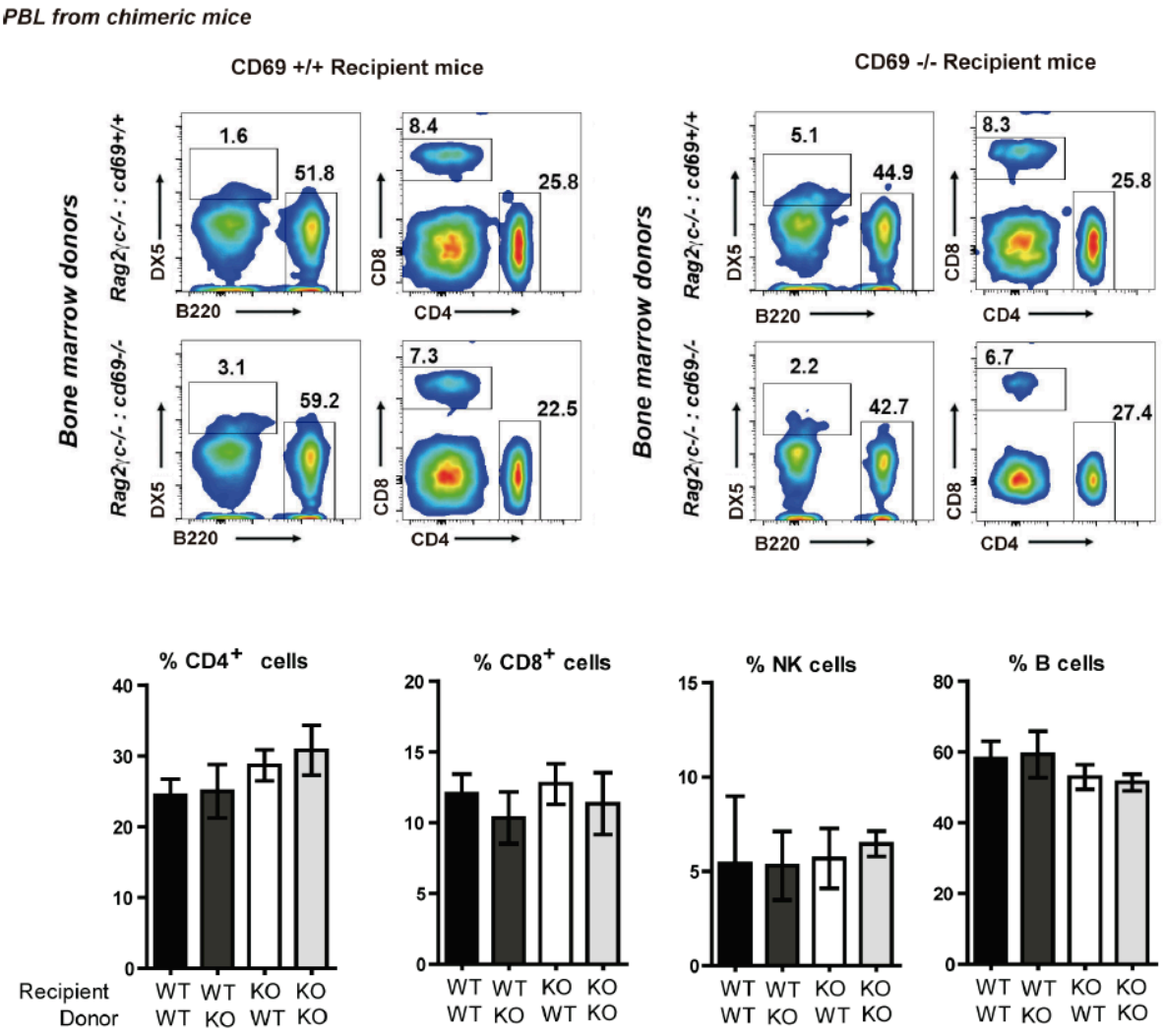

Figura 12. Reconstitución de animales quiméricos Rag2$^{-/-}$γc$^{-/-}$: CD69$^{-/-}$ o Rag2$^{-/-}$γc$^{-/-}$: CD69$^{+/+}$. Los ratones receptores WT y CD69$^{-/-}$ se trasplantaron con una mezcla de células de médula ósea de Rag2$^{-/-}$ γc$^{-/-}$ y CD69$^{-/-}$ (KO) o Rag2$^{-/-}$ γc$^{-/-}$ y CD69$^{+/+}$ (WT) en proporciones 3:1, respectivamente. Los diagramas de densidad del análisis por citometría de flujo representativos de cada grupo de quimeras, indican el porcentaje de reconstitución de las poblaciones linfoides después de 10 semanas. Los histogramas Análisis de citometría de flujo de células CD4^{+}, CD8^{+}, NK (DX5^{+}) y B (B220^{+}) en muestras de sangre periférica (*peripheral blood lymphocytes*, PBL) tras el tiempo necesario para la reconstitución (10 semanas) antes del inicio del tratamiento con PDF. (N≥8). No se encontraron diferencias estadísticamente significativas utilizando la prueba ANOVA de una vía y Bonferroni post Test para comparar los diferentes grupos por parejas.

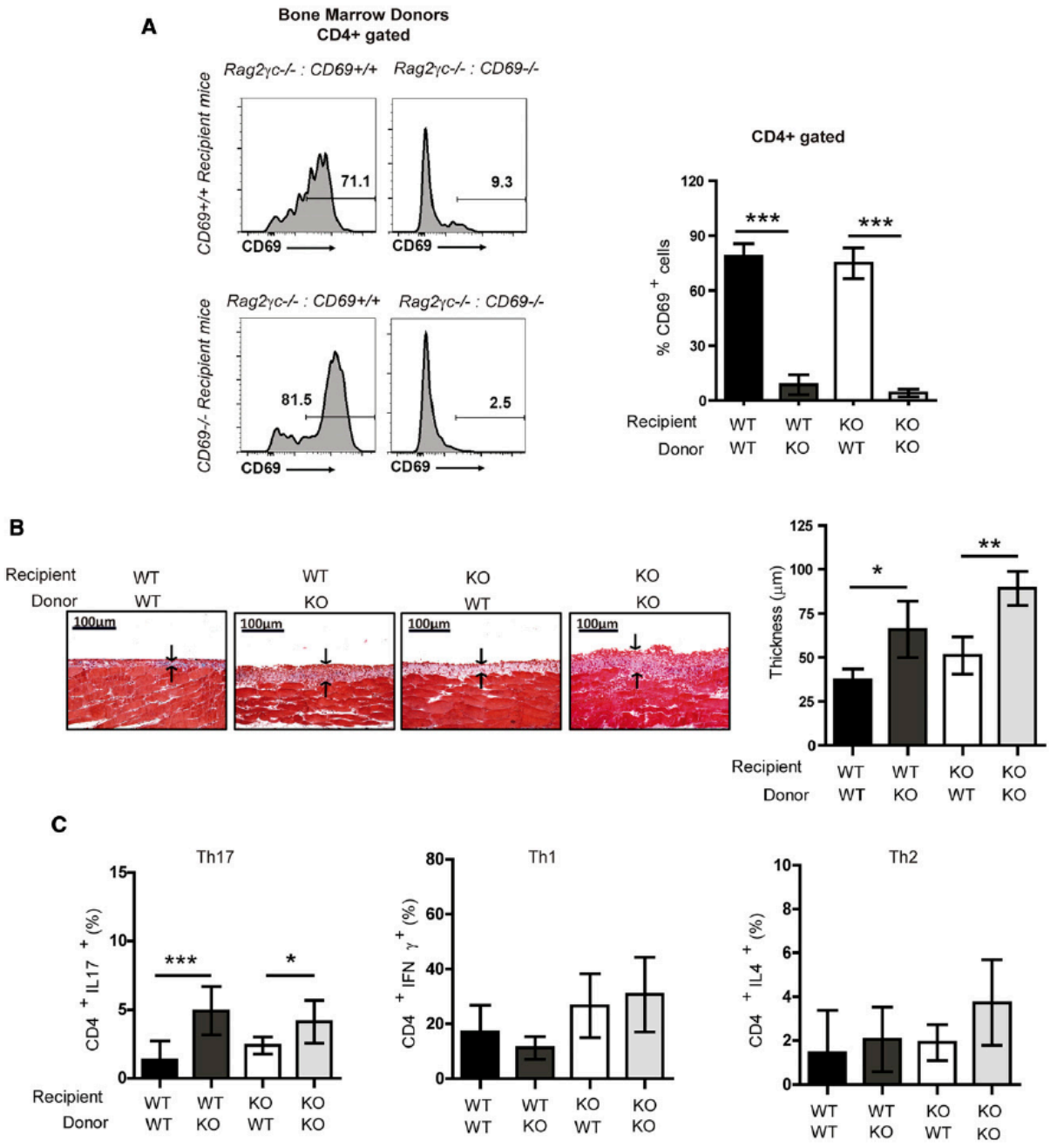

Figura 13: La expresión de CD69 en el compartimiento de linfoide regula la fibrosis peritoneal. Los ratones WT y CD69$^{-/-}$ se trasplantaron con una mezcla de precursores de BM de animales Rag2$^{-/-}$γc$^{-/-}$y CD69$^{-/-}$ (KO) o Rag2$^{-/-}$γc$^{-/-}$y CD69$^{+/+}$ (WT) como se describe en material y métodos. **(A)** Histograma representativo del análisis de citometría de flujo de células CD4^{+} CD69^{+} en sangre periférica de los animales quiméricos y la cuantificación correspondiente. (n=8). **(B)** Imágenes representativas de tinción con Tricómico de Masson en secciones de tejido peritoneal de ratones quiméricos tratados 40 días con PDF. Las flechas indican el grosor de la menbrana (n=4). **(C)** Análisis de citometría de flujo de células Th17 (CD4^{+} IL-17^{+}), Th1 (CD4^{+} IFN-γ^{+}) y Th2 (CD4^{+} IL-4^{+}) de la cavidad peritoneal (n =7). Los datos se analizaron por ANOVA y post-test de Bonferroni para comparar los diferentes grupos por pares (* P <0.05, ** P <0.01, *** P <0.001).

2. ESTUDIO DEL PAPEL DE LA MOLÉCULA CD69 EN LA FUNCIÓN DE LAS CÉLULAS TREG.

Las células T reguladoras Foxp3$^+$ son linfocitos T CD4$^+$ con actividad supresora que intervienen en el desarrollo de la tolerancia periférica y por tanto son esenciales para prevenir enfermedades inflamatorias autoinmunes y crónicas. Sin embargo, la falta de marcadores específicos y la insuficiente comprensión de la biología de estas células constituyen los dos mayores obstáculos para desarrollar protocolos de inmunoterapia para estas enfermedades. En este trabajo hemos analizado el papel de CD69 en la función de las células Treg Foxp3$^+$. Alrededor de la mitad de las Treg localizadas en los órganos linfoides expresan CD69 en homeostasis y es esta subpoblación de células Treg CD69$^+$ la que tiene mayores niveles de expresión de los marcadores asociados a procesos de supresión de la inflamación y por tanto son más proclives a intervenir en los procesos de generación de tolerancia. Nuestros resultados apoyan firmemente un papel de CD69 como un receptor crítico para controlar la función supresora de estas células, tanto en procesos fisiológicos cómo patológicos.

2.1. CD69 ESTÁ CONSTITUTIVAMENTE EXPRESADO EN UNA POBLACIÓN DE CÉLULAS TREG

Una subpoblación de entre treinta y cincuenta por ciento del total de Treg CD4$^+$CD25$^+$Foxp3$^+$ en el timo y los órganos linfoides secundarios expresan CD69 en su membrana constitutivamente (Figura 14A). El análisis fenotípico adicional de éstas poblaciones de Treg CD69$^+$ y CD69$^-$ procedentes de animales CD69$^{+/+}$ o CD69$^{-/-}$ en homeostasis, reveló que los marcadores inmunosupresores CTLA-4, ICOS, CD38 y GITR se expresaban más en la subpoblación de Treg CD69 $^+$ en estado estacionario en comparación con Treg CD69$^-$ o procedentes de ratones CD69$^{-/-}$ (Figura 14C), lo que sugiere que las características fenotípicas de las Treg CD69$^+$ las hace más proclives a desarrollar mejor su función supresora. Sin embargo, los niveles de expresión de otras proteínas relevantes para la función de las Treg, tales como CD25, CD86 o CD27, no se ven afectados en ausencia de CD69. Además, no observamos diferencias en la expresión del factor de transcripción Foxp3$^+$ o en el porcentaje de las Treg de animales CD69$^{-/-}$ o CD69$^{+/+}$ (Figura 14D), lo que sugiere que las Treg deficientes en CD69 podrían tener comprometida su función reguladora, mientras que la diferenciación de estas células, o al menos la expresión de Foxp3, parece no estar afectada.

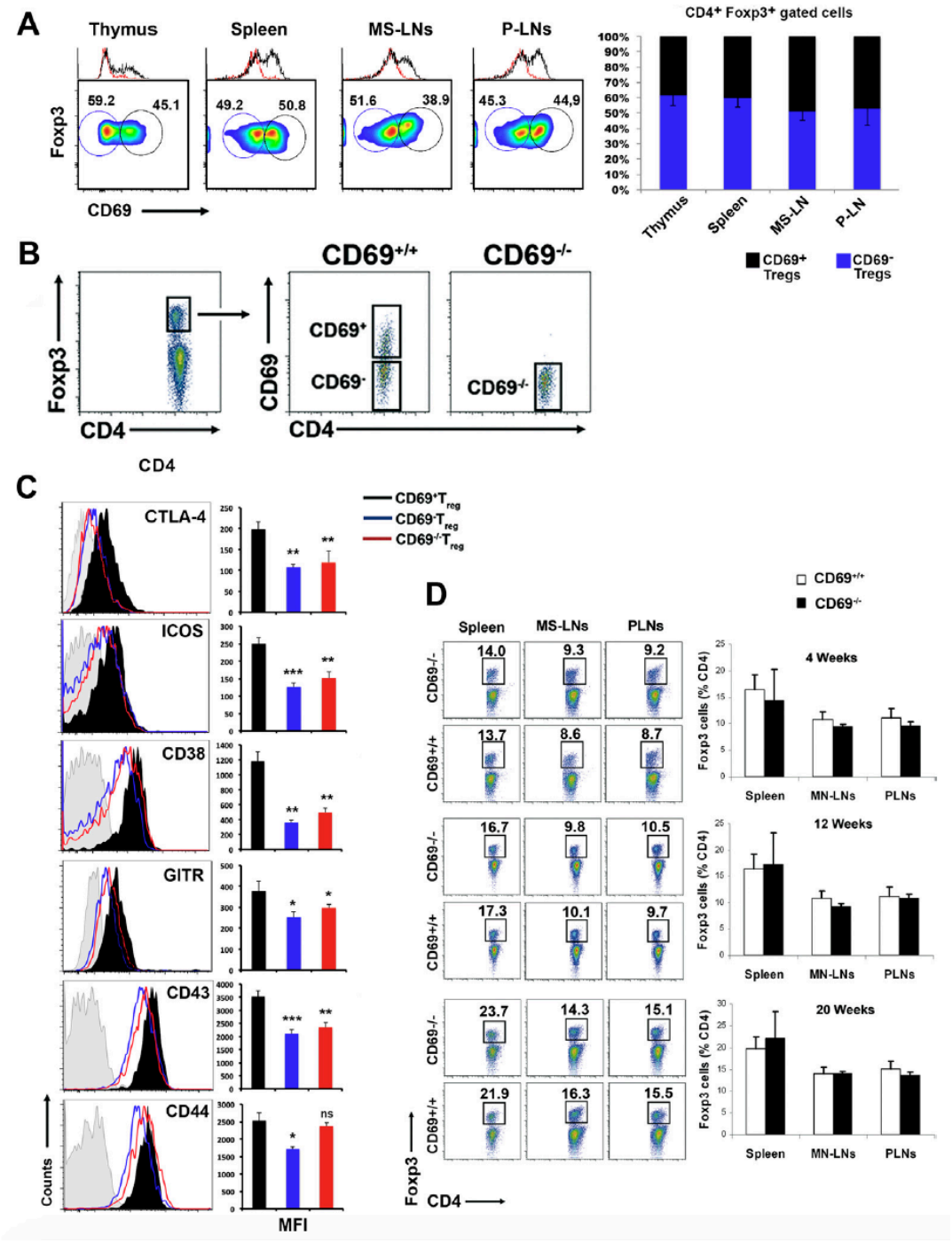

Figura 14: CD69 se expresa constitutivamente en una población de Treg. **(A)** Análisis por citometría de flujo de la expresión de CD69 en células $CD4^+$ $Foxp3^+$ en timo, bazo y ganglios mesentéricos (MS-LN) y periféricos (P-LN) de ratones $CD69^{+/+}$. Los histogramas representan la expresión de células $CD4^+$ $Foxp3^+$ $CD69^+$ (negro) y $CD69^-$ (azul). **(B)** Estrategia de análisis de los datos de FACS de células $CD4^+$ $Foxp3^+$ $CD69^+$ o $CD69^-$ de bazo de ratones $CD69^{+/+}$ y $CD69^{-/-}$. **(C)** Expresión de marcadores inmuno-supresores en Tregs $CD69^+$ (negro), $CD69^-$ (azul) y $CD69^{-/-}$ (rojo). Las áreas sombreadas en gris representan el control del isotipo de anticuerpo y los gráficos de barras muestran la media de la intensidad de la fluorescencia (MFI). **(D)** Análisis de citometría de flujo de células $CD4^+$ $Foxp3^+$ aisladas de ganglios linfáticos MS-LN y P-LN, y de bazo de ratones $Cd69^{+/+}$ y $Cd69^{-/-}$ de 4, 12 y 20 semanas de edad.

Cuantificación de los porcentajes de células T $CD4^{+}Foxp3^{+}$. Los datos son representativos de tres experimentos independientes. * P <0.05, ** P <0.01, *** P <0.001.

2.2. LAS CÉLULAS TREG $CD69^{-}$ TIENEN FUNCIÓN SUPRESORA DEFECTUOSA *IN VITRO*

Con el fin de evaluar el papel de CD69 en la función supresora de las Treg se llevaron a cabo ensayos de supresión de la función efectora de las células T. Para aislar las Tregs se emplearon animales reporteros de Foxp3, que expresan una forma monomérica de la proteína RFP en el locus de Foxp3 (Foxp3-$mRFP^{+}$), y fueron separadas por citometría de flujo (separación: *Sorting* en FACS Aria, BD) (Figura 15A). Para ello, se co-cultivaron células T convencionales (Tconv) de ratones $CD69^{+/+}$ con células Treg $CD4^{+}$Foxp3-$mRFP^{+}$ $CD69^{+}$ o $CD69^{-}$. Observamos una deficiencia marcada en la capacidad supresora de las Tregs Foxp3-$mRFP^{+}CD69^{-}$ en comparación con las Foxp3-$mRFP^{+}CD69^{+}$, ya que no eran capaces de suprimir la proliferación de las Tconv (Figura 15B).

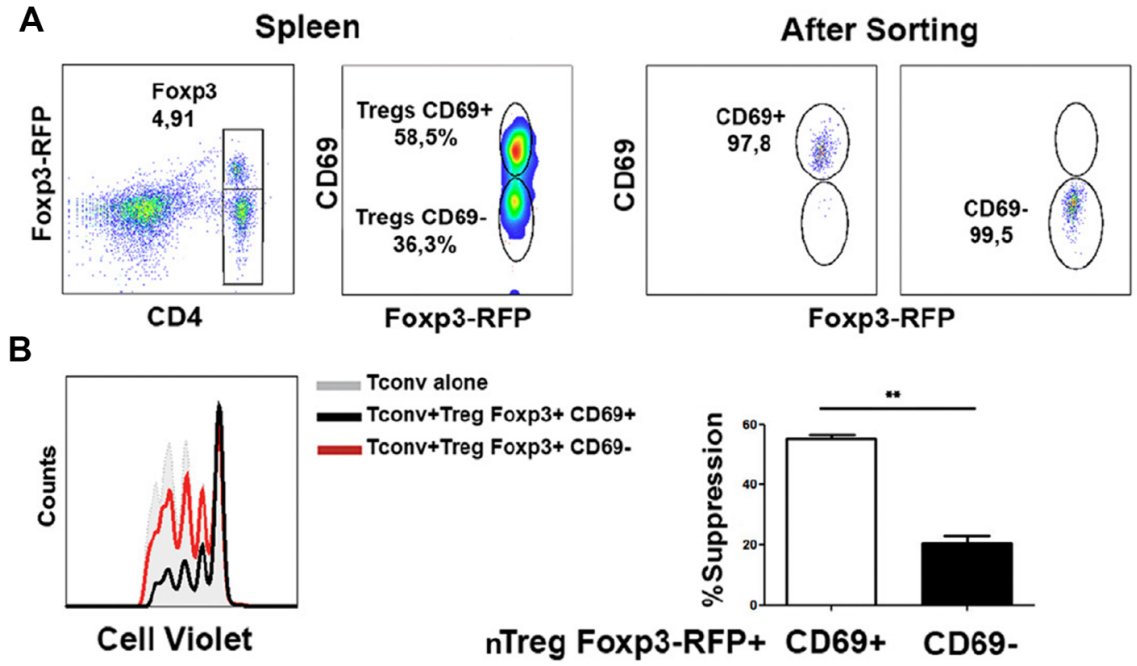

Figura 15: Las células Treg $CD69^{-}$ carecen de función supresora *in vitro*. (A) Estrategia de análisis de FACS para la purificación de las poblaciónes de células Treg $CD4^{+}$ Foxp3-$mRFP^{+}$ $CD69^{+}$ o $CD69^{-}$. **(B)** Histogramas representativos de la proliferación de células Tconv solas (sombra gris), Tconv con $CD4^{+}$ Foxp3-$mRFP^{+}$ $CD69^{+}$ (negro) o Tconv con $CD4^{+}$ Foxp3-$mRFP^{+}CD69^{-}$ (rojo), por incorporación y dilución del intercalante *Cell violet*. Cuantificación del porcentaje de supresión de células Treg en relación al porcentaje de proliferación de células Tconv. Los datos son representativos de tres experimentos independientes (n = 3). ** P <0,01.

2.3. La capacidad supresora de las Treg deficientes en CD69 está inhibida *in vivo* en protocolos de terapia celular

Para testar el papel de CD69 en la función supresora de las Tregs *in vivo* se desarrolló un modelo animal de asma en el que se generó tolerancia al antígeno en pulmón, mediante la inmunización intratraqueal (i.t.) del antígeno ovoalbumina (OVA) y la posterior exposición al antígeno inhalado. En este modelo los animales $CD69^{+/+}$ no desarrollan asma tras la exposición a OVA, debido a que tienen Tregs funcionales que inhiben la proliferación de las células Th2, causantes del asma alérgico. En cambio, los animales $CD69^{-/-}$ expuestos a OVA desarrollan una fuerte respuesta asmática con un aumento del reclutamiento de neutrófilos en los pulmones (Figura 16).

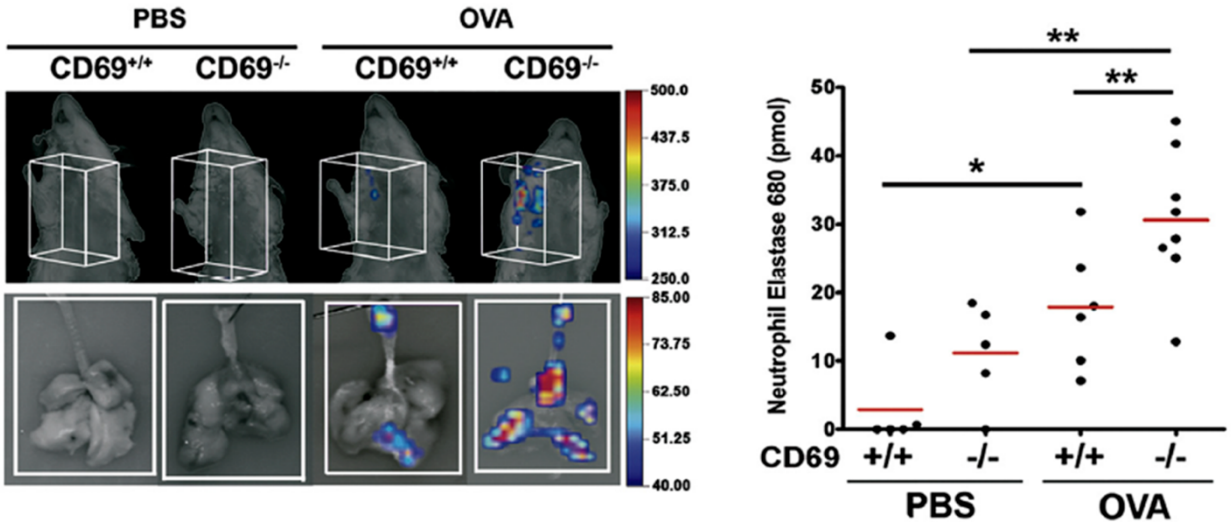

Figura 16. **Los animales $CD69^{-/-}$ muestran un aumento de inflamación pulmonar en un modelo de asma tolerogénico.** Los animales fueron sensibilizados con OVA intratraqueal y posteriormente intraperitonealmente. Después de 20 días los animales fueron expuestos a aerosol de OVA nebulizada. El grado de inflamación en los pulmones se valoró mediante Tomografía Molecular Fluorescente (*Molecular Fluorescence Tomography*, FMT) tras la inyección de una sonda de elastasa 680, específica de neutrófilos. Se muestra la señal de la sonda en el animal así como en los pulmones extraídos. Cuantificación de la señal de la sonda de elastasa en pico moles (pmol) en cada grupo de animales. Los datos son representativos de 3 experimentos independientes. * P <0.05, ** P <0.01, *** P <0.001.

Para demostrar que la expresión de CD69 en Tregs se requiere para restaurar la homeostasis en el pulmón y suprimir la inflamación provocada en respuesta a antígenos inhalados, inmunizamos ratones $CD69^{+/+}$ o $CD69^{-/-}$ con OVA. Se recolectaron MS-LN y las células se expandieron ex vivo con TGFβ1 e IL-2 en presencia de iAPCs pre-incubadas con OVAp. $5x10^6$células iTreg diferenciadas ex vivo se transfirieron a ratones receptores o $CD69^{-/-}$, 19 días después de inoculación i.t. con OVA. Después del tratamiento con iTreg, todos los grupos de ratones se sometieron a aerosol de OVA tres días consecutivos, 30 minutos cada grupo. Para analizar la inflamación en el pulmón se inyectó intravenoso (i.v.) la sonda de elastasa activada de neutrófilos, 12 horas antes del análisis por FMT (Figura 17A). El análisis de imágenes *in vivo* por tomografía cuantitativa indicó que ninguno de los ratones receptores desarrolló características de inflamación pulmonar cuando se inmunizaba con aerosol de PBS o estaban tratados con de Treg derivadas de ratones donantes $CD69^{+/+}$, mientras que se detectó una respuesta inflamatoria en los pulmones de $^{-}$ratones $CD69^{-/-}$ o los receptores tratados con Treg $CD69^{-/-}$ (Figura 17B y C). Además la inflamación de los receptores $CD69^{-/-}$ estaba completamente inhibida tras inmunoterapia con Treg $CD69^{+/+}$ (Figura 17B y C). En paralelo, se trató un grupo distinto de ratones con 2×10^5 células Treg $CD25^+$ obtenidas *ex vivo* de bazos ratones WT o $CD69^{-/-}$, purificadas mediante separación por *sorting*. Se analizó el porcentaje de neutrófilos de estos animales, obtenidos mediante lavados broncoalveolares (*Bronchoalveolar lavages*; BALS) 24 horas después de la última exposición a PBS u OVA. Los resultados confirmaron el experimento anterior, restableciéndose la tolerancia para los ratones $CD69^{-/-}$ expuestos a OVA tratados con pTreg $CD69^+$ obtenidas *ex vivo* (Figura 17D). Ya que CD69 controla los niveles de los receptores tipo 1 de esfingosina 1 fosfato ($S1P_1$) en la membrana del linfocito y de este modo su salida de los órganos linfoides a la circulación (Lamana et al., 2011), estudiamos la migración de las Tregs al pulmón, para descartar un posible efecto de la falta de CD69 en la migración al sitio de la inflamación. Cuantificamos las células Treg $CD4^+$ $Foxp3^+$ de los ganglios linfáticos del mediastino y BALS después de la transferencia de las pTregs encontrando un aumento en los números después de la exposición a OVA. No se detectaron diferencias significativas entre ratones WT y $CD69^{-/-}$transferidos con células $CD69^+$ o $CD69^-$, confirmando así una disfunción en las Treg $CD69^{-/-}$ en lugar de un defecto en su migración ratificando nuestros resultados anteriores (Figura 18).

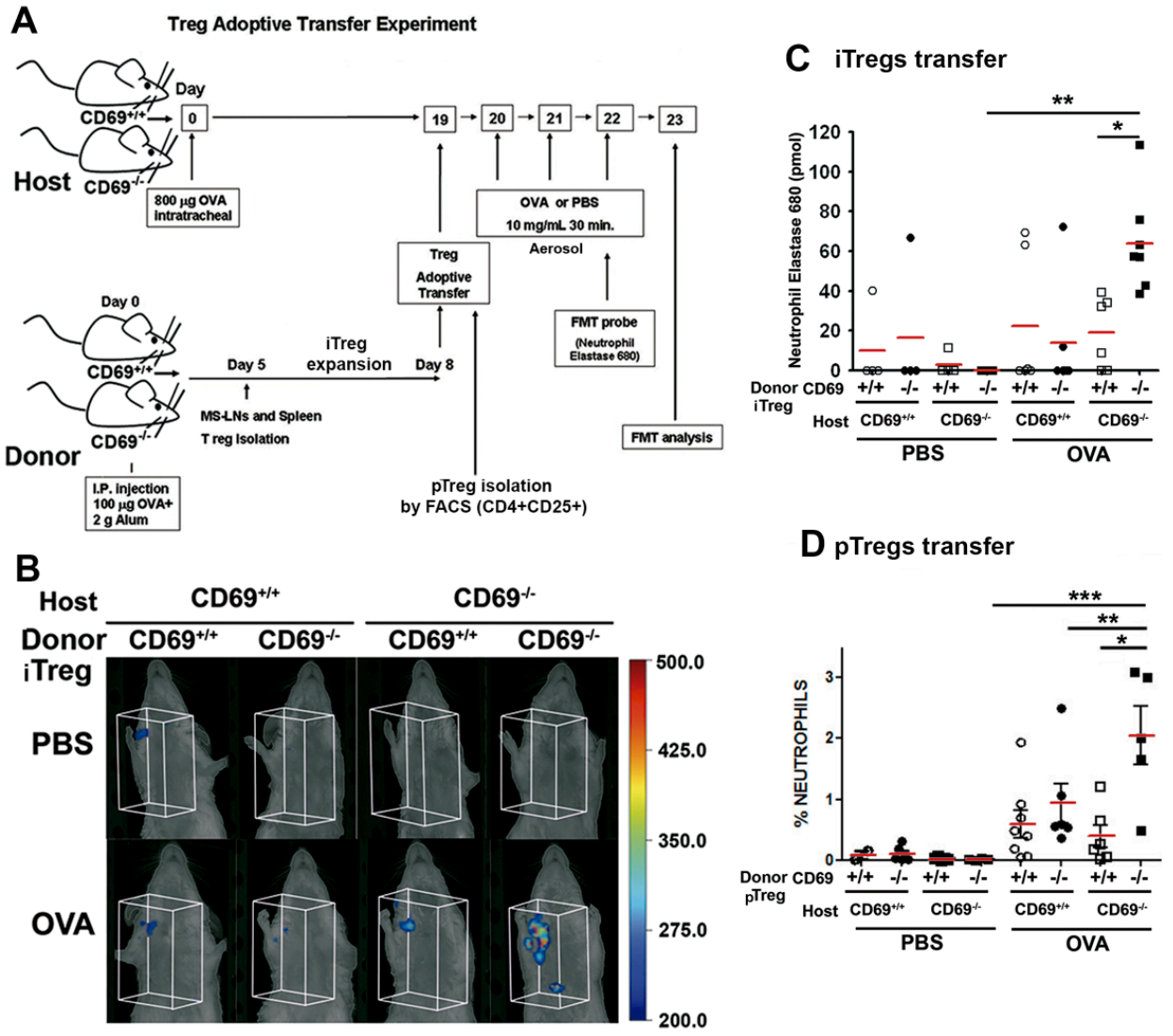

Figura 17. La terapia celular con Treg CD69^{+} restaura la tolerancia pulmonar en ratones CD69$^{-/-}$. (A) Esquema del experimento de transferencia de células iTreg o pTreg obtenidas de ratones CD69$^{+/+}$ y CD69$^{-/-}$ antes de la exposición a PBS u OVA. **(B)** Detección de neutrófilos activados en las vías respiratorias mediante FMT. Las regiones tridimensionales representan la actividad de la elastasa de neutrófilos en las vías respiratorias superiores y pulmón de ratones BALB/c CD69$^{+/+}$ y CD69$^{-/-}$ inmunizados con OVA y tratados con iTregs CD69$^{+/+}$ o CD69$^{-/-}$. Cuantificación de la fluorescencia emitida por la sonda activa de la elastasa de neutrófilos después del tratamiento con iTreg **(C).** Porcentaje de neutrófilos (CD11b^{+}Ly6G^{+}) analizados por FACS, tras la transferencia con pTreg **(D)**. Los datos son representativos de dos experimentos independientes (n= 4-7). Los datos se analizaron por ANOVA y post-test de Bonferroni para comparar los diferentes grupos por pares. * P <0,05, ** P <0,01, *** P <0,001.

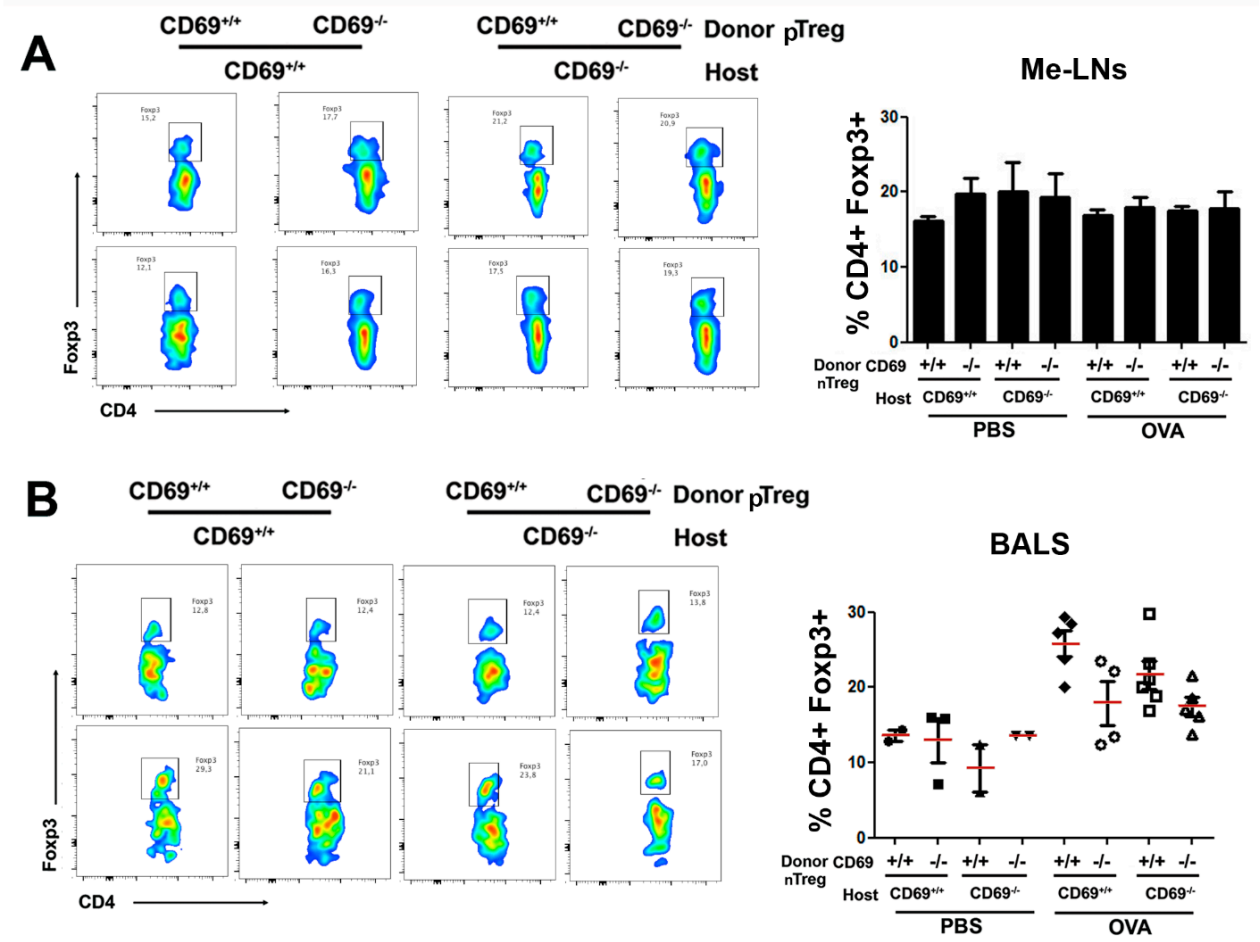

Figura 18. Análisis de la migración de las Tregs al pulmón después de los protocolos de transferencia. Se analizó las células $CD4^+$ $Foxp3^+$ de los ganglios del mediastino (Me-LN) (A) y BALS (B) después de la transferencia intravenosa de pTregs $CD4^+$ $CD25^+$ $CD69^+$ o $CD69^-$ aisladas ex vivo por FACS. Los números en los diagramas de citometría indican el porcentaje de $CD4^+$ $Foxp3^+$ en las regiones cuadradas. Los datos son representativos de dos experimentos independientes (n=5).

3. LA EXPRESIÓN DE CD69 ES NECESARIA PARA EL DESARROLLO DE LA POBLACIÓN DE TTREG

Las células T reguladoras derivadas del timo son clave para prevenir las enfermedades autoinmunes, pero los mecanismos implicados en su desarrollo aún no han sido esclarecidos del todo. En este trabajo se muestra que el receptor de lectina tipo C, CD69, controla el desarrollo de células tTreg, así como la homeostasis de las células Treg periféricas a través de un mecanismo en el que están implicados el miR-155, su promotor BIC y un gen diana de este miRNA, el supresor de la señalización por citoquinas 1 (*suppressor of cytokine signaling 1:* SOCS1).

3.1. EXPRESIÓN DE CD69 EN TTREGS DE ANIMALES CD69$^{+/+}$, CD69$^{+/-}$ Y CD69$^{-/-}$

Para determinar si CD69 es necesario para el desarrollo de tTreg en el timo, se analizó la expresión de CD69 en la membrana de tTreg procedentes de ratones CD69$^{+/+}$, CD69$^{+/-}$ y CD69$^{-/-}$ hermanos de camada y reporteros Foxp3-mRFP. De acuerdo con datos previos en ratones no reporteros C57BL/6 (Figura 14A) (Cortes et al., 2014), aproximadamente el 30% de tTreg que expresaban Foxp3-mRFP en el timo de animales WT también expresaban CD69 (Figura 19A). Este porcentaje era menor en los ratones Foxp3-mRFP CD69$^{+/-}$ no encontrándose en animales Foxp3-mRFP CD69$^{-/-}$, siendo similares las proporciones de timocitos simples positivos CD4^{+} (*simple positive*: CD4SP) y otras subpoblaciónes de timocitos en animales reporteros CD69 WT, CD69 heterocigotos y CD69 KO hermanos de camada (Figura 19A y B). Sin embargo, el número total de células y de CD4SP de los animales Foxp3-mRFP CD69$^{+/+}$ era alrededor del 30% superior a los otros grupos (Figura 19C y D). Estos resultados eran consistentes con datos previos que indicaban que la sobreexpresión de CD69 en el timo aumenta los niveles de timocitos SP, ya que CD69 está relacionado con el control de la migración de células a la periferia (Baeyens et al., 2015; Lamana et al., 2011). Además, los ratones adultos Foxp3-mRFP CD69$^{-/-}$ y CD69$^{+/-}$ mostraron una reducción marcada en la proporción y número de células tTreg en comparación con ratones reportero CD69$^{+/+}$ (FIgura 19E y F). Estos datos indicaban que CD69 podría desempeñar un papel importante en la regulación del desarrollo de tTreg, que podría estar enmascarado por los efectos de CD69 en la migración de los timocitos a la periferia. En paralelo, se encontró que ratones reportero adultos CD69$^{-/-}$ también presentaban una disminución en la proporción de Treg periféricas (pTreg) en comparación con los hermanos de camada CD69$^{+/+}$ (Figura 20). Sorprendentemente, estos datos no eran consistentes con los anteriormente obtenidos con ratones no reporteros (Figura 14D) (Cortes et al., 2014). Para aclarar las diferencias observadas entre el análisis por tinción de Foxp3 y los animales reporteros, se realizaron tinciones de Foxp3 en el timo y bazos de ratones Foxp3-mRFP (Figura 21A). Los datos obtenidos

ciertamente indicaban resultados dispares entre los dos métodos. La detección de Tregs por tinción exógena con anticuerpos anti-Foxp3 (Figura B y C) difería de la expresión endógena de Foxp3-mRFP en función del tejido, sobredimensionando ligeramente estas poblaciones (Figura 21D), lo que indicaba que el uso de anticuerpos anti-Foxp3 no es tan preciso como la expression endógena de los genes reportero. En resumen, CD69 podría estar jugando un papel importante también en el desarrollo de las células tTreg y en la homeostasis de las pTreg.

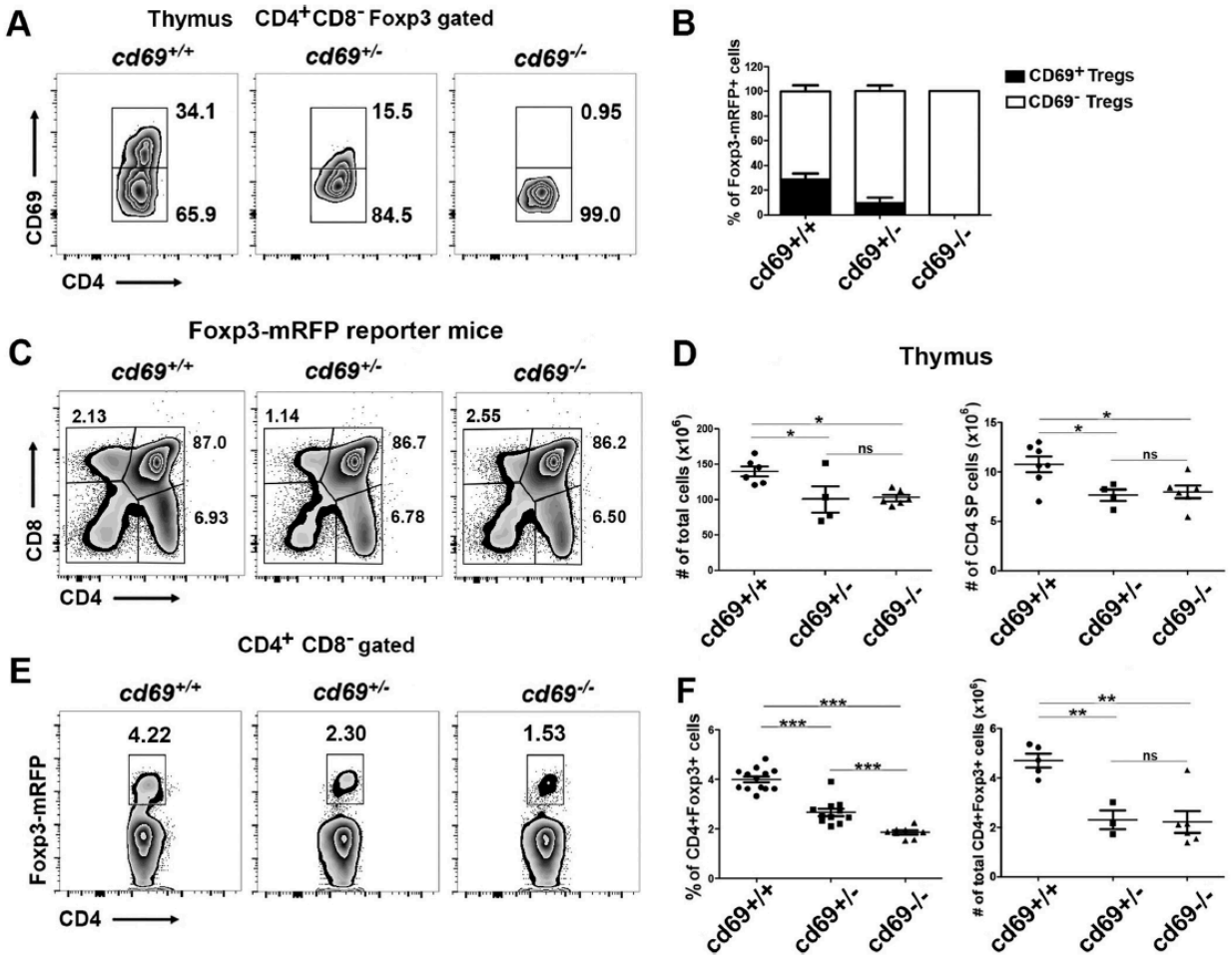

Figura 19. Se requiere expresión de CD69 para la diferenciación de células Treg derivadas de timo de ratones adultos. **(A)** Los gráficos de densidad de citometría de flujo muestran la expresión de CD69 en timocitos $CD4^+$ $CD8^-$ $Foxp3^+$ de ratones reporteros Foxp3-mRFP/$cd69^{+/+}$, Foxp3-mRFP/$CD69^{+/-}$ y Foxp3-mRFP/$CD69^{-/-}$ de 8-12 semanas de edad. Los números indican el porcentaje (%) de células en el recuadro. **(B)** El gráfico de barras muestra el porcentaje (± S.D.) de tTregs $CD69^+$ (negro) y $CD69^-$ (blanco) en el timo**. (C)** Análisis de los timocitos. Se muestran los porcentajes de los correspondientes precursors de células T derivadas de timo. **(D)** Número total de células del timo (izquierda) y número total de células CD4 SP (derecha) en reporteros hermanos de camada**. (E)** Análisis de la

expresión endógena de Foxp3 en tTreg en el timo de reporteros hermanos de camada. **(F)** Porcentajes (izquierda) y número de células totales (derecha) de $CD4^+$ $CD8^-$ $Foxp3^+$ tTreg. Datos correspondientes a 7 camadas de entre 3 y 12 crías cada una. Se analizó un total de 16 animales Foxp3-mRFP/$CD69^{+/+}$, 11 Foxp3-mRFP/$CD69^{+/-}$ y 12 ratones Foxp3-mRFP/$CD69^{-/-}$. Las barras de error muestran S.D. Los datos fueron analizados mediante ANOVA seguido de la prueba de Bonferroni para comparar los diferentes grupos por parejas: * P <0,05, ** P<0,01 y *** P<0,001.

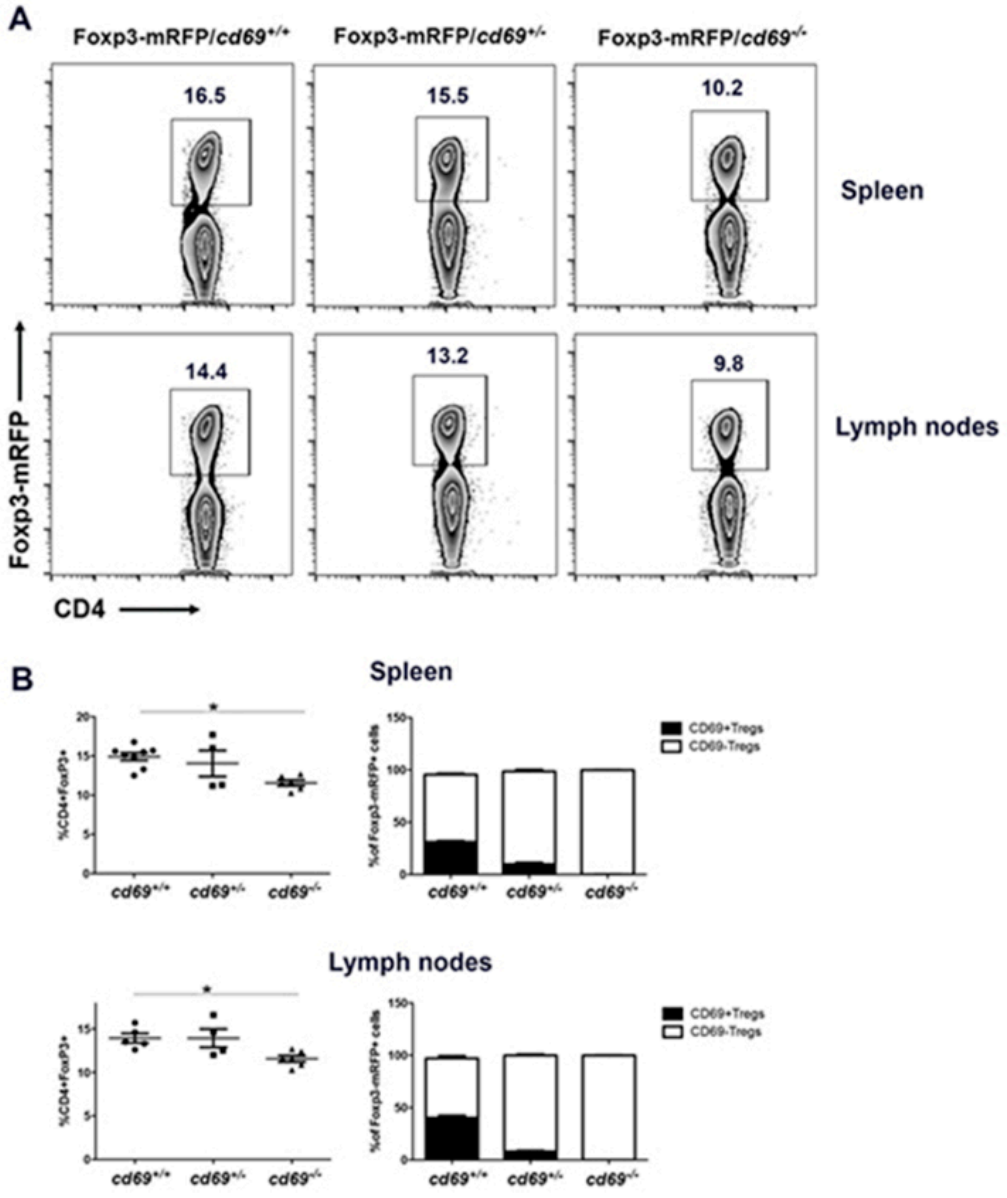

Figura 20. CD69 se require para la homeostasis de las pTregs en los órganos linfoides secundarios. (**A**) Análisis por citometría de flujo de las células $CD4^+$ $Foxp3^+$ en bazos (*spleen*) y ganglios periféricos (*lymph nodes*) de animales *cd69*$^{+/+}$, *cd69*$^{+/-}$ y *cd69*$^{-/-}$ reporteros Foxp3-mRFP y hermanos de camada de 8 a 12 semanas de edad. (**B**) Porcentajes de $CD4^+$ $Foxp3^+$ en los diferentes órganos. Los histogramas de barras representan el porcentaje de células $CD69^+$ (negro) y $CD69^-$ (blanco) dentro de las pTregs de bazos y ganglios. Los datos fueron analizados mediante ANOVA seguido de la prueba de Bonferroni para comparar los diferentes grupos: * P <0,05.

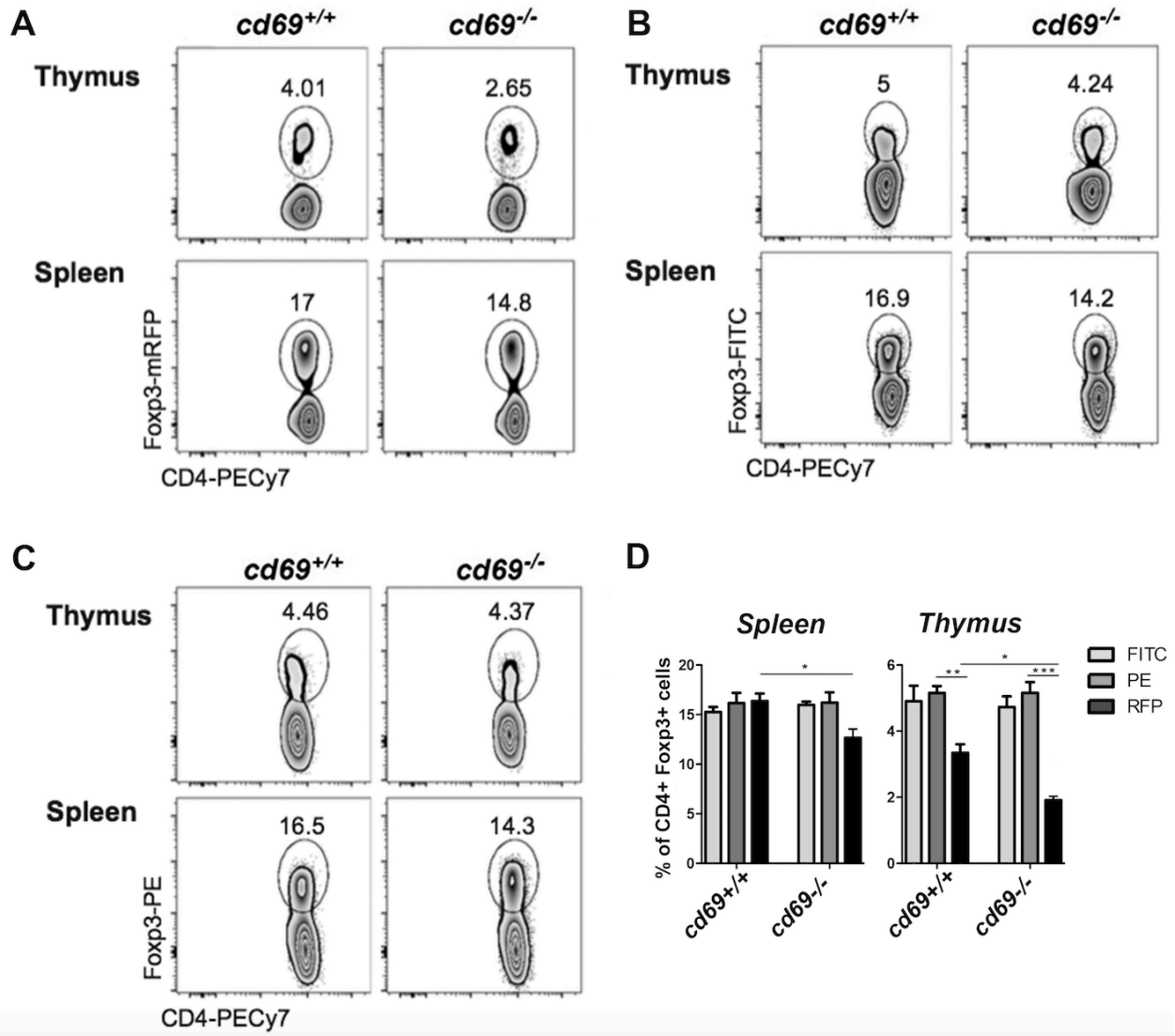

Figura 21. El uso de anticuerpos anti-Foxp3 no es equivalente a los niveles endógenos del factor de transcripción. Realizamos un marcaje de anti-Foxp3 con dos fluoróforos diferentes: PE y FITC (*fluorescein and phycoerythrin)* en células de timo y bazo de animales reporteros Foxp3-mRFP/*cd69*$^{+/+}$ y Foxp3-mRFP/*cd69*$^{-/-}$. **(A)** Análisis de los niveles endógenos de Foxp3^{+} en células CD4^{+} de animales transgénicos Foxp3-mRFP. Análisis de la expresión de Foxp3 tras tinción con anticuerpos anti-Foxp3 conjugados con PE (**B**) o FITC (**C**). EL porcentaje de células Foxp3+ se analizó en diferentes canales de emisión tras la adquisición de los datos de citometría de flujo (LRS Fortessa BD), después de su excitación con las diferentes longitudes de onda. (**D**) Los histogramas muestran la comparación entre las distintas técnicas de detección. Los datos fueron analizados mediante ANOVA seguido de la prueba de Bonferroni para comparar los diferentes grupos: * P <0,05, ** P<0,01 y *** P<0,001.

3.2. LA DELECIÓN DE CD69 INHIBE LA DIFERENCIACIÓN DE TTREG EN CULTIVOS DE LÓBULOS DE TIMO FETAL

Para determinar si la deficiencia en CD69 conduce a un desarrollo disminuido de tTreg, independientemente del estado de maduración tímica o de la migración de timocitos a la periferia mediado por $S1P_1$ y cuya expresión está asociada a la falta de CD69, se realizaron cultivos de lóbulos de timo fetal (*fetal thymus organ culture*: FTOC). Para ello utilizamos timos de embriones de ratón de entre 15 y 17 días de edad (E15-E17), y se analizaron los timocitos CD4SP totales y la diferenciación de tTreg durante 5 días de cultivo, comparando las diferencias entre lóbulos de timo de embriones de estadio E15-17 $CD69^{+/+}$ y $CD69^{-/-}$. Los FTOC de animales $CD69^{-/-}$ mostraron una marcada reducción en el porcentaje y en el valor absoluto de número de células tTreg $Foxp3^+$, con cambios insignificantes en el número total de células (Figura 22A y B). Estos datos indicaban que CD69 es requerido durante la diferenciación de tTreg en las primeras etapas del desarrollo. Para confirmar estos resultados, FTOCs de E15 fueron tratados durante 14 días con el anticuerpo anti-CD69 (2.2), que regula negativamente la expresión de CD69 en la membrana así como su señalización en el citoplasma. De acuerdo con los datos anteriores, los FTOCs procedentes de animales $CD69^{+/+}$ tratados con el anticuerpo 2.2 muestran proporciones notablemente menores de células tTreg $Foxp3^+$ que los FTOCs tratados con el anticuerpo control de isotipo (2.8), siendo el numero total de células de los FTOCs similar con los dos tratamientos (Figura 22C y D). Estos hallazgos son consistentes con trabajos previos que indicaban que los timocitos inmaduros $CD69^+$ son los precursores de lasTreg intratímicas en humanos y ratones (Martin-Gayo et al., 2010).

3.3 LA GENERACIÓN DE CÉLULAS TTREG Y PTREG A PARTIR DE PRECURSORES HEMATOPOIETICOS $CD69^{-/-}$ ESTÁ INHIBIDA

Para explorar en más detalle el papel de CD69 en los precursores hematopoiéticos y la diferenciación de las tTreg realizamos experimentos de reconstitución de médula ósea. Transferimos una mezcla de iguales proporciones de células madre hematopoiéticas de la médula ósea de animales Foxp3-mRFP/$CD69^{+/+}$/$CD45.1^+$ y Foxp3-mRFP/$CD69^{-/-}$/$CD45.2^+$ a animales receptores $Rag2^{-/-}$ $\gamma c^{-/-}$ tras irradiación sub-letal. Después de la reconstitución, se analizaron los porcentajes y números de células Treg $CD4^+$ $Foxp3^+$ $CD45.1^+$ derivados de precursores $CD69^+$ y $CD45.2^+$ de precursores $CD69^-$ (Figura 23A). El porcentaje de células Treg originadas de precursores $CD69^{-/-}$ era marcadamente más bajo en el timo, siendo iguales los números de células CD4SP en el timo (Figura 23B y C). Estos datos junto con los experimentos de FTOC confirman que CD69 tiene un importante papel para la correcta diferenciación de las células tTreg a partir de los precursores intratímicos.

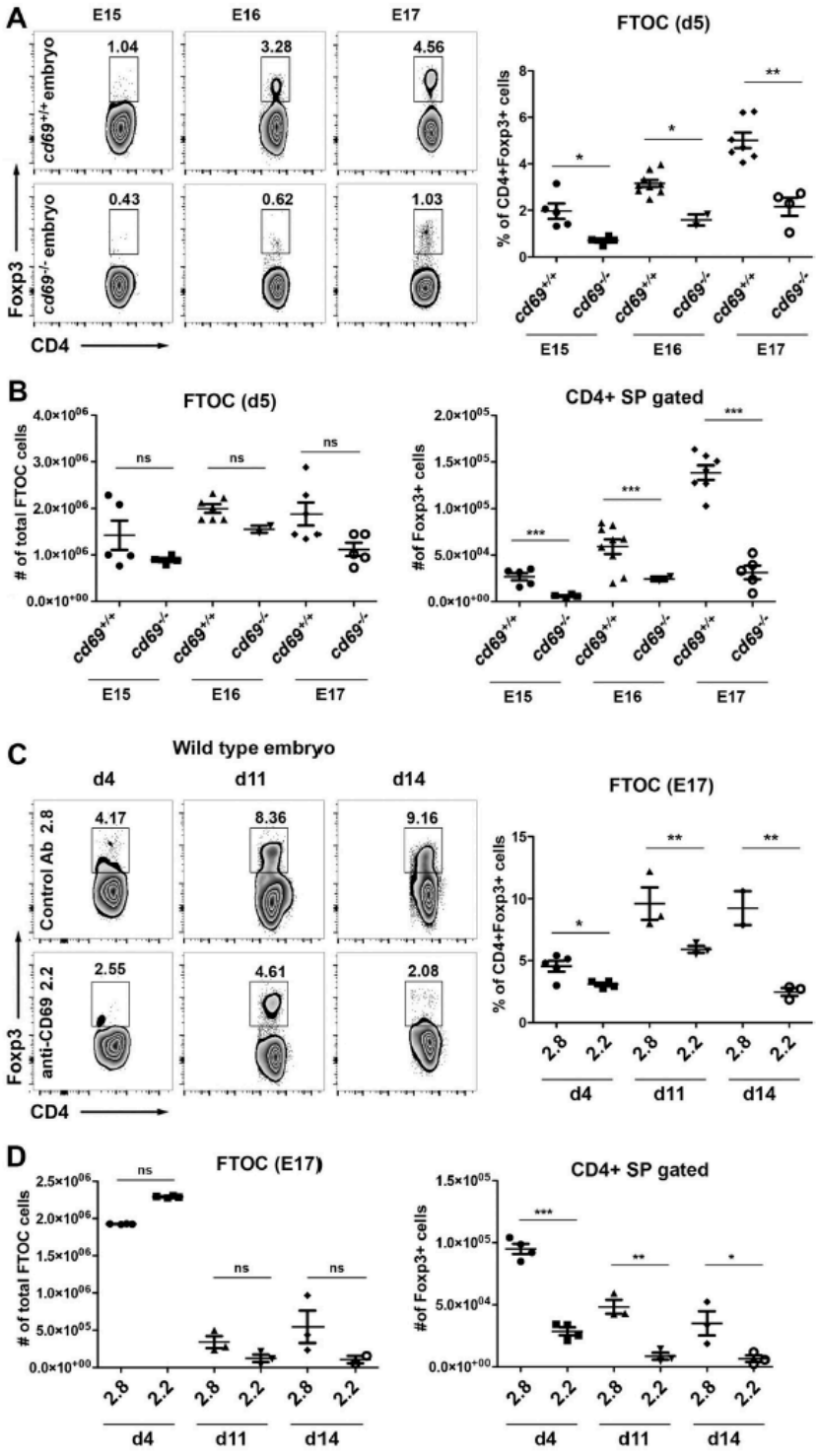

Figura 22. La expresión de CD69 es clave en la diferenciación embrionaria de tTregs. (A) Análisis por FACS representativos de FTOC de 5 días pertenecientes a embriones CD69$^{+/+}$ y Cd69$^{-/-}$ en fondo genético C57BL/6. Se analizaron los lóbulos tímicos de embriones de estadio 15 - 17 y los porcentajes de tTreg que desarrollaron. (**B**) Número total de células de los lóbulos de timo fetal y de CD4^{+} Foxp3^{+}. **(C)** FTOCs de embriones de 17 días (E17) de animales CD69$^{+/+}$, se mantuvieron 4-14 días en cultivo en presencia de anticuerpos monoclonales anti-CD69 (2.2) o

el anticuerpo control de isotipo (2.8). Las gráficas de densidad muestran el porcentaje de tTreg en los días 4, 11 y 14 de cultivo **(D)** Número total de células de los lóbulos de timo fetal y de $CD4^+$ $Foxp3^+$ en cada condición. Se analizaron un total de 31 y 36 embriones de cinco hembras $CD69^{+/+}$ y cuatro hembras $CD69^{-/-}$, respectivamente. Los 2 lóbulos de cada timo fetal se analizaron por separado. Las barras de error muestran la S.D. y los valores se calcularon en relación con los datos de los lóbulos control $CD69^{+/+}$ de cuatro ensayos FTOC independientes. * P <0,05, ** P <0,01, *** P <0,001 (prueba t de Student).

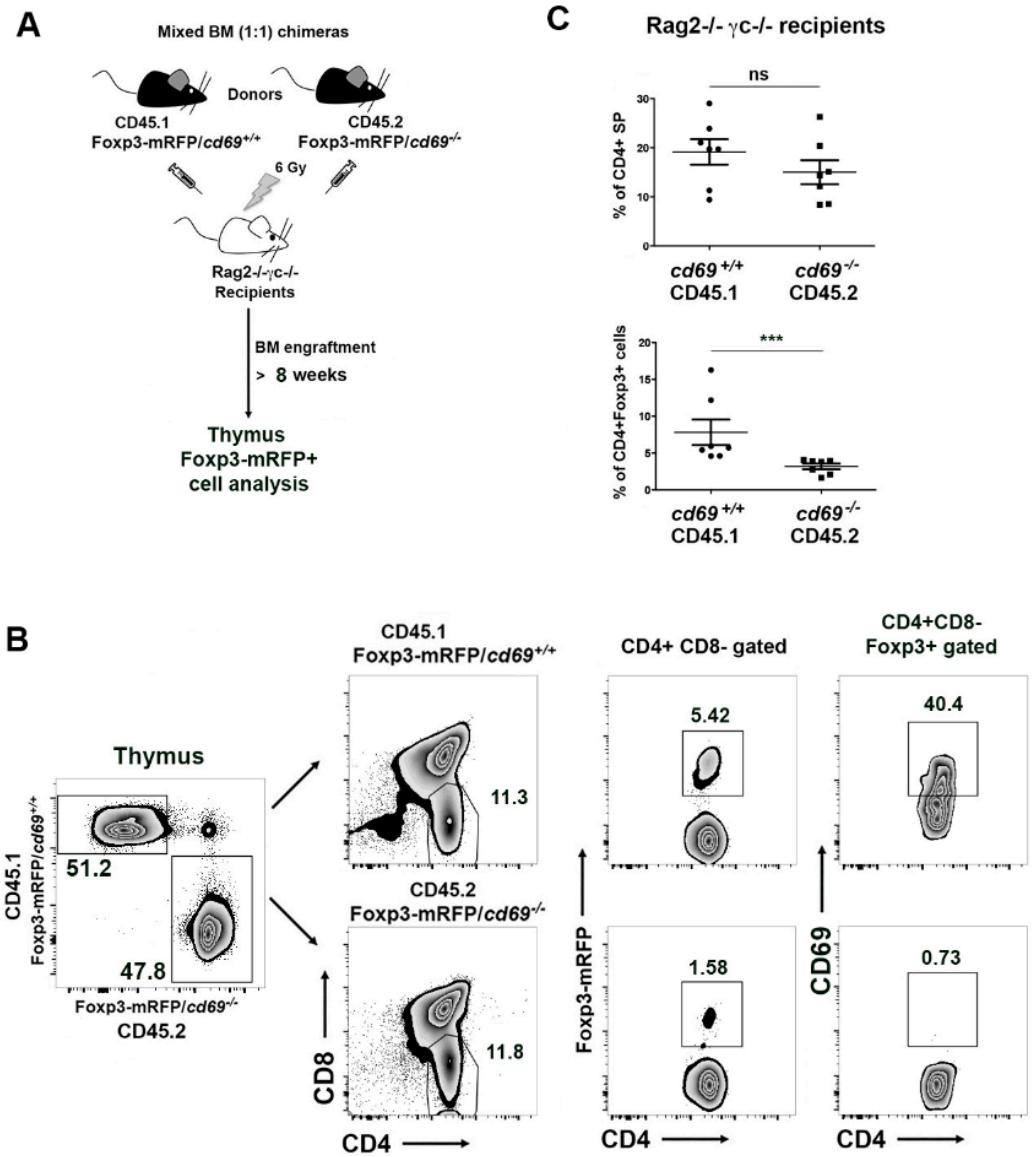

Figura 23: Los precursores hematopoyéticos $CD69^+$ tienen mayor potencial para el desarrollo de tTregs. **(A)** Esquema de la generación de quimeras; los receptores $Rag2^{-/-}$ $\gamma c^{-/-}$ irradiados fueron trasplantados con una mezcla de precursores de médula ósea CD45.1/Foxp3-mRFP/$CD69^{+/+}$ o CD45.2/Foxp3-mRFP/$CD69^{-/-}$ en una proporción 1:1. **(B)** Los diagramas representativos muestran la contribución de los diferentes precursores de médula ósea al

desarrollo de células tTreg y expresión de CD69 en tTreg determinado por FACS. **(C)** Porcentajes de células CD4SP y $CD4^+$ $CD8^-$ $Foxp3^+$ tTreg pertenecientes a los donantes CD45.1 o CD45.2 en el timo. Todos los datos son representativos de, al menos, 3 experimentos independientes con al menos 3 ratones receptores por grupo. Las barras de error muestran S.D. * P <0,05, ** P <0,01, *** P <0,001 (prueba t de Student).

3.4. La deficiencia en CD69 inhibe la señalización de STAT5 y la diferenciación de tTregs dependiente de la vía BIC/miR-155

Nuestro grupo ha demostrado anteriormente que CD69 activa la vía de señalización de Stat5 (Martín et al., 2010). Por ello, para investigar el mecanismo molecular que interviene en el desarrollo de tTreg mediado por CD69, se examinó la vía de señalización del transductor de señales y activador de la transcripción 5 (*signal transducer and activator of transcription 5*: Stat5) que estimula el promotor de Foxp3, induciendo el desarrollo de tTreg. Las poblaciones de tTregs, Foxp3-$mRFP^+$/$CD69^+$ y la Foxp3-$mRFP^+$/$CD69^-$ fueron separadas mediante *fluorescence-activated cell sorting* (FACS Aria, BD) de timos de animales WT. El análisis de la activación de Stat5 (fosforilación de Stat5 en la Tyr694) por citometría (Figura 24A) y western blot (WB) (Figura 24B), mostró una disminución de la fosforilación de STAT5 en las tTreg $CD69^-$ en condiciones basales, lo que indicaba que la expresión CD69 mantiene activa la vía de STAT5 en las tTreg en el timo. El análisis de las dos poblaciones de pTreg en el bazo confirmó estos resultados, por lo que también había una menor fosforilación de Stat5 en las pTreg $CD69^-$ de órganos linfoides secundarios (Figura 25A). Sin embargo, no encontramos variaciones en la expresión del factor de trascripción Foxp3 en tTreg (Figura 24C) o pTreg (Figura 25B) $CD69^+$ o $CD69^-$, lo que indicaba que la fosforilación de Stat5 inducida por CD69 podría actuar independiente de Foxp3 en las Treg. Para profundizar más en esta observación analizamos los niveles de expresión de miR-155 y su promotor BIC en ambas poblaciones celulares. Está descrito que éste miRNA interviene en los procesos de diferenciación de células Treg a través de la regulación de la expresión de su gen diana SOCS1 (Yao et al., 2012). Comprobamos que los niveles de miR-155 y su promotor BIC estaban significativamente disminuidos en las poblaciónes de tTreg (Figura Figura 24D) y pTreg (Figura 25B) $CD69^-$, mientras que su diana SOCS1, estaba aumentada tanto a nivel transcripcional (Figuras 24E y 25B) como de proteína por WB (Figuras 24F y 25B) en las Treg $CD69^-$.

Para confirmar estos resultados en células deficientes en CD69, analizamos la ruta de Stat5 en las poblaciones de tTreg de ratones de $CD69^{+/+}$, $CD69^{+/-}$ y $CD69^{-/-}$ Foxp3-mRFP. La fosforilación de Stat5 estaba parcialmente inhibida en las tTreg $CD69^{+/-}$ en comparación con las $CD69^{-/-}$, cuya vía de activación de Stat5 estaba casi completamente inhibida (Figura 25A). De acuerdo a lo anterior, las tTreg $CD69^{+/-}$ y $CD69^{-/-}$ presentaban niveles muy bajos de miR-155 en comparación con las tTregs $CD69^{+/+}$ (Figura 25B). Por consiguiente, el gen *socs1* estaba moderada y fuertemente expresado en tTreg $CD69^{+/-}$ y $CD69^{-/-}$,

respectivamente (Figura 25B). Nuestros datos sugieren que la pérdida de al menos un alelo de CD69 en las tTregs modifica drásticamente la expresión del receptor en la membrane (Figura 19A y B), de forma que impide la activación completa de la vía de Stat5, la transcripción de miR-155, la inhibición de SOCS-1 y la adecuada diferenciación de tTreg.

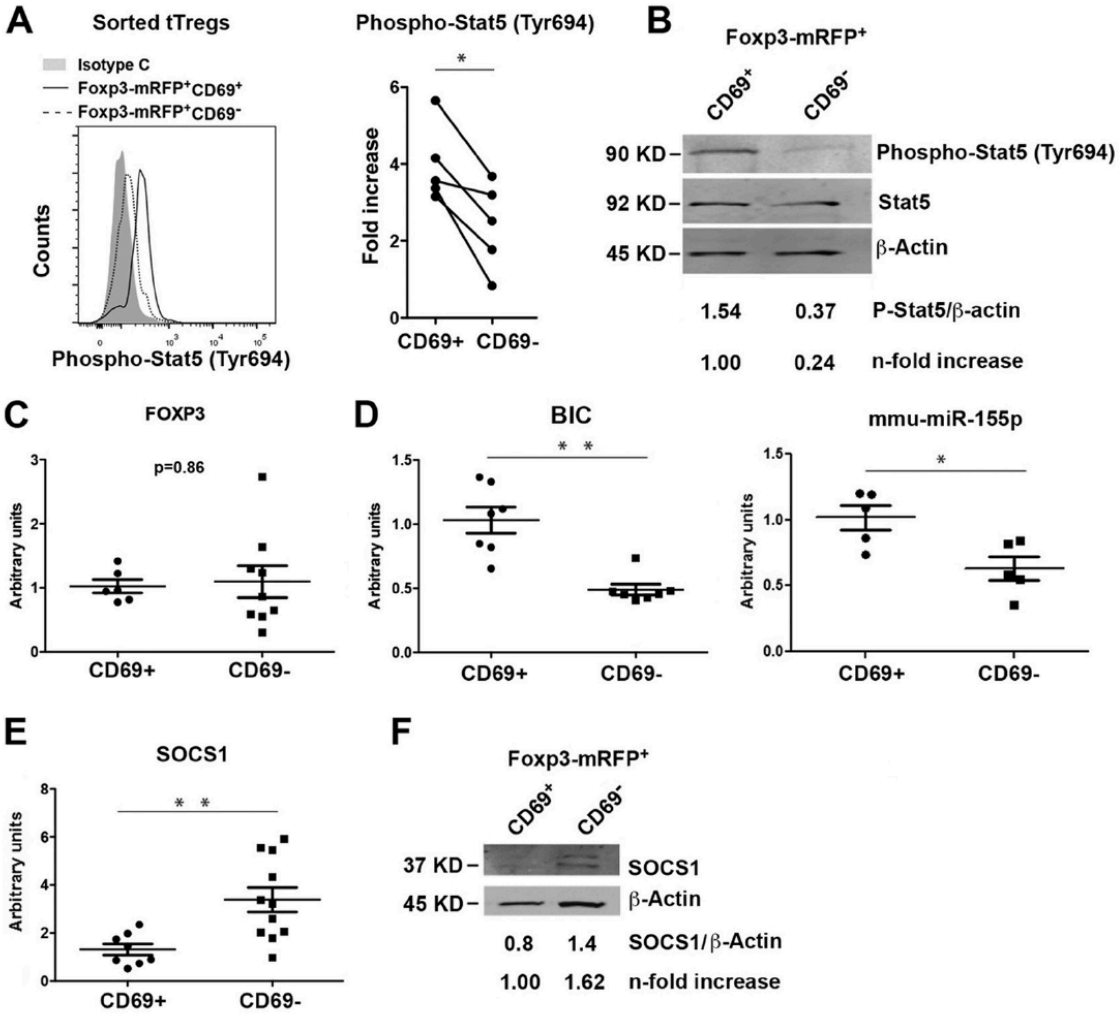

Figura 24. Activación de Stat5 y expresión de miR-155 y su proteína diana SOCS1 en células Treg CD69$^+$ y CD69$^-$. **(A)** Histograma representativo de los niveles de fosforilación de la Tyr694 de Stat5 analizados por FACS en células tTreg CD69 $^+$ o CD69$^-$. A la derecha, los niveles de fosforilación de Stat5 represantodos como la diferencia en la intensidad de la fluorescencia entre las células tratadas con el anticuerpo de Phospho-Stat 5 y las células tratadas con el anticuerpo control de isotipo. Las líneas enlazan los valores de Stat5 fosforilado en tTreg CD69$^+$ y CD69$^-$ aisladas del mismo ratón. **(B)** WB representantivo de la fosforilación de Stat5 en las mismas poblaciones de tTreg que en A. La cuantificación de los niveles de fosforilación se normalizaron por los niveles de proteína total Stat5 y el control de carga β-actina. **(C)** Analisis por q-PCR de la expresión relativa de Foxp3, **(D)** el promotor BIC, mmu-miR-155 y **(E)** SOCS1 en tTreg CD69$^+$ y CD69$^-$. La expresión en unidades arbitrarias (*Arbitrary Units*) se normalizó

con los niveles de éstas moléculas en tTreg CD69^{+}. **(F)** WB representantivo de la expresión de la proteína SOCS1 en células tTreg Foxp3mRFP^{+}CD69^{+} y CD69^{+} sorteadas. Los niveles de proteína de SOCS1 se normalizaron con el control de carga de β-actina (*n-fold increase*). Todos los experimentos se realizaron con células procedentes de al menos 4 sortings independientes de células de timo de animales reporteros CD69 WT. Los datos fueron analizados por la prueba t de Student (A - E) excepto para los análisis de WB, para los que se muestran geles representativos. Las barras de error muestran S.D. ** P <0,01, *** P <0,001.

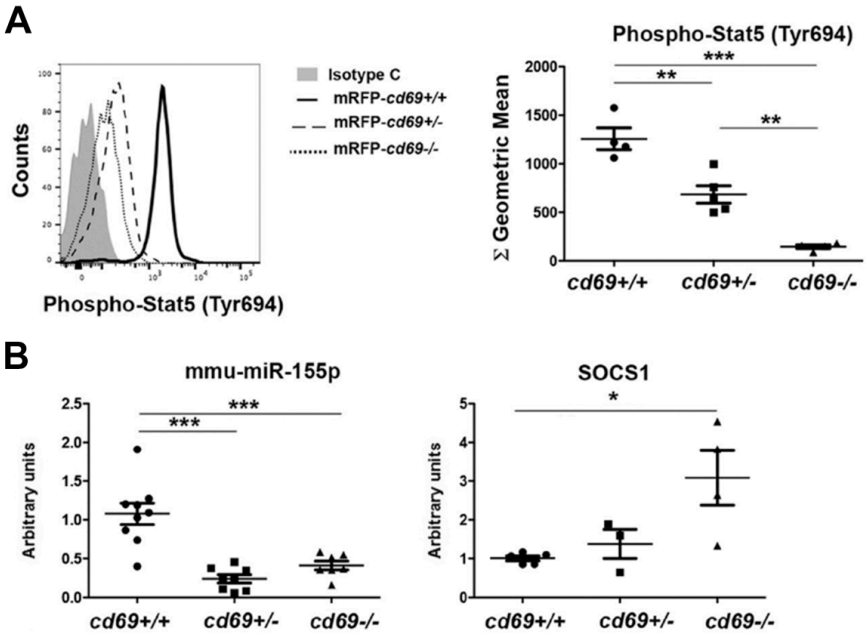

Figura 25: Niveles de fosforilación de Stat5 y expresión de miR-155 y SOCS1 en células tTreg procedentes de animales reportero Foxp3-RFP CD69$^{+/+}$, CD69$^{+/-}$ y CD69$^{-/-}$. (A) Histograma representativo del análisis por citometría de la fosforilación de STAT5 en tTreg de ratones Foxp3-RFP CD69$^{+/+}$, CD69$^{+/-}$ y CD69$^{-/-}$. Derecha, cuantificación de los niveles de fosforilación de Stat5 mostrados como media geométrica de la intensidad de fluorescencia. **(B)** Niveles transcripcionales del mmu-miR-155 y SOCS1 analizados por qPCR en células tTreg de ratones reportero Foxp3-RFP CD69$^{+/+}$, CD69$^{+/-}$ y CD69$^{-/-}$. Todos los datos están derivados de al menos 5 sortings independientes con 3 animales por separación. Las barras de error muestran S.D. Los datos fueron analizados mediante ANOVA seguido de la prueba de Bonferroni para comparar los diferentes grupos por parejas: * P <0,05, ** P<0,01 y *** P<0,001.

3.5. Los animales miR-155$^{-/-}$ presentan deficiencias en la generación de células Treg CD69^{+}

Ya que la expresión de CD69 regula la expresión de miR-155 en las tTregs, quisimos analizar si las tTregs deficientes en miR-155, que tienen graves deficiencias en tTregs y pTregs (Kohlhaas et al., 2009; Lu et al., 2009), desarrollaban a su vez Tregs CD69^{+}. Analizamos los niveles de células tTreg y pTreg de ratones miR-155$^{-/-}$ y, de acuerdo con el trabajo anterior, los ratones miR-155$^{-/-}$ mostraban un número muy reducido de tTreg y pTreg (Figuras 26A y C), así como una importante reducción en el desarrollo de Treg CD69^{+}, tanto en timo como en bazo (Figura 26A y C). En paralelo, analizamos la expresión del gen *cd69*

en los timocitos de los animales miR-155-/- encontrando, sorprendentemente, que la expresión del gen *cd69* estaba inhibida casi por completo en el timo de ratones miR-155$^{-/-}$, lo que sugería fuertemente que las dos moléculas CD69 y miR-155 podrían tener vías de regulación de la expresión comunes (Figura 26B). Por lo tanto, La sobre-expresión de SOCS-1 que regula negativamente la señalización de la vía de Stat5, podría estar inhibiendo la diferenciación de tTreg en ratones CD69$^{-/-}$ de manera similares a lo que sucede en los animales miR-155$^{-/-}$.

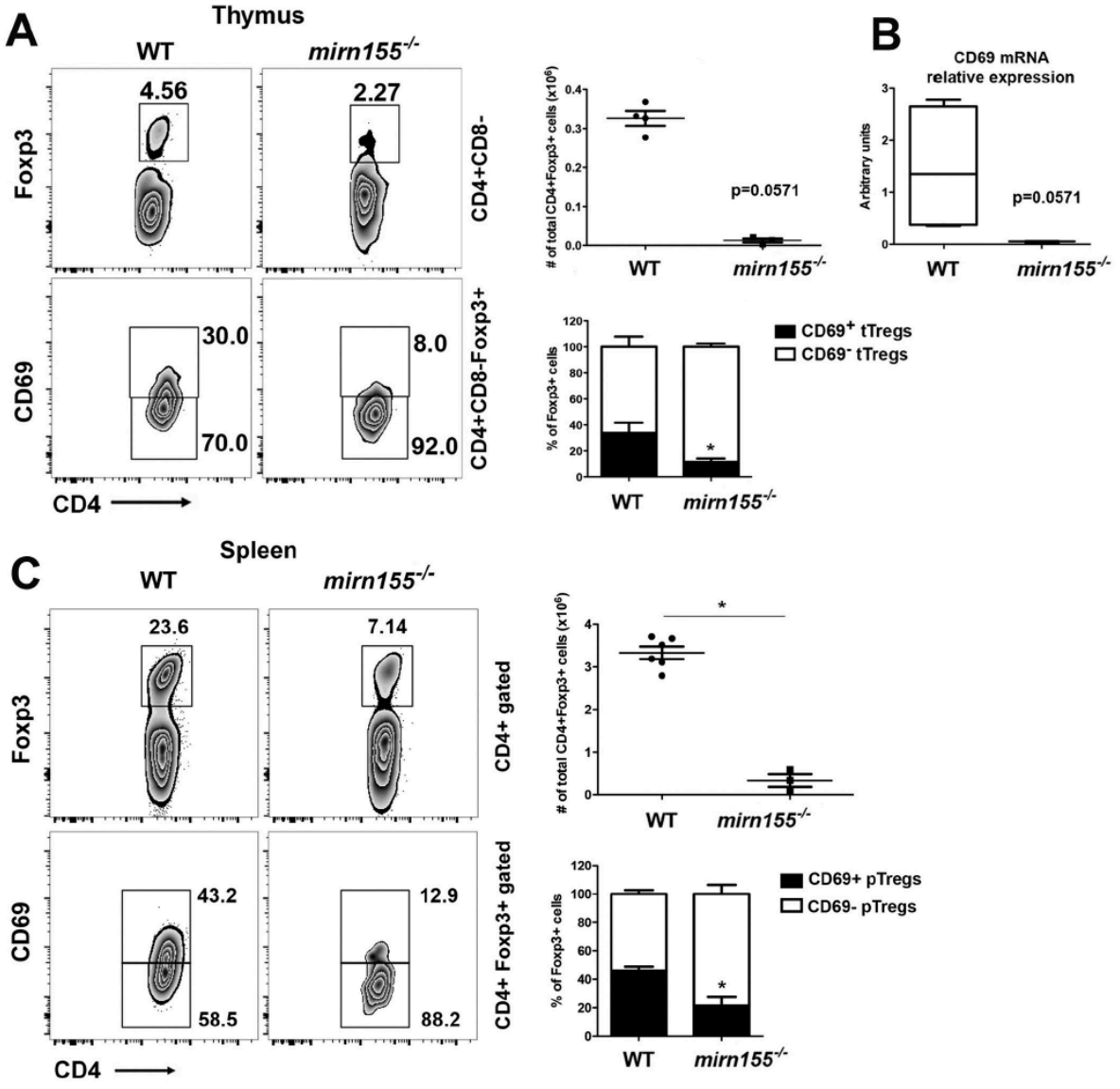

Figura 26: El desarrollo de Tregs CD69^{+} está inhibido en el timo y el bazo de ratones miR-155$^{-/-}$. Los gráficos de densidad y los histogramas muestran el porcentaje de células tTreg CD4^{+} CD8^{-} Foxp3^{+} y la expresión de CD69 en estas células **(A)** o en linfocitos de bazo CD4^{+} CD8^{-} Foxp3^{+} **(C),** de ratones WT o miR-155$^{-/-}$. Los números indican el porcentaje de células incluidas en los recuadros. **(B)** Análisis por qPCR de la expresión de *cd69* en unidades

arbitrarias en los timocitos de ratones WT o miR155$^{-/-}$. Se muestran los resultados de 5 ratones WT y 3 miR 155$^{-/-}$. Los datos se analizaron mediante t-Test, las barras de error muestran S.D. * P <0,05 (prueba t de Student).

3.6. LAS VÍAS DE IL-2Rγ Y LA DE CD69 SON IGUALMENTE NECESARIAS PARA EL DESARROLLO DE CÉLULAS TREG CD25^{+} INDUCIDAS *IN VITRO*

Para continuar con el estudio del papel no redundante de CD69 en el desarrollo de Treg inducidas *in vitro* (iTreg), se analizaron los niveles de Foxp3 en ausencia de la señalización mediada por la vía Jak3-Stat5. Cultivamos células T CD4^{+} vírgenes en condiciones de diferenciación de Treg con TGFβ e IL-2, en presencia de células presentadoras de antígeno. El uso de un inhibidor químico de Jak3 disminuyó la fosforilación Stat5 de las células iTreg CD69$^{+/+}$ a los niveles de las células iTreg CD69$^{-/-}$ (Figura 27A), sin embargo, el porcentaje de células Foxp3-RFP^{+} era comparable en ambos genotipos, incluso más alta en Treg CD69$^{-/-}$ independientemente de la inhibición de Jak3-Stat5 (Figura 27B), lo que indicaba que la vía de señalización Jak3-Stat5 no es necesaria para expresión de Foxp3 por las iTreg, corroborando los datos anteriores en tTreg (Figura 24C). Se ha descrito que la expresión de Foxp3 es dependiente de la cadena γ del receptor de la IL-2 (IL-2Rγc), por lo que los ratones IL-2Rγ$^{-/-}$ no tienen células Foxp3^{+} en el timo o el bazo (Fontenot et al., 2005). Sin embargo, la expresión de Treg CD25^{+} es detectable en el timo y el bazo de los ratones IL-2Rγ$^{-/-}$ (Fontenot et al., 2005). Nuestro objetivo fue abordar el papel de CD69 en el desarrollo de iTreg CD25^{+} en ausencia de las vías señalización IL-2Rγ/Foxp3. Para ello, generamos ratones doble knock-out para IL-2Rγ$^{-/-}$ y CD69$^{-/-}$. Analizamos los niveles de células iTreg CD25^{+} procedentes de ratones IL-2Rγ$^{-/-}$ o ratones IL-2Rγ$^{-/-}$/CD69$^{-/-}$ inducidas con TGF-β e IL-2 en presencia de inhibidores de Jak3, comprobando que disminuía la fosforilación de Stat5 en las células iTreg IL2Rγ$^{-/-}$ a los niveles de las IL2Rγ$^{-/-}$/CD69$^{-/-}$ (Figura 27C). Además, la diferenciación de las células iTreg CD25^{+} estaba completamente inhibida en iTreg procedentes de IL-2Rγ$^{-/-}$/CD69$^{-/-}$ e iTreg IL-2Rγ$^{-/-}$ tratadas con inhibidores de Jak3 (Figura 27D). Estos datos indican que, en ausencia de la vía de señalización IL-2Rγ/Foxp3, la activación de Jak3/Stat5 por parte de CD69 es fundamental para el desarrollo de células iTreg CD25^{+}. Se ha propuesto que el miR-155 podría regular diferentes funciones según el tipo celular y el contexto biológico, y la represión SOCS1 mediada por miR-155 regularía la diferenciación de las células Treg. (Lu et al., 2015). Se analizó la expresión de miR-155, SOCS1, T-bet y Eomes con el fin de investigar si otros genes diana de miR-155 estan afectados en iTreg diferenciadas en ausencia de señalización por Jak3-STAT5 activada a través de CD69. Se observó disminución de la expresión de miR-155 en células iTreg CD69$^{-/-}$ en comparación con células iTreg CD69$^{+/+}$ (Figura 28A), como ocurre con las tTreg procedentes de timos de animales CD69$^{-/-}$ (Figura 24D). Sin embargo, la inhibición de Jak3 no

contribuía a la inhibición de miR-155, sugiriendo que otras vías de señalización podrían contribuir a la regulación miR-155 en iTreg. Además, la expresión de SOCS1 estaba fuertemente inducida en las células iTreg CD69$^{-/-}$ en comparación con iTreg cd69 $^{+/+}$, pero no otros genes diana de miR-155 como T-bet o Eomes. Curiosamente, Jak3 inhibe la expresión de SOCS1, T-bet y Eomes en la ausencia de CD69 (Figura 28B y C), apoyando la hipótesis de que otros mecanismos dependientes CD69 podrían estar involucrados en la regulación de estos genes diana. En conjunto, estos datos sugerían que CD69 controla la expresión de SOCS1 y la diferenciación de Treg a través de la regulación la expresión de miR-155, sin descartar que otras moléculas puedan estar involucradas en el proceso.

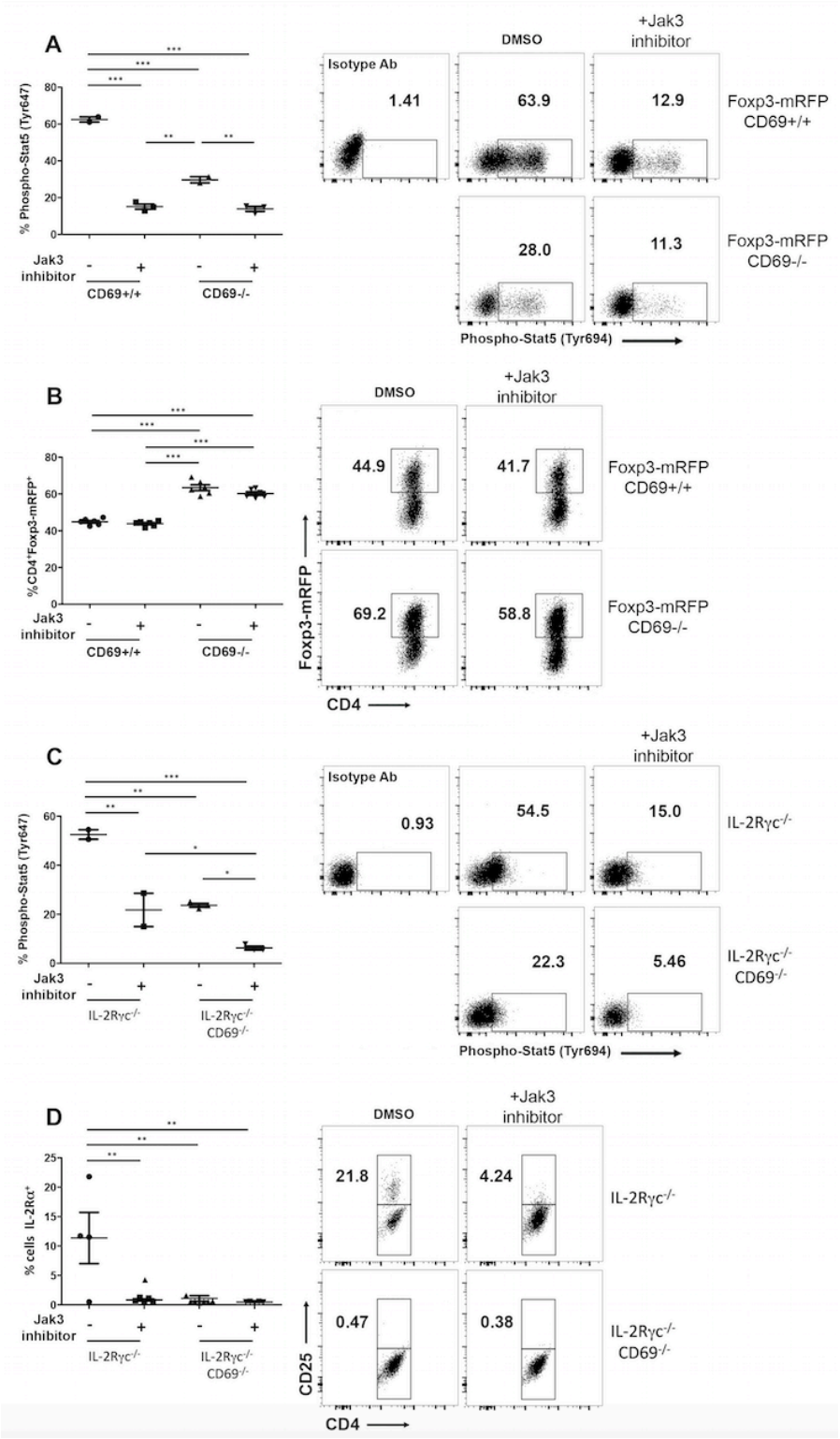

Figura 27. La expresión de CD69 rescata la diferenciación de iTreg en ausencia de la vía de IL-2Rγc/Foxp3. **(A)** Se cultivaron células T $CD4^{+}$ naïve de ratones Foxp3-mRFP $CD69^{+/+}$ o $CD69^{-/-}$ hermanos de camada en condiciones de diferenciación de células Treg durante 72 horas las últimos 9 horas se trataron con un inhibidor químico de Jak3 o con una concentración igual de DMSO Se muestran los porcentajes de células Phospho-Stat5 $^{+}$ y los niveles de

fosforilación Stat5 analizados por FACS y comparados con el anticuerpo control de isotipo. **(B)** Cuantificación de células Foxp3-mRFP^{+} tratadas cómo en A. (C) células T CD4^{+} vírgenes procedentes de ratones IL2Rγ$^{-/-}$CD69$^{+/+}$ e IL2Rγ$^{-/-}$/CD69$^{-/-}$ se cultivaron como en A y los porcentajes de células Phospho-Stat5^{+} y los niveles de fosforilación Stat5 fueron analizados por FACS. (D) Cuantificación de células Treg CD25^{+} mediante FACS. Los datos son de dos experimentos independientes (n=3) de cada genotipo. Las barras de error muestran S.D. Los datos fueron evaluados por ANOVA seguido de Bonferroni para comparar los diferentes grupos por parejas: * P <0,05, ** P <0,01, *** P <0,001.

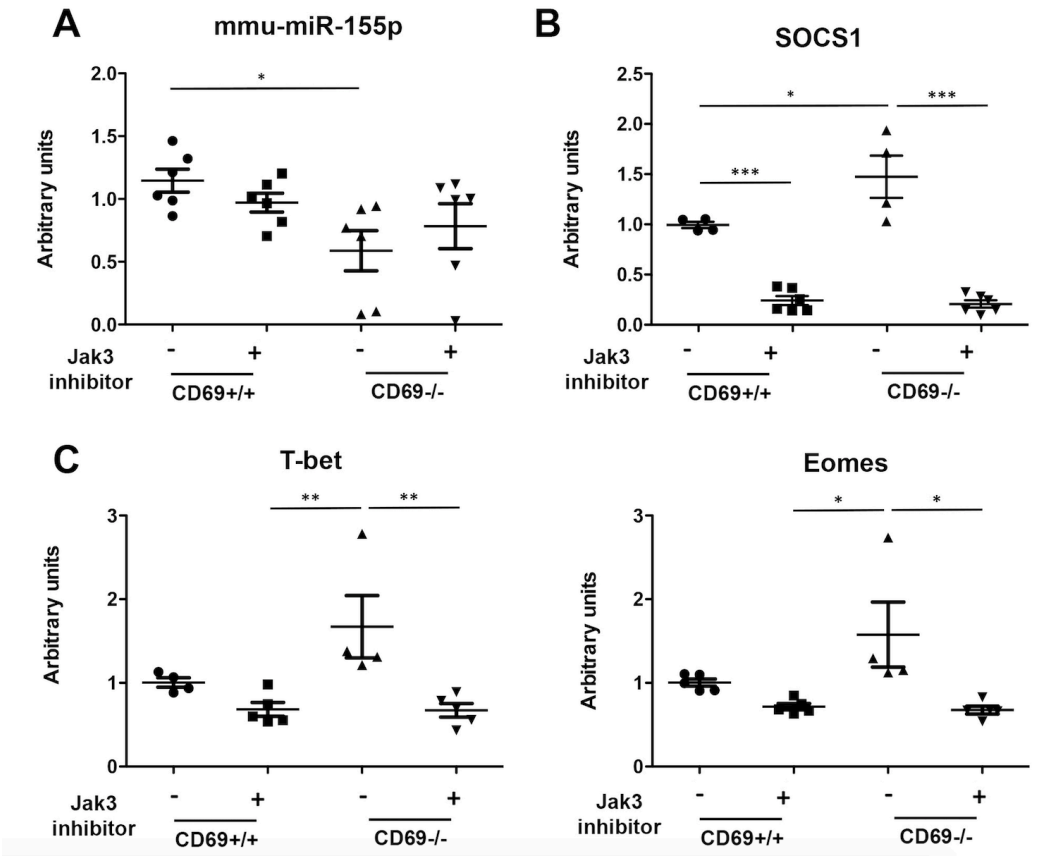

Figura 28. Expresión del miR-155 y genes diana en ausencia de señalización por Jak3/Stat5. Las células iTregs se cultivaron del mismo modo que en Figura 27 se trataron con un inhibidor de Jak3 las últimas 9 horas del cultivo. Se analizó por qPCR la expresión relativa de miR-155 (**A**), SOCS1 (**B**), T-bet y Eomes (**C**) en iTregs de animales *cd69*$^{+/+}$ o *cd69*$^{-/-}$. Se muestran los datos de dos experimentos independientes. Los datos fueron evaluados por ANOVA seguido de Bonferroni para comparar los diferentes grupos por parejas: * P <0,05, ** P <0,01, *** P <0,001.

3.7. LOS NIVELES DE EXPRESIÓN DE MIR-155 Y CD69 SE CO-REGULAN EN UN BUCLE DE RETROALIMENTACIÓN POSITIVO.

Las secuencias de los promotores de CD69 y BIC/miR-155 tienen varios sitios putativos de unión de Stat5 y del elemento AP-1 delante de la caja TATA. Además, el factor de transcripción AP-1, altamente inducido después de la estimulación por TCR, regula la activación de ambos promotores de CD69 y miR-155 (Castellanos et al., 1997; Yin et al., 2008b), lo que sugiere que ambos promotores pueden ser activados concomitantemente, por la misma vía TCR/CD3 (Figura 29).

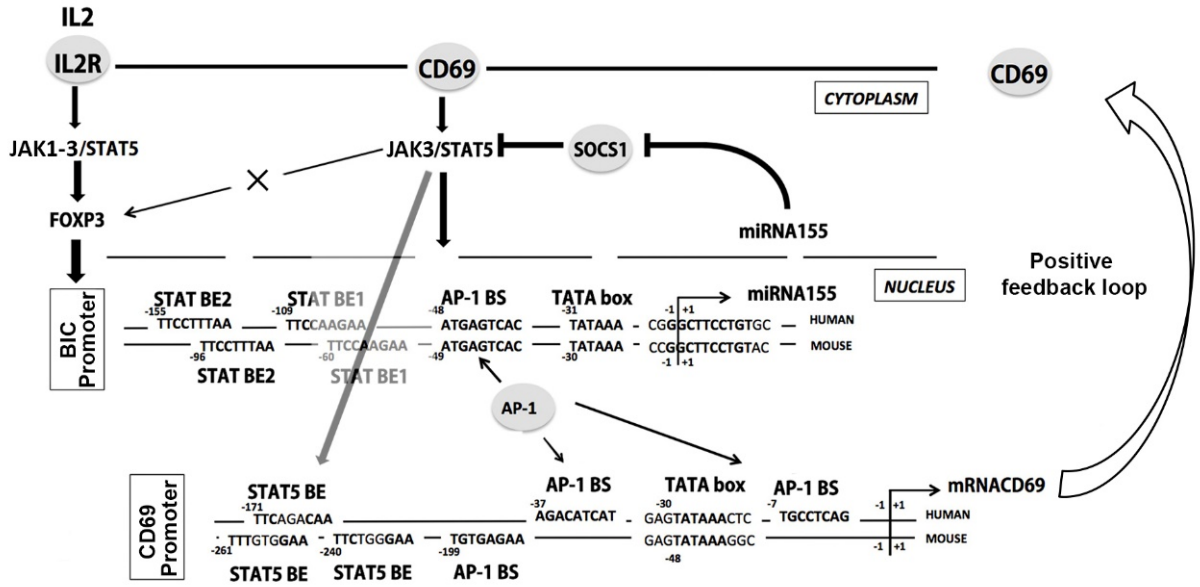

Figura 29: La señalización citoplasmática de CD69 regula la expresión de miR-155 en un bucle de retroalimentación positiva. La señalización concomitante de CD69 e IL-2R regula la expresion de miR-155. Se han encontrado secuencias conservadas para los promotores BIC y CD69 humanos y de ratón obtenidas a partir de GenBank (Mus gencus BIC noncoding mRNA. GenBank: AY096003.1; Homo sapiens (humano) MIR155 gen hospedador GenBank: NC_018932.2; Mus musculus CD69 antígeno GenBank: NC_000072.6, Molécula CD69 de Homo sapiens GenBank: NC_000012.12). Las secuencias promotoras BIC / miR-155 y CD69 comparten una organización similar de elementos de union a Stat5 y AP-1, con dos elementos putativos de union a STAT y el elemento AP-1 situados delante de la caja TATA. Las secuencias de consenso para sitios de unión de STAT y AP-1 se encuentran tanto en ratones como promotores humanos de CD69 y BIC. Los números indican la posición con respecto al codon de partida ATG dentro de cada promotor.

Para comprobar esta hipótesis, investigamos a continuación si la señalización mediada por CD69 regula la expresión de miR-155 en tTreg. Se separaron por sorting tTreg Foxp3^{+} de ratones Foxp3-mRFP CD69$^{+/+}$, expresando CD69 en estado estacionario, y se incubaron con el anticuerpo anti-CD69 (2.2), que

bloquea la expresión de CD69 en la membrana de la célula y por tanto amortigua su señalización (Esplugues et al., 2003). Como se describió anteriormente, observamos una fuerte disminución de la expresión en la membrana de CD69 en comparación con las células incubadas con el anticuerpo control de isotipo IgG1 (2.8) (Figura 30A). El análisis por qPCR reveló una disminución de la expresión del miR-155 en tTreg CD69^{+} tratadas con (2.2), a niveles comparables a tTreg CD69^{-} o tTreg procedentes de un animal CD69$^{-/-}$ (Figura 30B). Además, el bloqueo de CD69 con el anticuerpo 2.2 disminuyó la fosforilación de Stat5 (Figura 30C) provocando una activación de SOCS1 (Figura 30D), lo que significa que la expresión de CD69 es necesaria para la inhibición de SOCS1 dependiente de miR-155 y la formación de tTreg.

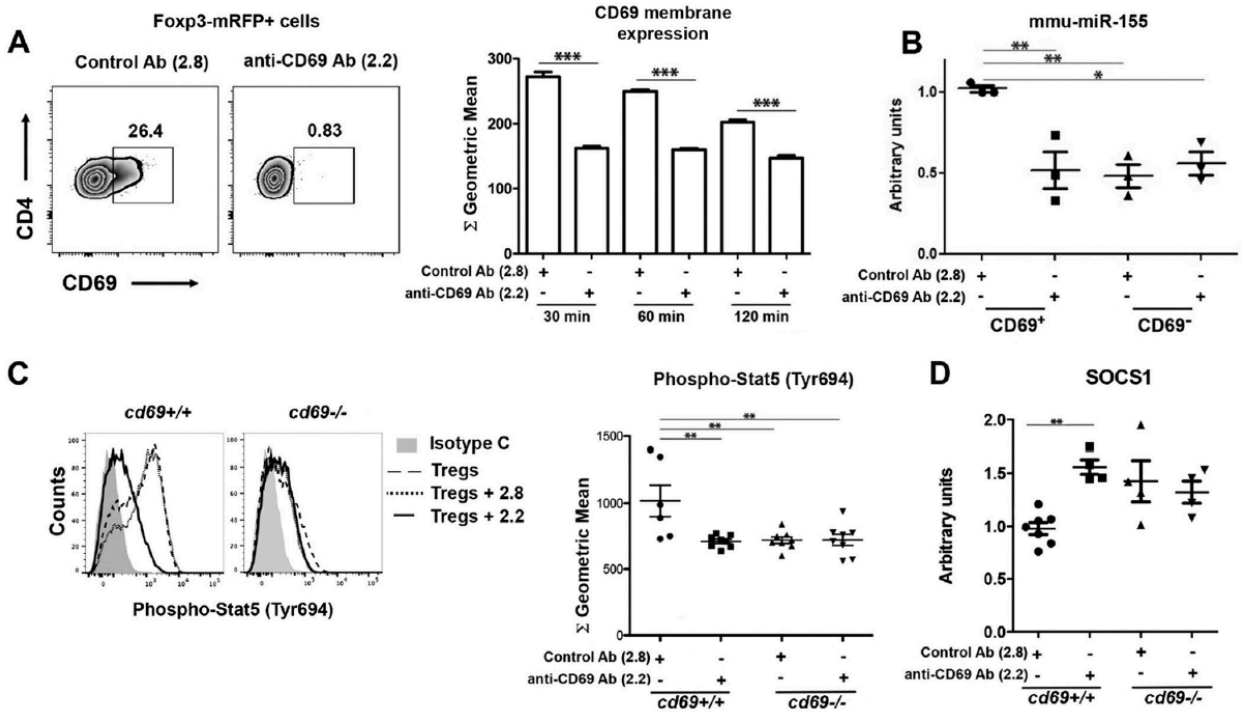

Figura 30: La señalización mediada por CD69 regula la expresión miR-155, Stat5 y SOSC1 en Treg. **(A)** Graficas de densidad representativas de la expresión de CD69 en células tTreg de ratones Foxp3-mRFP/CD69^{+} tratadas con anti-CD69 (2.2) o control de isotipo (2.8). Cuantificación de la expresión de CD69 en la membrana de la célula, expresada como la media geométrica de la intensidad de la fluorescencia (*Geometric-Mean*) después del tratamiento con los anticuerpos, analizado por FACS. **(B)** Análisis por qPCR de la expresión de mmu-miR-155 en tTreg Foxp3-mRFP^{+} CD69^{+} o CD69^{-} después del tratamiento con los anticuerpos. Los resultados se normalizaron por la expresión de snoRNA135 y la expresión relativa a las células CD69^{+} tratadas con 2.8. **(C)** Histograma representativo de la fosforilación de Stat5 en células iTreg CD69$^{+/+}$ o CD69$^{-/-}$ con anti-CD69 (2.2) o control de isotipo (2.8). La gráfica de puntos representa la cuantificación de los niveles de fosforilación de Stat5 expresados como la media geométrica de la intensidad de la fluorescencia. **(D)** Expresión trascripcional de SOCS1 analizada por qPCR. Los datos de A-B proceden de 3 *sorting* independientes (3 animales por *sorting*) y la diferenciación de iTreg procede de al menos 4 ratones por grupo (C-D). Los datos fueron analizados por ANOVA de 1 vía y se hizo el test Bonferroni para analizar por parejas los diferentes grupos experimentales (B). La expresión de CD69 después del

tratamiento con Ab fue analizada por la prueba t de Student (A). * P <0,05, ** P <0,01, *** P <0,001). Las barras corresponden a la media ± S.D de al menos 4 experimentos independientes.

Para verificar si estos hallazgos podrían extenderse a las células humanas, activamos linfocitos $CD4^+$ $CD25^+$ de sangre periférica humana (*peripheral blood lymphocytes*: PBLs) que posteriormente infectamos con vectores lentivirales (*lentiviral vectors*: LV), que expresan secuencias silenciadoras de la transcripción y la expresión de CD69 (shCD69-1 a -3). Los niveles de expresión en la membrana de CD69 fueron analizados por FACS y los niveles de hsa-miR-155 por qPCR. Las PBLs infectadas con lentivirus que expresan la secuencias shCD69 inhiben completamente la expresión de CD69 en comparación con las células infectadas con lentivirus control (Mock) (Figura 31A). El análisis del miR-155, en estas células en las que se ha silenciado la expresión de CD69, muestra una importante disminución de la expresión de miR-155, con cualquiera de las tres secuencias silenciadoras utilizadas (Figura 31B). Nuestros datos indicaban que en humanos CD69 y hsa-miR-155 se regulan conjuntamente como en las células de ratón. Paralelamente, se indujo la expresión de CD69 *in vitro* (Figura 31C) para corroborar que la vía Stat5 y hsa-miR-155 se activan junto con el receptor, mientras que SOCS1 es inhibido (Figura 31D). Para demostrar inequívocamente que el mecanismo molecular observado es funcional, se realizaron ensayos de pérdida y ganancia de función, en los que transfectamos Treg humanas con anti-hsa-miR-155 o hsa-pre-miR-155 para inhibir o sobre-expresar el miRNA, respectivamente. Primero transfectamos PBL humanos $CD4^+$ $CD25^+$, estimulados con anti-CD3, con el anti-hsa-miR-155-5p que bloquea la expresión del miRNA-155 o con anti-miRNA control (Figura 31E). Como consecuencia, la expresión de CD69 en PBLs activadas se inhibía dramáticamente después de la inhibición de hsa-miR-155 (Figura 31F). Además, la fosforilación de Stat5 se redujo y por lo tanto se incrementó la expresión génica de SOCS1 (Figura 31F), lo que indicaba que el bloqueo de miR-155 regula la ruta de señalización de CD69. Por el contrario, la sobrexpresión de hsa-pre-miR-155 (Figura 31G) en Tregs reveló un aumento significativo en la expresión de CD69, fosforilación de Stat5 e inhibición de la expresión de SOCS1 (Figura 31H). En resumen, estos resultados confirmaron nuestra hipótesis, la modulación recíproca del receptor CD69 y el miR-155 se lleva a cabo mediante un bucle de retroalimentación positiva (Figura 29) mediante la activación de elementos comunes en el promotor, y esta retroalimentación podría ser fundamental para mantener la diferenciación de tTreg y la homeostasis de pTreg en el organismo.

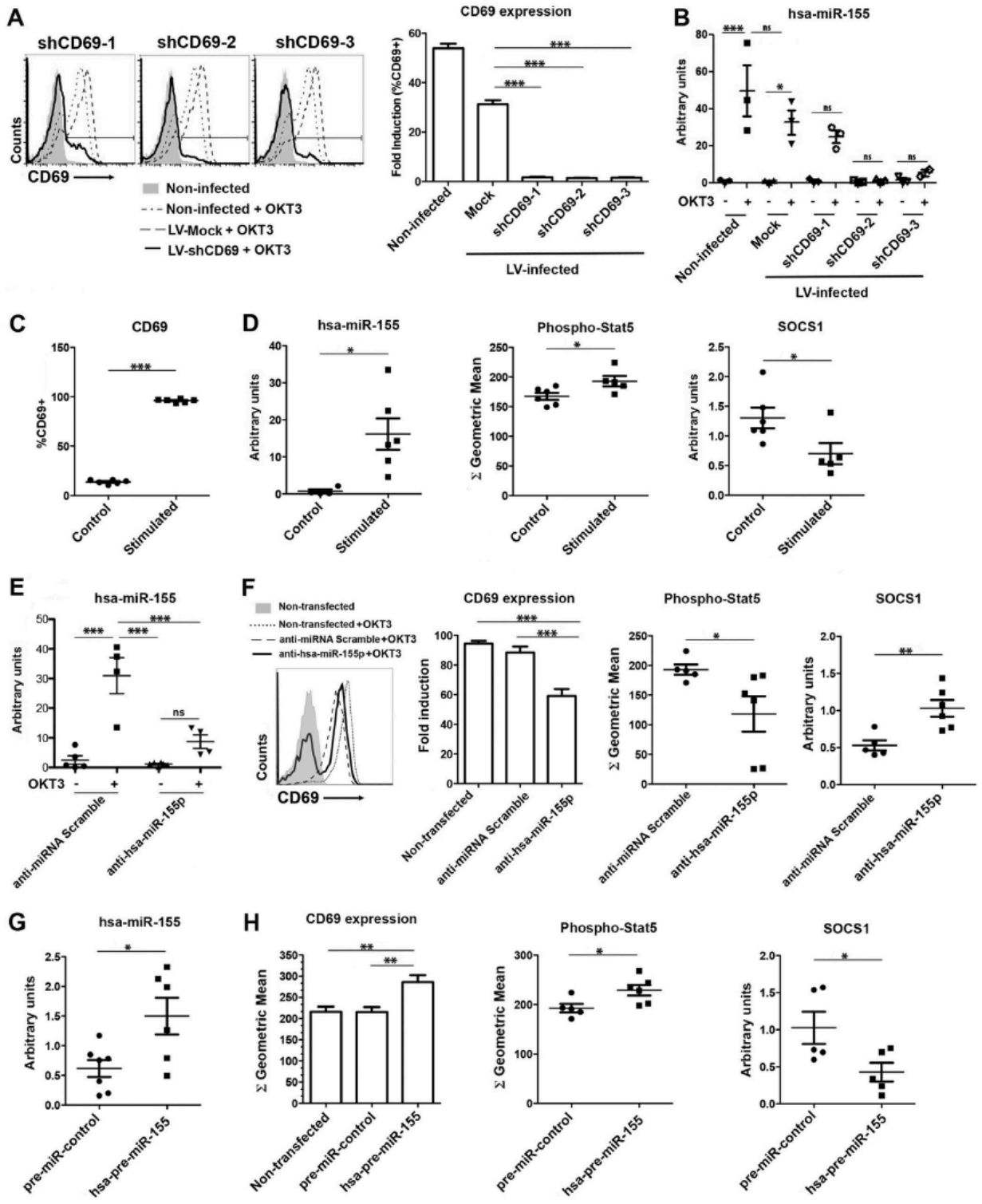

Figura 31. Co-regulación de la expresión de CD69 y miR-155 en Treg humanas. (A) Histogramas representativos de la expresión de CD69 después de la infección lentiviral con 3 secuencias silenciadoras diferentes de shCD69 o una secuencia sh control, estimuladas o no con anticuerpos humanos anti-CD3 (clon OKT3). Los histogramas representan la cuantificación de la inducción de CD69 en relación con las células no estimuladas. **(B)** Expresión de

hsa-miR-155 en células T $CD4^+$ humanas después de la infección con LV, analizado por q-PCR. **(C)** PBL humanas estimuladas o no con PMA/Iono durante 4 horas y cálculo del porcentaje de células $CD69^+$. **(D)** Niveles de fosforilación de Stat5 analizado por FACS**,** niveles de expresión de hsa-miR-155 y el gen SOCS1 humano analizados por qPCR. **(E)** PBL humanos transfectados con anti-hsa-miR-155-5p o anti-miRNA-Scramble y análisis de los niveles de expresión de miR-155 por qPCR. **(F)** Histogramas representativos y cuantificación de la expresión de CD69 y fosforilación de STAT5 analizados por FACS y expresión de SOCS1 analizado por qPCR en PBL $CD4^+$ tratados como en (E). **(G)** PBL humanos transfectados con hsa-pre-miR-155-5p o pre-miRNA-control y análisis de la expresión de hsa-miR-155 por qPCR. **(H)** Niveles de expresión de CD69, fosforilación de STAT5 y SOCS1 humano en PBL $CD4^+$ tratados como en (G). Los resultados de qPCRs para miRNA se normalizaron con la expresión de snoRNA135. Todos los datos son media ± DS. De al menos 3 donantes independientes de un total de diez donantes. Los datos se analizaron por ANOVA y Bonferroni post-test para comparar por parejas los diferentes grupos experimetales * P <0,05, ** P <0,01, *** P <0,001.

4. PAPEL DE CD69 EN LOS PROCESOS DE ANGIOGÉNESIS O NEOVASCULARIZACIÓN POST ISQUEMIA

La presencia de las células Th17 en procesos de angiogénesis y neovascularización está sobradamente demostrada ya que la inflamación producida en un proceso de isquemia induce el reclutamiento de neutrófilos y monocitos en la zona de la isquemia lo que favorece la secreción de IL-6 que potencia la diferenciación de los linfocitos T $CD4^+$ a células Th17, que producen TGF-β y VEGF, favoreciendo la neovascularización post-isquemia. Además las células Treg, puesto que regulan la función de las células Th17, también juegan un papel importante en los procesos de neovascularización(Hata et al., 2011; Zouggari et al., 2009). La mólecula CD69, como se ha demostrado en diversos trabajos publicados en el grupo y en esta tesis, tiene un papel fundamental en la regulación del balance entre las células Th17 y Treg, en condiciones tanto fisilógicas como patológicas(Cortes et al., 2014; Martin et al., 2010a; Martin et al., 2010b; Martin and Sanchez-Madrid, 2011; Sanchez-Diaz, 2016), por lo que nos planteamos si dicha molécula podría ejercer una función reguladora en la neovascularización post-isquemia y por lo tanto ser una posible diana para el tratamiento de las enfermedades que cursan con isquemia.

4.1 CINÉTICA DE LAS CÉLULAS TH17 Y TREG EN SANGRE Y ÓRGANOS LINFOIDES TRAS ISQUEMIA DE LA ARTERIA FEMORAL

Para estudiar el papel de CD69 en células Th17 y Treg en la neovascularización post-isquemia hemos utilizado el modelo de isquemia de la arteria femoral (*Himblimb ischemia model)*, ampliamente usado para el estudio de la enfermedad arterial periférica (PAD). En este modelo hemos evaluado los niveles de células Th17 y células Treg en animales $CD69^{+/+}$ y animales $CD69^{-/-}$ en sangre periférica 0, 1, 3 y 7 días post-isquemia y en ganglios linfáticos periféricos inguinales y popliteos 7 días post-isquemia, utilizando como control, los ganglios correspondientes de la extremidad contra-lateral sin isquemia. Encontramos que las células Treg se incrementaban un 25% en sangre de los animales BALB/c de ambos genotipos, 1 día post-isquemia, mientras que a día 7 habían disminuido en los animales WT, pero no en los animales que $CD69^{-/-}$ (Figura 32A). Además, en paralelo se producía un marcado incremento de células Th17 en sangre 7 días post-isquemia, en animales $CD69^{+/+}$ y animales $CD69^{-/-}$ (Figura 32A). En los ganglios linfáticos inguinales no encontramos ninguna variación significativa de estas poblaciones de células T en ninguno de los genotipos (Figura 32B y C). Sin embargo, los ganglios popliteos sí mostraron diferencias

en los niveles de células Th17 y Treg, indicando que la respuesta inmune adaptativa frente al proceso de isquemia se estaba llevando a cabo en estos órganos (Figura 32B).

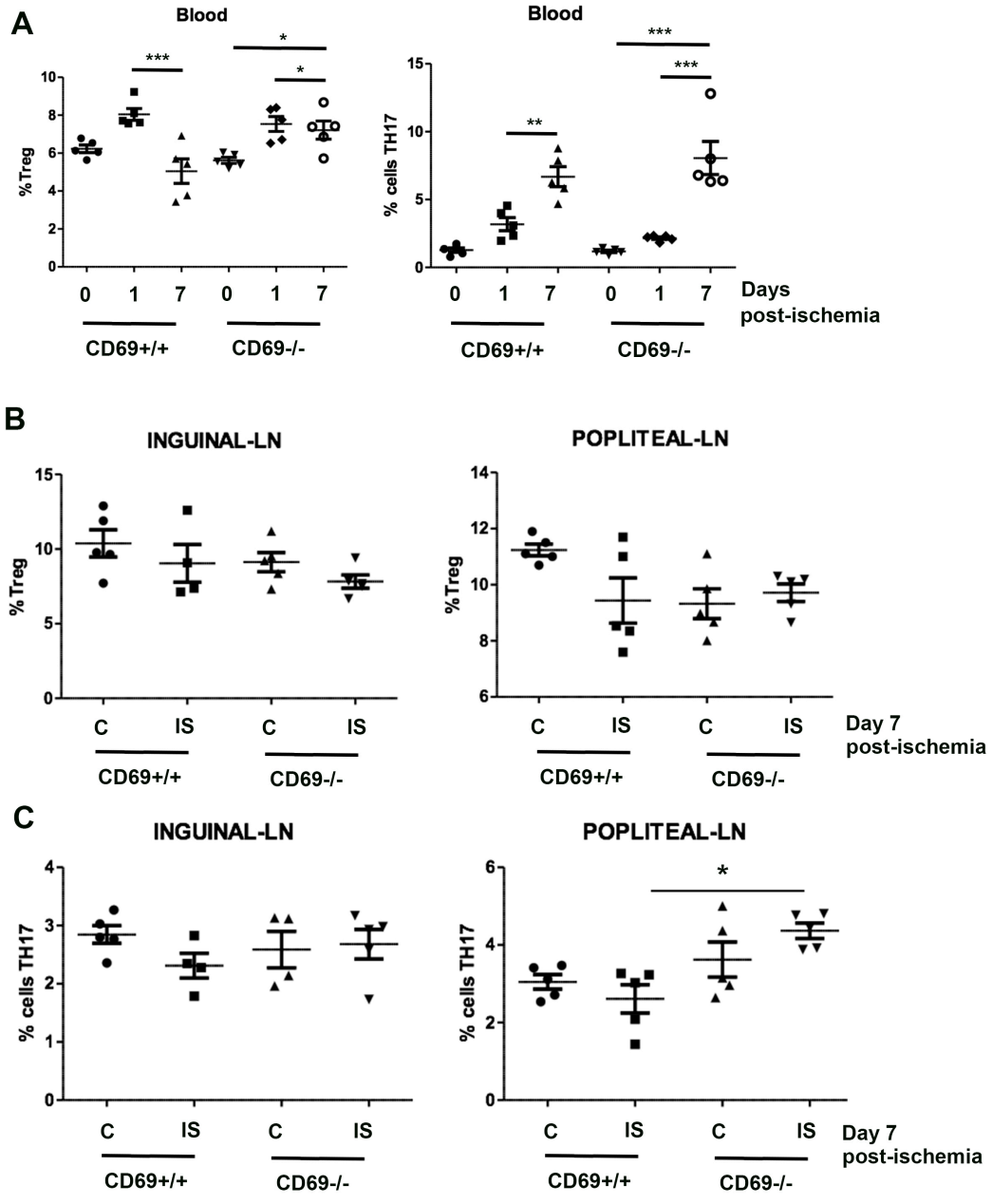

Figura 32. Análisis de las células Th17 y Treg en sangre y ganglios de animales post-isquemia de la arteria femoral. Los animales WT y KO (CD69$^{-/-}$) en fondo BALB/c fueron sometidos a isquemia de la arteria femoral en la extremidad inferior izquierda, dejando la derecha (contra-lateral) sin operar como control. Las células de sangre y ganglios linfáticos fueron analizadas por citometría de flujo. **(A)**. Porcentajes de células Treg y Th17 en sangre periférica antes de la isquemia (*0*) y 1 y 7 días post-isquemia. **(B)** Análisis de las Treg en glanglios linfáticos inguinales (*inguinal-LN*) y poplíteos (*popliteal-LN*) 7 días post-isquemia (*IS*) en la extremidad isquémica y la control (C: no isquémica). **(C)** Porcentajes de células Th17 en glanglios linfáticos inguinales y poplíteos 7 días post-isquemia. Los datos son representativos de 2 experimentos independientes (n=5).

El porcentaje de las células Treg de los gaglios poplíteos de los animales WT se encontraba disminuido en la extremidad isquémica con respecto a la contra-lateral no isquémica, mientras que los animales CD69$^{-/-}$ presentaban menor porcentaje de células Treg en ambas extremidades (Figura 32B). Por el contrario, los porcentajes de las células Th17 de los ganglios poplíteos de los animales CD69$^{-/-}$ eran muy altos en comparación con los de los animales WT (Figura 32C). Estos datos indicaban una mayor respuesta adaptativaTh17 en los ganglios poplíteos de los animales CD69$^{-/-}$ en comparación con los WT, en respuesta a la isquemia de la arteria femoral, poniendo de manifiesto un papel de estas células en esta patología.

4.2 LOS ANIMALES CD69$^{-/-}$ PRESENTAN UNA REVASCULARIZACIÓN ACELERADA

Los animales sometidos a isquemia de la arteria femoral recuperan la perfusión sanguínea en la extremidad aproximadamente después de un mes, dependiendo del fondo genético, por lo que es un modelo ideal para estudiar procesos de arteriogénesis *in vivo*. La evaluación de la revascularización en animales sometidos a isquemia en la extremidad posterior izquierda se realizó mediante ecografía de laser doppler. Esta técnica permite detectar el flujo sanguíneo en el animal vivo mediante la dispersión que sufre el láser al incidir sobre los glóbulos rojos en movimiento, lo que permite analizar las áreas isquémicas y las que están reperfundidas a lo largo de todo el proceso de revascularización. Las medidas de flujo periférico (*peripheral flows* FP) las representamos en *Flux* que son unidades arbitrarias comunes para todos los aparatos que realizan éste tipo de medidas. Hemos usado las unidades relativas RU, que calcula el flujo en función la media de los valores reales de flujo obtenidos en un espacio y tiempo determinados. El análisis de estos datos se representó como el ratio de reperfusión y se calculó realizando el cociente entre el flujo en la extremidad isquémica y el flujo de la extremidad no isquémica.
En primer lugar analizamos la recuperación de la perfusión en animales WT y CD69$^{-/-}$ en fondo BALB/c. En estos experimentos, los animales BALB/c CD69$^{-/-}$ mostraban una total recuperación de la reperfusión a día 7 post-isquemia, mientras que en los animales BALB/c CD69$^{+/+}$ la recuperación no era completa hasta el día 14 post-isquemia. Estos datos sugerían que CD69 podría tener un papel en la regulación de la arteriogénesis, ralentizando el proceso de neovascularización (Figura 33A). Para ahondar más en el papel de CD69 en la neovascularización realizamos quimeras hematopoyéticas en fondo C57BL/6, en las que el animal receptor es siempre WT para CD69 y los donantes expresan o no CD69 en las células hematopoiéticas. En las quimeras el receptor es un animal C57BL/6 CD69$^{+/+}$ y los donates son animales doble reportero (DR) ya que son doble transgénicos y expresan Foxp3-mRFP y IL-17eGFP; Foxp3-

mRFP/Th17eGFP/CD69$^{+/+}$ ó Foxp3-mRFP/Th17eGFP/CD69$^{-/-}$. En estas quimeras el endotelio siempre es WT para CD69, lo que permite estudiar el papel de CD69 únicamente en el compartimento hematopoiético. En los experimentos de isquemia, las quimeras reconstituidas con precursores de médula ósea procedentes de animales DR CD69$^{-/-}$ presentaron una reperfusión más rápida (Figura 33B) al igual que en los animales CD69$^{-/-}$ (Figura 33A), lo que indicaba que la expresión de CD69 en el compatimento leucocitario frena la neovascularización por isquemia (Figura 33B). Para intentar dilucidar si CD69 expresado específicamente en el compartimento linfoide influye en los procesos de neovascularicación, generamos quimeras mixtas con animales Rag2$^{-/-}$γc$^{-/-}$, en las que el receptor es siempre un animal WT para CD69 que carece de linfocitos T, B y NK y los precursores de medula ósea son una mezcla de animales Rag2$^{-/-}$γc$^{-/-}$ y animales DR WT o CD69$^{-/-}$, en proporciones 3:1 respectivamente. Con este tipo de quimeras conseguimos un endotelio WT como en el caso anterior, y al inyectar una mayor proporción de precursores mieloides de medula ósea Rag2$^{-/-}$γc$^{-/-}$, estos compiten en el nicho con los precursores de animales DR WT o CD69$^{-/-}$, desplazando el componente mieloide perteneciente al animal DR. Por lo tanto, estas quimeras constituyen un buen modelo para analizar el papel de CD69 únicamente en el compartimento linfoide. Tras la isquemia en estas quimeras mixtas comprobamos que la revascularización era también más rápida en los animales reconstituidos con precursores linfoides CD69$^{-/-}$ (Figura 33C). Por lo tanto, los tres modelos confirmaban un papel de las células Th17 en procesos de neovascularización, que parecían estar regulados por CD69 en estas células.

4.3. PAPEL DEL MIR-721 EN PROCESOS DE ANGIOGÉNESIS

Estudios previos en el laboratorio relacionan la expresión del miR-721 con procesos patológicos que cursan con un incremento de linfocitos Th17, como es el caso de la miocarditis autoinmune en el que se correlaciona un aumento de este miRNA con la respuesta Th17 que se desencadena tanto en pacientes de miocarditis, como en ratones a los se ha sometido al proceso de miocarditis experimental (Tesis doctoral de Adela Matesanz Marín, 2015). Debido a estas evidencias junto con los datos anteriores y a que hasta el momento la única diana validada para este miRNA es la proteína Meox2 (Pfaff et al., 2011), relacionada con procesos de inhibición de la angiogénesis a través de la vía de señalización de NFκB (Cantile et al., 2008; Chen and Gorski, 2008; Patel et al., 2005) nos planteamos estudiar este miRNA y su papel en los procesos de neovascularización. Los datos previos apuntaban a que el miR-721, a través de la inhibición de su diana Meox 2, podría ser uno de los implicados en la rápida revascularización observada en los animales deficientes en CD69 (Figura 33), ya que la respuesta Th17 en estos animales

está exacerbada en los animales CD69$^{-/-}$ (Figura 32A y B). Con objeto de comprobar esta hipótesis analizamos los niveles de este miRNA en los animales tras isquemia en la extremidad posterior izquierda, en suero, ganglios poplíteos y músculo. En paralelo analizamos la expresión de su diana Meox2 y la proteína Cux1 en músculo de quimeras hematopoiéticas C57BL/6.

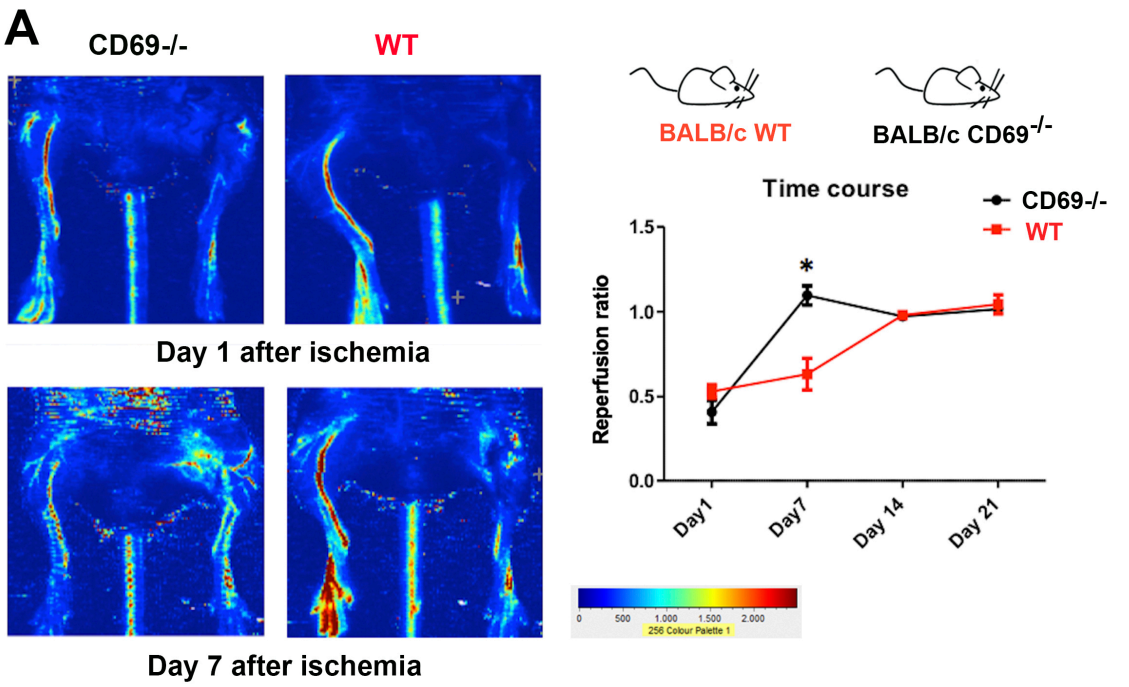
A
CD69-/-
WT
Day 1 after ischemia
Day 7 after ischemia
BALB/c WT
BALB/c CD69-/-
Time course
CD69-/-
WT
Reperfusion ratio
1.5
1.0
0.5
0.0
*
Day1
Day7
Day 14
Day 21
0
500
1.000
1.500
2.000
256 Colour Palette 1

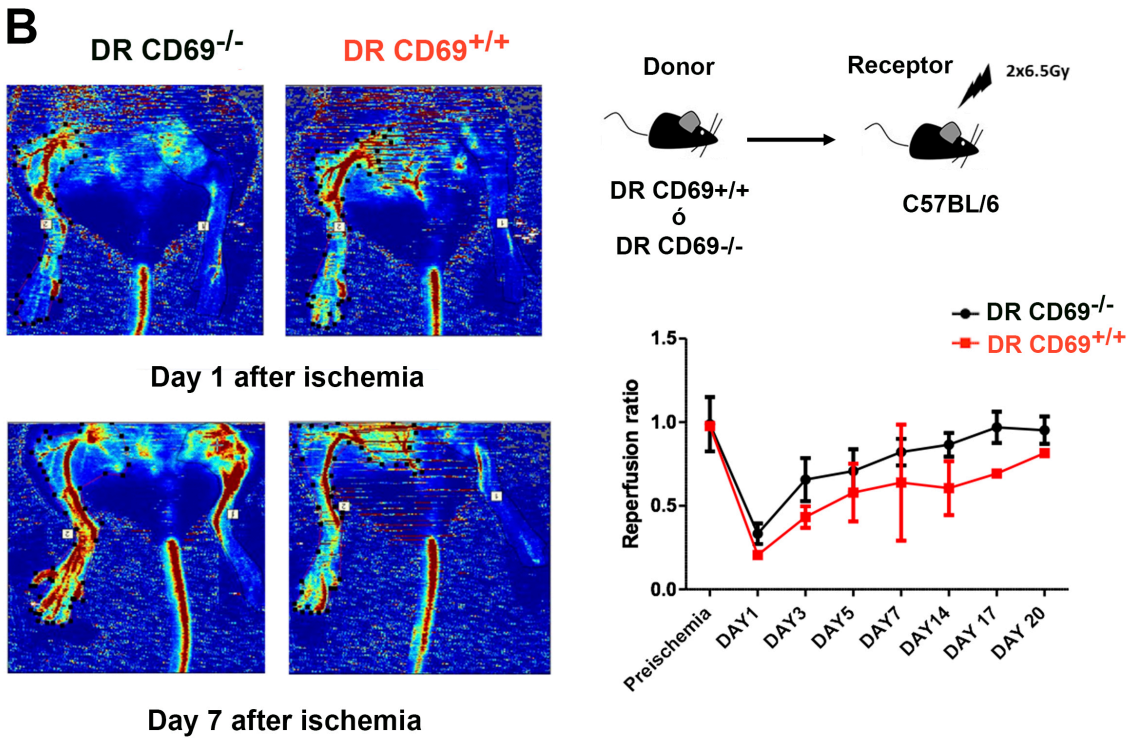
B
DR CD69-/-
DR CD69+/+
Day 1 after ischemia
Day 7 after ischemia
Donor
Receptor
2x6.5Gy
DR CD69+/+
ó
DR CD69-/-
C57BL/6
DR CD69-/-
DR CD69+/+
Reperfusion ratio
1.5
1.0
0.5
0.0
Preischemia
DAY1
DAY3
DAY5
DAY7
DAY14
DAY 17
DAY 20

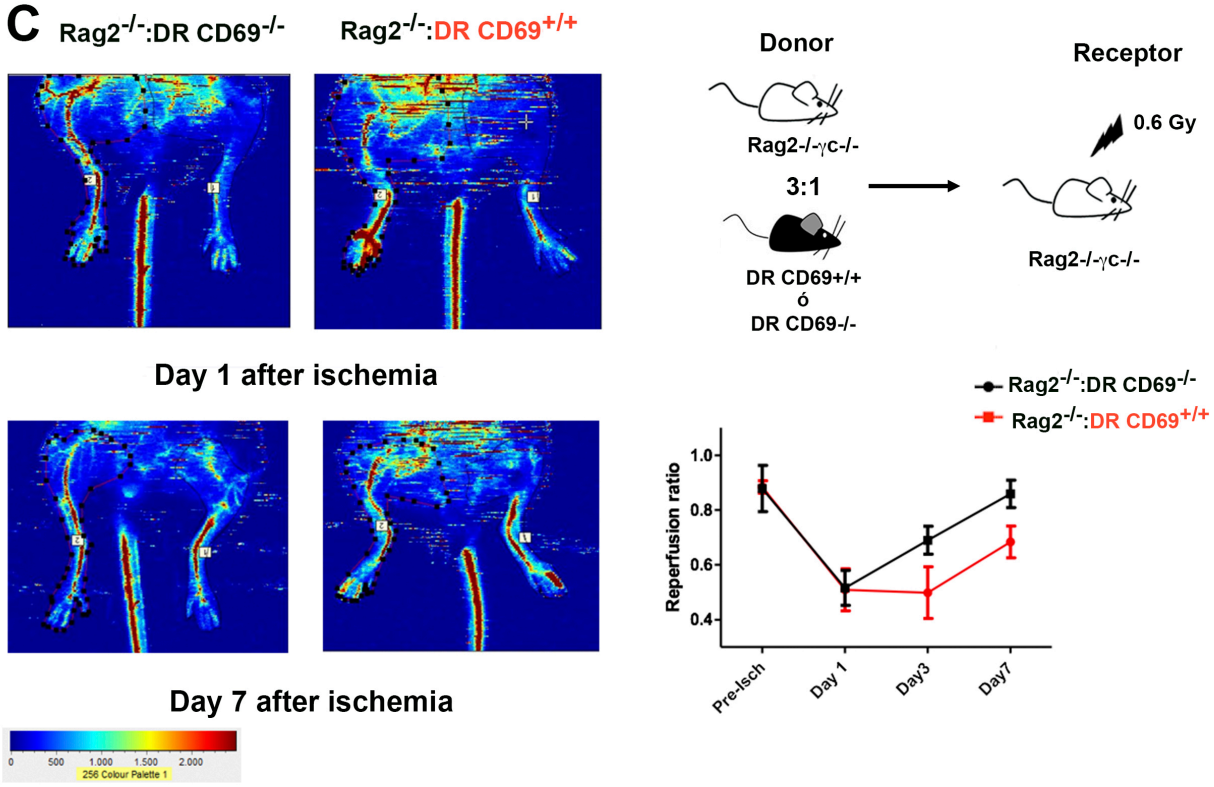

Figura 33. La expresión de CD69 en el compartimento linfoide ralentiza la neovascularización post-isquemia. (A) Imágenes representativas de un experimento de isquemia en animales BALB/c, obtenidas con un ecógrafo laser doppler antes y después de la isquemia. Cuantificación del experimento de isquemia en animales BALB/c, representado como el ratio de reperfusión (cociente entre la señal de doppler de la extremidad izquierda, isquémica y la derecha control, no isquémica). **(B)** El esquema ilustra la generación de quimeras en C57BL/6. Imágenes representativas de un experimento de isquemia en quimeras C57BL/6 y cuantificación del ratio de reperfusión. **(C)** El esquema ilustra la generación de las quimeras mixtas Rag2$^{-/-}$γc$^{-/-}$. Imágenes representativas de un experimento de isquemia en quimeras Rag2$^{-/-}$γc$^{-/-}$, y su cuantificación. Los datos son representativos de 2 experimentos independientes, n=5 animales por grupo (A), al menos 4 experimentos independientes con 5 a 7 animales por grupo experimental (B) y los experimentos con las quimeras Rag2$^{-/-}$γc$^{-/-}$, proceden de al menos 4 experimentos independientes con 3 a 7 animales por grupo experimental (C).

Tras análisis *in silico* de los genes diana de miR-721 en las bases de datos miRanda y PicTar, la proteína Cux1 se propone como diana putativa de miR-721, relacionada con procesos de proliferación y migración célular (Ripka et al., 2010; Truscott et al., 2007) y en la que además se encuentra expresado el tránscrito del miR-721 en sus intrones 3 y 4. Tras el análisis por qPCR en los diferentes tejidos, encontramos un incremento de la expresión del miR-721 en el suero de los animales BALB/c deficientes en CD69 tanto los niveles basales como después de la isquemia (Figura 35A). Encontramos un pico en los niveles de expresión de este miRNA en suero 7 días post-isquemia (Figura 35A), coincidiento con el pico de células Th17, que se producía en la sangre periférica de estos animales durante el proceso de la isquemia (Figura 32A). En los animales WT no se detectaron niveles significativos del miRNA en suero tras la isquemia. No se detectaron cambios entre WT y CD69$^{-/-}$ en la expresión del miR-721 en el ganglio poplíteo 28 días post-isquemia (Figura 33A), aunque es un tiempo demasiado largo para evaluar la respuesta T *helper* y por lo tanto, los niveles del miRNA. Sin embargo, en el músculo abductor de los animales BALB/c CD69$^{-/-}$ 28 días después de la isquemia, los niveles del miR-721 estaban muy elevados (Figura 35A), lo que indicaba que tanto el miRNA como las respuestas Th17 podían ser muy activas en este tejido en los animales CD69$^{-/-}$. En las quimeras C57BL/6 analizamos los niveles del miR-721 en suero los días 0, 1, 3 y 7 post-isquemia, encontrando un marcado incremento del miRNA en el suero de los animales deficientes en CD69 a partir del día 3 post-isquemia (Figura 35B). A su vez, los niveles de la diana Meox2 y la diana putativa del miRNA-721, Cux1, se encontraban inhibidas en el músculo isquémico de los animales CD69$^{-/-}$, mientras que el músculo isquémico de los animales WT presentaba ambas dianas elevadas (Figura 35C), lo que se correlaciona inversamente con los niveles del miRNA en suero a día 7 post-isquemía (Figura 35B) y con los niveles más elevados en sangre periférica de linfocitos Th17 en los animales deficientes para CD69 (Figura 32A).

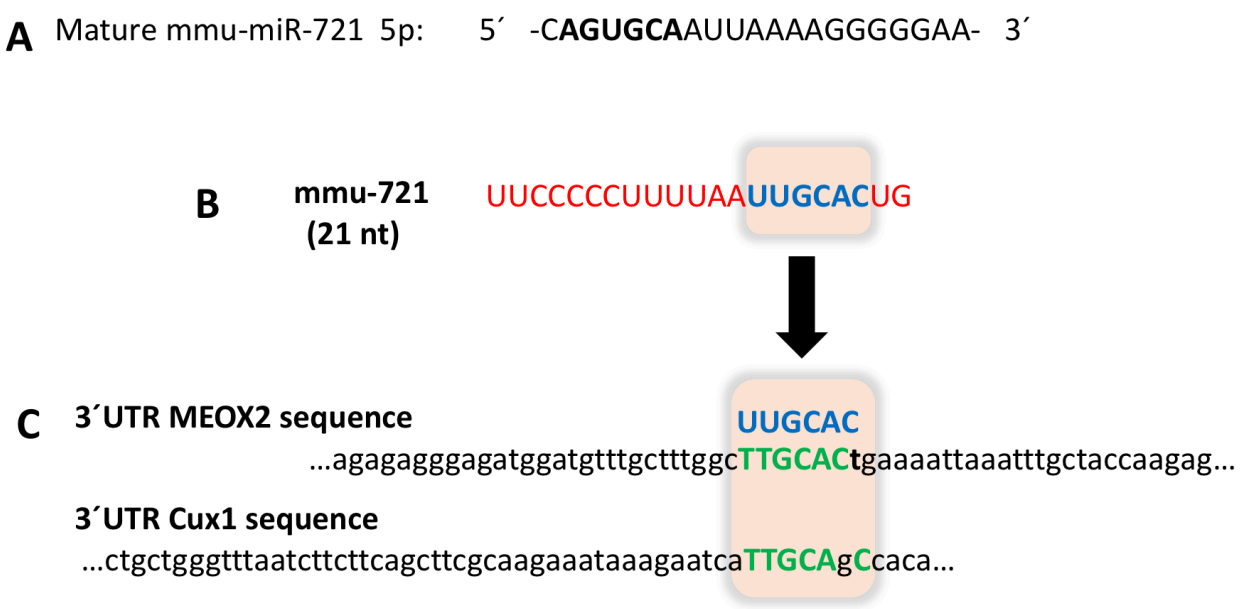

Figura 34. Secuencia de miR-721 y UTR de genes diana. (A) Secuencia madura 5p del microRNA-721 de ratón (mus musculus: mmu-miR-721 MIMAT0003515) de 21 nucleótidos (nt). **(B)** Secuencia reverso complementaria de miR-721 murino para ilustrar los sitios de unión a los UTR (*untranslate regions*) de los genes diana Meox2 y CUX1 **(C).** En rojo: la secuencia madura reverso complementaria del miR-721, en azul: secuencia de interacción con los UTR, en verde: dominio del gen diana que interacciona con el miRNA.

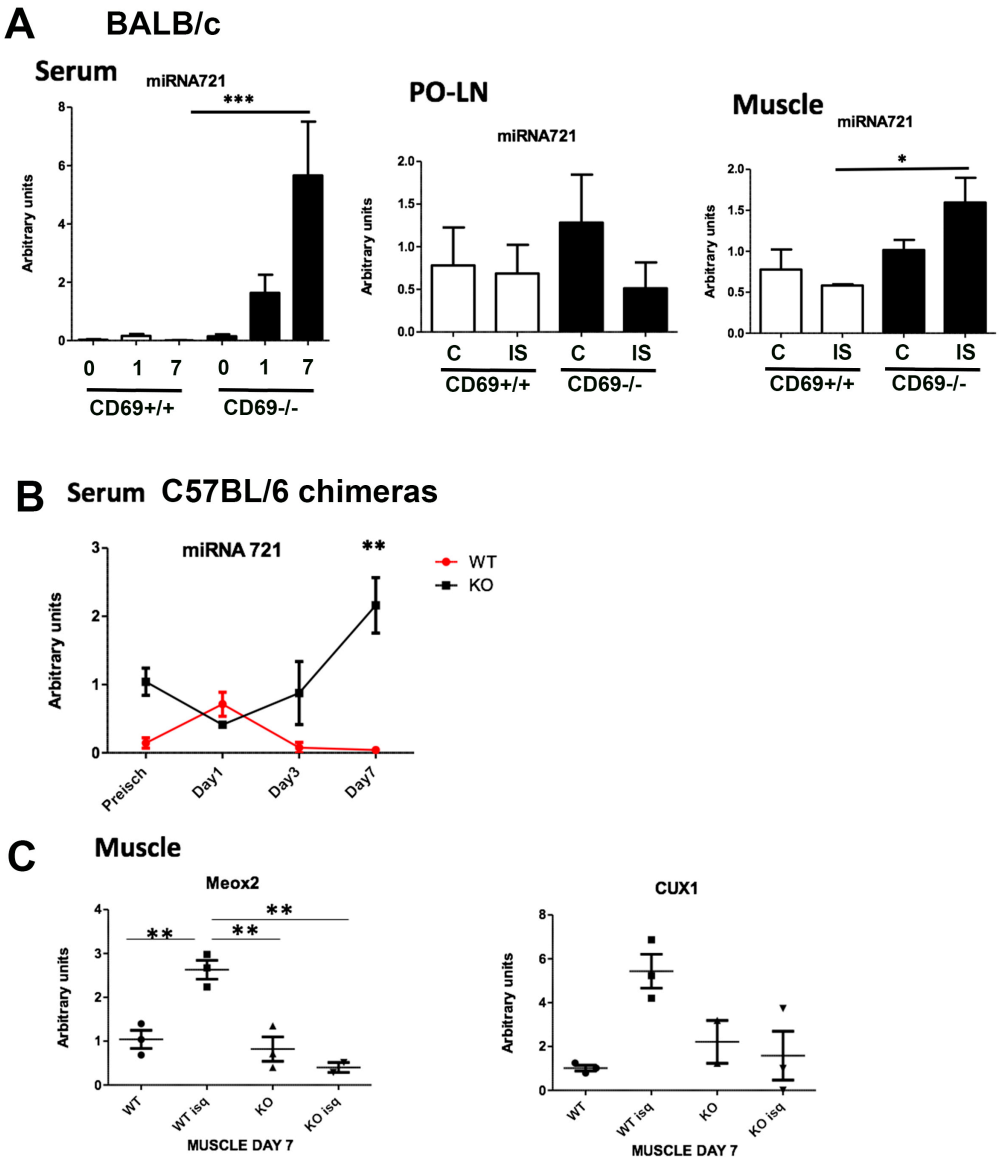

Figura 35. Análisis de la expresión del miR-721 y sus dianas en procesos de neo-vascularización post-squemia. **(A)** Niveles de expresión de miR-721 en la neo-vascularización post-isquemia en suero (*serum*), ganglios poplíteos (*PO-LN*) y músculo abductor (*muscle*) de animales BALB/c analizados por qPCR. Los valores fueron normalizados frente a los niveles en los animales WT a tiempo 0 de la isquemia. **(B)** Niveles de miR-721 en el el suero de quimeras hematopoiéticas C57BL/6 analizado por qPCR 0, 1, 3 y 7 días post-isquemia y normalizados frente a la expresión del miR-721 en el animal WT en condiciones basales. **(C)** Niveles de mRNA de las proteínas Meox2 y Cux1 en el músculo abductor de quimeras C57BL/6 7 días post-isquemia y analizados por qPCR normalizando por los niveles de mRNA de el músculo abductor WT de la extremidad no isquémica. Los datos proceden de 2 experimentos independientes con 5 y 3 animales por grupo (A), y de al menos 4 experimentos independientes con 5 a 7 animales por grupo experimental (B y C).

4.4 EVALUACIÓN DE LA REVASCULARIZACIÓN EN LOS MÚSCULOS DE LOS ANIMALES SOMETIDOS A PROCESO DE ISQUEMIA EN LAS EXTREMIDADES POSTERIORES

Para evaluar la neovascularización en los músculos de los animales DR sometidos a isquemia, hemos realizado tinciones inmunoistoquímicas, en las que hemos usado como marcador de angiogénesis la molécula CD31, que se encuentra expresada en las células endoteliales, además hemos analizado los niveles de expresión de la proteína Meox2 encontrandola también expresada en el endotelio y músculo de éstos animales. El marcador de angiogénesis CD31, se encuentra elevado significativamente, en la extremidad isquémica de los animales deficientes en CD69 en comparación con los niveles de CD31 encontrados en las extremidades isquémicas y no isquémicas de los animales WT (Figura 36A). La proteína Meox2 por el contrario se encuentra inhibida significativamente en el endotelio del tejido muscular isquémico de los ratones $CD69^{-/-}$, en comparación con la extremidad no isquémica y con la extremidad isquémica de los animales $CD69^{+/+}$ (Figura 36A). No hemos encontrado diferencias significativas con respecto a la expresión de Meox2 entre animales $CD69^{+/+}$ y $CD69^{-/-}$en la extremidades no isquémicas, por lo que pensamos que la proteína Meox2 se inhibe durante el proceso de isquemia en los animales deficientes en CD69 mediante su regulación por miR-721, que se induciría con el aumento de los linfocitos Th17 durante el proceso. Hemos calculado el ratio CD31/Meox2 como una medida del proceso de angiogénesis, ya que la expresión de ambas proteínas se correlacionan de manera antagónica para dar como resultado una mayor o menor revascularización post-isquemia (Figura 36B).

El ratio CD31/Meox2 es menor en los animales WT, que en los animales deficientes en CD69 en la extremidad no isquémica, aunque las diferencias no son significativas estadísticamente, si que encontramos diferencias significativas estadísticamente, con respecto al ratio CD31/Meox2 entre la extremidad no isquémica de los animales $CD69^{+/+}$y la extremidad isquémica de los animales $CD69^{-/-}$ indicando que el proceso de revascularización post isquémica es más activo en los animales $CD69^{-/-}$ (Figura 36B).

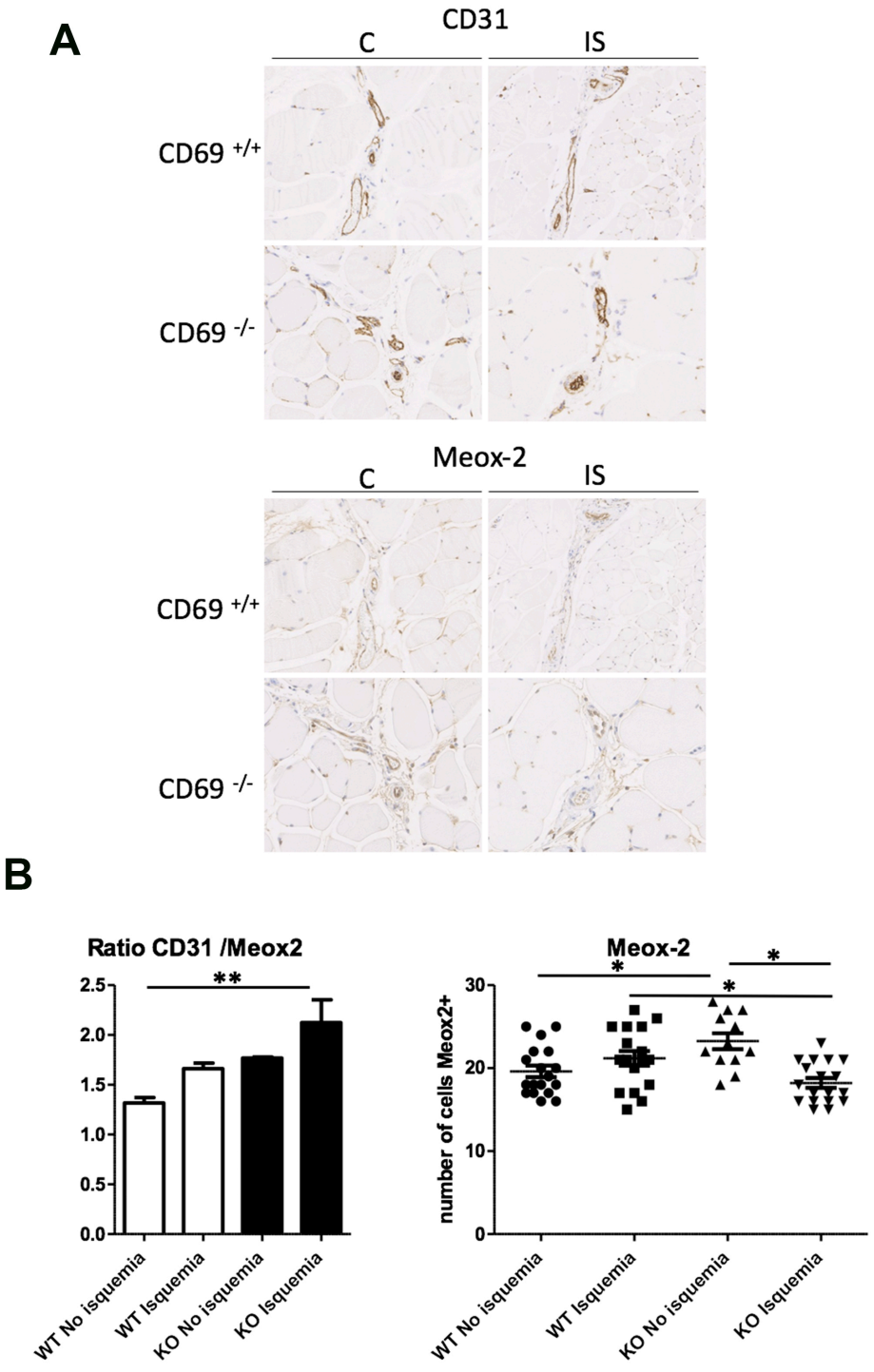

Figura 36. Análisis de CD31 y Meox2 en el endotelio del músculo con y sin isquemia. (A) Marcaje por inmunohistoquímica de CD31 (arriba) y Meox2 (abajo) en el tejido de la extremidad no isquémica contralateral (C) y la isquémica (IS) 7 días después de la isquemia. (B) Ratio CD31/Meox2 expresado como número de células $CD31^{+}$ entre el número de células $Meox2^{+}$ cuantificadas en cortes del músculo esquelético abductor. Los datos mostrados provienen de 2 experimentos de isquemia independientes realizados con animales DR, $CD69^{+/+}$ y $CD69^{-/-}$, sometidos a isquemia en la extremidad posterior izquierda y sacrificados a los 7 días post-isquemia.

4.5 Niveles de expresión de miR-721 y las proteínas Meox2 y Cux1 en células endoteliales.

Debido a las diferencias observadas con la técnica de doppler entre animales CD69$^{+/+}$ y animales CD69$^{-/-}$ en la neovascularización post-isquemia y a los datos obtenidos en los experimentos de inmunohistoquímica, en los que la proteína Meox2 se encuentra altamente expresada en el endotelio de los animales WT tras isquemia y con respecto a los animales deficientes en CD69, evaluamos los niveles de expresión del miR-721 y su diana Meox2 en células endoteliales procedentes de animales CD69$^{+/+}$ y animales CD69$^{-/-}$. Para ello purificamos células endoteliales de pulmón (*mouse lung endotelial cells*: MLEC) de ambos tipos de animales y analizamos por qPCR los niveles del miR-721, en estas células endoteliales en condiciones basales o estimuladas con phorbol 12-myristate 13-acetate (PMA) y Iomicina o con TNFα. Sorprendentemente y en todos los casos, el miR-721 sólo se encontró expresado en las MLEC procedentes de animales deficientes en CD69, donde además se inducía su expresión tras estimulación. El factor de transcripción Meox2, en concordancia con el comportamiento de la diana de un miRNA, se encontraba inhibido en las MLEC CD69$^{-/-}$ y muy expresado en las MLEC de animales CD69$^{+/+}$, sin embargo tras estimulación con TNFα, Meox2 también se expresaba en MLEC CD69$^{-/-}$ (Figura 37). La proteína Cux1 mostraba un comportamiento similar a Meox2 al analizar su expresión en las mismas condiciones, basales y de estimulación (Figura 37).

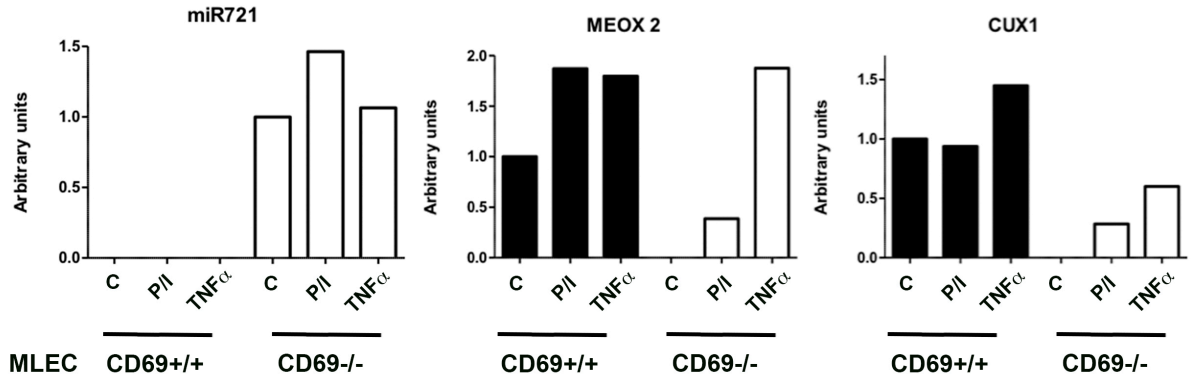

Figura 37. Niveles de expresión de miR-721 y los factores de transcripción Meox2 y Cux1 en MLEC. Análisis por qPCR de la expresión de miR-721, Meox2 y Cux1 en MLECs procedentes de ratones CD69$^{+/+}$ y CD69$^{-/-}$estimuladas o no con PMA+Ionomycin (P/I) o con TNFα. Los valores de expresión de Meox2 y Cux1 se normalizaron con respecto a su expresión en las MLEC CD69$^{+/+}$ no estimuladas, mientras que los niveles de expresión del miR-721 se normalizaron con respecto a la expresión en las MLEC deficientes en CD69, ya que no se encontró expresión en las MLEC CD69$^{+/+}$. Los datos son representativos de dos experimentos diferentes de células endoteliales extraídas de un *pull* de 8 a 10 pulmones de ratón por grupo experimental. En todos los casos la pureza de las células endoteliales de los cultivos se comprobó por FACS, considerando endoteliales las células CD31^{+} CD45.2^{-} y utilizándose únicamente las preparaciones de células con niveles de pureza mayores de 85%.

4.6 ANÁLISIS PROTEÓMICO POR SILAC DE LAS CÉLULAS ENDOTELIALES DE PULMÓN PROCEDENTES DE ANIMALES $CD69^{+/+}$ Y $CD69^{-/-}$

Las diferencias observadas en la neovascularización entre los ratones WT y KO para el gen CD69 en el modelo "Hindlimb Ischemia" y los diferentes patrones de expresión del miR-721 y su diana Meox2 observados en las células endoteliales, nos hace plantearnos, que sería necesario ver las proteínas diferencialmente expresadas entre los ratones WT y los ratones deficientes en CD69, que intervienen en el proceso de angiogénesis. Para abordar este reto decidimos hacer un experimento de marcaje metabolico SILAC (*Stable isotope labeling by/with amino acids in cell culture*). Una vez tengamos las posibles proteínas, dereguladas en el proceso de la angiogénesis, entre los ratones WT y KO para CD69, procederíamos a validarlas por métodos convencionales, como serían la Q-PCR y el WB.

Realizamos el experimento de SILAC como se describe en material y métodos y hemos encontrado 151 proteínas en los experimentos de SILAC y SILAC reverso, de las cuales hay 17 *up-reguladas* y 24 *down-reguladas* en el ratio silac KO/WT, considerando up-reguladas aquellas proteínas que presentan un ratio SILAC superior a 1.5 y down-reguladas las proteínas con un ratio SILAC inferior a 0.65 (Tabla 1).

De las proteínas encontradas, hay proteínas implicadas en diferentes procesos celulares y relacionadas con diferentes orgánulos celulares. Se puede destacar que en los animales KO hay un 59% de proteínas *up-reguladas* relacionadas con el citoesqueleto celular y que participan en funciones como la migración, adhesión, polarización y proyección celular, que son funciones íntimamente relacionadas con los procesos de angiogénesis, ademas hay un 14 % de proteínas, como por ejemplo la proteína Rho GDP-dissociation inhibitor 1, las proteinas con dominios LIM, presentes también en las proteínas con dominios *homeobox* (Cantile et al., 2008; Lisabeth et al., 2013) o la anexina 3 (Pan et al., 2015) que están directamente relacionadas con procesos de angiogénesis o neovascularización (Figura 38A y 38B), también encontramos proteinas up-reguladas relacionadas con la mitocondria, procesos de apoptosis celular y con la respuesta immune. Las proteínas down-reguladas en el KO, el 45% participan en diferentes procesos de metabolismo celular, hay un 19% de proteinas relacionadas con el citoesqueleto celular, pero en este caso intervendrían más en funciones relacionadas con la respuesta immune, tambien hay 19% de proteínas relacionadas con el sistema inmune y sólo un 10% relacionadas con proceso de angiogénesis, entre las que se puede destacar la galectina 3, relacionada con los procesos de migración de las células endoteliales mediante el reclutamiento de receptores de VEGF (Markowska et al., 2011) (Figura 39A Y 39B).

Tabla 1. Resultados del análisis de SILAC. Proteínas obtenidas en el esperimento de SILAC que compara MLEC procendentes de animales KO y WT para CD69. La tabla muestra las proteínas representadas al menos por 2 peptidos en el experimento de SILAC y el SILAC reverso. En Amarillo estan las proteínas up-reguladas o downregulas con ratios de SILAC por encima de 1.5 y 0.7 respectivamente y en rosa las proteínas que están potencialmente up o down reguladas pero en las que sus ratios de SILAC son próximos a los ratios considerados como up o down regulados. En blanco las proteinas que no estan diferencialmente expresadas.

Accession number	Protein Name	SILAC ratio	SILAC RSD	Mascot Score	Nº unique Peptides (ID)	Nº unique Peptides (QT)	Protein Coverage (%)
86476056	serine protease inhibitor A3G*	4,26	4,44	222	7	2	22,3
85861182	retinal dehydrogenase 1	3,64	14,43	97	7	3	16,4
6754706	MARCKS-related protein*	2,60	19,86	70	2	2	14,0
6755300	retinol-binding protein 1	2,49	14,40	119	5	2	40,0
113680348	fascin *	2,01	15,10	50	5	3	17,4
31543942	vinculin *	1,99	19,31	900	39	13	41,4
6755714	transgelin *	1,99	3,91	887	18	7	76,1
158937312	heat shock protein beta-1 *	1,91	13,32	89	5	2	34,0
9790219	destrin *	1,81	5,90	235	3	2	24,8
125347376	filamin-A *	1,66	15,55	1250	60	18	39,6
148747526	ras-related protein Rab-7a	1,65	17,92	316	6	2	40,6
145966915	filamin-B *	1,63	18,31	531	40	11	19,8
157951604	adenylyl cyclase-associated protein 1 *	1,62	14,87	52	2	2	7,4
6756085	zyxin *	1,61	19,88	61	3	2	6,9
7305395	purine nucleoside phosphorylase	1,61	18,90	211	8	5	39,8
83921612	thioredoxin domain-containing protein 5 precursor	1,58	11,65	193	6	3	24,2
15826844	serine (or cysteine) proteinase inhibitor, clade B, member 6b	1,53	17,71	198	7	2	24,9
6755372	40S ribosomal protein S3	1,51	17,31	115	8	3	41,2
6754910	nuclear migration protein nudC	1,49	9,83	62	3	2	11,1
158635992	PDZ and LIM domain protein 1	1,48	19,30	85	5	2	17,7
160707925	annexin A3	1,47	14,02	395	11	5	38,1
31980648	ATP synthase subunit beta, mitochondrial precursor	1,45	19,56	440	12	7	33,6
162461907	stress-70 protein, mitochondrial	1,43	3,39	113	8	2	15,6
47894398	tropomyosin alpha-4 chain	1,43	16,97	1123	16	8	52,0
149258501	PREDICTED: phosphate carrier protein, mitochondrial-like isoform 1	1,43	10,87	62	5	2	13,2
6671507	actin, aortic smooth muscle	1,40	10,69	39	3	3	5,6
6754084	glutathione S-transferase Mu 1	1,36	11,20	273	6	5	38,5
6678483	ubiquitin-like modifier-activating enzyme 1 isoform 1	1,34	22,29	86	9	2	13,8
31982030	rho GDP-dissociation inhibitor 1	1,33	7,37	316	4	2	28,4
21450625	eukaryotic initiation factor 4A-I isoform 1	1,33	14,08	173	7	3	23,9
21704156	caldesmon 1	1,32	15,89	59	11	3	22,5
6671509	actin, cytoplasmic 1	1,31	10,73	730	13	10	49,1
6755114	peroxiredoxin-5, mitochondrial precursor	1,30	6,46	82	4	2	33,3
6680748	ATP synthase subunit alpha, mitochondrial precursor	1,30	10,71	303	15	3	35,1
86198316	protein disulfide-isomerase A4 precursor	1,29	19,89	99	8	2	24,2

30519911	transgelin-2	1,29	19,07	367	13	6	63,8
6753556	cathepsin D precursor	1,28	6,24	87	5	2	13,2
110625979	elongation factor 1-gamma	1,28	6,22	141	9	2	18,1
146260280	heterogeneous nuclear ribonucleoprotein A/B isoform 1	1,27	14,42	237	3	2	11,7
9845257	histone H1.2	1,25	8,38	74	6	2	27,8
227116327	talin-1	1,25	16,14	714	32	6	13,3
9910548	SH3 domain-binding glutamic acid-rich-like protein	1,24	7,73	114	3	2	44,7
61743961	AHNAK nucleoprotein isoform 1	1,24	16,63	99	9	2	6,6
6671664	calnexin precursor	1,23	8,76	124	9	2	19,6
18250284	isocitrate dehydrogenase [NAD] subunit alpha, mitochondrial precursor	1,23	18,69	60	7	2	20,2
22165384	tubulin beta-4B chain	1,23	19,71	197	3	3	25,8
6753322	T-complex protein 1 subunit delta	1,22	20,00	58	7	2	17,3
112293266	heat shock 70 kDa protein 4	1,21	7,43	72	6	2	25,5
225579033	isocitrate dehydrogenase [NADP], mitochondrial precursor	1,20	2,11	156	5	2	18,4
19526818	phosphate carrier protein, mitochondrial precursor	1,20	14,60	86	5	2	19,9
6754994	poly(rC)-binding protein 1	1,19	14,16	110	6	3	25,0
183396771	60 kDa heat shock protein, mitochondrial	1,19	12,88	77	6	2	17,8
6755358	60S ribosomal protein L8	1,19	17,22	59	5	2	25,3
31981302	annexin A6 isoform a	1,18	10,79	235	9	2	19,3
226874906	14-3-3 protein epsilon	1,17	19,86	609	16	8	65,1
6756039	14-3-3 protein theta	1,16	14,24	342	5	2	23,3
114326446	myosin-9 isoform 1	1,15	19,40	773	44	7	25,3
6996913	annexin A2	1,14	19,48	194	8	4	27,7
31982186	malate dehydrogenase, mitochondrial precursor	1,14	19,16	848	11	4	37,9
359279904	tropomyosin alpha-3 chain isoform 3	1,12	11,08	356	10	5	53,2
18017605	ubiquitin-conjugating enzyme E2 N	1,12	19,53	69	2	2	16,4
6756041	14-3-3 protein zeta/delta isoform 1	1,11	18,98	286	8	3	46,1
19745150	NADH-cytochrome b5 reductase 3	1,11	19,19	135	4	2	15,3
84794552	phosphatidylethanolamine-binding protein 1	1,08	7,65	209	4	2	48,1
31543974	14-3-3 protein beta/alpha	1,07	19,80	167	5	12	40,2
45597447	superoxide dismutase [Cu-Zn]	1,06	18,67	87	3	2	29,2
7106439	tubulin beta-5 chain	1,06	16,67	1273	16	8	39,4
31981100	40S ribosomal protein S14	1,05	17,43	104	2	2	31,1
6754036	aspartate aminotransferase, mitochondrial	1,05	2,47	140	6	2	20,2
225543319	transitional endoplasmic reticulum ATPase	1,04	8,97	271	17	3	24,6
163838641	ATP synthase subunit gamma, mitochondrial isoform a	1,03	9,82	105	6	2	28,9
19745150	NADH-cytochrome b5 reductase 3	1,03	19,19	135	4	2	15,3
6678469	tubulin alpha-1C chain	1,02	18,74	1039	12	10	38,1

42415475	protein disulfide-isomerase precursor	1,02	11,69	215	16	3	36,9
6671549	peroxiredoxin-6	1,02	16,49	348	6	2	43,8
227500281	electron transfer flavoprotein subunit alpha, mitochondrial	1,01	12,51	66	4	2	26,4
6679439	peptidyl-prolyl cis-trans isomerase A	1,01	15,92	249	5	3	36,6
70794816	uncharacterized protein LOC433182	0,99	19,12	3189	20	15	53,2
32880197	heterogeneous nuclear ribonucleoproteins A2/B1 isoform 2	0,97	18,29	279	7	4	28,9
112293264	protein disulfide-isomerase A3 precursor	0,97	19,29	465	21	13	50,5
126032329	elongation factor 1-alpha 1	0,97	19,15	518	15	7	35,5
33563282	proteasome subunit alpha type-1	0,97	12,33	57	2	2	15,6
6679587	ras-related protein Rab-1A	0,96	16,39	281	6	2	35,1
15617203	chloride intracellular channel protein 1	0,96	13,70	262	4	3	26,1
40556608	heat shock protein HSP 90-beta	0,96	16,59	2645	18	10	27,5
117938334	spectrin beta chain, non-erythrocytic 1 isoform 2	0,96	7,37	108	13	2	10,3
6755863	endoplasmin precursor	0,95	19,18	1027	20	9	27,2
33859482	elongation factor 2	0,94	14,49	207	20	4	26,3
7305443	60S ribosomal protein L7a	0,93	20,00	168	7	2	32,7
13385942	citrate synthase, mitochondrial precursor	0,93	17,09	92	8	2	19,8
116089273	rab GDP dissociation inhibitor beta	0,92	19,65	285	7	3	24,0
70778976	phosphoglycerate kinase 1	0,91	17,22	575	17	6	52,3
33859640	transaldolase	0,91	16,56	81	6	4	20,2
31981690	heat shock cognate 71 kDa protein	0,90	18,54	1697	27	10	46,0
6679937	glyceraldehyde-3-phosphate dehydrogenase	0,89	18,15	672	12	3	47,1
6678682	galectin-1	0,89	18,54	574	5	3	32,6
6671539	fructose-bisphosphate aldolase A isoform 2	0,88	2,99	377	13	2	36,0
58037267	protein disulfide-isomerase A6 precursor	0,88	15,42	1213	9	3	31,2
6679078	nucleoside diphosphate kinase B	0,87	5,74	72	4	2	27,0
31982520	long-chain specific acyl-CoA dehydrogenase, mitochondrial precursor	0,86	8,93	120	6	2	18,8
31543976	14-3-3 protein gamma	0,86	19,78	110	3	3	36,8
6755040	profilin-1	0,85	16,43	1214	6	3	66,4
226958349	triosephosphate isomerase	0,85	14,98	733	7	5	36,1
293597567	fructose-bisphosphate aldolase A isoform 1precursor	0,85	16,24	749	13	3	37,1
84875537	nucleolin	0,85	16,05	26	6	2	14,1
6679961	myotrophin	0,83	19,04	83	2	2	22,0
6754524	L-lactate dehydrogenase A chain isoform 1	0,83	16,50	269	12	5	35,2
6752954	actin, cytoplasmic 2	0,82	15,67	3712	18	15	55,7
377833208	PREDICTED: protein disulfide-isomerase A6	0,81	19,32	1007	10	4	32,7
256000782	tropomyosin alpha-1 chain isoform 2	0,80	11,77	121	6	2	23,6

6680924	cofilin-1	0,79	19,76	132	5	3	44,0
51491845	clathrin heavy chain 1	0,79	11,01	134	14	2	12,5
6754254	heat shock protein HSP 90-alpha	0,78	11,02	1614	5	2	19,6
6753060	annexin A5	0,78	16,66	608	15	9	49,5
114326546	phosphoglycerate mutase 1	0,78	16,05	176	7	2	35,5
21313162	ras-related protein Rab-1B	0,78	17,07	207	2	2	37,3
6753036	aldehyde dehydrogenase, mitochondrial precursor	0,78	11,90	296	10	2	15,8
58037267	protein disulfide-isomerase A6 precursor	0,77	15,42	1213	9	3	31,2
31982755	vimentin	0,76	16,71	296	18	6	49,6
9845265	ubiquitin-60S ribosomal protein L40	0,76	17,32	48	2	2	36,7
70778915	moesin	0,75	19,14	478	22	6	43,0
6756037	14-3-3 protein eta	0,74	2,67	189	3	2	30,5
14192922	actin, alpha cardiac muscle 1	0,74	17,57	2200	5	4	48,8
19527028	vigilin	0,73	18,56	46	8	2	19,5
31981562	pyruvate kinase isozymes M1/M2 isoform 1	0,72	19,86	881	20	11	44,6
6678097	serpin B6 isoform b	0,70	13,64	98	4	2	13,2
6680836	calreticulin precursor	0,70	18,59	106	7	4	20,2
254540027	malate dehydrogenase, cytoplasmic	0,67	3,64	75	5	2	21,9
33859662	synaptic vesicle membrane protein VAT-1 homolog	0,67	10,27	155	7	2	17,7
254540166	78 kDa glucose-regulated protein precursor	0,66	18,06	1698	30	13	49,3
31543113	plastin-2	0,66	3,38	369	23	2	42,6
12963511	40S ribosomal protein S19	0,63	8,88	57	5	4	38,6
33563236	rho GDP-dissociation inhibitor 2	0,63	20,93	250	4	3	30,0
19526878	pyrroline-5-carboxylate reductase 2	0,62	21,05	73	4	2	11,9
6754696	macrophage migration inhibitory factor	0,61	10,58	307	2	2	15,7
255003735	60S ribosomal protein L10a	0,61	1,81	43	5	2	29,0
28372479	40S ribosomal protein S25	0,60	14,77	75	4	2	33,6
160707956	annexin A7	0,58	7,87	124	3	2	8,0
21361209	histone H4	0,57	6,34	145	5	2	50,5
10946870	alcohol dehydrogenase [NADP(+)]	0,57	19,78	102	8	2	40,6
124486895	6-phosphogluconate dehydrogenase, decarboxylating	0,56	15,79	405	8	3	32,1
309267832	PREDICTED: 60S ribosomal protein L5-like	0,55	12,70	92	3	2	16,7
6754450	fatty acid-binding protein, epidermal	0,54	9,28	110	4	2	26,7
9256624	phosphoglycerate mutase 2	0,51	6,28	66	2	2	8,7
124517663	annexin A1	0,48	15,58	653	11	3	47,7
31981273	cytosolic non-specific dipeptidase	0,47	15,68	264	8	3	22,9
110227377	macrophage-capping protein isoform 2	0,45	12,22	227	6	5	21,8
6754976	peroxiredoxin-1	0,42	15,07	719	13	6	52,3
33859580	galectin-3	0,39	8,72	156	5	2	26,5
161016799	annexin A4	0,37	17,77	303	8	2	39,2
10946574	creatine kinase B-type	0,31	18,94	159	2	2	6,8

4.7. Análisis funcional in silico de las proteínas obtenidas por SILAC

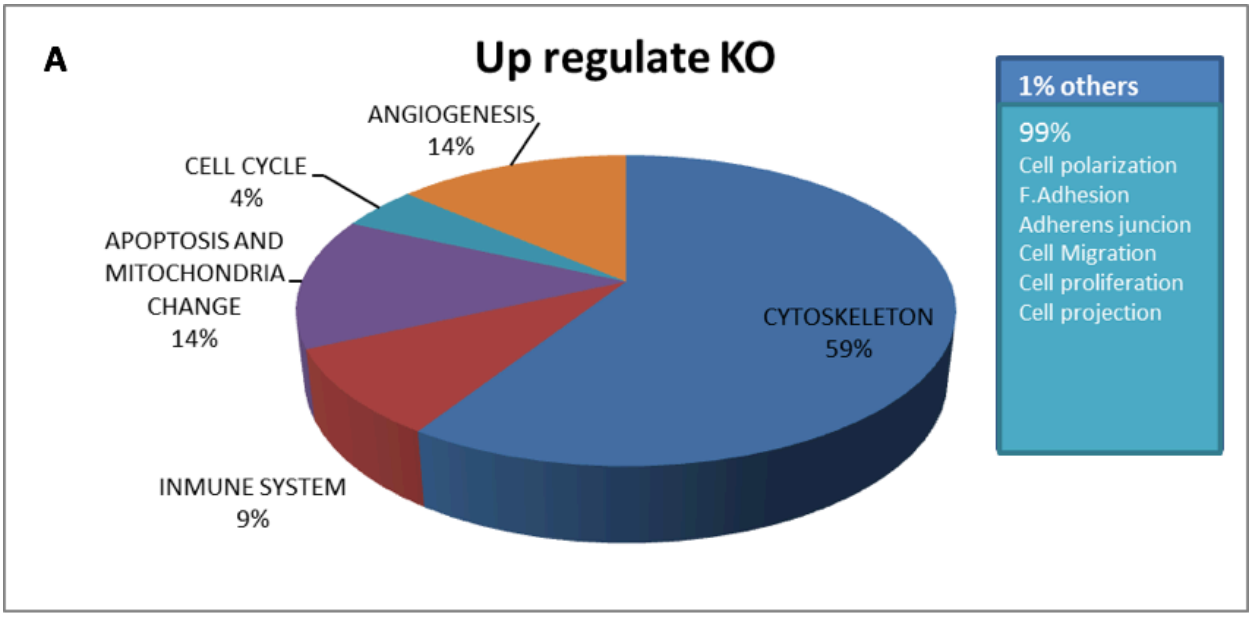

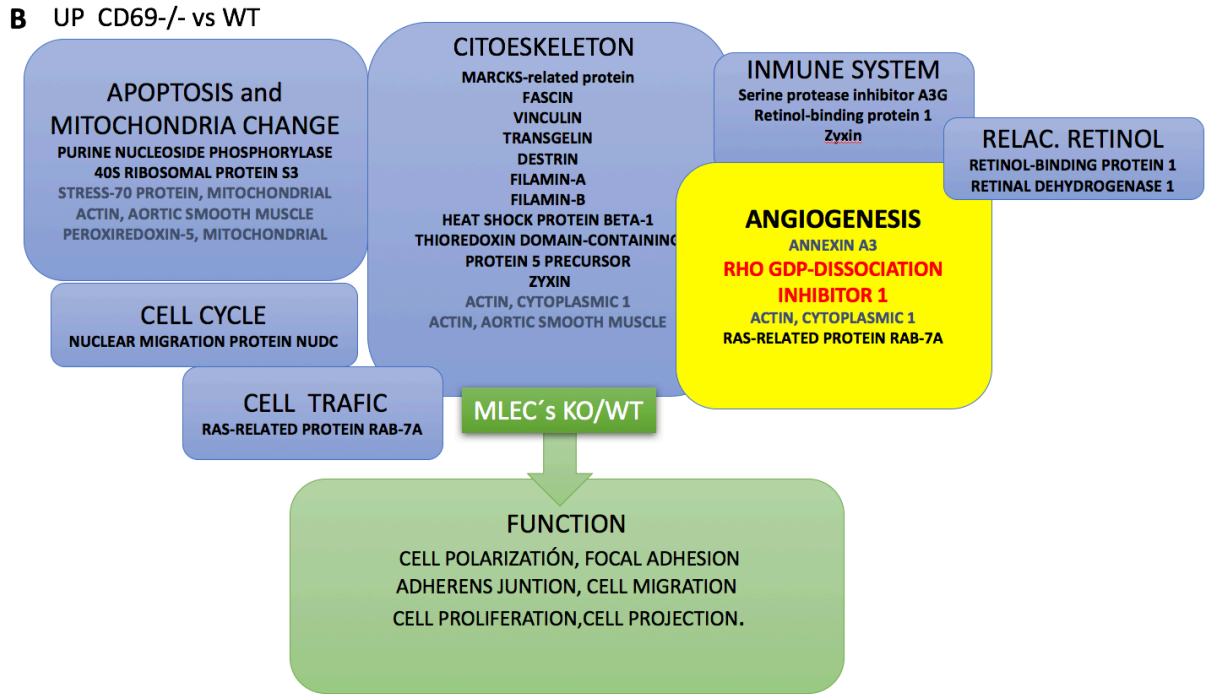

Figura 38. Resultados experimento de SILAC. Proteínas up-reguladas. (A) Analisis de las proteínas obtenidas mediante el experimento de SILAC agruclasificadas por las diferentes funciones que realizan en la célula y cuantificadas en función del porcentaje total de proteínas diferencialmente expresadas en las células endoteliales KO frente a las WT. Proteínas upreguladas en MLEC KO con respecto a las MLEC WT. **(B)** Esquema detallado de las proteínas up-reguladas en las MLEC KO frente a las WT en el que se muestran los procesos celulares en los que participan o están relacionadas y las funciones que realizan en dichos procesos.

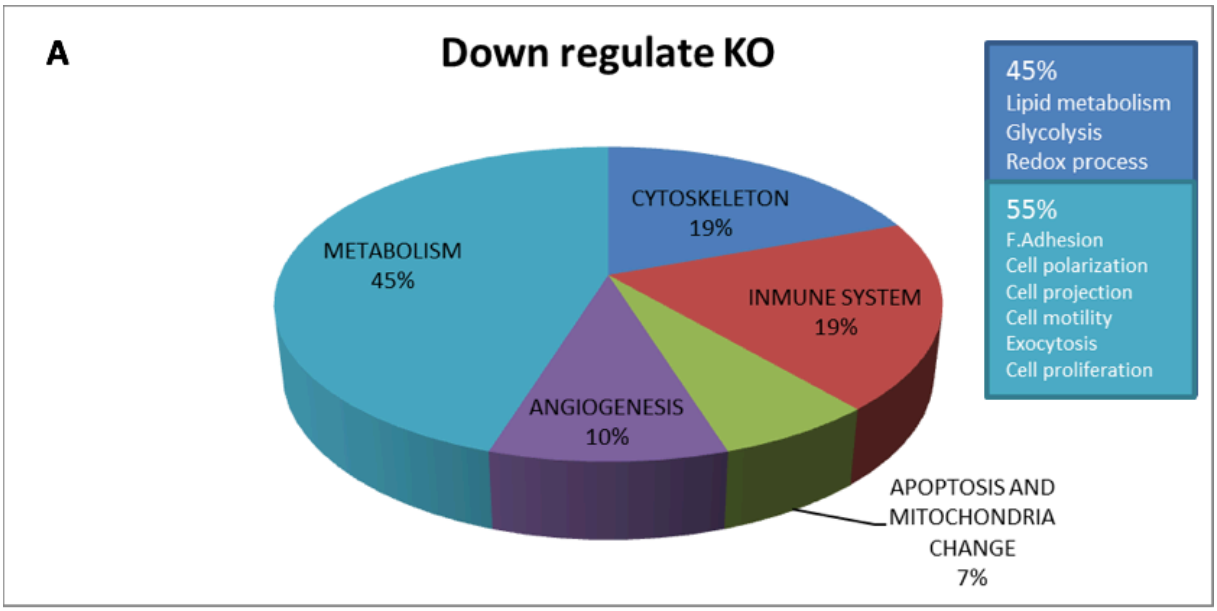

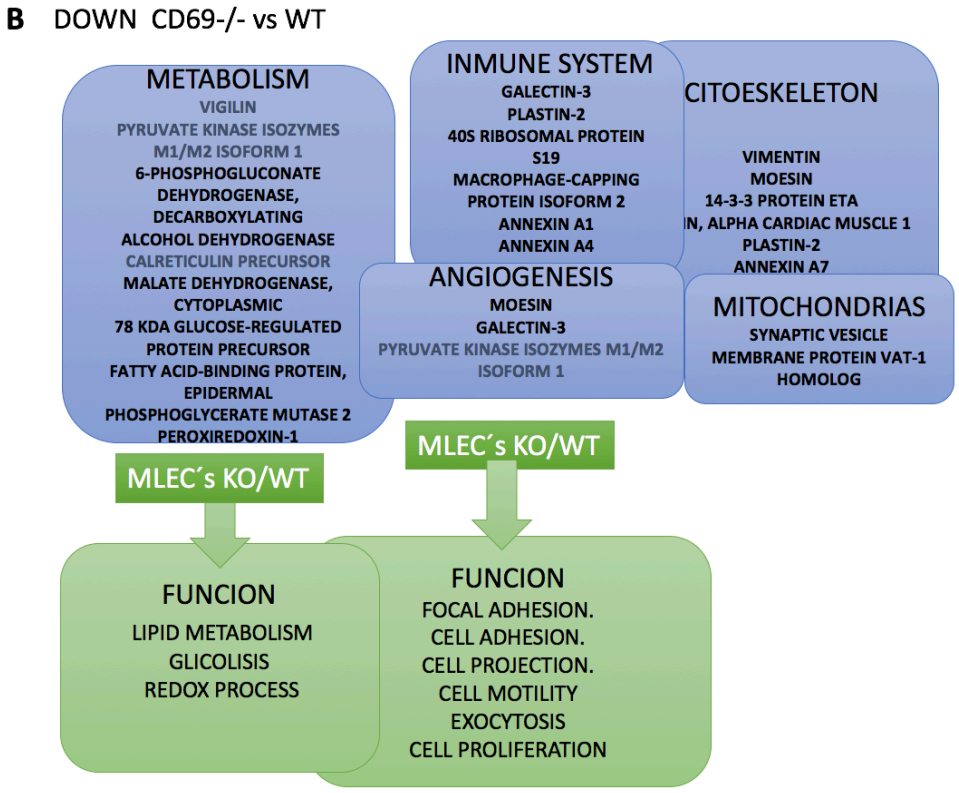

Figura 39. Resultados experimento de SILAC. Proteínas down-reguladas. (A) Analisis de las proteínas obtenidas mediante el experimento de SILAC clasificadas por las diferentes funciones que realizan en la célula y cuantificadas en función del porcentaje total de proteínas diferencialmente expresadas en las células endoteliales KO frente a las WT. Proteínas downreguladas en MLEC KO con respecto a las MLEC WT. **(B)** Esquema detallado de las proteínas down-reguladas en las MLEC KO frente a las WT en el que se muestran los procesos celulares en los que participan o están relacionadas y las funciones que realizan en dichos procesos.

4.8 LA ACTIVACIÓN DE LA VÍA AKT/HIF1α PARTICIPA EN EL PROCESO DE NEOVASCULARIZACIÓN POST-ISQUEMIA EN LOS ANIMALES DEFICIENTES EN CD69

Entre las proteínas up-reguladas en las células endoteliales de ratones deficientes en CD69 hemos encontrado la proteína *Rho GDP disociation factor 1* (Rho GDI 1) que inhibe la actividad de la proteína RhoA, impidiendo la disociación de la mólecula GDP de RhoA y, por lo tanto, que esta proteína esté activa para ejercer su función interaccionando con la proteína ROCK1 (Montalvo et al., 2013). Por lo tanto, Rho GDI 1 produce la degradación de RhoA y una acumulación en el citoplasma de la proteína ROCK1 en un pool inactivo, favoreciéndose la activación de la vía de AKT (Lisabeth et al., 2013). La activación de la ruta de AKT induce incremento de la proteína HIF1α, que favorece el incremento de la neovascularización. Para comprobar esta hipótesis analizamos por WB algunas de las proteínas implicadas en esta vía de activación que podrían estar implicadas en los procesos de neo-vascularización post-isquemia observados anteriormente. Hemos realizado WB de lisados de músculo de animales WT y deficientes en CD69, sometidos a isquemia de la extremidad posterior izquierda, comparando los niveles de expresión de las diferentes proteínas entre animales WT y KO para CD69 y entre la extremidad isquémica y no isquémica, 7 días después de la isquemia. Hemos encontrado una disminución de la proteína RhoA activada en los animales $CD69^{-/-}$ tanto en la extremidad isquémica como en la no isquémica, que se correlaciona con un acumulo de la quinasa ROCK1 en su forma inactiva (Figura 40A). La acumulación de ROCK1 inactivo conduce a un incremento de la activación/fosforilación de AKT y por tanto un incremento de la expresión de la proteína HIF1α en el tejido muscular de animales $CD69^{-/-}$ (Figura 40B), que podría explicar porqué observamos una revascularización más rápida en los animales deficientes en CD69 (Figura 33). Además, la inactivación de la proteína ROCK1 favorece la activación de las proteínas del citoesqueleto que pueden actuar como adaptadores reclutando otras proteínas como las kinasas al citoesqueleto, como la proteína kinasa 1 con dominios PDZ y LIM (*PDZ and LIM domain protein 1*: PDLIM1) que encontramos up-regulada en el SILAC en las MLEC $CD69^{-/-}$ (Tabla 1)$^{-}$. Las PDLIM1 interaccionan entre otras, con los receptores tipo efrina promoviendo la angiogénesis, ya que impiden la endocitosis de los receptores de VEGF (Lisabeth et al., 2013) activando esta vía y por lo tanto la activación de genes implicados en generación de nuevos vasos.

Recientemente se ha publicado que la molécula $S1P_1$, cuya expresión está upregulada en los animales deficientes en CD69 ya que esta molécula media la expresión de $S1P_1$ en la membrana, es capaz de inducir la vía de AKT/mTORc y activar la expresión de HIF1α, que conduciría a aumentar la angiogénesis en procesos de isquemia (Labiano and I., 2017). Los tejidos isquémicos y no isquémicos de $CD69^{-/-}$

presentan en efecto una mayor expresión de receptores $S1p_1$ así como la activación sostenida de la fosforilación de AKT y de expresión de HIF1α (Figura 40B). La expresión aumentada en condiciones basales podría indicar que estas vías están constitutivamente activadas en estos animales. Además el proceso es específico de $S1P_1$ ya que los niveles de otro receptor de la misma familia, el $S1P_3$ no están significativamente modificados en el proceso (Figura 40C). La endoglina, que también se encuentra elevada en los músculos de los animales deficientes para CD69 (Figura 40A), también podría estar activada a través de las PDLIM1. La endoglina es capaz de fijar PI3K a la membrana celular y mantener activada la vía de AKT promoviendo la formación y fijación de nuevos capilares. (Lee et al., 2012). En definitiva, estos datos preliminares parecen indicar que la mayor capacidad de regenerar el tejido vascular que presentan los animales deficientes en CD69 podría estar mediada por una mayor activación de la ruta PI3K/AKT, que a partir de diferentes mecamismos como el incremento de la expresión de HIFα o la inhición de la activación de las GTPasas RhoA/ROCK1 conduce a la activación de los mecanismos de angiogénesis. Además, todos los procesos descritos implican cambios en el citoesqueleto celular, que favorecen tanto la fijación de determinados tipos de proteínas en la membrana celular como el tráfico celular de diferentes proteínas y metabolitos para ejercer su función. Todos estos datos se correlacionan con los resultados obtenidos en el análisis proteómico del experimeto de SILAC, en los 59% de las proteínas diferencialmente expresadas y up-reguladas en las células endoteliales $CD69^{-/-}$, están relacionadas con el citoesqueleto, por lo que sería necesario un examen más exaustivo de los resultados obtenidos para comprender mejor el proceso de neo-vascularización en los animales deficientes en CD69.

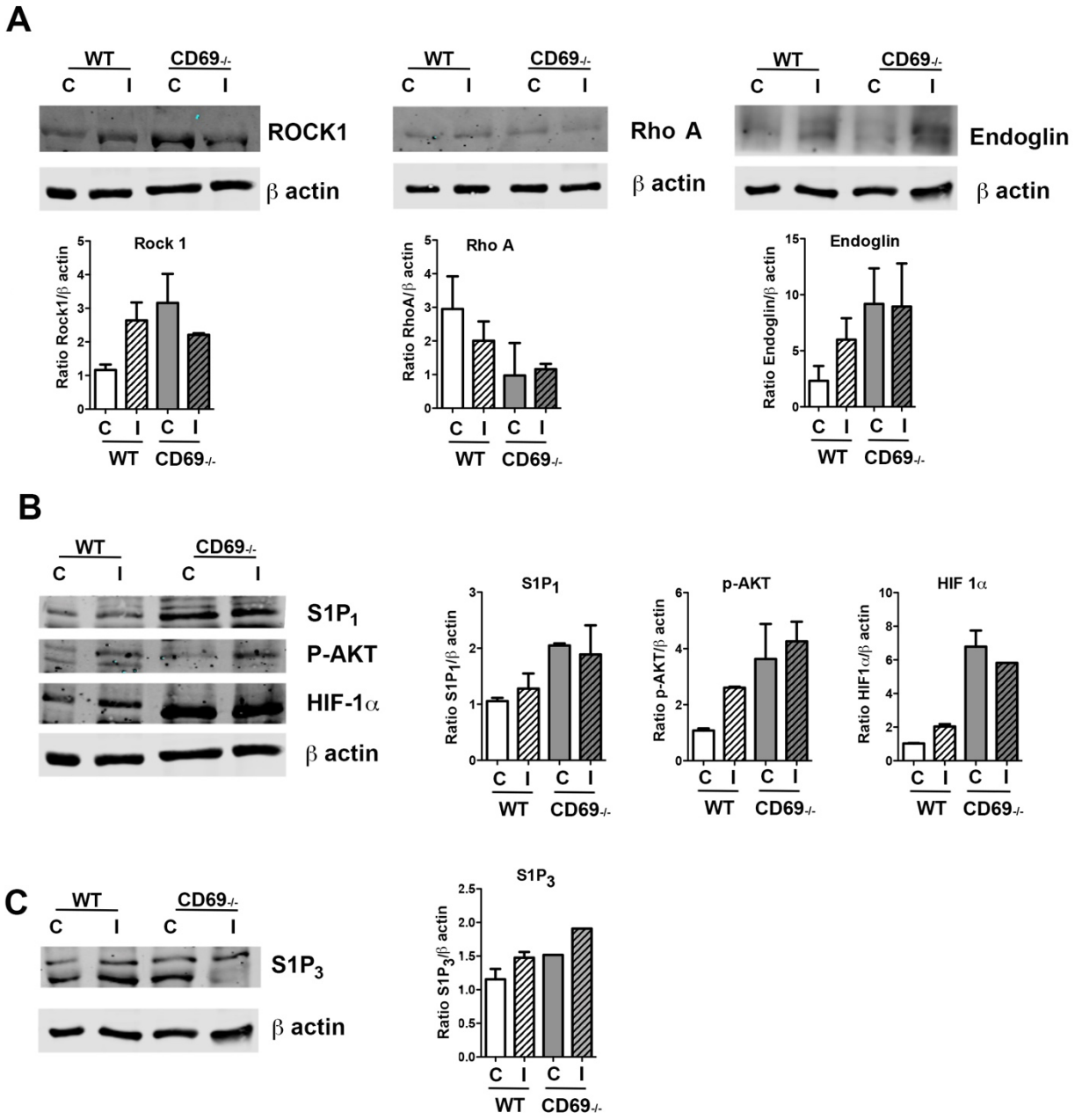

Figura 40. Las kinasas RhoA/ROCK1 intervienen en el proceso de neo-vascularización mediante el mantenimiento de la activación de la vía AKT/HIF1α. (A) WB representativos de las proteínas RhoA, ROCK1 y Endoglina en los músculos aductores procedentes de la extremidad control (C) y de la extrewmidad isquémica (I) de ratones WT o defiecientes en CD69 (arriba), cuantificación de las bandas de proteína, procedentes de al menos 4 músculos diferentes de cada tipo y normalizadas frente a β-actina (abajo). **(B)** WB representativos que muestran la ruta de activación de la proteína AKT anteriormente descrita con las proteínas $S1P_1$, P-AKT y HIF1α (izquierda). Cuantificación de las bandas de proteína, procedentes de al menos 4 músculos diferentes de cada tipo y normalizadas frente a β-actina (derecha)**. (C)** WB representativo de la proteína $S1P_3$, y su cuantificación, normalizada frente a β-actina.

IV. DISCUSIÓN

IV DISCUSIÓN

1. CD69 COMO MOLÉCULA INMUNOMODULADORA EN PROCESOS INFLAMATORIOS TANTO FISIOLÓGICOS COMO PATOLÓGICOS

En los últimos años, diversos estudios con animales deficientes en CD69 han puesto de manifiesto el papel de esta molécula en la modulación de la inflamación. La falta de CD69 en el comportamiento linfoide incrementa la inflamación en modelos animales como la artritis inducida por colágeno, el asma alérgica, la dermatitis de contacto, la miocarditis autoinmune o la colitis (Cruz-Adalia et al., 2010; Martin et al., 2010b; Radulovic et al., 2012; Radulovic et al., 2013; Sancho et al., 2003). Todos estos modelos animales desarrollados para el estudio de diferentes procesos patológicos cursan con un incremento de la población de linfocitos Th17, que está exacerbado en los animales deficientes en CD69. Además, estudios a nivel molecular demuestran que esta proteína, mediante la activación de vía de señalización Jak3/STAT5, inhibe la diferenciación de las células Th17 y favorece la activación de las células Treg, las cuales frenan la respuesta inflamatoria mediada por las células Th17 (Cortes et al., 2014; Martin et al., 2010a; Martin and Sanchez-Madrid, 2011). Por tanto, se puede considerar a CD69 como un regulador negativo de la inflamación mediada por células T, regulando el balance entre los linfocitos T reguladores y los linfocitos Th17 en procesos fisiológicos y patológicos (Martin and Sanchez-Madrid, 2011).

1.1 PAPEL DE CD69 EN ENFERMEDADES QUE CURSAN CON PROCESO FIBROPROLIFERATIVOS

En este trabajo se ha explorado el papel de CD69 en enfermedades que cursan con procesos fibro-proliferativos, como la fibrosis peritoneal inducida por un proceso de diálisis, y que hasta ahora nunca habían sido estudiadas en animales deficientes en CD69, así como en quimeras hematopoyéticas que expresan o no CD69 únicamente en el compartimento linfoide. Esto junto con los experimentos en los que se han bloqueado con anticuepos la expresión de CD69 en la membrana de la célula, ha permitido afirmar que CD69 modula la fibrosis peritoneal, a través de la regulación del balance de las poblaciones Th17/Treg. También se ha demostrado que la uremia contribuye modestamente al proceso fibro-proliferativo en la membrana peritoneal, siendo igualmente la molécula CD69 moduladora de la inflamación y posterior fibrosis en condiciones urémicas. A pesar de los hallazgos en modelos animales,

el efecto de la uremia en el peritoneo de los seres humanos es controvertido y la posible contribución de la uremia a la alteración de la de la PM, sigue siendo un tema sometido a debate

Los datos obtenidos muestran que la deficiencia de CD69 o el bloqueo de CD69 produce un aumento exacerbado de la fibrosis peritoneal en respuesta al PDF. Este resultado se correlaciona con el infiltrado inflamatorio y la hiperactivación local de las células Th17. Por el contrario, las respuestas mediadas por Th1 o Th2 parecen tener poca o ninguna relevancia en la fibrosis inducida por la dialysis peritoneal. El aumento de la fibrosis peritoneal en ratones $CD69^{-/-}$ se asocia con un aumento del ratio Th17/Tregs, que es causado por un aumentó de células Th17 en lugar de una disminución de Tregs. Se ha descrito que más importante que la proporción relativa de células Treg, es su actividad funcional, para lo que es necesaria la expresión de la molécula CD69 en éstas células, en la homeostasis inmune y en la modulación de la inflamación (Martin and Sanchez-Madrid, 2011). Por lo tanto, se puede especular que CD69 controla la fibrosis en el peritoneo limitando las respuestas Th17 y regulando la función de las células Treg. Los resultados obtenidos en este estudio han mostrado que los cambios peritoneales inducidos por la exposición a PDF, no sólo es exacerbada en tamaño sino también acelerada en los ratones $CD69^{-/-}$, y que la inflamación precede al proceso fibrótico. Los resultados indican claramente que la inflamación impulsa el proceso de fibrosis en la PM después de la exposición a PDF, y que éste proceso está desregulado en ratones $CD69^{-/-}$. Se ha observado que TGF-β esta up-regulado en la cavidad peritoneal de ratones $CD69^{-/-}$ expuestos a PDF. Esta citoquina juega un papel central en la diferenciación de los linajes Th17 y Treg. La exposición al TGF-β inclina a los linfocitos CD4 *naive* hacia el linaje Treg, mientras que la combinación de TGF-β e IL-6 hace que los progenitores adopten un papel Th17. La IL-6 en estos experimentos se indujo rápidamente en la cavidad peritoneal de ratones $CD69^{-/-}$ expuestos a PDF, y se mantuvo elevada durante los 40 días que duró el tratamiento. Esto podría explicar la fuerte polarización local hacia la diferenciación a linfocitos Th17 en respuesta a la exposición a PDF. En conclusión, los resultados demuestran que CD69 modula la respuesta inflamatoria mediada por Th17 incrementando la fibrosis peritoneal. Estos datos mejoran nuestra comprensión de los procesos fibróticos y podrían ayudar en el diseño de abordajes terapéuticos para prevenir los procesos fibro-proliferativos.

1.2 EL MANTENIMIENTO DE LA TOLERANCIA INMUNE MEDIADA POR LOS LINFOCITOS TREG FOXP3$^+$ REQUIERE LA EXPRESIÓN DE CD69

Se han descrito numerosas poblaciones de células Treg en función de los marcadores que expresan en su membrana, además de la población de células Treg CD4$^+$FoxP3$^+$CD25^{high}, se han caracterizado una población de células Treg humanas que expresan un péptido asociado a TGF-β (LAP, *latency-associated peptide*) en su membrana, y que no expresan FoxP3 pero sí el receptor tipo II de TGF-β y CD69. Asimismo, estas células son capaces de secretar IL-8, IL-9, IL-10, IF-γ y TGF-β y tienen capacidad supresora *in vivo* mediada por IL-10 y TGF-β (Gandhi et al., 2010). También hay Treg humanas que se que se encuentran localizadas en órganos linfoides secundarios y que tienen un fenotipo anérgico en comparación con las que se encuentra en sangre y médula ósea. La mayoría de las Treg de órganos linfoides secundarios Treg CD4$^+$ CD25$^+$ CD127$^-$ FoxP3$^+$, son también CD69$^+$ CD45RA$^+$, lo que las convierte en células Treg activadas policlonalmente, con similar función supresora pero que producen IL-2 y tienen mayor capacidad proliferativa *ex vivo* (Petersen et al., 2011). Además, también se ha demostrado recientemente que los donantes sanos con una población de células Treg CD69$^+$ NKGD$^+$ LAP$^+$ que expresan TGF-β e IL-10, tienen una capacidad supresora muy elevada, impidiendo fuertemente la activación y diferenciación de las células T-efectoras (Vitales-Noyola et al., 2015).

En este trabajo se ha identificado un tipo de células Treg que expresan CD69 constitutivamente en condiciones homeostáticas e inflamatorias, con mayor potencial supresor que las células Treg clásicas FoxP3$^+$. Estos datos son consistentes con la evidencia previa de que una población de timocitos con alta expresión de CD69 es la precursora de las células tTregs en humanos (Martin-Gayo et al., 2010). La población de Treg periféricas CD69$^+$ difiere de las Tregs CD69$^-$ en los niveles basales de expresión de marcadores como CD25, CTLA-4, ICOS, CD38 o GITR (Josefowicz et al., 2012). Las células tTregs FoxP3$^+$ CD69$^+$ es la población más efectiva a la hora de suprimir la proliferación de las células *Tconvs*, y la *down-regulation* del receptor CD69, mediante el tratamiento con anticuerpos bloqueantes de CD69, inhiben su potencial supresor, lo que indica que las células Tregs funcionales expresan constitutivamente CD69. Los resultados obtenidos indican que las Treg CD69$^+$ es la población con función supresora dentro del conjunto de las Tregs CD4$^+$ CD25$^+$ FoxP3$^+$. Sin embargo, también se ha descrito en diferentes modelos animales, sub-poblaciones de Tregs CD69$^+$ inducibles procedentes de poblaciones de Treg CD4$^+$ CD25$^-$ FoxP3$^-$, que expresan CD69 en su membrana tras la activación con OVA administrado por vía oral (Radulovic et al., 2012), o 2,4,6-trinitro-1-clorobenceno (Ring et al., 2010), después de la migración a órganos linfoides (Lieberman et al., 2012) o después de la inducción de tumores (Han et al., 2009). Estas Tregs ejercen su función principalmente a través de TGF-β1 unido a membrana mediante el péptido LAP.

El factor de transcripción FoxP3 ha sido postulado como marcador específico de linaje para Tregs; sin embargo, los datos son contradictorios, ya que algunos grupos definen a las Treg FoxP3^{+} como una población supresora (Kretschmer et al., 2005), y otros grupos definen una función supresora incompleta en esta población (Allan et al., 2007; Hill et al., 2007; Mucida et al., 2007). Los datos de este estudio revelan que, dentro de la población las células FoxP3^{+}, las células que expresan CD69 son las que tienen función supresora más potente, lo cual se ha demostrado mediante experimentos *in vitro* e *in vivo*. La regulación de la respuesta inmune a antígenos aéreos es fundamental para mantener la tolerancia inmune en los pulmones y la prevención de la enfermedad inflamatoria de las vías respiratorias (Bilate and Lafaille, 2012). En un trabajo previo en este grupo de investigación, se demostró que la expresión de CD69 en las células T efectoras regula negativamente las respuestas inflamatorias dirigidas por células Th2 y Th17 asociadas a asma alérgica y dermatitis de contacto (Martin et al., 2010b). Sin embargo, el papel de CD69 en el mantenimiento de la tolerancia pulmonar mediante el control de la función supresora de las células Treg, no se había explorado antes. Las células Treg son fundamentales para el mantenimiento de la tolerancia en las mucosa, y los defectos en el desarrollo o función de estas células, conducen a una inflamación de las vías respiratorias como las que cursan en enfermedades como las alergias y el asma (Curotto de Lafaille et al., 2008; de Heer et al., 2004; Mucida et al., 2005). Nuestros estudios con un modelo de tolerancia pulmonar muestran que las células Treg CD69$^{-/-}$ tienen un potencial disminuido para suprimir respuestas inflamatorias frente a antígenos específicos, lo que indica que la función supresora de las células Treg CD69$^{-/-}$ está afectada. Además, los experimentos de *adoptive tranfer* demuestran inequívocamente, que sólo la población de células Treg FoxP3^{+} CD69^{+}, es capaz de mantener la auto tolerancia en ratones CD69$^{-/-}$.

A pesar de que se han propuesto diversos mecanismos por los cuales las células Treg ejercen su función supresora, en este trabajo se ha demostrado que las células Tregs necesitan expresar CD69 para mantener la tolerancia inmune. Los resultados han demostrado que CD69 es una diana molecular clave para prevenir el desarrollo de la inflamación, mediante el control de la función supresora de las células Treg. La identificación de esta nueva población de Tregs CD69^{+}, abre el camino hacia el desarrollo de nuevas estrategias de aislamiento de células Treg con fines terapéuticos, enfocados a tratar enfermedades inflamatorias y autoinmunes crónicas.

1.3 CD69 CONTROLA LA DIFERENCIACIÓN DE LAS CÉLULAS TREG FOXP3$^+$ EN EL TIMO MEDIANTE LA EXPRESIÓN DE BIC/MIR-155

La implicación del microRNA 155 y su promotor BIC en el desarrollo de las células T reguladoras del timo (tTreg) FoxP3$^+$ está muy estudiada, contribuyendo al mantenimiento de la homeostasis de las células Treg y al control de la inflamación en procesos patológicos. Sin embargo, la vía de activación del miR-155 que conduce a la diferenciación de las células tTreg no se conoce. El hecho de que datos previos en humano que muestran que una población de linfocitos CD4$^+$, que expresa altos niveles de CD69 en el timo, es la que se diferencia a células tTreg (Martin-Gayo et al., 2010), junto con el hecho de que la expresión de CD69 sea fundamental para que las células Treg puedan ejercer su función supresora, genera la pregunta de si esta molécula interviene también en la diferenciación y homeostasis de las células Treg.

En éste estudio se ha mostrado que CD69 desempeña un papel clave en el desarrollo y la homeostasis de Tregs. Utilizando un modelo genético combinado de animales reportero Foxp3-mRFP$^+$ y CD69$^{-/-}$ y aproximaciones experimentales para la inhibición genética de ambas moléculas CD69 y miR-155, se ha demostrado que la activación de la vía CD69 promueve la fosforilación de STAT5, la expresión de BIC/miR-155, y la inhibición SOCS1. El papel de CD69 cómo regulador negativo de el sistema inmunitario, ha sido un tema controvertido durante los últimos años (Gonzalez-Amaro et al., 2013). Sin embargo, estudios muy recientes realizados por grupos independientes muestran que CD69 desempeña un papel crucial en la función supresora de Tregs murinas y humanas, así como en la generación de células Treg inducidas *in vitro* (Cortes et al., 2014; Lin et al., 2015; Radulovic et al., 2012; Wirnsberger et al., 2009). Sin embargo, el papel específico de CD69 en el desarrollo de las células Tregs en el timo hasta ahora no se había explorado.

Uno de los factores importantes que han limitado el estudio del papel de CD69 en la diferenciación de las células Treg, es el hecho de la salida de los linfocitos de los órganos linfoides, y en particular del timo, a la periferia (Feng et al., 2002; Matloubian et al., 2004; Nakayama et al., 2002; Weinreich and Hogquist, 2008). Aunque los procesos de selección de células T positivos y negativos del timo no se ven afectados por la deficiencia de CD69 (Lauzurica et al., 2000), esta molécula controla la salida de células T maduras a la periferia mediante la regulación negativa de los receptores $S1P_1$ (Matloubian et al., 2004; Shiow et al., 2006), por lo que se hace difícil analizar, qué parte de las diferencias observadas en el proceso de desarrollo de las células tTreg se debe a la presencia o ausencia de CD69, o a una mayor migración de células Treg maduras a la periferia, proceso mediado igualmente por CD69. En esta tesis, se ha

conseguido salvar el obstáculo derivado de los diferentes potenciales migratorios de las células CD69^{+} y CD69^{-}, mediante la realización de cultivos FTOC con lóbulos de timo de ratones reportero Foxp3-mRFP^{+}, y el estudio de la diferenciación de tTregs en ratones quiméricos. Se ha demostrado en ambos casos, que la expresión de CD69 es fundamental para el desarrollo de tTreg, ya que no se encuentran casi células Treg en cultivos FTOC de timos embrionarios procedentes de animales CD69$^{-/-}$ o de animales WT tratados con el anticuerpo 2.2. En las quimeras mixtas de médula ósea, prácticamente no se diferenciaron células Treg provenientes de precursores de CD69^{-}. En ambos sistemas, el número total de células dentro del timo no cambió, mientras que las proporciones de tTregs originadas a partir de precursores de CD69$^{-/-}$ estuvieron siempre disminuidas, lo que demuestra inequívocamente que éste efecto no se debe a un comportamiento migratorio diferente, si no a una defecto en la diferenciación de células Treg CD69^{-}. Se ha encontrado que pTregs Foxp3^{+} también están disminuidas en el bazo y ganglios linfáticos de ratones reportero Foxp3-mRFP^{+}/CD69$^{-/-}$ adultos en comparación con animales reportero CD69$^{+/+}$ y CD69$^{+/-}$ hermanos de camada. Además, las pTregs deficientes en CD69 tienen su función supresora defectuosa (Cortes et al., 2014). Por tanto, los defectos observados en los precursores deficientes en CD69 afectan tanto al desarrollo de tTreg cómo a la homeostasis de pTreg, lo que indica de manera clara que los precursores que expresan CD69 dan lugar a la población de pTreg CD69^{+} funcionalmente activas. En este sentido, existen diversos estudios que demuestran mediante dos enfoques diferentes en ratones y un estudio en humanos, que la expresión de CD69 en pTregs se requiere para mantener la tolerancia inmunológica. La deficiencia de CD69 en ratones compromete la colitis inducida por linfocitos T y el establecimiento de tolerancia oral después de exposición a antígeno (Radulovic et al., 2012); y las pTreg que expresan CD69^{+} son esenciales para la prevención de reacciones asmáticas a antígenos inofensivos (Cortes et al., 2014). Además, una población de Tregs CD69^{+} en la sangre de donantes humanos sanos, parece tener un importante papel inmuno-regulador (Vitales-Noyola et al., 2015).

La molécula CD69 interactúa con las proteínas Jak3/STAT5 de manera independiente a la vía de IL-2, inhibiendo así las respuestas de Th17 (Martin et al., 2010a) y controlando el potencial supresor de pTregs (Cortes et al., 2014). La fosforilación de STAT5 activa el factor de trascripción Foxp3, induciendo el desarrollo de tTreg (Burchill et al., 2008). Además, Foxp3 se une a un intrón dentro de la región promotora del gen BIC, favoreciendo la trascripción de miR-155 (Zheng et al., 2007). Los ratones miR-155 $^{-/-}$ y BIC$^{-/-}$ presentan un número de Treg Foxp3^{+}, inferior a los niveles encontrados en el timo y en los órganos linfoides secundarios de ratones WT, indicando un papel esencial de miR-155 en el desarrollo de Treg Foxp3^{+} (Kohlhaas et al., 2009; Lu et al., 2009). Se ha explorado la vía Jak3 /STAT5 por presentar

puntos comunes con los mecanismos de activación mediados por CD69 y por el miR-155, pudiendo ser ésta la responsable de los defectos observados en desarrollo de Treg en ratones deficientes en CD69. En este estudio se ha encontrado una fuerte inhibición de la fosforilación STAT5 en Treg Foxp3-mRFP^{+} CD69^{-} en comparación tTregs CD69^{+}. Además, los niveles de transcripción de BIC/miR-155 se reducen en Treg Foxp3-mRFP^{+} CD69^{-} en concordancia con estos datos; la diana del miR-155, SOCS1 está up-regulada a nivel de mRNA y de proteína. En un modelo de ratón en el que se sobreexpresa SOCS1, disminuye la fosforilación de STAT5 y se reduce la proporción de timocitos Foxp3^{+} a niveles similares a los observados en ratones miR-155$^{-/-}$ (Lu et al., 2009). El miR-155 inhibe la expresión de SOCS1, y favorece el desarrollo de tTreg Foxp3^{+} (Lu et al., 2009). Los resultados demuestran que la expresión de CD69 favorece la transcripción de BIC /miR-155, inhibe la expresión de SOCS1, y mantiene activo el proceso de diferenciación y función de las células Treg. Sin embargo, la señalización mediada por IL-2R, también activa la vía Jak3/STAT5. La expresión de Foxp3 es dependiente de la señalización de IL-2Rγc, ya que los ratones Il2rγ$^{-/-}$ no tienen células Foxp3^{+}, aunque sí tienen una pequeña proporción de células Tregs CD25^{+} (Fontenot et al., 2005). Nuestro estudio demuestra que la diferenciación de las células iTreg CD25^{+}, se inhibe de igual manera en los cultivos procedentes de animales Il2rγ$^{-/-}$ a los que se ha añadido un inhibidor de Jak3, que en cultivos de ratones Il2rγ$^{-/-}$/CD69$^{-/-}$, lo que indica que la activación de la vía de señalización Jak3/STAT5 a través de CD69 es esencial para el desarrollo de las células Tregs.

La proteína CD69 no aparece cómo diana de miR-155 en las diferentes bases de datos (PicTar, Targetscan o miRanda miRNA base) que predicen posibles dianas de un microRNA en función de las regiones 3´ UTR (*untranslated region*) de las diferentes proteínas. Además, no se ha encontrado mediante un análisis *in silico* de la región 3´UTR de CD69, ninguna secuencia a la que se pueda unir miR-155 (Ziegler et al., 1994). Sin embargo, varios estudios han demostrado una relación, "no canónica", en términos miRNA–proteína diana, entre miR-155 y la proteína CD69. Experimentos con ratones MRL/lpr en los que no se encuentran miRNAs, ya que son deficientes para la proteína Dicer, que interviene en el procesamiento de pre-miRNAs a miRNAs maduros. En estos ratones se encuentran niveles elevados de miR-155 y también una mayor expresión de CD69 (Divekar et al., 2011), lo que sugiere que existen mecanismos independientes de Dicer para la generación de miRNAS. En otro estudio con animales Dicer$^{-/-}$, se encontró una mayor expresión de CD69 después de la estimulación por TCR y una salida defectuosa a órganos linfoides periféricos (Zang et al., 2010). Como se ha descrito anteriormente para CD69, Dicer juega un papel clave en la diferenciación tTreg (Cobb et al., 2006) y la función Treg (Liston et al., 2008). En este sentido, CD69 se expresa en los linfocitos en estadios tempranos después de la estimulación

TCR/CD3 (Testi et al., 1989), y su cola citoplásmatica interactúa con moléculas Jak3/STAT5 (Martin and Sanchez-Madrid, 2011), activando la vía JaK3/STAT5 en pTregs (Cortes et al., 2014) y tTregs y, por lo tanto, inhibiendo la transcripción de SOCS1 (Figura 41). De forma similar, la señalización de IL-2 inducida por TCR desencadena la señalización de STAT5 y mejora la expresión de miR-155 dependiente de Foxp3, limitando la expresión de SOCS1 y promoviendo la homeostasis de Treg (Lu et al., 2009). Datos recientes muestran que los microRNAs podrían regular diferentes tipos de funciones en las células, modulando la expresión de diferentes genes diana en función del contexto biológico (Lu et al., 2015; Yin et al., 2008b). Se analizó la expresión de miR-155 y SOCS1 en ausencia de la activación mediada por la vía de señalización Jak3-STAT5 a través de CD69 en células iTreg, y se observó una disminución de la expresión de miR-155 y una up-regulación de SOCS1 en iTreg CD69$^{-/-}$ en comparación con iTreg CD69$^{+/+}$ (Figura 41). Sin embargo, la inhibición de Jak3 no contribuyó a disminuir la expresión de miR-155, sugiriendo que otros microRNAs y/o genes diana podrían estar implicados.

El análisis de los elementos de unión a STAT5 de las secuencias promotoras BIC/miR-155 y CD69 reveló que eran estructuralmente similares, conteniendo cada uno dos elementos putativos de unión a STAT y al elemento AP-1 delante de la caja TATA (Yin et al., 2008b). Además, se sabe que el factor de transcripción AP-1, altamente inducido después de la estimulación por TCR, regula la activación de ambos promotores (Castellanos et al., 1997; Yin et al., 2008b). Esto sugiere que ambos promotores pueden ser activados concurrentemente, en un bucle de retroalimentación positiva, por la vía de activación TCR/CD3. En éste trabajo se ha demostrado que los ratones reportero Foxp3-RFP^{+}/CD69$^{-/-}$ reducen drásticamente la población de células tTreg en el timo adulto. Las tTregs no pueden desarrollarse adecuadamente en cultivos FTOC a partir de timos embrionarios CD69$^{-/-}$ o tratados con el anticuerpo bloqueante de CD69 (2.2), y son los precursores de médula ósea CD69$^{-/-}$ los que no son capaces de desarrollar células Treg en quimeras de médula reconstituidas con una mezcla igualada de precursosres CD69$^{+/+}$ y CD69$^{-/-}$. Además, los datos *in vitro* confirman que la fosforilación de STAT5 se inhibe en tTregs deficientes en CD69 y provoca la inhibición de la vía BIC/miR-155, aumentando la expresión de SOCS1 y por lo tanto, disminuyendo el desarrollo de tTreg (Figura 41). Estos datos junto con los datos que muestran que la función supresora de Tregs está comprometida en ratones deficientes en CD69 (Cortes et al., 2014), indican que CD69 es una molécula clave en el desarrollo de Tregs Foxp3^{+} CD69 $^{+}$ en el timo, que darán lugar a la población de Treg de la periferia funcionalmente activas. Todos estos datos posicionan a la molécula CD69 en un papel esencial en el mantenimiento de la homeostasis inmune, en procesos tanto fisiológicos como patológicos.

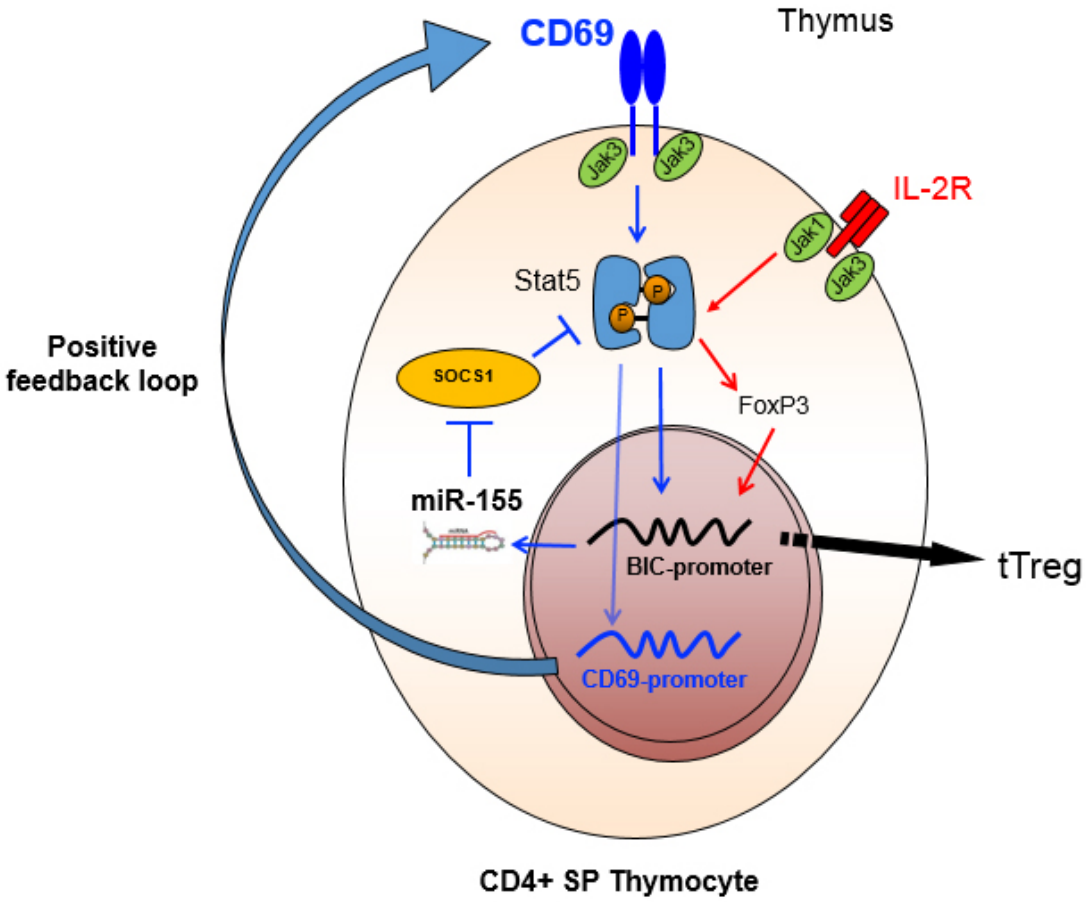

Figura 41. La diferenciación de las Tregs en el timo está regulada por CD69 y miR-155 mediante un "*positive feedback loop*". La activación de la vía Jak3/STAT5 mediada por CD69 conduce a la fosforilación, dimerización e internalización en el núcleo del factor de trascripción STAT5. Allí se une tanto al promotor de CD69 como al del miR-155 (BIC), favoreciendo la transcripción de ambas moléculas. La expresión del miR-155 propicia la inhibición de la expresión de su diana SOCS1, manteniendo activada la vía Jak3/STAT5. Por lo que ambas moléculas CD69 y miR-155 actúan conjuntamente para mantener activada esta vía y, por lo tanto, la generación de células T reguladoras en el timo.

2. PAPEL DE CD69 EN LA NEO-VASCULARIZACIÓN POST-ISQUEMIA

2.1. PAPEL DE LA INMUNIDAD ADAPTATIVA Y DE LOS MIRNAS EN LA NEO-ANGIOGÉNESIS

Las enfermedades cardiovasculares que cursan con isquemia, se encuentran entre las principales causas de muerte en todo el mundo, y son cada vez un problema más frecuente en la sociedad, debido al estilo de vida moderno y poco saludable. Aunque existen tratamientos para combatir los procesos patológicos que cursan con isquemia en enfermedades cardiovasculares, el conocimiento de los procesos que regulan este tipo de enfermedades, es necesario para prevenirlas y mejorar los tratamientos hasta ahora existentes.

El sistema inmune está implicado en el daño/reparación de tejidos isquémicos en procesos mediados tanto por la inmunidad innata como adquirida. El estudio de los factores que regulan los diferentes tipos de respuesta inmune puede ser crítico para controlar los procesos de re-vascularización post-isquemia. Diferentes estudios en animales con isquemia arterial, muestran que las células Th17 y Tregs modulan la neovascularización de un modo antagónico (Hata et al., 2011; Zouggari et al., 2009), lo que revela un papel de estos tipos celulares en enfermedades vasculares como la enfermedad arterial periférica (PAD), aunque los mecanismos que operan en esta regulación son completamente desconocidos.

CD69 puede regular negativamente la respuesta Th17 *in vivo* e *in vitro* (Martin et al., 2010a). En este trabajo, y apoyando el papel de CD69 como bloqueador temprano de la diferenciación Th17 mediante un mecanismo en el cual la rápida inducción de la molécula, seguida de la activación por antígeno, modifica el destino de la diferenciación de la célula T y previene la polarización hacia linfocitos Th17, se planteó conocer si CD69 tiene algún papel en la neo-vascularización post-isquemia. Para ello se ha utilizado el modelo *Hindlimb Ischemia* y animales BALB/c WT o deficientes en CD69, o quimeras hematopoyéticas en las que el componente linfoide expresa diferencialmente CD69 y el endotelio y el componente mieloide es WT. Los resultados han demostrado que la ausencia de CD69 en el compartimento linfoide ralentiza el proceso de neo-vascularización post-isquemia. Estos datos coinciden con el hecho de que CD69 inhibe la función y diferenciación de las células Th17 que, mediante la secreción de TGF-β y VEGF, favorecen la neo-vascularización post-isquemia (Hata et al., 2011). Se ha comprobado también que los niveles de células Th17 se elevan después de la isquemia en los experimentos con animales BALB/c y en ambos tipos de quimeras hematopoyéticas utlilizadas, y esta elevación de los niveles de células Th17, es mayor en los animales deficientes en CD69. En nuestro grupo de investigación se ha relacionado el incremento de los niveles de células Th17 con procesos

inflamatorios que generan patologías cardiovasculares como la miocarditis autoinmune (Cruz-Adalia et al., 2010). Además, recientemente y también en el grupo, se ha relacionado el miR-721 (tesis doctoral de Adela Matesán Marín, 2015) con la miocarditis autoinmune, encontrándose este microRNA elevado tanto en el suero como en el miocardio de ratones sometidos al proceso de miocarditis autoinmune, y en el suero de pacientes con esta enfermedad. Recientemente, se ha sido descrito el papel de miR-155 en el modelo animal de PAD. Este microRNA actúa de manera antagónica, como anti-angiogénico y pro-arteriogénico durante procesos de neovascularización adaptativa (Pankratz et al., 2015). Este hecho pone de manifiesto la influencia de miRNAs en la progresión de este tipo de enfermedades y subraya que los mecanismos moleculares regulados por los miRNAs derivados del sistema inmunitario, pueden regular el curso de las enfermedades cardiovasculares isquémicas. En el estudio que se ha llevado a cabo así como en el modelo de PAD que se ha puesto a punto en el laboratorio, no se ha encontrado ninguna variación de miR-155 durante el proceso de revascularización post-isquemia. En cambio, sí se ha observado una inducción de miR-721 que, como ocurre con la miocarditis autoinmune, se eleva en el suero y músculo isquémico de los animales sometidos a isquemia en la extremidad posterior derecha. Este hecho coincide con el incremento de los niveles de células Th17. Además, se ha observado que miR-721 se mantiene elevado durante más tiempo y a niveles mayores en los animales deficientes en CD69, y en las quimeras hematopoyéticas que no expresan CD69 en el compartimento linfoide. Todas estas enfermedades tienen en común el componente inflamatorio, que es regulado por células Th17 y células Treg (Ghoreschi et al., 2011). Esto permite que CD69 sea un candidato factible para el estudio de miRNAs relacionados con enfermedades cardiovasculares que cursan con isquemia. El miR-721 resulta un candidato muy interesante a la hora de intervenir en los procesos de neo-vascularización post-isquemia, ya que la única diana validada actualmente de este miRNA es la proteína Meox2 (Pfaff et al., 2011). Esta proteína está muy relacionada con procesos de angiogénesis o neo-vascularización, actuando como un regulador negativo de la misma (Douville et al., 2011; Patel et al., 2005; Wu et al., 2010). La proteína Meox2 pertenece a la familia de factores de transcripción con dominios Homeobox, relacionándose este tipo de estructuras con la regulación de procesos fisiológicos y patológicos relacionados con la vasculogénesis (Cantile et al., 2008). A esta familia de genes homeobox, también pertenece la proteína CUX1, descrita como un regulador negativo de los procesos angiogénicos tumorales. Su presencia se relaciona con una buena prognosis en determinados tumores de mama (Vadnais et al., 2013), aunque también se la relaciona como un inhibidor negativo de la apoptosis en cáncer de páncreas a través de la vía de PI3K/AKT, incrementando la agresividad de este tipo de tumores (Ripka et al., 2010)R. Es interesante destacar que en los intrones 3 y 4 de CUX1, es donde se encuentra

codificado miR-721 (miRNA data base). Aunque todavía no está descrito, es conocido que los miRNAs suelen regular también la expresión de las proteínas en las que se encuentran codificados. En este trabajo y debido a la relación de las proteínas con dominios homeobox con los procesos de angiogénesis (Cantile et al., 2008), se ha analizado la expresión de ambas proteínas en los músculos de los animales sometidos a isquemia de la extremidad posterior. Se ha encontrado que ambas proteínas se regulan de forma opuesta a miR-721, encontrándose elevadas en los músculos isquémicos de las quimeras hematopoyéticas que expresan CD69, donde la expresión de miR-721 es prácticamente nula. Es interesante destacar que en este tipo de quimeras, el músculo y el endotelio son WT, y la expresión diferencial de CD69 está determinada por las poblaciones mieloides y/o linfoides que se han generado en estos animales después del proceso de reconstitución. Por tanto, la expresión de este miRNA en el compartimento mieloide y/o linfoide de estos animales, estaría regulando la expresión en el tejido endotelial y muscular de estas proteínas y, en definitiva, interviniendo en el proceso de angiogénesis. Recientemente se ha demostrado en nuestro grupo de investigación (Tesis de Adela Matesanz, 2015), que miR-721 es secretado en la sangre por los linfocitos Th17 que acuden a los focos de inflamación, lo que podría permitir que este miRNA realizara sus funciones en las células diana del tejido dañado, hecho que explicaría los resultados obtenidos con las quimeras hematopoyéticas.

En este trabajo y mediante técnicas inmunohistoquímicas, se ha encontrado una expresión diferencial aumentada de la proteína Meox2 en el endotelio de músculo isquémico de animales WT, con respecto a los músculos de los animales deficientes en CD69, incluso en los músculos control que no habían sufrido isquemia. Además, se ha comprobado en células endoteliales extraídas de animales WT y deficientes en CD69, que miR-721 sólo se encuentra expresado en el endotelio de los animales deficientes en CD69. Asimismo, Meox2, que es la diana de miR-721, así como la diana putativa CUX1, se expresan en condiciones basales en células endoteliales WT, mientras que en las células endoteliales deficientes en CD69 sólo se expresan en condiciones de estimulación, apoyando una regulación de estas moléculas en procesos isquémicos *in vivo* por miR-721.

2.2 ANALISIS BIOANALITICO DE LA MOLÉCULA CD69 EN ANGIOGÉNESIS

Los procesos de regeneración vascular post-isquemia son muy complejos y en ellos están implicadas diferentes moléculas que incluyen proteínas, péptidos, miRNAS (Cantile et al., 2008; Gomez Sandoval et al., 2013; Urbich et al., 2008a; Urbich et al., 2008b) y diferentes metabolitos tales como radicales libres de oxígeno, óxido nítrico, etc. (Gomez Sandoval et al., 2013). Estas moléculas interaccionan con diferentes tipos celulares y con el estroma extracellular, en función de la extensión de la zona dañada y de las necesidades de aporte de oxígeno de los diferentes tejidos. Debido a la expresión diferencial de las proteínas Meox2 y CUX1 que se han encontrado en las células endoteliales de animales deficientes en CD69 en condiciones basales, y a datos preliminaries de nuestro grupo que indican que CD69 se expresa en el endotelio activado, se planteó la necesidad de conocer mejor las proteínas diferencialmente expresadas en las células endoteliales de animales WT o deficientes en CD69 en los experimentos con BABL/c donde el gen está delecionado en todos los tejidos. El objetivo fue comprender mejor los procesos de neovascualrización post-isquemia que están ocurriendo de manera diferente en estos animales, y así poder evaluar la influencia de CD69 en la neo-vascularización post-isquemia, bien como molécula inmuno-reguladora de la inflamación o como proteína que interviene en determinados procesos celulares que conducen a una ralentización de la angiogénesis. Para abordar este reto y debido a la complejidad de los mecanismos que rigen la angiogénesis, se consideró necesario un abordaje experimental que permitiera conocer procesos complicados desde el punto de vista biológico, en los que es necesario coordinar una plétora de diferentes tipos celulares y mecanismos moleculares, de manera amplia y ordenada, para poder comprender mejor lo que está ocurriendo en los procesos de formación de nuevos vasos. Con este fin, se utilizó la técnica de espectrometría de masas biológica al ser una técnica con una alta sensibilidad y robustez, lo que le confiere un gran potencial para responder a las incógnitas derivadas de la complejidad y dinámica de los procesos angiogénicos (Hernandez-Fernaud, 2013; Zanivan et al., 2012). En este trabajo se ha utilizado la aproximación proteómica SILAC, al permitir realizar un análisis no dirigido y de alta exactitud (Lopez Heras, 2014).

Los datos obtenidos con este abordaje experimental, han permitido proponer algunas hipótesis que muestran cómo CD69 interviene en los procesos de angiogénesis. La proteína *Rho GDP-disociation inhibitor 1* Rho GDI 1, upregulada en los animales deficientes en CD69, a través de la regulación de la actividad de las GTPasas RhoA/ROCK1 (Leffers et al., 1993), es capaz de activar la vía PI3K/AKT y favorecer procesos angiogénicos mediados por diferentes mecanismos. Por ejemplo, a través del incremento de la expresión de la proteína HIF1-α, que se upregula por los procesos de hipoxia que se generan en la isquemia (Schroedl et al., 2002). HIF1-α se ha relacionado recientemente con CD69 a

través del receptor $S1P_1$, el cual interviene en la regulación de la hipoxia producida durante el crecimiento tumoral. (Labiano and I., 2017). También relacionado con la activación de la vía PI3K/AKT/mTORc y el proceso de angiogénesis, se encontró la proteína endoglina (Lee et al., 2012), up-regulada en el tejido isquémico de los animales $CD69^{-/-}$. La endoglina interacciona con la proteína Zyxin, upregulada también en las MLEC procedentes de animales $CD69^{-/-}$, siendo capaz de regular la organización del citoesqueleto y permitiendo la interacción de PI3K y AKT, activando así el proceso de angiogénesis (Sanz-Rodriguez et al., 2004). La proteína Zyxin es una proteína con dominios LIM, las proteínas con este tipo de estructura son proteínas adaptadoras que sirven de enlace entre los diferentes compartimentos celulares mediante su interacción con el citoesqueleto, permitiendo la movilización e interacción de proteínas (Kadrmas and Beckerle, 2004). También se ha encontrado up-regulada en las MLEC $CD69^{-/-}$ la proteína PDZ LIM domain protein 1, cuya actividad está controlada por la proteína ROCK1 (Montalvo et al., 2013), que se encuentra inactiva en el tejido isquémico de los animales $CD69^{-/-}$. Esta proteína PDZ LIM domain protein 1 es capaz de interaccionar con la endoglina, manteniendo fijado en la membrana a PI3P, favoreciendo así su interacción con AKT (Lee et al., 2012). Por otro lado, las proteínas Zyxin y PDZ LIM domain protein 1 a través de sus dominios, interaccionan con los receptores de tipo efrina favoreciendo la angiogénesis mediante el reclutamiento de receptores VEGF (Lisabeth et al., 2013).

Otras proteínas que presentan dominios LIM son los factores de transcripción tipo homeobox, Meox2 y CUX1, aunque en este caso, este tipo de dominios están más implicados en la comunicación, mediante el citoesqueleto, entre el citoplasma celular y el núcleo, para promover así la expresión de determinados tipos de genes. Resulta interesante ver cómo este tipo de dominios juega un papel tan importante en los diferentes aspectos que regulan la angiogénesis, ya sea favoreciendo interacciones de proteínas en el citoplasma celular o interviniendo en la expresión de determinados tipos de genes.

Las proteínas desreguladas que se han identificado en este trabajo, son sólo una pequeña parte de las que nos ha proporcionado el experimento SILAC, pero constituyen un *cluster* muy compacto en el que se relaciona la mayor revascularización de los animales $CD69^{-/-}$ con la activación de la vía AKT/PI3K/mTORc, y con cambios celulares mediados por las proteínas con dominios LIM.

En definitiva, el papel de CD69 en los proceso de angiogénesis se debe a dos contribuciones distintas: Por un lado está la implicación del sistema inmune mediante el papel de esta proteína en la función y diferenciación de los linfocitos Th17 y en los miRNAs producidos por estas células; y otro aspecto menos explorado, que se refiere al endotelio diferencial que presentan los animales $CD69^{+/+}$ y $CD69^{-/-}$. En este

punto los resultados del experimento SILAC abren un campo de estudio muy amplio, y que se espera que pueda contribuir a dilucidar el papel de CD69 en la neovascularización post-isquemia. Este proceso parece estar íntimamente relacionado con cambios en el citoesqueleto y en el tráfico celular, ya que la mayor parte de las proteínas diferencialmente expresadas que se han encontrado en este experimento, están fuertemente vinculadas con estas funciones y estos orgánulos celulares.

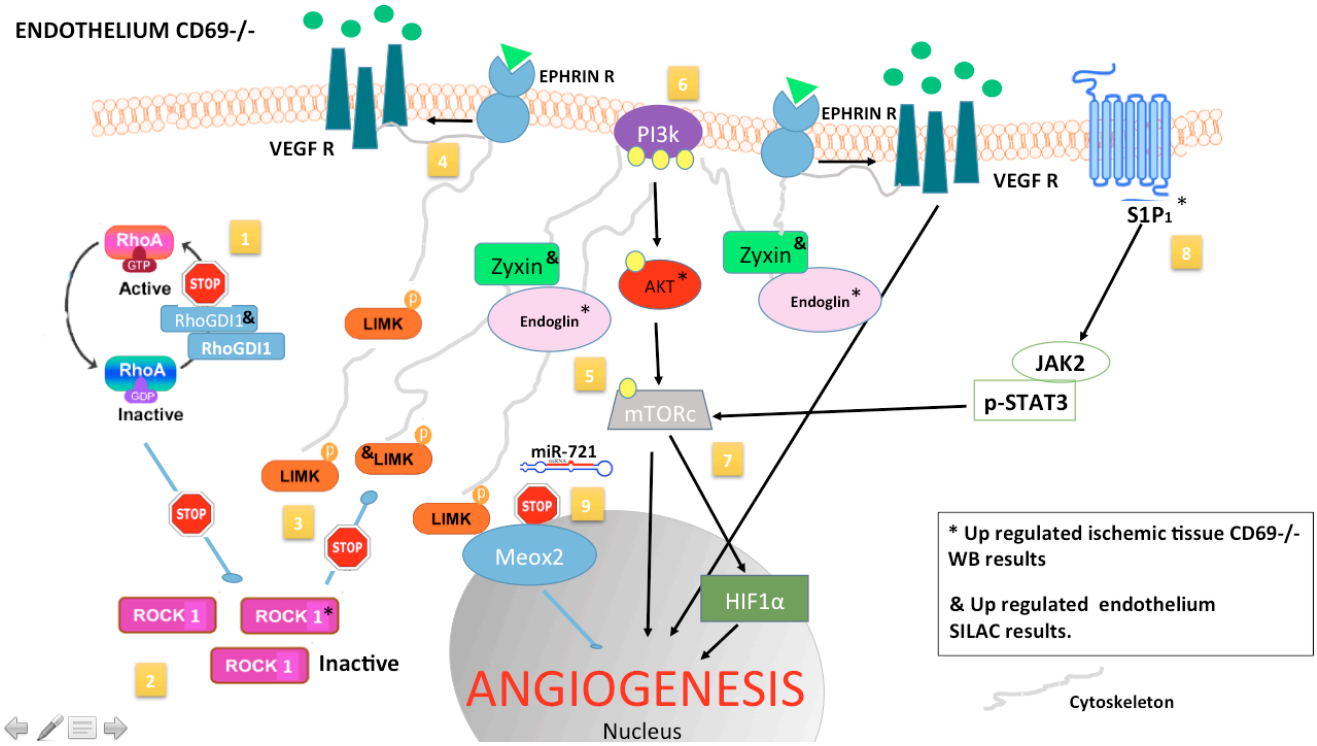

Figura 42. Esquema del papel de CD69 en la activación endotelial. (1) La proteína *Rho GDP dissociation inhibition* 1 Rho GDI 1 inhibe la fosforilación de la quinasa RhoA, que se inactiva y se degrada en el citoplasma. **(2)** La inactivación de la proteína Rho1, impide la activación de la kinasa ROCK1, que se acumula en el citoplasma en un pool inactivo. **(3)** La inactivación de ROCK1 favorece que las *PDZ-LIM Domain Kinasas* (LIMK), esten activas en el citoplasma. **(4)** La LIMK activa favorece que el receptor tipo efrina promueva, a través del citoesquelto, el reclutamiento de receptors de VEGF, que favorecen el proceso de angiogénesis**. (5)** y **(6**) La endoglina mediante su interacción con la proteína LIM domain Zyxin o con la proteína LIMK, mantiene unido *al Fosfatidil Inositol 3 P* (PI3K) a la membrana celular, manteniendo activada la vía de AKT/mTORc y favoreciendo la angiogénesis. **(7)** La activación de la vía de AKT/mTORC, incrementa la expression de la proteína HIF1α, implicada también en el proceso de neo-vascularización post-isquemia**. (8)** El receptor $S1P_1$ up-regulado en los animales $CD69^{-/-}$ favorece la activación de la ruta AKT/mTORc y el incremento de expresión de la proteína HIF1α. **(9)** miR-721 inhibe la expresión de su diana Meox2, favoreciendo la angiogénesis mediante la activación de la vía de NFKB.

V. CONCLUSIONES

V. CONCLUSIONES

1. La expresión de CD69 regula la respuesta Th17 en procesos fibro-proliferativos controlando la fibrosis en un modelo de diálisis peritoneal.

2. El antígeno CD69 es una molécula clave en la prevención del desarrollo de la inflamación, mediante el control de la función supresora de las células T reguladoras.

3. La población de células T reguladoras $CD69^{+}$ es fundamental para el mantenimiento de la homeostasis inmune y la regulación de las respuestas inflamatorias y autoinmunes mediadas por las células Th17.

4. La proteína CD69 es una molécula clave en el desarrollo de las células T reguladoras $Foxp3^{+}$ $CD69^{+}$ en el timo, que darán lugar a la población de células T reguladoras periféricas con capacidad supresora.

5. El mecanismo molecular que regula la diferenciación de las células T reguladoras en el timo está mediado por CD69 y miR-155 mediante un bucle de retroalimentación positivo.

6. La molécula CD69 interviene en el proceso de neo-vascularización post-isquemia mediante la regulación del balance Th17/Treg.

7. El microRNA-721, inducido tras la isquemia por las células Th17, promueve la neo-vascularización post-isquemia mediante la inhibición de la expresión de su diana Meox2.

8. Los resultados obtenidos mediante el análisis proteómico SILAC, indican claras diferencias entre el endotelio de los animales $CD69^{+/+}$ y el endotelio de animales $CD69^{-/-}$. Encontrando diferencialmente expresadas proteínas relacionadas con el citoesqueleto y el tráfico celular, que intervienen en la regulación de la angiogénesis.

9. Las proteínas adaptadoras con dominios LIM, inducidas en el endotelio deficiente en CD69, favorecen modificaciones en el citoesqueleto celular y el proceso de neo-vascularización post-isquemia mediante la activación de la vía PI3K/AKT/mTORc y la regulación de HIF-1α.

VI. REFERENCIAS

VI. REFERENCIAS

Allan, S.E., Crome, S.Q., Crellin, N.K., Passerini, L., Steiner, T.S., Bacchetta, R., Roncarolo, M.G., and Levings, M.K. (2007). Activation-induced FOXP3 in human T effector cells does not suppress proliferation or cytokine production. Int Immunol *19*, 345-354.

Asahara, T., Murohara, T., Sullivan, A., Silver, M., van der Zee, R., Li, T., Witzenbichler, B., Schatteman, G., and Isner, J.M. (1997). Isolation of putative progenitor endothelial cells for angiogenesis. Science *275*, 964-967.

Aujla, S.J., Chan, Y.R., Zheng, M., Fei, M., Askew, D.J., Pociask, D.A., Reinhart, T.A., McAllister, F., Edeal, J., Gaus, K., *et al.* (2008). IL-22 mediates mucosal host defense against Gram-negative bacterial pneumonia. Nat Med *14*, 275-281.

Baeyens, A., Fang, V., Chen, C., and Schwab, S.R. (2015). Exit Strategies: S1P Signaling and T Cell Migration. Trends Immunol *36*, 778-787.

Baltimore, D., Boldin, M.P., O'Connell, R.M., Rao, D.S., and Taganov, K.D. (2008). MicroRNAs: new regulators of immune cell development and function. Nat Immunol *9*, 839-845.

Barczyk, A., Pierzchala, W., and Sozanska, E. (2003). Interleukin-17 in sputum correlates with airway hyperresponsiveness to methacholine. Respiratory medicine *97*, 726-733.

Barthlott, T., Kohler, H., and Eichmann, K. (1997). Asynchronous coreceptor downregulation after positive thymic selection: prolonged maintenance of the double positive state in CD8 lineage differentiation due to sustained biosynthesis of the CD4 coreceptor. J Exp Med *185*, 357-362.

Bettelli, E., Korn, T., and Kuchroo, V.K. (2007). Th17: the third member of the effector T cell trilogy. Curr Opin Immunol *19*, 652-657.

Bieber, T., Rieger, A., Stingl, G., Sander, E., Wanek, P., and Strobel, I. (1992). CD69, an early activation antigen on lymphocytes, is constitutively expressed by human epidermal Langerhans cells. J Invest Dermatol *98*, 771-776.

Bilate, A.M., and Lafaille, J.J. (2012). Induced CD4+Foxp3+ regulatory T cells in immune tolerance. Annu Rev Immunol *30*, 733-758.

Brown, K.N., Trichel, A., and Barratt-Boyes, S.M. (2007). Parallel loss of myeloid and plasmacytoid dendritic cells from blood and lymphoid tissue in simian AIDS. J Immunol *178*, 6958-6967.

Bruneel, A., Labas, V., Mailloux, A., Sharma, S., Royer, N., Vinh, J., Pernet, P., Vaubourdolle, M., and Baudin, B. (2005). Proteomics of human umbilical vein endothelial cells applied to etoposide-induced apoptosis. Proteomics *5*, 3876-3884.

Burchill, M.A., Yang, J., Vang, K.B., Moon, J.J., Chu, H.H., Lio, C.W., Vegoe, A.L., Hsieh, C.S., Jenkins, M.K., and Farrar, M.A. (2008). Linked T cell receptor and cytokine signaling govern the development of the regulatory T cell repertoire. Immunity *28*, 112-121.

Burghoff, S., and Schrader, J. (2011). Secretome of human endothelial cells under shear stress. J Proteome Res *10*, 1160-1169.

Calin, G.A., Dumitru, C.D., Shimizu, M., Bichi, R., Zupo, S., Noch, E., Aldler, H., Rattan, S., Keating, M., Rai, K.*, et al.* (2002). Frequent deletions and down-regulation of micro- RNA genes miR15 and miR16 at 13q14 in chronic lymphocytic leukemia. Proc Natl Acad Sci U S A *99*, 15524-15529.

Canas, B., Lopez-Ferrer, D., Ramos-Fernandez, A., Camafeita, E., and Calvo, E. (2006). Mass spectrometry technologies for proteomics. Brief Funct Genomic Proteomic *4*, 295-320.

Cantile, M., Schiavo, G., Terracciano, L., and Cillo, C. (2008). Homeobox genes in normal and abnormal vasculogenesis. Nutr Metab Cardiovasc Dis *18*, 651-658.

Caspar-Bauguil, S., Saadawi, M., Negre-Salvayre, A., Thomsen, M., Salvayre, R., and Benoist, H. (1998). Mildly oxidized low-density lipoproteins suppress the proliferation of activated CD4+ T-lymphocytes and their interleukin 2 receptor expression in vitro. The Biochemical journal *330 (Pt 2)*, 659-666.

Castellanos, M.C., Munoz, C., Montoya, M.C., Lara-Pezzi, E., Lopez-Cabrera, M., and de Landazuri, M.O. (1997). Expression of the leukocyte early activation antigen CD69 is regulated by the transcription factor AP-1. J Immunol *159*, 5463-5473.

Castellanos Mdel, C., Lopez-Giral, S., Lopez-Cabrera, M., and de Landazuri, M.O. (2002). Multiple cis-acting elements regulate the expression of the early T cell activation antigen CD69. Eur J Immunol *32*, 3108-3117.

Cebrian, M., Yague, E., Rincon, M., Lopez-Botet, M., de Landazuri, M.O., and Sanchez-Madrid, F. (1988). Triggering of T cell proliferation through AIM, an activation inducer molecule expressed on activated human lymphocytes. J Exp Med *168*, 1621-1637.

Chen, W., Jin, W., Hardegen, N., Lei, K.J., Li, L., Marinos, N., McGrady, G., and Wahl, S.M. (2003). Conversion of peripheral CD4+CD25- naive T cells to CD4+CD25+ regulatory T cells by TGF-beta induction of transcription factor Foxp3. J Exp Med *198*, 1875-1886.

Chen, X., Ba, Y., Ma, L., Cai, X., Yin, Y., Wang, K., Guo, J., Zhang, Y., Chen, J., Guo, X.*, et al.* (2008). Characterization of microRNAs in serum: a novel class of biomarkers for diagnosis of cancer and other diseases. Cell research *18*, 997-1006.

Chen, Y., and Gorski, D.H. (2008). Regulation of angiogenesis through a microRNA (miR-130a) that down-regulates antiangiogenic homeobox genes GAX and HOXA5. Blood *111*, 1217-1226.

Childs, R.A., Galustian, C., Lawson, A.M., Dougan, G., Benwell, K., Frankel, G., and Feizi, T. (1999). Recombinant soluble human CD69 dimer produced in Escherichia coli: reevaluation of saccharide binding. Biochemical and biophysical research communications *266*, 19-23.

Cobb, B.S., Hertweck, A., Smith, J., O'Connor, E., Graf, D., Cook, T., Smale, S.T., Sakaguchi, S., Livesey, F.J., Fisher, A.G., and Merkenschlager, M. (2006). A role for Dicer in immune regulation. J Exp Med *203*, 2519-2527.

Collison, L.W., Workman, C.J., Kuo, T.T., Boyd, K., Wang, Y., Vignali, K.M., Cross, R., Sehy, D., Blumberg, R.S., and Vignali, D.A. (2007). The inhibitory cytokine IL-35 contributes to regulatory T-cell function. Nature *450*, 566-569.

Cortes, J.R., Sanchez-Diaz, R., Bovolenta, E.R., Barreiro, O., Lasarte, S., Matesanz-Marin, A., Toribio, M.L., Sanchez-Madrid, F., and Martin, P. (2014). Maintenance of immune tolerance by Foxp3+ regulatory T cells requires CD69 expression. J Autoimmun *55*, 51-62.

Costinean, S., Zanesi, N., Pekarsky, Y., Tili, E., Volinia, S., Heerema, N., and Croce, C.M. (2006). Pre-B cell proliferation and lymphoblastic leukemia/high-grade lymphoma in E(mu)-miR155 transgenic mice. Proc Natl Acad Sci U S A *103*, 7024-7029.

Couffinhal, T., Silver, M., Zheng, L.P., Kearney, M., Witzenbichler, B., and Isner, J.M. (1998). Mouse model of angiogenesis. Am J Pathol *152*, 1667-1679.

Coventry, B.J., Weeks, S.C., Heckford, S.E., Sykes, P.J., Bradley, J., and Skinner, J.M. (1996). Lack of IL-2 cytokine expression despite Il-2 messenger RNA transcription in tumor-infiltrating lymphocytes in primary human breast carcinoma: selective expression of early activation markers. J Immunol *156*, 3486-3492.

Cruz-Adalia, A., Jimenez-Borreguero, L.J., Ramirez-Huesca, M., Chico-Calero, I., Barreiro, O., Lopez-Conesa, E., Fresno, M., Sanchez-Madrid, F., and Martin, P. (2010). CD69 limits the severity of cardiomyopathy after autoimmune myocarditis. Circulation *122*, 1396-1404.

Curotto de Lafaille, M.A., Kutchukhidze, N., Shen, S., Ding, Y., Yee, H., and Lafaille, J.J. (2008). Adaptive Foxp3+ regulatory T cell-dependent and -independent control of allergic inflammation. Immunity *29*, 114-126.

D'Ambrosio, D., Cantrell, D.A., Frati, L., Santoni, A., and Testi, R. (1994). Involvement of p21ras activation in T cell CD69 expression. Eur J Immunol *24*, 616-620.

de Heer, H.J., Hammad, H., Soullie, T., Hijdra, D., Vos, N., Willart, M.A., Hoogsteden, H.C., and Lambrecht, B.N. (2004). Essential role of lung plasmacytoid dendritic cells in preventing asthmatic reactions to harmless inhaled antigen. J Exp Med *200*, 89-98.

de la Fuente, H., Cruz-Adalia, A., Martinez Del Hoyo, G., Cibrian-Vera, D., Bonay, P., Perez-Hernandez, D., Vazquez, J., Navarro, P., Gutierrez-Gallego, R., Ramirez-Huesca, M.*, et al.* (2014). The leukocyte activation receptor CD69 controls T cell differentiation through its interaction with galectin-1. Mol Cell Biol *34*, 2479-2487.

De Maria, R., Cifone, M.G., Trotta, R., Rippo, M.R., Festuccia, C., Santoni, A., and Testi, R. (1994). Triggering of human monocyte activation through CD69, a member of the natural killer cell gene complex family of signal transducing receptors. J Exp Med *180*, 1999-2004.

Deindl, E., and Schaper, W. (2005). The art of arteriogenesis. Cell biochemistry and biophysics *43*, 1-15.

Divekar, A.A., Dubey, S., Gangalum, P.R., and Singh, R.R. (2011). Dicer insufficiency and microRNA-155 overexpression in lupus regulatory T cells: an apparent paradox in the setting of an inflammatory milieu. J Immunol *186*, 924-930.

Doi, K., Ikeda, T., Marui, A., Kushibiki, T., Arai, Y., Hirose, K., Soga, Y., Iwakura, A., Ueyama, K., Yamahara, K.*, et al.* (2007). Enhanced angiogenesis by gelatin hydrogels incorporating basic fibroblast growth factor in rabbit model of hind limb ischemia. Heart and vessels *22*, 104-108.

Douville, J.M., Cheung, D.Y., Herbert, K.L., Moffatt, T., and Wigle, J.T. (2011). Mechanisms of MEOX1 and MEOX2 regulation of the cyclin dependent kinase inhibitors p21 and p16 in vascular endothelial cells. PLoS One *6*, e29099.

Drickamer, K., and Taylor, M.E. (1993). Biology of animal lectins. Annual review of cell biology *9*, 237-264.

Duerr, R.H., Taylor, K.D., Brant, S.R., Rioux, J.D., Silverberg, M.S., Daly, M.J., Steinhart, A.H., Abraham, C., Regueiro, M., Griffiths, A.*, et al.* (2006). A genome-wide association study identifies IL23R as an inflammatory bowel disease gene. Science *314*, 1461-1463.

Escribano, L., Orfao, A., Villarrubia, J., Martin, F., Madruga, J.I., Cuevas, M., Velasco, J.L., Rios, A., and San Miguel, J.F. (1997). Sequential immunophenotypic analysis of mast cells in a case of systemic mast cell disease evolving to a mast cell leukemia. Cytometry *30*, 98-102.

Esplugues, E., Sancho, D., Vega-Ramos, J., Martinez, C., Syrbe, U., Hamann, A., Engel, P., Sanchez-Madrid, F., and Lauzurica, P. (2003). Enhanced antitumor immunity in mice deficient in CD69. J Exp Med *197*, 1093-1106.

Fabbiano, S., Menacho-Marquez, M., Robles-Valero, J., Pericacho, M., Matesanz-Marin, A., Garcia-Macias, C., Sevilla, M.A., Montero, M.J., Alarcon, B., Lopez-Novoa, J.M*., et al.* (2015). Immunosuppression-Independent Role of Regulatory T Cells against Hypertension-Driven Renal Dysfunctions. Mol Cell Biol *35*, 3528-3546.

Feng, C., Woodside, K.J., Vance, B.A., El-Khoury, D., Canelles, M., Lee, J., Gress, R., Fowlkes, B.J., Shores, E.W., and Love, P.E. (2002). A potential role for CD69 in thymocyte emigration. Int Immunol *14*, 535-544.

Fontenot, J.D., Gavin, M.A., and Rudensky, A.Y. (2003). Foxp3 programs the development and function of CD4+CD25+ regulatory T cells. Nat Immunol *4*, 330-336.

Fontenot, J.D., Rasmussen, J.P., Gavin, M.A., and Rudensky, A.Y. (2005). A function for interleukin 2 in Foxp3-expressing regulatory T cells. Nat Immunol *6*, 1142-1151.

Franses, J.W., and Edelman, E.R. (2011). The evolution of endothelial regulatory paradigms in cancer biology and vascular repair. Cancer research *71*, 7339-7344.

Gandhi, R., Farez, M.F., Wang, Y., Kozoriz, D., Quintana, F.J., and Weiner, H.L. (2010). Cutting edge: human latency-associated peptide+ T cells: a novel regulatory T cell subset. J Immunol *184*, 4620-4624.

Garcia-Monzon, C., Moreno-Otero, R., Pajares, J.M., Garcia-Sanchez, A., Lopez-Botet, M., de Landazuri, M.O., and Sanchez-Madrid, F. (1990). Expression of a novel activation antigen on intrahepatic CD8+ T lymphocytes in viral chronic active hepatitis. Gastroenterology *98*, 1029-1035.

Gautier, A., Gauron, C., Volovitch, M., Bensimon, D., Jullien, L., and Vriz, S. (2014). How to control proteins with light in living systems. Nat Chem Biol *10*, 533-541.

Gavioli, R., Risso, A., Smilovich, D., Baldissarro, I., Capra, M.C., Bargellesi, A., and Cosulich, M.E. (1992). CD69 molecule in human neutrophils: its expression and role in signal-transducing mechanisms. Cellular immunology *142*, 186-196.

Ghoreschi, K., Laurence, A., Yang, X.P., Hirahara, K., and O'Shea, J.J. (2011). T helper 17 cell heterogeneity and pathogenicity in autoimmune disease. Trends Immunol *32*, 395-401.

Glimcher, L.H., and Murphy, K.M. (2000). Lineage commitment in the immune system: the T helper lymphocyte grows up. Genes & development *14*, 1693-1711.

Gomez Sandoval, Y.H., Levesque, L.O., Li, Y., and Anand-Srivastava, M.B. (2013). Role of epidermal growth factor receptor transactivation in endothelin-1-induced enhanced expression of Gi protein and proliferation in A10 vascular smooth muscle cells. Can J Physiol Pharmacol *91*, 221-227.

Gondek, D.C., Lu, L.F., Quezada, S.A., Sakaguchi, S., and Noelle, R.J. (2005). Cutting edge: contact-mediated suppression by CD4+CD25+ regulatory cells involves a granzyme B-dependent, perforin-independent mechanism. J Immunol *174*, 1783-1786.

Gonzalez-Amaro, R., Cortes, J.R., Sanchez-Madrid, F., and Martin, P. (2013). Is CD69 an effective brake to control inflammatory diseases? Trends in molecular medicine *19*, 625-632.

Gonzalez-Mateo, G.T., Loureiro-Alvarez, J., Rayego-Mateos, S., Ruiz-Ortega, M., Lopez-Cabrera, M., Selgas, R., and Aroeira, L.S. (2008). [Animal models of peritoneal dialysis: relevance, difficulties, and future]. Nefrologia *28 Suppl 6*, 17-22.

Gremel, G., Ryan, D., Rafferty, M., Lanigan, F., Hegarty, S., Lavelle, M., Murphy, I., Unwin, L., Joyce, C., Faller, W.*, et al.* (2011). Functional and prognostic relevance of the homeobox protein MSX2 in malignant melanoma. Br J Cancer *105*, 565-574.

Griffiths-Jones, S. (2004). The microRNA Registry. Nucleic acids research *32*, D109-111.

Grossman, W.J., Verbsky, J.W., Barchet, W., Colonna, M., Atkinson, J.P., and Ley, T.J. (2004). Human T regulatory cells can use the perforin pathway to cause autologous target cell death. Immunity *21*, 589-601.

Haasch, D., Chen, Y.W., Reilly, R.M., Chiou, X.G., Koterski, S., Smith, M.L., Kroeger, P., McWeeny, K., Halbert, D.N., Mollison, K.W.*, et al.* (2002). T cell activation induces a noncoding RNA transcript sensitive to inhibition by immunosuppressant drugs and encoded by the proto-oncogene, BIC. Cellular immunology *217*, 78-86.

Han, Y., Guo, Q., Zhang, M., Chen, Z., and Cao, X. (2009). CD69+ CD4+ CD25- T cells, a new subset of regulatory T cells, suppress T cell proliferation through membrane-bound TGF-beta 1. J Immunol *182*, 111-120.

Harrington, L.E., Mangan, P.R., and Weaver, C.T. (2006). Expanding the effector CD4 T-cell repertoire: the Th17 lineage. Curr Opin Immunol *18*, 349-356.

Hartnell, A., Robinson, D.S., Kay, A.B., and Wardlaw, A.J. (1993). CD69 is expressed by human eosinophils activated in vivo in asthma and in vitro by cytokines. Immunology *80*, 281-286.

Hata, T., Takahashi, M., Hida, S., Kawaguchi, M., Kashima, Y., Usui, F., Morimoto, H., Nishiyama, A., Izawa, A., Koyama, J.*, et al.* (2011). Critical role of Th17 cells in inflammation and neovascularization after ischaemia. Cardiovasc Res *90*, 364-372.

He, D., Wu, L., Kim, H.K., Li, H., Elmets, C.A., and Xu, H. (2006). CD8+ IL-17-producing T cells are important in effector functions for the elicitation of contact hypersensitivity responses. J Immunol *177*, 6852-6858.

Helisch, A., Wagner, S., Khan, N., Drinane, M., Wolfram, S., Heil, M., Ziegelhoeffer, T., Brandt, U., Pearlman, J.D., Swartz, H.M., and Schaper, W. (2006). Impact of mouse strain differences in innate hindlimb collateral vasculature. Arteriosclerosis, thrombosis, and vascular biology *26*, 520-526.

Hernandez-Fernaud, J.R.S.E.R.N.J.L.Z.S. (2013). Quantitative mass spectrometry-based proteomics in angiogenesis

. Proteomics Clin. Appl. *7*, 464–476

.

Heymans, S., Corsten, M.F., Verhesen, W., Carai, P., van Leeuwen, R.E., Custers, K., Peters, T., Hazebroek, M., Stoger, L., Wijnands, E.*, et al.* (2013). Macrophage microRNA-155 promotes cardiac hypertrophy and failure. Circulation *128*, 1420-1432.

Hill, J.A., Feuerer, M., Tash, K., Haxhinasto, S., Perez, J., Melamed, R., Mathis, D., and Benoist, C. (2007). Foxp3 transcription-factor-dependent and -independent regulation of the regulatory T cell transcriptional signature. Immunity *27*, 786-800.

Hori, S., Nomura, T., and Sakaguchi, S. (2003). Control of regulatory T cell development by the transcription factor Foxp3. Science *299*, 1057-1061.

Hsieh, C.S., Zheng, Y., Liang, Y., Fontenot, J.D., and Rudensky, A.Y. (2006). An intersection between the self-reactive regulatory and nonregulatory T cell receptor repertoires. Nat Immunol *7*, 401-410.

Ishikawa, S., Akakura, S., Abe, M., Terashima, K., Chijiiwa, K., Nishimura, H., Hirose, S., and Shirai, T. (1998). A subset of CD4+ T cells expressing early activation antigen CD69 in murine lupus: possible abnormal regulatory role for cytokine imbalance. J Immunol *161*, 1267-1273.

Ivanov, II, McKenzie, B.S., Zhou, L., Tadokoro, C.E., Lepelley, A., Lafaille, J.J., Cua, D.J., and Littman, D.R. (2006). The orphan nuclear receptor RORgammat directs the differentiation program of proinflammatory IL-17+ T helper cells. Cell *126*, 1121-1133.

J.R. González-Escalada, J.L.d.l.C.y.A.P.u.c.h.o. (1999).

Flujometría campimétrica por láser doppler. Un nuevo

procedimiento diagnóstico y evaluativo del dolor

. R e v. Soc. Esp. Dolor

6, 187-198.

Jordan, M.S., Boesteanu, A., Reed, A.J., Petrone, A.L., Holenbeck, A.E., Lerman, M.A., Naji, A., and Caton, A.J. (2001). Thymic selection of CD4+CD25+ regulatory T cells induced by an agonist self-peptide. Nat Immunol *2*, 301-306.

Jorge, I., Navarro, P., Martinez-Acedo, P., Nunez, E., Serrano, H., Alfranca, A., Redondo, J.M., and Vazquez, J. (2009). Statistical model to analyze quantitative proteomics data obtained by 18O/16O labeling and linear ion trap mass spectrometry: application to the study of vascular endothelial growth factor-induced angiogenesis in endothelial cells. Mol Cell Proteomics *8*, 1130-1149.

Josefowicz, S.Z., Lu, L.F., and Rudensky, A.Y. (2012). Regulatory T Cells: Mechanisms of Differentiation and Function. Annu Rev Immunol *30*, 531-564.

Kadrmas, J.L., and Beckerle, M.C. (2004). The LIM domain: from the cytoskeleton to the nucleus. Nat Rev Mol Cell Biol *5*, 920-931.

Kanegane, H., and Tosato, G. (1996). Activation of naive and memory T cells by interleukin-15. Blood *88*, 230-235.

Kebir, H., Kreymborg, K., Ifergan, I., Dodelet-Devillers, A., Cayrol, R., Bernard, M., Giuliani, F., Arbour, N., Becher, B., and Prat, A. (2007). Human TH17 lymphocytes promote blood-brain barrier disruption and central nervous system inflammation. Nat Med *13*, 1173-1175.

Kirkham, B.W., Lassere, M.N., Edmonds, J.P., Juhasz, K.M., Bird, P.A., Lee, C.S., Shnier, R., and Portek, I.J. (2006). Synovial membrane cytokine expression is predictive of joint damage progression in rheumatoid arthritis: a two-year prospective study (the DAMAGE study cohort). Arthritis Rheum *54*, 1122-1131.

Kluiver, J., van den Berg, A., de Jong, D., Blokzijl, T., Harms, G., Bouwman, E., Jacobs, S., Poppema, S., and Kroesen, B.J. (2007). Regulation of pri-microRNA BIC transcription and processing in Burkitt lymphoma. Oncogene *26*, 3769-3776.

Kmieciak, M., Gowda, M., Graham, L., Godder, K., Bear, H.D., Marincola, F.M., and Manjili, M.H. (2009). Human T cells express CD25 and Foxp3 upon activation and exhibit effector/memory phenotypes without any regulatory/suppressor function. Journal of translational medicine *7*, 89.

Kohlhaas, S., Garden, O.A., Scudamore, C., Turner, M., Okkenhaug, K., and Vigorito, E. (2009). Cutting edge: the Foxp3 target miR-155 contributes to the development of regulatory T cells. J Immunol *182*, 2578-2582.

Komiyama, Y., Nakae, S., Matsuki, T., Nambu, A., Ishigame, H., Kakuta, S., Sudo, K., and Iwakura, Y. (2006). IL-17 plays an important role in the development of experimental autoimmune encephalomyelitis. J Immunol *177*, 566-573.

Korn, T., Oukka, M., Kuchroo, V., and Bettelli, E. (2007). Th17 cells: effector T cells with inflammatory properties. Seminars in immunology *19*, 362-371.

Kosaka, N., Iguchi, H., and Ochiya, T. (2010). Circulating microRNA in body fluid: a new potential biomarker for cancer diagnosis and prognosis. Cancer Sci *101*, 2087-2092.

Kretschmer, K., Apostolou, I., Hawiger, D., Khazaie, K., Nussenzweig, M.C., and von Boehmer, H. (2005). Inducing and expanding regulatory T cell populations by foreign antigen. Nat Immunol *6*, 1219-1227.

Krueger, G.G., Langley, R.G., Leonardi, C., Yeilding, N., Guzzo, C., Wang, Y., Dooley, L.T., Lebwohl, M., and Group, C.P.S. (2007). A human interleukin-12/23 monoclonal antibody for the treatment of psoriasis. N Engl J Med *356*, 580-592.

Kruger, M., Moser, M., Ussar, S., Thievessen, I., Luber, C.A., Forner, F., Schmidt, S., Zanivan, S., Fassler, R., and Mann, M. (2008). SILAC mouse for quantitative proteomics uncovers kindlin-3 as an essential factor for red blood cell function. Cell *134*, 353-364.

Kubota, Y., Kleinman, H.K., Martin, G.R., and Lawley, T.J. (1988). Role of laminin and basement membrane in the morphological differentiation of human endothelial cells into capillary-like structures. The Journal of cell biology *107*, 1589-1598.

Labiano, S., Meléndez-Rodríguez, F., Palazón, A., Teijeira, Á., Garasa, S., Etxeberria,, and I., A., M. Á. (2017). CD69 is a direct HIF-1α target gene in hypoxia as a mechanism

enhancing expression on tumor-infiltrating T lymphocytes. OncoImmunology.

Laffon, A., Garcia-Vicuna, R., Humbria, A., Postigo, A.A., Corbi, A.L., de Landazuri, M.O., and Sanchez-Madrid, F. (1991). Upregulated expression and function of VLA-4 fibronectin receptors on human activated T cells in rheumatoid arthritis. J Clin Invest *88*, 546-552.

Lagos-Quintana, M., Rauhut, R., Lendeckel, W., and Tuschl, T. (2001). Identification of novel genes coding for small expressed RNAs. Science *294*, 853-858.

Lamana, A., Martin, P., de la Fuente, H., Martinez-Munoz, L., Cruz-Adalia, A., Ramirez-Huesca, M., Escribano, C., Gollmer, K., Mellado, M., Stein, J.V.*, et al.* (2011). CD69 modulates sphingosine-1-phosphate-induced migration of skin dendritic cells. J Invest Dermatol *doi:10.1038/jid.2011.54*.

Lampugnani, M.G. (1999). Cell migration into a wounded area in vitro. Methods Mol Biol *96*, 177-182.

Langrish, C.L., Chen, Y., Blumenschein, W.M., Mattson, J., Basham, B., Sedgwick, J.D., McClanahan, T., Kastelein, R.A., and Cua, D.J. (2005). IL-23 drives a pathogenic T cell population that induces autoimmune inflammation. J Exp Med *201*, 233-240.

Lau, N.C., Lim, L.P., Weinstein, E.G., and Bartel, D.P. (2001). An abundant class of tiny RNAs with probable regulatory roles in Caenorhabditis elegans. Science *294*, 858-862.

Lauzurica, P., Sancho, D., Torres, M., Albella, B., Marazuela, M., Merino, T., Bueren, J.A., Martinez, A.C., and Sanchez-Madrid, F. (2000). Phenotypic and functional characteristics of hematopoietic cell lineages in CD69-deficient mice. Blood *95*, 2312-2320.

Lawrie, C.H., Gal, S., Dunlop, H.M., Pushkaran, B., Liggins, A.P., Pulford, K., Banham, A.H., Pezzella, F., Boultwood, J., Wainscoat, J.S.*, et al.* (2008). Detection of elevated levels of tumour-associated microRNAs in serum of patients with diffuse large B-cell lymphoma. British journal of haematology *141*, 672-675.

Lee, N.Y., Golzio, C., Gatza, C.E., Sharma, A., Katsanis, N., and Blobe, G.C. (2012). Endoglin regulates PI3-kinase/Akt trafficking and signaling to alter endothelial capillary stability during angiogenesis. Molecular biology of the cell *23*, 2412-2423.

Lee, R.C., and Ambros, V. (2001). An extensive class of small RNAs in Caenorhabditis elegans. Science *294*, 862-864.

Lee, R.C., Feinbaum, R.L., and Ambros, V. (1993). The C. elegans heterochronic gene lin-4 encodes small RNAs with antisense complementarity to lin-14. Cell *75*, 843-854.

Leffers, H., Nielsen, M.S., Andersen, A.H., Honore, B., Madsen, P., Vandekerckhove, J., and Celis, J.E. (1993). Identification of two human Rho GDP dissociation inhibitor proteins whose overexpression leads to disruption of the actin cytoskeleton. Experimental cell research *209*, 165-174.

Lewis, B.P., Burge, C.B., and Bartel, D.P. (2005). Conserved seed pairing, often flanked by adenosines, indicates that thousands of human genes are microRNA targets. Cell *120*, 15-20.

Liappas, G., Gonzalez-Mateo, G.T., Majano, P., Sanchez-Tomero, J.A., Ruiz-Ortega, M., Rodrigues Diez, R., Martin, P., Sanchez-Diaz, R., Selgas, R., Lopez-Cabrera, M., and Aguilera Peralta, A. (2017). Corrigendum to "T Helper 17/Regulatory T Cell Balance and Experimental Models of Peritoneal Dialysis-Induced Damage". Biomed Res Int *2017*, 6130208.

Liddell, R.P., Patel, T.H., Weiss, C.R., Lee, D.S., Matsuhashi, T., Brown, P.R., Gabrielson, K.L., Rodriguez, E.R., Eng, J., Kimura, H., and Hofmann, L.V. (2005). Endovascular model of rabbit hindlimb ischemia: a platform to evaluate therapeutic angiogenesis. Journal of vascular and interventional radiology : JVIR *16*, 991-998.

Lieberman, S.M., Kim, J.S., Corbo-Rodgers, E., Kambayashi, T., Maltzman, J.S., Behrens, E.M., and Turka, L.A. (2012). Site-specific accumulation of recently activated CD4+ Foxp3+ regulatory T cells following adoptive transfer. Eur J Immunol *42*, 1429-1435.

Lin, C.R., Wei, T.W., Tsai, H.Y., Wu, Y.T., Wu, P.Y., and Chen, S.T. (2015). Glycosylation-dependent interaction between CD69 and S100A8/S100A9 complex is required for regulatory T-cell differentiation. FASEB journal : official publication of the Federation of American Societies for Experimental Biology.

Lio, C.W., and Hsieh, C.S. (2008). A two-step process for thymic regulatory T cell development. Immunity *28*, 100-111.

Lisabeth, E.M., Falivelli, G., and Pasquale, E.B. (2013). Eph receptor signaling and ephrins. Cold Spring Harb Perspect Biol *5*.

Liston, A., Lu, L.F., O'Carroll, D., Tarakhovsky, A., and Rudensky, A.Y. (2008). Dicer-dependent microRNA pathway safeguards regulatory T cell function. J Exp Med *205*, 1993-2004.

Liu, W., Gao, C., Zhou, B.G., and Li, W.M. (2006). Effects of adenovirus-mediated gene transfer of ICOSIg and CTLA4Ig fusion protein on experimental autoimmune myocarditis. Autoimmunity *39*, 83-92.

Lopez Heras, I.S.-D., R. ; Anunciação S. D.; Madrid, Y. Luque-Garcia J.L. and Camara C. (2014). Effect of Chitosan-Stabilized Selenium Nanoparticles on Cell Cycle Arrest

and Invasiveness in Hepatocarcinoma Cells Revealed by Quantitative

Proteomics. Nanomedicine & Nanotechnology.

Lopez-Cabrera, M., Munoz, E., Blazquez, M.V., Ursa, M.A., Santis, A.G., and Sanchez-Madrid, F. (1995). Transcriptional regulation of the gene encoding the human C-type lectin leukocyte receptor AIM/CD69 and functional characterization of its tumor necrosis factor-alpha-responsive elements. J Biol Chem *270*, 21545-21551.

Lopez-Cabrera, M., Santis, A.G., Fernandez-Ruiz, E., Blacher, R., Esch, F., Sanchez-Mateos, P., and Sanchez-Madrid, F. (1993). Molecular cloning, expression, and chromosomal localization of the human earliest lymphocyte activation antigen AIM/CD69, a new member of the C-type animal lectin superfamily of signal-transmitting receptors. J Exp Med *178*, 537-547.

Lopez-Ferrer, D., Ramos-Fernandez, A., Martinez-Bartolome, S., Garcia-Ruiz, P., and Vazquez, J. (2006). Quantitative proteomics using 16O/18O labeling and linear ion trap mass spectrometry. Proteomics *6 Suppl 1*, S4-11.

Lu, L.F., Gasteiger, G., Yu, I.S., Chaudhry, A., Hsin, J.P., Lu, Y., Bos, P.D., Lin, L.L., Zawislak, C.L., Cho, S.*, et al.* (2015). A Single miRNA-mRNA Interaction Affects the Immune Response in a Context- and Cell-Type-Specific Manner. Immunity *43*, 52-64.

Lu, L.F., Thai, T.H., Calado, D.P., Chaudhry, A., Kubo, M., Tanaka, K., Loeb, G.B., Lee, H., Yoshimura, A., Rajewsky, K., and Rudensky, A.Y. (2009). Foxp3-dependent microRNA155 confers competitive fitness to regulatory T cells by targeting SOCS1 protein. Immunity *30*, 80-91.

Lu, S.Y., Huang, X.J., Liu, K.Y., Liu, D.H., and Xu, L.P. (2012). High frequency of CD4+ CD25- CD69+ T cells is correlated with a low risk of acute graft-versus-host disease in allotransplants. Clinical transplantation *26*, E158-167.

Mack, D.G., Lanham, A.M., Palmer, B.E., Maier, L.A., and Fontenot, A.P. (2009). CD27 expression on CD4+ T cells differentiates effector from regulatory T cell subsets in the lung. J Immunol *182*, 7317-7324.

Mampaso, F., Sanchez-Madrid, F., Marcen, R., Molina, A., Pascual, J., Bricio, T., Martin, A., and Alvarez, V. (1993). Expression of adhesion molecules in allograft renal dysfunction. A distinct diagnostic pattern in rejection and cyclosporine nephrotoxicity. Transplantation *56*, 687-691.

Markowska, A.I., Jefferies, K.C., and Panjwani, N. (2011). Galectin-3 protein modulates cell surface expression and activation of vascular endothelial growth factor receptor 2 in human endothelial cells. J Biol Chem *286*, 29913-29921.

Marouga, R., David, S., and Hawkins, E. (2005). The development of the DIGE system: 2D fluorescence difference gel analysis technology. Analytical and bioanalytical chemistry *382*, 669-678.

Martin, P., Gomez, M., Lamana, A., Cruz-Adalia, A., Ramirez-Huesca, M., Ursa, M.A., Yanez-Mo, M., and Sanchez-Madrid, F. (2010a). CD69 association with Jak3/Stat5 proteins regulates Th17 cell differentiation. Mol Cell Biol *30*, 4877-4889.

Martin, P., Gomez, M., Lamana, A., Marin, A.M., Cortes, J.R., Ramirez-Huesca, M., Barreiro, O., Lopez-Romero, P., Gutierrez-Vazquez, C., de la Fuente, H.*, et al.* (2010b). The leukocyte activation antigen CD69 limits allergic asthma and skin contact hypersensitivity. J Allergy Clin Immunol *126*, 355-365, 365 e351-353.

Martin, P., and Sanchez-Madrid, F. (2011). CD69: an unexpected regulator of TH17 cell-driven inflammatory responses. Sci Signal *4*, pe14.

Martin-Gayo, E., Sierra-Filardi, E., Corbi, A.L., and Toribio, M.L. (2010). Plasmacytoid dendritic cells resident in human thymus drive natural Treg cell development. Blood *115*, 5366-5375.

Matloubian, M., Lo, C.G., Cinamon, G., Lesneski, M.J., Xu, Y., Brinkmann, V., Allende, M.L., Proia, R.L., and Cyster, J.G. (2004). Lymphocyte egress from thymus and peripheral lymphoid organs is dependent on S1P receptor 1. Nature *427*, 355-360.

Mattiske, S., Suetani, R.J., Neilsen, P.M., and Callen, D.F. (2012). The oncogenic role of miR-155 in breast cancer. Cancer Epidemiol Biomarkers Prev *21*, 1236-1243.

McInnes, I.B., Leung, B.P., Sturrock, R.D., Field, M., and Liew, F.Y. (1997). Interleukin-15 mediates T cell-dependent regulation of tumor necrosis factor-alpha production in rheumatoid arthritis. Nat Med *3*, 189-195.

Mellor, A.L., and Munn, D.H. (2004). IDO expression by dendritic cells: tolerance and tryptophan catabolism. Nat Rev Immunol *4*, 762-774.

Miranda, K.C., Huynh, T., Tay, Y., Ang, Y.S., Tam, W.L., Thomson, A.M., Lim, B., and Rigoutsos, I. (2006). A pattern-based method for the identification of MicroRNA binding sites and their corresponding heteroduplexes. Cell *126*, 1203-1217.

Mitchell, P.S., Parkin, R.K., Kroh, E.M., Fritz, B.R., Wyman, S.K., Pogosova-Agadjanyan, E.L., Peterson, A., Noteboom, J., O'Briant, K.C., Allen, A*., et al.* (2008). Circulating microRNAs as stable blood-based markers for cancer detection. Proc Natl Acad Sci U S A *105*, 10513-10518.

Molet, S., Hamid, Q., Davoine, F., Nutku, E., Taha, R., Page, N., Olivenstein, R., Elias, J., and Chakir, J. (2001). IL-17 is increased in asthmatic airways and induces human bronchial fibroblasts to produce cytokines. J Allergy Clin Immunol *108*, 430-438.

Montalvo, J., Spencer, C., Hackathorn, A., Masterjohn, K., Perkins, A., Doty, C., Arumugam, A., Ongusaha, P.P., Lakshmanaswamy, R., Liao, J.K*., et al.* (2013). ROCK1 & 2 perform overlapping and unique roles in angiogenesis and angiosarcoma tumor progression. Curr Mol Med *13*, 205-219.

Mosmann, T.R., and Coffman, R.L. (1989). TH1 and TH2 cells: different patterns of lymphokine secretion lead to different functional properties. Annu Rev Immunol *7*, 145-173.

Mucida, D., Kutchukhidze, N., Erazo, A., Russo, M., Lafaille, J.J., and Curotto de Lafaille, M.A. (2005). Oral tolerance in the absence of naturally occurring Tregs. J Clin Invest *115*, 1923-1933.

Mucida, D., Park, Y., Kim, G., Turovskaya, O., Scott, I., Kronenberg, M., and Cheroutre, H. (2007). Reciprocal TH17 and regulatory T cell differentiation mediated by retinoic acid. Science *317*, 256-260.

Nakae, S., Komiyama, Y., Nambu, A., Sudo, K., Iwase, M., Homma, I., Sekikawa, K., Asano, M., and Iwakura, Y. (2002). Antigen-specific T cell sensitization is impaired in IL-17-deficient mice, causing suppression of allergic cellular and humoral responses. Immunity *17*, 375-387.

Nakae, S., Nambu, A., Sudo, K., and Iwakura, Y. (2003). Suppression of immune induction of collagen-induced arthritis in IL-17-deficient mice. J Immunol *171*, 6173-6177.

Nakayama, T., Kasprowicz, D.J., Yamashita, M., Schubert, L.A., Gillard, G., Kimura, M., Didierlaurent, A., Koseki, H., and Ziegler, S.F. (2002). The generation of mature, single-positive thymocytes in vivo is dysregulated by CD69 blockade or overexpression. J Immunol *168*, 87-94.

Napolitani, G., Rinaldi, A., Bertoni, F., Sallusto, F., and Lanzavecchia, A. (2005). Selected Toll-like receptor agonist combinations synergistically trigger a T helper type 1-polarizing program in dendritic cells. Nat Immunol *6*, 769-776.

Nazari-Jahantigh, M., Wei, Y., Noels, H., Akhtar, S., Zhou, Z., Koenen, R.R., Heyll, K., Gremse, F., Kiessling, F., Grommes, J*., et al.* (2012). MicroRNA-155 promotes atherosclerosis by repressing Bcl6 in macrophages. J Clin Invest *122*, 4190-4202.

Nicosia, R.F., and Ottinetti, A. (1990a). Growth of microvessels in serum-free matrix culture of rat aorta. A quantitative assay of angiogenesis in vitro. Lab Invest *63*, 115-122.

Nicosia, R.F., and Ottinetti, A. (1990b). Modulation of microvascular growth and morphogenesis by reconstituted basement membrane gel in three-dimensional cultures of rat aorta: a comparative study of angiogenesis in matrigel, collagen, fibrin, and plasma clot. In vitro cellular & developmental biology : journal of the Tissue Culture Association *26*, 119-128.

Nikiforova, M.N., Tseng, G.C., Steward, D., Diorio, D., and Nikiforov, Y.E. (2008). MicroRNA expression profiling of thyroid tumors: biological significance and diagnostic utility. The Journal of clinical endocrinology and metabolism *93*, 1600-1608.

Nishikawa, K., Morii, T., Ako, H., Hamada, K., Saito, S., and Narita, N. (1992). In vivo expression of CD69 on lung eosinophils in eosinophilic pneumonia: CD69 as a possible activation marker for eosinophils. J Allergy Clin Immunol *90*, 169-174.

O'Connell, R.M., Kahn, D., Gibson, W.S., Round, J.L., Scholz, R.L., Chaudhuri, A.A., Kahn, M.E., Rao, D.S., and Baltimore, D. (2010). MicroRNA-155 promotes autoimmune inflammation by enhancing inflammatory T cell development. Immunity *33*, 607-619.

O'Connell, R.M., Rao, D.S., Chaudhuri, A.A., Boldin, M.P., Taganov, K.D., Nicoll, J., Paquette, R.L., and Baltimore, D. (2008). Sustained expression of microRNA-155 in hematopoietic stem cells causes a myeloproliferative disorder. J Exp Med *205*, 585-594.

O'Shea, J.J., and Paul, W.E. (2010). Mechanisms underlying lineage commitment and plasticity of helper CD4+ T cells. Science *327*, 1098-1102.

Ohkura, N., Kitagawa, Y., and Sakaguchi, S. (2013). Development and maintenance of regulatory T cells. Immunity *38*, 414-423.

Ong, S.E., Blagoev, B., Kratchmarova, I., Kristensen, D.B., Steen, H., Pandey, A., and Mann, M. (2002). Stable isotope labeling by amino acids in cell culture, SILAC, as a simple and accurate approach to expression proteomics. Mol Cell Proteomics *1*, 376-386.

Ouyang, W., Kolls, J.K., and Zheng, Y. (2008). The biological functions of T helper 17 cell effector cytokines in inflammation. Immunity *28*, 454-467.

Padilla, N.D., van Vliet, A.K., Schoots, I.G., Valls Seron, M., Maas, M.A., Peltenburg, E.E., de Vries, A., Niessen, H.W., Hack, C.E., and van Gulik, T.M. (2007). C-reactive protein and natural IgM antibodies are activators of complement in a rat model of intestinal ischemia and reperfusion. Surgery *142*, 722-733.

Pan, Q.Z., Pan, K., Wang, Q.J., Weng, D.S., Zhao, J.J., Zheng, H.X., Zhang, X.F., Jiang, S.S., Lv, L., Tang, Y.*, et al.* (2015). Annexin A3 as a potential target for immunotherapy of liver cancer stem-like cells. Stem Cells *33*, 354-366.

Pankratz, F., Bemtgen, X., Zeiser, R., Leonhardt, F., Kreuzaler, S., Hilgendorf, I., Smolka, C., Helbing, T., Hoefer, I., Esser, J.S.*, et al.* (2015). MicroRNA-155 Exerts Cell-Specific Antiangiogenic but Proarteriogenic Effects During Adaptive Neovascularization. Circulation *131*, 1575-1589.

Patel, S., Leal, A.D., and Gorski, D.H. (2005). The homeobox gene Gax inhibits angiogenesis through inhibition of nuclear factor-kappaB-dependent endothelial cell gene expression. Cancer research *65*, 1414-1424.

Petersen, C.C., Nederby, L., Roug, A.S., Skovbo, A., Peterslund, N.A., Hokland, P., Nielsen, B., and Hokland, M. (2011). Increased expression of CD69 on T cells as an early immune marker for human cytomegalovirus reactivation in chronic lymphocytic leukemia patients. Viral Immunol *24*, 165-169.

Pfaff, N., Fiedler, J., Holzmann, A., Schambach, A., Moritz, T., Cantz, T., and Thum, T. (2011). miRNA screening reveals a new miRNA family stimulating iPS cell generation via regulation of Meox2. EMBO reports *12*, 1153-1159.

Pillai, R.S. (2005). MicroRNA function: multiple mechanisms for a tiny RNA? Rna *11*, 1753-1761.

Powrie, F., and Coffman, R.L. (1993). Cytokine regulation of T-cell function: potential for therapeutic intervention. Immunol Today *14*, 270-274.

Qureshi, O.S., Zheng, Y., Nakamura, K., Attridge, K., Manzotti, C., Schmidt, E.M., Baker, J., Jeffery, L.E., Kaur, S., Briggs, Z.*, et al.* (2011). Trans-endocytosis of CD80 and CD86: a molecular basis for the cell-extrinsic function of CTLA-4. Science *332*, 600-603.

Radstake, T.R., van Bon, L., Broen, J., Wenink, M., Santegoets, K., Deng, Y., Hussaini, A., Simms, R., Cruikshank, W.W., and Lafyatis, R. (2009). Increased frequency and compromised function of T regulatory cells in systemic sclerosis (SSc) is related to a diminished CD69 and TGFbeta expression. PLoS One *4*, e5981.

Radulovic, K., Manta, C., Rossini, V., Holzmann, K., Kestler, H.A., Wegenka, U.M., Nakayama, T., and Niess, J.H. (2012). CD69 regulates type I IFN-induced tolerogenic signals to mucosal CD4 T cells that attenuate their colitogenic potential. J Immunol *188*, 2001-2013.

Radulovic, K., Rossini, V., Manta, C., Holzmann, K., Kestler, H.A., and Niess, J.H. (2013). The early activation marker CD69 regulates the expression of chemokines and CD4 T cell accumulation in intestine. PLoS One *8*, e65413.

Rangachari, M., Mauermann, N., Marty, R.R., Dirnhofer, S., Kurrer, M.O., Komnenovic, V., Penninger, J.M., and Eriksson, U. (2006). T-bet negatively regulates autoimmune myocarditis by suppressing local production of interleukin 17. J Exp Med *203*, 2009-2019.

Read, S., Malmstrom, V., and Powrie, F. (2000). Cytotoxic T lymphocyte-associated antigen 4 plays an essential role in the function of CD25(+)CD4(+) regulatory cells that control intestinal inflammation. J Exp Med *192*, 295-302.

Ring, S., Enk, A.H., and Mahnke, K. (2010). ATP activates regulatory T Cells in vivo during contact hypersensitivity reactions. J Immunol *184*, 3408-3416.

Ripka, S., Neesse, A., Riedel, J., Bug, E., Aigner, A., Poulsom, R., Fulda, S., Neoptolemos, J., Greenhalf, W., Barth, P.*, et al.* (2010). CUX1: target of Akt signalling and mediator of resistance to apoptosis in pancreatic cancer. Gut *59*, 1101-1110.

Rodriguez, A., Vigorito, E., Clare, S., Warren, M.V., Couttet, P., Soond, D.R., van Dongen, S., Grocock, R.J., Das, P.P., Miska, E.A.*, et al.* (2007). Requirement of bic/microRNA-155 for normal immune function. Science *316*, 608-611.

Rodriguez-Diez, M.C., Diez, N., Merino, I., Velis, J.M., Tienza, A., and Robles-Garcia, J.E. (2014). Simulators help improve student confidence to acquire skills in urology. Actas Urol Esp *38*, 367-372.

Roncarolo, M.G., Gregori, S., Battaglia, M., Bacchetta, R., Fleischhauer, K., and Levings, M.K. (2006). Interleukin-10-secreting type 1 regulatory T cells in rodents and humans. Immunol Rev *212*, 28-50.

Ruprecht, C.R., Gattorno, M., Ferlito, F., Gregorio, A., Martini, A., Lanzavecchia, A., and Sallusto, F. (2005). Coexpression of CD25 and CD27 identifies FoxP3+ regulatory T cells in inflamed synovia. J Exp Med *201*, 1793-1803.

Sanchez-Diaz, R.L., S.; Tsilingiri, K.; Matesanz-Marin, A.; Martin-Gayo, E.; Toribio, M.L.; Sanchez-Madrid, F.; Martin, P. (2016). CD69 contributes intrathymic natural regulatory T cell development through microRNA155 overexpression. *Unpublished*.

Sanchez-Mateos, P., Cebrian, M., Acevedo, A., Lopez-Botet, M., De Landazuri, M.O., and Sanchez-Madrid, F. (1989). Expression of a gp33/27,000 MW activation inducer molecule (AIM) on human lymphoid tissues. Induction of cell proliferation on thymocytes and B lymphocytes by anti-AIM antibodies. Immunology *68*, 72-79.

Sanchez-Mateos, P., and Sanchez-Madrid, F. (1991). Structure-function relationship and immunochemical mapping of external and intracellular antigenic sites on the lymphocyte activation inducer molecule, AIM/CD69. Eur J Immunol *21*, 2317-2325.

Sancho, D., Gomez, M., Viedma, F., Esplugues, E., Gordon-Alonso, M., Garcia-Lopez, M.A., de la Fuente, H., Martinez, A.C., Lauzurica, P., and Sanchez-Madrid, F. (2003). CD69 downregulates autoimmune reactivity through active transforming growth factor-beta production in collagen-induced arthritis. J Clin Invest *112*, 872-882.

Santis, A.G., Lopez-Cabrera, M., Hamann, J., Strauss, M., and Sanchez-Madrid, F. (1994). Structure of the gene coding for the human early lymphocyte activation antigen CD69: a C-type lectin receptor evolutionarily related with the gene families of natural killer cell-specific receptors. Eur J Immunol *24*, 1692-1697.

Sanz-Rodriguez, F., Guerrero-Esteo, M., Botella, L.M., Banville, D., Vary, C.P., and Bernabeu, C. (2004). Endoglin regulates cytoskeletal organization through binding to ZRP-1, a member of the Lim family of proteins. J Biol Chem *279*, 32858-32868.

Schnyder-Candrian, S., Togbe, D., Couillin, I., Mercier, I., Brombacher, F., Quesniaux, V., Fossiez, F., Ryffel, B., and Schnyder, B. (2006). Interleukin-17 is a negative regulator of established allergic asthma. J Exp Med *203*, 2715-2725.

Schroedl, C., McClintock, D.S., Budinger, G.R., and Chandel, N.S. (2002). Hypoxic but not anoxic stabilization of HIF-1alpha requires mitochondrial reactive oxygen species. American journal of physiology. Lung cellular and molecular physiology *283*, L922-931.

Seddiki, N., Santner-Nanan, B., Martinson, J., Zaunders, J., Sasson, S., Landay, A., Solomon, M., Selby, W., Alexander, S.I., Nanan, R.*, et al.* (2006). Expression of interleukin (IL)-2 and IL-7 receptors discriminates between human regulatory and activated T cells. J Exp Med *203*, 1693-1700.

Seppo Ylä-Herttuala, T.T.R., Ismo Vajanto, Juha Hartikainen (2007). Molecular Mechanisms of VEGF-Induced Angiogenesis. Journal of the American College of Cardiology *49*, 1015-1026

.

Shiow, L.R., Rosen, D.B., Brdickova, N., Xu, Y., An, J., Lanier, L.L., Cyster, J.G., and Matloubian, M. (2006). CD69 acts downstream of interferon-alpha/beta to inhibit S1P1 and lymphocyte egress from lymphoid organs. Nature *440*, 540-544.

Sica, V., Williams-Ignarro, S., de Nigris, F., D'Armiento, F.P., Lerman, L.O., Balestrieri, M.L., Maione, C., Palagiano, A., Rossiello, L., Ignarro, L.J., and Napoli, C. (2006). Autologous bone marrow cell therapy and metabolic intervention in ischemia-induced angiogenesis in the diabetic mouse hindlimb. Cell Cycle *5*, 2903-2908.

Sonderegger, I., Rohn, T.A., Kurrer, M.O., Iezzi, G., Zou, Y., Kastelein, R.A., Bachmann, M.F., and Kopf, M. (2006). Neutralization of IL-17 by active vaccination inhibits IL-23-dependent autoimmune myocarditis. Eur J Immunol *36*, 2849-2856.

Spellman, D.S., Deinhardt, K., Darie, C.C., Chao, M.V., and Neubert, T.A. (2008). Stable isotopic labeling by amino acids in cultured primary neurons: application to brain-derived neurotrophic factor-dependent phosphotyrosine-associated signaling. Mol Cell Proteomics *7*, 1067-1076.

Spinetti, G., Fortunato, O., Caporali, A., Shantikumar, S., Marchetti, M., Meloni, M., Descamps, B., Floris, I., Sangalli, E., Vono, R.*, et al.* (2013). MicroRNA-15a and microRNA-16 impair human circulating proangiogenic cell functions and are increased in the proangiogenic cells and serum of patients with critical limb ischemia. Circ Res *112*, 335-346.

Swat, W., Dessing, M., von Boehmer, H., and Kisielow, P. (1993). CD69 expression during selection and maturation of CD4+8+ thymocytes. Eur J Immunol *23*, 739-746.

Swierkosz, J.E., Marrack, P., and Kappler, J.W. (1979). Functional analysis of T cells expressing Ia antigens. I. Demonstration of helper T-cell heterogeneity. J Exp Med *150*, 1293-1309.

Szabo, S.J., Sullivan, B.M., Peng, S.L., and Glimcher, L.H. (2003). Molecular mechanisms regulating Th1 immune responses. Annu Rev Immunol *21*, 713-758.

Tada, T., Takemori, T., Okumura, K., Nonaka, M., and Tokuhisa, T. (1978). Two distinct types of helper T cells involved in the secondary antibody response: independent and synergistic effects of Ia- and Ia+ helper T cells. J Exp Med *147*, 446-458.

Taganov, K.D., Boldin, M.P., Chang, K.J., and Baltimore, D. (2006). NF-kappaB-dependent induction of microRNA miR-146, an inhibitor targeted to signaling proteins of innate immune responses. Proc Natl Acad Sci U S A *103*, 12481-12486.

Testi, R., D'Ambrosio, D., De Maria, R., and Santoni, A. (1994). The CD69 receptor: a multipurpose cell-surface trigger for hematopoietic cells. Immunol Today *15*, 479-483.

Testi, R., Phillips, J.H., and Lanier, L.L. (1989). T cell activation via Leu-23 (CD69). J Immunol *143*, 1123-1128.

Testi, R., Pulcinelli, F., Frati, L., Gazzaniga, P.P., and Santoni, A. (1990). CD69 is expressed on platelets and mediates platelet activation and aggregation. J Exp Med *172*, 701-707.

Thai, T.H., Calado, D.P., Casola, S., Ansel, K.M., Xiao, C., Xue, Y., Murphy, A., Frendewey, D., Valenzuela, D., Kutok, J.L.*, et al.* (2007). Regulation of the germinal center response by microRNA-155. Science *316*, 604-608.

Trinchieri, G., Pflanz, S., and Kastelein, R.A. (2003). The IL-12 family of heterodimeric cytokines: new players in the regulation of T cell responses. Immunity *19*, 641-644.

Truscott, M., Denault, J.B., Goulet, B., Leduy, L., Salvesen, G.S., and Nepveu, A. (2007). Carboxyl-terminal proteolytic processing of CUX1 by a caspase enables transcriptional activation in proliferating cells. J Biol Chem *282*, 30216-30226.

Turecek, F. (2002). Mass spectrometry in coupling with affinity capture-release and isotope-coded affinity tags for quantitative protein analysis. J Mass Spectrom *37*, 1-14.

Unutmaz, D., Pileri, P., and Abrignani, S. (1994). Antigen-independent activation of naive and memory resting T cells by a cytokine combination. J Exp Med *180*, 1159-1164.

Urbich, C., Dernbach, E., Rossig, L., Zeiher, A.M., and Dimmeler, S. (2008a). High glucose reduces cathepsin L activity and impairs invasion of circulating progenitor cells. J Mol Cell Cardiol *45*, 429-436.

Urbich, C., Kuehbacher, A., and Dimmeler, S. (2008b). Role of microRNAs in vascular diseases, inflammation, and angiogenesis. Cardiovasc Res *79*, 581-588.

Vadnais, C., Awan, A.A., Harada, R., Clermont, P.L., Leduy, L., Berube, G., and Nepveu, A. (2013). Long-range transcriptional regulation by the p110 CUX1 homeodomain protein on the ENCODE array. BMC Genomics *14*, 258.

Verano-Braga, T., Schwammle, V., Sylvester, M., Passos-Silva, D.G., Peluso, A.A., Etelvino, G.M., Santos, R.A., and Roepstorff, P. (2012). Time-resolved quantitative phosphoproteomics: new insights into Angiotensin-(1-7) signaling networks in human endothelial cells. J Proteome Res *11*, 3370-3381.

Vigorito, E., Perks, K.L., Abreu-Goodger, C., Bunting, S., Xiang, Z., Kohlhaas, S., Das, P.P., Miska, E.A., Rodriguez, A., Bradley, A*., et al.* (2007). microRNA-155 regulates the generation of immunoglobulin class-switched plasma cells. Immunity *27*, 847-859.

Vitales-Noyola, M., Doniz-Padilla, L., Alvarez-Quiroga, C., Monsivais-Urenda, A., Portillo-Salazar, H., and Gonzalez-Amaro, R. (2015). Quantitative and functional analysis of CD69(+) NKG2D(+) T regulatory cells in healthy subjects. Human immunology *76*, 511-518.

Wan, Y.Y., and Flavell, R.A. (2007). Regulatory T-cell functions are subverted and converted owing to attenuated Foxp3 expression. Nature *445*, 766-770.

Weaver, C.T., Harrington, L.E., Mangan, P.R., Gavrieli, M., and Murphy, K.M. (2006). Th17: an effector CD4 T cell lineage with regulatory T cell ties. Immunity *24*, 677-688.

Wei, Y., Nazari-Jahantigh, M., Chan, L., Zhu, M., Heyll, K., Corbalan-Campos, J., Hartmann, P., Thiemann, A., Weber, C., and Schober, A. (2013). The microRNA-342-5p fosters inflammatory macrophage activation through an Akt1- and microRNA-155-dependent pathway during atherosclerosis. Circulation *127*, 1609-1619.

Weinreich, M.A., and Hogquist, K.A. (2008). Thymic emigration: when and how T cells leave home. J Immunol *181*, 2265-2270.

Wheeler, G., Ntounia-Fousara, S., Granda, B., Rathjen, T., and Dalmay, T. (2006). Identification of new central nervous system specific mouse microRNAs. FEBS letters *580*, 2195-2200.

Wightman, B., Ha, I., and Ruvkun, G. (1993). Posttranscriptional regulation of the heterochronic gene lin-14 by lin-4 mediates temporal pattern formation in C. elegans. Cell *75*, 855-862.

Wirnsberger, G., Mair, F., and Klein, L. (2009). Regulatory T cell differentiation of thymocytes does not require a dedicated antigen-presenting cell but is under T cell-intrinsic developmental control. Proc Natl Acad Sci U S A *106*, 10278-10283.

Wu, Y., Han, W., and Liu, G.N. (2010). A DNA enzyme targeting Egr-1 inhibits rat vascular smooth muscle cell proliferation by down-regulation of cyclin D1 and TGF-beta1. Brazilian journal of medical and biological research = Revista brasileira de pesquisas medicas e biologicas *43*, 17-24.

Yang, X.O., Panopoulos, A.D., Nurieva, R., Chang, S.H., Wang, D., Watowich, S.S., and Dong, C. (2007). STAT3 regulates cytokine-mediated generation of inflammatory helper T cells. J Biol Chem *282*, 9358-9363.

Yang, Y., Bai, W., Zhang, L., Yin, G., Wang, X., Wang, J., Zhao, H., Han, Y., and Yao, Y.Q. (2008). Determination of microRNAs in mouse preimplantation embryos by microarray. Dev Dyn *237*, 2315-2327.

Yao, R., Ma, Y., Du, Y., Liao, M., Li, H., Liang, W., Yuan, J., Ma, Z., Yu, X., Xiao, H., and Liao, Y. (2011). The altered expression of inflammation-related microRNAs with microRNA-155 expression correlates with Th17 differentiation in patients with acute coronary syndrome. Cellular & molecular immunology *8*, 486-495.

Yao, R., Ma, Y.L., Liang, W., Li, H.H., Ma, Z.J., Yu, X., and Liao, Y.H. (2012). MicroRNA-155 modulates Treg and Th17 cells differentiation and Th17 cell function by targeting SOCS1. PLoS One *7*, e46082.

Yin, Q., McBride, J., Fewell, C., Lacey, M., Wang, X., Lin, Z., Cameron, J., and Flemington, E.K. (2008a). MicroRNA-155 is an Epstein-Barr virus-induced gene that modulates Epstein-Barr virus-regulated gene expression pathways. Journal of virology *82*, 5295-5306.

Yin, Q., Wang, X., McBride, J., Fewell, C., and Flemington, E. (2008b). B-cell receptor activation induces BIC/miR-155 expression through a conserved AP-1 element. J Biol Chem *283*, 2654-2662.

Yuyama, T., Yusa, S., Yoshizumi, K., Yamano, S., Murata, S., Hirose, T., Osanai, R., Onishi, Y., Osato, S., Sasaki, C*., et al.* (2002). Molecular epidemiology of VapA-positive Rhodococcus equi in thoroughbred horses in Kagoshima, Japan. The Journal of veterinary medical science *64*, 715-718.

Zajac, A.J., Blattman, J.N., Murali-Krishna, K., Sourdive, D.J., Suresh, M., Altman, J.D., and Ahmed, R. (1998). Viral immune evasion due to persistence of activated T cells without effector function. J Exp Med *188*, 2205-2213.

Zanivan, S., Krueger, M., and Mann, M. (2012). In vivo quantitative proteomics: the SILAC mouse. Methods Mol Biol *757*, 435-450.

Zernecke, A., Bidzhekov, K., Noels, H., Shagdarsuren, E., Gan, L., Denecke, B., Hristov, M., Koppel, T., Jahantigh, M.N., Lutgens, E*., et al.* (2009). Delivery of microRNA-126 by apoptotic bodies induces CXCL12-dependent vascular protection. Sci Signal *2*, ra81.

Zhang, Y., Liu, D., Chen, X., Li, J., Li, L., Bian, Z., Sun, F., Lu, J., Yin, Y., Cai, X*., et al.* (2010). Secreted monocytic miR-150 enhances targeted endothelial cell migration. Molecular cell *39*, 133-144.

Zheng, W., and Flavell, R.A. (1997). The transcription factor GATA-3 is necessary and sufficient for Th2 cytokine gene expression in CD4 T cells. Cell *89*, 587-596.

Zheng, Y., Josefowicz, S.Z., Kas, A., Chu, T.T., Gavin, M.A., and Rudensky, A.Y. (2007). Genome-wide analysis of Foxp3 target genes in developing and mature regulatory T cells. Nature *445*, 936-940.

Ziegler, S.F., Levin, S.D., Johnson, L., Copeland, N.G., Gilbert, D.J., Jenkins, N.A., Baker, E., Sutherland, G.R., Feldhaus, A.L., and Ramsdell, F. (1994). The mouse CD69 gene. Structure, expression, and mapping to the NK gene complex. J Immunol *152*, 1228-1236.

Zieske, L.R. (2006). A perspective on the use of iTRAQ reagent technology for protein complex and profiling studies. J Exp Bot *57*, 1501-1508.

Zingoni, A., Palmieri, G., Morrone, S., Carretero, M., Lopez-Botel, M., Piccoli, M., Frati, L., and Santoni, A. (2000). CD69-triggered ERK activation and functions are negatively regulated by CD94 / NKG2-A inhibitory receptor. Eur J Immunol *30*, 644-651.

Zouggari, Y., Ait-Oufella, H., Waeckel, L., Vilar, J., Loinard, C., Cochain, C., Recalde, A., Duriez, M., Levy, B.I., Lutgens, E.*, et al.* (2009). Regulatory T cells modulate postischemic neovascularization. Circulation *120*, 1415-1425.

VII. ANEXOS

Bioanalytical strategies for *in-vitro* and *in-vivo* evaluation of the toxicity induced by metallic nanoparticles

Jose L. Luque-Garcia, Raquel Sanchez-Díaz, Isabel Lopez-Heras, Pilar Martin, Carmen Camara

The increasing use of metallic nanoparticles (MNPs) in a wide variety of applications has led to an urgent need to evaluate the impact of these new materials on human health and the environment. To date, the potential toxicity of MNPs and their interaction mechanisms with cells and living organisms have not been fully addressed.

In this article, we discuss the different bioanalytical strategies that have been used for this purpose. We consider different methods aiming to evaluate cellular uptake and localization in cells and tissues, and *in-vitro* methods for the study of the toxicity induced by MNPs, considering different toxicity markers and high-throughput approaches for the identification of specific targets involved in the cell-MNP interaction. We also discuss special strategies related to the use of animal models to assess *in-vivo* toxicity of MNPs.

Keywords: Animal model; Bioanalytical strategy; Cellular uptake; Interaction mechanism; *In-vitro* assay; *In-vivo* assay; Metallic nanoparticle (MNP); Target identification; Toxicity assessment; Toxicity marker

Jose L. Luque-Garcia*, Raquel Sanchez-Díaz, Isabel Lopez-Heras, Carmen Camara
Department of Analytical Chemistry, Faculty of Chemistry, Complutense University of Madrid, Av. Complutense s/n, 28004 Madrid, Spain

Pilar Martin
Department of Vascular Biology and Inflammation, Fundacion Centro Nacional de Investigaciones Cardiovasculares Carlos III, Madrid, Spain

*Corresponding author.
Tel.: +34 913 944 318;
Fax: +34 913 944 329;
E-mail: jlluque@quim.ucm.es

1. Introduction

Nanoparticles (NPs) have received great attention for their use and applicability in many new consumer products. A recent estimate suggests that more than 1000 NP-containing consumer products are currently on the market. In addition, their ability to advance science with novel analytical and medical tools also makes them relevant to physical and life sciences [1].

NPs are generally defined as particles with at least one dimension of 1–100 nm. This smaller size gives them unique properties, especially because their specific surface area is larger and their reactivity is increased or different compared to bulk materials. These specific features are often linked with a potential toxicity [2]. Among the different kinds of NPs, metallic NPs (MNPs) are particularly used in many applications. The products and the applications of MNPs include electronics, optics, textiles, medical applications, cosmetics, food packaging, water-treatment technology, fuel cells, catalysts, biosensors and agents for environmental remediation [3,4]. As a result of these applications, exposure of MNPs to the environment and humans is becoming increasingly widespread. Consequently, different metals in the form of MNPs have gained increasing access to tissues, cells and biological molecules within the human body [5]. Human exposure to MNPs is most likely to occur during manufacturing processes, but inhalation of MNPs released to the atmosphere, ingestion of water or food containing MNPs and dermal exposure from various sources (e.g., body lotions and sunscreens) are possible [6].

To date, the impact of exposure to MNPs on human health and the environment has not been fully assessed [7]. Research efforts to assess the toxic potential of MNPs have presented some serious, far-reaching challenges and there remains an urgent

0165-9936/$ - see front matter © 2012 Elsevier Ltd. All rights reserved. doi:http://dx.doi.org/10.1016/j.trac.2012.11.004

need for well-designed studies that will generate data so that the risk of MNPs can be assessed [8].

Chemical composition, shape, size, stability, surface coating, functionalization and purity of MNPs are essential aspects for not only applications but also potential toxicity [9]. Particle chemistry is especially relevant; depending on their chemistry, NPs can show different cellular uptake and ability to catalyze the production of reactive oxygen species, which is directly related to toxicity [10]. Many studies have also suggested the importance of shape and crystallographic phase when evaluating the toxicity induced by MNPs [3,11]. Uptake and cellular distribution of NPs are greatly influenced by their size. It has been demonstrated that cellular internalization is more pronounced for smaller NPs as compared to equivalent larger NPs at the same dose [12]. In addition, smaller MNPs show greater reactivity because of their larger surface area [2]. Aggregation of MNPs mainly depends on surface charge, material type and size. The formation of MNP aggregates affects the degree of cell internalization and thus modifies the potential toxic effect [13]. It is also crucial to consider surface modification of NPs by proteins or ions present in the culture media or when using metals, organic molecules or polymers as surface coatings [12–14]. These modifications can dramatically change the physicochemical properties of MNPs, including their magnetic, electric, and optical properties and their chemical reactivity [15].

In order to correlate any toxic reaction with MNP type, it is indispensable to investigate if the NPs are attached to the cell surface or if they enter cells. If NPs are found in cells, their localization in different compartments (e.g., endosomes, lysosomes, mitochondria, nucleus or citosol) may also provide some answers regarding their potential toxicity [16]. It is also very important for understanding the complex processes that govern cellular uptake and intracellular fate of MNPs [17]. Finally, *in-vivo* studies are also needed to design specific, safe clinical trials to develop new strategies for applications of MNPs and also to evaluate their risk to the environment [18].

In this review, we present different analytical and bioanalytical strategies to study the interaction of MNPs with cells and living organisms in order to assess their potential toxicity. We start by discussing different options to evaluate cellular uptake and localization of MNPs by using atomic techniques and imaging approaches. We also review *in-vitro* assays to study the interaction of cells with MNPs considering those that aim to evaluate specific cellular pathways or cellular responses to MNP exposure and those based on high-throughput discovery platforms focused on identifying particular targets (genes and/or proteins) involved in the cell-MNP interaction. Finally, we review considerations about *in-vivo* assays depending on the different animal models that have been used to date.

2. Cellular uptake and localization of MNPs

When studying the interaction of MNPs with living organisms and cells, one of the key aspects is the evaluation of the cellular uptake and the localization of the MNPs within the cells and tissues. The quantification of MNPs and ions released from them is mainly carried out by sensitive analytical techniques [e.g., inductively coupled plasma-mass spectrometry (ICP-MS)] while localization, which requires spatial resolution analysis, is generally performed by different microscopic techniques.

2.1. Quantification of NPs and ions released from NPs using spectrometric techniques

ICP sources are regarded as excellent tools for elemental analysis. Many authors have used techniques based on ICP in order to provide a quantitative analysis of the uptake of MNPs in different organisms [19]. ICP-MS provides high sensitivity and robustness for quantifying metal composition in a large variety of samples. Christen and Fent used an ICP-MS equipped with an octopole reaction system to minimize possible interferences, and confirmed that the cytotoxicity induced by Ag-doped SiO_2 NPs was caused by Ag ions released from the NPs [7].

Other detectors have also been coupled to an ICP source for this purpose. The use of ICP with optical emission spectroscopy detection (ICP-OES) has been employed to perform cadmium analysis as an indication of the concentration of CdSe/ZnS quantum-dot (QD) NPs in plasma and organs of *Daphnia magna* after 48 h of exposure [20]. The impact of three metal-oxide NPs (nonporous SiO_2, mesoporous SiO_2 and anatase TiO_2 NPs) on the immune response of mast cells was evaluated using ICP-OES, showing that the cell-NP interaction depended on the chemically-modified surface of the NPs [21].

However, the direct analysis of MNPs using ICP as ionization source presents some drawbacks due to the limited availability of commercial standards for MNPs and the low nebulization efficiency. This technique is able to ionize and to atomize spherical NPs of 5–25 nm in aqueous and organic solutions [22]. However, MNP aggregates might not be effectively ionized in the plasma, and that can result in lower recoveries. In these cases of low ionization efficiency, electro-thermal vaporization (ETV) should be considered as an alternative sample-introduction system because it allows pre-digestion of the MNPs [23,24].

Another problem that has to be considered is the potential adsorption of the MNPs on the sample-introduction system, which can complicate the quantification of MNPs in real samples [25]. Thus, it is important to carry out a previous digestion, using a combination of acids and high temperature [26], to determine the total metal concentration of the tested element. In this way, the

concentration of Cd and Se were determined in *Arabidopsis thaliana* plants exposed to CdSe/ZnS QDs. Leaves and roots were thoroughly rinsed with Milli-Q water to remove material that was not adsorbed or integrated by the plant. The tissues were digested in concentrated nitric acid and 30% hydrogen peroxide (4:1) for 2 h using a hot plate [27]. Conventional digestion procedures can be very time consuming so the use of microwaves can minimize the time required for sample treatment. In addition, a closed microwave-digestion vessel might lower the risk of analyte losses compared to open digestion. The accumulation of TiO_2 NPs was observed in lung tissue of Wistar rats after analysis of the levels of Ti by digesting the sample with nitric acid and hydrogen peroxide prior to double-focusing (DF)-ICP-MS detection [28]. Differences between the bioaccumulation of Ag NPs and Ag microparticles in rat brain microvessel vascular endothelial cells (BMVECs) were evaluated by acid digestion with nitric acid prior to the analysis with ICP-MS. This study demonstrated that Ag NPs accumulate in cells more easily than microparticles [29].

Analytical methods based on acid digestion offer the possibility to reduce the matrix effects due to eliminating biological components present in the sample or stabilizing agents employed to avoid NP aggregation. However, this procedure makes it impossible to distinguish between metal species (MNPs taken up by the organism and other metal species). An alternative to digestion of solid samples is the use of ultrasound. The use of ultrasound-assisted extraction is a very promising methodology for metal species and MNPs. In addition, ultrasonic energy breaks up MNP aggregates [30]. However, as in digestion procedures, the chemical form of MNPs might alter due to the use of basic or acid solutions in the extractant. Using this approach, total Ti concentration was determined in fibroblasts exposed to TiO_2 NPs after sonication of trypsinized cells in an ultrasonic bath for 30 min [11].

Other techniques include furnace atomic absorption spectrometry (FAAS), used to determine the total Ag content in harvested THP-1 cells prior to acid digestion in 69% HNO_3 [31], or graphite furnace AAS (GF-AAS) [13], which are alternatives to ICP-based techniques.

Despite the numerous advantages offered by ICP-MS and other atomic techniques, it is important to emphasize that this technique by itself is unable to differentiate between metal species (e.g., MNPs or ions). Such differentiation requires previous treatments (e.g., filtration, centrifugation and sedimentation) that allow isolation of MNPs from solutions, or otherwise, the use of a separation technique coupled to the ICP-MS. Separation techniques [e.g., liquid chromatography (LC) or field-flow fractionation (FFF)] coupled to ICP-MS are among the most promising approaches. In this way, size-exclusion chromatography (SEC) columns and hydrodynamic chromatography (HDC) have been described in the literature as alternatives to separate MNPs of 10–80 nm [32,33].

Currently, FFF is a promising method for size separation of natural and engineered NPs, providing a wide dynamic range. Although an ultraviolet (UV) detector is the most common system used in combination with FFF, elemental information can be obtained by combining FFF with ICP-MS. One of the main advantages of FFF-ICP-MS is not only the possibility for multiple elemental detection, but also the higher sensitivity achieved (in the ng/L range) compared to UV detection. To provide complementary information, the FFF can also be coupled to a multi-angle light scattering (MAL) for particle-size characterization. The two FFF principles mainly used are sedimentation FFF (SedFFF) and the asymmetric flow FFF (AF4). SedFFF-ICP-OES has been employed to study size-based elemental distribution of air particles and MNPs (e.g., Al, Ti and Fe) [34].

In recent investigations about the toxicity of TiO_2 present in sunscreen products and the influence of polymer-coated CdSe/ZnS QDs to *Daphnia magna*, on-line FFF-ICP-MS was applied to characterize the particle size and the composition of MNPs [20,35]. In spite of the promising results obtained so far, there are still some aspects that require further investigation (e.g., problems related to membrane-particle interaction, the different behavior of MNPs according to their chemical structure, and the influence of eluents during the separation step, which can lead to erroneous size information and negatively affect recovery rates).

2.2. Determining the stability of MNPs

The aggregation state of MNPs is a crucial factor for experimentally assessing their toxic activity. In *in-vitro* studies, the influence of biological components present in the culture media on MNPs has been evaluated on many occasions (e.g., serum proteins, antibiotics, vitamins, and electrolytes may interact with MNPs to change their physicochemical properties and aggregation state. While serum proteins may absorb onto the surfaces of MNPs, changing their size and surface chemistry, the presence of electrolytes and the high ionic strength of the culture media may alter their aggregation state).

Due to the dimensions of MNPs, detection and characterization of MNPs is generally performed by microscopic techniques. Scanning electron microscopy (SEM), transmission EM (TEM) and atomic force microscopy (AFM) are the most commonly used techniques to visualize MNPs and their features, including aggregation state, dispersion, sorption and particle size.

Before evaluating the toxicity of Ag NPs in different cell lines, Mukherjee et al. used TEM and SEM to determine the stability of Ag NPs and their possible interaction with the culture media [5]. The aggregation state of Ag NPs was also studied by Oukarroum et al., whose TEM images showed an increase in the diameter of the

NPs in all the culture media tested for growing two types of green algae [36]. Although TEM images provide useful information about the morphology and the aggregation state of MNPs, these images might not completely represent the morphology of the MNPs under the real experimental conditions because TEM images are acquired on dried samples.

As an alternative, dynamic light scattering (DLS) can be combined with TEM, thus allowing the analysis of the MNPs in solution. The characterization of stable monodisperse and aggregated Si NPs by TEM and DLS was carried out to study the effect of these MNPs on macrophages and fibroblasts. The DLS results demonstrated that the mean hydrodynamic diameter of particles increased from 25 nm to 183 nm [2]. The analysis of Au NPs, synthesized in citrate media as reducing agent, by DLS revealed that the surfaces of the NPs were covered by citrate. As mentioned above, proteins and other biological molecules may bind to the surface of the MNPs. The absorption spectra of Au NPs in solution showed that not only were the Au NPs covered by citrate, but also proteins or lipids were adsorbed onto their surface [37].

2.3. Localization of MNPs into cells and living organisms using microscopic techniques

TEM is also considered an appropriate technique to discriminate between MNPs localized inside cells and tissues from those that are only externally attached. Obtaining reliable information about the intracellular localization of MNPs is important to establish NP-cell interactions. It is known that smaller NPs can enter more easily into cells than larger ones [38], which might explain the higher toxicity of smaller MNPs.

When it comes to design a protocol for TEM, it is very important to select the most suitable fixing agent. The most common fixings are aldehydes (glutaraldehyde and formaldehyde) and osmium tetroxide. Aldehydes react with amines and amino acids (lysine and arginine), generating cross-linked proteins, which preserve cellular structure. However, these fixing agents do not react with most lipids of the cellular membrane, leading to problems during fixing and processing. For this reason, osmium tetroxide is generally used as a secondary fixing, since it is able to react with unsaturated lipids and some proteins, thus stabilizing the membrane structures and also adding electron density to enhance the contrast.

Another important aspect is the choice of buffer, in which the fixing will be dissolved. It should maintain the cell in its physiological state, when possible. The most frequently used buffer is phosphate buffer saline (PBS). Buffers containing amine groups (e.g. Tris) should not be used because these groups might react with the fixing molecule. Typically, samples prepared for TEM analysis have to be dehydrated and embedded in resin (overnight with temperature) to allow ultrathin sections to be cut. Allouni et al. developed a protocol in which cells were fixed in 1.5% glutaraldehyde and 0.1 M Na-cacodylate buffer (pH 7.4), and post-fixed in 1% osmium tetraoxide. TEM images revealed that not only were TiO_2 NPs attached to the surface of the cells, but also they were in vesicles and distributed in the cytoplasm [11].

A mixture of glutaraldehyde and formaldehyde is also very commonly used as fixing agent. A fixing solution containing 3% paraformaldehyde and 0.5% glutaraldehyde was employed to visualize both the localization of SiO_2 NPs and Ag-doped SiO_2 NPs in fibroblast-like fathead minnow cells [17], and Au NPs in human lung carcinoma cells A549 [37].

In some cases, the resulting blocks embedded in resin are incubated in uranyl-acetate (1%-6%) to obtain a higher electron density and image contrast, which is especially useful for smaller particulate specimens. However, this stain is not recommended in the treatment of specimens that are unstable in acid conditions, due to the low pH of the solution [7,11].

Ultrahigh-resolution imaging (URI) is a promising technique for studying cell-NP interactions, as it allows direct visualization of both cells and MNPs without the need of an elaborate sample preparation and without the use of fluorescent tags. In URI, the illuminator is connected to the light source by a liquid light guide, which allows transport of light without loss of intensity, and minimizes the thermal impact on living systems. In a recent study, the cellular uptake of TiO_2 NPs by fibroblasts was investigated by combining SEM and TEM with URI. For URI analysis, cells were washed, fixed in 4% formaldehyde for 15 min at room temperature and, finally, a drop of mounting media was added to the slides and encased with a cover-slip. URI images showed that TiO_2 NPs appeared to be both taken up by and attached to the cells, mainly as agglomerates. The discrimination between MNPs attached to the cell from those internalized was performed by changing the focus plane in the URI microscope. As shown in Fig. 1, the agglomerates could be easily distinguished from other cellular components due to their brightness [11].

Dark-field microscopy (DFM) is able to provide a panoramic view of non-fluorescent NPs in cells since NPs appear as a bright image superimposed on a dark background. Because DF illumination has a very low background, low signals are sufficient to detect individual non-fluorescent NPs. Although there are limited studies on accumulation of non-fluorescent NPs at the single-cell level using DFM, this technique has been used in studies focused on Au NPs. As in URI, sample preparation is very straightforward when using DF imaging. The accumulation of Au NPs in cells has been observed in a time-course experiment. Cells were seeded on coverslips in 24-well plate, fixed in 4% paraformaldehyde for

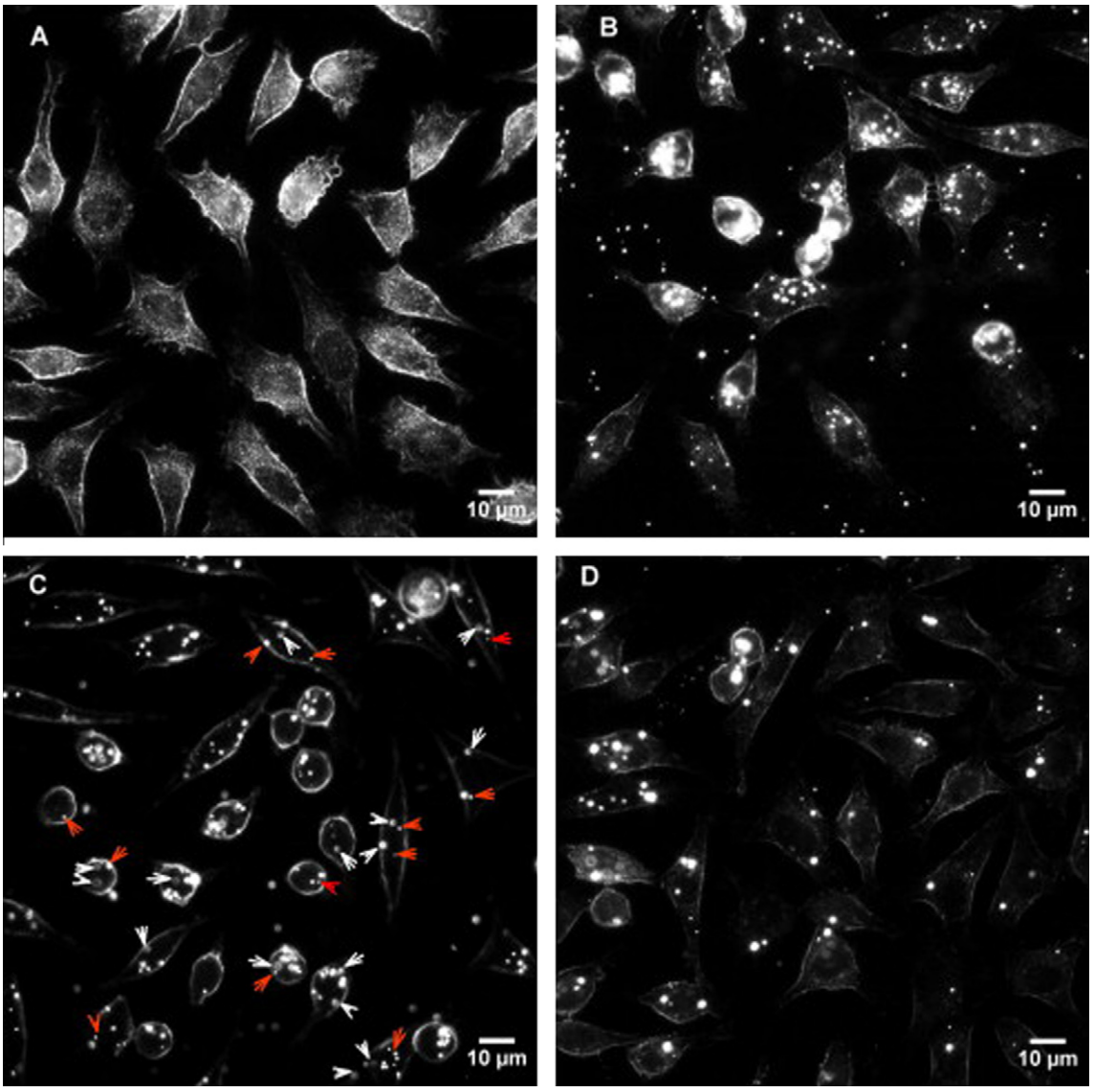

Figure 1. URI images of L929 fibroblasts at 100x magnification after 24-h exposure to 0.5 mg/L of TiO_2 NPs. Bright spots are NPs internalized or attached to the membrane. (A) Control cells. (B) Rutile, 40 nm. (C) Rutile and anatase mixture, <100 nm. (D) Anatase, 10 nm. White arrows (C) show agglomerates that appear to be attached to the cell membrane; red arrows point at agglomerates inside the cells (Reproduced with permission of Elsevier).

10 min after MNP exposure [26], and Au NPs embedded inside the cell were identified in their aggregated states [17].

Another option for visualizing MNPs is based on functionalization with fluorescent markers, which allows use of fluorescence microscopy. However, it is important to keep in mind that the attachment of a fluorochrome may alter the physicochemical properties of MNPs. MNPs can be easily functionalized by using specific fluorochromes, which have their own absorption and emission spectra [e.g., fluorescein isothiocyanate (FITC), ALEXA 488, BODIPY-FL, propidium iodide (PI), Mito-Tracker Red and rhodamine are among the fluorochromes commonly used in many bioapplications]. FITC presents maxima absorption in the blue-light range of the visible light spectrum (approximately at 488 nm). When FITC is irradiated at 488 nm, it fluoresces at 520 nm, emitting a greenish-yellow glow. Other fluorochromes (e.g., propidium iodide, ALEXA 488 and BODIPY-FL) have excitation and emission profiles similar to FITC. By contrast, rhodamine 123 and Mito-Tracker Red fluorochrome are excited by light in the green range and emit at red wavelengths.

Kurepa and co-workers synthesized Alizarin red S (ARS)-TiO_2 NP conjugates to study the uptake and the distribution of NPs in plants. The covalent surface modification of the MNPs was performed following a straightforward protocol in which the MNPs were mixed

with an ARS solution. The high surface reactivity of synthesized TiO_2 NPs (smaller than 20 nm) was very adequate in the formation of ARS-NP conjugates [38].

3. *In-vitro* cytotoxicity assays

Cytotoxicity assays are based on the idea that toxic agents affect basic functions of cells, and thus their toxicity can be evaluated by measuring cellular damage. It is known that the toxic effects of MNPs on a cell culture may differ, depending on the incubation time and the concentration of MNPs used. Many cytotoxic effects are due to the number of MNPs internalized in the cells rather than the total concentration of MNPs added to the cell-culture media. Generally, the amount of MNPs taken up by cells differs by several orders of magnitude from the amount of MNPs used in the cellular treatment [39]. The uptake efficiency depends on not only MNP concentration but also other properties of MNPs (e.g., size and shape). Exposure times and concentrations greatly vary from one study to another. Concentrations of the order of μg/L or a few mg/L are commonly used, while exposure times of 24–96 h are usually selected [6,9,40], although internalization of MNPs has been observed at shorter exposure times under certain conditions [15,41].

When performing a cytotoxicity assay, cell types are generally chosen by considering the organ in which the studied MNPs are accumulated in organisms. In this way, hepatic cells [42,43] and macrophages [2] are most commonly used, since MNPs tend to accumulate in liver and spleen. Other cell types (e.g., fibroblasts, which are the major cellular constituent of fibrous connective tissue) have also been used (e.g., to assess the effects of TiO_2 NPs released from implant materials) [11].

It is important to keep in mind that the toxic effects induced by MNPs may depend on the cell line tested and these effects may not necessarily be the same when exposing other cell lines to the same MNPs [5,44]. In this way, Patra et al. found that citrate-capped Au NPs induced toxicity in human carcinoma lung cells greater than in liver carcinoma cells at the same dosage [45]. The effects could even be the opposite, as shown by Chen et al., who found that SeNPs inhibit cellular growth in hepatocarcinoma cells but increase cell proliferation when using human fibroblasts [44].

Below, we describe several common assays that have been applied when evaluating the effect of MNPs in different cell lines, most of them involving the use of vital dyes, protease markers, and colorimetric, fluorescence, or luminescence detection.

3.1. Assessment of membrane integrity

The cell membrane is a thin, semi-permeable membrane that surrounds the cytoplasm of a cell and constitutes a functional barrier. Its function is to protect the integrity of the cell by controlling the traffic into and out of the cell, which is regulated by transporters, receptors and secretion pathways. Since cytotoxic compounds often compromise the cell membrane, assessing cell-membrane integrity is one of the most common ways to measure cell viability and cytotoxic effects. For this purpose, the so-called vital dyes (e.g., trypan blue and propidium iodide) are generally used, These compounds can freely cross the cell membrane when it has been compromised and stain intracellular components, but are excluded from the inside healthy cells [46]. Alternatively, membrane integrity can be evaluated by monitoring the presence in the culture media of substances that are normally sequestered inside healthy cells [5]. One commonly measured is lactate dehydrogenase (LDH) [47]. LDH leakage from damaged cells can be measured with a coupled enzymatic assay resulting in the conversion of a tetrazolium salt into a red formazan product. The intensity of the color produced is proportional to the number of cells with compromised plasma membranes [37]. There are several commercially available kits to carry out this assay, which does not involve any kind of sample preparation, since the substrate mixture is directly added to the culture media and the resulting reaction product (red formazan) is measured spectrophotometrically. Using this assay, Hussain et al. showed that LDH leakage for MoO_3, Al, Fe_3O_4, MnO_2, and W NPs did not produce cytotoxicity up to a concentration of 100 μg/mL in rat-liver cells, while Ag NPs were highly toxic at those concentrations in the same cells [10]. In the same manner, Gerloff et al. showed that only anatase-rutile-containing NPs, in contrast to the pure, fine TiO_2, induced cytotoxicity in human intestinal cells [3].

3.2. Measurement of cellular metabolic activity

An early indication of cellular damage is a reduction in metabolic activity. Thus, assays able to measure metabolic functions (e.g., ATP levels or mitochondrial activity) have been widely used to evaluate the toxicity of MNPs. One of the most widely-used methods is the 3-(4, 5-dimethyl-2-thiazolyl)-2,5-diphenyl-2H-tetrazolium bromide (MTT) assay [14,48], which measures the reducing potential of a cell. It is based on the capacity of healthy cells to reduce MTT to formazan by mitochondrial reductases. Formazan is a colored compound, whose absorbance can be measured spectrophotometrically at a wavelength of 500–600 nm. In this approach, cells are incubated with MTT (2–10 mg/L) for 4–5 h and then the formazan crystals are commonly dissolved in dimethyl sulfoxide (DMSO) (or other organic solvent) prior to colorimetric detection. It is important to consider the signal provided by the phenol red usually present in culture media. Thus, it is recommended to either use red-phenol-free media or to remove the media before dissolving the formazan

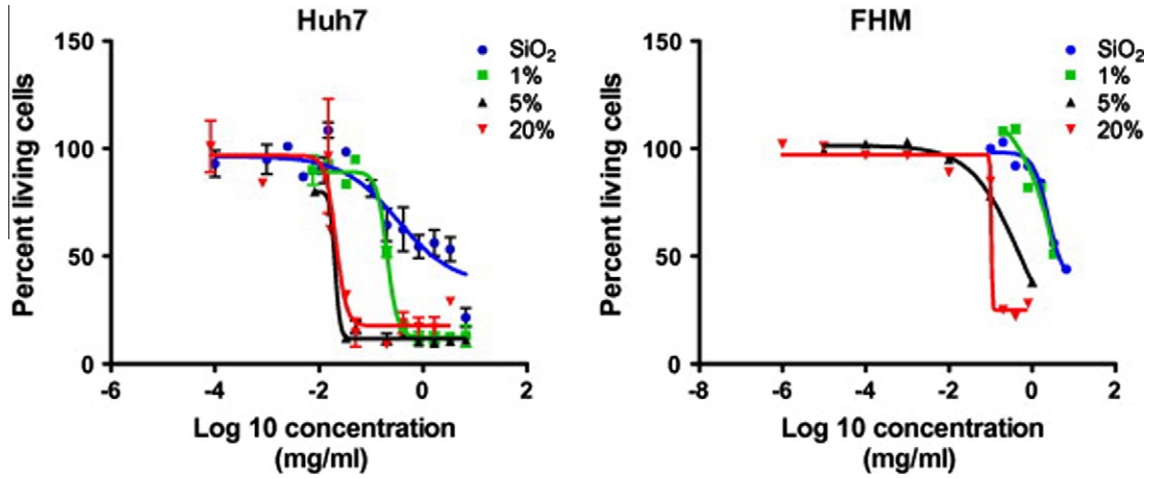

Figure 2. Cytotoxicity of NPs. Huh7 (left) and FHM (right) cells were treated for 24 h with different concentrations of SiO_2 NPs (blue dots); SiO_2 1% Ag NPs (green squares), SiO_2-5% Ag NPs (black triangle); and SiO_2-20% Ag NPs (red triangle) followed by assessing cell viability by MTT assay. Shown are the results of three independent experiments (Reproduced with permission of Elsevier).

crystals. The cytotoxicity of several MNPs has been evaluated by comparing the absorbance of formazan in control *versus* cells exposed to MNPs. Christen and Fent showed that human hepatic cells (Huh7) reacted more sensitively to SiO_2 NPs than fibroblast-like fish cells (FHM). Exposure of the two cell lines with SiO_2-Ag NPs, containing 1%, 5% and 20% of Ag demonstrated again that Huh7 cells were more sensitive than FHM cells (Fig. 2) [7]. Yuan et al. used the MTT assay to show how the viability of lung fibroblast exposed to ZnO decreased in a dose-dependent manner independently of the particle size [49]. Other close dyes [e.g., 3-(4,5-dimethylthiazol-2-yl)-5-(3-carboxymethoxyphenyl)-2-(4-sulfophenyl)-2H-tetrazolium (MTS), 2,3-bis-(2-methoxy-4-nitro-5-sulfophenyl)-2H-tetrazolium-5-carboxanilide (XTT) and water soluble tetrazolium salts (WSTs)] have also been used for the same purpose [3,6].

3.3. Evaluation of the oxidative stress

Oxidative stress is an imbalance of pro-oxidants and antioxidants. It is associated with increased production of oxidizing species or a significant decrease in the effectiveness of antioxidant defenses. One common way to analyze oxidative stress in cells is by measuring glutathione (GSH) levels. GSH is the major intracellular low-molecular-weight thiol that plays a critical role in cellular defense against oxidative stress. There are many commercially-available GSH-detection kits, mainly based on colorimetric and fluorimetric detection. One key step in this approach is the thorough wash of the cells with PBS to remove the excess of dye prior detection. GSH measurement is widely used in toxicological studies [50] and it has also been used to evaluate the toxicity of different MNPs. For example, GSH depletion has been observed in cells exposed to Ag NPs, although the degree of depletion greatly depended on the cell line tested [5].

When cells are exposed to environmental stress they can generate reactive oxygen species (ROS), both radical ROS (nitric acid and hydroxide radicals) and non-radical ROS (hydrogen peroxide). When the increase of ROS is too high and it overwhelms the antioxidant defense, cells are prone to suffer cell damage and even apoptosis. Several studies have linked the increase of the ROS level in cells with exposure to MNPs, so allowing use of the ROS level as a cytotoxicity marker. The most widely used method to measure the intracellular production of ROS is the dichlorodihydrofluorescein diacetate (DCFH-DA) assay [8]. DCFH-DA penetrates the cells, where it is hydrolyzed by unspecific esterases and converted into a stable green fluorescent product, 2′,7′-dichlorofluorescein (DCF), in the presence of oxidative species [53]. DCFH-DA is prepared in phenol red-free media and used at a final concentration of 10 μM. Cells are incubated with this reagent for 15–30 min and then washed twice with PBS prior to fluorimetric detection. It is important to carry out this assay in the dark to avoid the fluorophore fading. Using this approach, Konczol et al. demonstrated that the ROS production observed in alveolar epithelial cells increased after 24 h of incubation with Fe_3O_4 NPs in a concentration-dependent manner. This study also showed that the particle size did not affect the cytotoxicity of these MNPs [51].

Reaction of generated ROS with other fluorescent probes [e.g., dihydroethidium (DHE)] has also been used [52]. In addition, when ROS production increases, other intracellular events (e.g., lipid peroxidation) are initiated, so, by measuring these events, it is possible to evaluate the oxidative damage of cells exposed to MNPs. Malondialdehyde (MDA) formed from the breakdown of

polyunsaturated fatty acids, can be used as a convenient index for determining the extent of lipid peroxidation reactions. MDA formation can be measured by Western Blot [53], enzyme-linked immunosorbent assay (ELISA) or the traditional thiobarbituric acid reactive substances (TBARS) assay based on the reaction of MDA with thiobarbituric acid reactive substances to yield a fluorescent product [41]. After cell lysis, the cell extract is mixed with the reaction solution and incubated at 90°C for 1 h. The product formed is extracted with an organic solvent (e.g., butanol) and the fluorescence is measured in the organic phase. Addition of cadmium chloride to control cells can be used as positive control since it induces lipid peroxidation [52]. Passagne et al. used this assay to show how SiO_2 NPs affected the production of MDA, depending on the cell line tested and the particle size. While smaller NPs (20 nm) induced the formation of MDA in porcine tubular cells more than bigger NPs (100 nm), the effect of both NPs was not significantly different when using human kidney cells [52].

3.4. Measuring apoptosis induced by MNPs

As commented upon above, exposure of cells to MNPs can increase ROS production and lipid peroxidation, which ultimately can cause apoptosis. There are several strategies to evaluate the degree of apoptosis based on the measurement of different parameters. There are several protein markers of apoptosis, including Bax, Bcl2, p53 and caspases, which can be easily monitored using Western Blot with the appropriate antibodies [8,55], colorimetric assays [56] or real-time polymerase chain reaction (PCR) [38,58]. Apoptosis can also be visualized by studying nuclear morphology, particularly chromosome condensation, assessed using nuclear-specific dyes [e.g., 4́-6-diamidino-2-phenylindole (DAPI) and Hoechst] and fluorescence microscopy [54,55].

However, the technique generally chosen to evaluate apoptosis is flow cytometry. The most important factor that has to be considered when preparing samples for flow cytometry is the density of the cell suspension, which should be kept between 10^5–10^7 cells/mL to prevent clogging the narrow bores of the cytometer and its tubing.

Two common methods to evaluate apoptosis by flow cytometry are the measurement of the mitochondrial membrane potential and the annexin-V assay. Since mitochondria act as a point of integration for apoptotic signals originating from both extrinsic and intrinsic apoptotic pathways [57], loss of mitochondrial membrane potential can be associated with the activation of caspases and the initiation of apoptotic cascades [58]. To measure the percentage of cells with depolarized mitochondria, resuspended cells are incubated at 37°C for 10–15 min with a solution of 10 μg/mL JC-1 (5,5′,6,6′-tetrachloro-1,1′,3,3′-tetraethylbenzimidazolcabocyanine iodide). After incubation, cells are immediately centrifuged to remove the supernatant and the cell pellet is resuspended in PBS and then analyzed by flow cytometry. The membrane-permeant JC-1 dye exhibits potential-dependent accumulation in mitochondria, indicated by a fluorescence emission shift from green (~529 nm) to red (~590 nm). Consequently, mitochondrial depolarization is indicated by a decrease in the red/green fluorescence-intensity ratio. The potential-sensitive color shift is due to concentration-dependent formation of red fluorescent J-aggregates [54]. Using this method, Chen et al. demonstrated that Se NPs induced apoptosis in melanoma cells through mitochondrial-mediated pathways. In this study, the percentage of cells with depolarized mitochondria increased from 5.6% (control) to 9.3% when exposing the cells to 20 μM Se NPs, and up to 30.0% when using 40 μM Se NPs [56].

In apoptotic cells, phosphatidyl serine (PS) is translocated from the inner to the outer leaflet of the plasma membrane, so PS becomes exposed to the external cellular environment. Annexin-V labeled with a fluorophore (e.g., FITC) can selectively identify apoptotic cells by binding to the exposed PS on the outer leaflet of the membrane. The number of labeled cells can then be quantified by flow cytometry. Annexin-V-FITC is usually used together with PI to differentiate between apoptotic and dead cells. Cells are resuspended (10^6 cells/mL) in binding buffer (10 mM HEPES/NaOH, pH 7.5 containing 140 mM NaCl and 2.5 mM $CaCl_2$) and then incubated in the dark with annexin-V-FITC and PI for 10 min at room temperature [54]. Generally, fluorescence emitted by annexin-V-FITC and DNA-bound PI in each event is detected as green and red fluorescence, respectively.

Other fluorophores can also be conjugated to annexin-V [44]. This assay is generally used to confirm that the cell death observed after exposure to certain MNPs is generally caused by apoptosis [44,59]. It is important to mention that certain fluorochromes may be adsorbed on the surface of MNPs, which may cause fluorescence of the NPs, and quenching or enhancement of the fluorescence of fluorochromes, thus altering the results of the flow-cytometry assay. In addition, cellular internalization or deposition of MNPs may avoid the correct binding of the fluorochromes to their target molecules. As an example, the annexin-V assay may give false negatives as a result of NP deposition on the cellular membrane, which hinders the annexin-V from binding to PS.

3.5. Genotoxicity assessment

The potential DNA-damaging properties of MNPs have also been assessed in many cases using the Comet assay and the formamidopyrimidine glycosylase (Fpg)-modified Comet assay [3,51,54]. The Comet assay (also known as single-cell gel electrophoresis) is a rapid, sensitive, simple method for detecting DNA damage at the level of individual cells [60]. It involves encapsulation of single cells in low melting-point agarose. Then, cells are lysed to

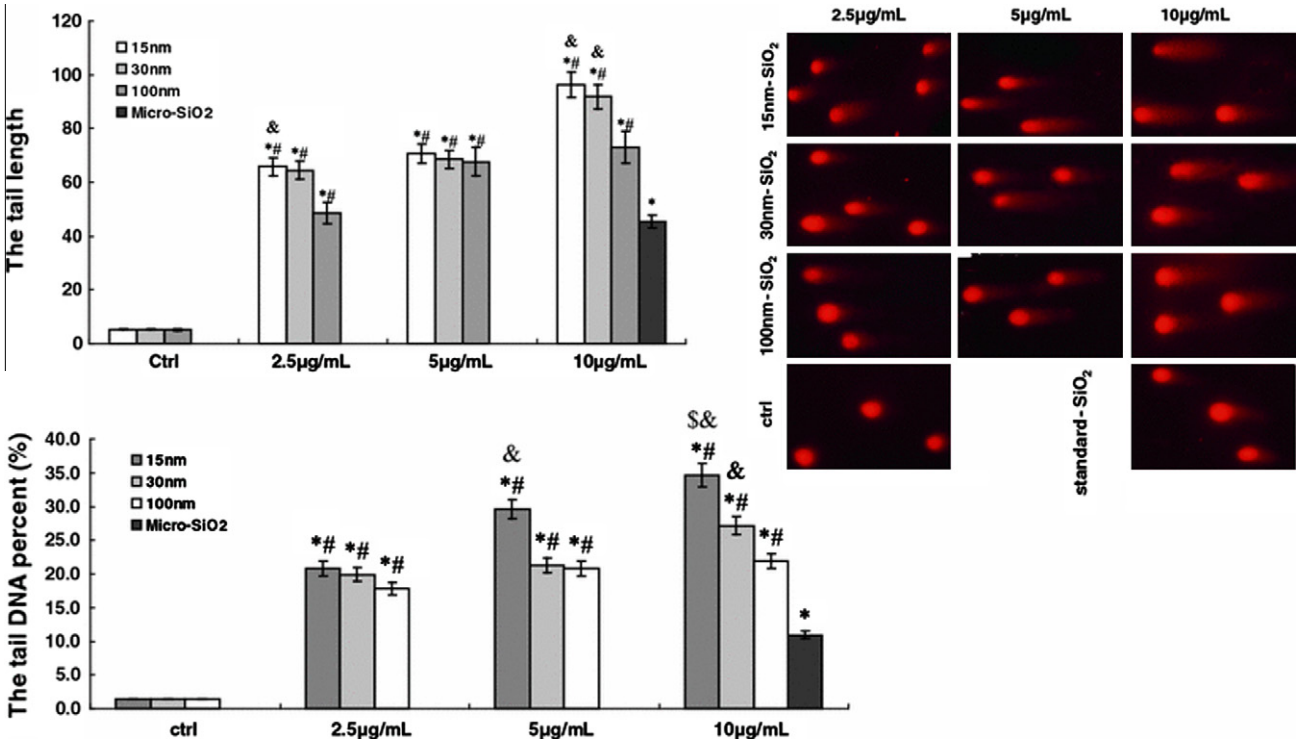

Figure 3. The effects of exposure to 15-nm, 30-nm, 100-nm or μm-sized SiO_2 particles on DNA damage in HaCaT (human keratinocytes) cells. Representative images and quantitative analysis of tail length or tail DNA percentage of comet in HaCaT cells. Values shown were the mean from 300 randomly selected comet images of each sample (Reproduced with permission of Springer).

form nucleoids containing supercoiled loops of DNA. Electrophoresis at high pH results in DNA structures resembling comets. It is important to reduce the pH after electrophoresis to avoid the contribution of alkali-labile sites, since they strongly decrease the sensitivity of the Comet assay. The extent of DNA migration depends directly on the DNA damage present in the cells. It should be noted that DNA lesions consisting of strand breaks after treatment with alkali, alone or in combination with certain enzymes (endonucleases), increase DNA migration, whereas DNA-DNA and DNA-protein cross-links retard DNA migration. This is followed by visual analysis with staining of DNA with ethidium bromide [54,61]. Other dyes (e.g., PI, Hoechst or DAPI) have also been used. The intensity of the comet tail relative to the head reflects the number of DNA breaks. Gong et al. used this assay to evaluate the effect of SiO_2 NPs of different particle size in human keratinocytes, showing a significant increase in the comet-tail length of cells exposed to smaller SiO_2 NPs (15 nm), which means an increased DNA damage in an NP-size-dependent manner (Fig. 3) [62].

Several studies used a modification of the Comet assay specifically to evaluate oxidative DNA damage. For this purpose, the endonuclease formamide pyrimidine glycosylase (Fpg) is generally used for detection of 8-OH guanine, other damaged purines, basic sites (AP sites) and ring-opened N-7 guanine adducts [63]. This endonuclease is added to the gel and incubated for 30 min at 37°C in a humidified chamber. It is important to prepare this enzyme in a buffer solution containing b-mercaptoethanol to preserve the enzyme and to take into consideration that the inclusion of sulfhydryl reagents in the reaction buffer would significantly increase background-DNA breakage. Gerloff et al. demonstrated that only anatase/rutile TiO_2 NPs significantly increased DNA-strand breakage while none of the anatase TiO_2 NPs induced oxidative DNA damage [3].

3.6. Use of microscopy to study cellular morphological alterations

Several studies derived from EM analyses have reported morphological alterations in the cell layer and/or cell shape after exposure to cytotoxic agents, so it is not surprising that the visualization of morphological alterations is considered a primary index of toxicity. Changes in the morphology of lung fibroblasts were examined by SEM after incubation with 20-nm ZnO NPs for 72 h. For this analysis, cells were washed with PBS and dehydrated in 35% alcohol for 10 min, followed by consecutive addition of ethanol solutions from 40% to 100%. Finally, the samples were dried in vacuum before SEM analysis. A very rough cell surface was observed in ZnO NP-treated cells, compared with control cells, which have a regular morphology and smooth surface. Moreover, the presence of nanosized pores of 20 nm in the plasma membrane indicated that ZnO NPs could have entered into the cells, thus affecting the inner structure and inducing apoptosis and/or necrosis [49].

Unlike SEM or TEM techniques, phase-contrast microscopy allows examination of living cells in their natural state without need for previous fixation or dehydration steps. Hussain et al. observed that increasing the concentration of Ag NPs in culture media led to morphological changes in rat-liver cells, which started to shrink, and became irregular in shape [10]. In the same way, the cellular morphology of epithelial carcinoma cells was observed in order to evaluate the cytotoxicity of Fe_3O_4 NPs with different surface functionalizations [14].

For a more exhaustive visualization of the morphological changes, cells may be fixed and differentiated using the hematoxylin-eosin method. Hematoxylin (blue-purple dye) stains nucleic acid and eosin (pink dye) stains proteins non-specifically. The required protocol for sample preparation is very straightforward. In a study of cytotoxicity of Fe NPs, HeLa cells were seeded on the glass coverslips in 24-well plate and incubated for 2 h with the NPs. Then, cells were fixed with 4% paraformaldehyde and stained with hematoxylin and eosin. In this case, no significant changes in cellular morphology were observed after exposure to Fe NPs [30], which could be due to the extremely short exposure time selected to carry out the study.

3.7. High-throughput discovery platforms

In addition to the assays commented before, which are mainly based on target-directed approaches, high-throughput discovery platforms based on gene- and protein-expression profiling can provide very useful information on the specific mechanisms of interaction of MNPs with cells. Gene expression is the term used to describe the transcription of the information contained within the DNA into messenger RNA (mRNA) molecules that are then translated into proteins. The study of the kinds and the amounts of mRNA produced by a cell under certain conditions, which are directly related to which genes are expressed, provides insights into how the cell responds to a particular perturbation.

A way to evaluate the expression of many genes in a single experiment is by using a DNA microarray, which is a collection of microscopic DNA spots immobilized in a solid surface. Each DNA spot contains picomoles of a specific DNA sequence, known as reporters (also known as probes or oligos), which can be a short section of a gene or other DNA element used to hybridize a cDNA or a cRNA. Probe-target hybridization is usually detected and quantified by detection of fluorophore, silver-labeled or chemiluminescence-labeled targets to determine relative abundance of nucleic-acid sequences in the target.

Hanagata et al. [64] carried out a whole genome-expression analysis to study the molecular responses of

lung epithelial cells to CuO NPs. After extraction of the RNA from cells exposed to CuO (or control cells), the RNAs were amplified and labeled with fluorescence probes (Cy3 and Cy5). Hybridization of the amplified RNAs with the DNA microarray was carried out for 18 h at 65°C. Then, the microarray was scanned to measure the fluorescence intensity of Cy3 and Cy5. Foreground and background median values of each spot were obtained from median values of the pixels included in each spot area. The difference between foreground and background values of each spot was established as the signal strength, and only spots with signal values >3 times the noise value were considered valid spots. The results indicated that change of gene expression involved in mitogen-activated protein-kinase (MAPK) pathways and cell-cycle progression in cells exposed to CuO NPs were similar to those in cells exposed to Cu ions [64]. With a similar approach, Mahmoudi et al. evaluated the toxicity of superparamagnetic iron oxide in different cell lines (heart, brain and kidney) [65] and Dua et al. the toxicity induced by mesoporous silica NPs, Fe_2O_3 NPs and ZnO NPs in kidney cells [66]. The findings using this approach have to be analyzed by powerful bioinformatics tools due to the large amount of data obtained. In addition, alternative methods (e.g., real time-PCR) are required for further validation of the identified targets. Examining changes in protein expression can also be very useful for better understanding of the effects of MNPs in cells [67].

Among all the proteomic approaches available, quantitative strategies are particularly attractive, since they allow for identification of differentially-expressed proteins in cells exposed to MNPs, compared to control cells. Although these approaches are extensively used in other research areas [68], they have been applied to study MNP toxicity in only a few studies. Yang et al. used two-dimensional differential gel electrophoresis (2D-DIGE) to identify proteins altered after exposure to SiO_2 NPs. In this study, control and cells exposed to SiO_2 NPs were differentially labeled with Cy3 and Cy5 dyes for comparison on the same gel. The labeling reaction was carried out for 30 min at 4°C in the dark and then quenched with a 50-fold molar excess of free lysine. The internal standard was labeled with Cy2 dye and use on all gels to aid image matching and cross-gel statistical analysis. The proteomic analysis revealed that 16 differentially-expressed proteins were induced by SiO_2 NPs exposure, and that the expression levels of these proteins were associated with the particle size [69].

Jeon et al. also used 2D-DIGE to analyze the hepatotoxicity induced by TiO_2 in liver cells, finding 15 altered proteins related to inflammation, apoptosis and antioxidative reaction [70]. Alternatives to 2D-DIGE [e.g., stable isotopic labeling by amino acids in cell culture (SILAC), isobaric tags for relative and absolute quantitation (iTRAQ) and label-free methods] should also be considered for future studies, since they generally provide better results than gel-based approaches [67].

4. *In-vivo* assessment of the toxicity of metallic nanoparticles

After *in-vitro* toxicity assays and before the pre-clinical studies, *in-vivo* assays to evaluate the toxicity of MNPs are needed to design specific and safe clinical trials to develop new strategies for the applied use of MNPs. This use includes diagnostic and/or therapeutic purposes, although large-scale use of MNPs also represents an increasing risk to health and the environment [18,71].

Several aspects of the physicochemical properties of MNPs are important to design these protocols and, of course, suitable for the biological organism in each case. The target organ in the organism chosen is also one of the major issues to test, so it is important to test hepatotoxicity, nephrotoxicity, pulmonary toxicity, spleen toxicity, immune-system activation, hematological toxicity and oxidative stress, among others [72,73]. Within the most important options to consider is the route of administering NPs, especially in higher vertebrates and mammals.

4.1. Routes of administration in common animal models

The acquisition pathway of MNPs by biological systems is determinant, in most cases, of the type and the extent of potential damage in different organs and tissues. We discuss below relevant routes of administration and doses in different animal model.

4.1.1. Skin absorption. This route of administration involves not only active absorption after direct application to the skin but also passive uptake of NPs through the skin (e.g., respiration after nebulization in a chamber or directly in the water for aquatic animals) [74].

The zebra fish is a genetically-tractable vertebrate-model organism commonly used for the *in-vivo* administration and testing of MNP toxicity. Compared to other vertebrate animal models, zebra fish have several benefits. Importantly, housing and maintenance are less expensive, making it an attractive model for preliminary studies of toxicity and/or environmental contamination. Moreover, the zebra-fish model for the assessment of toxicity is easily extrapolated to other vertebrates and humans. The short life cycle of this aquatic vertebrate makes it very suitable for the study of embryo viability and genetic malformations during treatment with NPs. Assessment of MNP toxicity in zebra fish includes immunohistochemical analysis, flow-cytometry studies to detect ROS and proteomic analysis for well-established cellular markers of stress [75]. Eurasian perch, oysters and the fruit fly share many of the zebra-fish

characteristics, so making them suitable models for toxicity studies, although they are used less frequently because their genetics are not well known.

4.1.2. Airways release. *In-vivo* toxicity of Ag NPs and Au NPs has been studied in models of sub-chronic inhalation, in trying to have a complete study of toxicity that measures the adsorption, distribution, metabolism and excretion (ADME) of MNPs *in-vivo* in rats [76]. These studies, although not very common, need to be done for commercial purposes and for the effects of MNPs in humans. The most important parameters are the lowest dose for an adverse effect (LOAEL) and the dose with no adverse toxicity effect included in the pre-clinical trial (NOAEL). These studies tested daily different doses (e.g., Au NPs in different groups of male and female rats with 6-h-inhalation treatment consecutively during three months). Airways, skin and mucosas (oral, nasal and genital) were checked daily and the rat's weights were monitored once a week. The analysis *pre-mortem* included biochemistry and hematologic parameters, nephrotoxicity and lung function. The *post-mortem* study comprised multi-organ histopathological analysis (including broncho-alveolar lavage). Au NPs accumulation in tissue was measured by AAS [76].

4.1.3. Systemic administration. Commonly used routes for systemic release of MNPs are intravenous (i.v.) and intraperitoneal (i.p.) injection. The systemic administration of MNPs by these two pathways allows study of their organ distribution after different time points. The organs are extracted from injected mice and accumulation of NPs is generally analyzed by ICP-MS and/or by fluorescent imaging with confocal microscopy. Interestingly, small silica-coated magnetic (50 nm) NPs containing rhodamine B isothiocyanate were recruited to the brain, through the blood-brain barrier [77], whereas Au NPs with a diameter of 100–250 nm were retained in different tissues and organs (e.g., liver, spleen, kidney, or lungs) [78].

Hematological and biochemical studies are also performed in these animals to test the toxicity of NPs in tissues and blood cells.

Another interesting approach with systemic administration of NPs is the evaluation of mutagenic potential, chromosomal aberrations and genotoxicity for germinal cell-viability studies [77,79].

4.1.4. Oral gavage. This route of administration has been studied using Cu NPs of different sizes after gavage of mice through naso-gastric probe. In this model of acute toxicity, the effect of the NPs was tested after short exposure to high doses. After determination of the LD_{50} (lethal doses determination for 50% of the population), a complete histopathology and hematology study has to be performed to describe the ADME parameters *in vivo* in the animal model.

Oral toxicity determination is important due to the putative use of NPs with food or orally-administrated drugs [80,81]. Moreover, oral uptake of NPs through drinking water pollutants or passive uptake from other routes of administration (e.g., airways or skin) must be taken into consideration to address the *in-vivo* toxicity of MNPs fully [82]. A single administration of NPs is performed in the acute exposure model for toxicity assessment of MNPs; hence, increasing doses of the different NPs and the control (vehicle) are administrated to the mice to detect the LD_{50}.

In an interesting study, Chen et al. tested two sizes of Cu NPs (25 nm and 17 nm), and compared the effect to that of soluble ionic Cu after administration through a nasogastric probe. This study revealed the importance of the size of the NPs for the induction of toxicity – larger NPs have a smaller surface area in contact with the organism and are, therefore, potentially less toxic than the smaller NPs or the ionic Cu. Another important conclusion from this work is that study of the different ways of administering NPs is essential to understand the difference and the specificity of the toxicity induced by MNPs. As an example, the interaction of NPs with H^+ in the stomach after oral administration promotes an increase in the release of HCO_3^-, which results in an increase of the pH in the stomach causing renal damage and electrolytic metabolic alterations [82].

Another important issue after oral administration of NPs is the different outcome depending on the use of males or females for toxicity tests. In this regard, males are more prone to produce H^+ in the stomach, so they are more susceptible to develop renal damage than females [83]. All these considerations mark the importance of designing an adequate experimental model for *in-vivo* toxicity. Moreover, deep knowledge of the biology of the selected animal is needed for proper assessment of the effect of the route of administration on the toxicity induced by MNPs [82].

4.2. Alternative ***in-vivo*** **models**

Other organisms (e.g., invertebrates), which permit the analysis of ADME-toxicity parameters, have also been used for the *in-vivo* evaluation of the toxicity of MNPs. An important benefit of these models is that there is no need to refer them to bioethical committees.

4.2.1. Invertebrate organisms. In an interesting study, Novak and collaborators proposed a terrestrial invertebrate, *Porcellio scaber* (Isopoda, Crustacea) to test toxicity of TiO_2 NPs orally administered [84]. They hypothesized that the TiO_2 NP toxicity could be due to the high doses, exposure time and the ability to distribute within the whole animal body after crossing gut epithelial-cell barriers. The route of administration by feeding the

animal with TiO_2 NPs within the food intake permitted the study of several parameters (e.g., general health score of the animals). Each individual was independently exposed and the feed rate was calculated by the relation between food consumption and weight increase of each animal each day of treatment. The ability of NPs to spread throughout the whole organism was evaluated by analyzing the membrane integrity of gut epithelial cells by immunohistochemistry [84,85].

The use of biomarker organisms of environmental contamination is another interesting model to test MNP-induced toxicity. In this test, freshwater crustacean *Daphnia magna* has been used as a contamination biomarker due to its sensitivity to changes in the ecosystem [86]. Moreover, *D. magna* is part of the trophic chain base revealing important information about the accumulation of toxic effects within the rest of the organisms in the ecosystem [87,88].

In a recent work, Asghari et al. evaluated the toxicity of different groups of colloidal Ag NPs under an acute, short-term exposure model. They determined the minimum dose of Ag NPs inducing lethality in *D. magna* after 48-h administration in water containers. The toxicity score was evaluated by determining lethal doses (LD_{10}, LD_{50} and LD_{90}), observation of birth defects and progression of paralysis. They concluded from these studies that the toxicity of Ag NPs depends on their nature and state of aggregation [89]. Similar studies have been performed by other groups to analyze the effects of Ag NPs ingested by *D. magna* [89,90].

There are benefits and disadvantages from using invertebrate models to test toxicity induced by MNPs. First, the protocols are technically easier than those for vertebrates and mammals so interpretation is easier. Invertebrates are big enough to obtain sufficient amounts of biological samples for histopathological analysis and other purposes. Another important issue is the possibility to obtain a large number of individuals to increase statistical significance. Conversely, the short experience with these models so far could be a disadvantage in using them in MNP tests. Another objection to using invertebrates is the lack of mathematical models to interpret the results properly and to extrapolate to the potential toxicity in humans. The last concern could be aggravated due to the low physiological correlation between vertebrates and invertebrates. Hence, the ideal situation for properly testing the toxicity of MNPs would be the use of both types of model animal, invertebrate and vertebrate.

4.2.2. Embryo models. Another important factor to be considered is the potential toxicity of MNPs during embryo development. To address this question, Clancy et al. developed a model of live chicken embryo in which MNPs were administered directly into the bloodstream. The use of fluorescent NPs allowed the study of their distribution throughout the whole body, as well as the aggregation behavior, by fluorescence spectroscopy.

NPs tended to aggregate and to accumulate in blood vessels of different sizes and in tissues with high angiogenic activity. Similarly to the toxicity studies in vertebrates, the toxicity in embryo models depended on the bio-distribution of the MNPs and their physicochemical properties: size, electrical charge, and surface modifications (e.g., chitosan and fluorescent particles) [91,92].

The data obtained from live chicken embryos could be extrapolated to adult animals, so being helpful for the development of toxicity protocols. Moreover, chicken embryo is a *bona fide* model for experimentation, as their use is not regulated by ethical committees, thus avoiding legal issues [92].

4.2.3. Prokaryotic organisms. A new biological model using prokaryotic organisms was recently proposed for MNP-toxicity studies. This model is based on using bacteria able to produce bioluminescence. Bioluminescence intensity is directly related to cellular metabolism, and this correlation is used to address the toxicity of NPs. A decrease in metabolic activity induced by exposure to MNPs would decrease the bioluminescence intensity, which would indicate an increase in the toxicity induced by MNPs.

The use of bacteria with these characteristics represents a new method to address the toxicity of different MNPs in a short time period by analyzing fluctuations of light emission [93]. This characteristic of luminous bacteria has been used in promising toxicity studies for Au NPs and carbon nanotubes in assays taking just 15 min [94]. The results obtained with the luminous bacteria were comparable to those obtained with other conventional approaches used to evaluate MNP-induced toxicity [95].

5. Conclusions

We have presented the different options used to evaluate the potential toxicity of MNPs using *in-vitro* and *in-vivo* assays. Although the number of articles aiming to assess the toxicity of MNPs is increasing, there is still an urgent need for standardized protocols allowing systematic study of the toxicity induced by particular types of MNP. As we have shown, not only are concentration and the exposure times parameters that have to be considered when assessing the toxicity of MNPs, but stability, particle size, shape and aggregation state are also significant factors. Moreover, when using *in-vitro* models, the behavior may be radically different, depending on the cell line tested.

As for the *in-vivo* models, it is important to choose not only the correct animal model but also the appropriate

route of administration, since the toxic response can greatly vary.

Also, it is important to mention that, although general toxicity assays have been shown to be very useful to evaluate MNP-induced toxicity, approaches focused on identifying specific targets (genes and/or proteins) may help not only to improve understanding of the interaction mechanisms of cells and organisms with MNPs, but also to design novel non-toxic MNPs.

Acknowledgements

This work was funded by grants from the Spanish Ministry of Economy and Competitiveness (CTQ2010-18644, CTQ2011-28328C02-01 and SAF2011-27330), and grants ANALISYC II and INDISNET 01592006 from *Comunidad de Madrid*. J.L.L.-G. was financially supported by the *Ramón y Cajal* program. I.L.-H. thanks the *Comunidad de Madrid* for a pre-doctoral scholarship.

References

[1] D. Cui, H. Gao, Biotechnol. Prog. 19 (2003) 683.
[2] V. Rabolli, L.C.J. Thomassen, F. Uwambayinema, J.A. Martens, D. Lison, Toxicol. Lett. 206 (2011) 197.
[3] K. Gerloff, I. Fenoglio, E. Carella, J. Kolling, C. Albrecht, A.W. Boots, I. Förster, R.P.F. Schins, Chem. Res. Toxicol. 25 (2012) 646.
[4] R.D. Handy, R. Owen, E. Valsami-Jones, Ecotoxicology 17 (2008) 315.
[5] S.G. Mukherjee, N. O'Claonadh, A. Casey, G. Chambers, Toxicol. Vitro 26 (2012) 238.
[6] M. Tarantola, D. Schnelder, E. Sunnick, H. Adam, S. Pierrat, C. Rosman, V. Breus, C. Sönnichsen, T. Basché, J. Wegener, A. Janshoff, ACS Nano 3 (2009) 213.
[7] V. Christen, K. Fent, Chemosphere 87 (2012) 423.
[8] H.A. Ngwa, A. Kanthasamy, Y. Gu, N. Fang, V. Anantharam, A.G. Kanthasamy, Toxicol. Appl. Pharmacol. 256 (2011) 227.
[9] M. Al-Rawi, S. Diabaté, C. Weiss, Arch. Toxicol. 85 (2011) 813.
[10] S.M. Hussain, K.L. Hess, J.M. Geahart, K.T. Geiss, J.J. Schlager, Toxicol. Vitro 19 (2005) 975.
[11] Z.E. Allouni, P.J. Høl, M.A. Cauqui, N.R. Gjerdet, M.R. Cimpan, Toxicol. Vitro 26 (2012) 469.
[12] M.J.D. Clift, B. Rothen-Rutishauser, D.M. Brown, R. Duffin, K. Donaldson, L. Proudfoot, K. Guy, V. Stone, Toxicol. Appl. Pharmacol. 232 (2008) 418.
[13] T. Morais, M.E. Soares, J.A. Duarte, L. Soares, S. Maia, P. Gomes, E. Pereira, S. Fraga, H. Carmo, M. de Lourdes Bastos, Eur. J. Pharm. Biopharm. 80 (2012) 185.
[14] M. Shen, H. Cai, X. Wang, X. Cao, K. Li, S.H. Wang, R. Guo, L. Zheng, G. Zhang, X. Shi, Nanotechnology 23 (2012) 105601.
[15] A. Albanese, W.C.W. Chan, ACS Nano 5 (2011) 5478.
[16] C. Brandenberger, M.J.D. Clift, D. Vanhecke, C. Mühlfeld, V. Stone, P. Gehr, B. Rothen-Rutishauser, Particle Fibre Toxicol. 7 (2010) 1.
[17] J.H. Park, J. Park, U. Dembereldorj, K. Cho, K. Lee, S.I. Yang, S.Y. Lee, S.W. Joo, Anal. Bioanal. Chem. 401 (2011) 1631.
[18] R. de Lima, A.B. Seabra, N. Duran, J. Appl. Toxicol. 32 (2012) 867.
[19] B.J. Marquis, S.A. Love, K.L. Braun, C.L. Haynes, Analyst (Cambridge, UK) 134 (2009) 425.
[20] H.E. Pace, E.K. Lesher, J.F. Ranville, Environ. Toxicol. Chem. 29 (2010) 1338.
[21] F. Watari, N. Takashi, A. Yokoyama, M. Uo, T. Akaska, Y. Sato, S. Abe, Y. Totsuka, K. Tohij, J.R. Soc, Interface 6 (2009) S371.
[22] R. Allabashi, W. Stach, A. de la Escosura-Muniz, L. Liste-Calleja, A. Merkoci, J. Nanopart. Res. 11 (2009) 2003.
[23] M.C. Wende, J.A.C. Broekaert, Fresenius' J. Anal. Chem. 370 (2001) 513.
[24] M. Resano, F. Vanhaecke, M.T.C. de Loos-Vollebregt, J. Anal. At. Spectrom. 23 (2008) 1450.
[25] A. Scheffer, C. Engelhard, M. Sperling, W. Buscher, Anal. Bioanal. Chem. 390 (2008) 249.
[26] W. Zhang, Y. Ji 2, J. Meng, X. Wu, H. Xu, PLoS ONE 7 (2012) e31957.
[27] D.A. Navarro, M.A. Bisson, D.S. Aga, J. Hazard. Mater. 211–212 (2012) 427.
[28] A. Sarmiento-Gonzalez, J.R. Encinar, J.M. Marchante-Gayon, A. Sanz-Medel, Anal. Bioanal. Chem. 393 (2009) 335.
[29] J.L. Tang, L. Xiong, S. Wang, J.Y. Wang, L. Liu, J. Li, F.Q. Yuan, T.F. Xi, J. Nanosci. Nanotechnol. 9 (2009) 4924.
[30] M.M. Song, W.J. Song, H. Bi, J. Wang, W.L. Wu, J. Sun, M. Yu, Biomaterials 31 (2010) 1509.
[31] Y. Hayashi, P. Engelmann, R. Foldbjerg, M. Szabo, I. Somogyi, E. Pollák, L. Molnár, H. Autrup, D.S. Sutherland, J. Scott-Fordsmand, L.H. Heckmann, Environ. Sci. Technol. 46 (2012) 4166.
[32] F. Liu, J. Chromatogr., A 1216 (2009) 9034.
[33] K. Teide, A.B.A. Boxall, X. Wang, D. Gore, D. Tiede, M. Baxter, H. David, S.P. Tear, J. Lewis, J. Anal At. Spectrom. 25 (2010) 1149.
[34] U. Kumtabtim, J. Shiowatana, A. Siripinyanond, J. Anal. At. Spectrom. (20) (2005) 1185.
[35] A. Samontha, J. Shiowatana, A. Siripinyanond, Anal. Bioanal. Chem. 399 (2011) 973.
[36] A. Oukarroum, S. Bras, F. Perreault, R. Popovic, Ecotoxicol. Environ. Safety 78 (2012) 80.
[37] S.Y. Choi, S. Jeong, S.H. Jang, J. Park, J.H. Park, K.S. Ock, S.Y. Lee, S.W. Joo, Toxicol. Vitro 26 (2012) 229.
[38] G.D. Zhang, Z. Yang, W. Lu, R. Zhang, Q. Huang, M. Tian, L. Li, D. Liang, C. Li, Biomaterials 30 (2009) 1928.
[39] J.G. Teeguarden, P.M. Hinderliter, G. Orr, B.D. Thrall, J.G. Pounds, Toxicol. Sci. 95 (2007) 300.
[40] A.M. Alkilany, P.K. Nagaria, C.R. Hexel, T.J. Shaw, C.J. Murphy, M.D. Wyatt, Small 5 (2009) 701.
[41] J. Chan, T. Ying, Y.F. Guang, L.X. Lin, T. Kai, Z.V. Fang, Y.X. Ting, L.F. Xing, Y.Y. Ji, Biol. Trace Elem. Res. 144 (2011) 183.
[42] T. Hasezaki, K. Isoda, M. Kondoh, Y. Tsutsumi, K. Yagi, Pharmazie 66 (2011) 698.
[43] X. Lu, J.C. Qian, H.J. Zhou, Q. Gan, W. Tang, J.X. Lu, Y. Yuan, C.S. Liu, Int. J. Nanomed. 6 (2011) 1889.
[44] H. Luo, F. Wang, Y. Bai, T. Chen, W. Zheng, Colloids Surf., B 94 (2012) 304.
[45] H.K. Patra, S. Banerjee, U. Chaudhuri, P. Lahiri, A.K. Dasgupta, Nanomed. Nanotechnol. 3 (2007) 111.
[46] R.M. Zucker, E.J. Massaro, K.M. Sanders, L.L. Degn, W.K. Boyes, Cytometry Part A 77A (2010) 677.
[47] X. Han, N. Corson, P. Wade-Mercer, R. Gelein, J. Jiang, M. Sahu, P. Biswas, J.N. Finkelstein, A. Elder, G. Oberdörster, Toxicology 297 (2012) 1.
[48] C. Uboldi, G. Giudetti, F. Broggi, D. Gilliland, J. Ponti, F. Rossi, Mutat. Res. 745 (2012) 11.
[49] J.-H. Yuan, Y. Chen, H.-X. Zha, L.-J. Song, C.-Y. Li, J.-Q. Li, X.-H. Xia, Colloids Surf., B 76 (2010) 145.
[50] C. Harris, J.M. Hansen, Methods Mol. Biol. 889 (2012) 325.
[51] M. Könczöl, S. Ebeling, E. Goldenberg, F. Treude, R. Gminski, R. Gieré, B. Grobéty, B. Rothen-Rutishauser, I. Merfort, V. Mersch-Sundermann, Chem. Res. Toxicol. 24 (2011) 1460.
[52] I. Passagne, M. Morille, M. Rousset, I. Pujalté, B. L'Azou, Toxicology 299 (2012) 112.
[53] J.J. Li, D. Hartono, C.-N. Omg, B.-H. Bay, L.-Y.L. Yung, Biomaterials 31 (2010) 5996.

[54] V. Sharma, D. Anderson, A. Dhawan, Apoptosis 17 (2012) 852.
[55] E.-J. Park, J. Yi, K.-H. Chung, D.-Y. Ryu, J. Choi, K. Park, Toxicol. Lett. 180 (2008) 222.
[56] J. Ahmad, M. Ahamed, M.J. Akhtar, S.A. Alrokayan, M.A. Siddiqui, J. Musarrat, A.A. Al-Khedhairy, Toxicol. Appl. Pharmacol. 259 (2012) 160.
[57] M. van Gurp, N. Festjens, G. van Loo, X. Saelens, P. Vandenabeele, Biochem. Biophys. Res. Commun. 304 (2003) 487.
[58] T. Chen, Y.-S. Wong, W. Zheng, Y. Bai, L. Huang, Coll. Surf. B 67 (2008) 26.
[59] K. Meyer, P. Rajanahalli, M. Ahamed, J.J. Rowe, Y. Hong, Toxicol. Vitro 25 (2011) 1721.
[60] S. Cotelle, J.F. Férard, Environ. Mol. Mutagen. 34 (1999) 246.
[61] R. Meena, M. Rani, R. Pal, P. Rajamani, Appl. Biochem. Biotechnol. 167 (2012) 791.
[62] C. Gong, G. Tao, L. Yang, J. Liu, H. He, Z. Zhuang, Mol. Biol. Rep. 39 (2012) 4915.
[63] G. Speit, P. Schütz, I. Bonzheim, K. Trenz, H. Hoffmann, Toxicol. Lett. 146 (2004) 151.
[64] N. Hanagata, F. Zhuang, S. Connolly, J. Li, N. Ogawa, M. Xu, ACS Nano 5 (2011) 9326.
[65] M. Mahmoudi, S. Laurent, M.A. Shokrgozar, M. Hosseinkhani, ACS nano 5 (2011) 7263.
[66] P. Dua, K.N. Chaudhari, C.H. Lee, N.K. Chaudhari, S.W. Hong, J.-S. Yu, S. Kim, D.-K. Lee, Bull. Korean Chem. Soc. 32 (2011) 2051.
[67] J.L. Luque-Garcia, P. Cabezas-Sanchez, C. Camara, Trends Anal. Chem. 30 (2011) 703.
[68] J.L. Luque-Garcia, J.L. Martinez-Torrecuadrada, C. Epifano, I. Babel, M. Cañamero, I. Casal, Proteomics 10 (2010) 940.
[69] X. Yang, J. Liu, H. He, L. Zhou, C. Gong, X. Wang, L. Yang, J. Yuan, H. Huang, L. He, B. Zhang, Z. Zhuang, Particle Fibre Toxicol. 7 (2010) 1.
[70] Y.-M. Jeon, S.-K. Park, M.-Y. Lee, J. Korean Soc, Appl. Biol. Chem. 54 (2011) 852.
[71] C.A. Simpson, K.J. Salleng, D.E. Cliffel, D.L. Feldheim, Nanomedicine (2012) http://dx.doi.org/10.1016/j.nano.2012.06.002.
[72] K.L. Aillon, Y. Xie, N. El-Gendy, C.J. Berkland, M.L. Forrest, Adv. Drug Deliv. Rev. 61 (2009) 457.
[73] V. Kumar, A. Kumari, P. Guleria, S.K. Yadav, Rev. Environ. Contam. Toxicol. 215 (2012) 39.
[74] R.J. Griffitt, J. Luo, J. Gao, J.C. Bonzongo, D.S. Barber, Environ. Toxicol. Chem. 27 (2008) 1972.
[75] Y.L. Hu, W. Qi, F. Han, J.Z. Shao, J.O. Gao, Int. J. Nanomed. 6 (2011) 3351.
[76] J.H. Sung, J.H. Ji, J.D. Park, M.Y. Song, K.S. Song, H.R. Ryu, J.U. Yoon, K.S. Jeon, J. Jeong, B.S. Han, Y.H. Chung, H.K. Chang, J.H. Lee, D.W. Kim, B.J. Kelman, I.J. Yu, Particle Fibre Toxicol. 8 (2011) 16.
[77] J.S. Kim, T.J. Yoon, K.N. Yu, B.G. Kim, S.J. Park, H.W. Kim, K.H. Lee, S.B. Park, J.K. Lee, M.H. Cho, Toxicol. Sci. 89 (2006) 338.
[78] W.H. De Jong, W.I. Hagens, P. Krystek, M.C. Burger, A.J. Sips, R.E. Geertsma, Biomaterials 29 (2008) 1912.
[79] H. Xie, M.M. Mason, J.P. Wise, Rev. Environ. Health 26 (2011) 251.
[80] G. Oberdorster, E. Oberdorster, J. Oberdorster, Environ. Health Perspect. 113 (2005) 823.
[81] G.M. Hodges, E.A. Carr, R.A. Hazzard, C. O'Reilly, K.E. Carr, J. Drug Target. 3 (1995) 57.
[82] Z. Chen, H. Meng, G. Xing, C. Chen, Y. Zhao, G. Jia, T. Wang, H. Yuan, C. Ye, F. Zhao, Z. Chai, C. Zhu, X. Fang, B. Ma, L. Wan, Toxicol. Lett. 163 (2006) 109.
[83] S.K. Lam, Clin. Gastroenterol. 14 (2000) 41.
[84] S. Novak, D. Drobne, A. Menard, Zookeys 176 (2012) 261.
[85] A. Jemec, D. Drobne, M. Remskar, K. Sepcic, T. Tisler, Environ. Toxicol. Chem. 27 (2008) 1904.
[86] D. Drobne, A. Jemec, Z. Pipan-Tkalec, Environ. Pollut. 157 (2009) 1157.
[87] S. Asghari, S.A. Johari, J.H. Lee, Y.S. Kim, Y.B. Jeon, H.J. Choi, M.C. Moon, L.J. Yu, J. Nanobiotechnol. 10 (2012) 14.
[88] A.J. Kennedy, M.S. Hull, A.J. Bednar, J.D. Goss, J.C. Gunter, J.L. Bouldin, P.J. Vikesland, J.A. Steevens, Environ. Sci. Technol. 44 (2010) 9571.
[89] H.J. Allen, C.A. Impellitteri, D.A. Macke, J.L. Heckman, H.C. Poynton, J.M. Lazorchak, S. Govindaswamy, D.L. Roose, M.N. Nadagouda, Environ. Toxicol. Chem. 29 (2010) 2742.
[90] S. Zhu, E. Oberdorster, M.L. Haasch, Marine, Environ. Res. 62 (2006) S5.
[91] A.A. Clancy, Y. Gregoriou, K. Yaehne, D.R. Cramb, Chem. Phys. Lett. 488 (2010) 99.
[92] M.Y. Wani, M.A. Hashim, F. Nabi, M.A. Malik, Adv. Phys. Chem. 2011 (2011) 1.
[93] S. Parvez, C. Venkataraman, S. Mukherji, Environ. Int. 32 (2006) 265.
[94] H. Zheng, L. Liu, Y. Lu, Y. Long, L. Wang, K.P. Ho, K.Y. Wong, Anal. Sci. 26 (2010) 125.
[95] J. Lappalainen, R. Juvonen, J. Nurmi, M. Karp, Chemosphere 45 (2001) 635.

Journal of Autoimmunity 55 (2014) 51–62

Contents lists available at ScienceDirect

Journal of Autoimmunity

journal homepage: www.elsevier.com/locate/jautimm

Maintenance of immune tolerance by Foxp3$^+$ regulatory T cells requires CD69 expression

José R. Cortés [a, 1], Raquel Sánchez-Díaz [a, 1], Elena R. Bovolenta [a], Olga Barreiro [a], Sandra Lasarte [a], Adela Matesanz-Marín [a], María L. Toribio [c], Francisco Sánchez-Madrid [a, b], Pilar Martín [a, *]

[a] Department of Vascular Biology and Inflammation, Centro Nacional de Investigaciones Cardiovasculares Carlos III (CNIC), Madrid 28029, Spain
[b] Servicio de Inmunología, Hospital de La Princesa, Universidad Autónoma de Madrid, Madrid 28006, Spain
[c] Centro de Biología Molecular Severo Ochoa, Consejo Superior de Investigaciones Científicas, Universidad Autónoma de Madrid, 28049, Spain

ARTICLE INFO

Article history:
Received 13 December 2013
Received in revised form
22 April 2014
Accepted 23 May 2014
Available online 14 June 2014

Keywords:
Regulatory T cells
Immune tolerance
FoxP3
CD69

ABSTRACT

Although FoxP3$^+$ regulatory T cells are key players in the maintenance of immune tolerance and autoimmunity, the lack of specific markers constitute an obstacle to their use for immunotherapy protocols. In this study, we have investigated the role of the C-type lectin receptor CD69 in the suppressor function of Tregs and maintenance of immune tolerance towards harmless inhaled antigens. We identified a novel FoxP3$^+$CD69$^+$ Treg subset capable to maintain immune tolerance and protect to developing inflammation. Although CD69$^+$ and CD69$^-$FoxP3$^+$ Tregs exist in homeostasis, only CD69-expressing Tregs express high levels of CTLA-4, ICOS, CD38 and GITR suppression-associated markers, secrete high amounts of TGFβ and have potent suppressor activity. This activity is regulated by STAT5 and ERK signaling pathways and is impaired by antibody-mediated down-regulation of CD69 expression. Moreover, immunotherapy with FoxP3$^+$CD69$^+$ Tregs restores the homeostasis in *Cd69*$^{-/-}$ mice, that fail to induce tolerance, and is also highly proficient in the prevention of inflammation. The identification of the FoxP3$^+$CD69$^+$ Treg subset paves the way toward the development of new therapeutic strategies to control immune homeostasis and autoimmunity.

1. Introduction

FoxP3$^+$ regulatory T (Treg) cells are a subset of CD4$^+$ T lymphocytes with suppressive activity, key mediator of peripheral tolerance and essential for preventing autoimmune and chronic inflammatory diseases. However, the lack of specific markers and insufficient understanding of Tregs biology constitute the two largest obstacles to develop immunotherapy protocols for the treatment of these diseases [1]. Treg cells inhibit proliferation and function of effector T cells through various mechanisms, including cell–cell contact and the production of anti-inflammatory cytokines such as TGF-β or IL-10. Tregs can develop in the thymus, or from naïve CD4$^+$ T cells in the periphery [2]. After antigen challenge lymph nodes are the sites of differentiation of effector T cells and/or Tregs, which upregulate specific adhesion and chemokine receptors and migrate to the inflamed tissue. This regulatory mechanism of cell migration is critical for a proper balance between the innate and adaptive immune responses in the inflamed tissue [3]. In this regard, $S1P_1$ has been described as an important molecule controlling lymphocyte egress from lymphoid organs and leukocyte receptor CD69 negatively regulates its expression [4].

The early leukocyte activation antigen CD69 is a membrane receptor from the family of type II C-type lectins. CD69 is rapidly induced after cell activation in all bone marrow derived cells except erythrocytes [5,6]. Expression of CD69 *in vivo* is restricted to positively selected thymocytes and leukocytes undergoing activation, particularly at inflammatory sites. Engagement of CD69 with monoclonal antibodies (mAbs) in the presence of phorbol esters induces a strong Ca^{2+} influx leading to the activation of ERK, induction of IL-2 and IFN-γ genes, and T cell proliferation [7,8]. However, *in vivo* studies with CD69-deficient mice revealed an unexpected immunoregulatory role [9]. A mouse model of lymphocyte-dependent collagen-induced arthritis (CIA) suggested

* Corresponding author. Department of Vascular Biology and Inflammation, Centro Nacional de Investigaciones Cardiovasculares Carlos III (CNIC), Melchor Fernández Almagro 3, Madrid E-28029, Spain. Tel.: +34 914 531 200; fax: +34 914 531 265.
E-mail addresses: pmartinf@cnic.es, pilar.pmartin@gmail.com (P. Martín).
[1] Those authors contributed equally to this work.

http://dx.doi.org/10.1016/j.jaut.2014.05.007
0896-8411/

that CD69 might act as a regulatory molecule by modulating TGF-β levels at the site of inflammation [10]. Since TGF-β participates in the differentiation both of regulatory T cells and of Th17 cells [11,12], CD69 might regulate the immune response at the stage of T cell differentiation. The balance between Th17 and Treg cells is critical for the regulation of the immune response by determining the net balance of pro- and anti-inflammatory cytokines at the inflammatory foci.

In this report we have analyzed the role of CD69 in the function of FoxP3$^+$ Tregs. We show that around half of the Tregs located in lymphoid organs express CD69 in steady state. CD69$^+$ Tregs express higher surface levels of suppression-associated markers than CD69$^-$ Tregs cells or Tregs from *Cd69*$^{-/-}$ mice, and have enhanced suppressor activity *in vitro* and in a mouse model of lung tolerance to harmless antigens. Our results strongly support a role for CD69 as a critical receptor for controlling Treg-suppressor function in both physiological and pathological immune responses, including autoimmunity and allergy.

2. Materials and methods

2.1. Animals

CD69-deficient mice were generated as described [13]. C57BL/6 Tg(TcraTcrb)425Cbn/J mice expressing a T-cell receptor specific for peptide 323–339 of OVA in the context of I-Ab (OTII mice) were purchased from the Jackson Laboratory (stock number 004194). OTII mice were backcrossed with CD69-deficient mice in the C57BL/6 background (OTKO mice). For *in vivo* tolerogenic asthma experiments, we used females 10–12 weeks old that were either littermates or age-matched offspring in BALB/c or OTII background. Foxp3-RFP reported mice were kindly provided by Dr. R.A. Flavell (Yale University). Mice were kept in SPF conditions at the Animal Facility of CNIC. Experimental procedures were approved by the CNIC Committee for Research Ethics and conducted under Animal Welfare and Health Spanish and European guidelines.

2.2. T-cell isolation

Single-cell suspensions were obtained from spleen or mesenteric lymph nodes and incubated with the following biotinylated antibodies: CD8, CD19, B220, MHCII, CD11c, IgM, DX5 and CD11b, followed by streptavidin Microbeads. CD4$^+$ T cells were negatively selected with auto-MACS Pro (Miltenyi) separator. The negative fraction was incubated with anti-CD25 biotin to obtain Tregs.

2.3. Treg cell suppression assays

Tconvs were cultured with coated a-CD3 antibody (1 μg/mL) plus indicated amounts of soluble a-CD28 or irradiated T cell–depleted splenocytes. For antigen-specific assays, CD4$^+$ T cells from OTII and OTKO mice were cultured in the presence of irradiated APC and OVAp (10 mg/mL). T cell proliferation was measured by [^{3}H]-thymidine incorporation for the last 16 h of culture or by CFSE or CellTraceViolet staining of CD4$^+$ Tconv cells.

2.4. Intracellular staining and FACS

Tregs or Tconv cells were treated with 1 μg/ml anti-CD3 (145-2C11) and anti-CD28 (37.51), and crosslinked with anti–Armenian Hamster IgG F(ab')2 (20 μg/mL). Activation was arrested by fixation with 4% formaldehyde and permeabilized with 90% methanol and cells were incubated with phospho-Akt, phospho-Erk and phospho-Stat5 from Cell Signaling.

2.5. In vitro differentiation of Tregs

OVA-specific TCR transgenic naïve T cells were obtained from OTII and OTKO mice and cultured for 72 h with irradiated APCs in the presence of 10 μg/ml OVAp, recombinant TGF-β1, and IL-2. *In vitro* differentiation of iTregs from C57BL/6 mice with normal TCR was performed from naïve CD4 T cells from CD69-proficient or deficient mice, co-cultured 120 h with WT splenic dendritic cells in the presence of plate-bound CD3 and soluble CD28 plus recombinant TGF-β1 and IL-2.

2.6. Tolerogenic challenge with harmless antigen

To analyze the *in vivo* function of Treg, we used a previously described tolerogenic model [14]. Briefly, at day 0, mice were i.t injected with 800 μg LPS-free OVA (Calbiochem). At day 20, mice received 3 OVA aerosols (10 mg/mL in PBS, generated using a jet nebulizer) of 30 min on 3 consecutive days. In some experiments, 10 days later after the i.t administration of OVA, the mice were immunized with OVA-alum (10 μg OVA adsorbed to 2 mg aluminum hydroxide) and 10 days later, mice were challenged with three daily 30-min OVA aerosols as described before.

2.7. Adoptive transfer experiments

Mice were intraperitoneally injected with 10 μg OVA in 2 mg alum, and 5 days later CD4$^+$ T cells were isolated and expanded *in vitro* with TGF-β and IL-2 in presence of irradiated APC and OVAp. iTreg cells were intravenously injected (5×10^6 cells) into *Cd69*$^{+/+}$ or *Cd69*$^{-/-}$ recipient mice previously intratracheally sensitized with OVA. The recipients were exposed to inhaled OVA (10 mg/mL) for 3 days. For the adoptive transfer experiment with natural Tregs, CD4$^+$CD25$^+$-CD69$^+$ or -CD69$^-$ Tregs were isolated by FACS sorting from spleens and 2×10^5 cells were i.v. transferred to *Cd69*$^{+/+}$ or *Cd69*$^{-/-}$ recipients.

2.8. Whole-mount staining of mouse tracheas

Tracheas were incubated with PBS containing 0.5% Triton X-100, 5% goat serum and primary antibodies [rabbit polyclonal anti-mouse CD31 (Abcam) and rat clone FJK-16s anti-mouse Foxp3 coupled to FITC (eBiosciences)]. Samples were washed with 0.3% Triton X-100 in PBS and stained with goat anti-rabbit Rhodamine Red-X (Molecular Probes). Stained samples were fixed with PFA 4% and mounted with Prolong® Gold antifade reagent (Molecular Probes, Life Technologies). Confocal z-stacks from the inner side of tracheas were obtained using a LSM 700 Laser Scanning Microscope equipped with a LD LCI Plan/Apochromat 25×/0.8 Imm Korr DIC M27 (Zeiss). Images were analyzed with Imaris v.7.3.1 (Bitplane).

2.9. In vivo FMT 1500 tomographic imaging and analysis

Mice were injected intravenously with 4 nmol of Neutrophil Elastase 680 FAST (PerkinElmer, Inc.). OVA-challenged and control mice were imaged using the FMT 1500 fluorescence tomography *in vivo* imaging system (PerkinElmer, Inc.). The collected fluorescence data were reconstructed by FMT 2500 system software version 1.1 for three-dimensional fluorescence quantification. The total amount of lung fluorescence (in picomols) was calculated relative to internal standards.

2.10. RNA extraction and micro fluidic card analysis

RNA was extracted using Absolutely RNA Nanoprep Kit (Agilent Technologies). 100–200 ng of total RNA was converted into cDNA

and loaded in a TaqMan® Array Micro Fluidic Card (Applied Biosystems). Relative gene expression was calculated with qbase software (Biogazelle) using Actb, B2m, Gapdh and Hprt1 as reference targets genes. Heat map images were generated with Gene Cluster 3.0 and Java Treeview software.

2.11. Statistical analysis

P values were calculated with the Student *t* test, and values below 0.05 were considered significant. Means of the experimental groups were compared by using One-way ANOVA. To account for multiple comparisons, the Tukey or Bonferroni post-test were used to compare selected pairs of means and all pairs of means, respectively. All statistical analyses were carried out with GraphPad Prism v5.

3. Results

3.1. CD69 is constitutively expressed by a subset of thymic and peripheral Tregs in steady state

A subpopulation of about fifty percent of total $CD4^+CD25^+FoxP3^+$ Treg cells in thymus and secondary lymphoid organs express CD69 on their membrane in steady state (Fig. 1A). Further phenotypic analysis of peripheral $CD4^+FoxP3^+$ gated $CD69^+$ and $CD69^-$ Tregs from *Cd69*$^{+/+}$ or *Cd69*$^{-/-}$ mice in homeostasis (Fig. 1B), revealed that the suppression-associated markers CTLA-4, ICOS, CD38 and GITR are expressed at higher levels in $CD69^+$-Tregs in steady state compared to $CD69^-$ Tregs or Tregs from *Cd69*$^{-/-}$ mice (Fig. 1C), suggesting that the phenotypic features of $CD69^+$ Tregs cells are consistent with an effector Treg phenotype. However, expression levels of other relevant proteins for Treg function, such as CD25, CD86 or CD27, are unaffected by CD69 expression (Supplementary Fig. S1). Interestingly, $CD4^+FoxP3^+$ Tregs homeostasis is not altered in peripheral lymphoid organs from *Cd69*$^{-/-}$ mice in comparison with *Cd69*$^{+/+}$ mice (Fig. 1D), indicating that, although Treg development seems not to be affected by the lack of CD69, their function could be dampened.

3.2. The suppressive function of Tregs is dependent on CD69 expression

We next assessed the role of CD69 in the suppressive function of Tregs. Naïve conventional T (Tconv) cells from *Cd69*$^{+/+}$ or *Cd69*$^{-/-}$ mice were co-cultured with $CD4^+CD25^+FoxP3^+$ Tregs of *Cd69*$^{+/+}$ or *Cd69*$^{-/-}$ mice and irradiated APCs (iAPCs). Suppressor function of CD69-deficient Tregs was diminished compared with Tregs from *Cd69*$^{+/+}$ mice (Fig. 2A). This effect was confirmed in the presence of CD3/CD28 antibodies suppression assays devoid of APCs (Supplementary Fig. S2). Tregs from *Cd69*$^{-/-}$ mice bearing OTII T-cell receptors (TCR) specific for OVA peptide showed almost no ability to inhibit Tconv proliferation in antigen-specific suppression cultures (Fig. 2B).

To confirm those results, we sorted $CD69^+$ and $CD69^-$ Tregs from *Cd69*$^{+/+}$ mice and compared them with the total $CD4^+CD25^+$ Tregs from *Cd69*$^{-/-}$ mice (referred hereafter as *Cd69*$^{-/-}$ Tregs) (see Supplementary Fig. S3A for sorting strategy). All Treg subpopulations have identical levels of $FoxP3^+$ (Supplementary Fig. S3B). $CD69^+$ Tregs showed the highest capacity to inhibit the proliferation of Tconvs, whereas $CD69^-$ and *Cd69*$^{-/-}$ Tregs showed a weaker suppressor function (Fig. 2C). The involvement of CD69 in Treg function was ascertained in *Cd69*$^{+/+}$ Tregs by addition of the anti-CD69 monoclonal antibody (*2.2*), which downregulates CD69 expression [15] and blocks the suppressive function (Fig. 2D). It is worth noting that CD69 expression in untreated $CD69^+$ Treg subpopulation was maintained at high levels *in vitro* after 3 days of co-culture with Tconv cells (Fig. 2, C–D), indicating that sustained CD69 expression is critical for the suppressive function of Tregs. We also analyzed the ability of Tregs differentiated *in vitro* (iTreg) to induce effector T cells suppression; although Treg differentiation process is not compromised in OTII *Cd69*$^{-/-}$ cells (Fig. 2E) or in *Cd69*$^{-/-}$ cells with normal TCR (Fig. 2G), these cells were unable to properly induce T cell suppression compared to OT-II-*Cd69*$^{+/+}$ iTregs (Fig. 2F) or B6 *Cd69*$^{+/+}$ iTregs (Fig. 2H), respectively. These data indicate that CD69 expression is also required for iTreg suppressive function. To further support these results, we analyzed the expression of CD69 in Tregs from Foxp3-RFP reported mice. As in the WT B6 mice, $CD69^+$ and $CD69^-$ Tregs maintain the same proportions in lymphoid organs and more importantly, Foxp3-RFP^+ $CD69^-$ Tregs showed almost no ability to suppress Tconv proliferation (Fig. 2I).

3.3. Activation of $CD69^+$ Tregs enhances STAT5 phosphorylation and decreases ERK phosphorylation

Activation of STAT5 has been reported to be required for Treg development and suppressive function [16]. To study the molecular mechanism of suppression by $FoxP3^+CD69^+$ Tregs, we stimulated sorted Tregs and naïve T cells through the TCR and measured the levels of STAT5, ERK and AKT phosphorylation by FACS. Naïve T cells from *Cd69*$^{+/+}$ or *Cd69*$^{-/-}$ mice showed no significant difference in STAT5, ERK or AKT phosphorylation (Fig. 3A). However STAT5 phosphorylation in *Cd69*$^{-/-}$ Tregs was inhibited, whereas phospho-ERK was enhanced at late time points and AKT activation was unaltered (Fig. 3B). These results are consistent with our previous results in Th17 cells, where STAT5 activation is partially inhibited in the absence of CD69 [13]. Addition of IL-2 abolished the differences in STAT5 phosphorylation between *Cd69*$^{+/+}$ and *Cd69*$^{-/-}$ Tregs (Fig. 3C), thus indicating that this cytokine restores the activation of the pathway.

To further study the role of ERK activation in the suppressor function of Tregs, Tregs isolated from *Cd69*$^{+/+}$ or *Cd69*$^{-/-}$ mice were treated with the ERK inhibitor U0126. ERK inhibition in Tregs from *Cd69*$^{-/-}$ mice restored their suppressor activity, whereas it had no detectable effect in Tregs from *Cd69*$^{+/+}$ mice (Fig. 3D). Moreover, sorted $CD69^-$ Tregs and *Cd69*$^{-/-}$ Tregs partially recovered their suppressor potential after pre-incubation with U0126 (Fig. 3E). To assess whether ERK inhibitors could also restore the suppressor potential of *Cd69*$^{-/-}$ Tregs *in vivo*, mice were given daily i.p. injection with the ERK inhibitor *ci 1040* [17]. *In vivo* inhibition of ERK phosphorylation in *Cd69*$^{-/-}$ mice (Supplementary Fig. S4) restored the suppressor capacity of Tregs isolated from *Cd69*$^{-/-}$ mice to the level detected for Tregs from *Cd69*$^{+/+}$ mice (Fig. 3F).

3.4. $CD69^+$ Tregs display specific cytokine, migratory and Treg cell-associated gene expression

We analyzed the secretion of TGF-β1 and IL-2, cytokines involved in the regulation of T cell proliferation. Sorted Tregs were stimulated with anti-CD3/CD28 mAbs. *Cd69*$^{-/-}$ Tregs secreted significantly less TGF-β1 than *Cd69*$^{+/+}$ Tregs (Fig. 4A). Moreover, lower levels of soluble TGF-β1 were found in co-cultures of *Cd69*$^{-/-}$ Tregs and Tconvs (Fig. 4B). IL-2 secretion was low in cultures of *Cd69*$^{+/+}$ and *Cd69*$^{-/-}$ Tregs, consistent with the notion that lack of IL-2 secretion is a typical feature of mature and functional Tregs [18] (Fig. 4A). However we observed increased IL-2 secretion in co-cultures of *Cd69*$^{-/-}$ Tregs and Tconvs (Fig. 4B), which could be a consequence of the higher proliferation rate of Tconvs in this

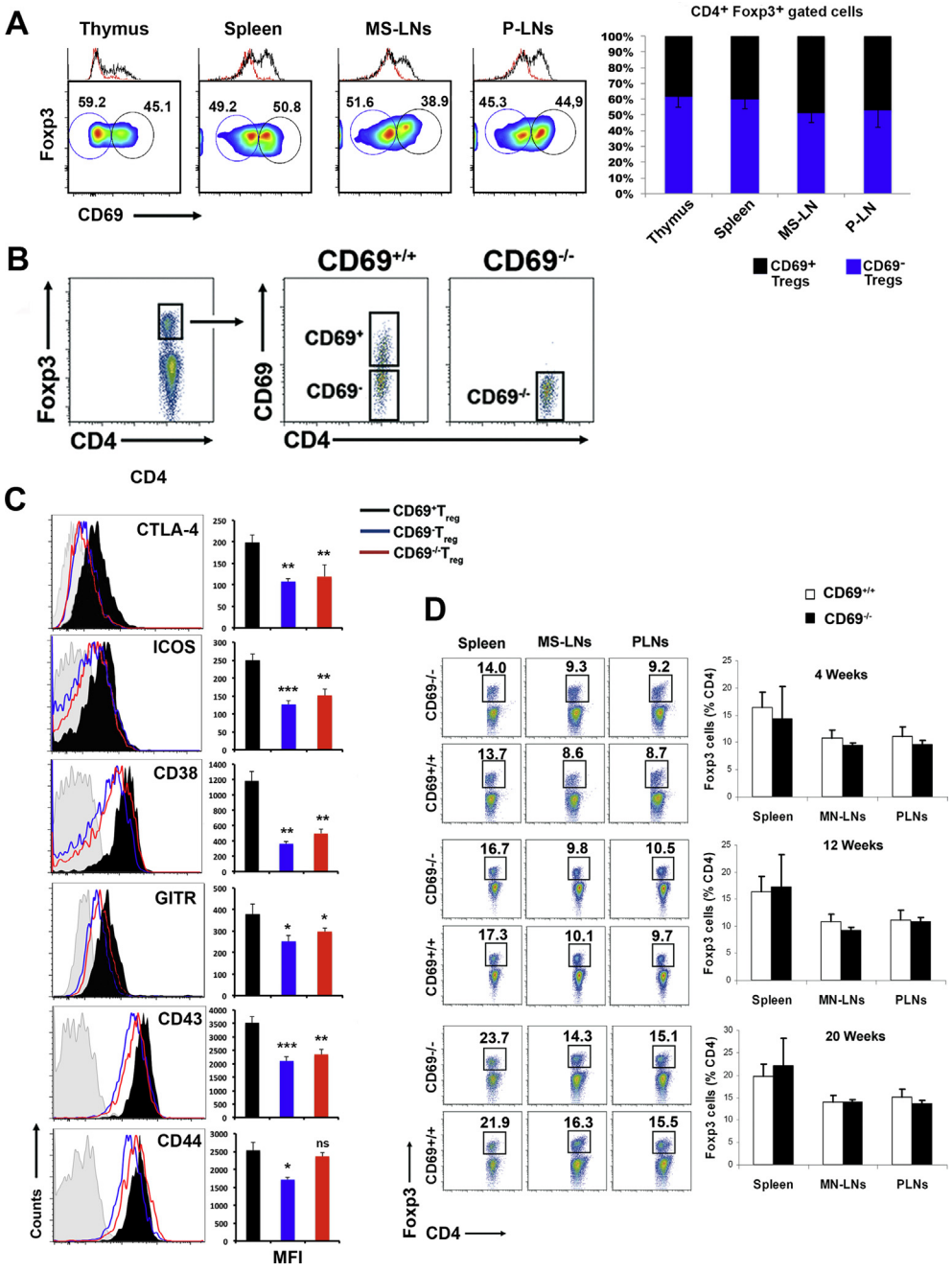

Fig. 1. CD69 is constitutively expressed by a subset of peripheral Tregs in steady state. (A) Left, density plots show CD69 expression in gated $CD4^+FoxP3^+$ cells in thymus, spleen, MS-LNs and PLNs from $Cd69^{+/+}$ mice. Histograms represent CD69 expression on $CD4^+FoxP3^+$ cells in $Cd69^{+/+}$ (black line) and $Cd69^{-/-}$ (red line) mice. Right, the bar chart shows the percentage of $CD69^+$ and $CD69^-$ Tregs within the indicated organs from $Cd69^{+/+}$ mice ± S.D. (B) FACS analysis of $CD4^+FoxP3^+CD69^+$ or -$CD69^-$ gated spleen cells from $Cd69^{+/+}$ and $Cd69^{-/-}$ mice. (C) Cell surface expression of Treg-related markers in $CD69^+$ and $CD69^-$ Tregs gated as in (B). Gray-shaded areas represent antibody isotype control and bar charts show mean fluorescence intensity (MFI) from $CD69^+$ (solid black), $CD69^-$ (blue) or $Cd69^{-/-}$ (red) Tregs. (D) $Cd69^{+/+}$ and $Cd69^{-/-}$ mice have comparable proportions of $CD4^+CD25^+FoxP3^+$ Treg cells in secondary lymphoid organs. Left panels, flow cytometry analysis of $CD4^+FoxP3^+$ cells isolated from spleen, mesenteric (MS-LNs) and peripheral (P-LNs) lymph nodes of $Cd69^{+/+}$ and $Cd69^{-/-}$ mice of 4, 12 and 20 weeks of age. Right panels, percentage of $FoxP3^+$ on gated $CD4^+$ T cells. Data are representative of three independents experiments ($n = 3$ each). Errors bars represent mean ± SD. $^*P < 0.05$, $^{**}P < 0.01$, $^{***}P < 0.001$.

condition (Fig. 2, A and B). Intracellular content of FoxP3 (Fig. 1B, and Supplementary Fig. S3B) as well as *Foxp3* mRNA levels (Fig. 4C) was the same in $CD69^+$, $CD69^-$ and $Cd69^{-/-}$ Tregs or in iTregs from $Cd69^{+/+}$ or $Cd69^{-/-}$ mice (Fig. 4D). Thus the functional differences between $CD69^+$ and $CD69^-$ Tregs are unrelated to FoxP3 expression.

To identify differential gene expression patterns we conducted TaqMan immune function gene expression analysis on sorted $CD69^+$, and $CD69^-$ Tregs (Fig. 4 E–G, and Supplementary Table S1). $CD69^+$ Tregs showed higher expression of cytokine genes involved in T cell differentiation and function such as *Il2*, *Il10*, *Il4* and *Ifnγ* (Fig. 4E). Expression of these transcripts was barely detected in $CD69^-$ Tregs. $CD69^+$ Tregs express higher levels of *Cxcl10*, *Cxcl11* and *Ccl5* and chemokine receptors *Cxcr3* and *Ccr2*, involved in the migration of Tregs to inflamed tissue [19]. $CD69^-$ Tregs express low levels of most of the receptors and

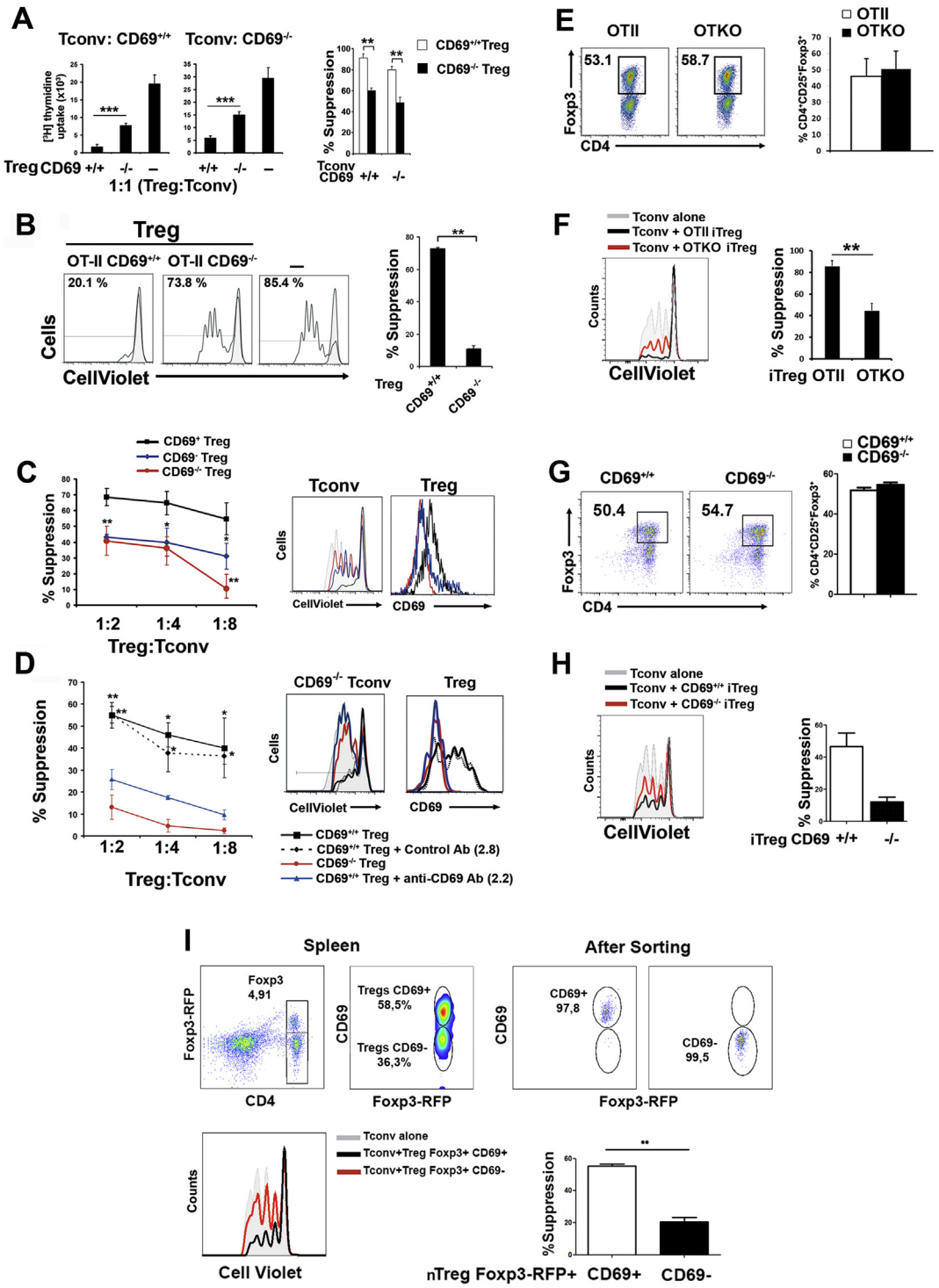

Fig. 2. Impaired suppressive function of CD69^{-} and *Cd69*$^{-/-}$ Tregs *in vitro*. (A) *In vitro* Treg polyclonal suppression assay of CD4^{+}FoxP3^{+} Treg cells from *Cd69*$^{+/+}$ and *Cd69*$^{-/-}$ mice and Tconv cells from *Cd69*$^{+/+}$ (left) and *Cd69*$^{-/-}$ (right) mice with coated anti-CD3 Ab in the presence of iAPCs; left panels show [^{3}H]thymidine uptake, and right panels show percentage of suppression relative to maximum Tconv proliferation in culture without Tregs. (B) FACS analysis of OT-II CD69$^{+/+}$ or OT-II CD69$^{-/-}$ Tregs suppression function under antigen-specific conditions (iAPCs and OVAp). CellViolet show proliferation of Tconvs and bar charts percentage of suppression. (C) Sorted CD69^{+} and CD69^{-} Tregs from *Cd69*$^{+/+}$ mice and *Cd69*$^{-/-}$ Tregs were tested in suppression assays with coated anti-CD3 and iAPCs. *Left*, Percentage suppression of Tconvs. *Center*, CellViolet shows Tconvs proliferation. *Right*, CD69 expression in Tregs co-cultures. (D) *In vitro* suppression function assay of CD69^{+} or CD69^{-} Tregs under polyclonal stimulus with or without anti-CD69 *2.2* or isotype control *2.8* mAbs. *Left*, percentage of suppression. *Center*, Tconv proliferation. *Right*, CD69 expression in gated Tregs. (E) FACS analysis of *in vitro* iTreg differentiation cultures of CD4^{+} naïve TCs from OT-II *Cd69*$^{+/+}$ or OT-II *Cd69*$^{-/-}$ mice. Bars show the percentage of CD4^{+}Foxp3^{+} iTregs obtained. (F) iTreg suppression assay of Tconvs cultured with OT-II *Cd69*$^{+/+}$ or OT-II *Cd69*$^{-/-}$ iTregs. (G) iTreg differentiation cultures with naive CD4^{+} T cells from B6 WT and CD69$^{-/-}$with normal TCR repertoire and cultured together with DCs, anti-CD3/CD28, TGF-β and IL-2 and (H) iTreg suppression assay of Tconvs cultured with iTregs WT and CD69$^{-/-}$ from B6 mice. (I) FACS analysis of splenic CD4^{+}Foxp3^{+} -CD69^{+} and -CD69^{-} natural Tregs from Foxp3-RFP reporter mice (*up left*). CD4^{+}Foxp3^{+} -CD69^{+} and -CD69^{-} nTregs were sorted (*up right*) and suppression assays of Tconvs were performed. CellViolet show proliferation of Tconvs and bar charts percentage of suppression (*lower panels*). Data are representative of three (A–C) or nine (D) independent experiments ($n = 3$). Errors bars represent mean ± SD. $^{*}P < 0.05$, $^{**}P < 0.01$, $^{***}P < 0.001$.

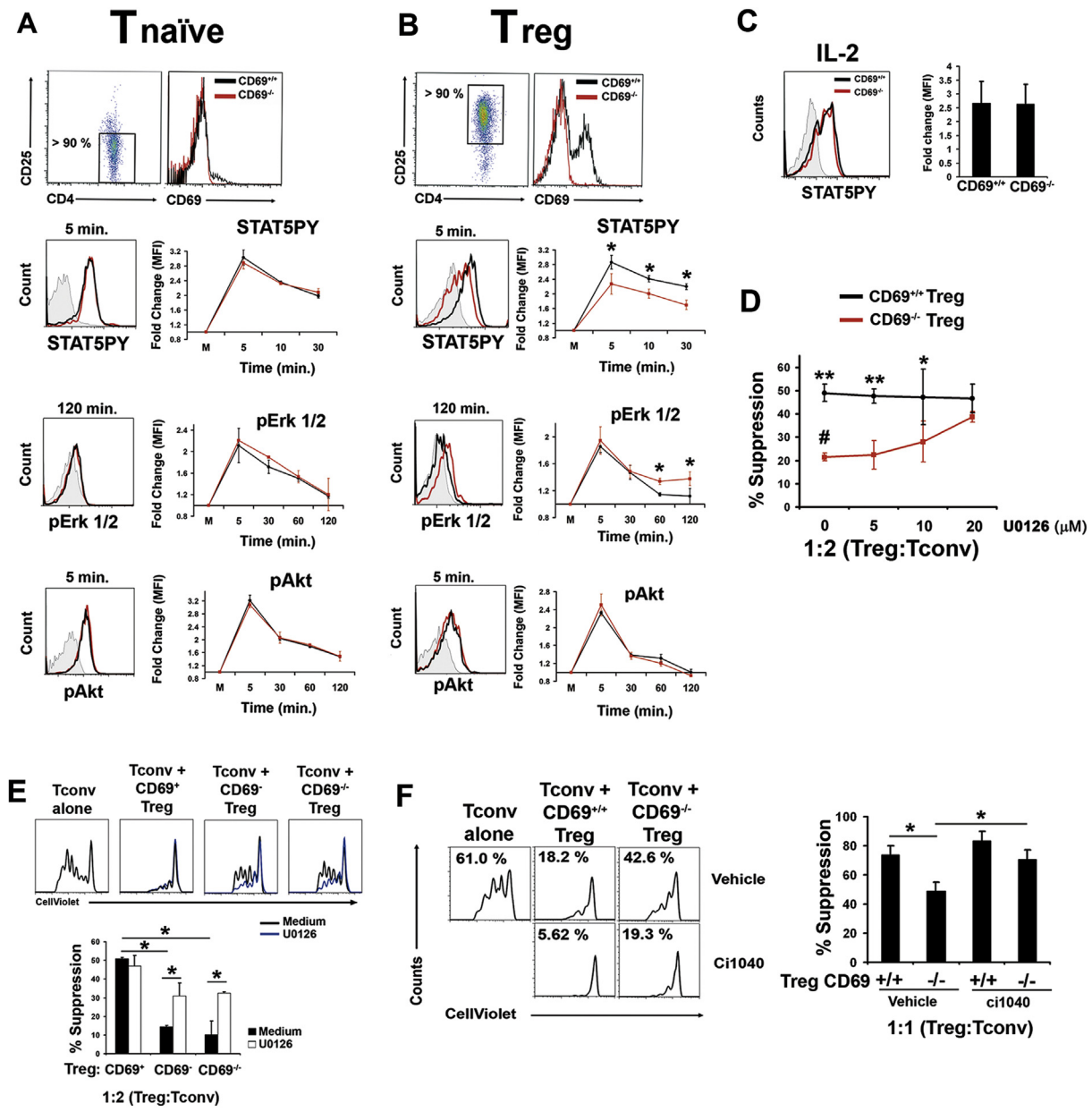

Fig. 3. STAT5 and Erk 1/2 activation controls the suppressor potential of Tregs. FACS analysis shows purity and CD69 expression of naïve T cells (A) and Tregs (B) from *Cd69*$^{+/+}$ or *Cd69*$^{-/-}$ mice. Kinetics of STAT5, Erk and Akt phosphorylation after TCR stimulation; gray histograms represent non-stimulated cells and phosphorylation was measured as MFI fold change. Data are representative of three independent experiments. (C) STAT5 phosphorylation in Tregs stimulated 30 min with IL-2. (D) *In vitro* suppression assays after pre-treatment of Tregs with the indicated concentrations of Erk inhibitor U0126 for 2 h. $^{*}P < 0.5$, $^{**}P < 0.01$ (comparison of *Cd69*$^{+/+}$ versus *Cd69*$^{-/-}$ Treg), $^{\#}P < 0.05$ (untreated CD69$^{-/-}$ Tregs versus 20 μM U0126 pre-treated CD69$^{-/-}$ Tregs). CellViolet indicate Tconv proliferation. (E) *In vitro* pre-treatment of Tregs with 20 μM U0126 partially restores suppressor ability of sorted CD69^{-} Tregs and *Cd69*$^{-/-}$ Tregs. *Upper histograms*, cell violet analysis of Tconv proliferation. *Lower,* percentage of suppression. (F) *In vivo* pre-treatment daily with 100 mg/kg of Erk inhibitor *ci1040* (100 mg/kg) or vehicle. Suppressor ability of derived Tregs was tested *in vitro*. *Left*, percentage of suppression. *Right*, Tconv proliferation in co-culture. Data are representative of at least 3 independent experiments. Errors bars represent mean ± SD. $^{*}P < 0.05$, $^{**}P < 0.01$.

chemokines analyzed (Fig. 4F). Analysis of surface receptor gene expression showed that CD69^{+} and CD69^{-} Tregs express similar levels of the membrane antigens analyzed (Supplementary Fig. S5A). CD69^{+} Tregs expressed high levels of *Tbx21* (*T-bet*), which together with *FoxP3* is important for the suppression of immune responses *in vivo* [20] (Supplementary Fig. S5B). Interestingly, expression of *Icos* and *FasL*, which are involved in immune-suppression pathways, was enhanced in CD69^{+} Tregs (Fig. 4G). These data indicate that CD69^{+} Tregs and CD69^{-} Tregs exist as two independent populations with different pattern of gene expression.

3.5. Tregs from *Cd69*$^{-/-}$ mice have reduced capacity to maintain immune tolerance and suppress inflammation in vivo

We next investigated the tolerogenic potential of *Cd69*$^{+/+}$ and *Cd69*$^{-/-}$ Tregs in a model of sensitization to inhaled harmless antigens. In this model, primary tolerogenic challenge by intratracheal (i.t.) injection of OVA did not lead to sensitization or lung inflammation upon repeated challenge with aerosolized OVA in *CD69*$^{+/+}$ mice. However, analysis of bronchoalveolar lavage (BAL) fluids as previously described [14] showed increased neutrophil and macrophage infiltration in *Cd69*$^{-/-}$ mice (Fig. 5A). Detection of

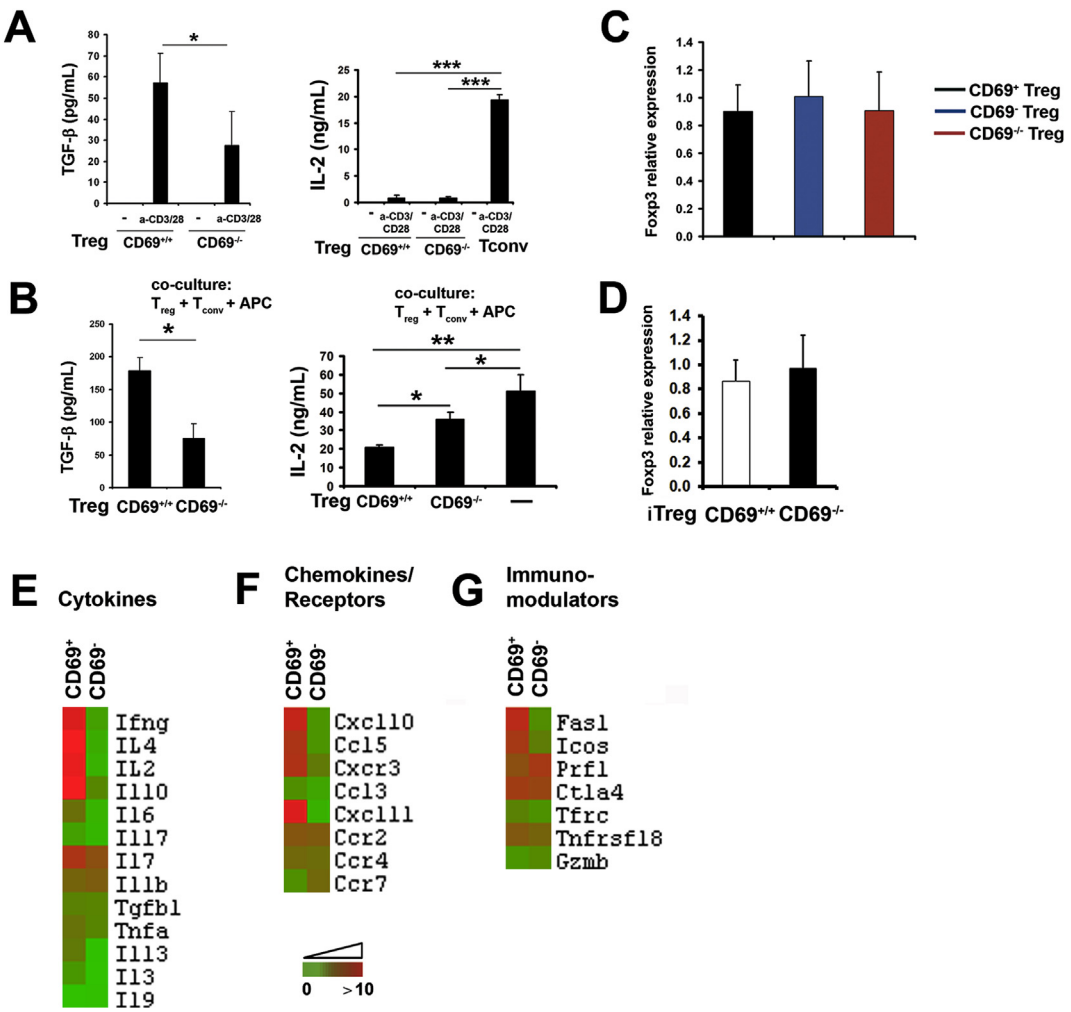

Fig. 4. CD69$^+$ Tregs secrete high amounts of TGF-β and express high levels of immune-suppression related genes. TGF-β and IL-2 secretion by Tregs after TCR stimulation with anti-CD3/CD28 for 48 h (A) or after co-culture with Tconvs and iAPCs (B) measured by ELISA. Results are representative of three independent experiments. (C–D) Relative *Foxp3* mRNA expression in *ex-vivo* sorted CD69$^+$ and CD69$^-$ Tregs from *Cd69*$^{+/+}$ mice, and *Cd69*$^-$ Tregs from *Cd69*$^{-/-}$ mice (C) or *in vitro* differentiated iTregs obtained from OT-II *Cd69*$^{+/+}$ or OT-II *Cd69*$^{-/-}$ mice (D). (E–G) qPCR analysis of immune-related genes in *ex-vivo* sorted CD69$^+$ and CD69$^-$ Tregs. Heat map represent fold increase to internal standards. Data are means from three biological samples. Errors bars represent mean ± SD. $^*P < 0.05$, $^{**}P < 0.01$, $^{***}P < 0.001$.

activated neutrophils by tomographic imaging after Neutrophil Elastase probe administration confirmed that only *Cd69*$^{-/-}$ mice developed inflammation under tolerogenic conditions, indicating that the absence of CD69 impairs the maintenance of tolerance in lungs (Fig. 5B). We found higher neutrophil infiltration in Me-LNs from OVA-sensitized *Cd69*$^{-/-}$ mice (Fig. 5C) and this was confirmed by tomographic imaging (Fig. 5D). Moreover, transgenic OTKO mice fail to establish lung tolerance, compared to OTII, after OVA exposure, similar to CD69$^{-/-}$ mice in BALB/c background (Fig. 5E). In a different experiment, after the i.t. tolerogenic challenge, mice were i.p. immunized with OVA, in order to study the induction of tolerance after immunization with the same antigen. After aerosol exposure to OVA mice developed airway inflammation, although the neutrophil infiltration was significantly higher in *Cd69*$^{-/-}$ mice than in *Cd69*$^{+/+}$ mice (Fig. 5F). Neutrophil infiltration in lungs and tracheas assessed by tomographic imaging was higher in OVA-treated *Cd69*$^{-/-}$ mice (Fig. 5G), indicating that CD69 expression is necessary for the maintenance of tolerance in a mouse model of airway inflammation.

The lack of CD69 expression on Tregs diminishes the potential to suppress inflammation in response to inhaled antigens (Fig. 5). To rule out an effect to differences in cell migration capacities of *Cd69*$^{+/+}$ and *Cd69*$^{-/-}$ Tregs after OVA challenge, we analyzed the content of CD4$^+$FoxP3$^+$ cells in BALS fluid (Fig. 6A) and Me-LNs (Fig. 6B) finding no significant differences in Tregs cell numbers between the two genotypes. Analysis of tracheas by whole mount staining confocal microscopy detected higher numbers of perivascular infiltrating neutrophils in *Cd69*$^{-/-}$ mice (Fig. 6C); however, we did not observe any differences in total numbers of FoxP3$^+$ cells migrating to this tissue, indicating that the migration of FoxP3$^+$ cells is not affected by CD69 expression (Fig. 6D). Moreover, we analyzed the expression levels of $S1P_1$ receptor, a molecule involved in T-cell migration regulated by CD69 expression on the membrane [4]. We did not find any differences in $S1P_1$ receptor expression levels between *Cd69*$^{-/-}$ and *Cd69*$^{-/-}$ Treg cell subsets (Supplementary Fig. S6).

3.6. *Cd69*$^{-/-}$ *Tregs show impaired function in cell therapy protocols*

To demonstrate that CD69 expression on Tregs is required to restore lung homeostasis and suppress inflammation in response to inhaled antigens, we immunized *Cd69*$^{+/+}$ or *Cd69*$^{-/-}$ mice with OVA. MS-LNs were collected and cells were *ex-vivo* expanded with TGF-β1 and IL-2 in the presence of iAPCs pre-incubated with OVAp.

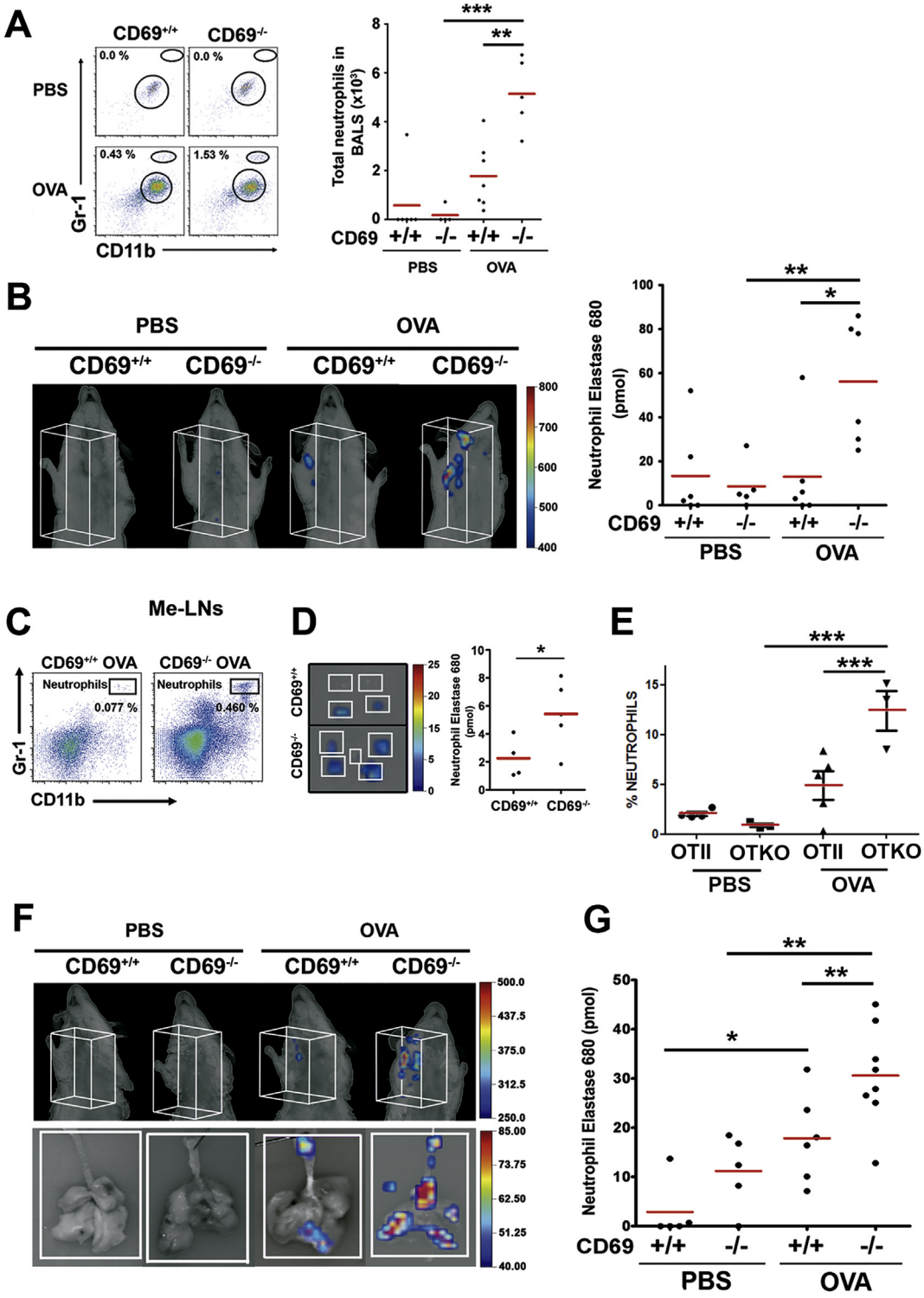

Fig. 5. *Cd69*$^{-/-}$ Tregs show impaired ability to suppress airway inflammation *in vivo* in a model of lung tolerance. (A) Mice were treated with OVA i.t. 20d before PBS or OVA-aerosolized challenge. *Left*, flow cytometry analysis of BALS cells stained with a-CD11b and a-Gr-1, showing the percentage of neutrophils. *Right*, absolute numbers of neutrophils recruited in BALS are shown (B) *In vivo* detection of activated neutrophils in airways by three-dimensional tomographic imaging in mice treated as in A (*left*). *Right*, quantification of Neutrophil Elastase 680 probe fluorescence activity. (C) FACS analysis of neutrophils in cell suspensions from Me-LNs. (D) *Left*, *ex vivo* tissue imaging of excised Me-LNs from OVA-challenged *Cd69*$^{+/+}$ and *Cd69*$^{-/-}$ mice. *Right*, quantification of Neutrophil Elastase 680 probe fluorescence activity in the individual lymph nodes excised from different mice (white boxes). Red bars represent means. (E) OTII and OTKO mice were injected i.t. with endotoxin free OVA previous nebulizations with PBS or OVA and percentage of neutrophils in BALS were analyzed 24 h after the last exposure to the antigen by FACS. (F–G) Mice were treated with OVA i.t. to induce tolerance and then with OVA i.p. before PBS or OVA-aerosolized challenge. Detection of neutrophils by tomographic imaging of airways *in vivo* or in resected lungs and tracheas (*lower panels*). (G) Neutrophil Elastase 680 probe fluorescence activity quantification. Data are representative of three (A–B) or two (E) independent experiments ($n = 5–7$). $^{*}P < 0.05$, $^{**}P < 0.01$, $^{***}P < 0.001$.

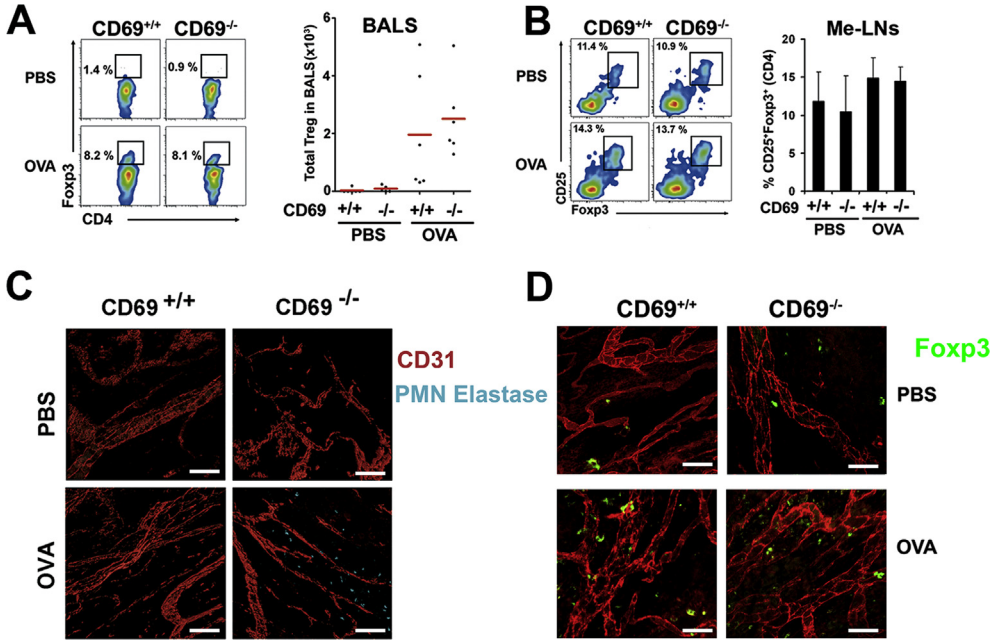

Fig. 6. Migratory behavior of FoxP3$^+$ cells to the airways and lymph nodes is not affected in *CD69*$^{-/-}$ mice. (A) FACS analysis of CD4$^+$FoxP3$^+$ Tregs in BALS from mice treated with OVA i.t. before PBS or OVA-aerosolized challenge. *Left*, numbers indicate the percentage of cells within squares in dot plots. *Right*, absolute cell numbers of Tregs; red bars indicate means. (B) Analysis of Tregs in Me-LNs from *Cd69*$^{+/+}$ and *Cd69*$^{-/-}$ mice treated as in (A). (C–D) Whole-mount staining with CD31 to visualize vasculature (red) from tracheas of mice treated as in A. (C) Neutrophil infiltration in the trachea analyzed by whole-mount staining as described under methods. Tissues were stained with a rabbit anti-mouse CD31 followed by a goat anti-rabbit Rhodamine Red-X to visualize vasculature (red). In parallel, Neutrophil elastase 680 fluorescent probe was detected with a 633 laser line (bright blue). Figure shows the three-dimensional isosurface rendering of confocal image stacks. Bars, 30 μm. (D) Whole-mount staining of Foxp3 (Tregs, green) and CD31 (vasculature, red) in tracheas from PBS or OVA-challenged *Cd69*$^{+/+}$ and *Cd69*$^{-/-}$ mice. Bars, 20 μm. Data are from three independent experiments ($n = 6$).

The derived *ex-vivo* iTreg-enriched cell suspensions (5×10^6) were adoptively transferred into recipient *Cd69*$^{+/+}$ or *Cd69*$^{-/-}$ mice on day 19 of i.t. injection with OVA (see scheme in Fig. 7A). After the treatment with iTregs, all groups of mice were aerosolized with OVA three consecutive days 30 min each and i.v. injected with the neutrophil elastase probe 12 h previous analysis. *In vivo* imaging analysis by quantitative tomography indicated that none of the recipient mice developed features of lung inflammation when challenged with PBS aerosol or transfer of Tregs derived from *Cd69*$^{+/+}$ donor mice. Interestingly, whereas an inflammatory response was detected in the lungs of *Cd69*$^{-/-}$ recipient mice treated with *Cd69*$^{-/-}$ donor Tregs, inflammation was completely abolished in *Cd69*$^{-/-}$ mice receiving immunotherapy with *Cd69*$^{+/+}$ Tregs (Fig. 7B and C). In parallel, a different group of mice was adoptively transferred with 2×10^5 freshly isolated CD25$^+$ natural Tregs cells from WT or CD69$^{-/-}$ mice, obtained from spleens by FACS sorting. Percentage of neutrophils in BALS was analyzed 24 h after the last exposure to PBS or OVA. Confirming the previous adoptive transfer experiment, the tolerance for OVA was restored in CD69$^{-/-}$ mice treated with CD69 expressing natural Tregs (Fig. 7D). To rule out a role in Treg migration, we analyzed CD4$^+$Foxp3$^+$ Treg cells in mediastinal lymph nodes and BALS after adoptive transfer experiment using nTregs. Although we find an increase in Treg numbers from BALS after OVA exposure, we do not detect any significant differences between WT and CD69$^{-/-}$ mice transferred with CD69$^+$ or CD69$^-$ nTreg cells (Supplementary Fig. S7), thus confirming our previous results pointing to a dysfunction in CD69$^{-/-}$ Tregs rather than a defect in their migration.

4. Discussion

Here we identify a unique CD69-constitutive expressing subset of Treg cells in homeostatic and inflammatory conditions with higher suppressor potential, than the classical FoxP3$^+$ Treg cell population as a whole. Consistent with previous evidence that a subset of thymocytes with high expression of CD69 is the precursor of human natural Tregs [21], the peripheral subset of CD69$^+$ Treg differs from CD69$^-$ Tregs in the basal expression levels of naturally occurring Treg markers, such as CD25, CTLA-4, ICOS, CD38 or GITR [22]. More importantly, FoxP3$^+$CD69$^+$-Tregs are the more effective subset suppressing Tconvs; and downregulation of the CD69 receptor after antibody treatment inhibited their suppressor potential, indicating that functional suppressor Tregs constitutively express CD69.

Our data support the notion that the CD69$^+$ Treg cell subset is the functional suppressive population within the classical CD4$^+$CD25$^+$FoxP3$^+$ Tregs. However, different subsets of inducible CD69$^+$ Tregs have also been reported in mice, CD4$^+$CD25$^-$FoxP3$^-$ Treg precursors, express CD69 on their membrane upon activation with oral OVA [23], 2,4,6-trinitro-1-chlorobenzene [24] or after migration within lymphoid organs [25] and tumor induction [26], and exert their function mainly through membrane-bound LAP/TGF-β1. Similarly, recent studies in humans have found the CD69$^+$CD4$^+$FoxP3$^-$LAP$^+$ Treg subset in peripheral blood [27], CD69$^+$CD71$^+$ Tregs after allospecific activation *in vitro* [28], and the diminished suppressive function of Tregs from systemic sclerosis patients, correlating with lower CD69 expression [29].

FoxP3 has been postulated as a master lineage specification factor for Tregs; however, the data are contradictory, with some groups postulating that FoxP3$^+$ T cells are a suppressive population [30] and others describing an incomplete suppressive function in this population [31–33]. Our data reveal that, within the FoxP3$^+$ cells, the CD69$^+$ subset is the most potent with suppressive capacity *in vitro* and *in vivo*. Recent data indicate that CD69 associates with the Jak3/STAT5 pathway, triggering STAT5 phosphorylation

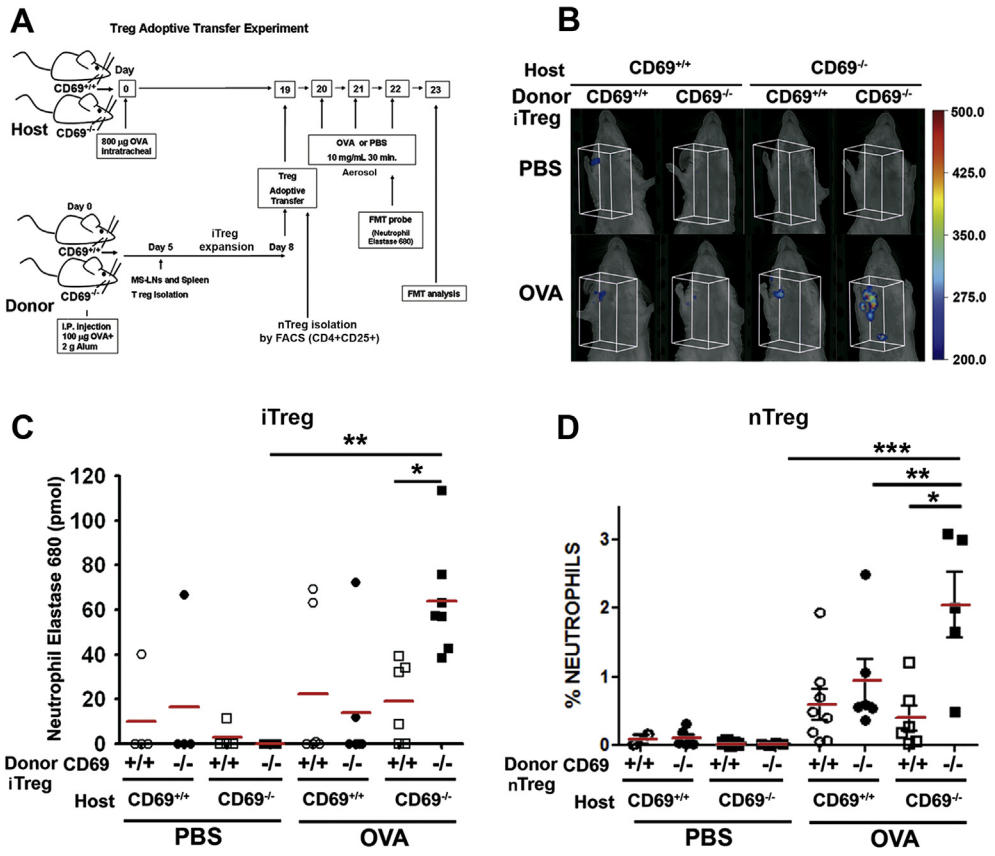

Fig. 7. Cell therapy with *Cd69*$^{+/+}$ Tregs restores lung tolerance in *Cd69*$^{-/-}$ mice. (A) Scheme depicting adoptive transfer with inducible iTregs or natural nTregs obtained from *Cd69*$^{+/+}$ and *Cd69*$^{-/-}$ mice before PBS or OVA-challenge. (B) Detection of activated neutrophils in airways by tomographic imaging. Three-dimensional regions represent neutrophil elastase activity in upper airways and lung (white boxes) of PBS or OVA-challenged *Cd69*$^{+/+}$ and *Cd69*$^{-/-}$ BALB/c mice treated with *ex vivo* expanded *Cd69*$^{+/+}$ or *Cd69*$^{-/-}$ iTregs. Quantification of Neutrophil Elastase 680 probe fluorescence activity after treatment with iTregs (C) or nTregs (D). Circles and squares indicate *Cd69*$^{+/+}$ and *Cd69*$^{-/-}$ host mice and white and black symbols indicate mice treated with exogenous *Cd69*$^{+/+}$ or *Cd69*$^{-/-}$ Tregs, respectively. Data are representative of two independent experiments ($n = 4$–7). $^{*}P < 0.05$, $^{**}P < 0.01$, $^{***}P < 0.001$.

[9,13], which can directly bind the Foxp3 promoter, thus playing a critical role in Treg development [16]. STAT5 phosphorylation, which is critical for Treg thymic differentiation, is diminished in *Cd69*$^{-/-}$ Tregs and lower strength of TCR or costimulatory signals is required to maintain FoxP3 expression on Tregs, through the inhibition of the AKT/mTOR pathway in a TGF-β independent manner [34,35]. Moreover, inhibition of the ERK MAPK pathway increases the frequency of FoxP3^{+} Tregs in a mechanism dependent on TGF-β signaling [36]. Here we show that, although the AKT pathway and FoxP3 expression at mRNA or protein levels are not altered in the absence of CD69 expression in Tregs, the ERK MAPK pathway remains phosphorylated only in CD69$^{-/-}$ Treg cells after long term TCR signaling. Since ERK is not active in CD69$^{+/+}$ Tregs, the pretreatment of Tregs during 2 h with ERK inhibitor may be effective only in CD69$^{-/-}$ Tregs with activated ERK, having no effect on CD69$^{+/+}$ Tregs with down-regulated ERK signaling. Therefore, inhibition of the ERK1/2 pathway in *Cd69*$^{-/-}$ Tregs restores their suppressive function *in vitro* and *in vivo* [37]. Interestingly, the secretion of TGF-β by CD69-deficient Tregs after TCR stimulation is significantly inhibited, indicating that CD69 exerts its immunoregulatory role through the control of the ERK MAPK pathway in a mechanism dependent on TGF-β.

The regulation of the immune response to aeroantigens is critical for maintaining immune tolerance in the lungs and preventing airway inflammatory disease [38]. In a previous work we demonstrated that CD69 expression in effector T cells negatively regulates Th2 and Th17 cell-driven inflammatory responses associated to allergic asthma and contact dermatitis [39]. However, the role of CD69 in the function of regulatory T cells and the maintenance of lung tolerance has not been before explored. Treg subset is central to the maintenance of mucosal tolerance, and defects in the development or function of these cells lead to exacerbated airway inflammation typical of allergies and asthma [14,40,41]. Our studies with a model of lung tolerance show that *Cd69*$^{-/-}$ Treg cells exhibited a diminished potential to suppress OVA-specific inflammatory responses, indicating that Treg function or migration to the lungs was impaired. Adoptive transfer experiments unequivocally demonstrate that only the FoxP3^{+}CD69^{+} Treg subset is able to maintain self tolerance in *Cd69*$^{-/-}$ mice. However, *in vivo* analysis of Treg migration to trachea, alveoli and mediastinal lymph nodes indicates an identical pattern of migration by CD69$^{+/+}$ and *Cd69*$^{-/-}$ Tregs. The rate of T cell migration to the inflamed tissue is also regulated by the S1P/S1P$_1$ pathway, and it has been demonstrated a role of CD69 in the negative regulation of S1P$_1$ expression levels in T cells [4,42] and Dendritic cells [43]. In contrast to our previous observations in *CD69*$^{-/-}$ Th17 cells [39], we have detected any significant difference in S1P$_1$ expression between *Cd69*$^{+/+}$ and *Cd69*$^{-/-}$ Tregs, suggesting that those are not altered by differential expression of S1P$_1$. Moreover, S1P$_1$ is an inhibitor of Treg cell function through AKT-mTOR pathway [44] and we have not found any differences in this signaling pathway by *Cd69*$^{+/+}$ and *Cd69*$^{-/-}$ Tregs, indicating that CD69 regulation of Tregs function or migration is independent on their expression of S1P$_1$.

5. Conclusions

Several mechanisms of suppression by Tregs have been proposed; however, Tregs need to express CD69 to sustain immune tolerance. Our results thus show that CD69 is a key molecular target for controlling Treg-suppressive function and development of inflammation. The identification of this new subset of CD69^{+} Tregs paves the way toward the development of new strategies of Treg cell isolation for therapeutic purposes towards chronic inflammatory and autoimmune diseases.

Author contributions

J.R.C. and R.S-D performed most experiments and analyzed the data; O.B. contributed confocal microscopy images, analyzed the data and reviewed the manuscript; E.R.B., S.L. and A.M-M. performed experiments; M.L.T. designed experiments and revised the manuscript; F.S-M. designed experiments and revised the manuscript; and P.M. conceived and coordinated the study, designed experiments, oversaw the data analysis and wrote the paper.

Conflict of interest

The authors declare that they have no conflict of interest.

Acknowledgments

The authors thank Dr. R.A. Flavell for kindly provided the Foxp3-RFP reporter mice, S. Bartlett for editorial assistance, R. Strippoli and M.A. del Pozo for kindly providing the Ci1040 ERK inhibitor and Mª Carmen Gómez de Frutos for technical help. This work was supported by funding from the Spanish Ministry of Economy and Competitiveness: SAF2011-27330 to P.M., SAF2010-15106 to M.L.T and SAF2011-25834 to F.S-M.; grant INDISNET (S2010/BMD-2332) from Comunidad de Madrid and RETICS *Enfermedades Cardiovasculares* (RD12/0042/0056) from Instituto de Salud Carlos III to P.M and F. S-M; and ERC-2011-AdG294340-GENTRIS to F.S-M. J.R.C. was supported by a CNIC post-doctoral fellowship, R. S-D is funded with a pre-doctoral fellowship from Comunidad de Madrid and E.R.B. and A.M-M. were supported by a FPI pre-doctoral fellowship from the Spanish Ministry of Economy and Competitiveness. The CNIC is supported by the Spanish Ministry of Economy and Competitiveness and the Pro CNIC Foundation.

Appendix A. Supplementary data

Supplementary data related to this article can be found online at http://dx.doi.org/10.1016/j.jaut.2014.05.007.

References

[1] Akdis CA, Akdis M. Mechanisms of allergen-specific immunotherapy. J Allergy Clin Immunol 2011;127:18–27. quiz 8–9.
[2] Sakaguchi S, Miyara M, Costantino CM, Hafler DA. FOXP3+ regulatory T cells in the human immune system. Nat Rev Immunol 2010;10:490–500.
[3] Barreiro O, Martin P, Gonzalez-Amaro R, Sanchez-Madrid F. Molecular cues guiding inflammatory responses. Cardiovasc Res 2010;86:174–82.
[4] Shiow LR, Rosen DB, Brdickova N, Xu Y, An J, Lanier LL, et al. CD69 acts downstream of interferon-alpha/beta to inhibit S1P1 and lymphocyte egress from lymphoid organs. Nature 2006;440:540–4.
[5] Lopez-Cabrera M, Santis AG, Fernandez-Ruiz E, Blacher R, Esch F, Sanchez-Mateos P, et al. Molecular cloning, expression, and chromosomal localization of the human earliest lymphocyte activation antigen AIM/CD69, a new member of the C-type animal lectin superfamily of signal-transmitting receptors. J Exp Med 1993;178:537–47.
[6] Testi R, D'Ambrosio D, De Maria R, Santoni A. The CD69 receptor: a multipurpose cell-surface trigger for hematopoietic cells. Immunol Today 1994;15:479–83.
[7] Zingoni A, Palmieri G, Morrone S, Carretero M, Lopez-Botel M, Piccoli M, et al. CD69-triggered ERK activation and functions are negatively regulated by CD94/NKG2-A inhibitory receptor. Eur J Immunol 2000;30:644–51.
[8] Cebrian M, Yague E, Rincon M, Lopez-Botet M, de Landazuri MO, Sanchez-Madrid F. Triggering of T cell proliferation through AIM, an activation inducer molecule expressed on activated human lymphocytes. J Exp Med 1988;168:1621–37.
[9] Martin P, Sanchez-Madrid F. CD69: an unexpected regulator of TH17 cell-driven inflammatory responses. Sci Signal 2011;4:pe14.
[10] Sancho D, Gomez M, Viedma F, Esplugues E, Gordon-Alonso M, Garcia-Lopez MA, et al. CD69 downregulates autoimmune reactivity through active transforming growth factor-beta production in collagen-induced arthritis. J Clin Invest 2003;112:872–82.
[11] Bettelli E, Carrier Y, Gao W, Korn T, Strom TB, Oukka M, et al. Reciprocal developmental pathways for the generation of pathogenic effector TH17 and regulatory T cells. Nature 2006;441:235–8.
[12] Veldhoen M, Hocking RJ, Atkins CJ, Locksley RM, Stockinger B. TGFbeta in the context of an inflammatory cytokine milieu supports de novo differentiation of IL-17-producing T cells. Immunity 2006;24:179–89.
[13] Martin P, Gomez M, Lamana A, Cruz-Adalia A, Ramirez-Huesca M, Ursa MA, et al. CD69 association with Jak3/Stat5 proteins regulates Th17 cell differentiation. Mol Cell Biol 2010;30:4877–89.
[14] de Heer HJ, Hammad H, Soullie T, Hijdra D, Vos N, Willart MA, et al. Essential role of lung plasmacytoid dendritic cells in preventing asthmatic reactions to harmless inhaled antigen. J Exp Med 2004;200:89–98.
[15] Sancho D, Gomez M, Martinez Del Hoyo G, Lamana A, Esplugues E, Lauzurica P, et al. CD69 targeting differentially affects the course of collagen-induced arthritis. J Leukoc Biol 2006;80:1233–41.
[16] Burchill MA, Yang J, Vogtenhuber C, Blazar BR, Farrar MA. IL-2 receptor beta-dependent STAT5 activation is required for the development of Foxp3+ regulatory T cells. J Immunol 2007;178:280–90.
[17] Sebolt-Leopold JS, Dudley DT, Herrera R, Van Becelaere K, Wiland A, Gowan RC, et al. Blockade of the MAP kinase pathway suppresses growth of colon tumors in vivo. Nat Med 1999;5:810–6.
[18] Campbell DJ, Koch MA. Phenotypical and functional specialization of FOXP3+ regulatory T cells. Nat Rev Immunol 2011;11:119–30.
[19] Lee JH, Kang SG, Kim CH. FoxP3+ T cells undergo conventional first switch to lymphoid tissue homing receptors in thymus but accelerated second switch to nonlymphoid tissue homing receptors in secondary lymphoid tissues. J Immunol 2007;178:301–11.
[20] Koch MA, Tucker-Heard G, Perdue NR, Killebrew JR, Urdahl KB, Campbell DJ. The transcription factor T-bet controls regulatory T cell homeostasis and function during type 1 inflammation. Nat Immunol 2009;10:595–602.
[21] Martin-Gayo E, Sierra-Filardi E, Corbi AL, Toribio ML. Plasmacytoid dendritic cells resident in human thymus drive natural Treg cell development. Blood 2010;115:5366–75.
[22] Josefowicz SZ, Lu LF, Rudensky AY. Regulatory t cells: mechanisms of differentiation and function. Annu Rev Immunol 2012;30:531–64.
[23] Radulovic K, Manta C, Rossini V, Holzmann K, Kestler HA, Wegenka UM, et al. CD69 regulates type I IFN-induced tolerogenic signals to mucosal CD4 T cells that attenuate their colitogenic potential. J Immunol 2012;188:2001–13.
[24] Ring S, Enk AH, Mahnke K. ATP activates regulatory T Cells in vivo during contact hypersensitivity reactions. J Immunol 2010;184:3408–16.
[25] Lieberman SM, Kim JS, Corbo-Rodgers E, Kambayashi T, Maltzman JS, Behrens EM, et al. Site-specific accumulation of recently activated CD4+ Foxp3+ regulatory T cells following adoptive transfer. Eur J Immunol 2012;42:1429–35.
[26] Han Y, Guo Q, Zhang M, Chen Z, Cao X. CD69+ CD4+ CD25- T cells, a new subset of regulatory T cells, suppress T cell proliferation through membrane-bound TGF-beta 1. J Immunol 2009;182:111–20.
[27] Gandhi R, Farez MF, Wang Y, Kozoriz D, Quintana FJ, Weiner HL. Cutting edge: human latency-associated peptide+ T cells: a novel regulatory T cell subset. J Immunol 2010;184:4620–4.
[28] Sagoo P, Ali N, Garg G, Nestle FO, Lechler RI, Lombardi G. Human regulatory T cells with alloantigen specificity are more potent inhibitors of alloimmune skin graft damage than polyclonal regulatory T cells. Sci Transl Med 2011;3:83ra42.
[29] Radstake TR, van Bon L, Broen J, Wenink M, Santegoets K, Deng Y, et al. Increased frequency and compromised function of T regulatory cells in systemic sclerosis (SSc) is related to a diminished CD69 and TGFbeta expression. PLoS One 2009;4:e5981.
[30] Kretschmer K, Apostolou I, Hawiger D, Khazaie K, Nussenzweig MC, von Boehmer H. Inducing and expanding regulatory T cell populations by foreign antigen. Nat Immunol 2005;6:1219–27.
[31] Hill JA, Feuerer M, Tash K, Haxhinasto S, Perez J, Melamed R, et al. Foxp3 transcription-factor-dependent and -independent regulation of the regulatory T cell transcriptional signature. Immunity 2007;27:786–800.
[32] Mucida D, Park Y, Kim G, Turovskaya O, Scott I, Kronenberg M, et al. Reciprocal TH17 and regulatory T cell differentiation mediated by retinoic acid. Science 2007;317:256–60.
[33] Allan SE, Crome SQ, Crellin NK, Passerini L, Steiner TS, Bacchetta R, et al. Activation-induced FOXP3 in human T effector cells does not suppress proliferation or cytokine production. Int Immunol 2007;19:345–54.
[34] Haxhinasto S, Mathis D, Benoist C. The AKT-mTOR axis regulates de novo differentiation of CD4+Foxp3+ cells. J Exp Med 2008;205:565–74.

[35] Sauer S, Bruno L, Hertweck A, Finlay D, Leleu M, Spivakov M, et al. T cell receptor signaling controls Foxp3 expression via PI3K, Akt, and mTOR. Proc Natl Acad Sci U S A 2008;105:7797–802.
[36] Gabrysova L, Christensen JR, Wu X, Kissenpfennig A, Malissen B, O'Garra A. Integrated T-cell receptor and costimulatory signals determine TGF-beta-dependent differentiation and maintenance of Foxp3+ regulatory T cells. Eur J Immunol 2011;41:1242–8.
[37] Zanin-Zhorov A, Cahalon L, Tal G, Margalit R, Lider O, Cohen IR. Heat shock protein 60 enhances CD4+ CD25+ regulatory T cell function via innate TLR2 signaling. J Clin Invest 2006;116:2022–32.
[38] Bilate AM, Lafaille JJ. Induced CD4(+)Foxp3(+) regulatory t cells in immune tolerance. Annu Rev Immunol 2012;30:733–58.
[39] Martin P, Gomez M, Lamana A, Marin AM, Cortes JR, Ramirez-Huesca M, et al. The leukocyte activation antigen CD69 limits allergic asthma and skin contact hypersensitivity. J Allergy Clin Immunol 2010;126:355–65. 65 e1–3.
[40] Mucida D, Kutchukhidze N, Erazo A, Russo M, Lafaille JJ, Curotto de Lafaille MA. Oral tolerance in the absence of naturally occurring Tregs. J Clin Invest 2005;115:1923–33.
[41] Curotto de Lafaille MA, Kutchukhidze N, Shen S, Ding Y, Yee H, Lafaille JJ. Adaptive Foxp3+ regulatory T cell-dependent and -independent control of allergic inflammation. Immunity 2008;29:114–26.
[42] Bankovich AJ, Shiow LR, Cyster JG. CD69 suppresses sphingosine 1-phosophate receptor-1 (S1P1) function through interaction with membrane helix 4. J Biol Chem 2010;285:22328–37.
[43] Lamana A, Martin P, de la Fuente H, Martinez-Munoz L, Cruz-Adalia A, Ramirez-Huesca M, et al. CD69 modulates sphingosine-1-phosphate-induced migration of skin dendritic cells. J Invest Dermatol 2011. http://dx.doi.org/10.1038/jid.2011.54.
[44] Liu G, Burns S, Huang G, Boyd K, Proia RL, Flavell RA, et al. The receptor S1P1 overrides regulatory T cell-mediated immune suppression through Akt-mTOR. Nat Immunol 2009;10:769–77.

Nanomedicine & Nanotechnology

Lopez-Heras et al., J Nanomed Nanotechnol 2014, 5:5
http://dx.doi.org/10.4172/2157-7439.1000226

Research Article Open Access

Effect of Chitosan-Stabilized Selenium Nanoparticles on Cell Cycle Arrest and Invasiveness in Hepatocarcinoma Cells Revealed by Quantitative Proteomics

Isabel Lopez-Heras[1], Raquel Sanchez-Diaz[1], Daniela S Anunciação[2], Yolanda Madrid[1], Jose L Luque-Garcia[1]*, Carmen Camara[1]

[1]*Department of Analytical Chemistry, Faculty of Chemistry, University Complutense of Madrid, Madrid, Spain*
[2]*Institute of Chemistry and Biotechnology, University Federal of Alagoas, Maceió, Brazil*

Abstract

Selenium nanoparticles have been recently proposed as a potential chemotherapeutic agent due to its low toxicity and its ability to arrest the cell cycle of cancer cells. However, the biochemical mechanisms associated to this effect have not yet been uncovered. We evaluate here the potential of chitosan-stabilized selenium nanoparticles to induce cell cycle arrest and to inhibit in-vitro invasiveness in HepG2 cells. In addition, we use a quantitative proteomic approach to identify potential protein targets involved in the mechanisms associated to selenium nanoparticles exposure. Our data suggest that the induction of the cell cycle arrest at the S phase is mediated by de-regulation of the eIF3 protein complex. We found additional de-regulated proteins upon selenium nanoparticles exposure that could also be involved in the overall inhibition of cell proliferation. These findings not only support the potential of chitosan-stabilized selenium nanoparticles as anti-cancer therapy but also provide a deeper insight into the mechanisms associated to their chemotherapeutic effects.

Keywords: Selenium nanoparticles; Cell cycle arrest; SILAC; eIF3 protein complex; Inhibition of invasiveness

Introduction

Selenium is one of the essential trace elements and has great importance in nutrition and medicine due to its antioxidant properties. The relationship between selenium intake/status and several health outcomes such as cancer, cardiovascular disease, diabetes and male fertility have been recently reviewed [1]. It is known that the dose and the chemical form of selenium have a significant influence on these beneficial effects [2].

Selenium nanoparticles (SeNPs), which are considered a novel Se compound, are attracting increasing attention of the scientific community due to their excellent antioxidants properties and low toxicity in comparison with other Se-species such as selenomethionine (SeMet) [3], selenium methyl selenocysteine (SeMeSeCys) [4] and selenite (Se IV) [5]. It has also been reported that SeNPs exhibit a great selectivity between cancer and normal cells showing a broad spectrum of growth inhibition for A375, CNE2, MCF-7 and HepG2 cancer cells This effect was more pronounced than when using Se IV at a similar concentration [6]. Recently, it has also been shown the anti-proliferative effect of SeNPs on HeLa, MDA-MB-231 and HepG2 cells in a dose-dependent manner by induction of cell cycle arrest [7,8]. However, the biomolecular mechanisms involved in this inhibitory effect have not yet been fully understood.

Proteomics is a powerful tool for describing complete proteomes at the organelle, cell, organ or tissue levels. Among all the proteomic approaches available, quantitative strategies are particularly attractive, since they allow for identification of differentially expressed proteins by comparing proteomes as affected by different conditions [9]. In this way, the identification of changes in individual proteins or group of proteins associated with SeNPs exposure could help to gain insight into the mechanisms of action of these NPs. Between the different alternatives for relative protein quantitation, stable isotopic labeling by amino acids in cell culture (SILAC) is one of the most reliable alternatives [10].

In this work, we investigated the potential cytotoxic effects of chitosan-stabilized selenium nanoparticles (Ch-SeNPs) and the biological mechanisms involved in the interaction of Ch-SeNPs with a human hepatocarcinoma (HepG2) cell line. We evaluated key parameters such as cellular viability, cellular uptake and localization, apoptosis and cell cycle pattern. In addition, we used SILAC for the identification of specific protein targets affected upon Ch-SeNPs exposure. Our data allowed us to dissect the mechanism by which Ch-SeNPs induce cell cycle arrest at the S phase. We conclude that Ch-SeNPs induced de-regulation of the eIF3 protein complex that affect the protein synthesis machinery inhibiting cell cycle progression. Finally, we demonstrated that exposure to Ch-SeNPs inhibit *in-vitro* invasiveness of HepG2 cells, thus supporting the idea of Ch-SeNPs as a potential chemotherapeutic agent [11].

Methods

Synthesis of Ch-SeNPs

Preparation of Ch-SeNPs was performed according to a previously described procedure [12] using chitosan polysaccharide as stabilizer and ascorbic acid as reducer. Synthesized Ch-SeNPs were stored at 4°C up to two months. Ch-SeNPs were characterized by TEM (see below).

Cell culture and treatment

Human hepatocarcinoma (HepG2) cells were maintained in Dulbecco´s Modified Eagle´s Medium (DMEM) supplemented with fetal bovine serum (10% v/v) and antibiotics in 5% CO_2 at 37°C. Ch-

***Corresponding author:** Jose L Luque-Garcia, Department of Analytical Chemistry, Faculty of Chemistry, University Complutense of Madrid, 28040, Madrid, Spain, Tel. 34913944212; E-mail: jlluque@quim.ucm.es

Received July 16, 2014; **Accepted** September 06, 2014; **Published** September 16, 2014

Citation: Lopez-Heras I, Sanchez-Diaz R, Anunciação DS, Madrid Y, Luque-Garcia JL, et al. (2014) Effect of Chitosan-Stabilized Selenium Nanoparticles on Cell Cycle Arrest and Invasiveness in Hepatocarcinoma Cells Revealed by Quantitative Proteomics. J Nanomed Nanotechnol 5: 226. doi: 10.4172/2157-7439.1000226

SeNPs of 50-60 nm diameter were added at different concentrations ranging from 0.1 to 20 μg ml^{-1} and incubated for 48 h. Cells were then washed twice in phosphate-buffered saline (PBS) and harvested using 0.25% trypsin/0.1% EDTA.

Transmission electron microscopy analysis

For characterization of the synthesized Ch-SeNPs, droplets of the dispersion were placed onto a holey carbon film on copper grids. Micrographs were obtained using the JEOL 1010 JEM transmission electron microscope (JEOL) operating at 100 kV. Internalization of the NPs in HepG2 cells was observed after treatment with 1 μg ml^{-1} Ch-SeNPs for 48 h. Following exposure, attached cells were washed with PBS and fixed *in situ* with glutaraldehyde (2.5% v/v) and *p*-formaldehyde (4% v/v) in PBS at 4°C for 4 h. Cells were then washed and stored in PBS at 4°C overnight. After post-fixation with osmium tetroxide (1% v/v) for 1 h at room temperature and in the dark, the cells were dehydrated in graded ethanol series (from 30% to 100% ethanol) and harvested with propylene oxide. Cell suspensions were centrifuged at 1500 rpm for 30 seconds and the propylene oxide was removed. The pellets were treated with a mixture of resin:acetone and finally, treated with 100% resin. The resulting blocks were incubated at 65°C for 48 h until complete embedding. Ultrathin sections were cut, transferred onto copper grids and examined by TEM.

Cell viability assay

Cell viability was measured by the MTT assay. Briefly, cells were seeded in a 96-well plate at a concentration of $5x10^4$ cells per well and exposed to Ch-SeNPs, Se IV or Ch-SeNPs synthesis media during 48 hours. 20 μl of 5 mg ml^{-1} MTT solution were added to the cells and incubated for 4 h at 37°C. Then, the media was removed and 100 μl of dimethyl sulfoxide was added. Absorbance was measured at 595 nm in a microplate reader.

Determination of internalized Ch-SeNPs by ICP-MS

Internalization of Ch-SeNPs was quantified in HepG2 cells exposed to 1 μg ml^{-1} Ch-SeNPs for 48 hours. After treatment, the exposure media, the PBS used for washing the cells and the cell pellet were digested in a microwave oven with a mixture of HNO_3 (65%) and H_2O_2 (35%) (2:1). Digested samples were appropriately diluted with distilled water and then Se was determined using an Agilent HP 7700x inductively coupled plasma-mass spectrometer (ICP-MS) (Agilent).

Flow cytometry analysis

Measurement of apoptosis in Ch-SeNPs and Se IV exposed cells was performed using an Annexin V-FITC kit (Sigma) following the manufacturer's instructions. Around $1x10^6$ cells were treated with 1 μg ml^{-1} Ch-SeNPs for 48 hours. Then, cells were washed with PBS and re-suspended in 1 ml binding buffer solution at pH 7.5 containing HEPES/NaOH (100 mM), NaCl (1.4 M) and $CaCl_2$ (25 mM). Annexin V-FITC conjugate (5 μl) and propidium iodide (10 μl) were added to 500 μl of the cell suspension in order to label the apoptotic and necrotic cells, respectively. Cells were incubated in the dark at room temperature, and immediately examined using a FACScan flow cytometer (Becton-Dickinson). For evaluating the cell cycle arrest after exposure to Ch-SeNPs or Se IV, $1x10^6$ HepG2 cells were re-suspended in 250 μl of PBS and mixed with an equal volume of a solution containing 60% ethanol (v/v) and 20 μg ml^{-1} of Hoechst 33258 reagent. Cells were incubated for at least 45 min at room temperature and the DNA content analyzed by flow cytometry.

Immunofluorescence assay

Cells were seeded onto cover slips and incubated with 1 μg ml^{-1} Ch-SeNPs for 48 h. Cells were washed with PBS, fixed with paraformaldehyde (4% v/v) in PBS for 10 min and permeabilized with Triton-X100 (0.1% v/v) in PBS for 15 min. Cells were blocked with bovine serum albumin (BSA, 2% w/v) for 1 h, followed by incubation with the primary antibody anti-eIF3a (1:100) (Bethyl) or anti-eIf3b (1:100) (BioLegends) for 40 min at room temperature on humid chamber. After three washings with PBS, cells were incubated with Alexa Fluor 586-labeled anti-rabbit lgG (1:1000) (Invitrogen) for 30 minutes at room temperature, followed by incubation with Alexa Fluor 488-labeled phalloidine (1:60) (Invitrogen) for 20 min at room temperature. Finally, VectaShield (Atom) was used for staining the nuclei with 4´,6-diamino-2-phenylindole (DAPI) and as a mounting media. Fluorescence microscopy was performed in a Motic AE31 epifluorescence microscope.

eIF3 gene knockdown

Human epithelial cervix carcinoma HeLa cells were seeded at $5x10^4$ cells/well in 24-well plates and transfected with either eIF3 (30 pmol) or scrambled control siRNA (30 pmol) (Santa Cruz) using lipofectamine (Sigma) (1 μl) as transfection reagent and reduced serum media (opti-MEM) as transfection media. Cells were incubated in the transfection media for 5 h. The transfection was stopped by adding complete DMEM 10% FBS. After incubation for 24 h at 37°C 5% CO_2, the cells were harvested for further analyses.

Western blotting

Whole total lysates were separated by SDS-PAGE and transferred to nitrocellulose membranes. Membranes were blocked in PBS-tween buffer (PBST, 0.05% v/v) containing 3% skim milk and incubated overnight at 4°C with the corresponding primary antibodies to the following: eukaryotic initiation factor 3 subunit b (eIF3/p116), 1:1000 (Biolegend), methyl tetrahydrofolate reductase 1 (MTHF1), 1:1000 (Santa Cruz). After washing with PBST, membranes were incubated with HRP-conjugated secondary antibodies (Santa Cruz) for 1 h at room temperature, and specific proteins were visualized by enhanced chemiluminescence detection.

Matrigel invasion assay

Invasion assay was performed using Matrigel in 24-well plates, as per manufacturer´s instructions. Briefly, Matrigel was mixed with culture media (1:1) and 200 μl of the mixture was placed in each well and polymerized for 30 min at 37°C. A suspension of $5x10^4$ cells previously exposed to Ch-SeNPs (0.5 and 1 μg/ml for 48h) was added to the bottom of the well. Invasion of HepG2 cells was observed after incubation at 37°C for 5 h by phase-contrast microscopy.

Protein identification and quantitation

HepG2 cells were grown in either 'light' ($^{12}C_6$-Lys and $^{12}C_6$-Arg) or 'heavy' ($^{13}C_6$-Lys and $^{13}C_6$-Arg) DMEM medium containing 10% dialyzed FBS and 100 units/ml of penicillin/streptomycin. Cells were grown for at least six doublings to allow full incorporation of labeled amino acids. Two large-scale SILAC replicates (10^7 cells per condition) were performed. Complete incorporation of $^{13}C_6$-Lys and $^{13}C_6$-Arg after six cell divisions in isotopically heavy medium was verified by MS of a protein digest. Cells labeled with "heavy" (direct SILAC) or "light" (reversed SILAC) amino acids were exposed to 1 μg ml^{-1} Ch-SeNPs for 48 hours. Cells grown with "heavy" and "light" medium were mixed in a 1:1 ratio before subsequent processing. Cells were lysed in a buffer containing 1% Triton X-100, 150 mM NaCl, 20 mM Tris, pH

8, 0.2 mM ethylene diamine tetraacetic acid (EDTA), 2 mM Na_3VO_4, 2 mM NaF, and protease inhibitors (Complete tablet; Roche). Proteins were then separated by SDS-PAGE on 10% SDS-polyacrylamide gels. After electrophoresis, the proteins were visualized by Coomassie blue staining and in-gel digested as previously described [13].

The peptide mixtures from the different in-gel tryptic digestion fractions were loaded onto a trap column (Reprosil C18, 3 µm particle size, 0.3 x 10 mm, 120 Å pore size, SGE) and then eluted to the analytical column (Acclaim PepMap 100, C18, 3 µm particle size, 75 µm x 150 mm, 100 Å pore size, Dionex, LC Packings) with a linear gradient of 5-95% ACN in 0.1% formic acid. The samples were delivered over 120 min by a nano-LC ultra 1D plus system (Eksigent) at a flow-rate of 200 nl/min, through the analytical column to a stainless steel nano-bore emitter (O.D. 150 um, I.D. 30 um Proxeon, Odense, Denmark). The peptides were scanned and fragmented with an LTQ XL linear ion trap mass spectrometer (Thermo Scientific, San Jose, CA) operated in data-dependent ZoomScan and MS/MS switching mode using the three most intense precursors detected in a survey scan from 400 to 1600 u (three µscans). ZoomScan mass window was set to 12 Da enabling monitoring of the entire $^{12}C/^{13}C$ isotopic envelope of most doubly and triply charged peptides. Singly charged ions were excluded for MS/MS analysis. Normalized collision energy was set to 35% and dynamic exclusion was applied during 3 min periods to avoid repetitive fragmentation of ions.

Generated raw files were converted to mgf files (Bioworks 3.3.1) for submission to the MASCOT database. A database containing the NCBInr *Homo Sapiens* sequences (as of November 2012, 35586 sequences) was searched using the MASCOT protein identification software (v2.3 Matrix Science). Search criteria included trypsin specificity with one missed cleavage allowed, and with methionine oxidation, $^{13}C_6$-Arg and $^{13}C_6$ –Lys as variable modifications. Minimum precursor and fragment-ion mass accuracies of 1.2 and 0.3 Da were used. To consider a protein as an accurate identification, at least one unique peptide (bold-red peptides meaning highest scoring peptide matching to protein with highest total score) with a Mascot score higher than 39 ($p<0.05$) and a minimum total protein score of 46 ($p<0.01$) were required. The false positive rate was calculated by searching the same spectra against the NCBInr *Homo sapiens* decoy database. Relative quantification ratios of identified proteins based on peak area were calculated using Quixot v.1.3.26 open-source software (http://150.244.205.155/mediawiki/index.php/QuiXot). Protein ratios obtained by Quixot were verified manually for all peptides. Functional processes and subcellular localization of the proteins identified by SILAC were assigned based on the biological knowledge available in Gene Ontology (GO) annotations.

Results

Synthesis, characterization and cytotoxicity of Ch-SeNPs

We used transmission electron microscopy (TEM) to characterize the synthesized Ch-SeNPs under different concentrations of chitosan in terms of particle size, morphology and aggregation. In all cases, Ch-SeNPs presented a spherical structure with particle size between 10 nm to 60 nm. However, the size distribution was significantly affected by the concentration of chitosan. 0.1% chitosan provided a homogeneous dispersion in which around 80-90% of the Ch-SeNPs had a size in the range 40-60 nm (Figure 1A) and thus, we selected this concentration for further experiments.

Figure 1B shows the viability of HepG2 cells exposed to different concentrations of Ch-SeNPs, Se IV and the synthesis media during 48 h. Cell viability decreased with increasing NPs concentration and exposure times. While the higher concentrations of Ch-SeNPs and Se IV concentrations caused an almost 100% decrease on cell viability, the lowest concentration did not significantly affect cell. In order to evaluate the effect of Ch-SeNPs but without drastically compromising the cell viability, we selected 1 µg ml^{-1} Ch-SeNPs for further experiments. Our data also pointed out that there were only a slight decreased in the viability of cells exposed to Se IV as compared to Ch-SeNPs and that the synthesis media (containing chitosan and ascorbic acid) did not significantly affect the viability of the cells.

Flow cytometry assays

Figure 2A shows the data obtained from flow cytometry analyses regarding the degree of apoptosis and necrosis in cells exposed to Ch-SeNPs and Se IV. We did not observe significant differences in the number of apoptotic or necrotic cell populations between control and cells exposed to Ch-SeNPs. However, cells exposed to Se IV showed a significant increase in apoptotic cells. We also used flow cytometry to further investigate the influence of Ch-SeNPs and Se IV exposure on the cell cycle patterns of HepG2 cells by measuring the content of DNA (Figures 2B and 2C). After exposure to Ch-SeNPs, the number of cells in G0/G1 decreased to the same point that the populations in S-G2/M increased. The number of cells in sub-G0 (apoptotic cells) significantly increased in cells exposed to Se IV, thus confirming the apoptosis assay.

Cellular uptake and localization of Ch-SeNPs

We determined the total Se content in the cell culture media, in the PBS washing solution and in the pellet of cells exposed to 1 µg ml^{-1} Ch-SeNPs for 48 h by ICP-MS. The data obtained showed that the majority of Se was found in the culture media and that only 1% of the total Se added was internalized by the cells after 48 h. Then we used TEM for investigating the cellular localization of Ch-SeNPs. As shown in Figure 3, Ch-SeNPs were uptaken by HepG2 cells, localized in vacuoles (Figure 3A), also distributed throughout the cytoplasm (Figure 3B) and in subcellular organelles such as mitochondria and the endoplasmic reticulum (ER) (Figures 3C and 3D). In addition, about 90% of cells exposed to Ch-SeNPs exhibit more than 2-fold increase in the number of vacuoles as compared to control cells (Figures 3E and 3F).

Quantitative proteomics

To identify the proteins altered after Ch-SeNPs exposure, we performed two large-scale SILAC experiments (Figure 4A). Mass spectrometry analysis identified a total of 1170 proteins with at least one unique peptide in the two SILAC experiments and a false discovery rate of 0.4% estimated from the number of hits against the reverse sequence/total hits ratio, $p>0.01$. However, only 650 proteins passed the criteria established for protein quantitation, which include identification of at least two unique peptides with a MASCOT score >39 for the peptides and >46 for the full protein. Out of these proteins, 481 were found in both replicates (Supplementary Information, Table S1). The global overlap between the two SILAC experiments was 69%. We then focused on proteins with at least 1.3-fold difference between control and exposed cells and with 20% as the maximum relative standard deviation between peptides within each protein. Most of the identified proteins had a SILAC ratio close to 1. Judge by this criteria, 41 proteins were considered significantly altered in Ch-SeNPs exposed HepG2 cells compared with control cells. Of these, 21 were up-regulated and 20 down-regulated (Table 1).

For an unbiased search of pathways involved in Ch-SeNPs exposure, we submitted the 41 altered proteins to knowledge-based

Accession number (gi)	Protein name	Common name	Mascot score	SILAC ratio	RSD[a]
94721250	VAMP (vesicle-associated membrane protein)-associated protein A, 33kDa	VAPA	275	2.75	5.02
167466173	heat shock 70kDa protein 1A	HSPA1A/HSPA1B	558	1.84	8.41
24307969	cytoplasmic FMR1 interacting protein 1	CYFIP1	171	1.65	16.83
4504041	guanine nucleotide binding protein (G protein), alpha inhibiting activity polypeptide 2	GNAI2	128	1.65	8.10
4757756	annexin A2	ANXA2	144	1.55	4.24
4826898	profilin 1	PFN1	46	1.51	16.24
28557709	phosphoribosyl pyrophosphate synthetase 1-like 1	PRPS1L1	74	1.50	1.86
9910382	translocase of outer mitochondrial membrane 22 homolog	TOMM22	119	1.47	1.44
4557797	non-metastatic cells 1, protein (NM23A) expressed in	NME1	189	1.42	12.59
14141152	heterogeneous nuclear ribonucleoprotein M	HNRNPM	548	1.36	2.28
5901922	cell division cycle 37 homolog	CDC37	151	1.34	11.49
38570062	golgi to ER traffic protein 4 homolog	GET4	52	1.35	0.77
22749415	STT3, subunit of the oligosaccharyltransferase complex, homolog A	STT3A	90	1.35	18.66
4504279	H3 histone, family 3B (H3.3B)	H3F3A/ H3F3B	83	1.34	0.29
42558250	cell cycle associated protein 1	CAPRIN1	98	1.33	3.43
4501857	acyl-CoA dehydrogenase, long chain	ACADL	89	1.33	0.06
20149560	syntaxin 4	STX4	35	1.32	1.03
33519426	thioredoxin reductase 1	TXNRD1	208	1.31	5.53
4503519	eukaryotic translation initiation factor 3, subunit F	EIF3F	314	1.30	8.40
8923390	coiled-coil-helix-coiled-coil-helix domain containing 3	CHCHD3	52	1.30	11.51
4503729	FK506 binding protein 4, 59kDa	FKBP4	195	1.30	15.51
4759302	VAMP (vesicle-associated membrane protein)-associated protein B and C	VAPB	189	-1.32	8.29
23397429	eukaryotic translation initiation factor 3, subunit M	EIF3M	264	-1.32	11.31
4503523	eukaryotic translation initiation factor 3, subunit D	EIF3D	154	-1.32	17.54
71773329	annexin A6	ANXA6	296	-1.33	15.72
18379349	vesicle amine transport protein 1 homolog	VAT1	416	-1.35	12.77
4501867	aconitase 2, mitocondrial	ACO2	124	-1.37	18.76
148491070	CTP synthase	CTPS	171	-1.37	14.43
223468663	aldo-keto reductase family 1, member B10 (aldose reductase)	AKR1B10	97	-1.41	10.77
13491174	MARCKS-like 1	MARCKSL1	122	-1.43	17.02
148727247	ubiquitin specific peptidase 5 (isopeptidase T)	USP5	96	-1.43	12.95
4757732	apoptosis-inducing factor, mitochondrion-associated, 1	AIFM1	131	-1.45	4.65
112363070	HSPA (heat shock 70kDa) binding protein, cytoplasmic cochaperone 1	HSPBP1	61	-1.47	19.94
91807122	annexin A8-like 2	ANXA8L2	497	-1.52	16.28
24308514	glutathione S-transferase alpha 5	GSTA5	57	-1.52	10.70
109134349	coatomer protein complex, subunit gamma 2	COPG2	132	-1.52	5.84
4506619	ribosomal protein L24	RPL24	71	-1.54	8.89
4503243	cytochrome P450, family 51, subfamily A, polypeptide 1	CYP51A1	355	-1.54	7.32
100913206	DEAH (Asp-Glu-Ala-His) box polypeptide 9	DHX9	179	-1.54	17.86
62241042	glutamyl-prolyl-tRNA synthetase	EPRS	95	-1.61	17.68
5453990	proteasome (prosome, macropain) activator subunit 1 (PA28 alpha)	PSME1	435	-2.27	11.86

[a]Relative standard deviation

Table 1: Differentially expressed proteins in HepG2 Cells after exposure with 1 μg ml^{-1} of Ch-SeNPs.

Ingenuity pathway analysis (IPA). This allowed us to identify enriched canonical pathways involved in cell growth, cell proliferation, protein synthesis, DNA replication, nucleic acid metabolism, post-translational modification and cellular death. We also classified the differentially expressed proteins to their molecular and cellular functions using the gene ontology (GO) database. We found altered proteins involved in cell cycle regulation, cellular compromise, cellular growth and proliferation, amino acid metabolism and cell morphology (Figure 4B).

Fluorescence microscopy inspection of eIF3a and eIF3b levels

Figure 5 shows the fluorescence microscopy images of HepG2 cells (control and exposed to 1.0 μg ml^{-1} Ch-SeNPs) prior an immunofluorescence assay to evaluate the level of expression of eIF3a and eIF3b subunits. The expression of both subunits appeared significantly inhibited after exposure to Ch-SeNPs for 48 h. These results are in agreement with the proteomic data obtained and suggest that exposure to Ch-SeNPs inhibit the levels of expression of the eIF3 complex.

eIF3 silencing

To support the idea that the mechanism by which Ch-SeNPs induce cell cycle arrest at the S phase is by inhibiting the expression of most subunits of the eIF3 complex, thus affecting the protein synthesis machinery, we investigated whether siRNA-mediated gene knockdown of the eIF3b subunit induces cell cycle arrest in a similar manner to Ch-SeNPs exposure in HeLa cells. After validating the suitability of the transfection (Figure 6A) by Western Blot, we analyzed the cell cycle pattern of transfected cells and cells exposed to Ch-SeNPs by flow cytometry (Figure 6B). Silencing of the eiF3b expression partially increased the cell population in S-G2/M phase while decreased the

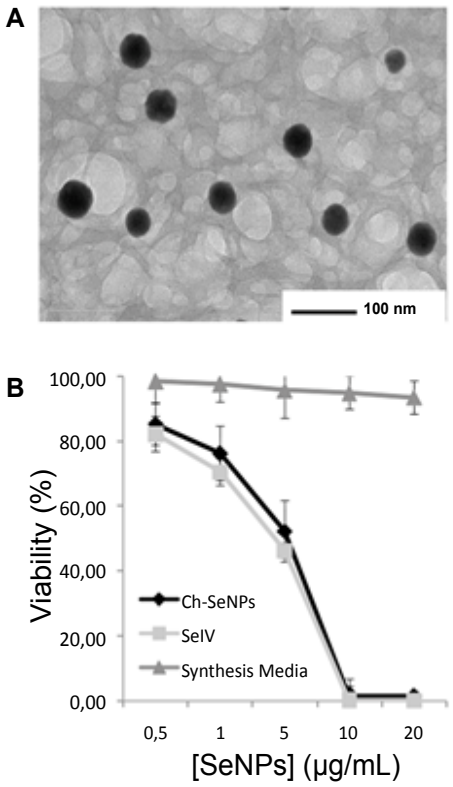

Figure 1: The use of 0.1% chitosan as stabilizer provided a homogeneous SeNPs suspension with around 80-90% of NPs in the range 40-60 nm. Cell viability of HepG2 cells exposed to Ch-SeNPs and Se IV decreased in a dose-dependent manner.
(A) Transmission electron microscopy of Ch-SeNPs synthesized in the presence of 0.1% chitosan.
(B) Cell viability of HepG2 cells exposed to different concentrations of Ch-SeNPs, Se IV and the synthesis media. The MTT assay showed that high concentrations (10-20 µg ml^{-1} of Ch-SeNPs and Se IV) caused an almost 100% decrease in the cell viability. Exposure conditions of 1 µg ml^{-1} of Ch-SeNPs induced a 30% decrease in cell viability and were selected for further experiments.

population in the G0/G1 phase. The differences observed as compared to control cells, were similar to those obtained after Ch-SeNPs exposure.

Matrigel assay

Figure 6C, shows the invasive behavior of HepG2 cells over matrigel cell culture. We observed that control cells migrated over the surface of matrigel forming large cellular branches, whereas cells exposed to 0.5 µg ml^{-1} Ch-SeNPs formed a less branched culture. The invasive behavior decreased with increasing concentrations of Ch-SeNPs and in fact, the morphology of cells exposed to 1.0 µg ml^{-1} Ch-SeNPs was very different from control cells, appearing round and individuals with no ramifications.

Discussion

In a previous report, Bai et al. demonstrated the capability of monosaccharides (glucose), oligosaccharides (sucrose) and polysaccharides (chitosan) to modify the size, morphology and stability of SeNPs in liquid dispersions. We used chitosan since previous studies have shown how encapsulation of Se IV into chitosan significantly improved the antioxidant properties and promoted a high retention of selenium in cells [12]. We observed that the size distribution of NPs was significantly affected by the concentration of polysaccharide used in synthesis reaction. 0.1% chitosan was the best concentration in terms of nanoparticles diameter and size distribution (Figure 1A). We did not observed significant differences in the TEM images as for changes in particle size and aggregation for Ch-SeNPs stored at 4°C for up to 2 months. Moreover, no flocculation was visually detected. We also examined the potential oxidation of Ch-SeNPs to Se IV weekly by centrifugation of the Ch-SeNPs suspension using 10 KDa cut-off filter. The total Se present in the liquid fraction was quantified by ICP-MS. We only found a low percentage of ionic Se (< 0.1%), thus showing the good stability of the synthesized Ch-SeNPs.

Ch-SeNPs induce cell cycle arrest

The viability of cells exposed to either Ch-SeNPs or Se IV decreased in a similar concentration-dependent manner (Figure 1B). However, we visually observed that while cells exposed to Ch-SeNPs seemed to have stopped dividing, cultures exposed to Se IV presented a significant number of dead floating cells. In order to confirm these differential effects, we carried out flow cytometry to evaluate both, apoptosis and cell cycle pattern. It is important to mention that the synthesis media composed by chitosan, ascorbic and acetic acid did not significantly influence the viability of HepG2 cells, which confirm that the effect observed in cells exposed to Ch-SeNPs was due to Ch-SeNPs themselves

Flow cytometry confirmed that the percentage of apoptotic or necrotic cell populations in cells exposed to Ch-SeNPs was not significantly different from control cells (Figure 2A), which correlates well with the absence of chromosome condensation and nuclear fragmentation, typical features for apoptotic cells, in our TEM images (Figure 3). However, cells exposed to Se IV presented a significant percentage of apoptotic cells, thus showing the higher toxicity exerted by Se IV as compared to Ch-SeNPs at this concentration.

We also investigated the influence of these NPs on the cell cycle patterns of HepG2 cells. The decrease of cell population in G0/G1 phase along with the increase in S-G2/M suggest that Ch-SeNPs induce cell cycle arrest at the S phase (Figures 2B and 2C), which is in agreement with a previous study carried out on HeLa and MDA-MB-231 cells [7]. In addition, a significant cell population of cells exposed to Se IV was found in the sub-G0 phase (Figure 2B), which is consistent with the apoptosis assay.

The data derived from the flow cytometry analyses supported the different effect induced by Ch-SeNPs in arresting the cell cycle of HepG2 cells as compared to the effect of Se IV, which, in contrast, induced apoptosis at the same tested concentration.

Internalization of Ch-SeNPs

When performing an *in vitro* study, the degree of cellular internalization is a potentially relevant factor for understanding the biological mechanisms affected by Ch-SeNPs exposure. Many authors have reported a close correlation between intracellular uptake and cytotoxic effects [14]. Our ICP-MS analysis showed that only 1% of Se was internalized after 48 h. These results showed how even small amounts of Ch-SeNPs could greatly alter cell functioning. We then used TEM for cellular localization of the internalized Ch-SeNPs with two purposes: (i) to discard the possibility of potential oxidation of Ch-SeNPs in contact with the cells or the culture media; and (ii) to confirm whether or not the Ch-SeNPs were really inside the cells or just attached to the cell membranes. Our TEM images showed Ch-SeNPs localized in vacuoles (Figure 3A), distributed throughout the cytoplasm (Figure 3B) and in subcellular organelles such as mitochondria and the

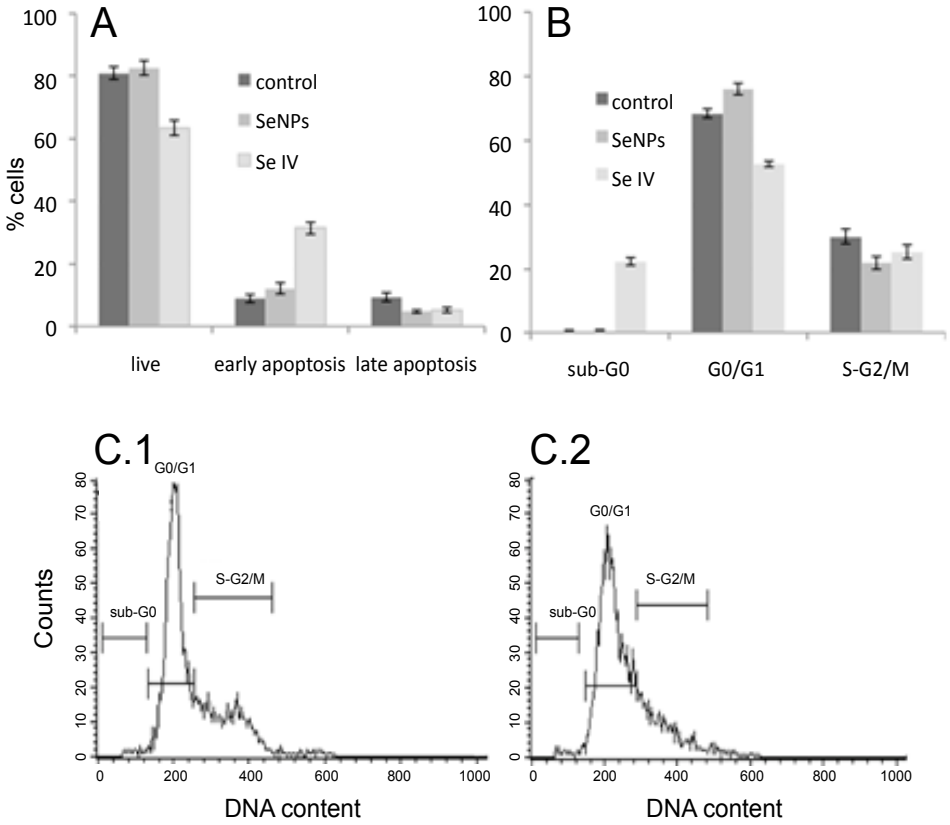

Figure 2: Ch-SeNPs exposure of HepG2 cells did not induce apoptosis but a cell cycle arrest at the S phase.
(A) Annexin-V-based flow cytometry analysis did not reveal a significant increase in apoptosis after Ch-SeNPs exposure. Se IV, in contrast, induce a significant increase of apoptotic cells.
(B) Measurement of the DNA content by flow cytometry of Ch-SeNPs-exposed cells showed that the number of cells in G0/G1 decrease to the same point that the populations in S-G2/M increase (C1) as compared to control cells (C2).

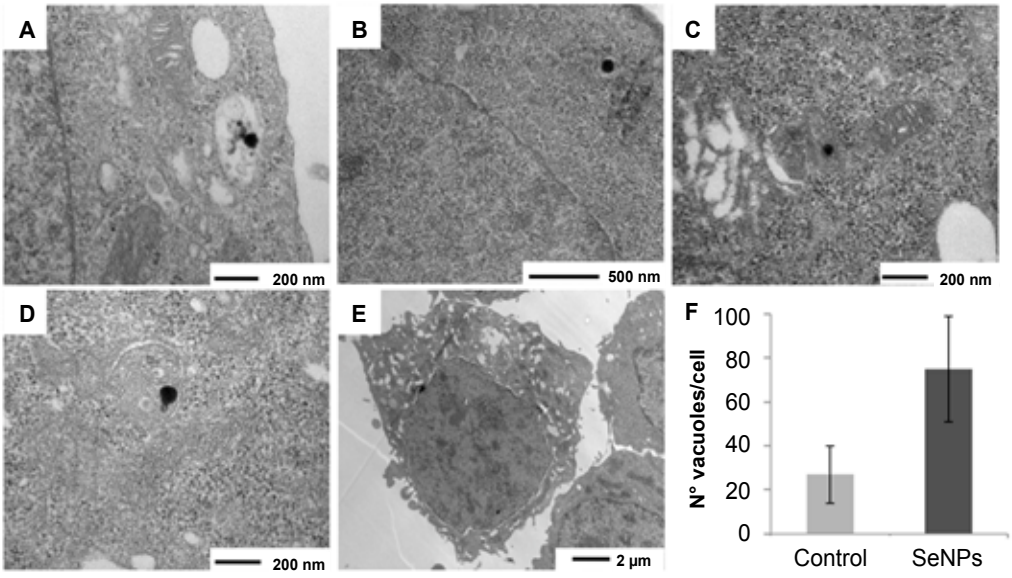

Figure 3: Transmission electron microscopy showed that Ch-SeNPs uptaked by HepG2 cells are localized in (A) vacuoles, (B) throughout the cytoplasm and in subcellular organelles such as (C) mitochondria and (D) the endoplasmic reticulum. As expected, Ch-SeNPs were not localized in the nuclei due to their particle size. (E, F) About 90% of cells exposed to Ch-SeNPs exhibit more than 2-fold increased in the number of vacuoles as compared to control cells.

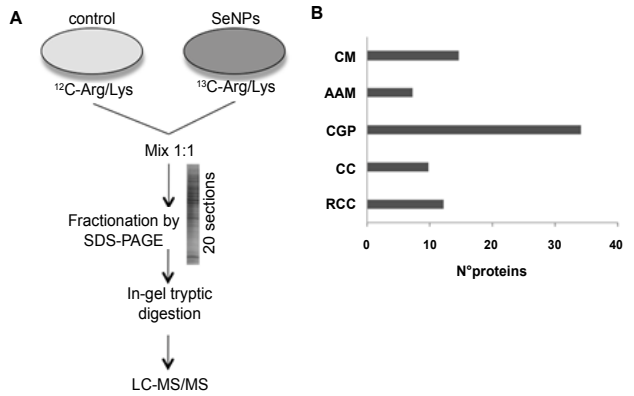

Figure 4: (A) A quantitative proteomic approach based on stable isotopic labeling by amino acids in cell culture (SILAC) identified a set of de-regulated proteins upon Ch-SeNPs exposure. (B) Altered proteins were involved in cell cycle regulation (RCC), cellular compromise (CC), cellular growth and proliferation (CGP), amino acid metabolism (AAM) and cell morphology (CM). Among these found de-regulated proteins, several subunits of the eIF3 protein complex, involved in the protein synthesis machinery, appeared down-regulated after Ch-SeNPs exposure.

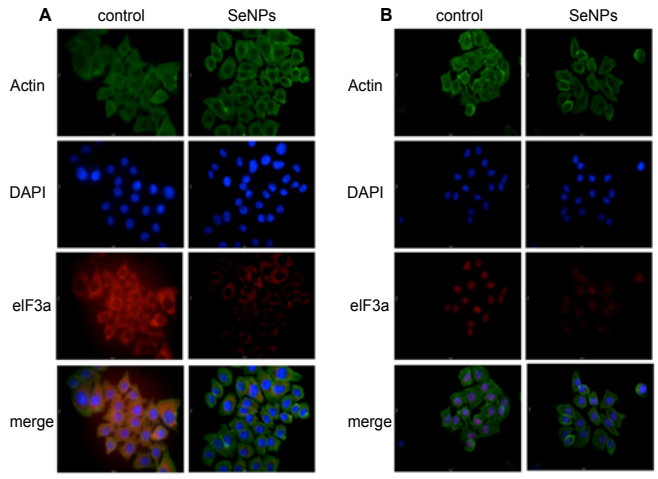

Figure 5: The expression of the eIF3 complex is altered after exposure of HepG2 cells to 1.0 μg ml^{-1} of Ch-SeNPs for 48 h. Control and HepG2 cells exposed to Ch-SeNPs were immunostained for actin filaments (green) with phalloidin, for nuclei (blue) with DAPI and for (a) eIF3a and (b) eIF3b (red). Note that both, eIF3a and eIF3b subunits staining intensities decrease significantly in cells exposed to Ch-SeNPs.

endoplasmic reticulum (ER) (Figures 3C and 3D). These two organelles play an important role in different processes including cellular energy supplying, differentiation and apoptosis [15]. As expected, Ch-SeNPs were not localized in the nuclei due to their particle size, thus reducing the possibility of DNA damage. In addition, a massive vacuolization was visualized in 90% of cells treated with Ch-SeNPs (Figures 3E and 3F). These results agree well with a previous study where formation of membrane fusion vesicles during active endocytosis was induced in breast adenocarcinoma cells exposed to SeNPs [16].

Ch-SeNPs exposure affects the expression of the eIF3 protein complex

After assessing the ability of Ch-SeNPs to induce cell cycle arrest, we used a quantitative proteomic approach for identifying differentially expressed proteins in control vs. Ch-SeNPs-exposed cells in order to gain a deeper insight into the biomolecular mechanisms involved. Our SILAC experiment reported the alteration of proteins involved in cell growth, cell development and protein synthesis by Ch-SeNPs exposure, which may be closely related with the cell cycle inhibitory effect observed in exposed HepG2 cells (Figure 4B). Protein synthesis is closely integrated with other metabolic pathways, influencing transcription, protein turnover and early development. Among the de-regulated proteins found in our SILAC experiments, we identified down-regulated two eukaryotic translation initiation factor 3 (eIF3) subunits (eIF3m and EiF3d). The eIF3 complex, formed by thirteen protein subunits, is considered the largest of the initiation factors, since the regulation of the protein synthesis and protein degradation machinery is coordinated through some eIF3 subunits [17]. eIF3 has two main roles in protein synthesis: first, eIF3 binds to the 40S ribosome and facilitates loading of the Met-tRNA/eIF2·GTP ternary complex to form the 43S pre-initiation complex; and secondly, eIF3 apparently assists eIF4 in recruiting mRNAs to the 43S complex [18].

The subunit eIF3m is associated to different mRNAs encoding proteins involved in nucleic acid metabolism, transporter proteins and proteins of unknown function [19]. It has been observed that the eIF3m subunit is highly expressed in many human cancer cell lines and its overexpression can be related to tumor progression. In addition, down-regulation of eIF3m reduces the proliferation of carcinogenic cells. Goh et al. silenced the expression of the eIF3m subunit by specific siRNA and confirmed the influence of eIF3m on cell proliferation, cell cycle progression and cell death in human colon cancer cell line HCT-116 by decreasing the CDC25A activity, which is required for progression from G1 to the S phase of the cell cycle [20]. Based on the evidences reported in previous studies, and the down-regulation of the eIF3m and eIF3d subunits observed in our SILAC approach after Ch-SeNPs exposure, we hypothesized that the inhibition of the expression of the eIF3 complex could be directly related with the inhibitory effect of Ch-SeNPs on the proliferation of HepG2 cells.

Another subunit, eIF3a, involved in cell proliferation and tissue development has also been found highly overexpressed in several human and murine cancer tissues [21,22]. In fact, many studies have reported the role of eIF3a as an early differentiation marker in human mammary carcinoma cells, although the role of this subunit in oncogenesis is still unclear. The eIF3b subunit is considered to be the major scaffolding subunit [23] and has an important role in human glioblastoma development [24]. In addition, it has been suggested that the protein synthesis machinery can be significantly inhibited in human colorectal cancer cells by decreasing the expression of the eIF3b subunit [25]. Since we did not identify either the eIF3a or the eIF3b subunit in our SILAC approach, we performed an immunofluorescence assay to evaluate the level of expression of these subunits after exposure to Ch-SeNPs (Figure 5). The expression of both subunits appeared significantly inhibited after exposure of HepG2 cells to Ch-SeNPs. These findings support the proteomic data obtained and suggest that exposure to Ch-SeNPs inhibit the levels of expression of the eIF3 complex, which is closely related to the inhibition of cell proliferation.

Unlike the other subunits, we found eIF3f overexpressed in our SILAC approach. Although this result may sound contradictory with our previous conclusions, interestingly, eIF3f is involved in the development and apoptosis of tumor cells by interaction with CDK11 [26]. In fact, it has been demonstrated that eIF3f appeared down-regulated in most human tumors and its ectopic expression inhibited translation and cellular protein synthesis in pancreatic cancer cells,

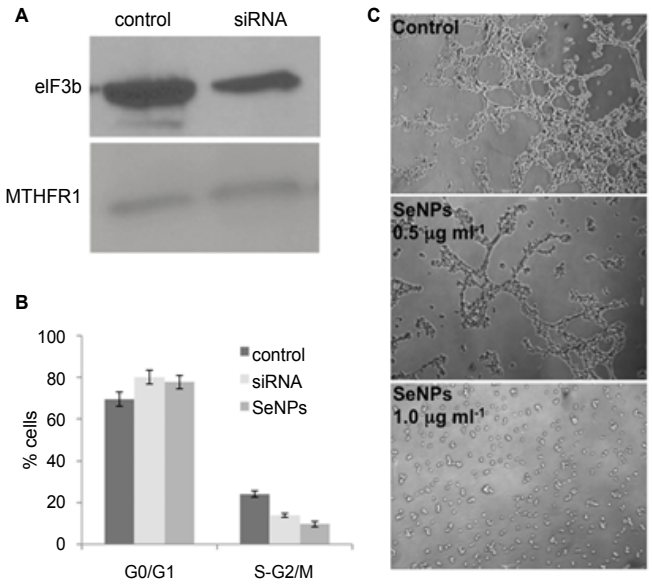

Figure 6: (A) siRNA knockdown of the eIF3b subunit induces cell cycle arrest in a similar manner to Ch-SeNPs in HeLa cells. The suitability of the transfection was validated by Western Blot using the methyl-tetrahydrofolate reductase (MTHFR1) as loading control since it showed a SILAC ratio closed to 1. (B) Silencing of the eiF3b expression partially increased the cell population in G2/M phase while decreased the population in the G0/G1 phase. The results obtained after knocking down eIF3b were similar to those obtained after Ch-SeNPs exposure. (C) The invasive behavior of HepG2 cells in a matrigel decrease in the presence of Ch-SeNPs. Cells exposed to 0.5 µg ml^{-1} Ch-SeNPs formed a less branched culture as compared to control cells. The morphology of cells exposed to 1.0 µg ml^{-1} Ch-SeNPs was very different from control cells, appearing round and individuals with no ramifications.

inducing them to enter apoptosis [27]. The fact that we found eIF3f up-regulated while other eIF3 subunits were down-regulated strongly support the idea that Ch-SeNPs induce cell cycle arrest at the S phase mediated by de-regulation of most subunits of the eIF3 complex, thus affecting the protein synthesis machinery. This hypothesis was investigated by silencing eIF3b subunit through a transfection assay. The similar cell cycle pattern among transfected cells and cells exposed to Ch-SeNPs (showing a slight increased of cell population in S-G2/M phase and a decreased of cells in G0/G1 phase) together with the different level of expression found for eIF3 subunits after Ch-SeNPs exposure that we showed previously, support the hypothesis that Ch-SeNPs induce eIF3-mediated cell cycle arrest (Figures 6A and 6B).

Differentially expressed proteins upon Ch-SeNPs exposure

In addition to some of the subunits of the eIF3 protein complex, we found other proteins altered in our SILAC approach that could also help to better understand the mechanisms involved in the cell interaction with Ch-SeNPs. One of the proteins that showed a higher up-regulation after Ch-SeNPs exposure was the VAPA (VAMP (vesicle-associated membrane protein)-associated protein A) protein. VAPs proteins are endoplasmic reticulum (ER)-resident membrane proteins that are broadly expressed in eukaryotic cells and are involved in stress signaling, membrane trafficking and ER homeostasis [28]. VAPA is related to the lateral diffusion inhibition of membrane proteins, and also is associated with intracellular vesicles so that the massive vacuolization found in cells exposed to Ch-SeNPs (Figure 3F) could be induced by VAPA up-regulation [29]. It has been reported that over expression of the VAPA isoform but not the B isoform (VAPB) inhibited ER-to-Golgi transport of membrane proteins. Interestingly, we found VAPB slightly down-regulated suggesting that this protein may also be involved in the pathway through which Ch-SeNPs inhibited protein synthesis.

Heat shock proteins (HSPs) constitute a group of chaperone proteins that play a pivotal role in the maintenance of protein homeostasis. In our SILAC approach, the expression of heat shock 70 kDa protein 1A (HSPA1A/HSPA1B) was highly up-regulated. This result is in agreement with previous studies in which HSP70 was dramatically up-regulated under environmental stress [30].

Cell division cycle 37 homolog (CDC37), a positive regulator of stability and/or activity of some protein kinases, appeared up-regulated in our experiment. This protein is involved in SAPK regulation, a stress-activated protein kinase dedicated to transmit environmental stress stimuli, which has a crucial role in cellular survival under stress conditions and inflammatory responses [31]. It is also worth mentioning that mammalian SAPK is related with the response of cancer cells to cytotoxic treatments [32].

Cytoplasmic FMR1 interacting protein 1 (Cyfip1) has been defined as a potential tumor suppressor that regulates invasive behavior. The loss of CYFIP1 expression has been correlated with tumor progression in epithelial and colon cancers [33]. Interestingly, we found this protein over-expressed after Ch-SeNPs exposure, thus showing the capability of Ch-SeNPs to raise the expression levels of certain tumor suppressors, such as in the case of the eIF3f subunit previously shown.

The apoptosis-inducing factor mitochondrion-associated 1 (AIF1) is involved in apoptosis because it induces the mitochondria to release cytochrome c and caspase-9. Down-regulation of AIF1 has been associated with low apoptosis ratio [34]. Interestingly, AIF1 appeared down-regulated after Ch-SeNPs exposure in our SILAC approach, which correlates well with the fact that no apoptosis was observed in cells exposed to Ch-SeNPs (Figure 2A).

Ch-SeNPs inhibit in-vitro invasiveness of HepG2 cells

We used matrigel cell culture, which has been widely used for in vitro studies on tumor growth [35], in order to evaluate the capacity of Ch-SeNPs to preclude cell invasion. It is known that the differentiation response on matrigel is dependent on the cell type being easily distinguished malignant and non-malignant cells by their morphology when they are cultured on the surface of this basement membrane matrix [36]. The images obtained under phase contrast microscopy (Figure 6C) showed that the exposure to Ch-SeNPs has a negative effect on invasive behavior of HepG2 cells. It can be observed how cells exposed to Ch-SeNPs appeared round and individuals with no ramifications as in the case of control cells.

Conclusions

To the best of our knowledge, this is the first time that a quantitative proteomic approach has been used to unravel the molecular mechanisms underlying the effects induced by SeNPs in cultured hepatocarcinoma cells. In summary, our data strongly suggest that the cell cycle of HepG2 cells is arrested at the S phase by alteration of the eIF3 protein complex expression as result of Ch-SeNPs exposure, which may hampers translation of mRNAs responsible for encoding proteins important for cell proliferation and oncogenesis. We have shown by different independent approaches how different eIF3 subunits, which are commonly found up-regulated in several types of tumors, are down-regulated after Ch-SeNPs exposure, except for eIF3f, which is the only eIF3 subunit that has been proposed as tumor suppressor and therefore

may also contribute to attenuate cell proliferation. In addition, we have demonstrated the ability of Ch-SeNPs to inhibit *in vitro* cell invasion and the de-regulation of other proteins that could also be involved in the overall inhibition of cell proliferation induced by Ch-SeNPs.

Acknowledgment

Authors thank the Spanish Ministry of Economy and Competitiveness (grants CTQ2010-18644 and CTQ2011-28328C02-01), the *Comunidad de Madrid* (Spain) and the European FEDER programme (grants AS2009/AGR-1464, ANALISYC-II, Interreg European Project Orque-Sudoe). The authors thank Maria Luisa Garcia and Agustin Fernandez for electron microscopy services (ICTS-CNME) and the Complutense University Flow Cytometry Core.

References

1. Fairweather-Tait SK, Bao Y, Broadley MR, Collings R, Ford D, et al. (2011) Selenium in human health and disease. Antioxid Redox Signal 14: 1337-1383.
2. Abdulah R, Miyazaki K, Nakazawa M, Koyama H (2005) Chemical forms of selenium for cancer prevention. J Trace Elem Med Biol 19: 141-150.
3. Wang H, Zhang J, Yu H (2007) Elemental selenium at nano size possesses lower toxicity without compromising the selenoenzymes: comparison with selenomethionine in mice. Free Radic Biol Med 42: 1524-1533.
4. Zhang J, Wang X, Xu T (2008) Elemental selenium at nano size (nano-Se) as a potential chemopreventive agent with reduced risk of selenium toxicity: comparison with Se-methylselenocysteine in mice. Toxicol Sci 101: 22-31.
5. Jin-Song Z, Xue-Yun G, Li-De Z, Yong-Ping B (2001) Biological effects of a nano red elemental selenium. Biofactors 15: 27-38.
6. Chen T, Wong YS, Zheng W, Bai Y, Huang L (2008) Selenium nanoparticles fabricated in *Undaria Pinnatifida* polysaccharide solutions induce mitochondria-mediated apoptosis in A375 human melanoma cells. Colloids Surf B Biointerfaces 67: 26-31.
7. Luo H, Wang F, Bai Y, Chen T, Zheng W (2012) Selenium nanoparticles inhibit the growth of HeLa and MDA-MB-231 cells through induction of S phase arrest. Colloids Surf B Biointerfaces 94: 304-308.
8. Estevez H, Garcia-Lidon JC, Luque-Garcia JL, Camara C (2014) Effects of chitosan-stabilized selenium nanoparticles on cell proliferation, apoptosis and cell cycle pattern in HepG2 cells: Comparison with other selenospecies. Colloids Surf B Biointerfaces 122C: 184-193.
9. Luque-Garcia JL, Cabezas-Sanchez P, Camara C (2011) Proteomics as a tool for examining the toxicity of heavy metals. Trends Anal Chem 30: 703-716.
10. Cuello S, Ramos S, Madrid Y, Luque-Garcia JL, Camara C (2012) Differential protein expression of hepatic cells associated with MeHg exposure: deepening into the molecular mechanisms of toxicity. Anal Bioanal Chem 404: 315-324.
11. Ren Y, Zhao T, Mao G, Zhang M, Li F, et al. (2013) Antitumor activity of hyaluronic acid-selenium nanoparticles in heps tumor mice models. Int J Biol Macromol 57: 57-62.
12. Bai Y, Wang Y, Zhou Y, Li W, Zheng W (2008) Modification and modulation of saccharides on elemental selenium nanoparticles in liquid phase. Materials Letters 62: 2311-2314.
13. Rivera-Torres J, Acín-Perez R, Cabezas-Sanchez P, Osorio FG, Gonzalez-Gomez C, et al. (2013) Identification of mitochondrial dysfunction in Hutchinson-Gilford progeria syndrome through use of stable isotope labeling with amino acids in cell culture. J Proteomics 91: 466-477.
14. Zhang M, Li J, Xing G, He R, Li W, et al. (2011) Variation in the internalization of differently sized nanoparticles induces different DNA-damaging effects on a macrophage cell line. Arch Toxicol 85: 1575-1588.
15. Green DR, Reed JC (1998) Mitochondria and apoptosis. Science 281: 1309-1312.
16. Huang Y, He L, Liu W, Fan C, et al. (2013) Selective cellular uptake and induction of apoptosis of cancer-targeted selenium nanoparticles. Biomaterials 34: 7106-7116.
17. Harris TE, Chi A, Shabanowitz J, Hunt DF, et al. (2006) mTOR-dependent stimulation of the association of eIF4G and eIF3 by insulin. EMBO J 25: 1659-1668.
18. Siridechadilok B, Fraser CS, Hall RJ, Doudna JA, Nogales E (2005) Structural roles for human translation factor eIF3 in initiation of protein synthesis. Science 310: 1513-1515.
19. Zhou C, Arslan F, Wee S, Krishnan S, Ivanov AR, et al. (2005) PCI proteins eIF3e and eIF3m define distinct translation initiation factor 3 complexes. BMC Biol 3: 14-29.
20. Gosh SH, Hong SH, Lee BC, Ju MH, Jeong JS, et al. (2011) eIF3m expression influences the regulation of tumorigenesis-related genes in human colon cancer. Oncogene 30: 398-409.
21. Pincheira R, Chen Q, Zhang JT (2001) Identification of a 170-kDa protein over-expressed in lung cancers. Br J Cancer 84: 1520-1527.
22. Liu Z, Dong Z, Yang Z, Chen Q, Pan Y, et al. (2007) Role of eIF3a (eIF3 p170) in intestinal cell differentiation and its association with early development. Differentiation 75: 652-661.
23. Fraser CS, Lee JY, Mayeur GL, Bushell M, Doudna JA, et al. (2004) The j-subunit of human translation initiation factor eIF3 is required for the stable binding of eIF3 and its subcomplexes to 40S ribosomal subunits in vitro. J Biol Chem 279: 8946-8956.
24. Liang H, Ding X, Zhou C, Zhang Y, Xu M, et al. (2012) Knockdown of eukaryotic translation initiation factors 3b (eIF3b) inhibits proliferation and promotes apoptosis in glioblastoma cells. Neurol Sci 33: 1057-1062.
25. Wang Z, Chen J, Sun J, Cui Z, Wu H (2012) RNA interference-mediated silencing of eukaryotic translation initiation factor 3, subunit b (eIF3b) gene expression inhibits proliferation of colon cancer cells. World J Surg Oncol 10: 119-127.
26. Beyaert R, Kidd VJ, Cornelis S, Van de Craen M, Denecker G, et al. (1997) Cleavage of PITSLRE kinases by ICE/CASP-1 and CPP32/CASP-3 during apoptosis induced by tumor necrosis factor. J Biol Chem 272: 11694-11697.
27. Shi J, Kahle A, Hershey JWB, Honchak BM, Warneke JA, et al. (2006) Decreased expression of eukaryotic initiation factor 3f deregulates translation and apoptosis in tumor cells. Oncogene 25: 4923-4936.
28. Amarillo R, Ramachandran S, Sabanay H, Lev S (2005) Differential regulation of endoplasmic reticulum structure through VAP-Nir protein interaction. J Biol Chem 280: 5934-5944.
29. Prosser DC, Tran D, Gougeon PY, Verly C, Ngsee JK (2008) FFAT rescues VAPA-mediated inhibition of ER-to-golgi transport and VAPB-mediated ER aggregation. J Cell Biol 121: 3052-3061.
30. De Maio A (1999) Heat shock proteins: facts, thoughts, and dreams. Shock 11: 1-12.
31. Tatebe H, Shiozaki K (2003) Identification of Cdc37 as a novel regulator of the stress-responsive mitogen-activated protein kinase. Mol Cell Biol 23: 5132-5142.
32. Kyriakis JM, Avruch J (2001) Mammalian mitogen-activated protein kinase signal transduction pathways activated by stress and inflammation. Physiol Rev 81: 807-869.
33. Silva JM, Ezhkova E, Silva J, Heart S, Castillo M, et al. (2009) Cyfip1 Is a Putative Invasion Suppressor in Epithelial Cancers. Cell 137: 1047-1061.
34. Susin SA, Lorenzo HK, Zamzami N, Marzo I, Snow BE, et al. (1999) Molecular characterization of mitochondrial apoptosis-inducing factor. Nature 397: 441-446.
35. Noel A, De Pauw-Gillet MC, Purnell G, Nusgens B, Lapierre CM, et al. (1993) Enhancement of tumorigenicity of human breast adenocarcinoma cells in nude mice by matrigel and fibroblasts. Br J Cancer 68: 909-915.
36. Marques MM, Martins MD, Franca CM (2006) Effect of matrigel on adenoid cystic carcinoma cell line differentiation. Int J Exp Pathol 87: 405-410.

Citation: Lopez-Heras I, Sanchez-Diaz R, Anunciação DS, Madrid Y, Luque-Garcia JL, et al. (2014) Effect of Chitosan-Stabilized Selenium Nanoparticles on Cell Cycle Arrest and Invasiveness in Hepatocarcinoma Cells Revealed by Quantitative Proteomics. J Nanomed Nanotechnol 5: 226. doi: 10.4172/2157-7439.1000226

Hindawi Publishing Corporation
BioMed Research International
Volume 2015, Article ID 416480, 9 pages
http://dx.doi.org/10.1155/2015/416480

Review Article

T Helper 17/Regulatory T Cell Balance and Experimental Models of Peritoneal Dialysis-Induced Damage

Georgios Liappas,[1,2] Guadalupe Tirma Gónzalez-Mateo,[1,2] Pedro Majano,[3] José Antonio Sánchez- Tomero,[4] Marta Ruiz-Ortega,[5] Raquel Rodrigues Díez,[5] Pilar Martín,[6] Raquel Sanchez-Díaz,[6] Rafael Selgas,[2] Manuel López-Cabrera,[1] and Abelardo Aguilera Peralta[3]

[1]*Department of Immunology, Centro de Biología Molecular Severo Ochoa (CBM), Consejo Superior de Investigaciones Científicas (CSIC), 28049 Madrid, Spain*
[2]*Department of Nephrology, Instituto de Investigación del Hospital Universitario La Paz (IdiPAZ), 28046 Madrid, Spain*
[3]*Department of Molecular Biology, Instituto de La Princesa (IP), 28006 Madrid, Spain*
[4]*Nephrology Service, Hospital Universitario de La Princesa (IP), 28006 Madrid, Spain*
[5]*Laboratory of Cellular Biology and Rare Diseases, Fundación Jiménez Díaz, Universidad Autónoma de Madrid (UAM), 28040 Madrid, Spain*
[6]*Department of Molecular and Vascular Inflammation, Centro Nacional de Investigaciones Cardiovasculares (CNIC), 28029 Madrid, Spain*

Correspondence should be addressed to Guadalupe Tirma Gónzalez-Mateo; guadalupe.gonzalez@idipaz.es and Abelardo Aguilera Peralta; abelardo.aguilera@salud.madrid.org

Received 18 September 2014; Accepted 29 December 2014

Academic Editor: Monica Fedele

Fibrosis is a general complication in many diseases. It is the main complication during peritoneal dialysis (PD) treatment, a therapy for renal failure disease. Local inflammation and mesothelial to mesenchymal transition (MMT) are well known key phenomena in peritoneal damage during PD. New data suggest that, in the peritoneal cavity, inflammatory changes may be regulated at least in part by a delicate balance between T helper 17 and regulatory T cells. This paper briefly reviews the implication of the Th17/Treg-axis in fibrotic diseases. Moreover, it compares current evidences described in PD animal experimental models, indicating a loss of Th17/Treg balance (Th17 predominance) leading to peritoneal damage during PD. In addition, considering the new clinical and animal experimental data, new therapeutic strategies to reduce the Th17 response and increase the regulatory T response are proposed. Thus, future goals should be to develop new clinical biomarkers to reverse this immune misbalance and reduce peritoneal fibrosis in PD.

1. Introduction

An effective inflammatory response is essential not only for the resolution of infections but also for wound healing after injury. The repair is mediated by the collaboration of various mechanisms launched by an acute inflammatory reaction. This process implicates the release of chemokines and cytokines and the migration of various cells of the immune system. If a sustained inflammatory reaction that is not resolved properly becomes chronic, it could lead to fibrosis due to the accumulation of extracellular matrix (ECM) components [1].

Peritoneal dialysis (PD) is a form of renal replacement therapy alternative to haemodialysis that is widely used around the world for patients suffering from renal failure disease [2, 3]. The process uses the peritoneum as a semipermeable membrane across which PD fluids (PDFs) and dissolved substances (electrolytes, urea, glucose, and other small molecules) are exchanged from the blood [4]. The peritoneal membrane (PM) acts as a protective barrier against injury

and pathogens, where humoural and cellular responses are generated. The treatment consists of the instillation and periodical renovation of a hyperosmotic PDF in the peritoneal cavity through a permanent installed catheter. However, the mechanical damage due to PDF instillation and the exposure of peritoneal cells to glucose degradation products (GDPs) and advanced glycation end products (AGEs) (due to the nonphysiological nature of this PDF) generates inflammation. Along these lines, it has been demonstrated *in vitro* that GDPs and AGEs stimulate NFκB-mediated transcription and the secretion of cytokines and chemokines by human peritoneal mesothelial cells [5]. In addition, the presence of the catheter [6] and peritonitis episodes during treatment [7] appears to be responsible for various alterations of the PM structure and functionality. The final consequence is the generation of vascular alterations [8] and peritoneal fibrosis [3, 9], leading to an ultrafiltration failure [10, 11] that impedes the dialysis process (Figure 1). Although in recent decades great effort has been made to improve catheter design [6] and the biocompatible solutions used [12–14], complications are still common [15, 16]. It has also been demonstrated that inflammation is present in PD patients. Increased serum concentrations of IL-6, TNF-α, VEGF, and C-reactive proteins have been reported in patients, suggesting that PD leads to increased systemic inflammation [17]. Moreover, there is evidence in animal models of chronic peritoneal exposure to PDF showing that this procedure induces PM inflammation and fibrosis [18]. The use of an anti-inflammatory drug (a Cox-2 inhibitor) reduced this peritoneal inflammatory response and consequently the fibrosis. This result confirms the role of inflammation in peritoneal fibrosis [19].

Inflammation is driven by various cell populations including macrophages, neutrophils, and lymphocyte subsets. The differentiation of T cells is crucial for immune and inflammatory responses and its regulation may be a therapeutic target to control peritoneal damage. It has been found that there are different rates between $CD4^+$ and $CD8^+$ cells in the peritoneum during PD with respect to healthy individuals [20]. It has been postulated that the presence of AGEs is responsible for an increase in the population of $CD8^+$ (T cytotoxic) lymphocytes [21]. Regarding $CD4^+$ (T helper) subsets, in general terms Th1 cells produce high levels of IFN-γ, while Th2 cells secrete predominantly IL-4 [22]. There is some controversy about the pattern of response that is generated in patients undergoing treatment with PDF. It is described that there is a deviation toward Th2 pattern of PD in stable patients [23]. However, during episodes of acute peritonitis, a Th1 immune response is developed [24, 25]. In addition to these two classical T helper cell subsets (Th1 and Th2), a third and fourth subpopulation, designated regulatory T (Treg) and T helper 17 (Th17) cells, have emerged as independent differentiation pathways [26, 27]. While the predominance of Th17 cells induces the secretion of a large number of proinflammatory cytokines, Treg cells restrict inflammatory responses and are associated with immune-tolerance [28]. Very little is known about the involvement of these subpopulations in the deterioration of the peritoneum during dialysis. The imbalance between these situations may cause fibroproliferative diseases and could be an important cause of morbidity and mortality.

In this review we discuss the implication of Th17 and Treg cells in kidney function and fibrotic diseases in different animal experimentation models. More specifically we will focus on the origin of peritoneal damage and its relationship with the intraperitoneal presence of these particular subsets of T lymphocytes, as well as on its clinical implication in peritoneal damage in PD patients, which frequently results in an inability to continue with the treatment.

2. T Helper 17 and Regulatory T Cell Differentiation and Their Plasticity

Th17 cells represent a subset of T helper cells that secrete mainly interleukin- (IL-) 17 as well as other proinflammatory cytokines, and they have been related to many autoimmune and chronic inflammatory diseases [29]. There is a balance between Th17 and Treg cells that depends on the activation of the transcription factor RORγt (factors retinoic acid receptor-related orphan receptor γt) and Stat3 (signal transducer and activator of transcription 3), or FoxP3 (forkhead box P3) and Stat5, respectively, which regulate the immune response through the secretion of pro- and anti-inflammatory cytokines [30–33]. On the other hand, the importance of Treg cells to the maintenance of peripheral tolerance under noninflammatory conditions throughout life has also been confirmed. In fact, mice lacking Treg cells presented a fatal inflammatory response [34, 35].

The main cytokines involved in Th17/Treg balance are the TGF-β (transforming growth factor beta) and IL-6 (interleukin-6) [27, 36, 37]. IL-6 is strongly induced in cells of the innate immune system upon stimulation of pattern recognition receptors such as toll like receptors (TLR) or C-type receptors. It has been shown that mice lacking IL-6 present a deficiency in the differentiation of effector T cells [38, 39]. TGF-β in the absence of IL-6 induces Foxp3, thus pushing T-cell differentiation away from the Th17 transcriptional program and decidedly toward the Treg lineage [33]. Moreover, in the central nervous system, TGF-β without the synergy of IL-6 will force T cells to differentiate through the T regulatory cell lineage [40]. In contrast, the proinflammatory cytokine IL-6 in the absence of TGF-β activates Stat3 by phosphorylating it, which overcomes Foxp3 inhibition of RORγt transcriptional activity. This process leads to the upregulation of the IL-23R, thus pushing T-cell differentiation toward a Th17 fate [33]. Therefore the cytokine environment is essential for the predominance of an inflammatory or an anti-inflammatory response (Figure 2).

3. Th17 and Tissue Fibrosis

Fibroproliferative diseases such as idiopathic pulmonary, liver, cardiovascular, and renal fibrosis are usually associated with chronic inflammation, as has been described previously [41–45]. When an inflammatory response becomes chronic, the accumulation of ECM is more extensive and the function of the organ is compromised. A number of studies have

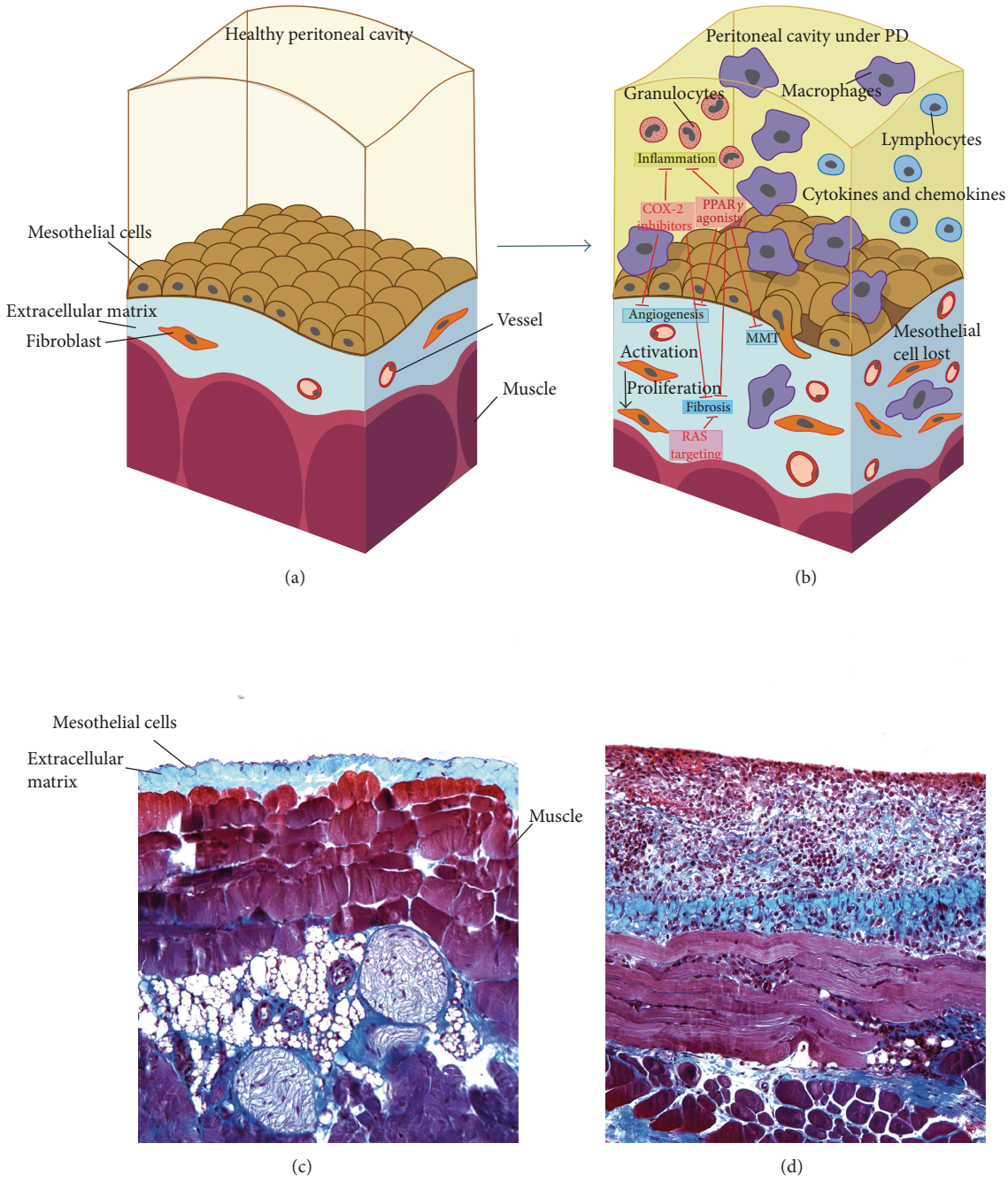

FIGURE 1: PM schemas and biopsies representing the normal peritoneal structure and its changes during PD. Possible therapeutic approaches. (a) and (b) are adapted with permission from Aguilera et al. (2013). *Available from* http://www.intechopen.com/books/the-latest-in-peritoneal-dialysis/the-mesothelial-to-mesenchymal-transition-a-pathogenic-and-therapeutic-key-for-peritoneal-membrane-f [80]. (a) Realistic representation of a healthy peritoneal cavity. A preservation of the mesothelial layer is clearly seen, only a few fibroblasts and vessels are visible, and only a small layer of extracellular matrix lies in the compact zone of the muscle layer. (b) After exposure to PD liquids, the structure of the PM starts to change dramatically with the appearance of more fibroblasts, macrophages, and inflammatory cytokines and finally with deposition of more extracellular matrix (ECM) cells. Inflammation and fibrosis will be the result of these changes. Some drugs like COX-2 inhibitors, PPRAγ agonists, or RAS targeting are possible therapeutic strategies to protect from PD complications such as inflammation, angiogenesis, fibrosis, and/or MMT. (c) A peritoneal biopsy of a mouse peritoneal membrane that was treated with physiological saline is shown as control. The PM is well preserved and fibrotic response is absent. (d) Peritoneal biopsy of a mouse PM that was exposed to PDF for 40 days. A significant fibrotic response can be observed with a larger ECM and many inflammatory cells.

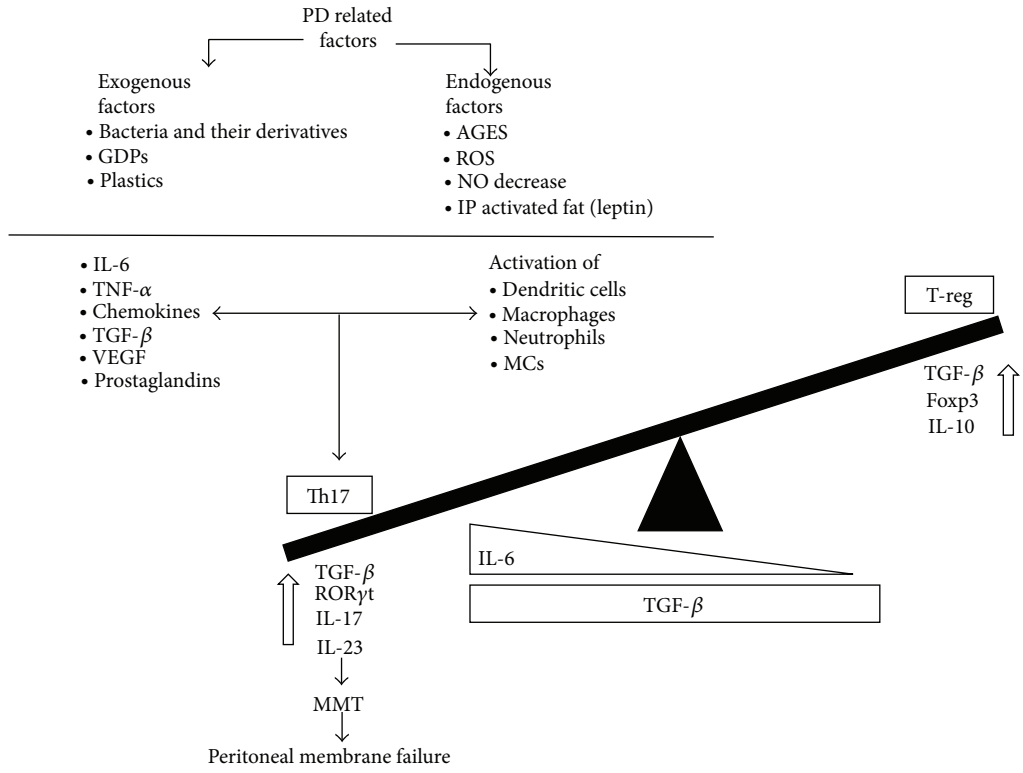

Figure 2: Mechanisms of Th17/Treg-balance in the peritoneal cavity in PD. Th17 predominance. In the peritoneal cavity local factors activate dendritic cells, macrophages, and neutrophils to produce proinflammatory molecules (IL-6, TNFα, TGF-β, VEGF, chemokines, and prostaglandins). Immune cells and proinflammatory molecules are reciprocally activated; thus cells induce proinflammatory molecule release and vice versa. These molecules activate Th17 cells and IL-17 production, which may result in fibrosis and MMT. This occurs in the presence of continuously high TGF-β levels. In contrast, in the presence of inactive immune cells together with low IL-6 levels, Treg cells are activated, releasing IL-10 and TGF-β that may block MMT. Abbreviations: GDPs: glucose-derived products. IP: intraperitoneal. AGEs: advanced glycation end products.

highlighted the roles of Th17/Treg/Th1/Th2 responses in the pathogenesis of tissue fibrosis [46, 47]. Among these responses, Th17 cells may mediate strong inflammation by producing a cocktail of cytokines such as IL-6, IL-17A, IL-17F, and IL-22, among which IL-17A has been characterized as the major effector cytokine in causing a sustained inflammatory response.

Recent studies have investigated the role of Th17 response in fibrosis. It has been reported that administration of IL-17A *in vitro* increased the synthesis and secretion of collagen in alveolar epithelial cells in a pulmonary fibrosis model. Moreover, all IL-17-associated signaling pathways were mainly activated in fibrotic lung biopsies, and a blockade of IL-17A attenuated tissue injury, inflammation, and fibrosis in acute and chronic injuries [48].

Furthermore, IL-17 has also been reported to be involved in the pathogenesis of chronic liver fibrosis [44, 49–51]. The same mechanism was proposed in another study on liver damage in chronic hepatitis B patients who presented an elevated Th17 cells population [52].

Th17 cells also play a crucial role in autoimmune myocarditis, as based on *in vitro* and *in vivo* experiments which confirm that IL-17 induced cardiac fibrosis by activating the protein kinase C-β/Erk1/2/NF-κB pathway [53]. Moreover, the regulatory molecule CD69, through the regulation of Th17 effector responses, limits myocardial inflammation, fibrosis, and subsequent heart failure [54].

Recent studies have shown the importance of Th17 cells, and the hallmark cytokine IL-17A, in immune-mediated glomerulonephritis, including experimental antimyeloperoxidase glomerulonephritis, crescentic glomerulonephritis, and lupus nephritis [55, 56]. Th17 cells participate in renal damage, as demonstrated by an experimental study in mice showing that Th17 cell injection caused albuminuria and neutrophils infiltration in the kidney [57]. Recent studies also show the presence of Th17 cells and elevated renal production of IL-17A in nonimmune experimental renal diseases, including a model of unilateral ureteral obstruction [58]. In experimental ischaemia reperfusion, neutrophils, but not Th17 cells, were the main sources of IL-17A and contribute to renal injury by natural killer T activation and IL-12/IFN-γ production [59]. In renal allograft rejection, positive staining for IL-17A has been detected in tubular cells [60], as we have observed in an experimental model of CCN2-mediated renal damage, suggesting that renal cells could produce this cytokine and contribute to extending the damage. With this model we recently demonstrated that a blockade of IL-17A diminished renal inflammation [58].

Based on all the above studies, IL-17 has been proposed as a drug target in many fibrotic diseases [61].

4. Regulatory T Cells and Tissue Fibrosis

Although an induced Th17 response is connected to fibrogenesis, a relative decrease in the number of Treg cells may also be involved in the pathogenesis of inflammatory and fibrotic diseases. The evaluation of these cells in the context of experimentally induced fibrosis has been challenging, and Treg depletion in mice has been demonstrated to attenuate the development of lung fibrosis [62]. Moreover, in an experimental animal model of cardiac fibrosis, the depletion of Treg cells and/or adoptive transfer of isolated Tregs ameliorated cardiac fibrosis, indicating a protective role of regulatory T cell in tissue fibrosis [63]. Recently, it has been reported that Treg cells are essential for preventing from accumulation of fibrocytes and collagen deposition in a pulmonary disease animal model. In this study, it was shown that a blockade of Treg cells increased the accumulation of solid collagen and progression of the disease [64]. Finally, in another study (Keloid fibrotic disease) the potential role of Treg cells in attenuating collagen synthesis was investigated. This group found that the imbalance of Tregs may contribute to the development of this fibrotic disease and that the correction of this imbalance may be of therapeutic value [65].

5. Th17 and Treg Lymphocyte Subsets in the Peritoneal Cavity on PD

PD-related factors locally stimulate Th17 cells and can be subdivided into two groups: exogenous and endogenous. The exogenous factors include bacteria and their derivatives, which enter into the peritoneal cavity through PD-catheter or via intestinal translocation and can provoke peritonitis episodes [66]. Peritoneal endogenous factors such as AGEs [67] could be involved in the induction of IL-17 levels by activating IL-6 and TGF-β proinflammatory cytokines, respectively. Although there is little data regarding how advanced glycation end products (AGEs) are implicated in peritoneal dialysis damage, their implication in posttransplantation and diabetic kidneys showed an induction of IL-6 and TGF-β, which are promoters of Th17 differentiation (Figure 2). Thus, it is plausible that the induced Th17 activity may have a poor fate in peritoneal damage during peritoneal dialysis. In nondiabetic PD patients, an elevation of IL-17 in peritoneal cavity effluents followed by a peritonitis episode was demonstrated [66], which is one of the main complications that lead to peritoneal fibrosis in PD patients [3].

Currently, it is accepted that mesothelial to mesenchymal transition (MMT) is a key process in PM survival in PD. Mesothelial cells lose their basolateral and basoapical polarity, acquiring a fibroblastoid phenotype with migration capacity. The cells invade the submesothelial compact zone where they synthesize ECM and VEGF, which are responsible for fibrosis and angiogenesis, respectively [68, 69]. IL-17 itself is capable of inducing epithelial to mesenchymal transition in bronchial cells [70]. Although this effect has not been demonstrated in the peritoneum, it is very likely that IL-17 also contributes to PM deterioration via MMT induction.

The definitive evidence on IL-17 involvement in PM damage on PD was recently provided by Rodrigues-Díez et al. (2014). This study demonstrated in both mice and human samples that IL-17 is overexpressed in peritoneal biopsies. This was the first report to demonstrate that IL-17 participates in the typical fibrotic changes suffered in PM during long-term PD (induced fibronectin, α-smooth muscle actin, and fibroblast specific protein-1 expression). Moreover, to better elucidate the effects of IL-17 on PM, intraperitoneal IL-17 was injected in mice, reproducing the changes that normally take place in PD patients. On the other hand, the use of a neutralizing IL-17A antibody injected intraperitoneally in mice exposed to PDF for 35 days blockaded the anatomical changes in the PM and reduced peritoneal fibrosis [71].

On the other hand, Treg cells are strongly connected with immune tolerance. Patients in end-stage renal disease with their suppressed immune response suffer impaired Treg cell responses [72]. Currently, there is not much evidence regarding the role of Treg cells in the peritoneal cavity during PD. To our knowledge, there is one study focusing on the function of Treg cells on peritoneal damage. This study concluded that rosiglitazone, a PPARγ agonist, augments the intraperitoneal IL-10 levels (Treg-associated cytokine), increases the recruitment of $CD4^+$ $CD25^+$ $FoxP3^+$ (regulatory T cells), and finally attenuates peritoneal fibrosis in an experimental mouse PD model [73].

Evidence suggests that Th17 cells share common progenitors with Treg cells and that the developmental pathways of these two subsets are reciprocally regulated [74]. In fact, it has been recently demonstrated that a reduction in IL-17 secretion due to Treg cell activation is associated with a diminished fibrotic response specifically in PD. The vitamin D pathway has been shown to regulate inflammatory responses. In regard to this, the effect of paricalcitol, a vitamin D receptor activator, was tested in a mouse model of PD to evaluate its effect on inflammatory cells and on the outcome of peritoneal fibrosis. It was found that the group that was treated with PDF presented increased levels of IL-17 cytokine in the peritoneal effluents compared with the group that was treated with paricalcitol diluted in the PDF. Moreover, the increased IL-17 concentration was perfectly correlated with the thickness of the peritoneum, meaning IL-17 is a profibrotic cytokine. This effect was related to an increased number of Tregs in the group that was treated with paricalcitol [75].

6. Therapeutic Approaches to Prevent Peritoneal Damage Using the Th17/Treg-Axis: From Animal Models to PD Patients

Accepting the evidence above that Th17 and Treg subsets are involved in peritoneal damage in PD, we propose the following therapeutic strategies.

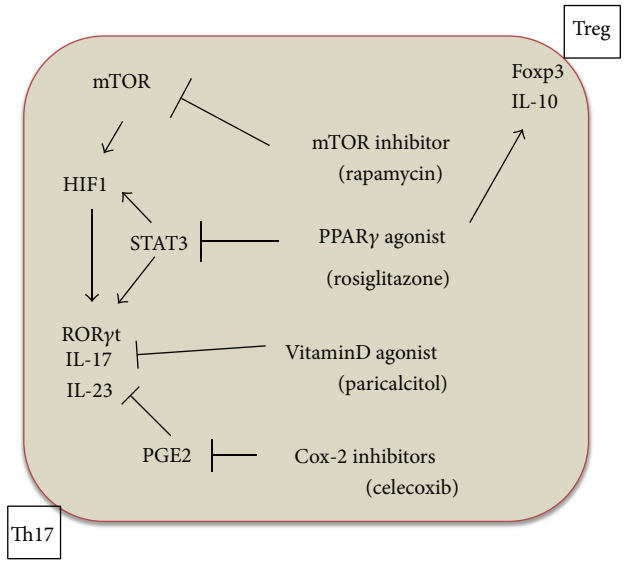

Figure 3: Therapeutic approaches to prevent peritoneal damage using the Th17/Treg-axis as a target. One of the most important modulators of Th17/Treg activity is the concentration of branch chain amino acids (BCAA). Although the data in relation to BCAA plasma levels in a uraemic state are contradictory, many articles indicate that these amino acids are decreased in uraemia due to systemic acidosis, inflammation, amino acid misbalances, and liquid overload. Normal or relative normal BCAA levels activate an mTOR (mammalian Target of Rapamycin) cascade including HIF1 and RORγt and subsequently IL-17 and IL-23 production. Rapamycin, an mTOR inhibitor, would block this cascade, thus providing an anti-inflammatory/antifibrotic and possibly anti-MMT effect. Moreover, PPARγ agonists can also inhibit Th17 differentiation through a direct blockade of Stat3 transcription factor and HIF-1. Ultimately RORγt is downregulated, and IL-17 and IL-23 production is decreased. However the PPRAγ agonists are also able to act on the anti-inflammatory cascade. In the peritoneal cavity in PD, rosiglitazone augments IL-10 levels and Treg activity (upregulation of $FoxP3^+$). This process could be one of the most important mechanisms by which PPRAγ agonists protect the PM. In addition, paricalcitol, a specific vitamin D activator, has been recently shown to inhibit IL-17 production and PM fibrosis and possibly decrease MMT. Finally, celecoxib, a Cox2 inhibitor, decreases IL-17 production by blocking the E2 prostaglandin levels and thus attenuates the PM damage induced by PDF.

6.1. Use Drugs and Molecular Strategies

6.1.1. mTOR Inhibitors. The mTOR inhibition by Rapamycin may diminish IL-17 production. The mTOR activation induces hypoxia induced factor-1 (HIF-1) and RORγt activation and subsequently IL-17 and IL-23 production [76]. Thus, these drugs may provide an anti-inflammatory/antifibrotic effect and possibly an anti-MMT action as was demonstrated by Aguilera et al. [77] (Figure 3).

6.1.2. Peroxisome Proliferator-Activated Receptors- (PPAR-) γ Agonists. The use of PPARγ agonists, for example, rosiglitazone, may be a therapeutic alternative to prevent peritoneal damage [78]. These receptors show a double protective effect. First, they inhibit the Th17 differentiation via a Stat3 cascade blockade, which results in a downregulation of RORγt and a decrease in IL-17 production [79]. Moreover, in an animal model study in which the effect of rosiglitazone in the preservation of the peritoneal membrane was investigated, it was found that rosiglitazone augmented the intraperitoneal IL-10 levels (Treg-associated cytokine) and increased the recruitment of $CD4^+$ $CD25^+$ $FoxP3^+$ (regulatory T cells) [73] (Figure 3).

6.1.3. Vitamin D Receptor Activators. Another interesting drug that could ultimately have a beneficial effect on PM in PD is paricalcitol. Using a mice PD model, it was demonstrated that the PM thickening was reduced in mice treated with paricalcitol in comparison with the nontreated group. Moreover, in the effluents of mice treated with paricalcitol, an increased number of Treg cells and lower IL-17 levels were found in comparison with the nontreated group. In addition, the IL-17 levels measured in peritoneal effluent showed a positive linear correlation with the PM thickness [75]. These data suggest a direct involvement of IL-17 in peritoneal injury and paricalcitol may act on this target (Figure 3).

6.1.4. COX-2 Inhibitors. Celecoxib, a cyclooxygenase- (Cox-) 2 inhibitor agent, was shown to prevent the PM damage in PD when administrated orally to a group of mice in PD, acting directly on the inflammatory cascade in general. After 5 weeks of treatment, the celecoxib group showed a fibrotic response similar to healthy controls, while the untreated group exposed to PD only developed considerable fibrosis [19] (Figure 3).

7. Discussion

One of the most devastating complications of PD treatment is peritoneal fibrosis. The endogenous and exogenous factors mentioned above related to PDF generate a chronic inflammatory response in the peritoneal cavity. The balance between Th17 and Treg cells is guided by proinflammatory cytokines secreted from Th17 cells and anti-inflammatory cytokines produced from regulatory T cells. Any factor that may alter this balance can lead to peritoneal deterioration and finally to peritoneal damage. The high levels of various proinflammatory molecules such as IL-6 and TGF-β cytokines during PD create an environment that induces a chronic inflammatory condition in the peritoneal cavity and generates peritoneal fibrosis. This emergent concept suggests that the immune imbalance is the fundamental key for PM deterioration in PD.

Moreover, Th17 signaling with high IL-17 levels has been implicated in the aetiology of several types of inflammatory and fibrotic diseases. Therefore, components of the IL-17 and Treg cells pathway are considered highly "druggable" and are important targets for the treatment of these inflammatory and fibrotic diseases. Current evidence indicates that IL-17 inhibition and Treg activation are logical therapeutic strategies for the treatment of animal peritoneal fibrosis [71, 73, 75].

In conclusion, the importance of developing new therapies to protect the peritoneal membrane blocking the IL-17 secretion or activating the Treg pathway has been demonstrated. Some novel therapeutic strategies tested in animal models and *in vitro* include the administration of m-Tor inhibitors, PPARγ agonists, vitamin D receptor activators, and Cox-2 inhibitors. Lessons learned from regulators of Th17/Treg-axis may aid in the future clinical implementation of these agents with the goal of reducing peritoneal fibrosis and improving patients' life undergoing PD.

8. Conclusion

PD-related factors are responsible for Th17 activation/Treg deactivation in the peritoneal cavity during peritoneal dialysis. The Th17/Treg-axis is important for maintaining the anatomical and functional integrity of the PM. Therefore, the Th17/Treg-axis may be considered a future therapeutic target.

Conflict of Interests

The authors declare that there is no conflict of interests regarding the publication of this paper.

Acknowledgments

This work was supported in part by grants from Ministerio de Economia y competitividad SAF2010-21249 to Manuel López-Cabrera, Comunidad Autónoma de Madrid 2010-BMD2321 (FIBROTEAM) to Manuel Lopez Cabrera, and Fondo de Investigaciones Santitarias RETICS 06/0016 and PI 09/0064 to Rafael Selgas and FIS 12/01175 to Abelardo Aguilera Peralta. Georgios Liappas is fully supported from European Union, Seventh Framework Program "EuTRiPD," under Grant Agreement PITN-GA-2011-287813. The authors would like to thank Juliette Siegfried and her team at ServingMed.com for editing the language of the paper.

References

[1] J. D. Williams, K. J. Craig, N. Topley et al., "Morphologic changes in the peritoneal membrane of patients with renal disease," *Journal of the American Society of Nephrology*, vol. 13, no. 2, pp. 470–479, 2002.

[2] C. Chaimovitz, "Peritoneal dialysis," *Kidney International*, vol. 45, no. 4, pp. 1226–1240, 1994.

[3] R. T. Krediet, "The peritoneal membrane in chronic peritoneal dialysis," *Kidney International*, vol. 55, no. 1, pp. 341–356, 1999.

[4] J. Waniewski, "Peritoneal fluid transport: mechanisms, pathways, methods of assessment," *Archives of Medical Research*, vol. 44, no. 8, pp. 576–583, 2013.

[5] J. Nevado, C. Peiró, S. Vallejo et al., "Amadori adducts activate nuclear factor-kappaB-related proinflammatory genes in cultured human peritoneal mesothelial cells," *British Journal of Pharmacology*, vol. 146, no. 2, pp. 268–279, 2005.

[6] G. R. Silberhumer, H. Pokorny, G. Györi, and F. Mühlbacher, "Surgical aspects of peritoneal dialysis," *Wiener Medizinische Wochenschrift*, vol. 163, no. 11-12, pp. 288–294, 2013.

[7] L. F. Fried, J. Bernardini, J. R. Johnston, and B. Piraino, "Peritonitis influences mortality in peritoneal dialysis patients," *Journal of the American Society of Nephrology*, vol. 7, no. 10, pp. 2176–2182, 1996.

[8] M. A. M. Mateijsen, A. C. van der Wal, P. M. E. M. Hendriks et al., "Vascular and interstitial changes in the peritoneum of CAPD patients with peritoneal sclerosis," *Peritoneal Dialysis International*, vol. 19, no. 6, pp. 517–525, 1999.

[9] L. S. Aroeira, A. Aguilera, J. A. Sánchez-Tomero et al., "Epithelial to mesenchymal transition and peritoneal membrane failure in peritoneal dialysis patients: Pathologic significance and potential therapeutic interventions," *Journal of the American Society of Nephrology*, vol. 18, no. 7, pp. 2004–2013, 2007.

[10] A. Lupo, C. Rugiu, A. Lapolla et al., "The dialytic failure of the peritoneal membrane," *Contributions to Nephrology*, vol. 131, pp. 90–96, 2001.

[11] J. Plum, S. Hermann, A. Fusshöller et al., "Peritoneal sclerosis in peritoneal dialysis patients related to dialysis settings and peritoneal transport properties," *Kidney International, Supplement*, vol. 59, no. 78, pp. S42–S47, 2001.

[12] O. Devuyst, P. J. Margetts, and N. Topley, "The pathophysiology of the peritoneal membrane," *Journal of the American Society of Nephrology*, vol. 21, no. 7, pp. 1077–1085, 2010.

[13] K. Wieczorowska-Tobis, A. Styszynski, A. Breborowicz, and D. G. Oreopoulos, "Comparison of the biocompatibility of phosphate-buffered saline alone, phosphate-buffered saline supplemented with glucose, and dianeal 3.86%," *Peritoneal Dialysis International*, vol. 21, no. 3, pp. S362–S364, 2001.

[14] C. J. Holmes, "Biocompatibility of peritoneal dialysis solutions," *Peritoneal Dialysis International*, vol. 13, no. 2, pp. 88–94, 1993.

[15] A. J. Collins, W. Hao, H. Xia et al., "Mortality risks of peritoneal dialysis and hemodialysis," *The American Journal of Kidney Diseases*, vol. 34, no. 6, pp. 1065–1074, 1999.

[16] R. Selgas, M.-J. Fernandez-Reyes, E. Bosque et al., "Functional longevity of the human peritoneum: how long is continuous peritoneal dialysis possible? Results of a prospective medium long-term study," *American Journal of Kidney Diseases*, vol. 23, no. 1, pp. 64–73, 1994.

[17] R. Pecoits-Filho, P. Stenvinkel, A. Yee-Moon Wang, O. Heimbürger, and B. Lindholm, "Chronic inflammation in peritoneal dialysis: the search for the holy grail?" *Peritoneal Dialysis International*, vol. 24, no. 4, pp. 327–339, 2004.

[18] G. T. González-Mateo, J. Loureiro, J. A. Jiménez-Hefferman et al., "Chronic exposure of mouse peritoneum to peritoneal dialysis fluid: structural and functional alterations of the peritoneal membrane," *Peritoneal Dialysis International*, vol. 29, no. 2, pp. 227–230, 2009.

[19] L. S. Aroeira, E. Lara-Pezzi, J. Loureiro et al., "Cyclooxygenase-2 mediates dialysate-induced alterations of the peritoneal membrane," *Journal of the American Society of Nephrology*, vol. 20, no. 3, pp. 582–592, 2009.

[20] I. Griveas, G. Visvardis, A. Fleva et al., "Lymphocytes subsets in the course of continuous ambulatory peritoneal dialysis (CAPD)," *Renal Failure*, vol. 26, no. 6, pp. 641–646, 2004.

[21] A. Glik and A. Douvdevani, "T lymphocytes: the 'cellular' arm of acquired immunity in the peritoneum," *Peritoneal Dialysis International*, vol. 26, no. 4, pp. 438–448, 2006.

[22] T. R. Mosmann and R. L. Coffman, "TH1 and TH2 cells: different patterns of lymphokine secretion lead to different functional properties," *Annual Review of Immunology*, vol. 7, pp. 145–173, 1989.

[23] T. Yokoyama, K. Nitta, K. Futatsuyama et al., "Identification of T helper cell subsets in continuous ambulatory peritoneal dialysis patients," *Nephron*, vol. 89, no. 2, pp. 215–218, 2001.

[24] A. Brauner, B. Hylander, and B. Wretlind, "Tumor necrosis factor-α, interleukin-1β, and interleukin-1 receptor antagonist in dialysate and serum from patients on continuous ambulatory peritoneal dialysis," *The American Journal of Kidney Diseases*, vol. 27, no. 3, pp. 402–408, 1996.

[25] H.-H. Wang and C.-Y. Lin, "Interleukin-12 and -18 levels in peritoneal dialysate effluent correlate with the outcome of peritonitis in patients undergoing peritoneal dialysis: implications for the type I/type II T-cell immune response," *American Journal of Kidney Diseases*, vol. 46, no. 2, pp. 328–338, 2005.

[26] P. Martín, M. Gómez, A. Lamana et al., "CD69 association with Jak3/Stat5 proteins regulates Th17 cell differentiation," *Molecular and Cellular Biology*, vol. 30, no. 20, pp. 4877–4889, 2010.

[27] E. Bettelli, Y. Carrier, W. Gao et al., "Reciprocal developmental pathways for the generation of pathogenic effector TH17 and regulatory T cells," *Nature*, vol. 441, no. 7090, pp. 235–238, 2006.

[28] D. R. Littman and A. Y. Rudensky, "Th17 and regulatory T cells in mediating and restraining inflammation," *Cell*, vol. 140, no. 6, pp. 845–858, 2010.

[29] J. C. Waite and D. Skokos, "Th17 response and inflammatory autoimmune diseases," *International Journal of Inflammation*, vol. 2012, Article ID 819467, 10 pages, 2012.

[30] I. I. Ivanov, B. S. McKenzie, L. Zhou et al., "The orphan nuclear receptor RORγt directs the differentiation program of proinflammatory IL-17$^+$ T helper cells," *Cell*, vol. 126, no. 6, pp. 1121–1133, 2006.

[31] T. J. Harris, J. F. Grosso, H.-R. Yen et al., "An in vivo requirement for STAT3 signaling in TH17 development and TH17-dependent autoimmunity," *Journal of Immunology*, vol. 179, no. 7, pp. 4313–4317, 2007.

[32] X. O. Yang, A. D. Panopoulos, R. Nurieva et al., "STAT3 regulates cytokine-mediated generation of inflammatory helper T cells," *Journal of Biological Chemistry*, vol. 282, no. 13, pp. 9358–9363, 2007.

[33] L. Zhou, J. E. Lopes, M. M. W. Chong et al., "TGF-B-induced Foxp3 inhibits T_H17 cell differentiation by antagonizing RORγt function," *Nature*, vol. 453, no. 7192, pp. 236–240, 2008.

[34] J. M. Kim, J. P. Rasmussen, and A. Y. Rudensky, "Regulatory T cells prevent catastrophic autoimmunity throughout the lifespan of mice," *Nature Immunology*, vol. 8, no. 2, pp. 191–197, 2007.

[35] K. Lahl, C. Loddenkemper, C. Drouin et al., "Selective depletion of Foxp3$^+$ regulatory T cells induces a scurfy-like disease," *Journal of Experimental Medicine*, vol. 204, no. 1, pp. 57–63, 2007.

[36] M. Veldhoen, R. J. Hocking, C. J. Atkins, R. M. Locksley, and B. Stockinger, "TGFβ in the context of an inflammatory cytokine milieu supports de novo differentiation of IL-17-producing T cells," *Immunity*, vol. 24, no. 2, pp. 179–189, 2006.

[37] P. R. Mangan, L. E. Harrington, D. B. O'Quinn et al., "Transforming growth factor-β induces development of the T_H17 lineage," *Nature*, vol. 441, no. 7090, pp. 231–234, 2006.

[38] H. P. Eugster, K. Frei, M. Kopf, H. Lassmann, and A. Fontana, "IL-6-deficient mice resist myelin oligodendrocyte glycoprotein-induced autoimmune encephalomyelitis," *European Journal of Immunology*, vol. 28, no. 7, pp. 2178–2187, 1998.

[39] E. B. Samoilova, J. L. Horton, B. Hilliard, T.-S. T. Liu, and Y. Chen, "IL-6-deficient mice are resistant to experimental autoimmune encephalomyelitis: roles of IL-6 in the activation and differentiation of autoreactive T cells," *Journal of Immunology*, vol. 161, no. 12, pp. 6480–6486, 1998.

[40] T. Korn, A. C. Anderson, E. Bettelli, and M. Oukka, "The dynamics of effector T cells and Foxp3$^+$ regulatory T cells in the promotion and regulation of autoimmune encephalomyelitis," *Journal of Neuroimmunology*, vol. 191, no. 1-2, pp. 51–60, 2007.

[41] S. Tamada, T. Asai, N. Kuwabara et al., "Molecular mechanisms and therapeutic strategies of chronic renal injury: the role of nuclear factor κB activation in the development of renal fibrosis," *Journal of Pharmacological Sciences*, vol. 100, no. 1, pp. 17–21, 2006.

[42] L. M. Blanco-Colio, J. L. Martín-Ventura, B. Munoz-Garcia et al., "TWEAK and Fn14. New players in the pathogenesis of atherosclerosis," *Frontiers in Bioscience*, vol. 12, no. 10, pp. 3648–3655, 2007.

[43] T. A. Wynn, "Cellular and molecular mechanisms of fibrosis," *The Journal of Pathology*, vol. 214, no. 2, pp. 199–210, 2008.

[44] Z. Tan, X. Qian, R. Jiang et al., "IL-17A plays a critical role in the pathogenesis of liver fibrosis through hepatic stellate cell activation," *Journal of Immunology*, vol. 191, no. 4, pp. 1835–1844, 2013.

[45] S. A. Hasan, B. Eksteen, D. Reid et al., "Role of IL-17A and neutrophils in fibrosis in experimental hypersensitivity pneumonitis," *The Journal of Allergy and Clinical Immunology*, vol. 131, no. 6, pp. 1663.e5–1673.e5, 2013.

[46] H.-Z. Yang, B. Cui, H.-Z. Liu et al., "Targeting TLR2 attenuates pulmonary inflammation and fibrosis by reversion of suppressive immune microenvironment," *The Journal of Immunology*, vol. 182, no. 1, pp. 692–702, 2009.

[47] K. J. Aitken, C. Tolg, T. Panchal et al., "Mammalian target of rapamycin (mTOR) induces proliferation and de-differentiation responses to three coordinate pathophysiologic stimuli (mechanical strain, hypoxia, and extracellular matrix remodeling) in rat bladder smooth muscle," *The American Journal of Pathology*, vol. 176, no. 1, pp. 304–319, 2010.

[48] S. Mi, Z. Li, H.-Z. Yang et al., "Blocking IL-17A promotes the resolution of pulmonary inflammation and fibrosis via TGF-beta1-dependent and -independent mechanisms," *Journal of Immunology*, vol. 187, no. 6, pp. 3003–3014, 2011.

[49] L. Wang, S. Chen, and K. Xu, "IL-17 expression is correlated with hepatitis B-related liver diseases and fibrosis," *International Journal of Molecular Medicine*, vol. 27, no. 3, pp. 385–392, 2011.

[50] A. Lemmers, C. Moreno, T. Gustot et al., "The interleukin-17 pathway is involved in human alcoholic liver disease," *Hepatology*, vol. 49, no. 2, pp. 646–657, 2009.

[51] D. Fenoglio, F. Bernuzzi, F. Battaglia et al., "Th17 and regulatory T lymphocytes in primary biliary cirrhosis and systemic sclerosis as models of autoimmune fibrotic diseases," *Autoimmunity Reviews*, vol. 12, no. 2, pp. 300–304, 2012.

[52] J.-Y. Zhang, Z. Zhang, F. Lin et al., "Interleukin-17-producing CD4$^+$ T cells increase with severity of liver damage in patients with chronic hepatitis B," *Hepatology*, vol. 51, no. 1, pp. 81–91, 2010.

[53] Y. Liu, H. Zhu, Z. Su et al., "IL-17 contributes to cardiac fibrosis following experimental autoimmune myocarditis by a PKCβ/Erk1/2/NF-κB-dependent signaling pathway," *International Immunology*, vol. 24, no. 10, pp. 605–612, 2012.

[54] A. Cruz-Adalia, L. J. Jiménez-Borreguero, M. Ramírez-Huesca et al., "CD69 limits the severity of cardiomyopathy after autoimmune myocarditis," *Circulation*, vol. 122, no. 14, pp. 1396–1404, 2010.

[55] A. R. Kitching and S. R. Holdsworth, "The emergence of Th17 cells as effectors of renal injury," *Journal of the American Society of Nephrology*, vol. 22, no. 2, pp. 235–238, 2011.

[56] J.-E. Turner, H.-J. Paust, O. M. Steinmetz, and U. Panzer, "The Th17 immune response in renal inflammation," *Kidney International*, vol. 77, no. 12, pp. 1070–1075, 2010.

[57] S. A. Summers, O. M. Steinmetz, M. Li et al., "Th1 and Th17 cells induce proliferative glomerulonephritis," *Journal of the American Society of Nephrology*, vol. 20, no. 12, pp. 2518–2524, 2009.

[58] R. Rodrigues-Díez, R. R. Rodrigues-Díez, S. Rayego-Mateos et al., "The C-terminal module IV of connective tissue growth factor is a novel immune modulator of the Th17 response," *Laboratory Investigation*, vol. 93, no. 7, pp. 812–824, 2013.

[59] L. Li, L. Huang, A. L. Vergis et al., "IL-17 produced by neutrophils regulates IFN-γ-mediated neutrophil migration in mouse kidney ischemia-reperfusion injury," *The Journal of Clinical Investigation*, vol. 120, no. 1, pp. 331–342, 2010.

[60] A. Loverre, T. Tataranni, G. Castellano et al., "IL-17 expression by tubular epithelial cells in renal transplant recipients with acute antibody-mediated rejection," *The American Journal of Transplantation*, vol. 11, no. 6, pp. 1248–1259, 2011.

[61] S. Ivanov and A. Lindén, "Interleukin-17 as a drug target in human disease," *Trends in Pharmacological Sciences*, vol. 30, no. 2, pp. 95–103, 2009.

[62] F. Liu, J. Liu, D. Weng et al., "CD4+CD25+Foxp3+ regulatory T cells depletion may attenuate the development of silica-induced lung fibrosis in mice," *PLoS ONE*, vol. 5, no. 11, Article ID e15404, 2010.

[63] Y. Cao, W. Xu, and S. Xiong, "Adoptive transfer of regulatory T Cells protects against Coxsackievirus B3-induced cardiac fibrosis," *PLoS ONE*, vol. 8, no. 9, Article ID e74955, 2013.

[64] X. Peng, M. W. Moore, H. Peng et al., "CD4+CD25+FoxP3+ regulatory tregs inhibit fibrocyte recruitment and fibrosis via suppression of FGF-9 production in the TGF-β1 exposed murine lung," *Frontiers in Pharmacology*, vol. 5, article 80, 2014.

[65] N. Murao, K.-I. Seino, T. Hayashi et al., "Treg-enriched CD4+ T cells attenuate collagen synthesis in keloid fibroblasts," *Experimental Dermatology*, vol. 23, no. 4, pp. 266–271, 2014.

[66] H.-H. Wang, T.-Y. Lee, and C.-Y. Lin, "Kinetics and involvement of interleukin-17 in the outcome of peritonitis in nondiabetic patients undergoing peritoneal dialysis," *Journal of the Chinese Medical Association*, vol. 74, no. 1, pp. 11–15, 2011.

[67] D. Maksić, M. Colić, V. Stanković-Popović, M. Radojević, and D. Bokonjić, "Systemic and intraperitoneal proinflammatory cytokines profiles in patients on chronic peritoneal dialysis," *Medicinski Pregled*, vol. 60, supplement 2, pp. 53–57, 2007.

[68] J. Loureiro, G. Gónzalez-Mateo, J. Jimenez-Heffernan, R. Selgas, M. López-Cabrera, and A. Aguilera Peralta, "Are the mesothelial-to-mesenchymal transition, sclerotic peritonitis syndromes, and encapsulating peritoneal sclerosis part of the same process?" *International Journal of Nephrology*, vol. 2013, Article ID 263285, 7 pages, 2013.

[69] M. Yáñez-Mó, E. Lara-Pezzi, R. Selgas et al., "Peritoneal dialysis and epithelial-to-mesenchymal transition of mesothelial cells," *The New England Journal of Medicine*, vol. 348, no. 5, pp. 403–413, 2003.

[70] X. Ji, J. Li, L. Xu et al., "IL4 and IL-17A provide a Th2/Th17-polarized inflammatory milieu in favor of TGF-β1 to induce bronchial epithelial-mesenchymal transition (EMT)," *International Journal of Clinical and Experimental Pathology*, vol. 6, no. 8, pp. 1481–1492, 2013.

[71] R. Rodrigues-Díez, L. S. Aroeira, M. Orejudo et al., "IL-17A is a novel player in dialysis-induced peritoneal damage," *Kidney International*, vol. 86, pp. 303–315, 2014.

[72] T. K. Hendrikx, E. A. F. J. Van Gurp, W. M. Mol et al., "End-stage renal failure and regulatory activities of CD4 +CD25bright+FoxP3+ T-cells," *Nephrology Dialysis Transplantation*, vol. 24, no. 6, pp. 1969–1978, 2009.

[73] P. Sandoval, J. Loureiro, G. González-Mateo et al., "PPAR-γ agonist rosiglitazone protects peritoneal membrane from dialysis fluid-induced damage," *Laboratory Investigation*, vol. 90, no. 10, pp. 1517–1532, 2010.

[74] A. Ueda, L. Zhou, and P. L. Stein, "Fyn promotes Th17 differentiation by regulating the kinetics of RORγt and Foxp3 expression," *Journal of Immunology*, vol. 188, no. 11, pp. 5247–5256, 2012.

[75] G. T. González-Mateo, V. Fernández-Míllara, T. Bellón et al., "Paricalcitol reduces peritoneal fibrosis in mice through the activation of regulatory T cells and reduction in IL-17 production," *PLoS ONE*, vol. 9, no. 10, Article ID e108477, 2014.

[76] A. Ikejiri, S. Nagai, N. Goda et al., "Dynamic regulation of Th17 differentiation by oxygen concentrations," *International Immunology*, vol. 24, no. 3, pp. 137–146, 2012.

[77] A. Aguilera, L. S. Aroeira, M. Ramírez-Huesca et al., "Effects of rapamycin on the epithelial-to-mesenchymal transition of human peritoneal mesothelial cells," *International Journal of Artificial Organs*, vol. 28, no. 2, pp. 164–169, 2005.

[78] S. G. Kim and W. H. Lee, "AMPK-dependent metabolic regulation by PPAR agonists," *PPAR Research*, vol. 2010, Article ID 549101, 10 pages, 2010.

[79] L. Klotz, S. Burgdorf, I. Dani et al., "The nuclear receptor PPARgamma selectively inhibits Th17 differentiation in a T cell-intrinsic fashion and suppresses CNS autoimmunity," *The Journal of Experimental Medicine*, vol. 206, no. 10, pp. 2079–2089, 2009.

[80] A. Aguilera, J. Loureiro, G. Gónzalez-Mateo, R. Selgas, and M. López-Cabrera, "The mesothelial to mesenchymal transition a pathogenic and therapeutic key for peritoneal membrane failure," in *The Latest in Peritoneal Dialysis*, chapter 2, InTech, 2013.

Immune-Regulatory Molecule CD69 Controls Peritoneal Fibrosis

Georgios Liappas,* Guadalupe Tirma González-Mateo,* Raquel Sánchez-Díaz,† Juan José Lazcano,† Sandra Lasarte,† Adela Matesanz-Marín,† Rafal Zur,‡ Evelina Ferrantelli,§ Laura García Ramírez,‖ Abelardo Aguilera,‖ Elena Fernández-Ruiz,‖ Robert H.J. Beelen,§ Rafael Selgas,¶ Francisco Sánchez-Madrid,†** Pilar Martín,† and Manuel López-Cabrera*

*Centro de Biología Molecular Severo Ochoa, Consejo Superior de Investigaciones Científicas Universidad Autónoma de Madrid, Madrid, Spain; †Signaling and Inflammation Program, Centro Nacional de Investigaciones Cardiovasculares, Madrid, Spain; ‡Department of Immunology and Oncology, Centro Nacional de Biotecnología Consejo Superior de Investigaciones Científicas, Madrid, Spain; §Department of Molecular Cell Biology and Immunology, Vrije Universiteit University Medical Center Vrije Universiteit Medisch Centrum, Amsterdam, The Netherlands; ‖Molecular Biology Unit and **Immunology Department, Hospital Universitario de la Princesa, Instituto de Investigación Sanitaria La Princesa, Madrid, Spain; and ¶Nephrology Department, Hospital Universitario La Paz, Instituto de Investigación Sanitaria La Paz, Madrid, Spain

ABSTRACT

Patients with ESRD undergoing peritoneal dialysis develop progressive peritoneal fibrosis, which may lead to technique failure. Recent data point to Th17-mediated inflammation as a key contributor in peritoneal damage. The leukocyte antigen CD69 modulates the setting and progression of autoimmune and inflammatory diseases by controlling the balance between Th17 and regulatory T cells (Tregs). However, the relevance of CD69 in tissue fibrosis remains largely unknown. Thus, we explored the role of CD69 in fibroproliferative responses using a mouse model of peritoneal fibrosis induced by dialysis fluid exposure under either normal or uremic status. We found that *cd69*$^{-/-}$ mice compared with wild-type (WT) mice showed enhanced fibrosis, mesothelial to mesenchymal transition, IL-17 production, and Th17 cell infiltration in response to dialysis fluid treatment. Uremia contributed partially to peritoneal inflammatory and fibrotic responses. Additionally, antibody–mediated CD69 blockade in WT mice mimicked the fibrotic response of *cd69*$^{-/-}$ mice. Finally, IL-17 blockade in *cd69*$^{-/-}$ mice decreased peritoneal fibrosis to the WT levels, and mixed bone marrow from *cd69*$^{-/-}$ and Rag2$^{-/-}{}_{\gamma}$c$^{-/-}$ mice transplanted into WT mice reproduced the severity of the response to dialysis fluid observed in *cd69*$^{-/-}$ mice, showing that CD69 exerts its regulatory function within the lymphocyte compartment. Overall, our results indicate that CD69 controls tissue fibrosis by regulating Th17-mediated inflammation.

J Am Soc Nephrol 27: 3561–3576, 2016. doi: 10.1681/ASN.2015080909

The peritoneum is a continuous membrane that lines the abdominal cavity and the organs located within this cavity.[1] Peritoneal membrane (PM) damage inflicted by mechanical trauma or other insults promotes an inflammatory response, which may lead to the development of fibrosis.[2,3] Extensive peritoneal fibrosis, such as that taking place in patients with encapsulating peritoneal sclerosis or postsurgical peritoneal adhesions, is a significant source for patient morbidity and mortality.[4,5]

Received August 18, 2015. Accepted March 7, 2016.

G.L., G.T.G.-M., and R.S.-D. contributed equally to this work.

Published online ahead of print. Publication date available at www.jasn.org.

Correspondence: Dr. Pilar Martín, Centro Nacional de Investigaciones Cardiovasculares (CNIC), Melchor Fernández Almagro 3, 28029 Madrid, Spain, or Dr. Manuel López-Cabrera, Centro de Biología Molecular Severo Ochoa, CSIC-UAM, C/Nicolás Cabrera number 1, Campus Cantoblanco, 28049 Madrid, Spain. Email: pmartinf@cnic.es or mlcabrera@cbm.csic.es

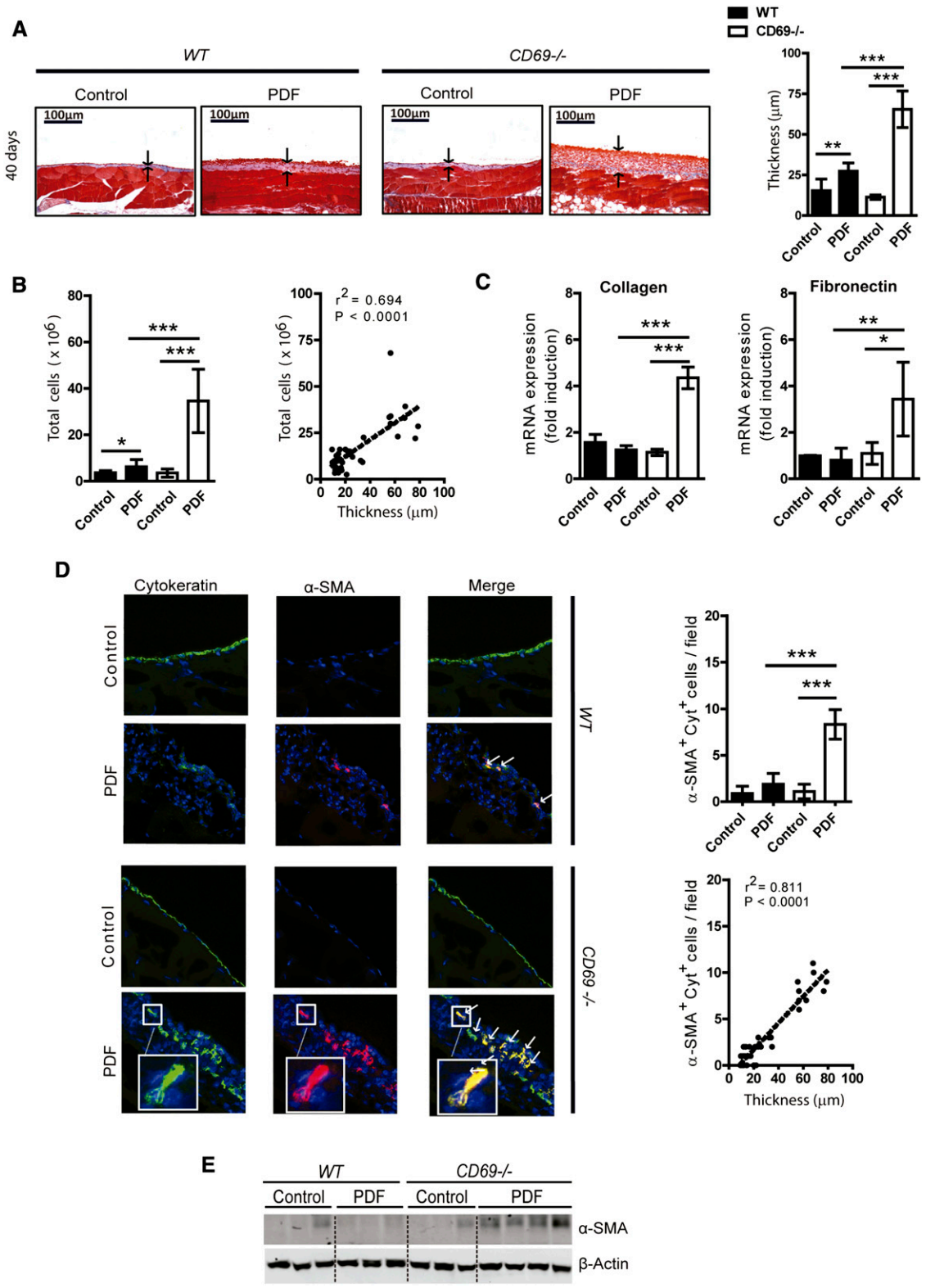

Figure 1. CD69 regulates fibrosis and MMT. (A) Representative images of fibrosis assessment by Masson Trichrome staining of PM sections from WT and *cd69*$^{-/-}$ mice treated for 40 days with PDF or saline as control. Thickness of PM, indicated with black arrows, was measured. Results are means±SDs ($n \geq 9$). Blue in the staining represents collagen depositions. Scale bars, 100 μm. (B) Quantification of total cells in peritoneal effluents from WT and *cd69*$^{-/-}$ mice treated as in A and correlation between total cell number and PM thickening (Spearman regression; $n \geq 9$). (C) Relative expression of collagen 1 and fibronectin mRNA in PM from WT and *cd69*$^{-/-}$ mice

Unfortunately, the precise mechanisms that contribute to the development of peritoneal fibroproliferative diseases are still poorly understood, hindering the development of efficient therapies.[2,6,7]

The study of peritoneal damage induced by the exposure to dialysis fluids has determined that mesothelial to mesenchymal transition (MMT) and inflammation establish a feedback loop. As a result of this feedback, the PM undergoes a remodeling with the accumulation of extracellular matrix.[3,8] Peritoneal dialysis (PD) is an RRT on the basis of the use of the PM as a semipermeable barrier across which ultrafiltration and diffusion take place.[3,9] Membrane failure is associated with structural alterations of the peritoneum, with fibrosis as the most constant feature of peritoneal deterioration. Myofibroblasts are the main responsible cells for peritoneal fibrosis, and they might have at least a dual origin from resident fibroblasts and mesothelial cells *via* MMT.[3,10,11] Peritoneal infections and the nonphysiologic nature of dialysis fluids induce chronic inflammation, which eventually leads to the development of fibrosis.[3,12,13] It has been suggested by some authors but not by others[14–16] that the uremic status of patients on PD may also affect the anatomy of the PM.

The immunologic mechanisms underlying PD–induced peritoneal fibrosis remain largely unknown. It has been recently shown that Th17– and more specifically, IL-17–mediated inflammatory response might play a central role in peritoneal damage.[17] In addition, it has been shown that pharmacologic treatments modulating Th17 response and/or enhancing regulatory T cell (Treg) response ameliorated peritoneal fibrosis and preserved membrane function.[18,19]

The antigen CD69 is a C–type lectin disulfide–linked homodimer that is rapidly expressed by most leukocytes *in vitro* on activation,[20,21] whereas *in vivo*, its expression is restricted to positively selected thymocytes, specific subsets of memory and Treg cells,[22,23] and leukocytes of chronic inflammatory infiltrates.[24,25] Studies using CD69-deficient models have shown that the absence of CD69 results in enhanced susceptibility to several inflammatory or autoimmune diseases.[26–30] These studies also indicate that CD69 contributes to the resolution of inflammation by regulating the balance between Th17 and Tregs.[31,32] The cytoplasmic tail of CD69 interacts with and activates the Jak3-Stat5 pathway, inhibiting the Stat3–dependent ROR(γ)t activation and therefore, modulating Th17 development and function.[30] Recently, a novel FoxP3$^+$CD69$^+$Treg subset, capable of maintaining immune homeostasis and providing protection from developing inflammation, has been identified.[33] Thus, CD69 might determine the outcome of immune responses by both limiting Th17 responses and regulating the function of Treg subset.

Given that CD69 controls the inflammatory response, we assessed whether CD69 acts as a regulator of fibrotic processes during peritoneal damage. In this study, we used an established animal model of peritoneal fibrosis in CD69-deficient mice. Our findings show that the expression of CD69 in the lymphoid compartment limits peritoneal fibrosis through modulation of the Th17-mediated inflammation.

RESULTS

CD69-Deficient Mice Develop an Exacerbated PD Fluid–Induced Fibroproliferative Response

To assess the role of CD69 in fibrosis, we have studied the peritoneal fibroproliferative response of C57BL/6 wild–type (WT) and *cd69*$^{-/-}$ mice in a model of peritoneal dialysis fluid (PDF) exposure at various time intervals (10, 20, and 40 days). This model elicits a moderate fibrotic response in C57BL/6 mice.[34,35] Analysis at day 10 showed no significant difference between the groups in terms of fibrosis and leukocyte infiltration (data not shown). After 20 days, there was a significant increase in PM thickness, and infiltrating cells were only in *cd69*$^{-/-}$ mice exposed to PDF compared with mice exposed to saline (Supplemental Figure 1). PM fibrosis and inflammatory infiltrate further increased in *cd69*$^{-/-}$ mice treated with PDF for 40 days, whereas in WT mice, thickness and infiltrate augmented only slightly but reached significant values at this time point (Figure 1, A and B). There was a strong correlation between peritoneal thickness and the number of infiltrating cells (Figure 1B). These data were verified by the detection of high levels of the major extracellular matrix components collagen 1 and fibronectin measured by quantitative PCR (qPCR) in peritoneal tissues from *cd69*$^{-/-}$ compared with WT mice exposed to PDF (Figure 1C). In the control groups, we did not detect α–smooth muscle actin (α-SMA) in the PM, and cytokeratin staining was confined to the preserved mesothelial cell monolayer (Figure 1D). In contrast, a greater accumulation of α-SMA fibroblasts was observed in the submesothelial compact region of *cd69*$^{-/-}$ compared with WT mice treated with PDF. A significant proportion of the myofibroblasts coexpressed cytokeratin, indicating that they were derived from local conversion of mesothelial cells (MMT) (Figure 1D). There was a strong correlation between peritoneal thickness

treated as in A. Data are means±SDs (n=3). (D) Representative images of immunofluorescence analysis of PM sections from WT and *cd69*$^{-/-}$ mice treated as in A, stained with antibodies to cytokeratin (green) or α-SMA (red), and counterstained with 4,6-diamidino-2-phenylindole (blue). Quantification of double-positive (α-SMA$^+$ Cyt$^+$) cells (yellow; indicated with arrows) was performed; 10 fields per mouse were usually scored. Data show means±SDs (n=9). Correlation between α-SMA$^+$ Cyt$^+$ cell counts and PM thickness was evaluated (Spearman regression; n=9). Magnification, ×200. (A–D) Differences were considered statistically significant for $P<0.05$ using one-way ANOVA. *$P<0.05$; **$P<0.01$; ***$P<0.001$. (E) Total protein extracts of PM from WT or *cd69*$^{-/-}$ mice ($n\geq3$) treated as in A were immunoblotted with antibodies to α-SMA and β-actin as loading control.

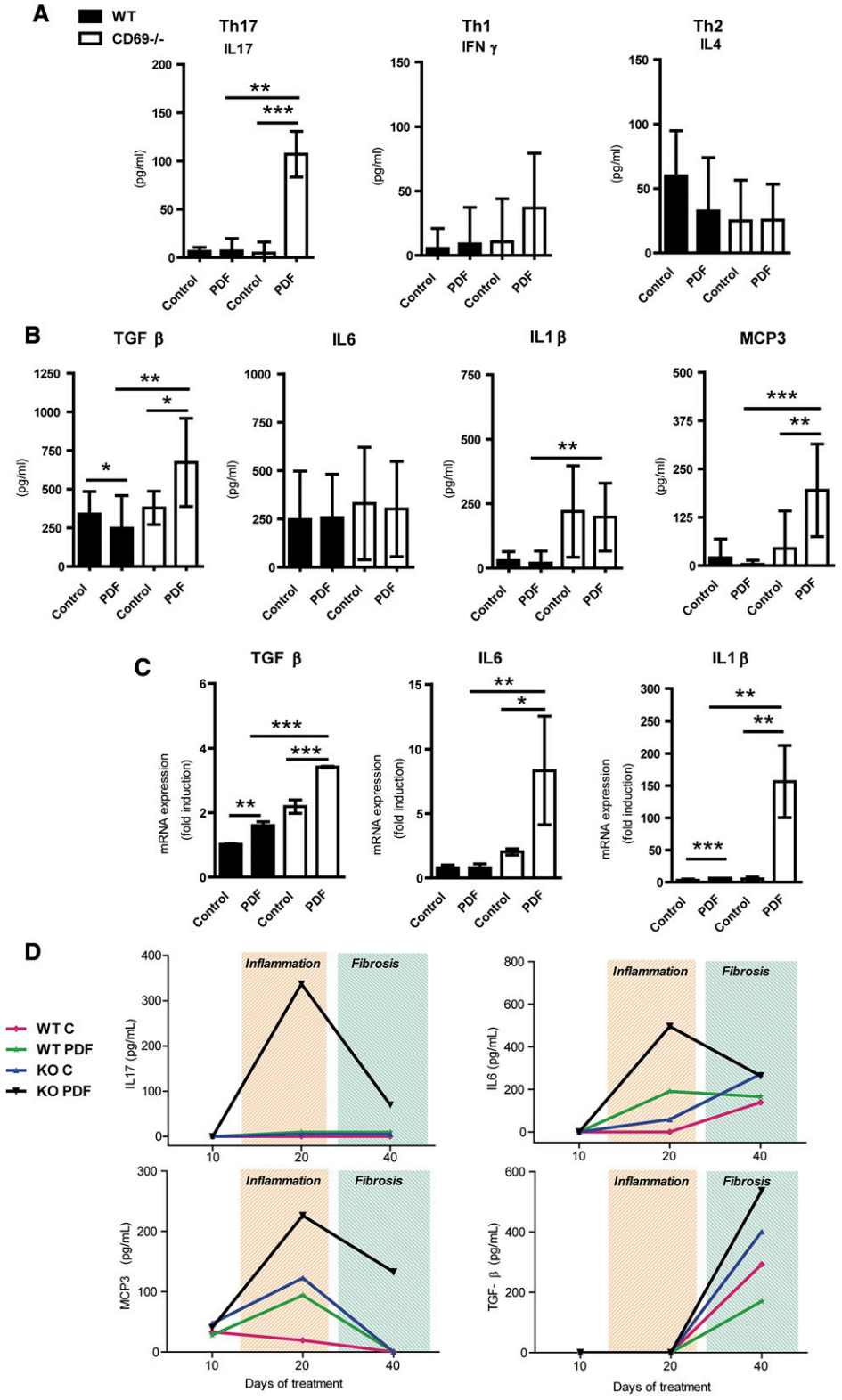

Figure 2. CD69 deficiency induces proinflammatory and profibrotic cytokine production in the peritoneum. (A) Concentration of the main cytokines released by Th17, Th1, and Th2 cells (IL-17, IFN-γ, and IL-4, respectively) was measured in the peritoneal effluents from WT and *cd69*$^{-/-}$ mice treated for 40 days with PDF or saline as control ($n \geq 8$). (B) Concentration of proinflammatory cytokines TGF-β, IL-6, IL-1β, and MCP3 as in A. (C) Relative mRNA expression of TGF-β, IL-6, and IL-1β was assessed by qPCR ($n \geq 3$) in PM tissue from WT and *cd69*$^{-/-}$ mice treated as in A. In A–C, data are means±SDs. *P* values <0.05 were considered statistically significant using one-

and the number of double-positive fibroblasts (Figure 1D). These data were confirmed by the analysis of α–SMA protein levels from peritoneal samples (Figure 1E). These results indicate that the inflammation/MMT axis drives the fibrotic process of the PM after PDF exposure and that this process is deregulated in *cd69*$^{-/-}$ mice.

CD69-Deficient Mice Show Enhanced Proinflammatory Milieu on PDF Exposure

At 40 days after PD treatment, the levels of IL-17 were greatly enhanced in the effluent of *cd69*$^{-/-}$ mice, whereas IFN-γ and IL-4 levels did not show any significant differences between groups (Figure 2A). Analysis of cytokines controlling Th17 differentiation revealed that TGF-β increased significantly in PDF–treated *cd69*$^{-/-}$ mice, whereas IL-6 did not show differences among groups, and IL-1β was increased in the effluent of both saline– and PDF–treated *cd69*$^{-/-}$ mice. MCP-3 expression was also increased in the effluents of PDF–exposed *cd69*$^{-/-}$ mice (Figure 2B). Interestingly, TGF-β, IL-6, and IL-1β cytokine–encoding transcripts from peritoneal tissue were significantly increased in PDF–treated *cd69*$^{-/-}$ mice compared with the WT (Figure 2C). These data indicated that TGF-β, but not IL-6 and IL-1β, was mostly locally produced.

Analysis of the effluents 20 days after PDF exposure showed a strong increase of the proinflammatory cytokines IL-17 and IL-6 in *cd69*$^{-/-}$ mice compared with WT mice (Supplemental Figure 2A). There was also increased expression of the chemokines GM-CSF; MIP1α; MIP1β; regulated upon activation, normal T cell expressed and secreted; and MCP-3 in PDF–treated *cd69*$^{-/-}$ mice (Supplemental Figure 2B). Comparison of the expression levels of these molecules at different time intervals showed that the inflammatory mediators (*e.g.*, IL-17, IL-6, and MCP-3) tended to peak at 20 days, whereas the profibrotic cytokine TGF-β was upregulated at 40 days (Figure 2D).

Analysis of the infiltrating cells in effluent and peritoneal tissue at 40 days showed that PDF exposure induced recruitment of CD4$^+$ and CD8$^+$ T lymphocytes in WT mice and to a greater extent, *cd69*$^{-/-}$ mice (Figure 3A, Supplemental Table 1). Quantification of the T helper subsets in the effluents revealed an increase in Th17 in PDF–treated WT mice that was exacerbated in *cd69*$^{-/-}$ mice (Figure 3B). Consistent with our previous results,[30] the Stat3 signaling pathway, involved in Th17 differentiation,[36] was enhanced in *cd69*$^{-/-}$ mice exposed to PDF, because protein levels were increased compared with the WT (Figure 3C). Moreover, 40 days after PD treatment, there was a small but significant increase in the number of CD4$^+$/FoxP3$^+$ (Treg) cells in *cd69*$^{-/-}$, and this increase was much lower compared with the total number of Th17 cells (Figure 3D). This resulted in an increased Th17-to-Treg ratio in WT and *cd69*$^{-/-}$ mice exposed to PDF. This ratio was higher in the *cd69*$^{-/-}$ mice (Figure 3D). The presence of an inflammatory response in PDF–treated *cd69*$^{-/-}$ mice was further substantiated by the strong recruitment of neutrophils and monocytes into the abdominal cavity and the peritoneal tissue (Figure 3E, Supplemental Table 1). Similar results were obtained in *cd69*$^{-/-}$ mice after 20 days of PD treatment (Supplemental Figure 3).

CD69 Controls Fibrosis under Uremic Conditions

We generated WT and *cd69*$^{-/-}$ uremic Foxp3-mRFP/IL-17A-eGFP mice (Figure 4A), which were treated with saline or PDF for 40 days. At the end of the study, a significant increase in PM thickness was observed in both WT and *cd69*$^{-/-}$ mice exposed to PDF compared with mice exposed to saline, and again, the fibrosis was exacerbated in *cd69*$^{-/-}$ mice (Figure 4B). The infiltrate increased in WT and *cd69*$^{-/-}$ mice exposed to PDF, but it reached statistical significance only in the *cd69*$^{-/-}$ group (Figure 4C). These data were confirmed by the detection of high levels of collagen 1 and fibronectin mRNAs as well as TGF-β–, IL-6–, and IL-1β–encoding transcripts in peritoneal tissues from *cd69*$^{-/-}$ compared with WT mice exposed to PDF (Figure 4, D and E). The level of IL-17 in the effluent was significantly increased in *cd69*$^{-/-}$ mice exposed to PDF, but in these uremic mice, the concentration of IL-17 was much lower than that in nonuremic mice at the same time point of treatment. IFN-γ and IL-4 levels did not show any significant differences between groups (Supplemental Figure 4). PDF induced recruitment of CD4$^+$ and CD8$^+$ T lymphocytes to similar extents in WT and *cd69*$^{-/-}$ mice (Supplemental Figure 5A). Th17 showed an increase in both PDF–treated WT and *cd69*$^{-/-}$ mice, but the number of Th17 was significantly higher in *cd69*$^{-/-}$ mice (Supplemental Figure 5B). The number of Tregs also increased in WT and *cd69*$^{-/-}$ mice treated with PDF, reaching statistical significance only in the *cd69*$^{-/-}$ group (Supplemental Figure 5B). Similarly, the increase of the Th17-to-Treg ratio reached statistical significance only in *cd69*$^{-/-}$ mice (Supplemental Figure 5B). The recruitment of monocytes and neutrophils was induced by PDF exposure to a similar extent in WT and *cd69*$^{-/-}$ mice (Supplemental Figure 5C). It was noteworthy that the number of cells in the infiltrates was generally smaller in nephrectomized than in nonuremic *cd69*$^{-/-}$ mice exposed to PDF, whereas the thickness was similar in both uremic and nonuremic *cd69*$^{-/-}$ mice. In contrast, uremic WT mice exposed to PDF showed increased fibrosis and infiltrate cell number compared with nonuremic WT mice. These data suggested that uremia accelerated the inflammatory process and that the

way ANOVA. *$P<0.05$; **$P<0.01$; ***$P<0.001$. (D) Time course analysis of the production of IL-17, IL-6, MCP3, and TGF-β in the peritoneal effluents from WT and *cd69*$^{-/-}$ mice (KO) treated for 10, 20, and 40 days with PDF or saline as control. Colored columns highlight whether a cytokine is important for either the initiation of inflammation or fibrosis.

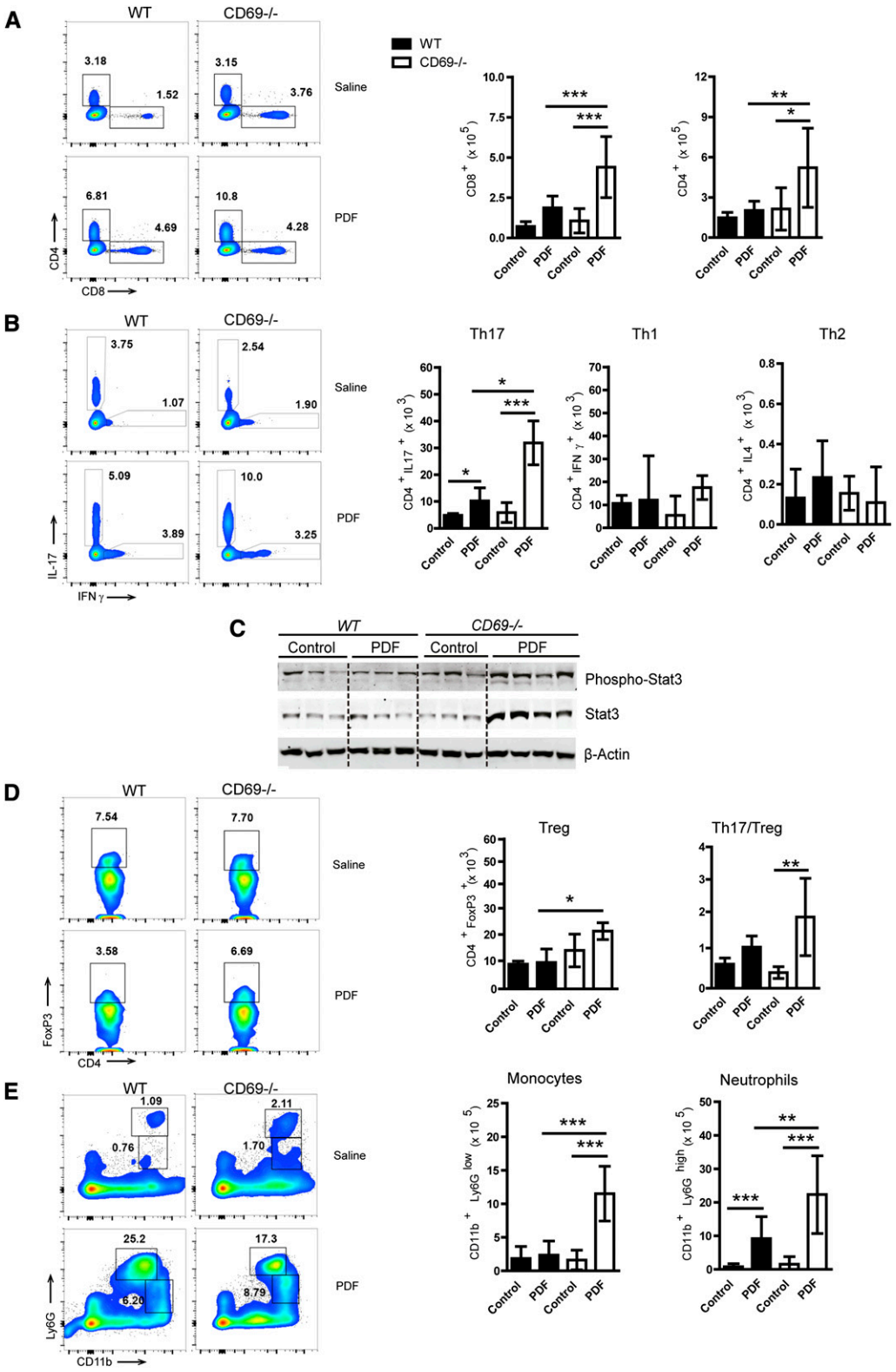

Figure 3. CD69 deficiency enhances the peritoneal recruitment of Th17 cells. (A) Quantitative analysis of $CD8^+$ and $CD4^+$ cells recruited to the peritoneal cavity of WT and *cd69*$^{-/-}$ mice in response to a 40-day treatment with PDF by flow cytometry. Representative density plot is shown with highlighted percentages of the corresponding lymphocytes. Total numbers of $CD8^+$ and $CD4^+$ cells in the peritoneal effluents, shown in the graphs, were calculated according to the flow cytometry results and total cell count in the same mouse. Data are means±SDs ($n \geq 6$). (B) Density plot of flow cytometry analysis of $CD4^+IL\text{-}17^+$ (Th17) and $CD4^+IFN\text{-}\gamma^+$ (Th1) cells. Numbers in quadrants

inflammation curve was in its decline phase in *cd69*$^{-/-}$ but not in WT mice exposed to PDF. Taken together, our results indicated that uremia contributed slightly to the final outcome of peritoneal alteration, confirming the regulatory role of CD69 in those processes.

Blockade of CD69 Mimics the Exacerbated Response of cd69$^{-/-}$ Mice to PD Fluid

To further show the relevance of CD69 in limiting peritoneal fibrosis, PDF–exposed WT mice were intraperitoneally injected with a neutralizing anti–CD69 antibody (mAb-2.2) or a mouse IgG1 isotype–matched control (mAb-2.8). PDF–exposed *cd69*$^{-/-}$ mice treated with mAb-2.2 served as positive control. WT mice treated with anti-CD69 exhibited increased peritoneal fibrosis in response to PDF exposure compared with WT mice treated with the control antibody and similar to *cd69*$^{-/-}$ treated with anti-CD69 mAb (Figure 5A). Quantification of the CD4$^+$ lymphocytes showed a clear increase, although it did not reach statistical significance (P=0.06), in Th17 but not in Th1 or Th2 in anti–CD69-treated WT and *cd69*$^{-/-}$ mice exposed to PDF (Figure 5B). Again, after PDF exposure, there was a significant increase in the number of Tregs in *cd69*$^{-/-}$ mice treated with anti-CD69 antibody (Figure 5C), but this increase was not observed in WT mice (Figure 5C). The enhanced inflammatory response in PDF-exposed mice treated with anti-CD69 was supported by a stronger recruitment of neutrophils and monocytes (Figure 5D). There was a strong correlation between thickness and the number of infiltrating Th17 cells (r=0.64; P=0.03), reinforcing the concept that Th17-mediated inflammation drives peritoneal fibrosis.

IL-17 Mediates the Exacerbated Response of cd69$^{-/-}$ Mice to PD Fluid

To show that IL-17 mediated the exacerbated inflammatory and fibrotic responses to PDF in *cd69*$^{-/-}$ mice, they were intraperitoneally injected with anti–IL-17 neutralizing mAb or a rat IgG2A isotype–matched control; *cd69*$^{-/-}$ mice treated with anti–IL-17 presented less peritoneal fibrosis in response to PDF compared with *cd69*$^{-/-}$ mice treated with the control antibody (Figure 6A).

An analysis of CD4$^+$ lymphocytes subpopulations showed a significant reduction in Th17 but not in Th1 or Th2 in anti–IL-17–treated *cd69*$^{-/-}$ mice exposed to PDF (Figure 6B). PDF–exposed *cd69*$^{-/-}$ mice treated with blocking anti–IL-17 antibody did not show a significant decrease of CD4$^+$/FoxP3$^+$ (Treg) cells (Figure 6C). However, the Th17-to-Treg ratio was reduced in *cd69*$^{-/-}$ mice treated with anti–IL-17 compared with mice treated with the control antibody (Figure 6D). Treatment with anti–IL-17 abrogated the expression of IL-17 in PDF–exposed *cd69*$^{-/-}$ mice (Figure 6E). The decreased inflammatory response in PDF–exposed *cd69*$^{-/-}$ mice treated with anti–IL-17 was shown by a reduction in neutrophil and monocyte recruitment (Figure 6F). These results strongly suggested that CD69 modulated the Th17–mediated inflammatory response in the peritoneal cavity and negatively regulated peritoneal fibrosis induced by PDF exposure.

CD69 within the Lymphocyte Compartment Regulates Fibrosis

WT and *cd69*$^{-/-}$ mice were reconstituted with mixed bone marrow (BM) cells from Rag2$^{-/-}{}_\gamma$c$^{-/-}$ and CD69$^{-/-}$ or Rag2$^{-/-}{}_\gamma$c$^{-/-}$ and WT cells in a proportion of 3:1, respectively. The myeloid cell subset of the chimeric mice belongs to the Rag2$^{-/-}{}_\gamma$c$^{-/-}$ double mutants, whereas the lymphocytic compartment belongs to WT or *cd69*$^{-/-}$ donors as shown by CD69 expression on the CD4$^+$ T cell subset (Figure 7A). WT or *cd69*$^{-/-}$ mice reconstituted with Rag2$^{-/-}{}_\gamma$c$^{-/-}$ and WT or CD69 KO BM cells had similar proportions of lymphocyte subpopulations (Supplemental Figure 6). Mice reconstituted with a mixture of BM cells from Rag2$^{-/-}{}_\gamma$c$^{-/-}$ and *cd69*$^{-/-}$ had greater PDF–induced peritoneal fibrosis than mice reconstituted with Rag2$^{-/-}{}_\gamma$c$^{-/-}$ and WT BM cells (Figure 7B), indicating that the expression of CD69 within the lymphocytes was critical to controlling the fibroproliferative response after PD treatment.

An analysis of the T helper subpopulations revealed a significant increase in Th17 but not in Th1 or Th2 cells in mice reconstituted with Rag2$^{-/-}{}_\gamma$c$^{-/-}$ and *cd69*$^{-/-}$ BM cells compared with mice reconstituted with Rag2$^{-/-}{}_\gamma$c$^{-/-}$ and WT BM cells on exposure to PDF (Figure 7C). Therefore, these data unequivocally show that CD69 expression within the lymphocyte compartment controls the Th17 response and the development of fibrosis in the peritoneum after PD treatment.

DISCUSSION

The pathophysiologic role of CD69 in fibroproliferative diseases had not been explored so far. By using complementary

indicate percentages of the corresponding cells. Total numbers of CD4$^+$IL-17$^+$ (Th17), CD4$^+$IFN-γ^+ (Th1), and CD4$^+$IL-4$^+$ (Th2) cells collected from the peritoneal cavity were quantified. Data are means±SDs (n≥6). (C) Immunoblotting analysis of total and phosphorylated Stat3 in total protein lysates of PM from WT and *cd69*$^{-/-}$ treated or not with PDF for 40 days (n≥3). β-Actin was used as loading control. (D) Density plot of flow cytometry analysis of CD4$^+$FoxP3$^+$ (Tregs) and their total quantification are shown. Th17-to-Treg ratio is shown. Data are means±SDs (n≥6). (E) Density plot of flow cytometry analysis of CD11b$^+$Ly6G^{low} (monocytes) and CD11b$^+$Ly6G^{high} (neutrophils) and their quantification are shown (n≥6). P values <0.05 were considered statistically significant using one-way ANOVA. *P<0.05; **P<0.01; ***P<0.001.

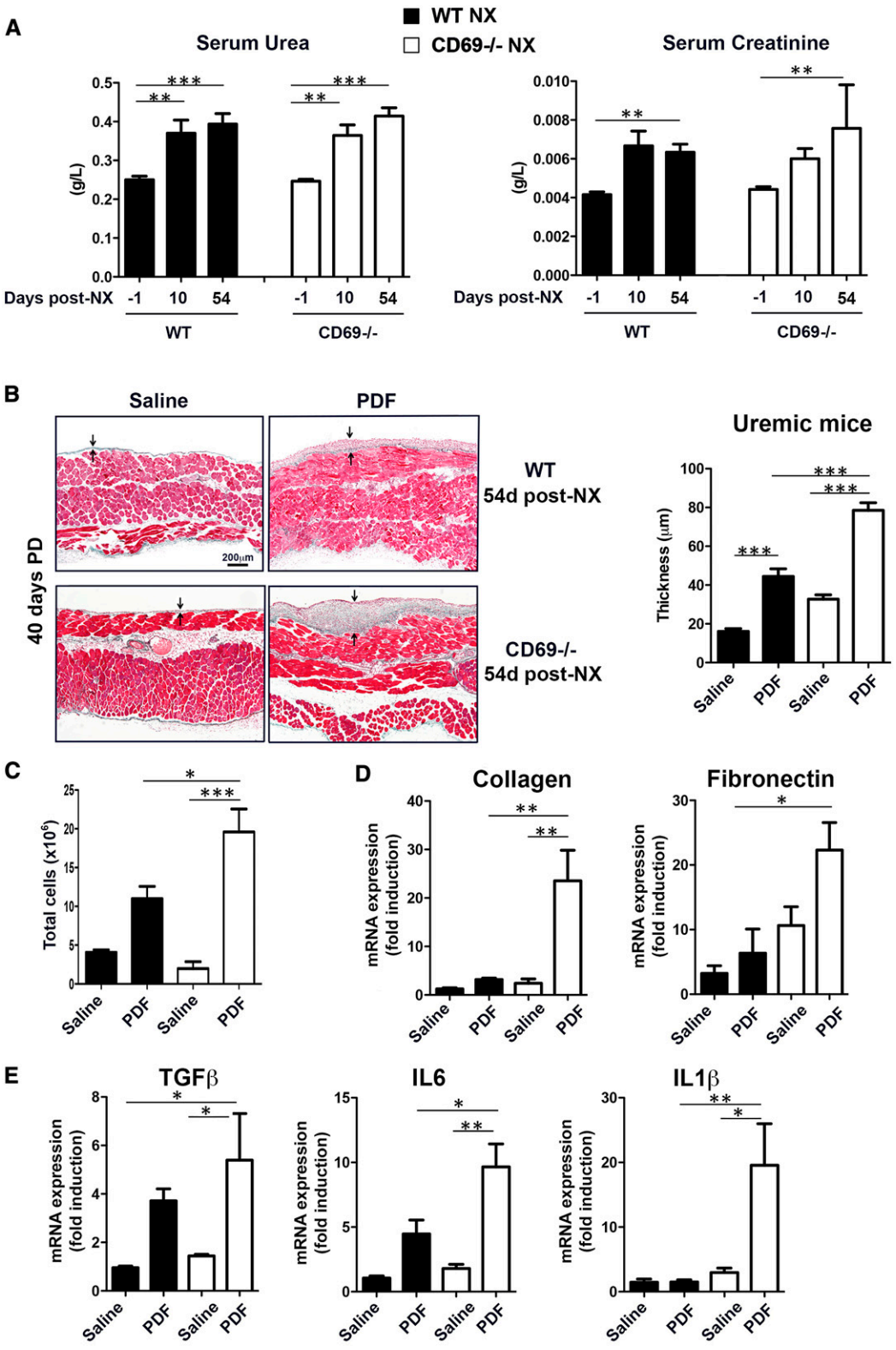

Figure 4. CD69 regulates fibrosis in mice with abnormal renal function. WT and cd69$^{-/-}$ mice undergo 5/6 nephrectomy before treatment with saline or PDF for a period of 40 days. (A) Serum levels of urea and creatinine were measured before and 10 and 54 days after 5/6 nephrectomy in groups throughout the treatment with saline or PDF. (B) Fibrosis assessment by Masson Trichrome staining in CD69$^{-/-}$ and WT mice 54 days postnephrectomy. Arrows indicate thickness of the PM. Right panel shows quantification of peritoneal fibrosis in uremic mice ($n \geq 10$). (C) Total cell counts of the peritoneal effluent in each group of mice. Fibrosis and inflammation in

experimental approaches in WT and *cd69*$^{-/-}$ mice as well as BM transplantation and *in vivo* blocking experiments, our results strongly indicate that CD69 modulates peritoneal fibrosis, at least in part, through regulation of the Th17/Treg balance. We also show that uremia contributes modestly to fibroproliferative response of the peritoneum and that CD69 also modulates the inflammation under the uremic status. Despite the findings in animal models,[37,38] the effect of uremia itself on the peritoneum in humans is controversial.[14–16] The possible contribution of uremia to the alteration of the PM anatomy and its transport characteristics is still a matter of debate.

The Th17 lineage has gained broad acceptance as a key mediator of various inflammatory and autoimmune pathologies.[39–44] Tregs are suppressors of activated T cell expansion and considered key regulators of adaptive immunity that mediates self-tolerance.[45] Recent evidence indicates that Th17 lineage and Tregs are developmentally related.[46] In addition, it was shown that plasticity between these two lineages as well as the pathogenic conversion of Tregs into Th17 cells occurred in autoimmune arthritis.[47] Our data show that CD69 deficiency or CD69 blockade results in exacerbated peritoneal fibrosis in response to PDF. This result correlates with enhanced inflammatory infiltrate and local hyperactivation of the Th17 cells. In contrast, Th1- or Th2-mediated responses seem to have little, if any, relevance in PD-induced fibrosis. The enhanced peritoneal fibrosis in *cd69*$^{-/-}$ mice is associated with an increase in the Th17-to-Tregs ratio, which is caused by augmented Th17 cells rather than a decrease of Tregs. Even more important than the relative proportion of Tregs is their functional stage. It has been described that the expression of CD69 on Tregs is required for the correct function of these cells in immune homeostasis and the modulation of inflammation.[33] Thus, it can be speculated that CD69 controls peritoneal fibrosis by limiting Th17 responses and regulating the function of Tregs.

Our results show that the peritoneal changes induced by PDF exposure are not only exacerbated in magnitude but also, accelerated over time intervals in *cd69*$^{-/-}$ mice and that inflammation precedes the fibrotic process. One of the most remarkable characteristics during peritoneal fibrosis is the progressive accumulation of myofibroblasts. Here, we show that the accumulation of myofibroblasts is greater in *cd69*$^{-/-}$ than in WT mice on PDF treatment. A significant proportion of these myofibroblasts derive from mesothelial cells *via* MMT. Recently, the concept of MMT as a key process in peritoneal fibrosis has been challenged by a lineage-tracing study.[11] However, another lineage tracing–based study confirmed the mesothelial origin of a subpopulation of peritoneal fibroblasts.[48] Thus, the role of MMT in peritoneal fibrosis is still a matter of debate and will require additional studies.[49] Independent of the precise origin of the myofibroblasts, our results clearly indicate that inflammation drives the fibrotic process of the PM after PDF exposure and that this process is deregulated in cd69$^{-/-}$ mice.

We have observed that TGF-β is strongly upregulated in the peritoneal cavity of *cd69*$^{-/-}$ mice exposed to PDF. This cytokine plays a central role in the differentiation of Th17 and Treg lineages, because it causes uncommitted progenitors to pass through an intermediate stage.[50] Exposure to TGF-β alone skews precursors toward the Treg lineage, whereas the combination of TGF-β and IL-6 causes progenitors to adopt a Th17 signature.[46] We have observed that IL-6 was rapidly induced at 20 days in the peritoneal cavity of *cd69*$^{-/-}$ mice exposed to PDF, and it remained high at 40 days. These data might explain the strong local polarization toward Th17 differentiation in response to PDF exposure.

In conclusion, our findings show that CD69 modulates Th17–mediated inflammatory responses and negatively regulates peritoneal fibrosis. These data improve our understanding of fibrotic processes and might help in the design of new therapeutic approaches in preventing fibroproliferative-associated diseases.

CONCISE METHODS

Mice

The *cd69*$^{-/-}$ mice were generated in the 129/Sv background as described[51] and backcrossed onto C57BL/6 for at least 12 generations. *cd69*$^{-/-}$ and wild type mice used for experiments were 8-12-week old females, and were either littermates or age-matched offspring of littermates in the C57BL/6 background. Double reporter mice (BL6 background) expressing Foxp3-mRFP (monomeric red fluorescence protein inserted in the *foxp3* locus) and IL-17A-eGFP (enhanced green fluorescent protein (eGFP) inserted in the *Il17a* locus), were kindly provided by Dr. R. Flavell. We generated *cd69*$^{-/-}$/Foxp3-mRFP/IL-17A-eGFP mice after backcrossing double reporter with C57/BL6 *cd69*$^{-/-}$ mice. Rag2$^{-/-}{}_{\gamma}$c$^{-/-}$ double–KO mice were provided by Dr. M.L. Toribio. Animals were housed and used in specific pathogen–free conditions at the CNIC animal facility. All animal procedures were approved by the ethics committee of the Comunidad Autónoma de Madrid and conducted in accordance with the institutional guidelines that comply with the *Directive of the European Parliament and of the Council on the Protection of Animals Used for Scientific Purposes*.[52]

peritoneal tissue from uremic WT and CD69$^{-/-}$ mice were assessed by qPCR analysis of (D) collagen 1 and fibronectin and (E) proinflammatory cytokines, respectively. Bars are means±SDs ($n \geq 6$). P values <0.05 were considered statistically significant using one–way ANOVA test, and Bonferroni post-tests were used to compare selected pairs of means and all pairs of means, respectively. NX, nephrectomy. *$P<0.05$; **$P<0.01$; ***$P<0.001$.

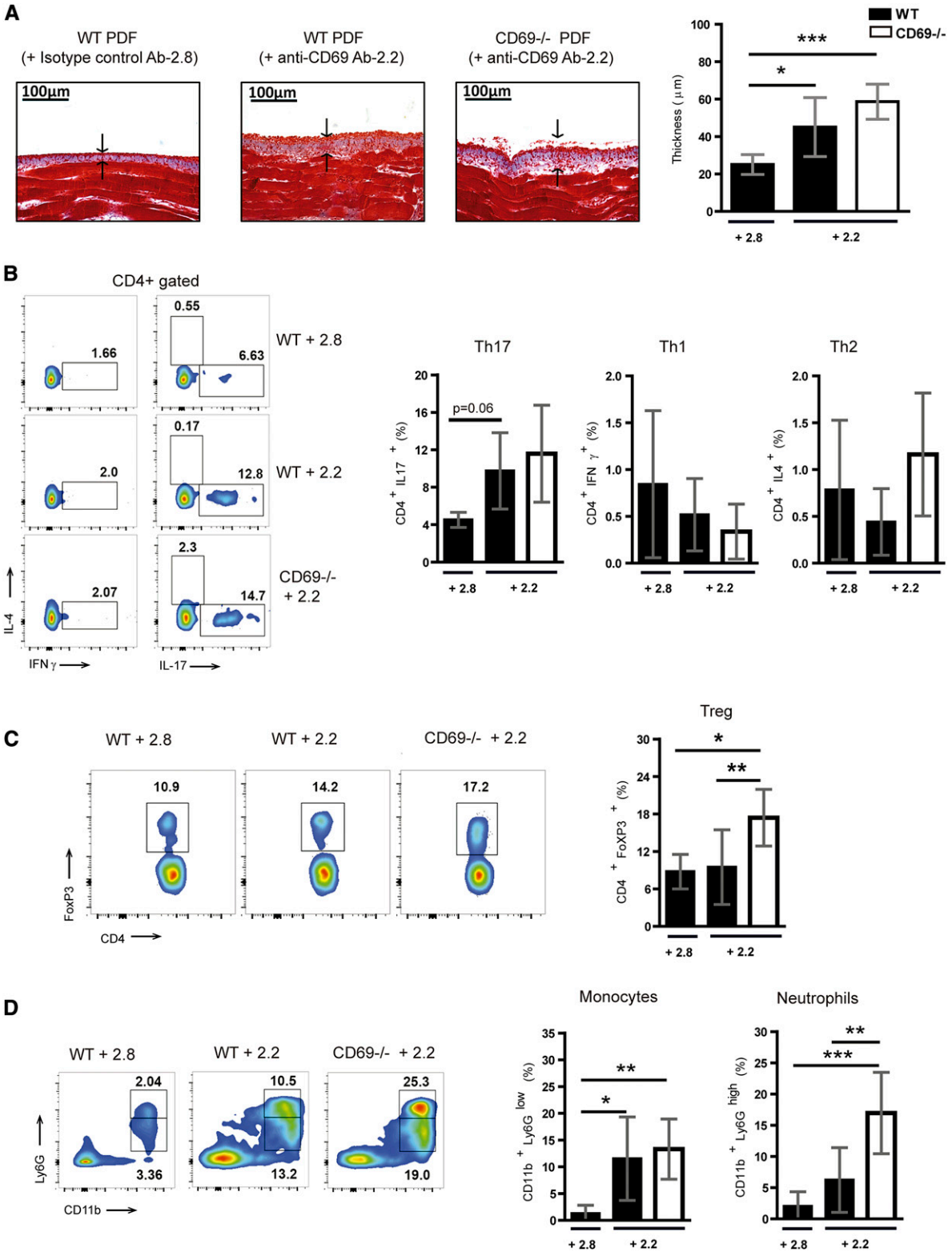

Figure 5. CD69 blockade in WT mice reproduces the CD69$^{-/-}$ phenotype. WT and *cd69*$^{-/-}$ mice were subject to a 40-day PDF treatment combined with either anti-CD69 antibody (Ab-2.2 or +2.2) treatment (in the case of both genotypes) or isotype control antibody (Ab-2.8 or +2.8) treatment as control (in the case of WT alone). The antibody was applied every 5 days (100 μg per mouse). (A) Representative pictures of Masson Trichrome staining of PM sections from the three groups. The PM thickness, indicated with arrows, was quantified. Data are means±SDs ($n \geq 5$). Scale bars, 100 μm. (B and C) Representative density plots of flow cytometry analysis and

Animal Surgeries and PDF Treatment

Catheter implantation was performed as described elsewhere.[53] We used four groups of mice throughout the project. The control WT and cd69$^{-/-}$ groups received 2 ml physiologic saline (n=10 per group) *via* a catheter. In addition, the treated WT and cd69$^{-/-}$ groups received 2 ml standard PDF (PDF-4; 25% glucose; pH 5.5; Stay Safe; Fresenius Medical Care) daily through the catheter (n=10 per group). The mice were treated for various time intervals (10, 20, and 40 days). To study the mechanism of the CD69 receptor in tissue fibrosis, we performed a comparison between the WT and cd69$^{-/-}$ PDF groups. The experiment was repeated a minimum of two times.

To make mice uremic, 5/6 nephrectomy was performed under isoflurane anesthesia (4% for induction and 2%–3% for maintenance); 0.05–0.1 mg/kg buprenorphine (Temgesic) was injected intramuscularly 15–30 minutes preoperatively, and eye drops were given. The animal was shaved in the abdomen, and it was placed on a heating pad. A ventral midline incision was made through the skin followed by an incision along the linea alba. Through the laparotomy, the left kidney was released from its capsule by using surgical forceps and wet cotton swabs. At this point, the kidney could be easily positioned on top of the peritoneum and was placed on a wound pad. The anterior one third and posterior one third parts of the kidney were impaired by using a monopolar electric blade. The remaining functional one third of the left kidney is placed back into its original position in the abdominal cavity. Following the same procedure, the right kidney was also removed from the abdominal cavity and released from the capsule. A total ligation with insoluble suture was applied that included the kidney vein, artery, and urethra. After the ligation, the right kidney was totally removed from the body. A volume of 200 μl blood was drawn *via* facial vein puncture at day −1 and at days 10 and 54 postnephrectomy (end point). At all of the time points, serum samples were analyzed for urea and creatinine levels. Measurements were performed by using the Dimension RxL Max Integrated Chemistry System.

BM Chimera Mice

WT and *cd69*$^{-/-}$ females, which were 10–12 weeks old, were lethally γ-irradiated with two doses of 6.5 Gy and intravenously administered a mixture of 4×10^6 BM cells from Rag2$^{-/-}{}_{\gamma}$c$^{-/-}$ and *cd69*$^{-/-}$ or Rag2$^{-/-}{}_{\gamma}$c$^{-/-}$ and WT cells in a proportion of 3:1, respectively. The Rag2$^{-/-}{}_{\gamma}$c$^{-/-}$ double–mutant mice are completely alymphoid (they lack T, B, and NK subsets), which gives specificity to our assay: the myeloid cell subset will belong to the Rag2$^{-/-}{}_{\gamma}$c$^{-/-}$ double mutants, whereas the lymphocyte compartment will belong only to WT or *cd69*$^{-/-}$ donors. Reconstitution of the immune system by the donors was analyzed 6 weeks after the BM transplant, and reconstituted mice were subsequently analyzed 40 days after PD treatment.

Anti–IL-17 Administration and Neutralization

PD–instilled *cd69*$^{-/-}$ mice were treated with a neutralizing antibody against IL-17A or its corresponding control (mouse IgG1-K Isotype). Anti–IL-17A antibody (100 μg per mouse; eBioscience, San Diego, CA) was instilled in the peritoneal cavity *via* a catheter every 5 days for a total period of 40 days. A control group was created by treating PDF–instilled *cd69*$^{-/-}$ mice with mouse IgG1-K Isotype (eBioscience) at the same concentration.

Anti-CD69 Administration and Neutralization

Murine mAb-2.2 antibody (IgG1-K), specific for mouse CD69, was generated as previously described.[54,55] It was purified from concentrated supernatants obtained in an INTEGRA CL 350 Flask (Integra Biosciences AG) using a protein G column (Pharmacia Biotech). Purified antibody was dialyzed extensively against PBS, tested for endotoxin (levels were <0.1 ng/ml), and stored at −20°C. PDF–treated WT mice were treated with a neutralizing antibody mAb-2.2 against CD69. mAb-2.2 can completely block CD69 receptors in all mouse compartments. mAb-2.2 (100 μg per mouse) was instilled in the peritoneal cavity through a catheter every 5 days for a total of 40 days. As control groups, WT PDF–instilled mice were treated with a mouse mAb-2.8 isotype, and *cd69*$^{-/-}$ PDF mice were treated with neutralizing antibody mAb-2.2.

FACS Analyses

Cell suspensions obtained from peritoneal lavage and membranes were stained with fluorochrome–conjugated mouse–specific antibodies against CD3, CD45, CD4, CD8α, B220, CD11c, CD11b, Ly6C, CD69, Ly6G, IFN-γ, IL-4, and IL-17 (BD Biosciences Pharmingen, San Diego, CA) and FoxP3 (eBiosciences). Before intracellular staining, cells were restimulated for 4 hours with 50 ng/ml PMA and 500 ng/ml ionomycin in the presence of 1 μg/ml Brefeldin A. Samples were analyzed in a BD FACS Canto II (BD Biosciences, San Jose, CA) flow cytometer, and additional analyses were performed using FlowJo software.

Real-Time qPCR

cDNA for real-time qPCR was generated from 0.5 μg total RNA using the High Capacity cDNA Reverse Transcription Kit (Applied Biosystems, Foster City, CA) in a final reaction volume of 10 μl. The qPCR reactions were performed in triplicate using 10 μl each cDNA at 1:40 dilution, 10 μM each oligonucleotide, and HOT FIREPol qPCR Mix (Solis BioDyne) or Power SYBR Green PCR Master Mix in a total volume of 8 μl in MicroAmp Optical 384-Well Plates (Applied Biosystems). PCR reactions were performed using the ABI PRISM 7900HT (Applied Biosystems). The amount of amplified DNA was measured through the emission of light by SYBR Green Dye, intercalating in synthesized double–stranded DNA. All samples were

quantification of T cell subsets in the peritoneal effluents ($n\geq5$): (B) Th17 (CD4$^+$IL-17$^+$), Th1 (CD4$^+$IFN-γ^+), and Th2 (CD4$^+$IL-4$^+$) and (C) Tregs (CD4$^+$Foxp3$^+$). Percentages of the subpopulations are shown above the corresponding quadrant in the graph. (D) Representative density plots of flow cytometry analysis and quantification of CD11b$^+$Ly6G^{low} (monocytes) and CD11b$^+$Ly6G^{high} (neutrophils) cells in the peritoneal effluents ($n\geq5$). Percentages of the subpopulations are shown above the corresponding quadrant in the graph. Data are means±SDs ($n\geq5$). P values <0.05 are considered statistically significant using one-way ANOVA. *P<0.05; **P<0.01; ***P<0.001.

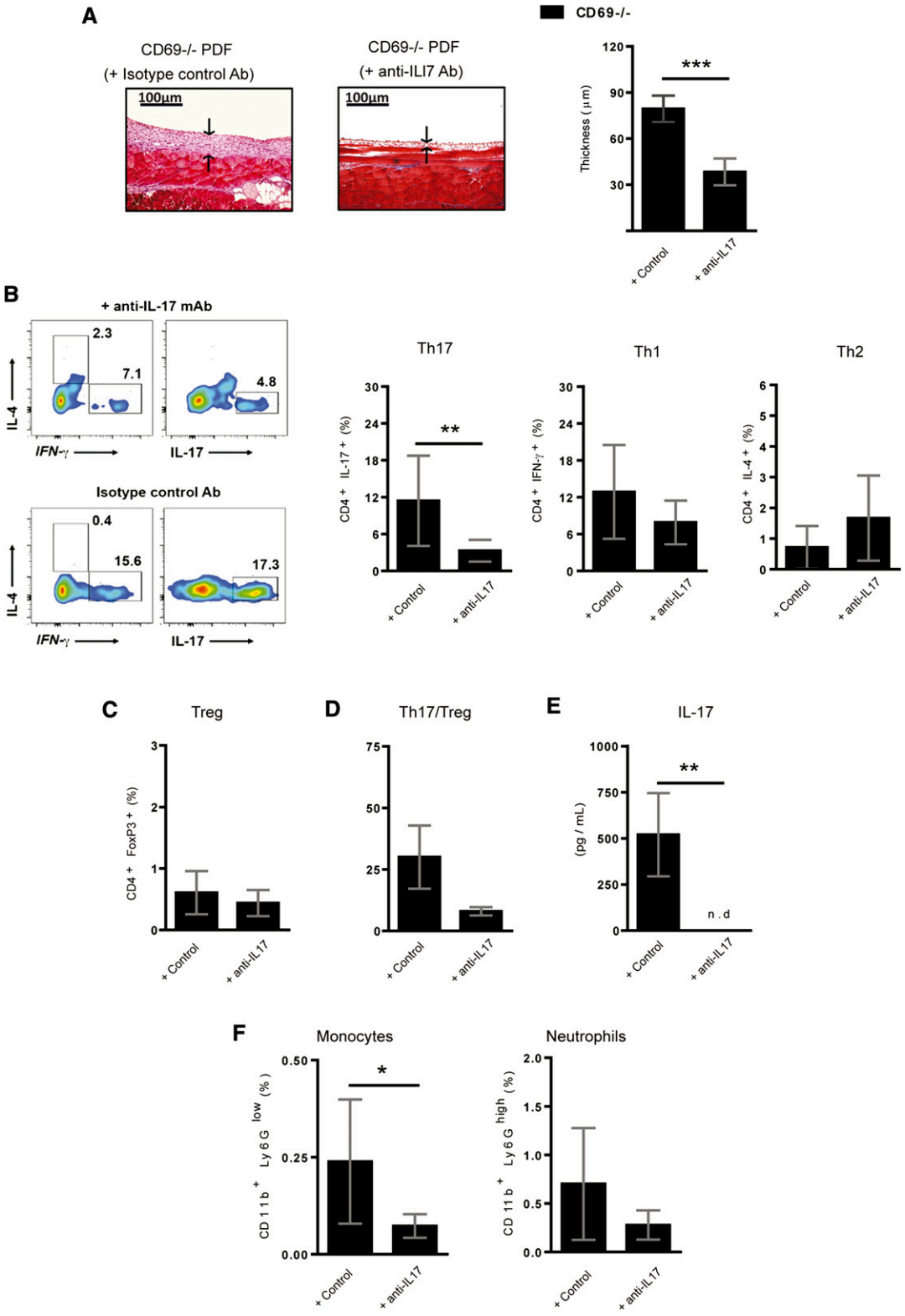

Figure 6. Neutralization of IL-17 in PDF–treated *cd69*$^{-/-}$ mice attenuates peritoneal fibrosis. The *cd69*$^{-/-}$ mice were subject to a 40-day exposure to PDF and simultaneously treated with either a neutralizing antibody against IL-17 (anti–IL-17) or its corresponding control antibody. The antibody was applied every 5 days (100 μg per mouse). (A) Representative pictures of Masson Trichrome–stained sections of PM from both *cd69*$^{-/-}$ groups. PM is indicated with arrows. PM thickness was measured, and quantification is represented on the graph. Data are means±SDs ($n \geq 5$). (B) Flow cytometry analysis of Th17 ($CD4^+IL\text{-}17^+$), Th1 ($CD4^+IFN\text{-}\gamma^+$), and Th2 ($CD4^+IL\text{-}4^+$)

measured in triplicate. SDS v2.2 software was used to analyze the results. Specific amplification was controlled by melting curve analysis. The data were analyzed by using the comparative Ct Method ($\Delta\Delta$Ct). The *x*-fold change in mRNA expression was quantified relative to control WT samples from the same experiment. β-Actin and GAPDH mRNAs was used as housekeeping genes. The primers that were used in this study were as follows: *collagen*, forward: CCAGAGTGGAACAGCGATTAC and reverse: GCAGGCGAGATGGCTTATTT; *fibronectin*, forward: GCAAACCTATAGCTGAGAAGTC and reverse: CAAGTACAGTCCACCATCATC; *TGF-β*, forward: GGAACTCTACCAGAAATATAGCAACAATTC and reverse: TGTAATCCGTCTCCTTGGTTCAG; *IL-6*, forward: GAGGATACCACTCCCAACAGACC and reverse: AAGTGCATCATCGTTGTTCATACA; *IL-1β*, forward: TGGTGTGTGACGTTCCATT and reverse: CAGCACGAGGCTTTTTTGTTG; *β-actin*, forward: AAGGAGATTACTTGCTCTGGCTCCTA and reverse: ACTCATCGTACTTCCTGCTTGCTGAT; and *GAPDH*, forward: AGCTTGTCATCAACGGGAAG and reverse: TTTGATGTTAGTGGGGTCTCG.

Immunoblotting

Lysates of PM were prepared in PD buffer (40 mM Tris HCl [20 mM, pH 8.0], 0.5 M NaCl, 6 mM EDTA, 6 mM de EGTA, and 0.1% NP40) containing the protease inhibitor cocktail (Complete; Roche, Basel, Switzerland). Proteins (30 μg) were size separated on 10% SDS polyacrylamide gels and transferred onto Trans-Blot Nitrocellulose Membranes (Bio-Rad, Hercules, CA). Primary antibodies for immunoblotting were as follows: anti–β-actin (Santa Cruz Biotechnology, Santa Cruz, CA), anti-Stat3 (Santa Cruz Biotechnology), antiphospho-Stat3 (Cell Signaling Technology, Danvers, MA), and α-SMA (Sigma-Aldrich, St. Louis, MO).

FlowCytomix

To determine the quantity of cytokines and chemokines, the peritoneal cavity was washed with 2 ml saline immediately after the mice were euthanized. The solution was centrifuged, and the supernatant was analyzed for cytokine and chemokine production using the FlowCytomix technique (Bender MedSystems GmbH). Data were analyzed using the FlowCytomix Pro 2.2 software (Bender MedSystems GmbH).

Masson Trichrome Staining

Parietal peritoneal biopsies were collected from the opposite side of the catheter installation. The biopsies were fixed in Bouin solution, embedded in paraffin, cut into 5-μm sections, and stained with Masson Trichrome. The PM thickness was determined using a microscope (Leica CTR6000 with a Leica Microsystems LAS-AF6000; Leica Microsystems, Buffalo Grove, IL). Microphotographs were obtained using an Olympus BX41 Clinical Microscope (Olympus, Tokyo, Japan) and an Olympus DP20 Digital Camera (Olympus) using cell acquisition software. The peritoneal thickness in each mouse was calculated by the median of measurement taken every 50 μm from one extreme to the other of the biopsy. The result was used to calculate the group thickness.

Immunofluorescence

Biopsies of mice were frozen in optimal cutting temperature compound and cut into 5-μm sections. To identify the mesothelial cells, we used a mouse anticytokeratin 8/18 (clone 5D3; Novocastra, Newcastle, United Kingdom), which was stained with anti-IgG1–specific Zenon Fab Fragments (Invitrogen, Carlsbad, CA) according to the manufacturer's instructions. Mesenchymal cells were stained with α-SMA (ab5694–100; Abcam, Inc., Cambridge, MA) and Zenon Fab Fragments. Nuclei were stained with 4,6-diamidino-2-phenylindole. The microscopy was performed with a fluorescence microscope (Leica CTR6000 with LAS-AF6000 software; Leica Microsystems) or a confocal microscope (Leica TCS SPE with LAS-AF software, version 2.0.1, build 2043; Leica Microsystems).

Statistical Analyses

P values were calculated with the *t* test, and values <0.05 were considered significant. Means of the experimental groups were compared by using one-way ANOVA. To account for multiple comparisons, the Tukey or Bonferroni post-tests were used to compare selected pairs of means and all pairs of means, respectively. All statistical analyses were carried out with GraphPad Prism 5.03 (GraphPad Software, La Jolla, CA). Correlations were assessed using Spearman correlation tests (GraphPad Prism 5.03).

ACKNOWLEDGMENTS

The authors thank Juliette Siegfried and her team at ServingMed.com for editing the manuscript and Dr. Richard Flavell for kindly providing the *foxp3*-mRFP/*Il17a*-eGFP double reporter mice.

G.L. and E.F. were supported by the European Union Seventh Framework Program EuTRiPD under grant PITN-GA-2011-287813. G.T.G.-M. is funded by Consejo Superior de Investigaciones Científicas. R.S.-D. is funded with a predoctoral fellowship from Comunidad de Madrid, and S.L. is funded with a fellowship from Redes Temáticas de Investigación Cooperativa en Salud (RETICS) Enfermedades Cardiovasculares from Instituto de Salud Carlos III. R.Z. received the laCaixa Foundation International Fellowship (laCaixa/Centro Nacional de Biotecnología). A.A. was supported by grant FIS 12/01175 from the

cells in the peritoneal effluents from indicated groups and representative density plots. Percentages of the analyzed cells are shown above the corresponding quadrants. (C) Percentage of Tregs in the peritoneal effluents was measured by flow cytometry, and (D) Th17-to-Treg ratio is shown. (E) Quantification of IL-17 concentration in the peritoneal effluents by ELISA. (F) Percentages of $CD11b^{+}Ly6G^{low}$ (monocytes; left panel) and $CD11b^{+}Ly6G^{high}$ (neutrophils; right panel) in the peritoneal effluents from the indicated groups quantified by flow cytometry. Data are means±SDs ($n \geq 8$). *P* values <0.05 were considered statistically significant using the *t* test. n.d., not detectable. **P*<0.05; ***P*<0.01; ****P*<0.001.

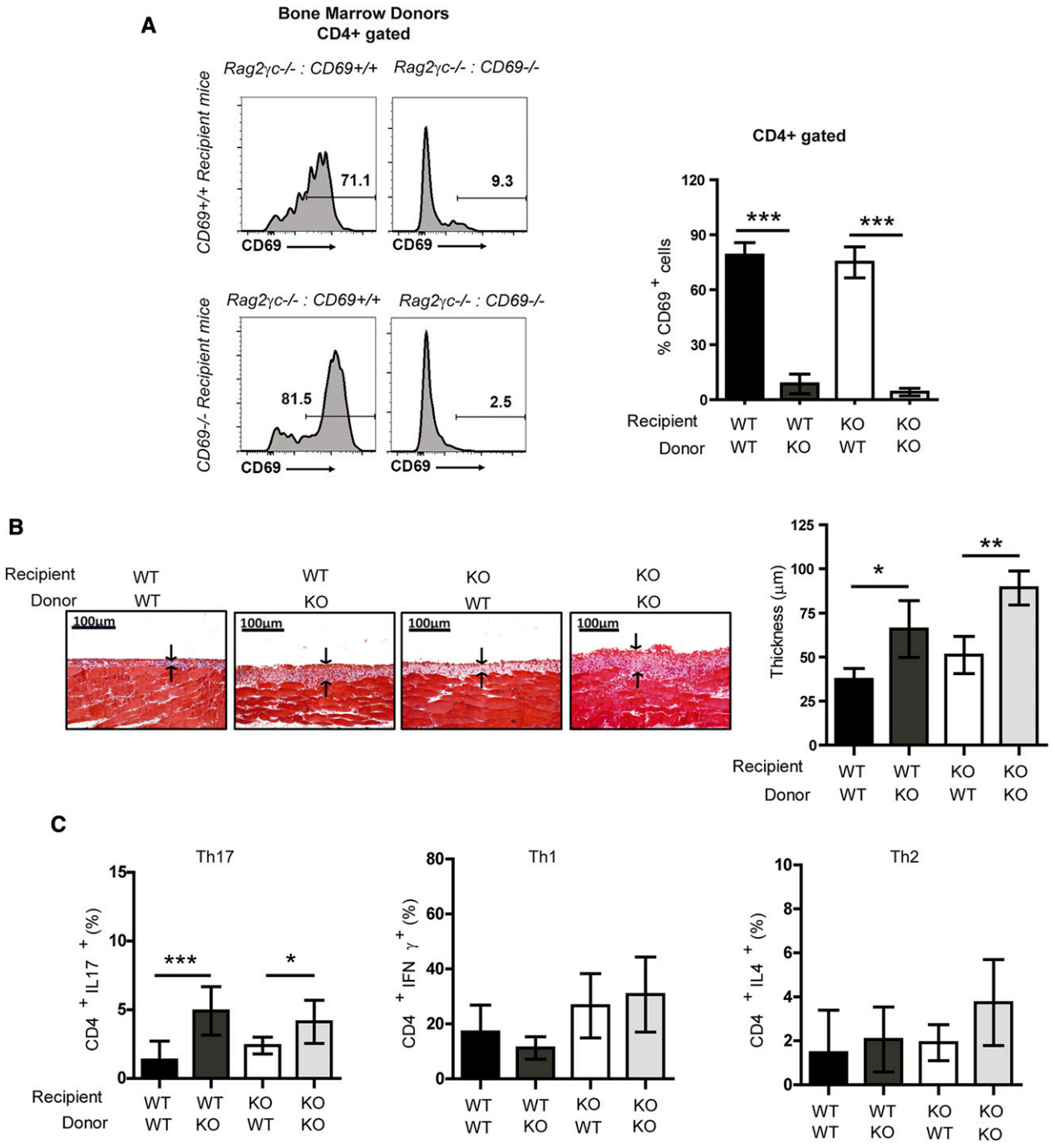

Figure 7. CD69 expression within the lymphocyte compartment drives peritoneal fibrosis. WT and *cd69*$^{-/-}$ (KO) mice were transplanted with a mixture of BM cells from either Rag2$^{-/-}{}_{\gamma}$c$^{-/-}$ and CD69$^{-/-}$ (KO) or Rag2$^{-/-}{}_{\gamma}$c$^{-/-}$ and CD69$^{+/+}$ (WT) cells as described in Concise Methods. (A) Representative histogram plot of flow cytometry analysis of CD4^{+} CD69^{+} cells in peripheral blood from four chimeric groups and the corresponding quantification. Data are means±SDs (n≥8). (B) Representative pictures of Masson Trichrome staining of peritoneal tissue sections from reconstituted mice subjected to a 40-day exposure to PDF. PM is indicated with arrows. PM thickness was measured. Data are means±SDs (n≥4). (C) Flow cytometry analysis of Th17 (CD4^{+}IL-17^{+}), Th1 (CD4^{+}IFN-γ^{+}), and Th2 (CD4^{+}IL-4^{+}) cells from the peritoneal cavity. Data are means±SDs (n≥7). P values <0.05 were considered statistically significant using one-way ANOVA. *P<0.05; **P<0.01; ***P<0.001.

Fondo de Investigaciones Santitarias. R.S. was supported by grants RETICS 06/0016 and PI 09/0064 from the Fondo de Investigaciones Santitarias. Grants SAF2011-25834 (to F.S.-M.), SAF2011-27330 (to P.M.), and INDISNET 01592006 (to F.S.-M. and P.M.) were from the Comunidad de Madrid and RETICS Enfermedades Cardiovasculares from the Instituto de Salud Carlos III, and grant ERC-2011-AdG294340-GENTRIS

from the European Research Council (European Commission) was to F.S.-M. M.L.-C. was supported, in part, by Ministerio de Economia y Competitividad grant SAF2013-47611-R and funding from Comunidad Autónoma de Madrid 2010-BMD2321 (FIBROTEAM). The Centro Nacional de Investigaciones Cardiovasculares (CNIC) is supported by the Spanish Ministry of Economy and Competitiveness (MINECO) and the Pro-CNIC Foundation, and a Severo Ochoa Center of Excellence (MINECO award SEV-2015-0505).

DISCLOSURES

None.

REFERENCES

1. Di Paolo N, Sacchi G: Atlas of peritoneal histology. *Perit Dial Int* 20 [Suppl 3]: S5–S96, 2000
2. Maciver AH, McCall M, James Shapiro AM: Intra-abdominal adhesions: Cellular mechanisms and strategies for prevention. *Int J Surg* 9: 589–594, 2011
3. Devuyst O, Margetts PJ, Topley N: The pathophysiology of the peritoneal membrane. *J Am Soc Nephrol* 21: 1077–1085, 2010
4. Moinuddin Z, Summers A, Van Dellen D, Augustine T, Herrick SE: Encapsulating peritoneal sclerosis-a rare but devastating peritoneal disease. *Front Physiol* 5: 470, 2014
5. Hellebrekers BW, Kooistra T: Pathogenesis of postoperative adhesion formation. *Br J Surg* 98: 1503–1516, 2011
6. Kawanishi H, Moriishi M: Encapsulating peritoneal sclerosis: Prevention and treatment. *Perit Dial Int* 27[Suppl 2]: S289–S292, 2007
7. González-Mateo GT, Aroeira LS, López-Cabrera M, Ruiz-Ortega M, Ortiz A, Selgas R: Pharmacological modulation of peritoneal injury induced by dialysis fluids: Is it an option? *Nephrol Dial Transplant* 27: 478–481, 2012
8. Aroeira LS, Aguilera A, Sánchez-Tomero JA, Bajo MA, del Peso G, Jiménez-Heffernan JA, Selgas R, López-Cabrera M: Epithelial to mesenchymal transition and peritoneal membrane failure in peritoneal dialysis patients: Pathologic significance and potential therapeutic interventions. *J Am Soc Nephrol* 18: 2004–2013, 2007
9. Chaimovitz C: Peritoneal dialysis. *Kidney Int* 45: 1226–1240, 1994
10. Yáñez-Mó M, Lara-Pezzi E, Selgas R, Ramírez-Huesca M, Domínguez-Jiménez C, Jiménez-Heffernan JA, Aguilera A, Sánchez-Tomero JA, Bajo MA, Alvarez V, Castro MA, del Peso G, Cirujeda A, Gamallo C, Sánchez-Madrid F, López-Cabrera M: Peritoneal dialysis and epithelial-to-mesenchymal transition of mesothelial cells. *N Engl J Med* 348: 403–413, 2003
11. Chen YT, Chang YT, Pan SY, Chou YH, Chang FC, Yeh PY, Liu YH, Chiang WC, Chen YM, Wu KD, Tsai TJ, Duffield JS, Lin SL: Lineage tracing reveals distinctive fates for mesothelial cells and submesothelial fibroblasts during peritoneal injury. *J Am Soc Nephrol* 25: 2847–2858, 2014
12. García-López E, Lindholm B, Davies S: An update on peritoneal dialysis solutions. *Nat Rev Nephrol* 8: 224–233, 2012
13. Morgan LW, Wieslander A, Davies M, Horiuchi T, Ohta Y, Beavis MJ, Craig KJ, Williams JD, Topley N: Glucose degradation products (GDP) retard remesothelialization independently of D-glucose concentration. *Kidney Int* 64: 1854–1866, 2003
14. Williams JD, Craig KJ, Topley N, Von Ruhland C, Fallon M, Newman GR, Mackenzie RK, Williams GT; Peritoneal Biopsy Study Group: Morphologic changes in the peritoneal membrane of patients with renal disease. *J Am Soc Nephrol* 13: 470–479, 2002
15. Plum J, Hermann S, Fusshöller A, Schoenicke G, Donner A, Röhrborn A, Grabensee B: Peritoneal sclerosis in peritoneal dialysis patients related to dialysis settings and peritoneal transport properties. *Kidney Int Suppl* 78: S42–S47, 2001
16. Jiménez-Heffernan JA, Aguilera A, Aroeira LS, Lara-Pezzi E, Bajo MA, del Peso G, Ramírez M, Gamallo C, Sánchez-Tomero JA, Alvarez V, López-Cabrera M, Selgas R: Immunohistochemical characterization of fibroblast subpopulations in normal peritoneal tissue and in peritoneal dialysis-induced fibrosis. *Virchows Arch* 444: 247–256, 2004
17. Rodrigues-Díez R, Aroeira LS, Orejudo M, Bajo MA, Heffernan JJ, Rodrigues-Díez RR, Rayego-Mateos S, Ortiz A, Gonzalez-Mateo G, López-Cabrera M, Selgas R, Egido J, Ruiz-Ortega M: IL-17A is a novel player in dialysis-induced peritoneal damage. *Kidney Int* 86: 303–315, 2014
18. Sandoval P, Loureiro J, González-Mateo G, Pérez-Lozano ML, Maldonado-Rodríguez A, Sánchez-Tomero JA, Mendoza L, Santamaría B, Ortiz A, Ruíz-Ortega M, Selgas R, Martín P, Sánchez-Madrid F, Aguilera A, López-Cabrera M: PPAR-γ agonist rosiglitazone protects peritoneal membrane from dialysis fluid-induced damage. *Lab Invest* 90: 1517–1532, 2010
19. González-Mateo GT, Fernández-Míllara V, Bellón T, Liappas G, Ruiz-Ortega M, López-Cabrera M, Selgas R, Aroeira LS: Paricalcitol reduces peritoneal fibrosis in mice through the activation of regulatory T cells and reduction in IL-17 production. *PLoS One* 9: e108477, 2014
20. Testi R, Phillips JH, Lanier LL: T cell activation via Leu-23 (CD69). *J Immunol* 143: 1123–1128, 1989
21. Cebrián M, Yagüe E, Rincón M, López-Botet M, de Landázuri MO, Sánchez-Madrid F: Triggering of T cell proliferation through AIM, an activation inducer molecule expressed on activated human lymphocytes. *J Exp Med* 168: 1621–1637, 1988
22. Okhrimenko A, Grün JR, Westendorf K, Fang Z, Reinke S, von Roth P, Wassilew G, Kühl AA, Kudernatsch R, Demski S, Scheibenbogen C, Tokoyoda K, McGrath MA, Raftery MJ, Schönrich G, Serra A, Chang HD, Radbruch A, Dong J: Human memory T cells from the bone marrow are resting and maintain long-lasting systemic memory. *Proc Natl Acad Sci U S A* 111: 9229–9234, 2014
23. Shinoda K, Tokoyoda K, Hanazawa A, Hayashizaki K, Zehentmeier S, Hosokawa H, Iwamura C, Koseki H, Tumes DJ, Radbruch A, Nakayama T: Type II membrane protein CD69 regulates the formation of resting T-helper memory. *Proc Natl Acad Sci U S A* 109: 7409–7414, 2012
24. Laffón A, García-Vicuña R, Humbría A, Postigo AA, Corbí AL, de Landázuri MO, Sánchez-Madrid F: Upregulated expression and function of VLA-4 fibronectin receptors on human activated T cells in rheumatoid arthritis. *J Clin Invest* 88: 546–552, 1991
25. García-Monzón C, Moreno-Otero R, Pajares JM, García-Sánchez A, López-Botet M, de Landázuri MO, Sánchez-Madrid F: Expression of a novel activation antigen on intrahepatic CD8+ T lymphocytes in viral chronic active hepatitis. *Gastroenterology* 98: 1029–1035, 1990
26. Sancho D, Gómez M, Viedma F, Esplugues E, Gordón-Alonso M, García-López MA, de la Fuente H, Martínez-A C, Lauzurica P, Sánchez-Madrid F: CD69 downregulates autoimmune reactivity through active transforming growth factor-beta production in collagen-induced arthritis. *J Clin Invest* 112: 872–882, 2003
27. Martin P, Gómez M, Lamana A, Matesanz Marín A, Cortés JR, Ramírez-Huesca M, Barreiro O, López-Romero P, Gutiérrez-Vázquez C, de la Fuente H, Cruz-Adalia A, Sánchez-Madrid F: The leukocyte activation antigen CD69 limits allergic asthma and skin contact hypersensitivity. *J Allergy Clin Immunol* 126: 355–365, 2010
28. Cruz-Adalia A, Jiménez-Borreguero LJ, Ramírez-Huesca M, Chico-Calero I, Barreiro O, López-Conesa E, Fresno M, Sánchez-Madrid F, Martín P: CD69 limits the severity of cardiomyopathy after autoimmune myocarditis. *Circulation* 122: 1396–1404, 2010
29. Radulovic K, Manta C, Rossini V, Holzmann K, Kestler HA, Wegenka UM, Nakayama T, Niess JH: CD69 regulates type I IFN-induced tolerogenic signals to mucosal CD4 T cells that attenuate their colitogenic potential. *J Immunol* 188: 2001–2013, 2012

30. Martín P, Gómez M, Lamana A, Cruz-Adalia A, Ramírez-Huesca M, Ursa MA, Yáñez-Mo M, Sánchez-Madrid F: CD69 association with Jak3/Stat5 proteins regulates Th17 cell differentiation. *Mol Cell Biol* 30: 4877–4889, 2010
31. Martín P, Sánchez-Madrid F: CD69: An unexpected regulator of TH17 cell-driven inflammatory responses. *Sci Signal* 4: pe14, 2011
32. González-Amaro R, Cortés JR, Sánchez-Madrid F, Martín P: Is CD69 an effective brake to control inflammatory diseases? *Trends Mol Med* 19: 625–632, 2013
33. Cortés JR, Sánchez-Díaz R, Bovolenta ER, Barreiro O, Lasarte S, Matesanz-Marín A, Toribio ML, Sánchez-Madrid F, Martín P: Maintenance of immune tolerance by Foxp3+ regulatory T cells requires CD69 expression. *J Autoimmun* 55: 51–62, 2014
34. Walkin L, Herrick SE, Summers A, Brenchley PE, Hoff CM, Korstanje R, Margetts PJ: The role of mouse strain differences in the susceptibility to fibrosis: A systematic review. *Fibrogenesis Tissue Repair* 6: 18, 2013
35. Busnadiego O, Loureiro-Álvarez J, Sandoval P, Lagares D, Dotor J, Pérez-Lozano ML, López-Armada MJ, Lamas S, López-Cabrera M, Rodríguez-Pascual F: A pathogenetic role for endothelin-1 in peritoneal dialysis-associated fibrosis. *J Am Soc Nephrol* 26: 173–182, 2015
36. Stockinger B: Good for Goose, but not for Gander: IL-2 interferes with Th17 differentiation. *Immunity* 26: 278–279, 2007
37. Combet S, Ferrier ML, Van Landschoot M, Stoenoiu M, Moulin P, Miyata T, Lameire N, Devuyst O: Chronic uremia induces permeability changes, increased nitric oxide synthase expression, and structural modifications in the peritoneum. *J Am Soc Nephrol* 12: 2146–2157, 2001
38. Ferrantelli E, Liappas G, Keuning ED, Vila Cuenca M, González-Mateo G, Verkaik M, López-Cabrera M, Beelen RH: A novel mouse model of peritoneal dialysis: Combination of uraemia and long-term exposure to PD fluid. *BioMed Res Int* 2015: 106902, 2015
39. Peck A, Mellins ED: Plasticity of T-cell phenotype and function: The T helper type 17 example. *Immunology* 129: 147–153, 2010
40. Liang SC, Long AJ, Bennett F, Whitters MJ, Karim R, Collins M, Goldman SJ, Dunussi-Joannopoulos K, Williams CM, Wright JF, Fouser LA: An IL-17F/A heterodimer protein is produced by mouse Th17 cells and induces airway neutrophil recruitment. *J Immunol* 179: 7791–7799, 2007
41. Rangachari M, Mauermann N, Marty RR, Dirnhofer S, Kurrer MO, Komnenovic V, Penninger JM, Eriksson U: T-bet negatively regulates autoimmune myocarditis by suppressing local production of interleukin 17. *J Exp Med* 203: 2009–2019, 2006
42. He D, Wu L, Kim HK, Li H, Elmets CA, Xu H: CD8+ IL-17-producing T cells are important in effector functions for the elicitation of contact hypersensitivity responses. *J Immunol* 177: 6852–6858, 2006
43. Nakae S, Nambu A, Sudo K, Iwakura Y: Suppression of immune induction of collagen-induced arthritis in IL-17-deficient mice. *J Immunol* 171: 6173–6177, 2003
44. Komiyama Y, Nakae S, Matsuki T, Nambu A, Ishigame H, Kakuta S, Sudo K, Iwakura Y: IL-17 plays an important role in the development of experimental autoimmune encephalomyelitis. *J Immunol* 177: 566–573, 2006
45. Sakaguchi S: Naturally arising CD4+ regulatory t cells for immunologic self-tolerance and negative control of immune responses. *Annu Rev Immunol* 22: 531–562, 2004
46. Bettelli E, Carrier Y, Gao W, Korn T, Strom TB, Oukka M, Weiner HL, Kuchroo VK: Reciprocal developmental pathways for the generation of pathogenic effector TH17 and regulatory T cells. *Nature* 441: 235–238, 2006
47. Komatsu N, Okamoto K, Sawa S, Nakashima T, Oh-hora M, Kodama T, Tanaka S, Bluestone JA, Takayanagi H: Pathogenic conversion of Foxp3+ T cells into TH17 cells in autoimmune arthritis. *Nat Med* 20: 62–68, 2014
48. Lua I, Li Y, Pappoe LS, Asahina K: Myofibroblastic conversion and regeneration of mesothelial cells in peritoneal and liver fibrosis. *Am J Pathol* 185: 3258–3273, 2015
49. Liu Y, Dong Z, Liu H, Zhu J, Liu F, Chen G: Transition of mesothelial cell to fibroblast in peritoneal dialysis: EMT, stem cell or bystander? *Perit Dial Int* 35: 14–25, 2015
50. Zhou L, Lopes JE, Chong MM, Ivanov II, Min R, Victora GD, Shen Y, Du J, Rubtsov YP, Rudensky AY, Ziegler SF, Littman DR: TGF-beta-induced Foxp3 inhibits T(H)17 cell differentiation by antagonizing RORgammat function. *Nature* 453: 236–240, 2008
51. Lauzurica P, Sancho D, Torres M, Albella B, Marazuela M, Merino T, Bueren JA, Martínez-A C, Sánchez-Madrid F: Phenotypic and functional characteristics of hematopoietic cell lineages in CD69-deficient mice. *Blood* 95: 2312–2320, 2000
52. Directive 2010/63/EU of the European Parliament and of the Council of 22 September 2010 on the Protection of Animals Used for Scientific Purposes. *Official Journal of the European Union* 53: 33–79, 2010
53. González-Mateo GT, Loureiro J, Jiménez-Hefferman JA, Bajo MA, Selgas R, López-Cabrera M, Aroeira LS: Chronic exposure of mouse peritoneum to peritoneal dialysis fluid: Structural and functional alterations of the peritoneal membrane. *Perit Dial Int* 29: 227–230, 2009
54. Esplugues E, Sancho D, Vega-Ramos J, Martínez C, Syrbe U, Hamann A, Engel P, Sánchez-Madrid F, Lauzurica P: Enhanced antitumor immunity in mice deficient in CD69. *J Exp Med* 197: 1093–1106, 2003
55. Sancho D, Gómez M, Martinez Del Hoyo G, Lamana A, Esplugues E, Lauzurica P, Martinez-A C, Sánchez-Madrid F: CD69 targeting differentially affects the course of collagen-induced arthritis. *J Leukoc Biol* 80: 1233–1241, 2006

This article contains supplemental material online at http://jasn.asnjournals.org/lookup/suppl/doi:10.1681/ASN.2015080909/-/DCSupplemental.

Supplementary Table S1: Flow cytometry analysis of the percentage of different cell populations in the peritoneal membrane tissue of WT and *cd69-/-* mice after 40 days of treatment with PDF or saline as control. Data are means ± SEM.

	WT		$CD69^{-/-}$	
(%)	Control	PDF	Control	PDF
$CD11b^{+}Gr\text{-}1^{+}$ (monocytes)	0.05 ± 0.02	0.18 ± 0.09	0.05 ± 0.01 @	0.21 ± 0.05 @
$CD11b^{+}Gr\text{-}1^{high}$ (neutrophils)	0.04 ± 0.01	0.20 ± 0.11	0.03 ± 0.01 £	0.34 ± 0.07 £
$B220^{+}$ (B cells)	8.12 ± 1.87 £	20.0 ± 2.21 £, $	9.26 ± 1.19 @	4.99 ± 0.98 @, $
cDCs (c dendritic cells)	0.04 ± 0.01 @	0.12 ± 0.03 @	0.03 ± 0.01	0.10 ± 0.02
pDCs (p dendritic cells)	0.57 ± 0.19	1.68 ± 0.60	0.32 ± 0.08 &	1.97 ± 0.40 &
$CD4^{+}$ (T cells)	0.04 ± 0.02 @	0.26 ± 0.08 @	0.04 ± 0.01 &	0.21 ± 0.04 &
$CD8^{+}$ (T cells)	0.04 ± 0.02 &, *	0.18 ± 0.04 &, *	0.05 ± 0.01 &, ©	0.14 ± 0.02 &, ©

@: $p < 0.05$; **&:** $p < 0.01$; **£:** $p < 0.001$; **$:** $p < 0.001$: WT PDF vs. $cd69^{-/-}$ PDF; ***:** $p < 0.01$: WT Control vs. WT PDF, **©:** $p < 0.01$: $CD69^{-/-}$ Control vs. $cd69^{-/-}$ PDF

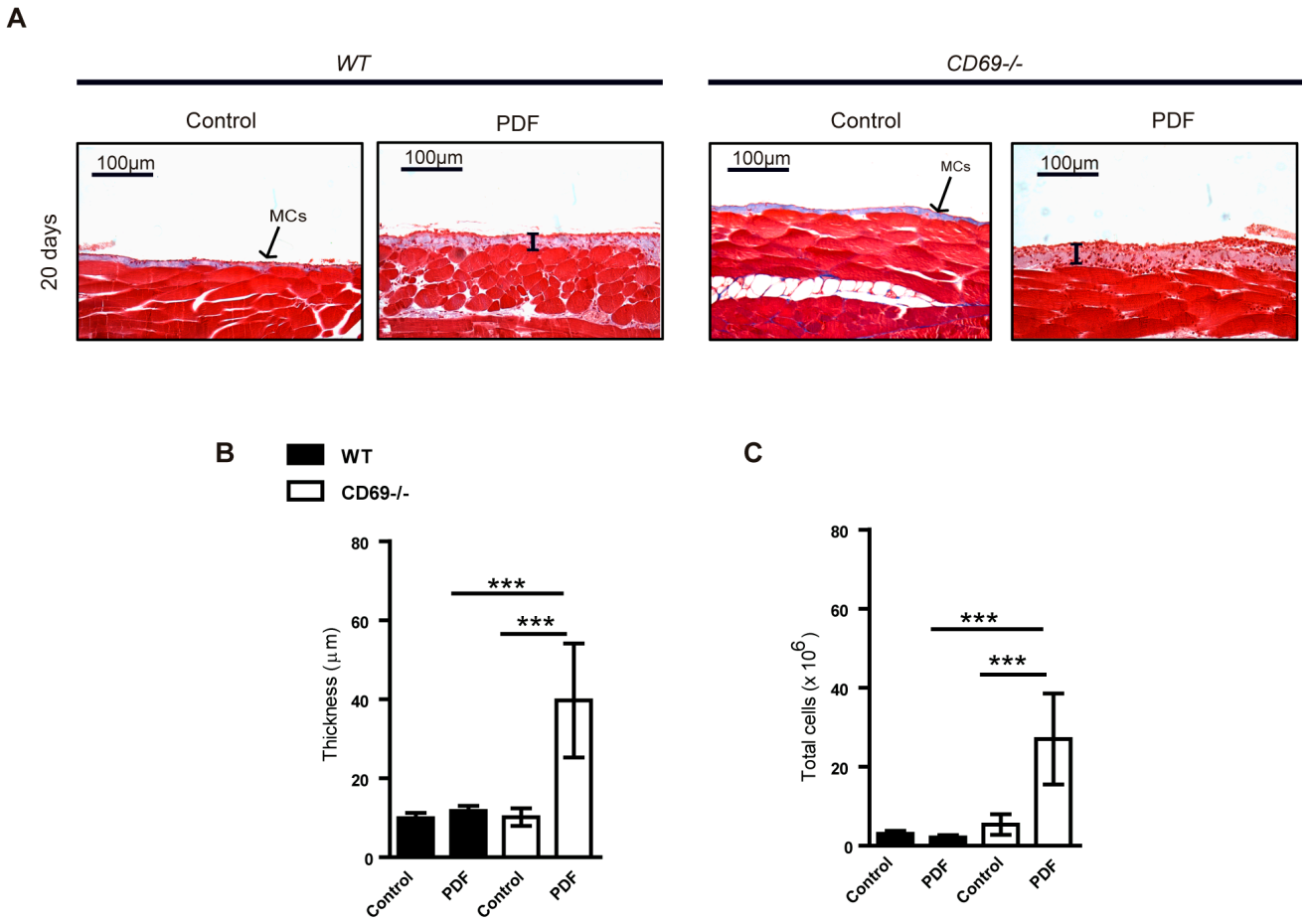

Supplementary Figure S1: PDF treatment of WT and *cd69*$^{-/-}$ mice (20 days). (**A**) Trichrome Massons staining of peritoneal tissue in *cd69*$^{-/-}$ and WT mice treated or not with PDF. (**B**) Peritoneal membrane thickness. (**C**) Total cell counts (x 10^6) in the peritoneal cavity effluents. Data are means ± SD (n≥5). P values p <0.05 are considered statistically significant one-way Anova test. *p <0.05, **p <0.01, ***p <0.001.

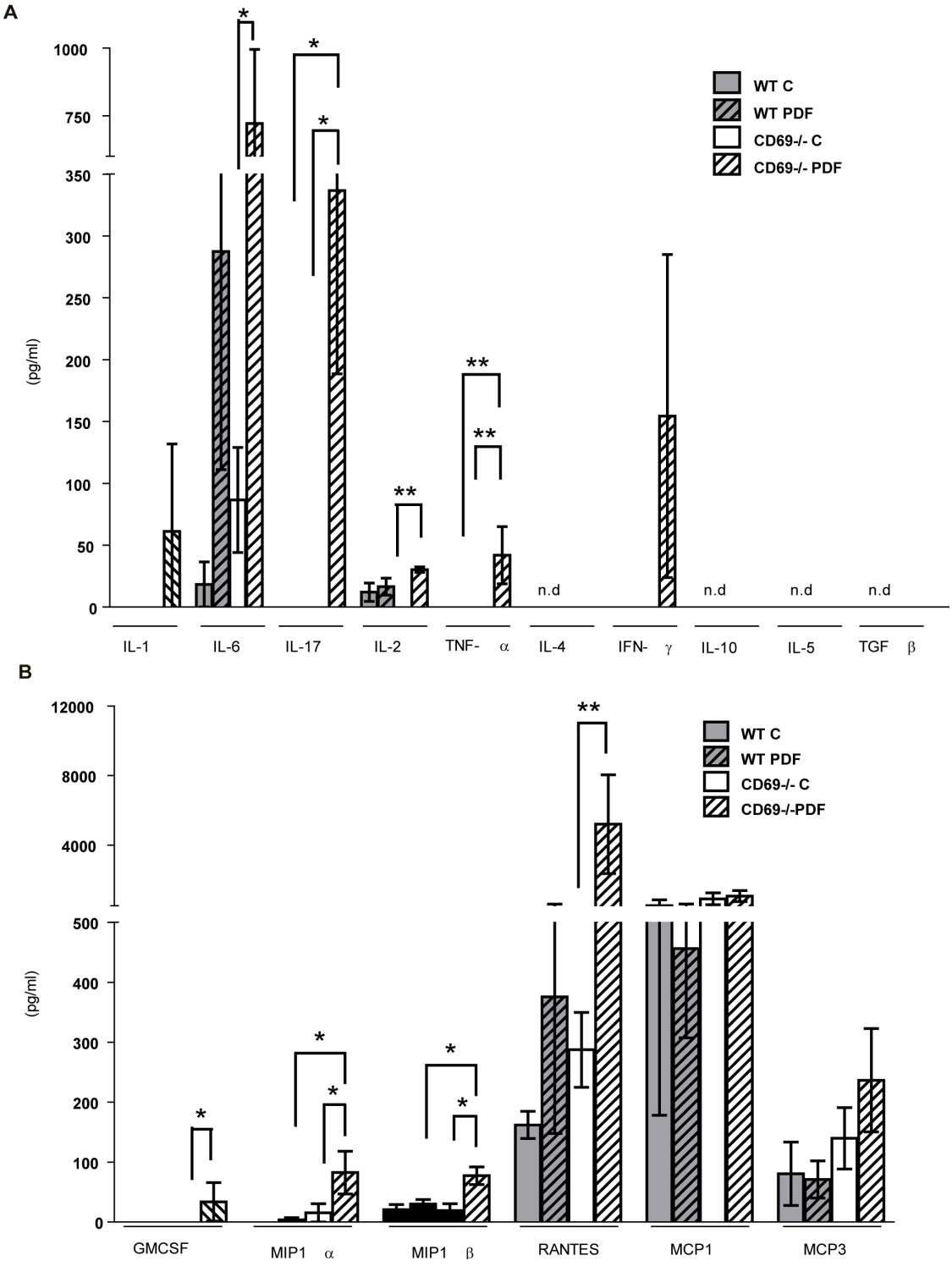

Supplementary Figure S2: Analysis of (**A**) cytokine and (**B**) chemokine profiles released in the peritoneal cavity after 20 days of PDF treatment. Production of pro-inflammatory cytokines and chemokines was assessed by Flow Cytomix cytokine array and analyzed by FACS. Bars are means ± SD ($n \geq 5$). P values $p < 0.05$ are considered statistically significant using one-way Anova test. *$p < 0.05$, **$p < 0.01$, ***$p < 0.001$.

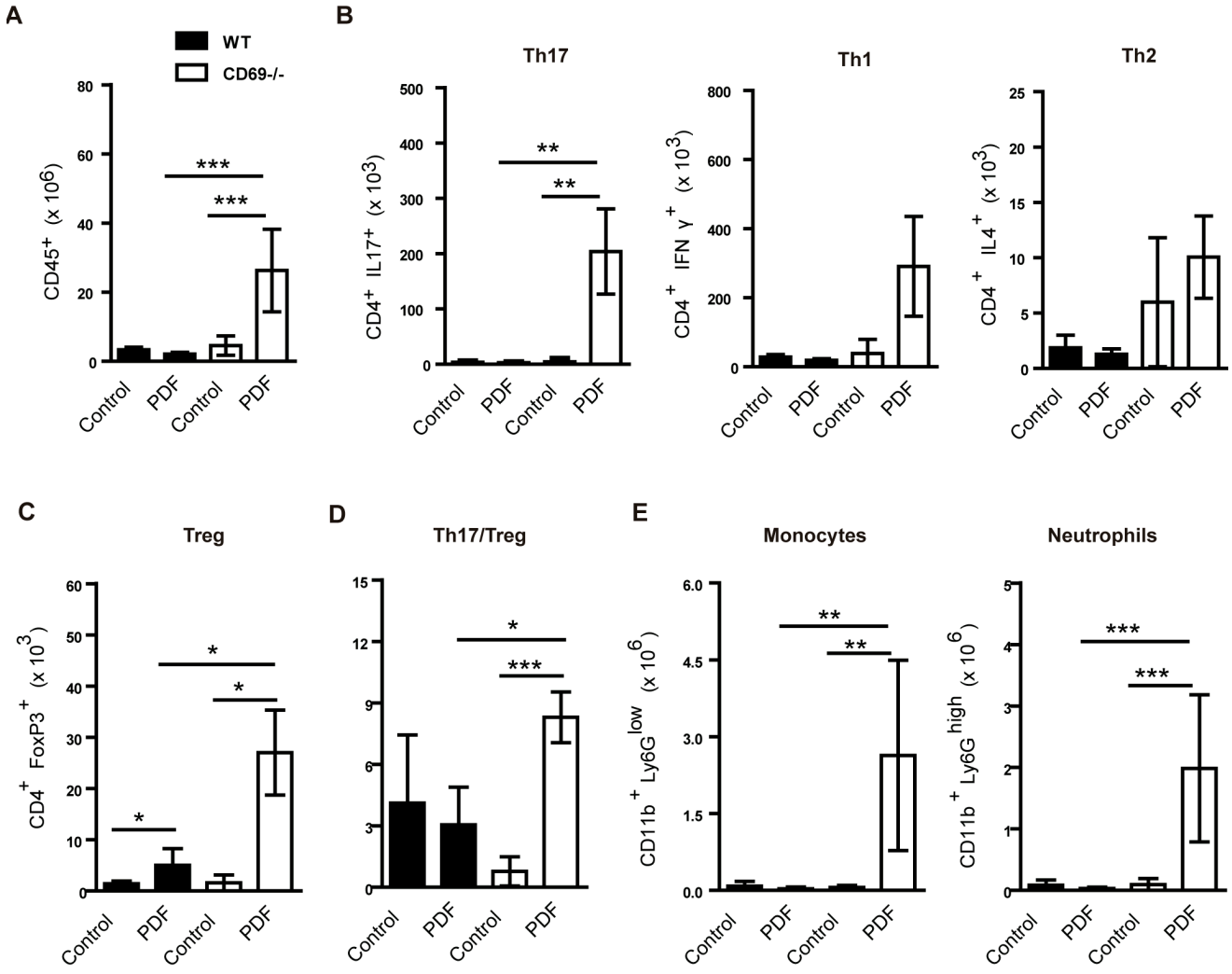

Supplementary Figure S3: (**A-C**) Quantification of flow-cytometry analysis of the expression of total number of (**A**) $CD45^+$, (**B**) Th17, Th1 and Th2 and (**C**) Treg cells after 20 days treatment with saline or PDF. (**D**). Ratio between the total Th17 and regulatory T cells in all groups. (**E**) $CD11b^+Ly6G^{low}$ (monocytes) and $CD11b^+Ly6G^{high}$ (neutrophils) in the peritoneal effluents from indicated groups. P values $p < 0.05$ are considered statistically significant using one-way Anova test. *p <0.05, **p <0.01, ***p <0.001.

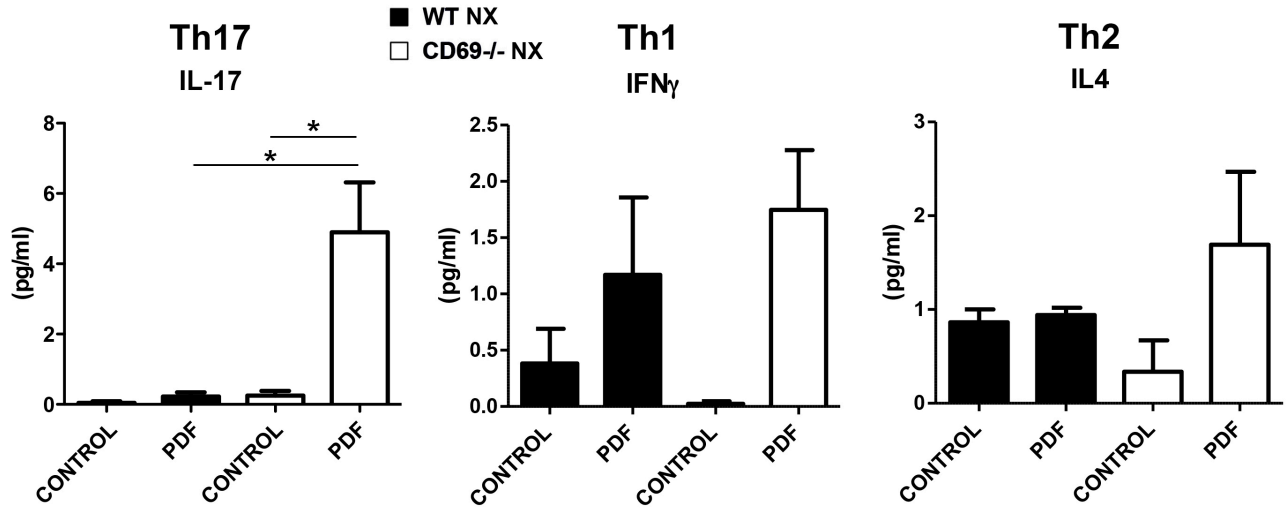

Supplementary Figure S4. Analysis of cytokine expression in the peritoneal cavity of uremic WT and *cd69*$^{-/-}$ mice. Mice undergo 5/6 nephrectomy before treatment with saline or PDF for a period of 40 days. Production of T helper-associated cytokines was assessed by multiplexed flow cytometric bead array. Bars are means ± SD ($n \geq 6$). P values $p < 0.05$ were considered statistically significant using one-way Anova test, and Bonferroni post-test were used to compare selected pairs of means and all pairs of means, respectively (*$p < 0.05$, **$p < 0.01$, ***$p < 0.001$).

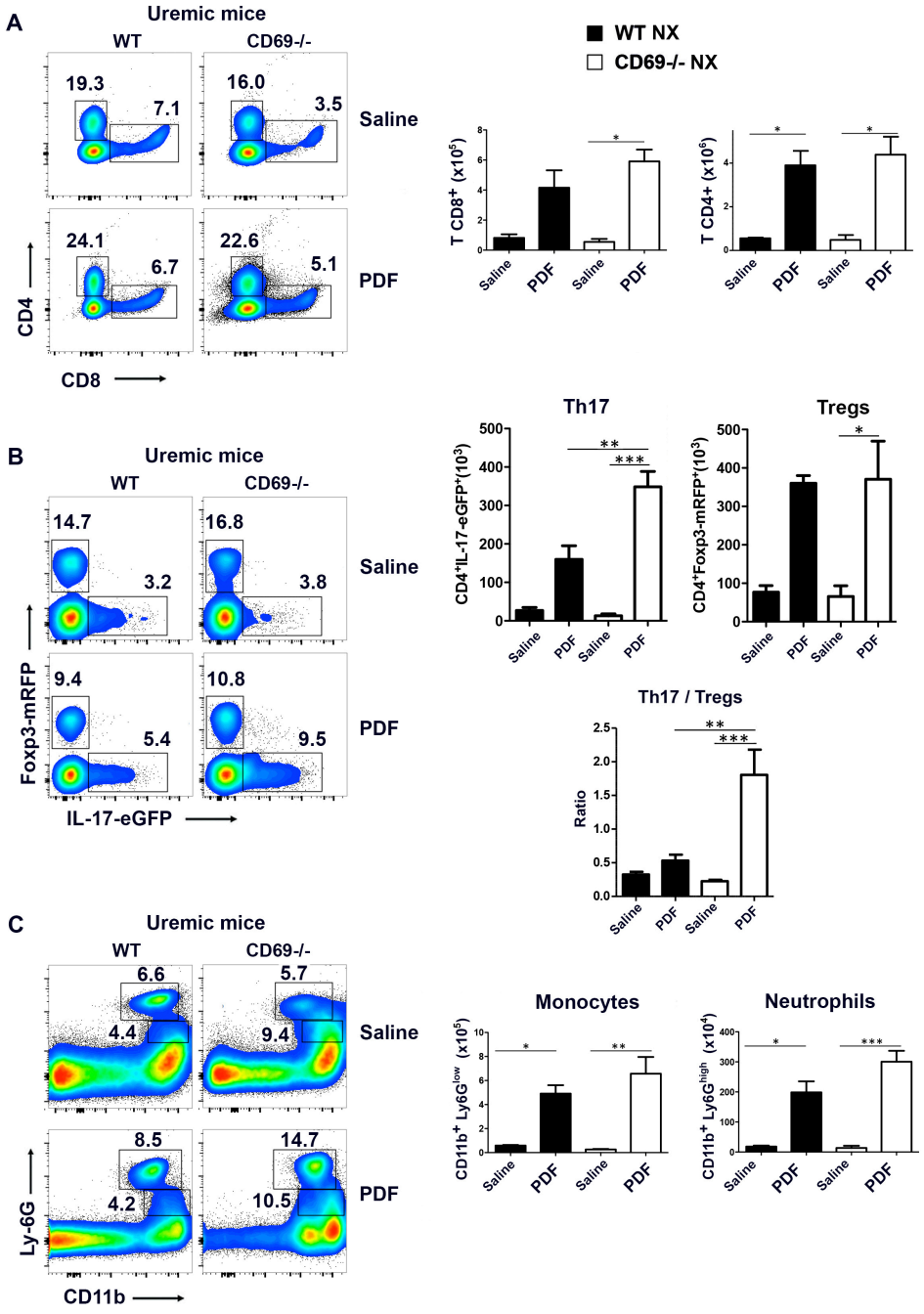

Supplementary Figure S5. Density plots of flow-cytometry analysis in peritoneal effluents from uremic cd69-/- double reporter (cd69-/-dRep) mice (Foxp3-mRFP in foxp3 locus and IL-17A-eGFP in Il17a locus) or wt littermates (cd69+/+dRep). (**A**) Total numbers of CD8+ and CD4+ T cells were assessed in mice treated during 40 days with saline or PDF. (**B**) Analysis of CD4+FoxP3-RFP (Tregs) and IL-17eGFP from indicated groups. The Th17/Treg ratio is shown. (**C**) CD11b+Ly6Glow (monocytes) and CD11b+Ly6Ghigh (neutrophils) quantification in peritoneal effluents. P values p <0.05 are considered statistically significant using one-way Anova test. *p <0.05, **p <0.01, ***p <0.001.

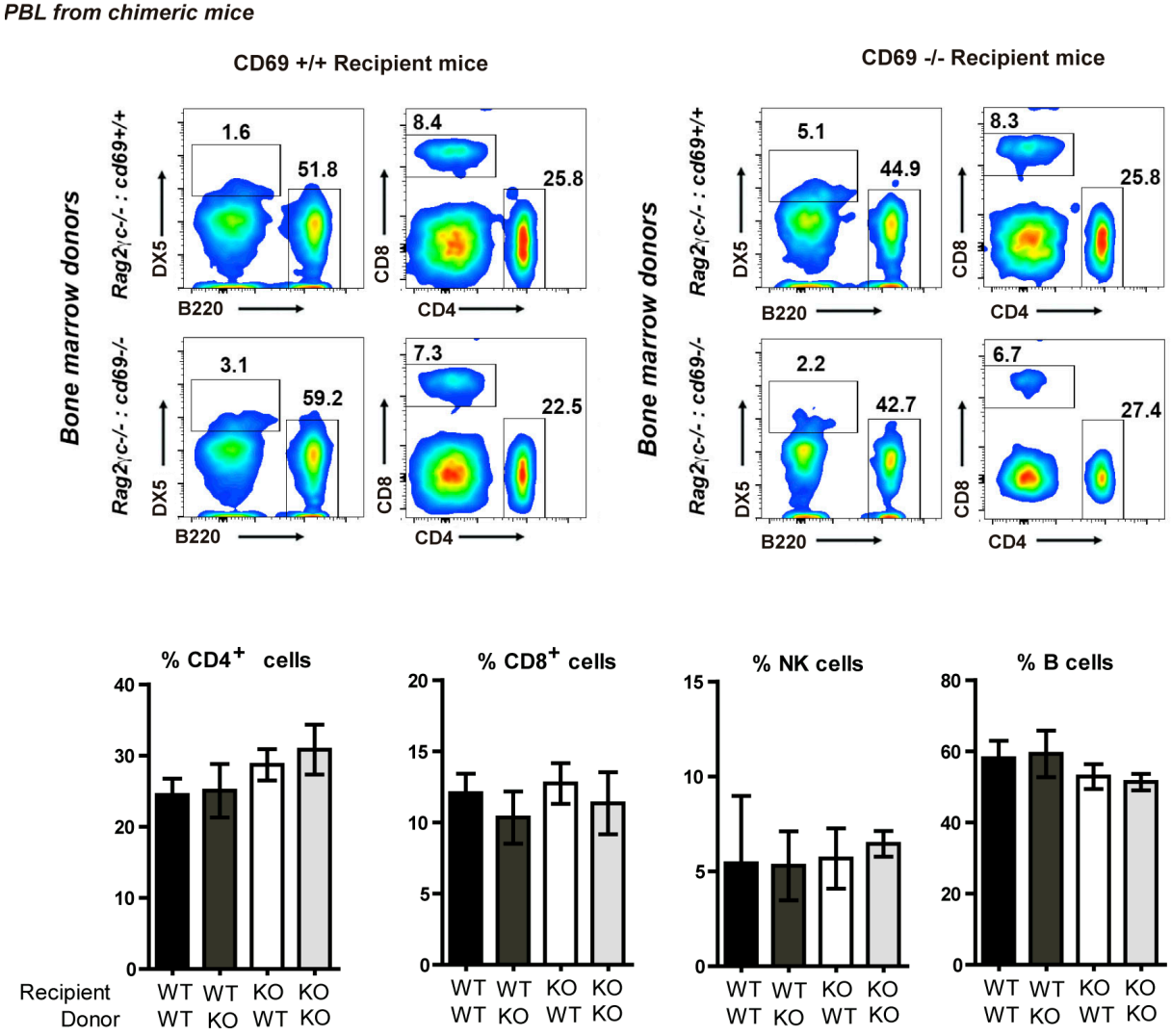

Supplementary Figure S6: WT and *cd69*$^{-/-}$ recipient mice were transplanted with a mixture of BM cells from Rag2$^{-/-}\gamma c^{-/-}$ and cd69$^{-/-}$ or Rag2$^{-/-}\gamma c^{-/-}$ and cd69$^{+/+}$ (WT) cells as described in the Material and Methods section. In the following graphs recipient mice are WT or KO for CD69 alone and donor mice are WT or KO mixed with Rag2$^{-/-}\gamma c^{-/-}$ cells. Flow-cytometry analysis of CD4^{+}, CD8^{+}, NK (DX5^{+}) and B (B220^{+}) cells in peripheral blood (PBL) samples in reconstituted mice before the initiation of PDF treatment. ($n \geq 8$). No statistically significant differences were found using one-way Anova test.

Thymus-derived Treg cell development is regulated by C-type-lectin–mediated BIC/miRNA155 expression

Running Title: C-type lectin regulates tTreg development

Authors:

Raquel Sánchez-Díaz[a,e], Rafael Blanco-Dominguez[a], Sandra Lasarte[a,e], Katerina Tsilingiri[a], Enrique Martín-Gayo[b], Beatriz Linillos-Pradillo[a] Hortensia de la Fuente[c,e], Francisco Sánchez-Madrid[c,e], Rinako Nakagawa[d], María L. Toribio[b], & Pilar Martín[a,e].

[a]Signaling & Inflammation Program, Centro Nacional de Investigaciones Cardiovasculares (CNIC), Madrid, Spain, 28029.

[b]Centro de Biología Molecular Severo Ochoa, Consejo Superior de Investigaciones Científicas, Universidad Autónoma de Madrid, Spain., 28049.

[c]Department of Immunology, Hospital de La Princesa, Madrid, Spain, 28006.

[d]Immunity and Cancer Laboratory, The Francis Crick Institute, London, WC2A 3LY, UK

[e]CIBER de Enfermedades Cardiovasculares, Instituto de Salud Carlos III, Spain, 28029.

Corresponding author. Tel: +34 914531200; Email: pmartinf@cnic.es

Keywords: Regulatory T cells development, C-type lectin, miRNA-155, Autoimmunity

Abstract

Thymus-derived regulatory T cells (tTregs) are key to prevent autoimmune diseases but the mechanisms involved in their development remain unsolved. Here, we show that the C-type lectin receptor CD69 controls tTreg cell development and peripheral Treg homeostasis through the regulation of BIC/miR-155 and its target, the suppressor of cytokine signaling 1 (SOCS-1). Using Foxp3-mRFP/*cd69*$^{+/-}$ or /*cd69*$^{-/-}$ reporter mice, shRNA-mediated silencing and miR-155 transfection approaches, we found that CD69 deficiency impaired the signal transducer and activator of transcription 5 (STAT5) pathway in Foxp3^{+} cells. This results in BIC/miR-155 inhibition, increased SOCS-1 expression and severely impaired tTregs development in embryos, adults and Rag2$^{-/-}\gamma c^{-/-}$ hematopoietic chimeras reconstituted with *cd69*$^{-/-}$ stem cells. Accordingly, *mirn155*$^{-/-}$ mice have impaired development of CD69^{+} tTreg cells and overexpression of miR-155 induced CD69 pathway, suggesting that both molecules might be concomitantly activated, in a positive feedback loop. Moreover, *in vitro*-inducible CD25^{+} Tregs (iTregs) development is inhibited in *Il2rγ*$^{-/-}$ /*cd69*$^{-/-}$ mice. Our data highlight the contribution of CD69 as a non-redundant key regulator of BIC/miR-155-dependent Treg development and homeostasis.

Introduction

Regulatory T (Treg) cells are a specialized subset of lymphocytes with a dominant role in the prevention of autoimmune diseases (1). Treg subtypes have been classified according to their origin in the thymus, peripheral lymphoid organs or *in vitro*, and have been extensively characterized; however, the mechanisms that regulate their generation in the thymus remain poorly understood. Understanding how thymus-derived Treg cells (tTregs) (2) become a distinct lineage is crucial for the development of strategies to control immune responses by targeting these cells (3). A central event in tTreg differentiation is the induction of the transcription factor Foxp3 by early signals delivered from the TCR, which results in transcriptional activation and enhanced function of the IL-2 signaling pathway(4). Among other mechanisms, Foxp3 expression is promoted by miR-155 through the inhibition of SOCS1 (suppressor of cytokine signaling 1), enhancing activation and binding of STAT5 (signal transducer and activator of transcription 5) to the Foxp3 promoter and the Foxp3-CNS (conserved non-coding sequence) (5, 6). In a positive feedback loop, Foxp3 increases expression of miR-155 by binding to an intronic element of BIC, the gene encoding the miR-155 precursor transcript. Nevertheless, the mechanisms by which miRNAs impact tTreg differentiation and function are not fully elucidated and the data are somewhat contradictory. For example, Dicer, a member of the RNAseIII complex that processes pre-miRNAs into mature miRNAs, plays a key role in tTreg differentiation (7) and function (8); however, lack of Dicer is linked to enhanced miR-155 expression in MRL/lpr mice (9), suggesting that there are Dicer-independent mechanisms for miRNA regulation in Tregs. The Tregs of Lupus-prone mice have an altered phenotype, low levels of Dicer, and a weak suppressive capacity linked to the expression of the C-type lectin

receptor CD69 (9). Moreover, increased CD69 expression has been detected in activated *Dicer*$^{-/-}$ TCs, which show defective egress from lymphoid organs (10). In addition, CD4^{+}CD8^{+} thymocytes include a CD69^{high}TCR^{high} Treg cell progenitor subpopulation, indicating that CD69 expression is relevant to tTreg differentiation (11). We hypothesized that CD69, which contributes to the maintenance of immunological tolerance through the regulation of Treg function, makes a substantial contribution to Treg development in the thymus. The C-type lectin CD69 is expressed constitutively by a subpopulation of peripheral Tregs (pTregs) and tTregs (12). Here, we report that CD69 is required for the development of Tregs in the thymus through the promotion of STAT5 phosphorylation and the transcription of BIC/miR-155. FoxP3-mRFP/c*d69*$^{-/-}$ reporter mice have a significantly below-normal number of tTregs, and Treg differentiation was also impaired in FTOC cultures of *cd69*$^{-/-}$ embryonic thymuses or wild-type embryonic thymuses treated with anti-CD69. Consistently, FoxP3^{+} tTregs are poorly generated from c*d69*$^{-/-}$ precursors in mixed bone marrow chimeras. Impairment of STAT5 phosphorylation in FoxP3-mRFP/c*d69*$^{-/-}$ tTregs leads to enhanced transcription of SOCS-1 and inhibition of miR-155-dependent tTreg development. CD69 thus maintains miR-155-dependent tTreg development through a positive feedback regulatory mechanism, giving rise to a functional pTreg cell subset. Our results strongly support a role for CD69 as a critical receptor in the control of Treg development and homeostasis.

Results

CD69 expression is required for development of the tTreg subset

To determine whether CD69 is necessary for tTreg development in the thymus, we analyzed CD69 membrane expression in tTregs from *cd69*$^{+/+}$, *cd69*$^{+/-}$, and *cd69*$^{-/-}$ littermates bearing a Foxp3-mRFP reporter gene (monomeric red fluorescent protein inserted in the *foxp3* locus). In agreement with previous data in non-reporter mice (12), about 30% of tTregs expressing Foxp3-mRFP in wild-type thymus also express CD69 (Fig. 1A and B). This percentage is lower in Foxp3-mRFP/*cd69*$^{+/-}$ heterozygous mice and this subset is absent in Foxp3-mRFP/*cd69*$^{-/-}$ deficient mice (Fig. 1A and B). The proportions of CD4^{+} single-positive (CD4SP) thymocytes and the other thymocyte subsets are unaffected in c*d69*-heterozygous and -deficient reporter littermates (Fig. 1C); but, compared with Foxp3-mRFP/*cd69*$^{+/+}$ mice, both genotypes showed a 30% lower cellularity of total and CD4SP thymocytes (Fig. 1D). These results are consistent with previous data showing that the overexpression of CD69 in the thymus increases the levels of SP thymocytes controlling egress to the periphery (13, 14). However, Foxp3-mRFP/*cd69*$^{-/-}$ and *cd69*$^{+/-}$ mice showed a marked reduction in the proportion of tTregs compared with *cd69*$^{+/+}$ adult reporter mice (Fig. 1E and F), while total tTreg numbers were not altered in the *cd69*$^{+/-}$ and *cd69*$^{-/-}$ deficient groups (Fig. 1F), indicating that CD69 could be playing an important role in the regulation of tTreg development masked by thymocyte egress defects in Foxp3-mRFP/*cd69*$^{-/-}$ mice. In addition, we found that *cd69*$^{-/-}$ adult reporter mice showed also a reduction in the proportion of peripheral Tregs (pTregs) compared with *cd69*$^{+/+}$ littermates (Fig. S1A and B). This data is not consistent with the previously reported in non-reporter mice (12). To clarify the differences observed with Foxp3 reporter mice, we performed

Foxp3 staining in thymus and spleens from Foxp3-mRFP mice. The data indicate that exogenous staining with anti-Foxp3 antibodies differs from the endogenous print of Foxp3-mRFP depending on the tissue (Fig. S2), suggesting that the use of anti-Foxp3 antibodies is not always as accurate as the use of reporter genes. In summary, CD69 could be playing a role in both, tTreg development and pTreg homeostasis.

Deletion of CD69 inhibits tTreg differentiation in fetal thymus organ cultures

To determine if *cd69*-deficiency leads to a decreased tTreg development, independently of the thymic maturation state or sphingosine 1-phosphate receptor-1 ($S1P_1$)-induced thymocyte egress capacity, we performed a fetal thymus organ culture (FTOC) assay on thymuses from 15-17-day-old mouse embryos (E15-E17), and analyzed total CD4SP thymocytes and tTreg differentiation over 5 days of culture. Compared with $cd69^{+/+}$ FTOCs, $cd69^{-/-}$ E15-17 FTOCs displayed a marked reduction in the proportion and absolute cell numbers of $Foxp3^+$ tTregs, with insignificant changes in total cell numbers (Fig. 2A and B), indicating that CD69 is required during tTreg differentiation at early stages of development. To confirm these results, we treated E15 FTOCs with an anti-CD69 monoclonal antibody (2.2), which downregulates CD69 expression and hence blocks downstream signaling (15) and monitored Treg development over 14 days of culture. Consistent with the $cd69^{-/-}$ FTOC data, throughout the culture period anti-CD69-treated FTOCs showed notably lower proportions and cell numbers of $Foxp3^+$ tTregs than FTOCs treated with isotype control antibody (2.8) (Fig. 2C and D), whereas total FTOC cell numbers were unaltered by either treatment (Fig. 2D). These findings are consistent with previous evidence indicating that immature activated $CD69^+$ thymocytes are the precursors of intrathymic Tregs in humans and mice (11, 16).

Defective tTreg and pTreg generation from *cd69*$^{-/-}$ progenitors is a cell-autonomous defect

To further explore the role of CD69 in tTreg differentiation, we transferred bone marrow (BM) hematopoietic stem cells from Foxp3-mRFP/*cd69*$^{+/+}$ or Foxp3-mRFP/*cd69*$^{-/-}$ littermates into lethally γ-irradiated C57BL/6 recipients (Fig. 3A). Twelve weeks after reconstitution, percentages and numbers of CD4^{+}Foxp3^{+} Tregs derived from *cd69*$^{-/-}$ BM precursors were markedly lower in the thymus (Fig. 3A) and blood (Fig. S3) than those derived from *cd69*$^{+/+}$ precursors, indicating an impaired Treg regeneration capacity of *cd69*$^{-/-}$ BM hematopoietic stem cells. Moreover, we analyzed the potential of these precursors to differentiate to tTregs in sublethally irradiated Rag2$^{-/-}$γc$^{-/-}$ recipients, which lack lymphoid cells (Fig. 3B). Because Rag2$^{-/-}$γc$^{-/-}$ recipient mice lack NK cells, we depleted donor BM precursors of T cells before transplant to avoid graft versus host disease (17). As before, *cd69*$^{-/-}$ BM precursors had the lowest tTreg regeneration potential, even though in both systems there were no differences in CD4SP cell numbers between thymus of chimeric mice from *cd69*$^{+/+}$ and *cd69*$^{-/-}$ BM precursors (Fig. 3A and B). These results suggest that the differences observed in the percentage of CD4^{+}Foxp3^{+} tTregs in the thymus are due to impaired differentiation of this cell subset and not to a defective thymocyte egress (Fig. 3A and B).

Finally, to definitely rule out that the differences observed are due to differential egress between *cd69*$^{+/+}$ and *cd69*$^{-/-}$ thymocytes (Fig. 1D), we generated mixed BM chimeric mice by reconstituting sublethally irradiated Rag2$^{-/-}$γc$^{-/-}$ mice with a 1:1 mixture of wild-type (B6SJL) CD45.1 and *cd69*$^{-/-}$ CD45.2 BM hematopoietic stem cells from either Foxp3-

reporter (Fig. 3C) or non-reporter mice (Fig. S4A). Thymuses, spleens, lymph nodes and blood were harvested starting from 8 to 10 weeks after transfer. $CD4^+Foxp3^+$ Tregs generated from *cd69*$^{+/+}$ and *cd69*$^{-/-}$ precursors were analyzed separately (Fig. 3D, Fig. S4B and Fig. S5). We detected a marked difference in the frequencies of $CD4^+Foxp3^+$ tTregs and pTregs originating from the two precursors in both models, with a lower proportion of Tregs derived from *cd69*$^{-/-}$ CD45.2 $CD4^+$ SP precursors than from *cd69*$^{+/+}$ CD45.1 precursors (Fig. 3D and E, Fig. S4C and Fig.S5A-C); this occurred even though $CD4^+$ SP cells originating from both precursors in equal proportions in the thymus (Fig. 3E), spleens (Fig. S5A) and lymph nodes (Fig. S5B). These data indicate that *cd69*$^{+/+}$ BM hematopoietic stem cells are necessary for the generation of $CD4^+Foxp3^+$ tTregs and subsequently pTreg homeostasis. Our data are consistent with the finding that Treg precursors in human thymus form part of the $CD69^+$ thymocyte cell subset (11).

CD69 deficiency impairs STAT5 signaling and BIC/miR-155-dependent tTreg differentiation

To investigate the mechanism of CD69-modulated tTreg development, we examined the Stat5 pathway that stimulates *foxp3* promoter, inducing tTreg development (4). Sorted Foxp3-mRFP$^+$-CD69$^+$ and -CD69$^-$ Tregs from wild type reporter mice (Fig. S6), were analyzed by intracellular staining and western blot. The analysis showed diminished STAT5 phosphorylation in sorted CD69$^-$ tTregs in steady state (Fig. 4A and B), indicating that CD69 expression maintains STAT5 bystander activation of tTregs within the thymus. The analysis of spleen sorted pTregs confirmed diminished STAT5 phosphorylation in secondary lymphoid organs (Fig. S7A). Although we detected no differences in Foxp3 activation or expression between CD69 expressing and non-expressing tTregs (Fig. 4C and

179 Fig. 1E) or pTregs (12), the transcriptional activation of *bic* was abrogated in CD69$^-$ tTregs,
180 and consequently miR-155 expression was inhibited in those cells (Fig. 4D) and pTregs
181 (Fig. S7B). It has been reported that miR-155 inhibits the expression of suppressor of
182 cytokine signaling 1 (SOCS-1), supporting Foxp3$^+$ tTreg development (6). Importantly,
183 *socs-1* gene and protein expression were both upregulated in CD69$^-$ tTregs (Fig. 4E and F)
184 and pTregs (Fig. S7B), which had very low levels of miR-155. Moreover, we analyzed
185 STAT5 pathway in sorted tTregs from *cd69*$^{+/+}$, *cd69*$^{+/-}$ and *cd69*$^{-/-}$ Foxp3-mRFP-reporter
186 mice. STAT5 phosphorylation is partially inhibited in *cd69*$^{+/-}$ compared to *cd69*$^{-/-}$ tTregs,
187 that have almost abrogated the pathway (Fig. 4G). Thus, *cd69*$^{+/-}$ and *cd69*$^{-/-}$ tTregs have
188 very low levels of miR-155 compared to *cd69*$^{+/+}$. Accordingly, *socs-1* gene is modestly and
189 strongly upregulated in *cd69*$^{+/-}$ and *cd69*$^{-/-}$ tTregs, respectively (Fig. 4H). Our data suggest
190 that the loss of at least one *cd69* allele modifies at least in part the expression of the
191 receptor on the membrane (Fig. 1A and B), but is sufficient to prevent fully activation of
192 STAT5 pathway, miR-155 transcription, SOCS-1 inhibition and proper differentiation of
193 tTregs.
194 The overexpression of SOCS-1 regulates STAT5 signaling reducing the proportion of
195 tTregs in *cd69*$^{-/-}$ mice to levels similar to *mirn155*$^{-/-}$ mice (6). We analyzed the
196 CD69$^+$/CD69$^-$ ratio within tTreg and pTreg cells from *mirn155*$^{-/-}$ mice (Fig. 5A and C).
197 Consistent with the previous work, *mirn155*$^{-/-}$ mice display impaired numbers of tTregs and
198 pTregs, as well as an important reduction in the development of CD69$^+$ Tregs, both in
199 thymus (Fig. 5A) and spleens (Fig. 5C). Interestingly, *cd69* gene expression was almost
200 abrogated in the thymus of *mirn155*$^{-/-}$ mice (Fig. 5B), suggesting that *cd69* and *mirn155*
201 could have common regulation pathways.

202 In agreement, we found that *cd69*$^{+/-}$ and *cd69*$^{-/-}$ thymic precursors are less able to
203 differentiate towards tTregs than CD69-proficient precursors in the same mice (Fig. 1F and
204 Fig. 3E). These data thus strongly suggest that the maintenance of miR-155 expression in
205 tTregs is dependent on CD69-induced STAT5 phosphorylation, reflecting a unique
206 property of CD69 in the development of tTregs.
207
208 **Both IL-2R$\gamma$and CD69 signaling is required for the development of *in vitro*-inducible**
209 **CD25^{+} Treg cells**
210 To further explore the non-redundant role of CD69 in the development of *in vitro*-inducible
211 Tregs (iTregs), we analyzed the levels of Foxp3 in the absence of Jak3-STAT5 signaling.
212 We cultured CD4 naïve T cells under Treg-skewed conditions with TGFβ plus IL-2 in the
213 presence of antigen presenting cells. The use of Jak3 chemical inhibitors decreased STAT-5
214 phosphorylation in *cd69*$^{+/+}$ iTreg cells to *cd69*$^{-/-}$ iTreg levels (Fig. 6A), however the
215 percentage of Foxp3-mRFP^{+} cells is comparable in both genotypes, even high in *cd69*$^{-/-}$
216 Tregs cultures and independently of Jak-STAT5 inhibition (Fig.6B), indicating that Jak3-
217 STAT5 signaling pathway is not required for Foxp3 expression of inducible Tregs,
218 corroborating previous data in tTregs (Fig. 4C).
219 It has been described that Foxp3 expression is dependent of IL-2Rγc, thus *Il2r*$\gamma^{-/-}$ mice had
220 no detectable Foxp3^{+} cells in thymus or spleen (18). However, the expression of CD25^{+}
221 Tregs is detectable in thymus and spleen of those mice (18). We aimed to address the role
222 of CD69 in the development of CD25^{+} iTregs in the absence of IL-2Rγ/Foxp3 signaling
223 pathways. For that purpose, we generated the double knock-out mice *Il2r*$\gamma^{-/-}$/*cd69*$^{-/-}$. We
224 analyzed the levels of CD25^{+} iTreg cells after induction with TGFβ plus IL-2 in the

presence of Jak3 inhibitors in cells from *Il2rγ*$^{-/-}$ mice compared to *Il2rγ*$^{-/-}$/*cd69*$^{-/-}$ mice. Jak3 inhibition decreased STAT-5 phosphorylation in *Il2rγ*$^{-/-}$ iTreg cells to the levels of *Il2rγ*$^{-/-}$/*cd69*$^{-/-}$ Tregs (Fig. 6C). Interestingly, the differentiation of CD25^{+} iTreg cells is completely abolished in both, *Il2rγ*$^{-/-}$/*cd69*$^{-/-}$ iTregs and *Il2rγ*$^{-/-}$ iTreg plus Jak3 inhibitors (Fig. 6D). These data indicate that, in the absence of IL-2Rγ/Foxp3 pathway, CD69-induced Jak3-STAT5 activation is pivotal for the development of CD25^{+} iTreg cells.

It has been proposed that miR-155 could regulate different cell type functions depending on the biological context, and miR-155 mediated SOCS-1 repression regulates the competitive fitness of Treg cells (19). We analyzed the expression of *mir-155*, *socs-1*, *T-bet* and *Eomes* in order to investigate if other miR-155 target genes are affected in iTregs differentiation in the absence of Jak3-STAT5 signaling pathway activation through CD69. We observed diminished expression of miR-155 in *cd69*$^{-/-}$ compared to *cd69*$^{+/+}$ iTreg cells (Fig. S8A), as in *ex-vivo* CD69^{-} Thymus-derived Tregs (Fig. 4D and G). However, Jak3 inhibition does not contribute to miR-155 inhibition (Fig. S8A), suggesting that other signaling pathways could contribute to miR-155 regulation in iTregs. Moreover, *socs-1* expression is strongly induced in *cd69*$^{-/-}$ iTreg cells compared to *cd69*$^{+/+}$ iTregs (Fig. S8B), but not other miR-155 target genes as *T-bet* and *Eomes* (Fig. S8C). Interestingly, Jak3 inhibits the expression of *socs-1*, *T-bet* and *Eomes* in the absence of CD69 (Fig. S8B and C), supporting the hypothesis that other CD69-dependent mechanisms could be involved in the regulation of those target genes. Altogether, these data suggest that CD69 controls *socs-1* expression and Tregs differentiation through miR-155 regulation, although other molecules could be involved in the process.

Expression levels of miR-155 and CD69 are co-regulated in a positive feedback loop

CD69 and BIC/miR-155 promoter sequences have two putative STAT5 binding elements upstream of the TATA box and AP-1 element (20) (Fig. S9). Moreover, the transcription factor AP-1, highly induced after TCR stimulation, regulates the activation of both promoters (20, 21), suggesting that both promoters might be concomitantly activated, in a positive feedback loop, by the same TCR/CD3 triggered pathway (Fig. S9). To test this hypothesis, we next investigated whether CD69 downstream signaling regulates miR-155 expression in tTregs. Sorted Foxp3^{+} tTregs from Foxp3-mRFP/*cd69*$^{+/+}$ mice, expressing CD69 in steady state, were incubated with anti-CD69 antibody (2.2), which downregulates CD69 membrane expression and dampens its signaling (22) (Fig. 7A). As described above, we observed strong CD69 dampening on the membrane compared with cells incubated with control mouse IgG1 mAb (2.8) (Fig. 7A). qPCR analysis revealed decreased miR-155 expression in 2.2-treated CD69^{+} tTregs (Fig. 7B), to levels comparable to CD69^{-} or *cd69*$^{-/-}$ tTregs (Fig. 7B and Fig. 4D and H). Moreover, CD69 blockade with 2.2 Abs impairs STAT5 phosphorylation (Fig. 7C) and prevents SOCS1 inhibition (Fig. 7D), meaning that CD69 expression is necessary for miR-155-dependent inhibition of SOCS1 and *bona fide* formation of tTregs.

To verify whether these findings could be extended to human cells, activated CD4^{+}CD25^{+} PBLs were infected with lentiviruses (LV) carrying different shCD69 sequences (shCD69-1 to -3). Endogenous levels of membrane CD69 and hsa-miR-155 were analyzed by FACS and qPCR, respectively (Fig. 8A and B). LV infection of PBLs with three shCD69 sequences fully inhibited CD69 expression compared to Mock LV infection (Fig. 8A), inducing loss of hsa-miR-155 transcription (Fig. 8B). Our data indicate that human CD69 and hsa-miR-155 are regulated together as in mouse cells. In parallel, we induced the

272 expression of CD69 in vitro (Fig. 8C) to corroborate that the STAT5 pathway and hsa-miR-
273 155 are activated together with the receptor, whereas SOCS1 is inhibited (Fig. 8D).
274 To test this mechanism functionally, we performed loss and gain of function assays by
275 transfecting human Tregs with anti-hsa-miR-155 or hsa-pre-miR-155. First, we transfected
276 control and anti-CD3 (OKT3)-stimulated $CD4^{+}CD25^{+}$ human PBLs with anti-hsa-miR-
277 155-5p or scrambled anti-miRNA (Fig. 8E). CD69 expression in activated PBLs drops
278 dramatically after inhibition of hsa-miR-155 (Fig. 8F). Moreover, STAT5 activation was
279 reduced and, in agreement, *socs1* gene expression was enhanced, indicating that miR-155
280 blockade regulates CD69 signaling pathway. By contrast, overexpression of hsa-miR-155
281 in $CD69^{-}$ Tregs (Fig. 8G) revealed a significant increase in the expression of CD69, STAT5
282 activation and *socs1* inhibition (Fig. 8H). Thus, the reciprocal modulation of the C-type
283 lectin and miR-155 in a positive feedback loop could be pivotal to maintain tTregs fitness
284 and pTregs homeostasis.
285
286

Discussion

In this study we have shown that the C-type lectin CD69 plays a key role in the development and homeostasis of Tregs. Using a combined genetic model of Foxp3-reporter and *cd69*-knockout mice and genetic inhibition approaches, we unequivocally demonstrate that the activation of CD69 pathway promotes STAT5 phosphorylation, BIC/miR-155 expression and SOCS-1 inhibition. The role of CD69 as a negative regulator of the immune system has remained a controversial issue during the last years (23). However, very recent studies by independent groups, show that CD69 plays a crucial role in the suppressor function of mice and human Tregs, as well as in the generation of *in vitro*-induced Treg cells (12, 16, 24-26). Nevertheless, the specific role of the C-type lectin in the development of Tregs in the thymus remains elusive.

A major issue that has limited this study has been the key role of CD69 in the egress of lymphocytes from lymphoid organs and in particular from the thymus to periphery (13, 14, 27-29). Although thymic positive and negative T-cell selection processes are unaffected by CD69 deficiency (30), CD69 controls the egress of mature T cells into the periphery via cortico-medullary blood vessels, through the negative regulation of $S1P_1$ receptors (27, 28), making it not an easy task to study its role in the development of Tregs in the thymus. With the help of Foxp3-reporter mice, we have performed the study of tTregs differentiation in FTOC and in mixed chimeric mice to avoid the effects derived from the different migratory potential of $CD69^+$ and $CD69^-$ cells. We demonstrate that the expression of the C-type lectin CD69 is pivotal for tTregs development as they are virtually absent in FTOC cultures from *cd69*$^{-/-}$ or anti-CD69-treated embryonic thymuses, or in mixed bone marrow chimeras from c*d69*$^{-/-}$ precursors. In both systems, total numbers of cells within the thymus do not

change, whereas tTregs proportions originated from CD69^{-} precursors are consistently diminished, demonstrating unequivocally that this effect is not due to a different migratory behavior.

We have found that Foxp3^{+}pTregs are also diminished after analysis of spleen and lymph nodes from adult Foxp3-mRFP/*cd69*$^{-/-}$ reporter compared to *cd69*$^{+/+}$ and *cd69*$^{+/-}$ littermates. In addition, CD69-deficient pTregs have defective suppressive function (12). Thus, defects observed in CD69 deficient precursors affect both, tTreg development and pTreg homeostasis, strongly indicating that CD69 proficient precursors give rise to the CD69^{+} functionally active pTreg subset. In this regard, two different genetic approaches in mice and a recent study in humans indicate that CD69 expression in pTregs is required to maintain immunological tolerance. CD69-deficiency in mice compromises T-cell induced colitis and the establishment of oral tolerance after antigen challenge in vivo (24), and CD69^{+} pTregs are essential for the prevention of asthmatic reactions to harmless antigens (12). Furthermore, a subset of CD69^{+} Tregs in the blood of healthy human donors seems to have a relevant immune-regulatory role (25).

The C-type lectin CD69 interacts with Jak3/STAT5 proteins independently of the IL-2 pathway, thus inhibiting Th17 responses (31) and controlling the suppressor potential of pTregs (12). STAT5 phosphorylation stimulates *foxp3* promoter, inducing tTreg development (4), and Foxp3 binds to an intron within the promoter region of the miR-155 host gene *bic* in Tregs (32). *Mirn155*$^{-/-}$ and *bic*$^{-/-}$ mice both have below normal Foxp3^{+} Treg numbers in thymus and secondary lymphoid organs, indicating an essential role for miR-155 in the development of Foxp3^{+} Tregs (5, 6). We have explored if this pathway could be the responsible for the defects observed in Treg development in *cd69*-deficient mice, finding a strong inhibition of STAT5 phosphorylation in freshly isolated Foxp3-mRFP^{+}-

334 CD69^{-} compared to -CD69^{+} tTregs. Moreover, bic/miR155 transcriptional levels are
335 reduced in Foxp3-mRFP^{+}-CD69^{-} Tregs and consequently, its target SOCS-1 is up-regulated
336 both at mRNA and protein levels. In a mouse model of SOCS-1 overexpression, negative
337 regulation of STAT5 signaling reduces the proportion of Foxp3^{+} thymocytes to levels
338 similar to those seen in *mirn155*$^{-/-}$ mice (6). MiR-155 inhibits SOCS1 expression,
339 enhancing Foxp3^{+} tTreg development (6). Our data demonstrate that CD69 expression
340 enhanced BIC/miR-155 transcription, inhibits SOCS-1 and therefore maintains Tregs
341 differentiation and fitness of Tregs. However, IL-2R signaling also activates Jak/STAT5
342 pathway in Tregs, specifically Foxp3 expression is dependent on IL-2Rγc signaling as
343 *Il2rγ*$^{-/-}$ mice have no detectable Foxp3^{+} cells, although a small proportion of CD25^{+} Tregs
344 are still detectable in these mice (18). Our study shows that the differentiation of CD25^{+}
345 iTreg cells is inhibited in *Il2rγ*$^{-/-}$ cultures plus Jak3 inhibitors or *Il2rγ*$^{-/-}$/*cd69*$^{-/-}$ mice,
346 indicating that Jak3-STAT5 signaling pathway activation through CD69 is essential for the
347 development of Tregs.
348 CD69 does not appear as a miR-155 target in the PicTar, Targetscan or miRanda miRNA
349 target prediction databases, and there are no miR-155 target sequences in the CD69
350 3´untranslated region (UTR) (33). However, several studies have shown a correlation
351 between Dicer, a member of the RNAseIII complex that processes pre-miRNAs into mature
352 miRNAs, miR-155 regulation, and CD69 expression. Tregs from MRL/lpr mice are Dicer
353 insufficient, and yet overexpress miR-155 and show increased CD69 expression (9),
354 suggesting that there are Dicer-alternative mechanisms for miRNA regulation. In another
355 study, *Dicer*$^{-/-}$ TCs showed increased CD69 expression after TCR stimulation and,
356 consequently, defective egress from lymphoid organs (10). As we described for CD69

357 above, Dicer plays a key role in tTreg differentiation (7) and Treg function (8). In this
358 regard, CD69 is expressed in lymphocytes early after TCR/CD3 stimulation (34) and its
359 cytoplasmic tail interacts with Jak3/STAT5 molecules (35), triggering this pathway in
360 pTregs (12) and tTregs and therefore inhibiting SOCS-1 transcription and protein
361 expression. Similarly, TCR-induced IL-2 signaling triggers STAT5 signaling and enhances
362 Foxp3-dependent miR-155 expression, limiting SOCS-1 expression and promoting Treg
363 homeostasis (6). Recent data shows that microRNAs could regulate different cell type
364 functions modulating different target genes, depending on the biological context (19). We
365 analyzed the expression of miR-155 and *SOCS1* in the absence of Jak3-STAT5 signaling
366 pathway activation through CD69 in the differentiation of iTreg cells. miR-155 expression
367 is inhibited and SOCS-1 is up-regulated in *cd69*$^{-/-}$ compared to *cd69*$^{+/+}$ iTreg cells, however
368 Jak3 inhibition does not contribute to miR-155 dampening suggesting that other
369 microRNAs and/or target genes could be involved. Interestingly, the STAT5 binding
370 elements of the BIC/miR-155 and CD69 promoter sequences are similar, with each
371 containing two putative STAT binding elements upstream of the TATA box and AP-1
372 element (20). Moreover, the transcription factor AP-1, highly induced after TCR
373 stimulation, regulates the activation of both promoters (20, 21). This suggests that both
374 promoters might be concomitantly activated, in a positive feedback loop, by the same
375 TCR/CD3 triggered pathway.
376 Our present study shows that Foxp3-RFP/*cd69*$^{-/-}$ reporter mice have dramatically reduced
377 tTreg cell population in adult thymus. Moreover, tTregs are unable to develop properly in
378 FTOC cultures from *cd69*$^{-/-}$ or anti-CD69-treated embryonic thymuses, or in mixed bone
379 marrow chimeras from c*d69*$^{-/-}$ precursors. The *in vitro* data confirm that phosphorylation of
380 STAT5 is abrogated in CD69-deficient tTregs and results in inhibition of the BIC/miR-155

pathway, increased SOCS-1 expression and impaired tTreg development. Our previous studies show that the suppressor function of Tregs is compromised in *cd69*-deficient mice (12), indicating that CD69 is a key molecule in the development of $Foxp3^{+}CD69^{+}$ Tregs in the thymus that will give rise to the functionally active subset of Tregs in the periphery. Therefore, we postulated the C-type lectin CD69 as a pivotal molecule for the maintenance of immune homeostasis in health and disease.

Material and Methods

Mice. *cd69*$^{-/-}$ mice were generated in the 129/Sv background as described (31), and backcrossed onto C57BL/6 for at least 12 generations. C57BL/6.Ly5.1 mice (CD45.1^{+}) were purchased from The Jackson Laboratory (B6.SJL-Ptprc^{a} Pepc^{b}/BoyJ: 002014). Rag2$^{-/-}$ γc$^{-/-}$ (Rag2/Il2rg) mice were provided by the Dr. ML. Toribio´s laboratory (Centro de Biología Molecular, CSIC, Spain) and were intercrossed with C57BL/6 mice to generate the *Il2rγ*$^{-/-}$ mice that were subsequently intercrossed with *cd69*$^{-/-}$ mice, to generate the *Il2rγ*$^{-/-}$/*cd69*$^{-/-}$ mice. FoxP3-mRFP reporter mice (FIR mice, C57BL/6 background) were generated and provided by the Flavell laboratory (Yale University School of Medicine, New Haven, CT) (36), and were intercrossed with the *cd69*$^{-/-}$ mice to generate the Foxp3-mRFP/*cd69*$^{+/+}$ wild-type, Foxp3-mRFP/*cd69*$^{+/-}$ heterozygous, and Foxp3-mRFP/*cd69*$^{-/-}$ *CD69*-deficient littermates. Animals were housed and used in specific pathogen-free (SPF) conditions at the CNIC animal facility. *mirn155*$^{-/-}$ mice were provided by Dr. R. Nakagawa (The Francis Crick Institute, London). All animal procedures were approved by the ethics committee of the *Comunidad Autónoma de Madrid* and conducted in accordance with the institutional guidelines that comply with the European Institutes of Health´s; *Directive 2010/63/EU of the European Parliament and the Council on the Protection of Animals Used for Scientific Purposes (Official Journal of the European Union. Vol. 53:33-79, 2010).*

Intracellular staining and FACS. Single-cell suspensions were obtained from adult or fetal thymuses and incubated in FACS buffer (PBS 0.5% BSA, 1μM EDTA, 0.1% NaN_3) with fluorochrome-conjugated mouse-specific antibodies against CD4, CD8, CD69,

414 CD45.1 and CD45.2. All antibodies were purchased from BD Biosciences. For Foxp3
415 intracellular staining, we used the Foxp3 staining kit (eBioscience). $CD69^{+}$- and $CD69^{-}$-
416 Foxp3-$mRFP^{+}$ tTreg cells were sorted from Foxp3-mRFP/*cd69*$^{+/+}$ thymus using a
417 FACSAria III (BD). For intracellular STAT5 staining, sorted tTregs were fixed with 0.2%
418 paraformaldehyde and permeabilized with 90% methanol, and cells were incubated with
419 anti-Phospho-Stat5 (Tyr694) (Cell Signaling), Alexa Fluor 647 IgG1 Isotype Control and
420 Alexa Fluor 647 anti-phospho-STAT5 (pY694) (Beckton Dickinson). Human PBLs were
421 obtained after Ficoll separation from buffy coats and maintained in RPMI medium
422 supplemented with 10% FCS, 20 mM HEPES, L-glutamine, antibiotics, non-essential
423 aminoacids, sodium pyruvate and □-mercaptoethanol. Treated PBLs were incubated with
424 fluorochrome-conjugated human-specific antibodies against CD4, CD25 and CD69 (BD
425 Biosciences) and Foxp3 (Miltenyi Biotec). Cells were analyzed in an LSRFortessa^{TM} flow
426 cytometer (BD) equipped with four lasers (405, 488, 561 and 640 nm), and the data were
427 processed with FlowJo v10.0.4 (Tree Star).
428
429 **Fetal Thymus Organ Culture.** Uteri were removed female mice at the indicated
430 gestational time points and the embryos were placed in a Petri dish with fresh cold PBS for
431 extraction of thymuses. To place the fetal thymus lobes in culture, we placed 0.8 µm
432 nitrocellulose membrane filters (Millipore) on top of 12-7 mm Gelfoam sponges embedded
433 in pre-warmed IMDM medium (supplemented with 10% FCS, L-glutamine, antibiotics, and
434 β-mercaptoethanol). FTOCs were maintained for 4 to 14 days with medium replaced every
435 3 days. Anti-CD69 monoclonal antibody (2.2) or the isotype control antibody (2.8) was
436 added (50µg/ml) to the culture medium as indicated and replaced every 3 days. At the end

of the culture period, single-cell suspensions were prepared from the lobes, and cells were counted and analyzed by FACS.

Western blotting. Lysates of sorted $CD69^+$- and $CD69^-$-Foxp3-$mRFP^+$ tTreg cells were prepared in PD buffer (40mM Tris HCl pH 8.0, 0.5M NaCl, 6 mM EDTA, 6 mM EGTA, 0.1% NP40) containing protease inhibitor cocktail (Complete Mini, Roche). Proteins (20 µg) were size-separated on 12% SDS-polyacrylamide gels and transferred onto Trans-Blot nitrocellulose membranes (BioRad). Primary antibodies for immunoblot were as follows: anti-β-actin, anti-SOCS-1 and anti-STAT5 (Santa Cruz); anti-phospho-STAT5 (Cell signaling). Quantitative assessment of protein expression was performed with the Odyssey scanner and analyzed with Image Studio Lite v4.0 western blot analysis software (LI-COR).

***In vitro* differentiation of Tregs**. Inducible Tregs were differentiated from Foxp3-mRFP/*cd69*$^{+/+}$, Foxp3-mRFP/*cd69*$^{-/-}$, *Il2rγ*$^{-/-}$/*cd69*$^{-/-}$ and *Il2rγ*$^{-/-}$ mice. Naïve CD4 T cells from these mice were isolated and co-cultured 72h with irradiated antigen presenting cells in the presence of plate bound anti-CD3 (2µg/ml) and soluble anti-CD28 (2µg/ml) plus recombinant TGF-β1(10ng/ml) and IL-2 (2ng/ml). The last 9 hours the cells were incubated with or without JAK 3 inhibitor I (CAS 202475-60-3 – Calbiochem) (10µg/ml). For experiments with inhibitor antibodies, after differentiation Treg cells were cultured 4h with anti-2.2 Ab or 2.8 isotype control.

459 **RNA extraction and gene expression analysis.** RNA and microRNA were extracted from
460 2- to -6x10^4 sorted mouse tTregs or 10^6 human PBLs with the miRNeasy mini kit (Qiagen),
461 followed by DNAse treatment with the Turbo DNAse-free kit (Ambion). For analysis of
462 SOCS-1, Foxp3 and BIC transcripts, reverse transcription was performed using the High
463 Capacity cDNA reverse transcription kit (Applied Biosystems). SOCS-1 and Foxp3 gene
464 expression was analyzed by real-time PCR using SYBR green PCR mix (Applied
465 Biosystems). Mouse and human *Gapdh* genes were used as the endogenous control. The
466 following primers were used to amplified murine genes: *Socs-1*, (F) 5′-
467 CTGCGGTTCTATTGGGGAC-3′, (R) 5′-AAAAGGCAGTCGAAGGTCTCG-3′; *Foxp3*,
468 (F) 5′-CACCCAGGAAAGACAG CAACC-3′, (R) 5′-GCAAGAGCTCTTGTCCATTGA-
469 3′; *cd69*, (F) 5′-CCCTTGGGCTGTGTTAATAGTG-3′, (R) 5′-
470 AACTTCTCGTACAAGCCTGGG-3′ and *Gapdh*, (F) 5′-TGAAGCAGGCATCTGAGGG-
471 3′, (R) 5′-CGAAGGTGGAAGAGTGGGAG-3′. The following primers were used to
472 amplified human genes: *socs-1,* (F) 5′-TTTTCGCCCTTAGCGTGAAGA-3′, (R) *5′-*
473 GAGGCAGTCGAAGCTCTCG-3′, and *gapdh* (F) *5′*-AATGGACTGGTCGTGGAG-*3′,*
474 (R) 5′-CCCTCCAGGGGATCGTTTG-*3′*. BIC gene expression was analyzed by real-time
475 PCR using TaqMan Universal PCR Master mix and specific TaqMan probe and primers for
476 *bic* (assays ID Mm01716204-m1 and ID Hs01374570-m1) (Applied Biosystems).
477 Expression of microRNA was analyzed using TaqMan MicroRNA Reverse Transcription
478 Kit, individual TaqMan MicroRNA Assays for mmu-miR-155-5p (Ref. 002571) and hsa-
479 miR-155-5p (Ref. 002287) and TaqMan Universal PCR Master mix (Applied Biosystems).
480 sno135 snRNA (Ref. 001230) was used as the endogenous control. Real-time Quantitative

PCR analysis was performed with an ABI Prism 7900HT 384 thermal cycler (Applied Biosystems). Relative gene expression was determined using the $2^{-\Delta\Delta_{CT}}$ method.

Chimeric mice. Eight-twelve-week-old Rag2$^{-/-}$ γc$^{-/-}$ recipient mice were irradiated with one split dose of 6.5 Gy γ-radiation, whereas C57BL/6 recipients were irradiated with two split 6.5 Gy doses. The mice were i.v. injected with bone marrow cells from Foxp3-mRFP/*cd69*$^{+/+}$ or Foxp3-mRFP/*cd69*$^{-/-}$ littermates. In mixed chimeras, irradiated Rag2$^{-/-}$ γc$^{-/-}$ recipients were transplanted with a mixture of CD45.1 *cd69*$^{+/+}$ or CD45.2 *cd69*$^{-/-}$ bone marrow precursors from non-reporter or reporter Foxp3-mRFP^{+}, at a ratio of 1:1. After at least 10 weeks, the contribution of the different donor bone marrow precursors to the tTreg subset was determined by FACS.

Transient transfection. PBLs (10^6) cells were transiently transfected for 4 hours with 50 pM of anti-miR-155 (AM12601 Ambion) by Lipotransfectin (Niborlab) according to the manufacturer´s instructions. As a negative control, random anti-miR sequence control (AM1701 negative control #1 Ambion) was included in the assay. Transfected cells were stimulated with plate-bound anti-CD3 antibody (OKT3; 3 ug/mL) for 24 hours. When indicated, PBLs ($0.5x10^6$) cells were transfected for 7h with 50 pM of Pre-miR-hsa- miR-155 or Pre-miR negative control (Ambion) by Lipofectamine RNA iMAX (Invitrogen). Transfected cells were stimulated with PMA during 4 h with 50ng/ml phorbol myristate acetate (PMA) and 750ng/ml ionomycin (P+I). After stimulation, the levels of CD69 and phospho-Stat5 were monitored by flow cytometry and transcriptional levels of hsa-miR-155 and *socs1* were monitored by qPCR.

504

505 **Plasmids.** The pLKO lentiviral plasmids containing shCD69 sequences were from Sigma
506 Aldrich (TRCN0000057693; TRCN0000057694; TRCN0000057695) and the pLKO
507 lentiviral control plasmid is a pLKO empty vector from Sigma Aldrich (Ref. SHC001). The
508 shCD69 sequences used were as follows: SHCD69-1 (5′-3′):
509 CCGGGCATGGAATGTGAGAAGAATTCTCGAGAATTCTTCTCACATTCCATGCTT
510 TTTG; SHCD69-2 (5′-3′):
511 CCGGAGGCCAATACACATTCTCAATCTCGAGATTGAGAATGTGTATTGGCCTTT
512 TTTG; SHCD69-3 (5′-3′):
513 CCGGGTGGTCAAATGGCAAAGAATTCTCGAGAATTCTTTGCCATTTGACCACTT
514 TTTG.

515

516 **LV production, titration, and infection.** HEK-293 cells were cultured in DMEM
517 containing 10% FBS (Sigma Aldrich) and L-glutamine plus antibiotics. HEK-293 were
518 transiently transfected by the calcium phosphate method with 3 HIV-derived plasmids and
519 the VSV pseudotyped LV system (provided by F. Sánchez-Madrid, Hospital de la Princesa,
520 Spain) to obtain LV expressing the shCD69 sequences. The supernatant containing LV
521 particles was collected 48 hours after removal of the calcium phosphate precipitate and
522 ultracentrifugated for 2 hours (Optima L-100 XP Ultracentrifuge Beckman). LVs were
523 collected by adding cold PBS and were titrated by qPCR. PBLs isolated from healthy
524 donors were infected with LV particles (MOI=10) for 5 hours. Subsequently, virus-
525 containing medium was replaced with fresh complete RPMI medium supplemented with
526 10% FBS. After 12 hours, infected cells were selected with puromycin for 48 hours.
527 Selected cells were stimulated with plate-bound anti-CD3 antibody (OKT3; 3 µg/mL) for

24 hours. After stimulation, the levels of CD69 were monitored by flow cytometry and levels of miRNA 155 were monitored by Taqman qPCR.

Statistical analysis. Experiments were performed according to a randomized complete block design (treatments and different time points have been taken into account) or a fully randomized design. To determine significant differences, P values were calculated by Student's t test as appropriate, and differences were considered significant values at $P<0.05$. Means of more than two experimental groups were compared by 1-way ANOVA. To account for multiple comparisons, the Tukey was used to compared selected pairs of means, and the Bo; ;nferroni post-test was used to compare all pairs of means. All statistical analyses were carried out with Prism v5 (GraphPad Software). Each experiment was repeated at least three times, unless otherwise indicated in the figure legends.

Acknowledgements

We thank S. Bartlett for editorial assistance and Prof. Richard A. Flavell (Yale University, New Haven, CT) for kindly provided the *foxp3*-mRFP reporter mice. This study was funded by grant from the Spanish Ministry of Economy and Competitiveness (SAF2013-44857-R to M.L.T); grant INDISNET 01592006 from the *Comunidad de Madrid* to P.M. and FSM; grant from Instituto de Salud Carlos III (PI-FIS-2016-9488 to P.M) and CIBER de Enfermedades Cardiovasculares to. F.S-M and P.M.; Fundació La Marató TV3 (20152330 31) to P.M. and F.S-M. R.S.D. was funded by a predoctoral fellowship from the Comunidad de Madrid; S.L. was funded by a contract from the RETICS *Enfermedades Cardiovasculares* (Instituto de Salud Carlos III); K.T. is co-funded by the EU Marie Curie Program (COFUND CNIC IPP). The research has been co-financed by FEDER. The CNIC is supported by the Ministry of Economy, Industry and Competitiveness (MINECO) and the Pro CNIC Foundation, and is a Severo Ochoa Center of Excellence (MINECO award SEV-2015-0505).

Authors contributions

R.S-D. and R.B-D. performed research and analyzed the data; S.L., K.T., H. dlF., B.L-P. and E.M-G. performed research; R. N. contributed with *mirn155*$^{-/-}$ mice; F.S-M. and M.L.T. designed research and analyzed the data.; P.M. designed research, collect and analyzed the data and wrote the paper.

Competing financial interests

The authors declare no that they have no competing interest.

References

1. Campbell, D. J., and M. A. Koch. 2011. Phenotypical and functional specialization of FOXP3+ regulatory T cells. *Nat Rev Immunol* 11: 119-130.
2. Abbas, A. K., C. Benoist, J. A. Bluestone, D. J. Campbell, S. Ghosh, S. Hori, S. Jiang, V. K. Kuchroo, D. Mathis, M. G. Roncarolo, A. Rudensky, S. Sakaguchi, E. M. Shevach, D. A. Vignali, and S. F. Ziegler. 2013. Regulatory T cells: recommendations to simplify the nomenclature. *Nat Immunol* 14: 307-308.
3. Josefowicz, S. Z., L. F. Lu, and A. Y. Rudensky. 2012. Regulatory T Cells: Mechanisms of Differentiation and Function. *Annu Rev Immunol* 30: 531-564.
4. Burchill, M. A., J. Yang, K. B. Vang, J. J. Moon, H. H. Chu, C. W. Lio, A. L. Vegoe, C. S. Hsieh, M. K. Jenkins, and M. A. Farrar. 2008. Linked T cell receptor and cytokine signaling govern the development of the regulatory T cell repertoire. *Immunity* 28: 112-121.
5. Kohlhaas, S., O. A. Garden, C. Scudamore, M. Turner, K. Okkenhaug, and E. Vigorito. 2009. Cutting edge: the Foxp3 target miR-155 contributes to the development of regulatory T cells. *J Immunol* 182: 2578-2582.
6. Lu, L. F., T. H. Thai, D. P. Calado, A. Chaudhry, M. Kubo, K. Tanaka, G. B. Loeb, H. Lee, A. Yoshimura, K. Rajewsky, and A. Y. Rudensky. 2009. Foxp3-dependent microRNA155 confers competitive fitness to regulatory T cells by targeting SOCS1 protein. *Immunity* 30: 80-91.
7. Cobb, B. S., A. Hertweck, J. Smith, E. O'Connor, D. Graf, T. Cook, S. T. Smale, S. Sakaguchi, F. J. Livesey, A. G. Fisher, and M. Merkenschlager. 2006. A role for Dicer in immune regulation. *J Exp Med* 203: 2519-2527.
8. Liston, A., L. F. Lu, D. O'Carroll, A. Tarakhovsky, and A. Y. Rudensky. 2008. Dicer-dependent microRNA pathway safeguards regulatory T cell function. *J Exp Med* 205: 1993-2004.
9. Divekar, A. A., S. Dubey, P. R. Gangalum, and R. R. Singh. 2011. Dicer insufficiency and microRNA-155 overexpression in lupus regulatory T cells: an apparent paradox in the setting of an inflammatory milieu. *J Immunol* 186: 924-930.
10. Zhang, N., and M. J. Bevan. 2010. Dicer controls CD8+ T-cell activation, migration, and survival. *Proc Natl Acad Sci U S A* 107: 21629-21634.
11. Martin-Gayo, E., E. Sierra-Filardi, A. L. Corbi, and M. L. Toribio. 2010. Plasmacytoid dendritic cells resident in human thymus drive natural Treg cell development. *Blood* 115: 5366-5375.
12. Cortes, J. R., R. Sanchez-Diaz, E. R. Bovolenta, O. Barreiro, S. Lasarte, A. Matesanz-Marin, M. L. Toribio, F. Sanchez-Madrid, and P. Martin. 2014. Maintenance of immune tolerance by Foxp3+ regulatory T cells requires CD69 expression. *J Autoimmun* 55: 51-62.
13. Feng, C., K. J. Woodside, B. A. Vance, D. El-Khoury, M. Canelles, J. Lee, R. Gress, B. J. Fowlkes, E. W. Shores, and P. E. Love. 2002. A potential role for CD69 in thymocyte emigration. *Int Immunol* 14: 535-544.
14. Nakayama, T., D. J. Kasprowicz, M. Yamashita, L. A. Schubert, G. Gillard, M. Kimura, A. Didierlaurent, H. Koseki, and S. F. Ziegler. 2002. The generation of mature, single-positive thymocytes in vivo is dysregulated by CD69 blockade or overexpression. *J Immunol* 168: 87-94.

15. Lamana, A., D. Sancho, A. Cruz-Adalia, G. M. del Hoyo, A. M. Herrera, M. Feria, F. Diaz-Gonzalez, M. Gomez, and F. Sanchez-Madrid. 2006. The role of CD69 in acute neutrophil-mediated inflammation. *Eur J Immunol* 36: 2632-2638.
16. Wirnsberger, G., F. Mair, and L. Klein. 2009. Regulatory T cell differentiation of thymocytes does not require a dedicated antigen-presenting cell but is under T cell-intrinsic developmental control. *Proc Natl Acad Sci U S A* 106: 10278-10283.
17. Noval Rivas, M., M. Hazzan, K. Weatherly, F. Gaudray, I. Salmon, and M. Y. Braun. 2010. NK cell regulation of CD4 T cell-mediated graft-versus-host disease. *J Immunol* 184: 6790-6798.
18. Fontenot, J. D., J. P. Rasmussen, M. A. Gavin, and A. Y. Rudensky. 2005. A function for interleukin 2 in Foxp3-expressing regulatory T cells. *Nat Immunol* 6: 1142-1151.
19. Lu, L. F., G. Gasteiger, I. S. Yu, A. Chaudhry, J. P. Hsin, Y. Lu, P. D. Bos, L. L. Lin, C. L. Zawislak, S. Cho, J. C. Sun, C. S. Leslie, S. W. Lin, and A. Y. Rudensky. 2015. A Single miRNA-mRNA Interaction Affects the Immune Response in a Context- and Cell-Type-Specific Manner. *Immunity* 43: 52-64.
20. Yin, Q., X. Wang, J. McBride, C. Fewell, and E. Flemington. 2008. B-cell receptor activation induces BIC/miR-155 expression through a conserved AP-1 element. *J Biol Chem* 283: 2654-2662.
21. Castellanos, M. C., C. Munoz, M. C. Montoya, E. Lara-Pezzi, M. Lopez-Cabrera, and M. O. de Landazuri. 1997. Expression of the leukocyte early activation antigen CD69 is regulated by the transcription factor AP-1. *J Immunol* 159: 5463-5473.
22. Esplugues, E., D. Sancho, J. Vega-Ramos, C. Martinez, U. Syrbe, A. Hamann, P. Engel, F. Sanchez-Madrid, and P. Lauzurica. 2003. Enhanced antitumor immunity in mice deficient in CD69. *J Exp Med* 197: 1093-1106.
23. Gonzalez-Amaro, R., J. R. Cortes, F. Sanchez-Madrid, and P. Martin. 2013. Is CD69 an effective brake to control inflammatory diseases? *Trends in molecular medicine* 19: 625-632.
24. Radulovic, K., C. Manta, V. Rossini, K. Holzmann, H. A. Kestler, U. M. Wegenka, T. Nakayama, and J. H. Niess. 2012. CD69 regulates type I IFN-induced tolerogenic signals to mucosal CD4 T cells that attenuate their colitogenic potential. *J Immunol* 188: 2001-2013.
25. Vitales-Noyola, M., L. Doniz-Padilla, C. Alvarez-Quiroga, A. Monsivais-Urenda, H. Portillo-Salazar, and R. Gonzalez-Amaro. 2015. Quantitative and functional analysis of CD69(+) NKG2D(+) T regulatory cells in healthy subjects. *Human immunology* 76: 511-518.
26. Lin, C. R., T. W. Wei, H. Y. Tsai, Y. T. Wu, P. Y. Wu, and S. T. Chen. 2015. Glycosylation-dependent interaction between CD69 and S100A8/S100A9 complex is required for regulatory T-cell differentiation. *FASEB journal : official publication of the Federation of American Societies for Experimental Biology*.
27. Matloubian, M., C. G. Lo, G. Cinamon, M. J. Lesneski, Y. Xu, V. Brinkmann, M. L. Allende, R. L. Proia, and J. G. Cyster. 2004. Lymphocyte egress from thymus and peripheral lymphoid organs is dependent on S1P receptor 1. *Nature* 427: 355-360.
28. Shiow, L. R., D. B. Rosen, N. Brdickova, Y. Xu, J. An, L. L. Lanier, J. G. Cyster, and M. Matloubian. 2006. CD69 acts downstream of interferon-alpha/beta to inhibit S1P1 and lymphocyte egress from lymphoid organs. *Nature* 440: 540-544.

29. Weinreich, M. A., and K. A. Hogquist. 2008. Thymic emigration: when and how T cells leave home. *J Immunol* 181: 2265-2270.
30. Lauzurica, P., D. Sancho, M. Torres, B. Albella, M. Marazuela, T. Merino, J. A. Bueren, A. C. Martinez, and F. Sanchez-Madrid. 2000. Phenotypic and functional characteristics of hematopoietic cell lineages in CD69-deficient mice. *Blood* 95: 2312-2320.
31. Martin, P., M. Gomez, A. Lamana, A. Cruz-Adalia, M. Ramirez-Huesca, M. A. Ursa, M. Yanez-Mo, and F. Sanchez-Madrid. 2010. CD69 association with Jak3/Stat5 proteins regulates Th17 cell differentiation. *Mol Cell Biol* 30: 4877-4889.
32. Zheng, Y., S. Z. Josefowicz, A. Kas, T. T. Chu, M. A. Gavin, and A. Y. Rudensky. 2007. Genome-wide analysis of Foxp3 target genes in developing and mature regulatory T cells. *Nature* 445: 936-940.
33. Ziegler, S. F., S. D. Levin, L. Johnson, N. G. Copeland, D. J. Gilbert, N. A. Jenkins, E. Baker, G. R. Sutherland, A. L. Feldhaus, and F. Ramsdell. 1994. The mouse CD69 gene. Structure, expression, and mapping to the NK gene complex. *J Immunol* 152: 1228-1236.
34. Testi, R., J. H. Phillips, and L. L. Lanier. 1989. T cell activation via Leu-23 (CD69). *J Immunol* 143: 1123-1128.
35. Martin, P., and F. Sanchez-Madrid. 2011. CD69: an unexpected regulator of TH17 cell-driven inflammatory responses. *Sci Signal* 4: pe14.
36. Wan, Y. Y., and R. A. Flavell. 2005. Identifying Foxp3-expressing suppressor T cells with a bicistronic reporter. *Proc Natl Acad Sci U S A* 102: 5126-5131.

685 **Figure legends**

686

687 **Figure 1. CD69 expression is required for thymus-derived Treg cell homeostasis in**
688 **adult mice.** (A) Density plots show CD69 expression in $CD4^+CD8^-Foxp3^+$ gated
689 thymocytes from 8-12-week-old Foxp3-mRFP/*cd69*$^{+/+}$ (wild type), Foxp3-mRFP/*cd69*$^{+/-}$
690 (heterozygous), and Foxp3-mRFP/*cd69*$^{-/-}$ (deficient) reporter littermates. Numbers indicate
691 the proportions (%) of gated cells. (B) The bar chart shows the percentage (± S.D.) of
692 $CD69^+$ (black) and $CD69^-$ (white) tTregs within the thymus of the indicated *reporter* mice.
693 (C) Flow cytometry analysis of thymocyte subsets in 8-10-week-old *reporter* littermates.
694 The percentages of thymus-derived T cell subsets are shown. (D) Cellularity of the thymus
695 (left) and total number of CD4 SP cells (right) in *reporter* littermates. (E) Analysis of
696 endogenous Foxp3 expression in tTregs in the thymuses of *reporter* littermates. (F)
697 Percentages (left) and total cell number (right) of gated $CD4^+CD8^-Foxp3^+$ tTregs in adult
698 *reporter* littermates. Data are from at least 7 litters with 3 to 12 littermates each. A total of
699 16 Foxp3-mRFP/*cd69*$^{+/+}$ (wild type), 11 Foxp3-mRFP/*cd69*$^{+/-}$ (heterozygous), and 12
700 Foxp3-mRFP/*cd69*$^{-/-}$ (deficient) mice were analyzed. Error bars show S.D. Data were
701 evaluated by ANOVA followed by Bonferroni's multiple comparison test: * $P < 0.05$, ** P
702 < 0.01, *** $P < 0.001$.

703

704 **Figure 2. tTregs differentiation in fetal thymus organ culture requires CD69**
705 **expression.** (A) Representative density plots of 5 days FTOC from *Cd69*$^{+/+}$ and *Cd69*$^{-/-}$
706 embryo in the C57BL/6 background. Embryonic thymuses were removed from 15 to 17
707 days old embryos and the percentages of tTregs development in the lobes were analysed by
708 FACS. (B) Cellularity of foetal thymus lobes (left) and total cell number of $CD4^+Foxp3^+$

(right) from *Cd69*$^{+/+}$ and *Cd69*$^{-/-}$ embryos. (C) FTOCs from wild type 17 days old embryos (E17) were maintained up to 14 days in culture in the presence of anti-CD69 monoclonal antibody (2.2) or the isotype control antibody (2.8). Density plots shows the percentage of tTregs on days 4, 11 and 14 after culture. (D) Cellularity of foetal thymus lobes (left) and total number of CD4^{+}Foxp3^{+} cells (right) en each condition. A total of 31 and 36 embryos from five *Cd69*$^{+/+}$ and four *Cd69*$^{-/-}$ females respectively, were analysed. The 2 lobes from each fetal thymus were analysed separately. Error bars show S.D. Values are calculated relative to data for *Cd69*$^{+/+}$ control lobes from four independent FTOC assays. * $P < 0.05$, ** $P < 0.01$, *** $P < 0.001$ (Student's t-test).

Figure 3. CD69^{+} hematopoietic stem cells are more prone to develop tTregs after reconstitution. (A) Eight to twelve-week-old C57BL/6 (A) or Rag2$^{-/-}$ γc$^{-/-}$ (B) recipient mice received two or one split doses of 6,5 Gy γ-radiation respectively and were i.v. injected with bone marrow cells from Foxp3-mRFP/*cd69*$^{+/+}$ or Foxp3-mRFP/*cd69*$^{-/-}$ littermates. (C) In mixed chimeras, irradiated Rag2$^{-/-}$γc$^{-/-}$ recipients were transplanted with a mixture of CD45.1-Foxp3-mRFP/*cd69*$^{+/+}$ or CD45.2-Foxp3-mRFP/*cd69*$^{-/-}$ bone marrow precursors at a ratio of 1:1. After at least 10 wks (D), the contribution of the different donor bone marrow precursors to tTreg cells development and CD69 expression in tTregs were determined by FACS (A-D). (E) Percentages of gated CD4^{+} SP cells and CD4^{+}CD8^{-}Foxp3^{+} tTregs within CD45.1 or CD45.2 donors in the thymus. All data are representative of at least 3 independent experiments with at least 3 recipient mice per group or 6 recipient mice for mixed chimeras. Error bars show S.D. * $P < 0.05$, ** $P < 0.01$, *** $P < 0.001$ (Student's t-test).

Figure 4. Expression of miR-155 and target proteins in CD69$^+$ deficient and proficient Treg cells.

(A) Left, representative histogram showing the levels of STAT5 phosphorylation analyzed by FACS in CD69$^+$ or CD69$^-$ sorted tTregs cells. *Right*, the levels of STAT5 phosphorylation shown as the fold difference compared with isotype control-treated cells. Lines link measurements of CD69$^+$ and CD69$^-$ tTregs from the same mouse. **(**B) Representative WB showing the levels of STAT5 phosphorylation in tTregs sorted as in A. Phosphorylation levels are normalized to STAT5 and β–actin total protein levels. q-PCR analysis of the relative expression of Foxp3 (C), BIC promoter, mmu-miR-155 **(**D) and *socs-1* **(**E) in CD69$^+$ and CD69$^-$ tTregs. Expression was normalized to the levels in CD69$^+$ tTregs. **(**F) Representative WB of SOCS1 protein expression in CD69$^+$ and CD69$^-$ Foxp3mRFP$^+$ sorted tTreg cells. SOCS1 levels are normalized to mean β–actin levels from of at least 4 independent sortings. (G) Left, representative histogram showing the levels of STAT5 phosphorylation in sorted tTregs cells from *cd69*$^{+/+}$, *cd69*$^{+/-}$ and *cd69*$^{-/-}$ Foxp3-reporter mice. *Right*, quantification of STAT5 phosphorylation levels shown as Geometric mean fluorescence intensity. (H) mmumiR-155 and *socs1* transcriptional levels analyzed by qPCR in tTregs cells from *cd69*$^{+/+}$, *cd69*$^{+/-}$ and *cd69*$^{-/-}$ Foxp3-reporter mice. All data are derived from at least 5 independent sortings/experiments (3 animals per sorting). Data were analyzed by t-test (A-E) except for WB analyses, for which representative gels are shown. Error bars show S.D. ** $P < 0.01$, *** $P < 0.001$ (Student's t-test). (G-H) Data were analyzed by ANOVA followed by Bonferroni's multiple comparison test: * $P < 0.05$, ** $P < 0.01$, *** $P < 0.001$.

Figure 5. CD69$^+$ Treg development was impaired in the thymus and spleen of *mirn155*$^{-/-}$ mice

Density plots show CD4$^+$CD8$^-$Foxp3$^+$ tTregs and CD69 expression in gated CD4$^+$CD8$^-$ Foxp3$^+$ gated thymocytes (A) or splenocytes (C), from wild type (WT) or *mirn155*$^{-/-}$ mice. Numbers indicate the proportions (%) of gated cells. The bar chart shows total cell number (upper) of gated CD4$^+$CD8$^-$Foxp3$^+$ tTregs and the percentage (± S.D.) of CD69$^+$ (black) and CD69$^-$ (white) tTregs (lower) within the thymus from WT or *mirn155*$^{-/-}$ mice. (B) *cd69* relative expression in thymocytes from WT or *mirn155*$^{-/-}$ mice analysed by qPCR. All data are derived from 5 mice WT and 3 *mirn155*$^{-/-}$. Data were analyzed by t-Test. Error bars show S.D. * $P < 0.05$ (Student's t-test).

Figure 6. CD69 expression rescues iTreg differentiation in the absence of IL-2Rγc/Foxp3 signaling pathway. (A) Naïve CD4$^+$ T cells from Foxp3-mRFP/*cd69*$^{+/+}$ or Foxp3-mRFP/*cd69*$^{-/-}$ littermates were cultured for 72 hours under Treg-skewed conditions and treated with a chemical Jak3 inhibitor or an equal concentration of DMSO for the last 9 hours. The percentages of Phospho-STAT5$^+$ cells and the levels of STAT5 phosphorylation analyzed by FACS and compared to and isotype Ab are shown. (B) Quantification of reporter Foxp3-mRFP$^+$ cells treated as in A. (C) Naïve CD4$^+$ T cells from *Il2rγ*$^{-/-}$/*cd69*$^{-/-}$ and *Il2rγ*$^{-/-}$ mice were cultured as in A and the percentages of Phospho-STAT5$^+$ cells and the levels of STAT5 phosphorylation were analyzed by FACS. (D) Quantification of CD25$^+$ Treg cells were analyzed by FACS. Data are from two independent experiment (n=3

from each genotype). Error bars show S.D. Data were evaluated by ANOVA followed by Bonferroni's multiple comparison test: * $P < 0.05$, ** $P < 0.01$, *** $P < 0.001$.

Figure 7. CD69 downstream signaling regulates miR-155, STAT5 and *socs1* expression in Tregs. (A) *Left*, representative plots of CD69 expression in sorted mouse Foxp3-mRFP/*cd69*$^{+/+}$ tTregs cells treated with anti-CD69 2.2 or 2.8 isotype control. *Right*, CD69 expression after Ab treatment analyzed by FACS. Bars correspond to the mean ± S.D. of one representative experiment of four. (B) qPCR analysis of mmu-miR-155 expression in sorted CD69^{+} or CD69^{-} Foxp3-mRFP^{+} tTregs after Ab treatment. Results are normalized by snoRNA135 expression and the expression was relative to 2.8-treated CD69^{+} cells. (C) Left, representative histogram showing the levels of STAT5 phosphorylation in iTreg cells from *cd69*$^{+/+}$ or *cd69*$^{-/-}$ reporter mice treated with anti-CD69 2.2 or 2.8 isotype control. *Right*, quantification of STAT5 phosphorylation levels shown as Geometric mean fluorescence intensity. (D) *socs1* transcriptional levels were analyzed by qPCR. Data from A-B are derived from 3 independent sortings/experiments (3 animals per sorting) and iTregs differentiated from at least 4 mice per group (C-D). Data was analyzed by 1-way ANOVA and Bonferroni's post-test (B). CD69 expression after Ab treatment was analyzed by t test (A). * $P < 0.05$, ** $P < 0.01$, *** $P < 0.001$ (Student's t-test).

Figure 8. Co-regulation of CD69 and miR-155 expression in human Tregs. (A) *Left*, Representative histograms of CD69 expression after LV infection with 3 different shCD69 sequences (1-3) or a sh control sequence, stimulated or not with human anti-CD3 Abs (OKT3 clone). *Right*, CD69 fold induction relative to non-stimulated cells. (B) q-PCR analysis of hsa-miR-155 expression in human CD4^{+} T cells after LV infection. (C) Human

PBLs were stimulated or not with PMA/Iono for 4 hours and the percentage of $CD69^+$ cells and phospho-Stat5 (D) were analyzed by FACS. (D) hsa-miR-155 and human *socs1* gene expression were analyzed by qPCR. (E) Human PBLs were transfected with anti-hsa-miR-155-5p or anti-miRNA Scramble and hsa-miR-155 expression was analyzed by qPCR. (F) Representative histograms and quantification of CD69 expression, STAT5 phosphorylation and human socs-1 transcription in $CD4^+$ PBLs treated as in (E). (G) Human PBLs were transfected with hsa-pre-miR-155-5p or pre-miRNA-control and hsa-miR-155 expression was analyzed by qPCR. (H) CD69 expression, STAT5 phosphorylation and human socs-1 transcription in $CD4^+$ PBLs treated as in (G). Results from miRNA qPCRs are normalized to snoRNA135 expression. All data are mean ± S.D. of at least 3 independent donors from a total of ten donors. Data was analyzed by 1-way ANOVA and Bonferroni's post-test or by t-test. * $P < 0.05$, ** $P < 0.01$, *** $P < 0.001$.

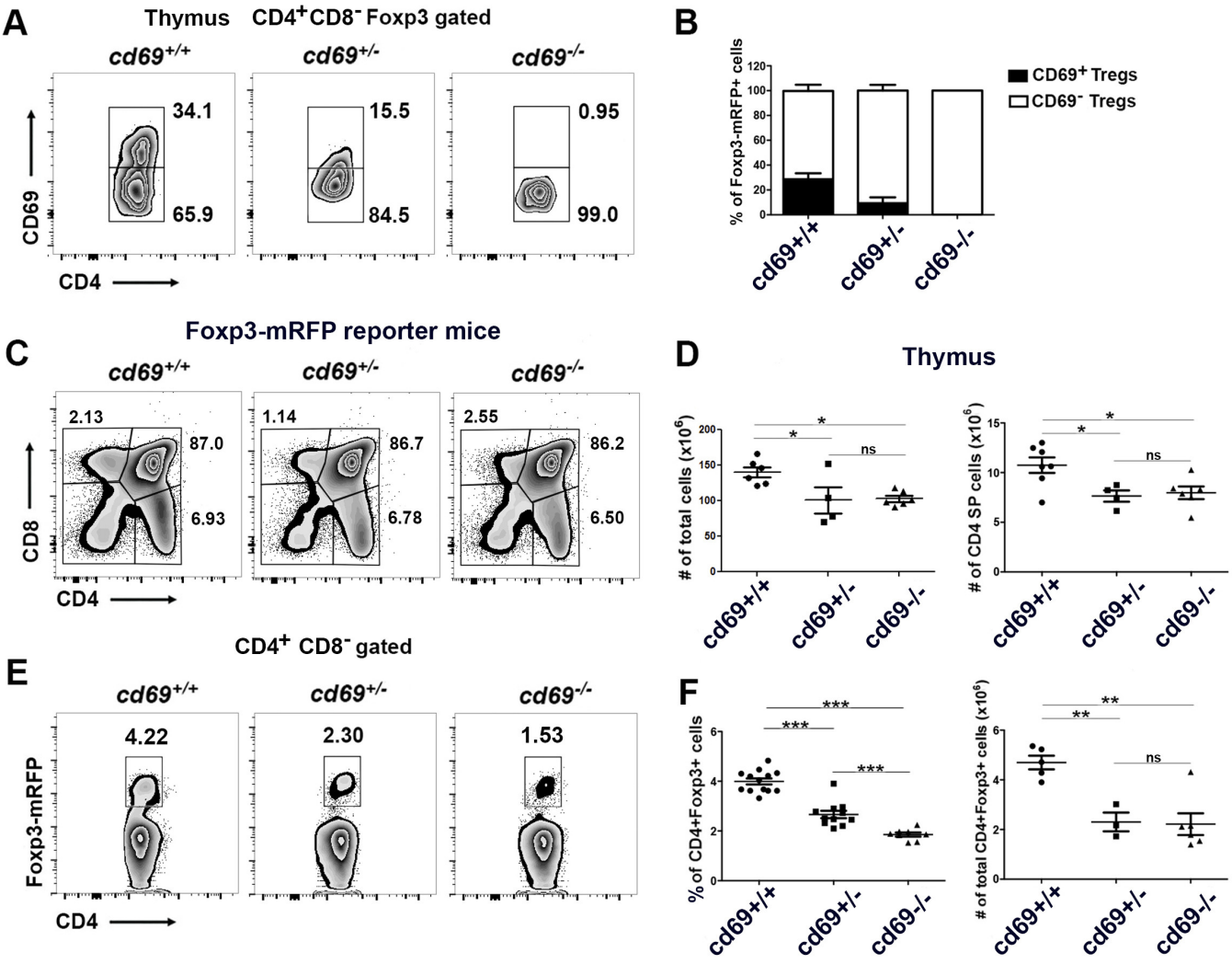

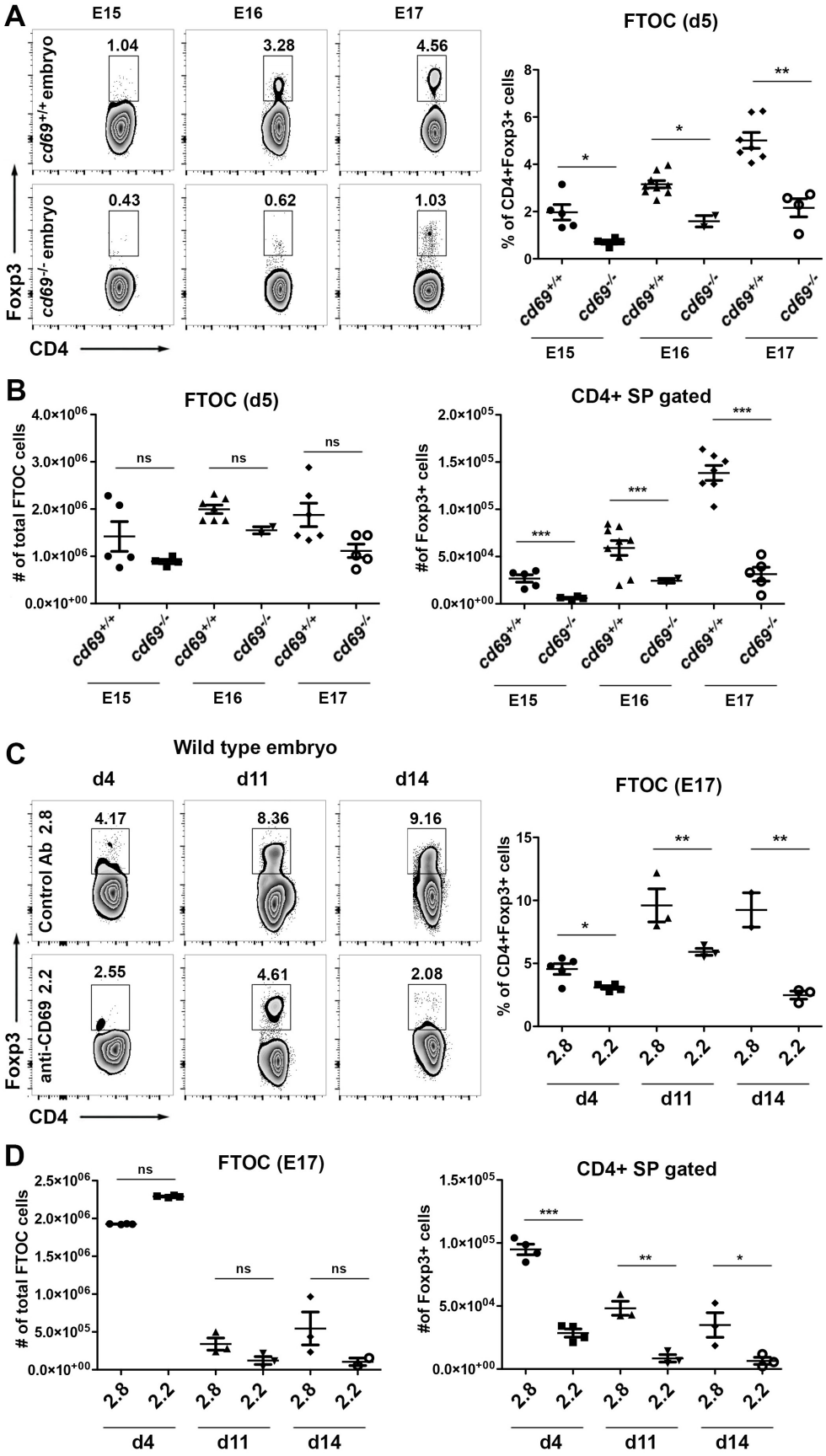

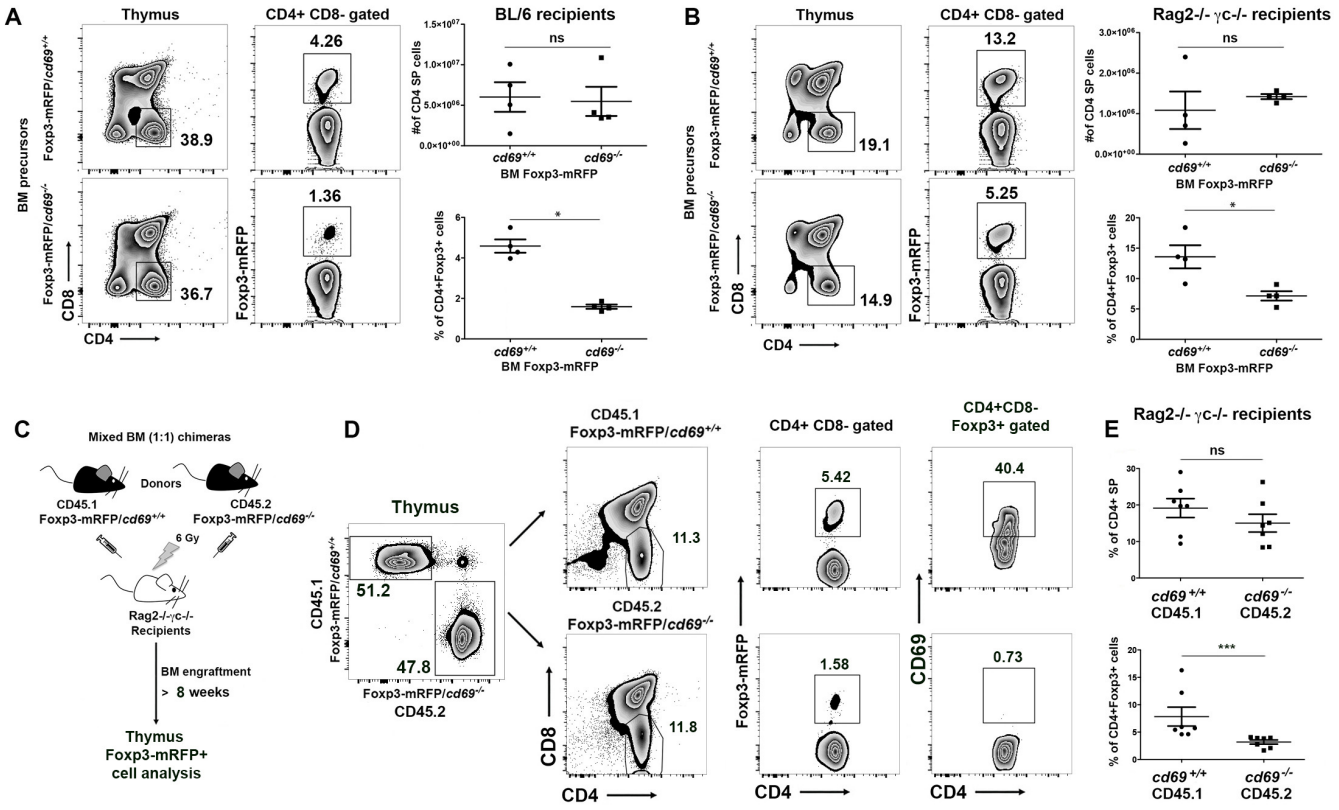

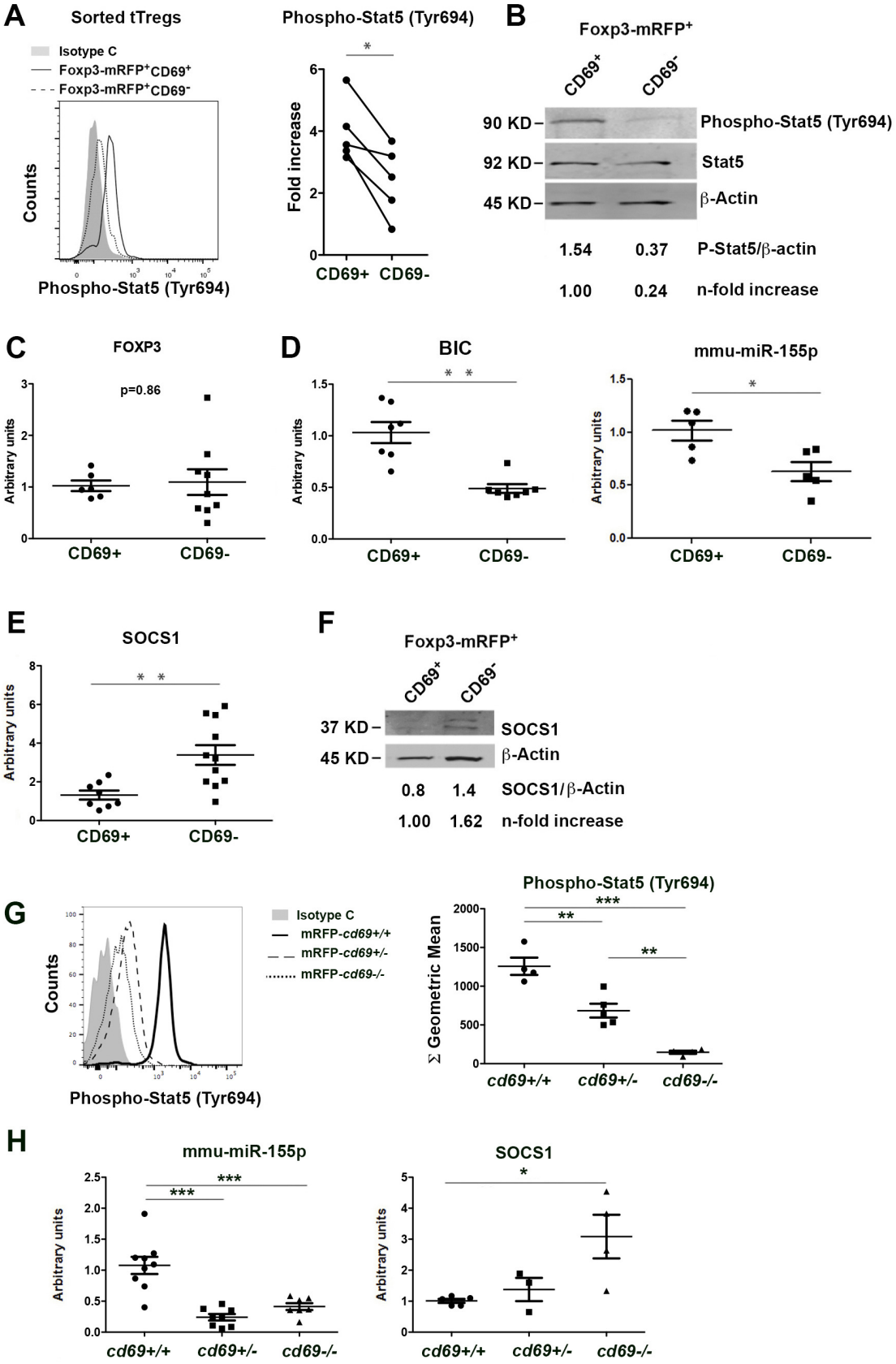

Molecular and Cellular Biology